CHAPTER 2: BLAST, FRAGMENT, AND SHOCK LOADS

CHAPTER 2 BLAST, FRAGMENT, AND SHOCK LOADS

CHAPTER 2 BLAST, FRAGMENT, AND SHOCK LOADS 2-1

INTRODUCTION 2-1
2-1 PURPOSE. 2-1
2-2 OBJECTIVE 2-1
2-3 BACKGROUND. 2-1
2-4 SCOPE. 2-2
2-5 FORMAT. 2-4
2-6 CHAPTER CONTENTS. 2-4
2-7 EFFECTS OF EXPLOSIVE OUTPUT. 2-4
BLAST LOADS 2-5
2-8 BLAST PHENOMENA. 2-5
2-8.1 General. 2-5
2-8.2 Explosive Materials. 2-6
2-9 TNT EQUIVALENCY. 2-6
2-10 BLAST-LOADING CATEGORIES. 2-7
2-10.1 Unconfined Explosion. 2-7
2-10.2 Confined Explosion. 2-8
2-11 BLAST LOADING PROTECTION. 2-8
2-12 BLAST-WAVE PHENOMENA. 2-9
2-13 UNCONFINED EXPLOSIONS 2-10
2-13.1 Free Air Burst. 2-10
2-13.2 Air Burst. 2-12
2-13.3 Surface Burst. 2-13
2-13.4 Multiple Explosions. 2-14
2-14 CONFINED EXPLOSIONS. 2-15
2-14.1 Effects of Confinement. 2-15
2-14.2 Shock Pressures. 2-16
2-14.3 Gas Pressures. 2-23

2-14.4 Leakage Pressures. 2-27
2-15 EXTERNAL BLAST LOADS ON STRUCTURES. 2-30
2-15.1 General. 2-30
2-15.2 Forces Acting on Structures. 2-30
2-15.3 Above-Ground Rectangular Structure without Openings. 2-32
2-15.4 Above Ground Rectangular Structures with Openings. 2-36
2-15.5 Pressure Buildup in Structures. 2-43
PRIMARY AND SECONDARY FRAGMENTS 2-287
2-16 GENERAL. 2-287
2-17 PRIMARY FRAGMENTS. 2-287
2-17.1 General. 2-287
2-17.2 Initial Fragment Velocity. 2-288
2-17.3 Fragment Mass Distribution. 2-290
2-17.4 Variation of Fragment Velocity with Distance. 2-293
2-17.5 Primary Fragments - Shape, Caliber Density and Impact Angle. 2-294
2-18 SECONDARY FRAGMENTS. 2-297
2-18.1 General. 2-297
2-18.2 Velocity of Unconstrained Secondary Fragments. 2-298
2-18.3 Velocity of Constrained Secondary Fragments. 2-301
2-19 FRAGMENT TRAJECTORIES. 2-303
SHOCK LOADS 2-326
2-20 INTRODUCTION. 2-326
2-21 GROUND SHOCK. 2-327
2-21.1 Introduction. 2-327
2-21.2 Air Blast-Induced Ground Shock. 2-328
2-21.3 Direct-Induced Ground Motion. 2-329
2-22 AIR SHOCK. 2-331
2-22.1 Introduction. 2-331
2-22.2 Method of Analysis. 2-331
2-23 STRUCTURE MOTIONS. 2-333
2-23.1 Introduction. 2-333

2-23.2 Net Ground Shock. 2-333
2-23.3 Maximum Structure Motion. 2-334
2-24 SHOCK RESPONSE SPECTRA. 2-335
2-24.1 Introduction. 2-335
2-24.2 Definition of Shock Spectra Grid. 2-335
2-24.3 Response Spectra. 2-336

CHAPTER 2 BLAST, FRAGMENT, AND SHOCK LOADS: FIGURES

Figure 2-1 Blast Loading Categories 2-45
Figure 2-2 Free-Field Pressure-Time Variation 2-46
Figure 2-3 Peak Incident Pressure versus Peak Dynamic Pressure, Density of Air Behind the Shock Front, and Particle Velocity 2-47
Figure 2-4 Free-Air Burst Blast Environment 2-48
Figure 2-5 Pressure-Time Variation for a Free-Air Burst 2-49
Figure 2-6 Peak Incident Pressure versus the Ratio of Normal Reflected Pressure/Incident Pressure for a Free-Air Burst 2-50
Figure 2-7 Positive Phase Shock Wave Parameters for a Spherical TNT Explosion in Free Air at Sea Level 2-51
Figure 2-8 Negative Phase Shock Wave Parameters for a Spherical TNT Explosion in Free Air at Sea Level 2-52
Figure 2-9 Variation of Reflected Pressure as a Function of Angle of Incidence ... 2-53
Figure 2-10 Variation of Scaled Reflected Impulse as a Function of Angle of Incidence 2-54
Figure 2-11 Air Burst Blast Environment 2-55
Figure 2-12 Pressure-Time Variation for Air Burst 2-55
Figure 2-13 Scaled Height of Triple Point 2-56
Figure 2-14 Surface Burst Blast Environment 2-57
Figure 2-15 Positive Phase Shock Wave Parameters for a Hemispherical TNT Explosion on the Surface at Sea Level 2-58
Figure 2-16 Negative Phase Shock Wave Parameters for a Hemispherical TNT Explosion on the Surface at Sea Level 2-59
Figure 2-17 Explosive Shapes 2-60
Figure 2-18 Peak Positive Incident Pressure and Scaled Impulse for an Explosion on the Surface at Sea Level, Composition A-3 and A-5 2-61
Figure 2-19 Peak Positive Incident Pressure and Scaled Impulse for an Explosion on the Surface at Sea Level, Composition B 2-62
Figure 2-20 Peak Positive Incident Pressure and Scaled Impulse for an Explosion on the Surface at Sea Level, Composition C-4 and Guanidine Nitrate 2-63

Figure 2-21 Peak Positive Incident Pressure and Scaled Impulse for an Explosion on the Surface at Sea Level, Cyclotol 70/30 and 64 M42 Grenades 2-64

Figure 2-22 Peak Positive Incident Pressure and Scaled Impulse for an Explosion on the Surface at Sea Level, HMX and M483 155mm ICM Projectile 2-65

Figure 2-23 Peak Positive Incident Pressure and Scaled Impulse for an Explosion on the Surface at Sea Level, Lead Azide (dextrinated) and Lead Styphnate 2-66

Figure 2-24 Peak Positive Incident Pressure and Scaled Impulse for an Explosion on the Surface at Sea Level, LX-14 2-67

Figure 2-25 Peak Positive Incident Pressure and Scaled Impulse for an Explosion on the Surface at Sea Level, Octol 75/25 and M718/741 RAAM 2-68

Figure 2-26 Peak Positive Incident Pressure and Scaled Impulse for an Explosion on the Surface at Sea Level, Nitrocellulose 2-69

Figure 2-27 Peak Positive Incident Pressure and Scaled Impulse for an Explosion on the Surface at Sea Level, Nitroglycerine and PBXC-203 2-70

Figure 2-28 Peak Positive Incident Pressure and Scaled Impulse for an Explosion on the Surface at Sea Level, RDX Slurry and RDX 98/2 2-71

Figure 2-29 Peak Positive Incident Pressure and Scaled Impulse for an Explosion on the Surface at Sea Level, TNT 2-72

Figure 2-30 Peak Positive Incident Pressure and Scaled Impulse for an Explosion on the Surface at Sea Level, Tetracene and Nitroguanidine 2-73

Figure 2-31 Peak Positive Incident Pressure and Scaled Impulse for an Explosion on the Surface at Sea Level, Benite Propellant and Black Powder 2-74

Figure 2-32 Peak Positive Incident Pressure and Scaled Impulse for an Explosion on the Surface at Sea Level, BS-NACO Propellant 2-75

Figure 2-33 Peak Positive Incident Pressure and Scaled Impulse for an Explosion on the Surface at Sea Level, DIGL-RP I5420, I5421, and I5422 Propellants 2-76

Figure 2-34 Peak Positive Incident Pressure and Scaled Impulse for an Explosion on the Surface at Sea Level, MI and M26 EI Propellants 2-77

Figure 2-35 Peak Positive Incident Pressure and Scaled Impulse for an Explosion on the Surface at Sea Level, M26 EI Propellant 2-78

Figure 2-36 Peak Positive Incident Pressure and Scaled Impulse for an Explosion on the Surface at Sea Level, M30 AI Propellant 2-79

Figure 2-37 Peak Positive Incident Pressure and Scaled Impulse for an Explosion on the Surface at Sea Level, M30 AI Propellant and M31 AI EI Slotted Stick Propellant 2-80

Figure 2-38 Peak Positive Incident Pressure and Scaled Impulse for an Explosion on the Surface at Sea Level, M31AIEI Slotted Stick Propellant and N5 Propellant 2-81

Figure 2-39 Peak Positive Incident Pressure and Scaled Impulse for an Explosion on the Surface at Sea Level, N5 Propellant 2-82

Figure 2-40 Peak Positive Incident Pressure and Scaled Impulse for an Explosion on the Surface at Sea Level, M6 Propellant 2-83

Figure 2-41 Peak Positive Incident Pressure and Scaled Impulse for an Explosion on the Surface at Sea Level, 2.75in Rocket Grain and WC844 Ball Powder 2-84

Figure 2-42 Peak Positive Incident Pressure and Scaled Impulse for an Explosion on the Surface at Sea Level, XM37 RAP Propellant 2-85

Figure 2-43 Peak Positive Incident Pressure and Scaled Impulse for an Explosion on the Surface at Sea Level, XM37 RAP Propellant, continued 2-86

Figure 2-44 Peak Positive Incident Pressure and Scaled Impulse for an Explosion on the Surface at Sea Level, JA-2 (L5460) Propellant and M10 Propellant 2-87

Figure 2-45 Peak Positive Incident Pressure and Scaled Impulse for an Explosion on the Surface at Sea Level, M10 Propellant and 105mm M314-A3 2-88

Figure 2-46 Peak Positive Incident Pressure and Scaled Impulse for an Explosion on the Surface at Sea Level, I559 Igniter Mixture and I560 Subigniter Mixture 2-89

Figure 2-47 Peak Positive Incident Pressure and Scaled Impulse for an Explosion on the Surface at Sea Level, I560 Subigniter Mixture and R284 Tracer Mixture 2-90

Figure 2-48 Peak Positive Incident Pressure and Scaled Impulse for an Explosion on the Surface at Sea Level, M314-A3 First Fire Composition and M49-A1 Trip Flare Composition 2-91

Figure 2-49 Peak Positive Incident Pressure and Scaled Impulse for an Explosion on the Surface at Sea Level, M49-A1 Trip Flare Composition 2-92

Figure 2-50 Confined Explosion Structures 2-93

Figure 2-51 Barrier and Cubicle Configurations and Parameters..... 2-94
Figure 2-52 Average Peak Reflected Pressure (*N* = 1, *l/L* = 0.10, *h/H* = 0.10)..... 2-95
Figure 2-53 Average Peak Reflected Pressure (*N* = 1, *l/L* = 0.25 and 0.75, *h/H* = 0.10)..... 2-96
Figure 2-54 Average Peak Reflected Pressure (*N* = 1, *l/L* = 0.50, *h/H* = 0.10)..... 2-97
Figure 2-55 Average Peak Reflected Pressure (*N* = 1, *l/L* = 0.10, *h/H* = 0.25)..... 2-98
Figure 2-56 Average Peak Reflected Pressure (*N* = 1, *l/L* = 0.25 and 0.75, *h/H* = 0.25)..... 2-99
Figure 2-57 Average Peak Reflected Pressure (*N* = 1, *l/L* = 0.50, *h/H* = 0.25)..... 2-100
Figure 2-58 Average Peak Reflected Pressure (*N* = 1, *l/L* = 0.10, *h/H* = 0.50)..... 2-101
Figure 2-59 Average Peak Reflected Pressure (*N* = 1, *l/L* = 0.25 and 0.75, *h/H* = 0.50)..... 2-102
Figure 2-60 Average Peak Reflected Pressure (*N* = 1, *l/L* = 0.50, *h/H* = 0.50)..... 2-103
Figure 2-61 Average Peak Reflected Pressure (*N* = 1, *l/L* = 0.10, *h/H* = 0.75)..... 2-104
Figure 2-62 Average Peak Reflected Pressure (*N* = 1, *l/L* = 0.25 and 0.75, *h/H* = 0.75)..... 2-105
Figure 2-63 Average Peak Reflected Pressure (*N* = 1, *l/L* = 0.50, *h/H* = 0.75)..... 2-106
Figure 2-64 Average Peak Reflected Pressure (*N* = 2, *l/L* = 0.10, *h/H* = 0.10)..... 2-107
Figure 2-65 Average Peak Reflected Pressure (*N* = 2, *l/L* = 0.25, *h/H* = 0.10)..... 2-108
Figure 2-66 Average Peak Reflected Pressure (*N* = 2, *l/L* = 0.50, *h/H* = 0.10)..... 2-109
Figure 2-67 Average Peak Reflected Pressure (*N* = 2, *l/L* = 0.75, *h/H* = 0.10)..... 2-110
Figure 2-68 Average Peak Reflected Pressure (*N* = 2, *l/L* = 0.10, *h/H* = 0.25)..... 2-111
Figure 2-69 Average Peak Reflected Pressure (*N* = 2, *l/L* = 0.25, *h/H* = 0.25)..... 2-112
Figure 2-70 Average Peak Reflected Pressure (*N* = 2, *l/L* = 0.50, *h/H* = 0.25)..... 2-113
Figure 2-71 Average Peak Reflected Pressure (*N* = 2, *l/L* = 0.75, *h/H* = 0.25)..... 2-114
Figure 2-72 Average Peak Reflected Pressure (*N* = 2, *l/L* = 0.10, *h/H* = 0.50)..... 2-115
Figure 2-73 Average Peak Reflected Pressure (*N* = 2, *l/L* = 0.25, *h/H* = 0.50)..... 2-116
Figure 2-74 Average Peak Reflected Pressure (*N* = 2, *l/L* = 0.50, *h/H* = 0.50)..... 2-117
Figure 2-75 Average Peak Reflected Pressure (*N* = 2, *l/L* = 0.75, *h/H* = 0.50)..... 2-118
Figure 2-76 Average Peak Reflected Pressure (*N* = 2, *l/L* = 0.10, *h/H* = 0.75)..... 2-119
Figure 2-77 Average Peak Reflected Pressure (*N* = 2, *l/L* = 0.25, *h/H* = 0.75)..... 2-120
Figure 2-78 Average Peak Reflected Pressure (*N* = 2, *l/L* = 0.50, *h/H* = 0.75)..... 2-121
Figure 2-79 Average Peak Reflected Pressure (*N* = 2, *l/L* = 0.75, *h/H* = 0.75)..... 2-122

Figure 2-80 Average Peak Reflected Pressure (*N* = 3, *l/L* = 0.10, *h/H* = 0.10)..... 2-123
Figure 2-81 Average Peak Reflected Pressure (*N* = 3, *l/L* = 0.25 and 0.75, *h/H* = 0.10)..... 2-124
Figure 2-82 Average Peak Reflected Pressure (*N* = 3, *l/L* = 0.50, *h/H* = 0.10)..... 2-125
Figure 2-83 Average Peak Reflected Pressure (*N* = 3, *l/L* = 0.10, *h/H* = 0.25)..... 2-126
Figure 2-84 Average Peak Reflected Pressure (*N* = 3, *l/L* = 0.25 and 0.75, *h/H* = 0.25)..... 2-127
Figure 2-85 Average Peak Reflected Pressure (*N* = 3, *l/L* = 0.50, *h/H* = 0.25)..... 2-128
Figure 2-86 Average Peak Reflected Pressure (*N* = 3, *l/L* = 0.10, *h/H* = 0.50)..... 2-129
Figure 2-87 Average Peak Reflected Pressure (*N* = 3, *l/L* = 0.25 and 0.75, *h/H* = 0.50)..... 2-130
Figure 2-88 Average Peak Reflected Pressure (*N* = 3, *l/L* = 0.50, *h/H* = 0.50)..... 2-131
Figure 2-89 Average Peak Reflected Pressure (*N* = 3, *l/L* = 0.10, *h/H* = 0.75)..... 2-132
Figure 2-90 Average Peak Reflected Pressure (*N* = 3, *l/L* = 0.25 and 0.75, *h/H* = 0.75)..... 2-133
Figure 2-91 Average Peak Reflected Pressure (*N* = 3, *l/L* = 0.50, *h/H* = 0.75)..... 2-134
Figure 2-92 Average Peak Reflected Pressure (*N* = 4, *l/L* = 0.10, *h/H* = 0.10)..... 2-135
Figure 2-93 Average Peak Reflected Pressure (*N* = 4, *l/L* = 0.25 and 0.75, *h/H* = 0.10)..... 2-136
Figure 2-94 Average Peak Reflected Pressure (*N* = 4, *l/L* = 0.50, *h/H* = 0.10)..... 2-137
Figure 2-95 Average Peak Reflected Pressure (*N* = 4, *l/L* = 0.10, *h/H* = 0.25 and 0.75)..... 2-138
Figure 2-96 Average Peak Reflected Pressure (*N* = 4, *l/L* = 0.25 and 0.75, *h/H* = 0.25 and 0.75)..... 2-139
Figure 2-97 Average Peak Reflected Pressure (*N* = 4, *l/L* = 0.50, *h/H* = 0.25 and 0.75)..... 2-140
Figure 2-98 Average Peak Reflected Pressure (*N* = 4, *l/L* = 0.10, *h/H* = 0.50)..... 2-141
Figure 2-99 Average Peak Reflected Pressure (*N* = 4, *l/L* = 0.25 and 0.75, *h/H* = 0.50)..... 2-142
Figure 2-100 Average Peak Reflected Pressure (*N* = 4, *l/L* = 0.50, *h/H* = 0.50)..... 2-143
Figure 2-101 Scaled Average Unit Reflected Impulse (*N* = 1, *l/L* = 0.10, *h/H* = 0.10)..... 2-144
Figure 2-102 Scaled Average Unit Reflected Impulse (*N* = 1, *l/L* = 0.25 and 0.75, *h/H* = 0.10)..... 2-145

Figure 2-103 Scaled Average Unit Reflected Impulse (*N* = 1, *l/L* = 0.50, *h/H* = 0.10) 2-146
Figure 2-104 Scaled Average Unit Reflected Impulse (*N* = 1, *l/L* = 0.10, *h/H* = 0.25) 2-147
Figure 2-105 Scaled Average Unit Reflected Impulse (*N* = 1, *l/L* = 0.25 and 0.75, *h/H* = 0.25) 2-148
Figure 2-106 Scaled Average Unit Reflected Impulse (*N* = 1, *l/L* = 0.50, *h/H* = 0.25) 2-149
Figure 2-107 Scaled Average Unit Reflected Impulse (*N* = 1, *l/L* = 0.10, *h/H* = 0.50) 2-150
Figure 2-108 Scaled Average Unit Reflected Impulse (*N* = 1, *l/L* = 0.25 and 0.75, *h/H* = 0.50) 2-151
Figure 2-109 Scaled Average Unit Reflected Impulse (*N* = 1, *l/L* = 0.50, *h/H* = 0.50) 2-152
Figure 2-110 Scaled Average Unit Reflected Impulse (*N* = 1, *l/L* = 0.10, *h/H* = 0.75) 2-153
Figure 2-111 Scaled Average Unit Reflected Impulse (*N* = 1, *l/L* = 0.25 and 0.75, *h/H* = 0.75) 2-154
Figure 2-112 Scaled Average Unit Reflected Impulse (*N* = 1, *l/L* = 0.50, *h/H* = 0.75) 2-155
Figure 2-113 Scaled Average Unit Reflected Impulse (*N* = 2, *l/L* = 0.10, *h/H* = 0.10) 2-156
Figure 2-114 Scaled Average Unit Reflected Impulse (*N* = 2, *l/L* = 0.25, *h/H* = 0.10) 2-157
Figure 2-115 Scaled Average Unit Reflected Impulse (*N* = 2, *l/L* = 0.50, *h/H* = 0.10) 2-158
Figure 2-116 Scaled Average Unit Reflected Impulse (*N* = 2, *l/L* = 0.75, *h/H* = 0.10) 2-159
Figure 2-117 Scaled Average Unit Reflected Impulse (*N* = 2, *l/L* = 0.10, *h/H* = 0.25) 2-160
Figure 2-118 Scaled Average Unit Reflected Impulse (*N* = 2, *l/L* = 0.25, *h/H* = 0.25) 2-161
Figure 2-119 Scaled Average Unit Reflected Impulse (*N* = 2, *l/L* = 0.50, *h/H* = 0.25) 2-162
Figure 2-120 Scaled Average Unit Reflected Impulse (*N* = 2, *l/L* = 0.75, *h/H* = 0.25) 2-163

Figure 2-121 Scaled Average Unit Reflected Impulse (*N* = 2, *l/L* = 0.10, *h/H* = 0.50) 2-164
Figure 2-122 Scaled Average Unit Reflected Impulse (*N* = 2, *l/L* = 0.25, *h/H* = 0.50) 2-165
Figure 2-123 Scaled Average Unit Reflected Impulse (*N* = 2, *l/L* = 0.50, *h/H* = 0.50) 2-166
Figure 2-124 Scaled Average Unit Reflected Impulse (*N* = 2, *l/L* = 0.75, *h/H* = 0.50) 2-167
Figure 2-125 Scaled Average Unit Reflected Impulse (*N* = 2, *l/L* = 0.10, *h/H* = 0.75) 2-168
Figure 2-126 Scaled Average Unit Reflected Impulse (*N* = 2, *l/L* = 0.25, *h/H* = 0.75) 2-169
Figure 2-127 Scaled Average Unit Reflected Impulse (*N* = 2, *l/L* = 0.50, *h/H* = 0.75) 2-170
Figure 2-128 Scaled Average Unit Reflected Impulse (*N* = 2, *l/L* = 0.75, *h/H* = 0.75) 2-171
Figure 2-129 Scaled Average Unit Reflected Impulse (*N* = 3, *l/L* = 0.10, *h/H* = 0.10) 2-172
Figure 2-130 Scaled Average Unit Reflected Impulse (*N* = 3, *l/L* = 0.25 and 0.75, *h/H* = 0.10) 2-173
Figure 2-131 Scaled Average Unit Reflected Impulse (*N* = 3, *l/L* = 0.50, *h/H* = 0.10) 2-174
Figure 2-132 Scaled Average Unit Reflected Impulse (*N* = 3, *l/L* = 0.10, *h/H* = 0.25) 2-175
Figure 2-133 Scaled Average Unit Reflected Impulse (*N* = 3, *l/L* = 0.25 and 0.75, *h/H* = 0.25) 2-176
Figure 2-134 Scaled Average Unit Reflected Impulse (*N* = 3, *l/L* = 0.50, *h/H* = 0.25) 2-177
Figure 2-135 Scaled Average Unit Reflected Impulse (*N* = 3, *l/L* = 0.10, *h/H* = 0.50) 2-178
Figure 2-136 Scaled Average Unit Reflected Impulse (*N* = 3, *l/L* = 0.25 and 0.75, *h/H* = 0.50) 2-179
Figure 2-137 Scaled Average Unit Reflected Impulse (*N* = 3, *l/L* = 0.50, *h/H* = 0.50) 2-180
Figure 2-138 Scaled Average Unit Reflected Impulse (*N* = 3, *l/L* = 0.10, *h/H* = 0.75) 2-181

Figure 2-139 Scaled Average Unit Reflected Impulse (N = 3, l/L = 0.25 and 0.75, h/H = 0.75) 2-182
Figure 2-140 Scaled Average Unit Reflected Impulse (N = 3, l/L = 0.50, h/H = 0.75) 2-183
Figure 2-141 Scaled Average Unit Reflected Impulse (N = 4, l/L = 0.10, h/H = 0.10) 2-184
Figure 2-142 Scaled Average Unit Reflected Impulse (N = 4, l/L = 0.25 and 0.75, h/H = 0.10) 2-185
Figure 2-143 Scaled Average Unit Reflected Impulse (N = 4, l/L = 0.50, h/H = 0.10) 2-186
Figure 2-144 Scaled Average Unit Reflected Impulse (N = 4, l/L = 0.10, h/H = 0.25 and 0.75) 2-187
Figure 2-145 Scaled Average Unit Reflected Impulse (N = 4, l/L = 0.25 and 0.75, h/H = 0.25 and 0.75) 2-188
Figure 2-146 Scaled Average Unit Reflected Impulse (N = 4, l/L = 0.50, h/H = 0.25 and 0.75) 2-189
Figure 2-147 Scaled Average Unit Reflected Impulse (N = 4, l/L = 0.10, h/H = 0.50) 2-190
Figure 2-148 Scaled Average Unit Reflected Impulse (N = 4, l/L = 0.25 and 0.75, h/H = 0.50) 2-191
Figure 2-149 Scaled Average Unit Reflected Impulse (N = 4, l/L = 0.50, h/H = 0.50) 2-192
Figure 2-150 Reflection Factor for Shock Loads on Frangible Elements 2-193
Figure 2-151 Pressure-Time Variation for a Partially Vented Explosion 2-194
Figure 2-152 Peak Gas Pressure Produced by a TNT Detonation in a Partially Contained Chamber 2-195
Figure 2-153 Scaled Gas Impulse (W/V_f = 0.002, $i_r/W^{1/3}$ = 20) 2-196
Figure 2-154 Scaled Gas Impulse (W/V_f = 0.002, $i_r/W^{1/3}$ = 100) 2-197
Figure 2-155 Scaled Gas Impulse (W/V_f = 0.002, $i_r/W^{1/3}$ = 600) 2-198
Figure 2-156 Scaled Gas Impulse (W/V_f = 0.015, $i_r/W^{1/3}$ = 20) 2-199
Figure 2-157 Scaled Gas Impulse (W/V_f = 0.015, $i_r/W^{1/3}$ = 100) 2-200
Figure 2-158 Scaled Gas Impulse (W/V_f = 0.015, $i_r/W^{1/3}$ = 600) 2-201
Figure 2-159 Scaled Gas Impulse (W/V_f = 0.15, $i_r/W^{1/3}$ = 20) 2-202
Figure 2-160 Scaled Gas Impulse (W/V_f = 0.15, $i_r/W^{1/3}$ = 100) 2-203
Figure 2-161 Scaled Gas Impulse (W/V_f = 0.15, $i_r/W^{1/3}$ = 600) 2-204

Figure 2-162 Scaled Gas Impulse (W/V_f = 1.0, $i_r/W^{1/3}$ = 100) 2-205
Figure 2-163 Scaled Gas Impulse (W/V_f = 1.0, $i_r/W^{1/3}$ = 600) 2-206
Figure 2-164 Scaled Gas Impulse (W/V_f = 1.0, $i_r/W^{1/3}$ = 2000) 2-207
Figure 2-165 Combined Shock and Gas Pressures 2-208
Figure 2-166 TNT Conversion Factor for Charges 2-209
Figure 2-167 Fully Vented Three-Wall Cubicles and Direction of Blast Wave Propagation 2-210
Figure 2-168 Envelope Curves for Peak Positive Pressure Outside Three-Wall Cubicles without a Roof 2-211
Figure 2-169 Envelope Curves for Peak Positive Pressure Outside Three-Wall Cubicles with a Roof 2-212
Figure 2-170 Envelope Curves for Maximum Peak Pressure Outside Three-Wall Cubicles 2-213
Figure 2-171 Scaled Peak Positive Impulse Out the Open Front of Cubic Three-Wall Cubicle without a Roof 2-214
Figure 2-172 Scaled Peak Positive Impulse Out the Open Front of Rectangular Three-Wall Cubicle without a Roof 2-215
Figure 2-173 Scaled Peak Positive Impulse Behind Sidewall of Cubic Three-Wall Cubicle without a Roof 2-216
Figure 2-174 Scaled Peak Positive Impulse Behind Sidewall of Rectangular Three-Wall Cubicle without a Roof 2-217
Figure 2-175 Scaled Peak Positive Impulse Behind Backwall of Cubic Three-Wall Cubicle without a Roof 2-218
Figure 2-176 Scaled Peak Positive Impulse Behind Backwall of Rectangular Three-Wall Cubicle without a Roof 2-219
Figure 2-177 Scaled Peak Positive Impulse Out the Open Front of Cubic Three-Wall Cubicle with a Roof 2-220
Figure 2-178 Scaled Peak Positive Impulse Out the Open Front of Rectangular Three-Wall Cubicle with a Roof 2-221
Figure 2-179 Scaled Peak Positive Impulse Behind Sidewall of Cubic Three-Wall Cubicle with a Roof 2-222
Figure 2-180 Scaled Peak Positive Impulse Behind Sidewall of Rectangular Three-Wall Cubicle with a Roof 2-223
Figure 2-181 Scaled Peak Positive Impulse Behind Backwall of Cubic Three-Wall Cubicle with a Roof 2-224

Figure 2-182 Scaled Peak Positive Impulse Behind Backwall of Rectangular Three-Wall Cubicle with a Roof 2-225
Figure 2-183 Four Wall Cubicle Vented Through its Roof 2-226
Figure 2-184 Peak Positive Pressure Outside of a Four-Wall Cubicle Vented Through Its Roof 2-227
Figure 2-185 Scaled Positive Impulse Outside of a Four-Wall Cubicle Vented Through Its Roof 2-228
Figure 2-186 Four Wall Cubicle Vented Through a Wall and Direction of Blast Wave Propagation 2-229
Figure 2-187 Peak Positive Pressure at the Front of a Partially Vented Four-Wall Cubicle 2-230
Figure 2-188 Peak Positive Pressure at the Side of a Partially Vented Four-Wall Cubicle 2-231
Figure 2-189 Peak Positive Pressure at the Back of a Partially Vented Four-Wall Cubicle 2-232
Figure 2-190 Idealized Pressure-Time Variation 2-233
Figure 2-191 Front Wall Loading 2-234
Figure 2-192 Velocity of Sound in Reflected Overpressure Region versus Peak Incident Overpressure 2-235
Figure 2-193 Reflected Pressure Coefficient versus Angle of Incidence 2-236
Figure 2-194 (a) Reflected Scaled Impulse versus Angle of Incidence 2-237
Figure 2-195 Roof and Side Wall Loading 2-239
Figure 2-196 Peak Equivalent Uniform Roof Pressures 2-240
Figure 2-197 Scaled Rise Time of Equivalent Uniform Positive Roof Pressures 2-241
Figure 2-198 Scaled Duration of Equivalent Uniform Roof Pressures 2-242
Figure 2-199 Rear Wall Loading 2-243
Figure 2-200 Idealized Structure Configuration for Interior Blast Loads 2-244
Figure 2-201 Idealized Interior Blast Loads 2-245
Figure 2-202 Sub-Division of Typical Front Wall with Openings 2-245
Figure 2-203 Maximum Average Pressure on Interior Face of Front Wall (W/H = 3/4) 2-246
Figure 2-204 Maximum Average Pressure on Interior Face of Front Wall (W/H = 3/2) 2-247
Figure 2-205 Maximum Average Pressure on Interior Face of Front Wall (W/H = 3) 2-248

Figure 2-206 Maximum Average Pressure on Interior Face of Front Wall (*W*/*H* = 6) 2-249

Figure 2-207 Arrival Time, T_1, for Interior Front Wall Blast Load (*W/H* = 3/4 and 3/2)..... 2-250

Figure 2-208 Arrival Time, T_1, for Interior Front Wall Blast Load (*W/H* = 3 and 6) ... 2-251

Figure 2-209 Idealized Rise Time, T_2 - T_1, for Interior Front Wall Blast Load (*W/H* = 3/4 and 3/2)..... 2-252

Figure 2-210 Idealized Rise Time, T_2 - T_1, for Interior Front Wall Blast Load (*W/H* = 3 and 6) 2-253

Figure 2-211 Idealized Duration, T_3 - T_1, for Interior Front Wall Blast Load (*W/H* = 3/4 and 3/2)..... 2-254

Figure 2-212 Idealized Duration, T_3 - T_1, for Interior Front Wall Blast Load (*W/H* = 3 and 6)..... 2-255

Figure 2-213 Idealized Times T_1 and T_2 for Interior Side Wall Blast Load 2-256

Figure 2-214 Idealized Times T_3 and T_4 for Interior Side Wall Blast Load (*L/H* = 1, *W/H* = 3/4) 2-257

Figure 2-215 Idealized Times T_3 and T_4 for Interior Side Wall Blast Load (*L/H* = 1, *W/H* = 3/2) 2-258

Figure 2-216 Idealized Times T_3 and T_4 for Interior Side Wall Blast Load (*L/H* = 1, *W/H* = 3) 2-259

Figure 2-217 Idealized Times T_3 and T_4 for Interior Side Wall Blast Load (*L/H* = 1, *W/H* = 6) 2-260

Figure 2-218 Idealized Times T_3 and T_4 for Interior Side Wall Blast Load (*L/H* = 2, *W/H* = 3/4) 2-261

Figure 2-219 Idealized Times T_3 and T_4 for Interior Side Wall Blast Load (*L/H* = 2, *W/H* = 3/2) 2-262

Figure 2-220 Idealized Times T_3 and T_4 for Interior Side Wall Blast Load (*L/H* = 2, *W/H* = 3) 2-263

Figure 2-221 Idealized Times T_3 and T_4 for Interior Side Wall Blast Load (*L/H* = 2, *W/H* = 6) 2-264

Figure 2-222 Idealized Times T_3 and T_4 for Interior Side Wall Blast Load (*L/H* = 4, *W/H* = 3/4) 2-265

Figure 2-223 Idealized Times T_3 and T_4 for Interior Side Wall Blast Load (*L/H* = 4, *W/H* = 3/2) 2-266

Figure 2-224 Idealized Times T_3 and T_4 for Interior Side Wall Blast Load (*L/H* = 4, *W/H* = 3) 2-267

Figure 2-225 Idealized Times T_3 and T_4 for Interior Side Wall Blast Load (L/H = 4, W/H = 6) 2-268

Figure 2-226 Idealized Times T_3 and T_4 for Interior Side Wall Blast Load (L/H = 8, W/H = 3/4) 2-269

Figure 2-227 Idealized Times T_3 and T_4 for Interior Side Wall Blast Load (L/H = 8, W/H = 3/2) 2-270

Figure 2-228 Idealized Times T_3 and T_4 for Interior Side Wall Blast Load (L/H = 8, W/H = 3) 2-271

Figure 2-229 Idealized Times T_3 and T_4 for Interior Side Wall Blast Load (L/H = 8, W/H = 6) 2-272

Figure 2-230 Idealized Pressure Coefficient for Back Wall Interior Blast Load (L/H = 1 and 2) 2-273

Figure 2-231 Idealized Pressure Coefficient for Back Wall Interior Blast Load (L/H = 4 and 8) 2-274

Figure 2-232 Arrival Time, T_1, for Interior Back Wall Blast Load (W/H = 3/4 and 3/2) 2-275

Figure 2-233 Arrival Time, T_1, for Interior Back Wall Blast Load (W/H = 3 and 6) 2-276

Figure 2-234 Idealized Time $T_2 - T_1$ for Interior Back Wall Blast Load 2-277

Figure 2-235 Leakage Pressure Coefficient versus Pressure Differential 2-278

Figure 2-236 Explosive Outer Casing Separated By Incompressible Fluid 2-305

Figure 2-237 Initial Velocity of Primary Fragments for Various Geometries 2-306

Figure 2-238 M_A/B versus Cylindrical Casing Geometry 2-307

Figure 2-239 Design Fragment Weight versus Design Confidence Level ($0.3 \leq C_L \leq 1$) 2-308

Figure 2-240 Design Fragment Weight versus Design Confidence Level ($0.986 \leq C_L \leq 1$) 2-309

Figure 2-241 B^2N_T/W_C versus Casing Geometry 2-310

Figure 2-242 Equivalent Cylindrical Explosive Casings 2-311

Figure 2-243 Variation of Primary Fragment Velocity with Distance 2-312

Figure 2-244 Primary Fragment Shapes 2-313

Figure 2-245 Relationship between Fragment Weight and Fragment Diameter 2-314

Figure 2-246 Interaction of Blast Wave with an Irregular Object 2-315

Figure 2-247 Idealized Pressure-Time Loading on an Irregular Fragment 2-315

Figure 2-248 Nondimensional Object Velocity, $\overline{V}$, as a Function of Pressure and Impulse 2-316

Figure 2-249 Target Shape Factor for Unconstrained Fragments 2-317
Figure 2-250 Specific Acquired Impulse versus Distance 2-318
Figure 2-251 Scaled Fragment Velocities for Constrained Fragments 2-319
Figure 2-252 Fragment Range Prediction 2-320
Figure 2-253 Net Ground Motions Produced By an Explosion at the Ground Surface 2-338
Figure 2-254 Typical Response Shock Spectra 2-339

CHAPTER 2 BLAST, FRAGMENT, AND SHOCK LOADS: TABLES

Table 2-1 Heat of Detonation and Heat of Combustion 2-279
Table 2-2 List of Illustrations of Peak Incident Pressure and Impulse Produced By Surface Detonation of Various Explosives 2-280
Table 2-3 List of Illustrations for Average Peak Reflected Pressure and Scaled Average Unit Reflected Impulse..... 2-286
Table 2-4 List of Illustrations for Interior Side Wall Idealized Times T_3 and T_4.... 2-286
Table 2-5 Specific Weight and Gurney Energy Constant for Various Explosives..... 2-321
Table 2-6 Initial Velocity of Primary Fragments for Various Geometries..... 2-322
Table 2-7 Mott Scaling Constants for Mild Steel Casings and Various Explosives..... 2-324
Table 2-8 Drag Coefficient, C_D, for Various Shapes 2-325
Table 2-9 Steel Toughness..... 2-325
Table 2-10 Mass Density for Typical Soils and Rocks 2-340
Table 2-11 Typical Seismic Velocities for Soils and Rocks..... 2-341
Table 2-12 Coefficient of Friction for Concrete Foundation and Underlying Soils. 2-341

CHAPTER 2 BLAST, FRAGMENT, AND SHOCK LOADS

INTRODUCTION

2-1 PURPOSE.

The purpose of this manual is to present methods of design for protective construction used in facilities for development, testing, production, storage, maintenance, modification, inspection, demilitarization, and disposal of explosive materials.

2-2 OBJECTIVE.

The primary objectives are to establish design procedures and construction techniques whereby propagation of explosion (from one structure or part of a structure to another) or mass detonation can be prevented and to provide protection for personnel and valuable equipment.

The secondary objectives are to:

(1) Establish the blast load parameters required for design of protective structures.

(2) Provide methods for calculating the dynamic response of structural elements including reinforced concrete, and structural steel.

(3) Establish construction details and procedures necessary to afford the required strength to resist the applied blast loads.

(4) Establish guidelines for siting explosive facilities to obtain maximum cost effectiveness in both the planning and structural arrangements, providing closures, and preventing damage to interior portions of structures because of structural motion, shock, and fragment perforation.

2-3 BACKGROUND.

For the first 60 years of the 20th century, criteria and methods based upon results of catastrophic events were used for the design of explosive facilities. The criteria and methods did not include a detailed or reliable quantitative basis for assessing the degree of protection afforded by the protective facility. In the late 1960's quantitative procedures were set forth in the first edition of the present manual, "Structures to Resist the Effects of Accidental Explosions." This manual was based on extensive research and development programs which permitted a more reliable approach to current and future design requirements. Since the original publication of this manual, more extensive testing and development programs have taken place. This additional research included work with materials other than reinforced concrete which was the principal construction material referenced in the initial version of the manual.

Modern methods for the manufacture and storage of explosive materials, which include many exotic chemicals, fuels, and propellants, require less space for a given quantity of explosive material than was previously needed. Such concentration of explosives increases the possibility of the propagation of accidental explosions (one accidental explosion causing the detonation of other explosive materials). It is evident that a requirement for more accurate design techniques is essential. This manual describes rational design methods to provide the required structural protection.

These design methods account for the close-in effects of a detonation including the high pressures and the nonuniformity of blast loading on protective structures or barriers. These methods also account for intermediate and far-range effects for the design of structures located away from the explosion. The dynamic response of structures, constructed of various materials, or combination of materials, can be calculated, and details are given to provide the strength and ductility required by the design. The design approach is directed primarily toward protective structures subjected to the effects of a high explosive detonation. However, this approach is general, and it is applicable to the design of other explosive environments as well as other explosive materials as mentioned above.

The design techniques set forth in this manual are based upon the results of numerous full- and small-scale structural response and explosive effects tests of various materials conducted in conjunction with the development of this manual and/or related projects.

2-4 SCOPE.

It is not the intent of this manual to establish safety criteria. Applicable documents should be consulted for this purpose. Response predictions for personnel and equipment are included for information.

In this manual an effort is made to cover the more probable design situations. However, sufficient general information on protective design techniques has been included in order that application of the basic theory can be made to situations other than those which were fully considered.

This manual is applicable to the design of protective structures subjected to the effects associated with high explosive detonations. For these design situations, the manual will apply for explosive quantities less than 25,000 pounds for close-in effects. However, this manual is also applicable to other situations such as far- or intermediate-range effects. For these latter cases the design procedures were originally developed for explosive quantities in the order of 500,000 pounds which is the maximum quantity of high explosive approved for aboveground storage facilities in the Department of Defense manual, "DoD Ammunition and Explosives Safety Standards," DOD 6055.09-M. **1**\ However, DOD 6055.09-M currently addresses explosive quantities of up to 5,000,000 lbs, and the design procedures in this document have been extrapolated for designs to resist accidental explosions on ships of 5,000,000 lbs or more. Although some disasters have involved very high explosive quantities (such as Port Chicago in 1944 which involved around 10,000,000 pounds of explosives), limited testing has been

completed at such high quantities (e.g. the Middle North Series used 1,000,000 lbs TNT, and the Minor Scale and Misty Picture used the equivalent of 8,000,000 lbs TNT). /**1**/ Since tests were primarily directed toward the response of structural steel and reinforced concrete elements to blast overpressures, this manual concentrates on design procedures and techniques for these materials. However, this does not imply that concrete and steel are the only useful materials for protective construction. Tests to establish the response of wood, brick blocks, and plastics, as well as the blast attenuating and mass effects of soil are contemplated. The results of these tests may require, at a later date, the supplementation of these design methods for these and other materials.

Other manuals are available to design protective structures against the effects of high explosive or nuclear detonations. The procedures in these manuals will quite often complement this manual and should be consulted for specific applications.

Computer programs, which are consistent with procedures and techniques contained in the manual, have been approved by the appropriate representative of the US Army, the US Navy, the US Air Force and the Department of Defense Explosives Safety Board (DDESB). These programs are available through the following repositories:

(1) Department of the Army
Commander and Director
U.S. Army Engineer Research and Development Center
Post Office Box 631
Vicksburg, Mississippi 39180-0631
Attn: WESKA

(2) Department of the Navy
Commanding Officer
Naval Facilities Engineering and Expeditionary Warfare Center
1000 23rd Avenue
Port Hueneme, California 93043
Attn: Code CI7

(3) Department of the Air Force
Aerospace Structures
Information and Analysis Center
Wright Patterson Air Force Base
Ohio 45433
Attn: AFFDL/FBR

If any modifications to these programs are required, they will be submitted for review by DDESB and the above services. Upon concurrence of the revisions, the necessary changes will be made and notification of the changes will be made by the individual repositories.

2-5 FORMAT.

This manual is subdivided into six specific chapters dealing with various aspects of design. The titles of these chapters are as follows:

Chapter 1 Introduction

Chapter 2 Blast, Fragment, and Shock Loads

Chapter 3 Principles of Dynamic Analysis

Chapter 4 Reinforced Concrete Design

Chapter 5 Structural Steel Design

Chapter 6 Special Considerations in Explosive Facility Design

When applicable, illustrative examples are included in the Appendices.

Commonly accepted symbols are used as much as possible. However, protective design involves many different scientific and engineering fields, and, therefore, no attempt is made to standardize completely all the symbols used. Each symbol is defined where it is first used, and in the list of symbols at the end of each chapter.

2-6 CHAPTER CONTENTS.

This chapter contains the procedures for determining explosive output and associated structure loadings, fragment effects, and the structural motion effects associated with accidental explosions. These procedures are contained in the following sections: Section 2-8 through 2-15 deal with the loadings associated with the blast phenomena. These data include, in addition to the determination of the effects of the explosive output, methods for determining blast loads acting on the exterior of and within structures. Sections 2-16 through 2-19 cover the formation of fragments which can be projected by an explosion and include both primary and secondary fragments effects. Sections 2-20 to 2-24 present the method for determining the structural motions, including both ground and air shock effects.

2-7 EFFECTS OF EXPLOSIVE OUTPUT.

In the design of protective structures to resist the effects of accidental explosions, the principal effects of the explosive output to be considered are blast overpressures (hereafter referred to as blast pressures or pressures), fragments generated by the explosion, and the shock loads produced by the shock wave transmitted through the air or ground. Of these three parameters, the blast pressures are usually the governing factor in the determination of the structure response. However, in some situations, fragments and/or shock loads may be just as important as the pressures in determining the configuration of the facility.

The quantitative data presented pertain to the blast output of bare trinitrotoluene (TNT) spherical or hemispherical charges considered as point source explosions, and other

explosives that have been specifically tested. These data can be extended by appropriate means, including testing, to include other potentially mass-detonating materials (solid, liquid, or gas) of varying shape. If these methods and procedures are to be adapted for use in analyzing the blast-wave effects caused by energetic materials which differ appreciably from those on which these predictions are based, it is the responsibility of the blast analyst to establish applicability of these procedures with respect to the boundary conditions associated with the scenario analyzed.

BLAST LOADS

2-8 BLAST PHENOMENA.

2-8.1 General.

Bare, solid explosives must detonate to produce any explosive effect other than a fire. The term detonation refers to a very rapid and stable chemical reaction which proceeds through the explosive material at a speed, called the detonation velocity, which is supersonic in the unreacted explosive. Detonation velocities range from 22,000 to 28,000 feet per second for most high explosives. The detonation wave rapidly converts the solid or liquid explosive into a very hot, dense, high-pressure gas, and the volume of this gas which had been the explosive material is then the source of strong blast waves in air. Pressures immediately behind the detonation front range from 2,700,000 to 4,900,000 psi. Only about one-third of the total chemical energy available in most high explosives is released in the detonation process. The remaining two-thirds is released more slowly in explosions in air as the detonation products mix with air and burn. This afterburning process has only a slight effect on blast wave properties because it is so much slower than detonation.

The blast effects of an explosion are in the form of a shock wave composed of a high-intensity shock front which expands outward from the surface of the explosive into the surrounding air. As the wave expands, it decays in strength, lengthens in duration, and decreases in velocity. These phenomena are caused by spherical divergence as well as by the fact that the chemical reaction is completed, except for some afterburning associated with the hot explosion products mixing with the surrounding atmosphere.

As the wave expands in air, the front impinges on structures located within its path and then the entire structure is engulfed by the shock pressures. The magnitude and distribution of the blast loads on the structure arising from these pressures are a function of the following factors: (1) explosive properties, namely type of explosive material, energy output (high or low order detonation), and weight of explosive; (2) the location of the detonation relative to the protective structures; and (3) the magnitude and reinforcement of the pressure by its interaction with the ground barrier, or the structure itself. The first of these three factors are discussed in Sections 2-8.2 and 2-9 below and the latter two factors are discussed throughout the remainder of this section.

2-8.2 Explosive Materials.

Explosive materials may be classified according to their physical state: solids, liquids, or gases. Solid explosives are primarily high explosives; however, other materials such as flammable chemicals and propellants may also be classified as potentially explosive materials. Liquid and gaseous explosives encompass a wide variety of substances used in the manufacture of chemicals, fuels, and propellants. The blast pressure environment produced will vary not only among the different materials but may also differ for a particular material. Such factors as methods and procedures used in manufacturing, storage, and handling, in addition to specific individual physical and chemical characteristics, may alter the blast effects of an explosive material.

The blast effects of solid materials are best known. This is particularly true for high-explosive materials. The blast pressures, impulses, durations, and other blast effects of an explosion have been well established. These effects are contained in this chapter.

Unlike high-explosive materials, other solid, liquid, and gaseous explosive materials will exhibit a variation of their blast pressure output. An explosion of these materials is in many cases incomplete, and only a portion of the total mass of the explosive (effective charge weight) is involved in the detonation process. The remainder of the mass is usually consumed by deflagration resulting in a large amount of the material's chemical energy being dissipated as thermal energy which, in turn, may cause fires or thermal radiation damage.

2-9 TNT EQUIVALENCY.

The major quantity of blast effects data presented in this manual pertains to the blast pressures output of bare spherical TNT explosive. These data can be extended to include other potentially mass-detonating materials (Class 1.1) by relating the explosive energy of the "effective charge weight" of those materials to that of an equivalent weight of TNT. In addition to the energy output, other factors may affect the equivalency of material compared to TNT. These factors include the material shape (flat, square, round, etc.), the number of explosive items, explosive confinement (casing, containers, etc.), and the pressure range being considered (close-in, intermediate or far ranges). These other factors will be discussed later in this manual.

For blast resistant design, the effects of the energy output on explosive material, of a specific shape, relative to that of TNT, of similar shape, can be expressed as function of the heat of detonation of the various materials as follows:

$$W_E = \frac{H^d_{EXP}}{H^d_{TNT}} W_{EXP} \qquad 2\text{-}1$$

where

W_E = *effective charge weight*
W_{EXP} = *weight of the explosive in question*
H^d_{EXP} = *heat of detonation of explosive in question*
H^d_{TNT} = *heat of detonation of TNT*

The heats of detonation of some of the more commonly used explosives are listed in Table 2-1 (+).

The above equation for the effective charge weight is related primarily to the blast output associated with the shock effects of unconfined detonations (Section 2-13). The effective charge weight produced by the confinement effects of explosions (Section 2-14) will differ. These differences will be discussed later in this manual.

2-10 BLAST-LOADING CATEGORIES.

Blast loads on structures can be divided into two main groups based on the confinement of the explosive charge (unconfined and confined explosions) and can be subdivided based on the blast loading produced within the donor structure or acting on acceptor structures. These blast loading categories are illustrated in Figure 2-1 (+). Figure 2-1 gives the six blast loading categories possible. Figure 2-1 also shows the five possible pressure loads associated with the blast load categories, the location of the explosive charge which would produce these pressure loads, and the protective structures subjected to these loads.

The blast load categories and the resulting pressure loads listed in Figure 2-1 (+) are qualitatively and, quantitatively defined below and in subsequent sections, respectively.

2-10.1 Unconfined Explosion.

2-10.1.1 Free Air Burst Explosion.

An explosion, which occurs in free air, produces an initial output whose shock wave propagates away from the center of the detonation, striking the protective structure without intermediate amplification of its wave.

2-10.1.2 Air Burst Explosion.

An explosion which is located at a distance from and above the protective structure so that the ground reflections of the initial wave occur prior to the arrival of the blast wave at the protective structure. As used in this manual, an air burst is limited to an explosion which occurs at a height above the ground not more than three times the height of a one or two-story building.

2-10.1.3 Surface Burst Explosion.

A surface burst explosion will occur when the detonation is located close to, or on the ground so that the initial shock is amplified at the point of detonation due to the ground reflections.

2-10.2 Confined Explosion.

2-10.2.1 Fully Vented Explosion.

A fully vented explosion will be produced within or immediately adjacent to a barrier or cubicle type structure with one or more surfaces open to the atmosphere. The initial wave, which is amplified by the non-frangible portions of the structure, and the products of detonation are totally vented to the atmosphere forming a shock wave (leakage pressures) which propagates away from the structure.

2-10.2.2 Partially Confined Explosion.

A partially confined explosion will be produced within a barrier or cubicle type structure with limited size openings and/or frangible surfaces. The initial wave, which is amplified by the frangible and non-frangible portion of the structure, and the products of detonation are vented to the atmosphere after a finite period of time. The confinement of the detonation products, which consist of the accumulation of high temperatures and gaseous products, is associated with a buildup of quasi-static pressure (hereafter referred to as gas pressure). This pressure has a long duration in comparison to that of the shock pressure.

2-10.2.3 Fully Confined Explosions.

Full confinement of an explosion is associated with either total or near total containment of the explosion by a barrier structure. Internal blast loads will consist of unvented shock loads and very long duration gas pressures which are a function of the degree of containment. The magnitude of the leakage pressures will usually be small and will only affect those facilities immediately outside the containment structure.

2-11 BLAST LOADING PROTECTION.

Protection of personnel and valuable equipment (acceptor system) will usually involve protective shelters located away from the detonation. Their design may involve one or more of the following blast-loading categories: free-air burst, air burst, surface burst, and exterior or leakage pressures from either vented or partially confined explosions. These shelters are usually enclosed buildings located at pressure ranges of a few hundred pounds per square inch (psi) or less. Depending on the shelter design pressures, these structures can be either above, below, or at ground surface. In this manual, primary consideration is given to above-ground shelters. However, some consideration is given in Chapter 6 regarding shelters positioned at other locations. For the third type of pressure loading of Figure 2-1 (+) (interior shock pressure), protection is required when the shelter is located immediately adjacent to the explosion. The

reflected pressure there may be in thousands of psi, but with pressure durations usually small. The acceptor portion of such an explosive system may include other explosive materials and/or personnel. The structure associated with the fifth pressure-loading type is a containment type building and is usually used to prevent escape of toxic chemicals, radiological and/or biological materials, or to limit blast pressures at the exterior to a level consistent with personnel protection.

Of the six categories, those from air bursts are seldom encountered and the free air burst is the least likely to occur. The possibility of such blast environments exists where potentially explosive materials are stored at heights adjacent to or away from protective structures such as in manufacturing (process or storage tanks) or missile sites. In the latter, the rocket propellant would be a source of explosive danger to the ground crew and control facilities.

The other four blast-loading categories can occur in most explosive manufacturing and storage facilities. In such installations, transportation of explosive materials between buildings either by rail, vehicle, or in the case of liquid or gases, through piping, is a possibility. Also, storage and handling of explosives within buildings are common occurrences.

Although the blast-loading categories can be separated and classified individually, no clear-cut limits differentiate each category. In most explosive facilities, the various blast environments will overlap, and judgment should be used in the application of the following recommendations for determining the blast parameters consistent with the various blast-loading categories.

2-12 BLAST-WAVE PHENOMENA.

The violent release of energy from a detonation converts the explosive material into a very high pressure gas at very high temperatures. A pressure front associated with the high pressure gas propagates radially into the surrounding atmosphere as a strong shock wave, driven and supported by the hot gases. The shock front, termed the blast wave, is characterized by an almost instantaneous rise from ambient pressure to a peak incident pressure P_{so} (Figure 2-2 (+)).

This pressure increase or shock front travels radially from the burst point with a diminishing shock velocity *U,* which is always in excess of the sonic velocity of the medium. Gas molecules behind the front move at lower flow velocities, termed particle velocities *u*. These latter particle velocities are associated with the dynamic pressures formed by the winds from the passage of the shock front, which have a maximum pressure, $q_{o.}$. As the shock front expands into increasingly larger volumes of the medium, the peak incident pressures at the fronts decrease and the durations of the pressures increase. The shock velocity, peak particle velocity, and peak dynamic pressure, vary as the peak incident pressure varies, as shown in Figure 2-3 (+).

At any point away from the burst, the pressure disturbance has the shape shown in Figure 2-2 (+). The shock front arrives at a given location at time t_A and, after the rise to

the peak value, P_{so} the incident pressure decays to the ambient value in time to which is the positive phase duration. This is followed by a negative phase with a duration t_o^- that is usually much longer than the positive phase and characterized by a negative pressure (below ambient pressure) having a maximum value of P_{so}^-, as well as a reversal of the particle flow. The negative phase is usually less important in a design than is the positive phase, and its amplitude P_s^- must, in all cases, be less than ambient atmosphere pressure p_o. The incident impulse associated with the blast wave is the integrated area under the pressure-time curve and is denoted as i_s for the positive phase and i_s^- for the negative phase.

An additional parameter of the blast wave, the wave length, is sometimes required in the analysis of structures. The positive wave length L_w^+ is that length at a given distance from the detonation which, at a particular instant of time, is experiencing positive pressure. The negative wave length L_w^- is similarly defined for negative pressures.

The above treatment of the blast wave phenomena is general. In subsequent sections of this chapter, the magnitude of the various parameters is presented depending upon the category of the detonation as previously described: free air burst, surface burst, exterior or leakage pressures, or interior or high pressure blast loading.

2-13 UNCONFINED EXPLOSIONS.

2-13.1 Free Air Burst.

When a detonation occurs adjacent to and above a protective structure such that no amplification of the initial shock wave occurs between the explosive source and the protective structure, then the blast loads acting on the structure are free-air blast pressures (Figure 2-4 (+)).

As the incident wave moves radially away from the center of the explosion, it will impact with the structure, and, upon impact, the initial wave (pressure and impulse) is reinforced and reflected (Figure 2-5 (+)). The reflected pressure pulse of Figure 2-5 is typical for infinite plane reflectors.

When the shock wave impinges on a surface oriented so that a line which describes the path of travel of the wave is normal to the surface, then the point of initial contact is said to sustain the maximum (normal reflected) pressure and impulse. Figure 2-6 (+) presents the ratios of the normal reflected pressures to the incident pressures as a function of the incident pressures.

The peak pressure and impulse patterns on the structure vary with distance from a maximum at the normal distance R_A to a minimum (incident pressure) where the plane of the structure's surface is perpendicular to the shock front. The positive phase pressures, impulses, durations, and other parameters of this shock environment for a spherical TNT explosions are given in Figure 2-7 (+) versus the scaled distance ($Z = R/W^{1/3}$).

The smallest scaled distance of 0.136 ft/lb$^{1/3}$ represents the radius of the spherical TNT explosive and, therefore, represents the surface of the explosive. Some parameters have been extrapolated to the charge surface, which are shown as dashed portions of the curves. These dashed curves represent an upper limit of scatter in experimental data and variation in theoretical predictions, giving for design purposes conservative limits for these parameters.

In some blast loading situations, negative blast wave parameters (Figure 2-8 (+)) are needed to predict the loading-time function of the blast wave acting on a structure. This is particularly true in flexible type protective structures (usually steel-frame structures) where the overall motion of the structure will be affected by the phasing of the blast loads acting on the various structure surfaces. The effects of the negative phase parameters are usually not important for the design of the more rigid type structures (reinforced concrete).

The curves presented in Figure 2-7 (+) and Figure 2-8 (+), which give the blast wave parameters as a function of scaled distance, extend only to a scaled distance Z = 100 ft/lb$^{1/3}$. For most protective structures, or even light structures, damage is relatively superficial beyond this scaled distance, consisting at most of broken windows or deformation of light panels or blow-out walls. But, the curves are also not extended beyond these levels because the blast wave properties start to be seriously affected by atmospheric conditions so that overpressures are very much less or very much more than the "ideal" parameters transmitted through a homogeneous atmosphere.

In the low pressure region, the pressure varies as a function of sound velocity with altitude above the ground surface. At very far distances from an explosion (Z= 1000 ft/lb$^{1/3}$), the peak pressures (really sound pressures at these levels) can be ten times greater, or more than ten times less than the ideal pressures for a homogenous atmosphere.

Even with enhancement caused by real atmospheric conditions (also called blast focusing), the pressures are still quite low and structural damage should be superficial. If it is necessary to predict such low levels, one should obtain and study more detailed reports listed in the bibliography.

The variation of the pressure and impulse patterns on the surface of a structure between the maximum and minimum values is a function of the angle of incidence. This angle is formed by the line which defines the normal distance R_A between the point of detonation and the structure, and line R (slant distance) which defines the path of shock propagation between the center of the explosion and any other point in question on the structure surface (Figure 2-4 (+)).

The effects of the angle of incidence on the peak reflected pressure $P_{r\alpha}$ and the reflected impulse $i_{r\alpha}$ are shown in Figure 2-9 (+) and Figure 2-10 (+), respectively. The figures are plots of the angle of incidence versus the peak reflected pressure or the reflected impulse as a function of the scaled normal distance between the charge and the surface in question. The usual load condition involves the ground surface and,

therefore, this normal scaled distance is referred to as the scaled height of charge above the ground ($H_c/W^{1/3}$). All other blast parameters are obtained from Figure 2-7 (+) and Figure 2-8 (+) for the scaled slant distance $R/W^{1/3}$ to the point in question.

2-13.2 Air Burst.

The air burst environment is produced by detonations which occur above the ground surface and at a distance away from the protective structure so that the initial shock wave, propagating away from the explosion, impinges on the ground surface prior to arrival at the structure. As the shock wave continues to propagate outward along the ground surface, a front known as the Mach front (Figure 2-11 (+)) is formed by the interaction of the initial wave (incident wave) and the reflected wave. This reflected wave is the result of the reinforcement of the incident wave by the ground surface.

Some variation of the pressures over the height of the Mach front occurs, but for design purposes, this variation can be neglected and the shock considered as a plane wave over the full height of the front. The blast parameters in the Mach front are calculated at the ground surface. The pressure-time variation of the Mach front (Figure 2-12a (+)) is similar to that of the incident wave except that the magnitude of the blast parameters are somewhat larger.

The height of the Mach front increases as the wave propagates away from the center of the detonation. This increase in height is referred to as the path of the triple point and is formed by the intersection of the initial, reflected, and Mach waves. A protected structure is considered to be subjected to a plane wave (uniform pressure) when the height of the triple point exceeds the height of the structure. The scaled height of the triple point $H_T/W^{1/3}$ versus scaled ground distance Z_G and scaled charge height $H_c/W^{1/3}$ is plotted in Figure 2-13 (+).

If the height of the triple point does not extend above the height of the structure, then the magnitude of the applied loads will vary with the height of the point being considered. Above the triple point, the pressure-time variation consists of an interaction of the incident and reflected incident wave pressures resulting in a pressure-time variation (Figure 2-12b (+)) different from that of the Mach incident wave pressures. The magnitude of pressures above the triple point is smaller than that of the Mach front. In most practical design situations, the location of the detonation will be far enough away from the structure so as not to produce this pressure variation. An exception may exist for multistory buildings even though these buildings are usually located at very low-pressure ranges where the triple point is high.

In determining the magnitude of the air blast loads acting on the surface of an above-ground protective structure, the peak incident blast pressures in the Mach wave acting on the ground surface immediately before the structure are calculated first. The peak reflected pressure $P_{r\alpha}$ is determined for this point from Figure 2-9 (+) using the scaled height of charge above the ground $H_c/W^{1/3}$ and the angle of incidence α.

A similar procedure is used with Figure 2-10 (+) to determine the impulse $i_{r\alpha}$ of the blast wave acting on the ground surface immediately before the structure. An estimate of the other blast parameters may be obtained from Figure 2-7 (+) and Figure 2-8 (+) by setting the values of $P_{r\alpha}$ and $i_{r\alpha}$ equal to the values of the peak incident pressure P_{so} and incident impulse i_s of the Mach wave, respectively. The scaled distances corresponding to P_{so} and i_s are determined from Figure 2-7. The scaled distance corresponding to P_{so} is used to obtain values of P_r, P_{so}^-, $t_A/W^{1/3}$, U, $L_W/W^{1/3}$ and $L_W^-/W^{1/3}$ while the scaled distance corresponding to i_s is used to obtain values of i_r, i_s^-, i_r^-, $t_o/W^{1/3}$ and $t_o^-/W^{1/3}$.

2-13.3 Surface Burst.

A charge located on, or very near the ground surface, is considered to be a surface burst. The initial wave of the explosion is reflected and reinforced by the ground surface to produce a reflected wave. Unlike the air burst, the reflected wave merges with the incident wave at the point of detonation to form a single wave, similar in nature to the Mach wave of the air burst but essentially hemispherical in shape (Figure 2-14 (+)).

The positive phase parameters of the surface burst environment for hemispherical TNT explosions are given in Figure 2-15 (+) while the negative phase parameters are given in Figure 2-16 (+). A comparison of these parameters with those of free-air explosions (Figure 2-7 (+) and Figure 2-8 (+)) indicate that, at a given distance from a detonation of the same weight of explosive, all of the parameters of the surface burst environment are larger than those for the free-air environment.

As for the case of air bursts, protected structures subjected to the explosive output of a surface burst will usually be located in the pressure range where the plane wave (Figure 2-14 (+)) concept can be applied. Therefore, for a surface burst, the blast loads acting on structure surface are calculated as described for an air burst except that the incident pressures and other positive phase parameters of the free-field shock environment are obtained from Figure 2-15 (+), and theoretical negative phase blast parameters are shown in Figure 2-16 (+).

As for the case of an air burst, the curves presented in Figure 2-15 (+) and Figure 2-16 (+) which give the blast wave parameters as a function of scaled distance, extend only to a scaled distance Z = 100 ft/lb$^{1/3}$ (see Section 2-13.1).

Blast parameters for explosives detonated on the ground surface other than hemispherical TNT are listed in Table 2-2 (+/+/+/+/+/+). These explosives include both uncased and cased high explosives, propellants and propelling charges as well as pyrotechnic mixtures. The various shapes of the explosive materials are given in Figure 2-17 (+). The blast parameters for the various explosives are illustrated in Figure 2-18 through Figure 2-49. For each explosive material considered, the peak incident pressure P_{so} and scaled incident impulse $i_s/W^{1/3}$ is presented as a function of the scaled ground distance $Z_G = R_G/W^{1/3}$ from the point of detonation. The charge weight W is equal to the actual weight of the explosive material under consideration increased by the required factor of safety (20 percent).

An estimate of the blast parameters other than incident pressure and impulse, may be obtained from Figure 2-15 (+) and Figure 2-16 (+). The scaled ground distance corresponding to the incident pressure P_{so} is used to obtain the values of P_r, P_{so}^-, P_r^-, $t_A/W^{1/3}$, U, $L_w/W^{1/3}$ and $L_w^-/W^{1/3}$. In addition, this scaled ground distance $Z_G = R_G/W^{1/3}$ is used to calculate the equivalent TNT design charge weight W for pressure using the actual ground distance R_G. The absolute values of the scaled blast parameters are obtained by multiplying the scaled values by the equivalent TNT design charge weight.

The scaled ground distance corresponding to the incident impulse requires a graphical solution. The point corresponding to the scaled incident impulse and scaled ground distance for the explosive material in question is plotted on Figure 2-15 (+). A 45 degree line is drawn through this point. The point where the line intersects the scaled impulse curve corresponds to the scaled impulse and scaled ground distance for the equivalent TNT charge. This scaled ground distance is then used to obtain the values of $i_r/W^{1/3}$, $i_s/W^{1/3}$, $i_r^-/W^{1/3}$, $t_o/W^{1/3}$ and $t_o^-/W^{1/3}$. In addition, this scaled ground distance and the actual ground distance is used to calculate the equivalent TNT design charge weight for impulse. The absolute values of the scaled blast parameters are obtained by multiplying the scaled values by the equivalent TNT design charge weight.

It may be noted that the above data for explosives other than TNT is limited to surface bursts with container shapes indicated in Figure 2-17 (+). This data should not be extrapolated for scaled distances less than those indicated on Figure 2-18 through Figure 2-49 . In addition, the blast pressure and impulse for propellants and, in particular, the pyrotechnic mixtures were obtained from tests which utilized booster charges to initiate the explosive material. Therefore, the blast parameters for both of these materials should be considered as upper limits.

2-13.4 Multiple Explosions.

When two or more explosions of similar material occur several milliseconds apart, the blast wave of the initial explosion will propagate ahead of the waves resulting from the subsequent explosions, with the phasing of the propagation of these latter waves being governed by the initiation time and orientation of the individual explosives. If the time delay between explosions is not too large, the blast waves produced by the subsequent explosions will eventually overtake and merge with that of the initial detonation. The distance from the explosion at which this merger occurs will depend on: (1) the magnitude of the individual explosions, (2) the time delays between the initiation of the explosions, (3) the separation distances between and orientation of the explosives, and (4) obstructions between the explosives themselves and other obstructions between the explosives and other parts of the facility (buildings, walls, barricades, terrain, etc.) which will distort, hinder, and generally interfere with wave propagation.

The pressure time relationships associated with the wave propagation will depend upon the interaction of the individual waves themselves. After all the waves have merged, the pressures associated with the common or merged wave will have a pressure-time relationship which is similar to that produced by a single explosion (Figure 2-12 (+)).

However, at closer distances to the explosion, the pressure-time relationship will be more closely represented by a pressure-time curve with multiple peak pressures (similar to that occurring above the triple point (Figure 2-12). The multiple peak pressures represent the interaction as the various waves reach the point in question. At distances even closer to the explosion, the time history of the pressures acting on the ground surface may consist of a series of completely separate blast loads. This loading condition is a result of the arrival of the subsequent blast waves at a particular point during or after the occurrence of the negative phase pressures produced by the initial wave at that point.

The latter pressure-time relationship is most likely to occur at high pressures close to the explosions, while the multiple peak pressure pulse is normally associated with low pressures at far distances. However, in many instances, the multiple peak pressure pulse will occur at high pressures, in particular where the individual explosives are positioned close together, e.g., in a cubicle or other storage facility.

2-14 CONFINED EXPLOSIONS.

2-14.1 Effects of Confinement.

When an explosion occurs within a structure, the peak pressures associated with the initial shock front (free-air pressures) will be extremely high and, in turn, will be amplified by their reflections within the structure. In addition, and depending upon the degree of confinement, the effects of the high temperatures and accumulation of gaseous products produced by the chemical process involved in the explosion will exert additional pressures and increase the load duration within the structure. The combined effects of these pressures may eventually destroy the structure unless the structure is designed to sustain the effects of the internal pressures. Provisions for venting of these pressures will reduce their magnitude as well as their duration.

The use of cubicle-type structures (Figure 2-50a (+)), or other similar barriers with one or more surfaces either sufficiently frangible or open to the atmosphere, will provide some degree of venting depending on the opening size. This type of structure will permit the blast wave from an internal explosion to spill over onto the surrounding ground surface, thereby, significantly reducing the magnitude and duration of the internal pressures. The exterior pressures are quite often referred to as "leakage" pressures, while the pressures reflected and reinforced within the structure are termed interior "shock pressures." The pressures associated with the accumulation of the gaseous products and temperature rise are identified as "gas" pressures. For the design of most fully vented cubicle type structures, the effects of the gas pressure may be neglected.

Detonation in an enclosed structure with relatively small openings (Figure 2-50b (+)) is associated with both shock and gas pressures whose magnitudes are a maximum. The duration of the gas pressure and, therefore, the impulse of the gas pressure is a function of the size of the opening. It should be noted that the onset of the gas pressure does not necessarily coincide with the onset of the shock pressure. Further, it takes a finite length of time after the onset for the gas pressure to reach its maximum value.

However, these times are very small and, for design purposes of most confined structures, they may be treated as instantaneous.

The term "frangible" pertains to those elements of a protective structure which fail and whose strength and mass are such as to reduce the amplification of the shock pressures and the confinement of the explosive gases. To reduce the amplification of the shock pressures, frangible elements must fail so as to relieve quickly the interior pressures acting on those surfaces and minimize their reflection to the non-frangible elements of the structure. Blast tests of glass panels have shown that a true frangible material does not exist and that some reflection of the initial blast pressures may be expected from very weak and light elements. Further, the buildup of gas pressures is a function of the ratio of the weight of the charge to the volume of the confining structure and the venting area. As stated, this pressure buildup will not begin until sometime after the onset of the shock pressures. Therefore, an element which is not considered frangible for the shock pressure may be frangible for gas pressures.

In addition to being dependent upon the physical properties of an element, frangibility will also be a function of the magnitude of the applied blast loads and, therefore, a function of the quantity of explosive being contained and the distance from the frangible element. Although frangibility is imperfectly understood and difficult to measure, in general, it can be assumed that if a closure's resistance to outward motion is equal to or less than 25 pounds per square foot of surface area, the resistance can be neglected since the time to reach failure is practically zero. In this case, frangibility can be stated solely in terms of the weight (inertial force) of the vent area closure. For resistances greater than 25 psf, the evaluation of frangibility must include the effects of resistance in addition to the weight of an element. The combined effects of the inertial force and the resistance can be accounted for by performing a dynamic analysis and determining the time to reach failure. However, if the blast pressure is very large in comparison to the resistance of the element, the effects of the resistance can be neglected without introducing significant errors. Therefore, it is advantageous to use vent closures that are light and inherently weak and/or weakly supported; such as, corrugated metal decking supported on steel joists, metal panels for walls, plexiglass or thin fiberglass panels supported by wood or lightweight steel frames or gypsum board panels.

In the following paragraphs of this section, a simple cantilever barrier as well as cubicle-type and containment type structures will be discussed. The cubicles are assumed to have one or more surfaces which are open or frangible while the containment structures are either totally enclosed or have small size openings. The effects of the inertia of frangible elements of these structures will be discussed in subsequent sections.

2-14.2 Shock Pressures.

2-14.2.1 Blast Loadings.

When an explosion occurs within a cubicle or containment-type structure, the peak pressures as well as the impulse associated with the shock front will be extremely high and will be amplified by the confining structure. Because of the close-in effects of the

explosion and the reinforcement of blast pressures due to the reflections within the structure, the distribution of the shock loads on any one surface will be non-uniform with the structural surface closest to the explosion subjected to the maximum load.

An approximate method for the calculation of the internal shock pressures has been developed using theoretical procedures based on semi-empirical blast data and on the results of response tests on slabs. The calculated average shock pressures have been compared with those obtained from the results of tests of a scale-model steel cubicle and have shown good agreement for a wide range of cubicle configurations. This method consists of the determination of the peak pressures and impulses acting at various points of each interior surface and then integrating to obtain the total shock load. In order to simplify the calculation of the response of a protective structure wall to these applied loads, the peak pressures and total impulses are assumed to be uniformly distributed on the surface. The peak average pressure and the total average impulse are given for any wall surface. The actual distribution of the blast loads is highly irregular, because of the multiple reflections and time phasing and results in localized high shear stresses in the element. The use of the average blast loads, when designing, is predicated on the ability of the element to transfer these localized loads to regions of lower stress. Reinforced concrete with properly designed shear reinforcement and steel plates exhibit this characteristic.

The parameters which are necessary to determine the average shock loads are the structure's configuration and size, charge weight, and charge location. Figure 2-51 (+) shows many possible simple barriers, cubicle configurations, and containment type structures as well as the definition of the various parameters pertaining to each. Surfaces depicted are not frangible for determining the shock loadings. The effects of frangibility will be discussed later.

Because of the wide range of required parameters, the procedure for the determination of the shock loads was programmed for solutions on a digital computer. The results of these calculations are presented in Figure 2-52 through Figure 2-100 for the average peak reflected pressures p_r and Figure 2-101 through Figure 2-149 for the average scaled unit impulse $i_r/W^{1/3}$. These shock loads are presented as a function of the parameters defining the configurations presented in Figure 2-51 (+). Each illustration is for a particular combination of values of h/H, l/L, and N reflecting surfaces adjacent to the surface for which the shock loads are being calculated. The wall (if any) parallel and opposite to the surface in question has a negligible contribution to the shock loads for the range of parameters used and was therefore not considered.

The general procedure for use of the above illustrations is as follows:

1. From Figure 2-51 (+), select the particular surface of the structure which conforms to the protective structure given and note the number of adjacent reflecting surfaces *N* as indicated in parenthesis.

2. Determine the values of the parameters indicated for the selected surface of the structure in Item 1 above and calculate the following quantities: h/H, l/L, L/H, L/R_A, and $Z_A = R_A/W^{1/3}$.

3. Refer to Table 2-3 (+) for the proper peak reflected pressure and impulse charts conforming to the number of adjacent reflected surfaces N and the values of l/L and h/H of Item 2 above, and enter the charts to determine the values of p_r and $i_r/W^{1/3}$.

In most cases, the above procedure will require interpolation for one or more of the parameters which define a given situation, in order to obtain the correct average reflected pressure and average reflected impulse. Examples of this interpolation procedure are given in Appendix 2A.

Because of the limitations in the range of the test data and the limited number of values of the parameters given in the above shock load charts, extrapolation of the data given in Figure 2-52 through Figure 2-149 may be required for some of the parameters involved. However, the limiting values as given in the charts for other parameters will not require extrapolation. The values of the average shock loads corresponding to the values of the parameters, which exceed their limiting values (as defined by the charts), will be approximately equal to those corresponding to the limiting values. The following are recommended procedures which will be applicable in most cases for either extrapolation or establishing the limits of impulse loads corresponding to values of the various parameters which exceed the limits of the charts:

1. To extrapolate beyond the limiting values of Z_A, plot a curve of values of p_r versus Z_A for constant values of L/R_A, L/H, h/H and l/L. Extrapolate curve to include the value of p_r corresponding to the value of Z_A required. Repeat similarly for value of $i_r/W^{1/3}$.

2. To extrapolate beyond the limiting values of L/R_A, extrapolate the given curve of p_r versus L/R_A for constant values of Z_A, L/H, h/H and l/L to include the value of p_r corresponding to the value of L/R_A required. Repeat this extrapolation for value of $i_r/W^{1/3}$.

3. Values of p_r and $i_r/W^{1/3}$ corresponding to values of L/H greater than 5 shall be taken as equal to those corresponding to $L/H = 6$ for actual values of Z_A, h/H, and l/L but with a fictitious value of L/R_A in which R_A is the actual value and L is a fictitious value equal to $5H$.

4. Values of p_r and $i_r/W^{1/3}$ corresponding to values of l/L less than 0.10 and greater than 0.75 shall be taken as equal to those corresponding to $l/L = 0.10$ and 0.75, respectively.

5. Values of p_r and $i_r/W^{1/3}$ corresponding to values of h/H less than 0.10 and greater than 0.75 shall be taken as equal to those corresponding to $h/H =$ 0.10 and 0.75, respectively.

An open distribution computer program, SHOCK, is available which executes the interpolation procedure using numerical tables equivalent to Figure 2-52 through Figure 2-149. This program may be obtained from NAVFAC EXWC using the contact information listed in Section 2-4.

A protective element subjected to high intensity shock pressures may be designed for the impulse rather than the pressure pulse only if the duration of the applied pressure acting on the element is short in comparison to its response time. However, if the time to reach maximum displacement is equal to, or less than, three times the load duration, then a simplified pressure pulse representing the full pressure-time relationship should be used for these cases. The actual pressure-time relationship resulting from a pressure distribution on the element is highly irregular because of the multiple reflections and time phasing. For these cases, the pressure-time relationship may be approximated by a fictitious right triangular pressure pulse. The average peak reflected pressure of the pulse is obtained from Figure 2-52 through Figure 2-100 and the average impulse from Figure 2-101 through Figure 2-149 and a fictitious duration t_o is established as a function of the reflected pressure p_r and impulse i_r acting on the element.

$$t_o = 2i_r / p_r \qquad 2\text{-}2$$

The above solution for the average shock load does not account for increased blast effects produced by contact charges. Therefore, if the values of the average shock loads given in Figure 2-52 through Figure 2-149 are to be applicable, a separation distance between the element and explosive must be maintained. This separation is measured between the surface of the element and the surface of either the actual charge or the spherical equivalent, whichever results in the larger normal distance between the element's surface and the center of the explosive (the radius r of a spherical TNT charge is $r = 0.136\ W^{1/3}$ where r is (ft) and W is (lb). For the purposes of design, the following separation distances are recommended for various charge weights:

Weight of Explosive (lb)	Separation Distance (ft)
up to 500	1.0
501 to 1,000	1.5
1,001 to 2,000	2.0
2,001 to 3,000	2.5
above 3,000	3.0

The above separation distances do not apply to floor slabs or other similar structural elements placed on grade. However, a separation distance of at least one foot should be maintained to minimize the size of craters associated with contact explosions.

It should be noted that these separation distances do not necessarily conform to those specified by other government regulations; their use in a particular design must be approved by the cognizant military construction agency.

Average shock loads over entire wall or roof slabs were discussed above. An approximate method may be used to calculate shock loads over surfaces other than an entire wall. These surfaces might include a blast door, panel, column, or other such items found inside any shaped structure.

The method assumes a fictitious strip centered in front of the charge having a width equal to the normal distance R_A and a height equal to that of the structure. This is the maximum representative area that may be considered. Average shock loads can be determined on entire area or any surface falling within the boundaries of the representative area.

The procedure for determining the shock loads consists of partitioning the surface under consideration into subareas. These subareas do not need to be the same size. The angle of incidence to the center of each subarea is calculated. The reflected pressure and scaled impulse are determined for each subarea using Figure 2-9 (+) and Figure 2-10 (+) respectively. A weighted average with respect to area is taken for both pressure and scaled impulse.

Both the pressure and the impulse are multiplied by a factor of 1.75 to account for secondary shocks. Idealized duration is calculated using Equation 2-2.

2-14.2.2 Frangibility.

A frangible element, as defined here, is an element that exhibits a resistance to internal shock loads equal to or less than 25 pounds per square foot and will undergo significant displacement during the loading time of the shock pressures and, thereby, reduce the effects of the shock pressures acting on both the frangible panel itself and reflections to other elements of the structure.

The following are design procedures for determining the magnitude of applied shock pressures acting on the frangible element, which will contribute to the displacement of the frangible element:

(1) Determine the peak average reflected pressure P_r and average impulse i_r acting on the frangible element assuming that the element is rigid (Figure 2-52 through Figure 2-149).

(2) Calculate the unit weight (lb/ft^2) of the frangible element and divide this weight by the sixth root of charge weight (lb), $W_F/W^{1/6}$.

(3) Determine the fictitious scaled distance Z from Figure 2-7 (+), which corresponds to the average impulse determined in Step 1.

(4) Utilize Figure 2-150 (+) to determine the value of the Reflection factor f_r of average impulse using the value of $W_F/W^{1/6}$ from Step 2 and the fictitious scaled distance of Step 3 (may require interpolation).

(5) Calculate the value of the average impulse acting on the frangible element and contributing to its translation by multiplying the values of i_r and f_r of Steps 1 and 4 respectively.

(6) The peak average pressure acting on the frangible element is assumed to equal P_r in Step 1.

The step by step procedure for determining the shock loads being reflected from a frangible element to an adjacent element is to:

(1) Determine the average peak reflected pressure P_r and the average reflected impulse i_r acting on the element in question, assuming that the adjoining frangible element will remain in place (Figure 2-52 through Figure 2-149).

(2) Determine the average impulse acting on the element in question assuming that the adjoining frangible element is removed (Figure 2-52 through Figure 2-149).

(3) Subtract the average impulse determined in Step 2 from the average impulse determined in Step 1.

(4) Calculate the unit weight (lb/ft^2) of the frangible element and divide this weight by the sixth root of the charge weight (lb), $W_F/W^{1/6}$.

(5) Calculate the normal scaled distance Z between the center of the charge and the surface of the frangible element.

(6) Utilize Figure 2-150 (+) to determine the value of the Reflection fraction f_r of the average impulse using the value of $W_F/W^{1/6}$ and scaled distance of Steps 4 and 5, respectively (may require interpolation).

(7) Determine the magnitude of the impulse load reflected to the element in question from the frangible element by multiplying the value of the average impulse of Step 3 by the value of f_r of Step 6.

(8) Determine the total impulse load acting on the element in question by adding the impulse loads determined in Steps 2 and 7.

(9) The peak average reflected pressure of the shock loads acting on the element is P_r in Step 1.

In the above procedure, it is assumed that the frangible element will remain intact while being loaded by shock pressures. If the element fails while being loaded by shock

pressures, then the portion of the shock impulse displacing the element as well as that portion of the impulse being reflected to other elements will be reduced because of additional venting area produced by the element's "break up."

2-14.2.3 TNT Equivalency.

The shock loads presented in Figure 2-52 through Figure 2-149 pertain to the blast effects of bare spherical TNT explosives and must be extended to include other potentially mass-detonating materials. However, only a limited amount of testing has been performed to determine the TNT equivalency of confined explosives. Therefore, as an interim procedure, it is suggested that the determination of shock pressures for confined explosives other than TNT utilize equivalencies based on Equation 2-1.

The above relationship assumes that the explosive in question is a bare charge and spherical in shape. If the charge is not spherical, then it is suggested that the explosive be subdivided into several segments which will have approximately equal dimensions and that the reflected impulse for any segment be calculated, as previously discussed. The reflected impulse of the total charge is then determined by multiplying the impulse of the individual segment by the total number of segments. The peak average reflected pressure is calculated assuming the total charge has a spherical shape. The impulse load for multiple explosives is obtained in a similar manner except that the locations of the individual charges are considered in calculating their individual impulse load. The total impulse load is determined by adding together the individual impulse loads from each charge. The average peak reflected pressure is calculated using the total weight of the explosive charges located at the centroid of the individual charges.

The explosive casing will have an effect on the magnitude of the shock pressures. These effects are dependent on the properties of the casing such as material, thickness, shape, etc. A review of a limited amount of surface detonated test data has indicated that the effects of the casing are not severe and, therefore, for design purposes it is recommended that casing effects be neglected.

2-14.2.4 Multiple Explosions.

The blast pressures and impulse loads, acting on various elements of cubicle or other similar structures, which are produced by multiple explosions, will usually differ from those produced by a single explosion of the same amount of explosives.

Although the magnitude of the total combined impulse produced by the multiple explosions will usually be larger than that produced by the single explosion, the damage to a protective element due to the impulse of the multiple detonation may be either greater, equal to, or less than that produced by the impulse of the single explosion. For a given total impulse, the degree of damage to a protective element will be defined by the duration of the entire load relative to the response time of the element (time to reach maximum deflection).

A minimum amount of theoretical and experimental data is available concerning the degree of damage sustained by structural elements due to multiple explosions.

However, results of response tests of reinforced concrete slabs have indicated that if the total combined duration of the blast loads produced by simultaneously or near simultaneously exploded charges is equal to or less than one-third the response time (time to reach maximum deflection) of the element, then the total combined impulse acting on the element can be estimated by numerically adding the impulse loads produced by the individual explosions. However, if the total combined duration of the blast loads is greater than one-third the response time, the actual pressure-time relationship of the combined loads approximated by a fictitious right triangular pressure pulse (similar to that of a single explosion) should be considered. The blast loads produced by charges that are not simultaneously or near simultaneously exploded may be considered as two or more impulse loads, two or more pressure-time loads, or a combination of impulse and pressure-time loads depending on the time delay and the duration of the individual loads compared to the response time of the element. A load or group of loads should be treated as an impulse load if the duration (one load or the combined duration of two or more loads) of the loading is less than one-third the time interval between the on-set of the load or group of loads and the response time of the member.

The duration of the blast loads due to multiple explosions may be approximated by considering the interrelationship between (a) the time intervals between individual explosions, (b) arrival times of the blast waves of the individual explosions at the element and (c) the fictitious duration of the pressure load from individual explosions. Because of the many variables involved, a relationship cannot be given to obtain the duration of the blast loads due to multiple explosions. Each situation will require a series of computations involving the time increments outlined above.

2-14.3 Gas Pressures.

2-14.3.1 Blast Loadings.

When an explosion occurs within a confined area, gaseous products will accumulate and temperature within the structure will rise, thereby forming blast pressures whose magnitude is generally less than that of the shock pressure but whose duration is significantly longer. The magnitude of the gas pressures as well as their durations is a function of the size of the vent openings in the structure. For very small openings or no openings at all, the duration of the gas pressures will be very long in comparison to the fundamental periods of the structure's elements and, therefore, may be considered as a long duration load similar to that associated with a nuclear event.

These conditions usually occur in total or near containment type structures. In the former, the internal blast pressures must be contained because of the presence of toxic or other harmful materials in the structure. In near containment structures, the leakage of pressure flow out of the structure usually must be limited because either personnel or frangible structure are located immediately adjacent to the donor structure. In other cases, however, openings in structures may be quite large, thereby minimizing the products' accumulation and limiting the temperature rise, hence producing gas

pressures with limited duration or no duration at all. The structures without gas pressure buildup are referred to as fully vented structures.

A typical pressure-time record at a point on the interior surface of a partially vented chamber is shown in Figure 2-151 (+). The high peaks are the multiple reflections associated with shock pressures. The gas pressure, denoted as p_g, is used as the basis for design and is a function of the charge weight and the contained net volume of the chamber. Figure 2-152 (+) shows an experimentally fitted curve based upon test results of partially vented chambers with small venting areas where the vent properties ranged between:

$$0 \leq A_f/V^{2/3} \leq 0.022 \qquad 2\text{-}3$$

The values of A and V_f are the chamber's total vent area and free volume, which are equal to the total volume minus the volume of all interior equipment, structural elements, etc. The maximum gas pressure, P_g, is plotted against the charge weight to free volume ratio.

Figure 2-153 through Figure 2-164 provide the relationship of the gas pressure scaled impulse $i_g/W^{1/3}$ as a function of the charge weight to free volume ratio W/V_f, scaled value of the vent opening $A/V_f^{2/3}$, the scaled unit weight of the frangible wall or vent cover $W_F/W^{1/3}$ over the opening, and the scaled average reflected impulse $i_r/W^{1/3}$ of the shock pressures acting on the frangible wall (Section 2-14.2.2) or a non-frangible wall with a vent cover over the opening. (The curves in Figure 2-153 through Figure 2-164 for $W_F/W^{1/3} = 0$ were obtained from data with $A/V_f^{2/3} \leq 1.0$. However, even lightweight frangible panels displace slowly enough that the majority of the gas impulse is developed before significant venting ($A/V_f^{2/3} > 1$) can occur.) For a full containment type structure, the impulse of the gas pressure will be infinite in comparison to the response time of the elements (long duration load). For near containment type structures where venting is permitted through vent openings without covers, the impulse loads of the gas pressures are determined using the scaled weight of the cover equal to zero. The impulse loads of the gas pressures in rooms with a frangible wall or vent cover is discussed in Section 2-14.3.2. The effects on the gas pressure impulse caused by the scaled shock impulse loads $i_r/W^{1/3}$ vary, where increasing shock impulse acting on a vent cover or frangible wall allows gas pressures to vent more quickly and reduces the scaled gas pressure. The gas impulse loads will have greater variance at lower shock impulse loads than at higher loads. Interpolation will be required between Figure 2-153 through Figure 2-164 for the variation of scaled gas impulse as a function of the scaled shock impulse loads and charge weight to free volume ratio. This interpolation can be performed in a manner similar to the interpolation for the shock pressures on walls of cubicles as illustrated in Appendix 2A.

An open distribution computer program, FRANG, is available which executes the interpolation procedure. This program may be obtained from NAVFAC EXWC using the contact information listed in Section 2-4.

The actual duration and the pressure-time variation of the gas pressures is not required for the analysis of most structural elements. Similar to the shock pressures, the actual pressure-time relationship can be approximated by a fictitious right triangular pulse. The peak gas pressure is obtained from Figure 2-152 (+) and the impulse from Figure 2-153 through Figure 2-164 and the fictitious duration is calculated from the following:

$$t_g = 2i_g / P_g \qquad \text{2-4}$$

Figure 2-165a (+) illustrates an idealized pressure-time curve considering both the shock and gas pressures. As the duration of the gas pressures approaches that of the shock pressures, the effects of the gas pressures on the response of the elements diminishes until the duration of both the shock and gas pressures are equal and the structure is said to be fully vented.

If a chamber is relatively small and/or square in plan area, then the magnitude of the gas pressure acting on an individual element will not vary significantly. For design purposes the gas pressures may be considered to be uniform on all members. When the chamber is quite long in one direction and the explosion occurs at one end of the structure, the magnitude of the gas pressures will initially vary along the length of the structure. At the end where the explosion occurs, the peak gas pressure is P_{g1} (Figure 2-165b (+)), which decays to P_{g2} after a finite time, and finally decays to zero. The gas pressure P_{g2} is based on the total volume of the structure and is obtained from Figure 2-152 (+) and the time for this pressure to decay to zero is calculated from Equation 2-4 using the impulse obtained from Figure 2-153 through Figure 2-164 based on the total volume of the structure. The peak gas pressure P_{g1} is obtained from Figure 2-152 (+) based on a pseudo volume (Figure 2-165b) whose length is equal to its width and the height is the actual height of the structure. The time t_p for the gas pressure to decay from P_{g1} to P_{g2} is taken as the actual length of the structure minus the width divided by the velocity of sound (1.12 ft/msec). At the end of the room where the explosion occurs, the peak gas pressures (P_{g1}, Figure 2-165b (+)) will be a maximum and, after a finite time, it will decay to a value (P_{g2}, Figure 2-165b) that is consistent with full volume of the structure; after which the gas pressure will decay to zero.

2-14.3.2 Frangibility.

Similar to shock pressures, an element can be considered frangible if it is designed such that its resistance to internal blast forces does not exceed 25 psf and that it will undergo significant displacement during the shock and gas loading phases. Figure 2-153 through Figure 2-164 present the method for determining the gas pressure impulse acting on the interior surfaces of the donor structure. These impulse loads will

vary as the mass of the frangible wall or cover over the vent opening varies; that is, the heavier the vent opening cover, the larger the gas pressure impulse.

2-14.3.3 TNT Equivalency.

The data presented in Figure 2-152 (+) and Figure 2-153 (+) through Figure 2-164 (+) are for TNT only and must be extended to include other potentially mass-detonating materials. Similar to the shock pressures, only a limited amount of data is available regarding the TNT equivalency of confined explosions and in particular the effects produced on gas pressures. It has been suggested that the TNT equivalency of explosives relating to gas pressures is a function of both the heat of detonation as well as the heat of combustion, while for the shock pressures, the TNT equivalency is a function of the former only. A relationship has been developed based on a limited amount of testing as follows:

$$W_{E_g} = \frac{\phi\left[H^c_{EXP} - H^d_{EXP}\right] + H^d_{EXP}}{\phi\left[H^c_{TNT} - H^d_{TNT}\right] + H^d_{TNT}} W_{EXP} \qquad \text{2-5}$$

where

W_{Eg} = *effective charge weight for gas pressure*
H^c_{TNT} = *heat of combustion of TNT*
H^c_{EXP} = *heat of combustion of explosive in question*
ϕ = *TNT conversion factor (Figure 2-166 (+))*
H^d_{TNT} = *heat of detonation of TNT*
H^d_{EXP} = *heat of detonation of explosion in question*
W_{EXP} = *weight of explosive in question*

Gas pressures will be increased because of casings, in particular, if the casing is combustible. Since only unrelated data are available concerning the effects on gas pressures by the casing, a method of compensating for these effects is to adjust the heat of combustion of the given explosive material in Equation 5 to account for the heat of combustion of the casing material. This adjustment should be made by chemically combining the heat of combustion of the explosive and casing.

2-14.3.4 Multiple Explosions.

The gas pressure produced by the release of the gaseous products of multiple explosions in a confined area may be approximated by considering the explosion to be produced by a single explosive whose weight is equal to the combined weights of the individual charges. This approximation is accurate if the individual charges are positioned in the immediate vicinity of one another and if near simultaneous detonation of the individual charges occurs. If the individual charges are not close to one another and/or positioned at one end of the structure, the magnitude of the gas pressures will

initially vary along the length or width of the structure. This variation may be determined in a manner similar to that described in Section 2-14.3.1.

2-14.4 Leakage Pressures.

2-14.4.1 Introduction.

When an explosion occurs inside a vented chamber, shock pressures escape to the outside along with venting of the gas pressures. Trailing shocks overrun and coalesce with the lead shock at some distance to form a single diverging shock wave. Close to the structure, the blast pressures are affected by the structure itself, as the shock pressures spill around the edges of the structure and form highly turbulent vortices. At further distances, this effect is no longer present and the shock pressure decreases with increasing distances. The leakage pressures are enhanced compared to a free-air explosion in the direction of venting (front) and reduced to the side and rear. The enhancement of pressures in the front and reduction of pressures to the side and rear are less extreme as the distance away from the structure is increased.

The blast environment outside a cubicle containing fully and partially vented explosions is presented in this section. Pressures and impulses acting on the ground surface are provided as a function of distance from the explosion, direction (front, side, back) relative to the vent opening in the structure, area of the vent opening, and volume of the structure. For design purposes, the remaining pressure and impulse values may be obtained from Figure 2-15 (+) and Figure 2-16 (+) in the following manner. Once the incident pressure has been calculated, an equivalent scaled distance corresponding to this pressure may be determined from Figure 2-15. This equivalent scaled distance may then be applied to determine the value of the other pressure variables in Figure 2-15 and Figure 2-16. Similarly, once the incident impulse has been calculated, an equivalent scaled distance corresponding to this impulse may be determined from Figure 2-15. This equivalent scaled distance is then applied to determine the value of the other impulse variables in Figure 2-15 and Figure 2-16.

Explosions in three and four wall cubicles are considered. Three wall cubicles are fully vented structures. The blast environment is furnished for cubicles with or without roofs. Four wall cubicles with a vent opening located either in the roof or one wall are considered. The size of the vent opening is varied from that of a fully vented cubicle through a full range of partially vented structures.

The data presented is based on tests in which the vent openings were completely open. There were no frangible covers over the vent area which might inhibit the pressure flow. Vent openings in protective structures are normally covered with frangible panels for weather protection, separation of operations, etc. These panels will affect the leakage pressures. However, it is assumed that these frangible panels will reduce the shock pressures leaking through the opening to a greater extent than the increase in the internal gas pressure buildup. Therefore, use of this data will predict conservative leakage pressures from cubicles with frangible covers.

2-14.4.2 Fully Vented Three Wall Cubicles.

For cubicle-type structures where full venting is provided through the frangible or open portion of the structure, the resulting blast wave exterior of the cubicle will be appreciably modified as compared to an unbarricaded detonation. As the blast wave propagates out from the center of the explosion, the shock front will collide with the interior surfaces of the structure. These collisions will reflect and reinforce the initial loads (pressure and impulse). Eventually these pressures will spill over and around the blast walls, and in the event of rapid collapse of frangible walls, through the structure to the surrounding area. The exterior pressures will not initially have a definite shock front but will, at some distance from the structure, shock-up with frontal pressures similar to those produced by a surface burst. The pressure distance gradients away from the explosion will vary in all directions. This variation is defined by the configuration (shape, openings, etc.) of the protective structure containing the explosion.

A series of tests have been performed on three wall cubicle type structures illustrated in Figure 2-167 (+). Cubic and rectangular three wall cubicles with and without a roof were tested. The results indicated that several parameters were important:

(1) Direction. Three directions illustrated in Figure 2-167 (+) are considered. The direction normal to the open wall is called the front. The directions perpendicular to the front normal are called the sides. The direction opposite the normal to the open wall is called the back. The blast pressures out the front are greater than that to the side which, in turn, are greater than that to the back.

(2) Structure geometry. Differences were found in the blast environment depending upon whether the shape of the structure was cubic or rectangular. This was true for pressure and impulse measurements to the side and back, and only impulse to the front. There were no differences in pressure out the front for the cubicle and rectangular structures. The difference in pressures to the side and back occur only close to the structure. Far from the structure, there is no effect on pressure in any direction due to structure shape. However, impulse does not converge with distance for differences in cubicle shape.

(3) Charge weight to volume ratio W/V and distance. The ratio W/V does not have an effect on the pressure to the front of any cubicle. There is an effect of W/V on pressure to the side and back of all cubicles, but only close to the structure. For a particular W/V, the pressure is affected differently for a cubic or rectangular structure. Thus, the effect on pressure close in depends both on structure size and W/V. But, for further out, neither affect the pressures. For all values of Z, there is a measured effect of W/V on impulse.

(4) Venting through the roof. For any direction, cubicle shape, and W/V value, there are differences in blast pressure and impulse based solely on whether or not venting could occur through the roof.

(5) Scaled distance *Z*. Both blast pressure and scaled impulse are affected by scaled distance from the explosion. This parameter is not independent of other factors.

The pressure variation in the front, side, and back direction of any three wall cubicle without a roof is given in Figure 2-168 (+), while for a three wall cubicle with a roof the pressure variation is given in Figure 2-169 (+). Due to interferences from the side and back walls which cause complex vortices near the structure and coalescence of shock waves in close, there is a maximum pressure produced in the side and back directions. These pressures are a function of the charge weight to cubicle volume ratio, *W*/*V*, and the configuration of the cubicle. The maximum peak pressures in the side or back direction of three wall cubicles with or without a roof are given in Figure 2-170 (+).

The scaled peak positive impulse in the front, side, and back direction of three wall cubicles is given in Figure 2-171 through Figure 2-182. The scaled impulse is given as a function of scaled distance from the explosion for various values of charge weight to structure volume ratio. The curves are presented in two groups; three wall cubicles without roofs and then cubicles with roofs. For each direction, the impulse is given for explosions in cubic and rectangular cubicles, respectively.

2-14.4.3 Partially Vented Four Wall Cubicles - Vent Opening in Roof.

Four wall cubicles with a vent openings located in the roof will produce blast pressures on the ground surface which are symmetric about the vent opening. Leakage pressures were determined for a below ground cubicle with its roof flush with the ground surface (Figure 2-183a (+)). Figure 2-183b (+) shows the above-ground four wall cubicle. The vent opening was centrally located in the roof, and various vent areas were considered. The blast pressure was determined to be a strong function of the vent area divided by the structure volume to the two-thirds power ($A/V^{2/3}$) and the scaled distance, and a very weak function of the charge weight to volume ratio *W*/*V,* which can be ignored with negligible error.

The leakage pressures resulting from an explosion in a partially vented belowground cubicle with a vent opening in its roof are given in Figure 2-184 (+/+), and the impulses are given in Figure 2-185 (+). The scaled ground distance, as indicated in Figure 2-183a (+), is used in these charts for below-ground structures.

Figure 2-184 (+/+) and Figure 2-185 (+) may also be used to determine the pressure and impulse acting on the ground surface for above-ground four wall cubicles (Figure 2-183b (+)). For an above-ground structure, the shock front must travel a longer distance than a below-ground structure. Therefore, the scaled distance that must be used in Figure 2-184 (+/+) and Figure 2-185 (+) is approximated by the addition of the slant and horizontal distances indicated in Figure 2-183b (+).

The figures, which are based on NCEL Technical Report R-828 (Reference 30 in the Chapter 2 Bibliography; NCEL since renamed NAVFAC EXWC), are useful in selecting the degree of venting required to limit leakage pressures outside roof-vented four wall

cubicles to a specified safe level at given distances. The blast load acting on a structure may be obtained from the pressure and impulse on the ground surface using the procedures given in this document. Thus, an adjacent structure may be designed to resist a blast load resulting from a given vent opening or the vent opening may be varied to suit the capacity of an adjacent structure.

2-14.4.4 Partially Vented Four Wall Cubicle - Vent Opening Through Wall.

Leakage pressures resulting from an explosion in a partially vented four wall cubicle where the vent opening is located in a wall (Figure 2-186 (+)) have not been documented. These leakage pressures have a variation in direction similar to a three wall cubicle with a roof and a variation with vent opening similar to a roof-vented four wall cubicle. Extrapolations of the data for these types of cubicles have resulted in Figure 2-187 (+) through Figure 2-189 (+). These figures present a reasonable estimate of the pressures produced in the front, side, and back directions (Figure 2-186 (+)). In addition to direction, these pressures are a function of scaled distance and the vent area divided by the volume to the two-thirds power ($A/V^{2/3}$).

2-15 EXTERNAL BLAST LOADS ON STRUCTURES.

2-15.1 General.

The blast loading on a structure caused by a high-explosive detonation is dependent upon several factors:

(1) The magnitude of the explosion.

(2) The location of the explosion relative to the structure in question (unconfined or confined).

(3) The geometrical configuration of the structure.

(4) The structure orientation with respect to the explosion and the ground surface (above, flush with, or below the ground).

The procedures presented here for the determination of the external blast loads on structures are restricted to rectangular structures positioned above the ground surface where the structure will be subjected to a plane wave shock front. The procedures can be extended to include structures of other shapes (cylindrical, arch, spherical, etc.), as well as structures positioned at and below the ground surface.

2-15.2 Forces Acting on Structures.

The forces acting on a structure associated with a plane shock wave are dependent upon both the peak pressure and the impulse of the incident shock pressures and dynamic pressures acting in the free-field. The peak pressures and impulses associated with the free-field shock wave have been presented for various explosives.

For each pressure range there is a particle, or wind velocity associated with the blast wave that causes a dynamic pressure on objects in the path of the wave. In the free field, these dynamic pressures are essentially functions of the air density and particle velocity. For typical conditions, standard relationships have been established between the peak incident shock pressure (P_{so}), the peak dynamic pressure (q_o), the air particle velocity, and the air density behind the shock front. The magnitudes of the dynamic pressures, particle velocity and air density are solely a function of the peak incident shock pressure, and, therefore, independent of the explosion size. Figure 2-3 (+) gives the values of the parameters versus the peak incident shock pressure. Of the three parameters, the dynamic pressure is the most important for determining the loads on structures.

For design purposes, it is necessary to establish the variation or decay of both the incident shock and dynamic pressures with time since the effects on the structure subjected to a blast loading depend upon the full pressure history of the loading. The pressure history from the incident shock wave (Figure 2-190 (+)) is characterized by an abrupt rise in pressure to a peak value, a period of decay to ambient pressure, and a period in which the pressure drops below ambient (negative pressure phase).

The rate of decay of the incident shock pressure and dynamic pressure, after the passage of the shock front, is a function of the peak pressure (both positive and negative phases) and the size of the detonation. For design purposes, the actual shape of the pressure history may be approximated with an equivalent right triangular pressure pulse. The actual positive phase duration is replaced by a fictitious duration t_{of} that is expressed as a function of the total positive impulse i and peak pressure P as shown in Equation 2-6.

$$t_{of} = 2i/P \qquad 2\text{-}6$$

The above relationship for the equivalent triangular pulse is applicable to the incident as well as the reflected shock pressures. However, in the case of the latter, the value of the pressure and impulse used with Equation 2-6 is equivalent to that associated with the reflected wave. The fictitious duration of the dynamic pressure may be assumed to be equal to that of the incident shock pressure.

A similar procedure is used to determine the pressure history for the negative phase of the blast load. The equivalent triangular pressure-time curve for the negative phase has a fictitious duration t_{of}^- given by Equation 2-7, where i^- and p^- are the total impulse and the peak pressure, respectively, of the negative pulse of either the incident or reflected shock wave. The equivalent pressure history begins at zero after the positive phase has ended, reduces linearly to the peak negative pressure p^- at a time equal to 25% of t_{of}^-, and then rises linearly to zero at time t_{of}^- after the end of the positive phase blast load. The effects of the dynamic pressure in the negative phase region usually may be neglected for analysis of structural elements where the negative phase loading is minimal or the rebound response is not critical.

$$t_{of}^{-} = 2i^{-}/P^{-} \qquad (2\text{-}7)$$

Since the fictitious duration of the positive phase will be smaller in magnitude than the actual duration, a time gap will occur between the fictitious duration and the onset of the negative phase. This time gap, which is illustrated in Figure 2-190 (+), should be maintained in an analysis for consistency of the onset of the various load phasings.

2-15.3 Above-Ground Rectangular Structure without Openings.

2-15.3.1 General.

For any given set of free-field incident and dynamic pressure pulses, the forces imparted to an above-ground structure can be divided into four general components: (a) the force resulting from the incident pressure, (b) the force associated with the dynamic pressures, (c) the force resulting from the reflection of the incident pressure impinging upon the surface of interest, and (d) the pressures associated with the negative phase of the shock wave. The relative significance of each of these components is dependent upon the geometrical configuration and size of the structure, the orientation of the structure relative to the shock front, and the design purpose of the blast loads.

The interaction of the incident blast wave with a structure is a complicated process. To reduce the complex problem of blast to reasonable terms, it will be assumed that (a) the structure is generally rectangular in shape, (b) the incident pressure of interest is 200 psi or less, (c) the structure being loaded is in the region of the Mach stem, and (d) the Mach stem extends above the height of the building.

2-15.3.2 Front Wall Loads.

For a rectangular above-ground structure at low pressure ranges, the pressure history on the side of the structure facing the detonation (front face) when this side is parallel to the shock front (normal reflection) is illustrated in Figure 2-191a (+). At the moment the incident shock front strikes the front wall, the pressure immediately rises from zero to the normal reflected pressure, P_r, which is a function of the incident pressure (Figure 2-15 (+)). The clearing time, t_c, required to relieve the reflected pressure is represented as:

$$t_c = \frac{4S}{(1+R)C_r} \qquad (2\text{-}8)$$

where

S = clearing distance and is equal to H or W/2 (Figure 2-191a (+)), whichever is the smallest
H = height of the structure

R = *ratio of S/G where G is equal to H or W/2 (Figure 2-191 (+)), whichever is larger*
C_r = *sound velocity in reflected region (Figure 2-192 (+))*

The peak pressure acting on the front wall after time t_c is the algebraic sum of the peak incident shock pressure P_s and the peak drag pressure, equal to the peak dynamic pressure q multiplied by the drag coefficient C_D of the structure. This is shown in Equation 2-9.

$$P = P_s + C_D q \qquad 2\text{-}9$$

The peak dynamic pressure is calculated based on P_s using Figure 2-3 (+). The drag coefficient C_D, which gives the relationship between the dynamic pressure and the total translational pressure in the direction of the wind produced by the dynamic pressure, varies with the Mach number (or with the Reynold's number at low incident pressures) and the relative geometry of the structure. A value of C_D=1 for the front wall is considered adequate for the pressure ranges considered in this manual. At higher pressure ranges, the duration of the reflected pressure t_{rf} may be less than the clearing time t_c causing the above procedure to be inaccurate. Therefore, a second pressure-time curve must be constructed (dotted triangle as indicated in Figure 2-191a (+)) based on the reflected shock pressure without clearing using the total reflected pressure impulse i_r from Figure 2-15 (+) (Figure 2-191a). The fictitious duration t_{rf} for the normal reflected wave is calculated from:

$$t_{rf} = 2i_r / P_r \qquad 2\text{-}10$$

where P_r is the peak normal reflected pressure (Figure 2-15 (+)). The curve (see Figure 2-191a (+)) that gives the smallest value of the impulse (area under curve) should be used in calculating the wall loading.

If the shock front approaches the structure at an oblique angle (Figure 2-191b (+)), then the peak pressure will be a function of the incident pressure and the incident angle between the front and the front wall α, and is obtained from Figure 2-193 (+). The peak reflected impulse $i_{r\alpha}$ is obtained from Figure 2-194 (+/+). The equivalent triangular pressure pulse has a fictitious duration t_{rf} calculated using Equation 2-11.

$$t_{rf} = 2i_{r\alpha} / P_{r\alpha} \qquad 2\text{-}11$$

Usually only the positive pulse of the pressure-time relationship of Figure 2-191b (+) is utilized for the front wall design since the negative pulse seldom affects the design. For determining the overall motion of the structure, the effects of negative pressures should be included. The peak negative reflected pressure (Figure 2-190 (+)) and reflected

impulse are obtained from Figure 2-16 (+) and correspond to the peak incident pressure (Figure 2-15 (+)) acting on the front wall. The rise time and decay of the negative pressures are similarly calculated as described in Section 2-15.2.

2-15.3.3 Roof and Side Walls.

As the shock front traverses a structure, a pressure is imparted to the roof slab and side walls equal to the incident shock pressure at a given time at any specified point reduced by a negative drag pressure. The portion of the surface loaded at a particular time is dependent upon the magnitude of the shock front incident pressure, the location of the shock front, and the wavelength (L_w and L_w^-) of the positive and negative shock pressure pulses. Values for L_w and L_w^- can be determined from Figure 2-15 (+) and Figure 2-16 (+) for the typical case of a surface burst.

To determine accurately the overall loading on a surface, a step-by-step analysis of the shock wave propagation across the surface should be made. This analysis includes an integration of the pressures at various points (Figure 2-195a (+)) on the surface and at various times to determine the equivalent uniform incident pressure acting on a span L as a function of time (Figure 2-195b (+)). Since the regions of maximum stress in the component vary along the span length as the shock front traverses the surface, , the component should be designed with constant cross sectional properties along the span length to ensure it will respond as intended when it is designed using the equivalent uniform pressure.

As the shock wave traverses the roof or side walls, the peak value of the incident pressure decays and the wave length increases. As illustrated in Figure 2-195b (+), the equivalent uniform pressure will increase linearly from time t_f, when the blast wave reaches the beginning of the component (point f), to time t_d, when the peak equivalent uniform pressure is reached. The equivalent uniform pressure will then decrease to zero when the blast load at point b in Figure 2-195a (+) on the component decreases to zero.

To simplify the calculations, the equivalent uniform pressure has been expressed as a function of the blast wave parameters at point f in Figure 2-195a (+). The equivalent load factor C_E, the rise time, and duration of the equivalent uniform pressure are obtained from Figure 2-196 (+), Figure 2-197 (+), and Figure 2-198 (+), respectively, as a function of the wave length-span ratio L_{wf}/L.

The peak value of the pressure acting on the roof P_R is the sum of contribution of the equivalent uniform pressure and drag pressure:

$$P_R = C_E P_{sof} + C_D q_{of} \qquad 2\text{-}12$$

where P_{sof} is the incident pressure occurring at point f and q_{of} is the dynamic pressure calculated from Figure 2-3 (+) with P_{so} equal to $C_E\, P_{sof}$.

The drag coefficient C_D for the roof and side walls is a function of the peak dynamic pressure. Recommended values are as follows:

Peak dynamic pressure	Drag coefficient
0-25 psi	-0.40
25-50 psi	-0.30
50-130 psi	-0.20

The data presented above for the equivalent uniform roof and side wall blast pressures are used principally for the design of individual elements. For overall motions of a structure, the effects of the negative phase pressures should be included. The equivalent load factor C_E for the peak equivalent uniform negative pressure is obtained from Figure 2-196 (+) as a function of the wavelength span ratio L_{wf}/L. The value of the negative pressure acting on the roof, P_R^- is equal to $C_E^- P_{sof}$ where the value of C_E^- is a negative value. The value of the equivalent negative pressure duration t_{of} is obtained from Figure 2-198 (+).The value is not a function of the peak incident pressure at point f. The rise time of the negative phase is equal to 0.25 t_{of}.

If a side wall is positioned at an oblique angle to the shock front, then blast loads acting on the side wall are calculated in the same manner as that described for front walls.

2-15.3.4 Rear Wall.

As the shock front passes over the rear edges of the roof and/or side walls, the pressure front will expand, forming secondary waves which propagate over the rear wall. In the case of long buildings, the secondary wave enveloping the back wall essentially results from the spillover from the roof and the side walls. In both cases, the secondary waves are reinforced due to their impingement with reflecting surfaces. The reinforcement of the secondary wave from the roof is produced by its reflection from the ground surface at the base of the rear wall, and the reinforcement of the secondary waves from the side walls is produced by their collision near the center of the wall and/or their interaction with the wave from the roof. Little information is available on the overall effects on the rear wall loading produced by the reflections of the secondary waves.

In most design cases, the primary reason for determining the blast loads acting on the rear wall is to determine the overall drag effects (both front and rear wall loadings) on the building. For this purpose, a procedure may be used where the blast loading on the rear wall (Figure 2-199a (+)) is calculated with the equivalent uniform method used for computing the blast loads on the roof and side walls. Here the peak pressure of the equivalent uniform pressure-time curve (Figure 2-199b (+)) is calculated using the peak

pressure applied at the back edge of the roof slab P_{sob}. The equivalent uniform load factors C_E and C_E^- are based on a wavelength span ratio L_{wf}/L where the wave length is calculated at the back edge of the roof slab and L is equal to the height of the rear wall H_s. A similar approach is used to calculate the rise times and durations of both the positive and negative phases.

Like the roof and side walls, the blast loads acting on the rear wall are a function of the drag pressures in addition to the incident shock pressure. The dynamic pressure is calculated based on the equivalent pressure $C_E\ P_{sob}$ and the recommended drag coefficients are the same as used for the roof and side walls.

In the event that the back wall is positioned at an oblique angle to the shock front, peak incident pressure at point b should be calculated at the mid-width of the back wall.

2-15.3.5 Multiple Explosions.

The blast loads produced by multiple explosions acting on structures located far from the explosions may consist of a series of separate pressure pulses, rather than a single pulse blast load. However, the multiple pressure-pulse loading is usually associated with weights of explosives which are very small (several pounds) and, therefore, will not be the usual design situation. For large charge weights, however, the single pressure pulse loading with multiple peak pressures will occur. At the present time no specific method has been devised which will enable one to evaluate this type of blast loading. In the interim, it is suggested that the multiple peak pressure type loading be replaced by the pressure-pulse which is associated with the merged shock wave. The parameters of this shock wave and corresponding pressures are determined assuming a single explosion, the explosive weight of which is equal to the combined weight of the individual charges.

2-15.4 Above Ground Rectangular Structures with Openings.

2-15.4.1 General.

Two structural configurations are usually encountered when blast loads are determined on structures with unsealed or unprotected openings in exterior surfaces. The first configuration assumes that interior blast pressure must be calculated based on exterior blast load entering the building through windows, doors, or other openings located in multiple sides of the structure. The second configuration assumes that interior blast pressure can be calculated based only on the exterior blast load entering the building through openings located in the front face of the structure. The blast load entering through the remaining surfaces is assumed to have a negligible effect. The second configuration is considered most representative since interior partitions will restrict the flow of the blast wave through the structure. Increased interior blast loads are produced due to the reflection of the blast wave on interior components. The interior blast loads associated with the second configuration are primarily discussed in this section with comments regarding the loads pertaining to the first configuration.

When a shock front strikes the front wall of a structure, the incident pressure is amplified. Windows and doors will fail almost immediately (approximately one millisecond) after the onset of the shock front unless they were designed to resist the applied load. As a result, blast pressures will flow into the structure through these openings. This sudden release of high pressure will cause a shock front to form inside of each opening. Each individual front will expand and tend to combine into a single front which will further expand throughout the structure's interior. This interior shock is initially weaker than the incident pressure at the building's exterior. However, the interior pressure will tend to get stronger due to reflections off interior building components.

An idealized structure configuration is shown in Figure 2-200 (+). The incident shock front arriving at the front wall of the structure has an incident pressure P_{so} and wave length L_w. As the shock front sweeps across the structure, blast pressures enter the interior of the building through the opening in the front wall of area A_o. The area of multiple openings are added to obtain a fictitious single opening located at the center of the front wall. The blast pressures entering the building first load the interior surface of the front wall, followed by the interior surface of the side walls and roof, and finally the interior surface of the back wall. The idealized pressure-time load curves for these surfaces are presented in Figure 2-201 (+). The procedures necessary to obtain the magnitude of the parameters given on the idealized load curves for a particular explosion are presented in the remainder of this section. Except for the front wall, the blast pressures acting on the exterior of the structure are not affected by the opening and are determined according to the procedures of the previous section.

The primary purpose of this section is to provide the blast loading on the interior surface of an exterior wall so that the maximum outward motion of the wall may be determined. It is not the intent to use these interior loads to reduce the exterior positive phase loading. Except for the front wall, accurate phasing of the interior and exterior blast loads are not possible. The interior loads will always lag the exterior positive phase loading and, due to reflections off interior components, the duration of the interior load is always longer. For design, the interior blast loads should be added to the negative phase exterior loading to obtain the maximum outward motion (negative response) of a side wall, roof or back wall. The maximum positive response should be determined for the exterior positive phase loading without any reductions due to internal pressures. In most instances, interior partitions are required to withstand the blast pressures leaking into a structure. The procedures presented in this section may be used to determine the design blast load acting on these elements. An interior partition located parallel to the front wall will reflect the shock front and, therefore, is considered as a back wall. The length of the side wall would then be taken as the distance between the front wall and this partition. An interior partition(s) perpendicular to and framing into the front wall may be considered as a side wall(s). The length of the front wall would then be taken as the distance between an interior partition and a side wall or between two interior partitions. In both cases, only the openings located between these partition walls would be considered as the vent opening.

The procedures presented in this section to determine interior blast loads acting on a structure with an opening in the front wall were developed for a shock front striking the front wall head-on. For the same size opening in a front wall, this orientation of the approaching shock front results in the most severe interior shock wave effects. The use of these procedures for shock fronts approaching at all other angles will result in conservative estimates of the blast loadings acting on the interior of the structure.

2-15.4.2 Exterior Front Wall Loads.

The time required for reflected pressures to clear a solid front wall is expressed in multiples of the time necessary for a rarefaction wave to sweep the wall. When walls with openings are considered, clearing takes place around the edges of the opening in addition to the edges of the wall. Depending upon the size of the overall wall and the openings, the clearing time of the reflected pressures may be significantly reduced.

The pressure-time relationship of the applied blast load acting on the front wall of a structure with openings is the same as that of a solid front wall (Figure 2-191 (+)) except the clearing time will be reduced. To evaluate this reduced time, the value of *S'* is introduced into Equation 2-8. This value is the weighted average distance that the rarefaction wave must travel to cover the wall assuming immediate access of the incident shock to the interior of the structure. If frangible covers (windows, doors) do not fail immediately, the clearing time should not be reduced.

The method for evaluating *S'* is illustrated in Figure 2-202 (+) where the face of the front wall is divided into rectangular areas. These areas are determined by the location and dimensions of the openings in the wall, and by consideration of the direction along which the reflected pressure clears around the area in the shortest possible time. The individual areas are labeled depending upon the number and location of the clearing sides of the individual areas. Clearing factors δ_n are established for these areas as follows:

Area	δ_n	Number of Clearing Sides
1	1.0	Two adjacent sides
2	0.5	Two opposite sides
3	1.0	One side
4	1.0	None

The weighted average clearing distance *S'* is expressed as:

$$S' = \frac{\sum \delta_n h_n A_n}{A_f} \leq S \qquad 2\text{-}13$$

where

S' = *weighted average clearing distance with openings*
δ_n = *clearing factor*
h_n = *average clearing distance for individual areas as follows:*
Area 1 - width or height of area, whichever is smaller
Area 2 - distance between opposite sides where clearing occurs
Area 3 - distance between side where clearing occurs and opposite side
Area 4 - same as Area 1
A_n = *area of individual wall subdivision*
A_f = *net area of the wall excluding openings*

The clearing time t'_c for a front wall with opening is calculated from Equation 2-8 in which *S'* is substituted for *S* or

$$t'_c = \frac{4S'}{(1+R)C_r} \qquad 2\text{-}14$$

where all components of Equation 2-14 have been previously defined. It should be realized that the load acting on the front wall with openings is still the same as that shown in Figure 2-191 (+) except with the reduced clearing time, t'_c. The curve which represents the wall loading is still the curve in Figure 2-191 which gives the lower impulse (i.e., the curve based on t'_c or t_{rf}).

As previously stated, window breakage will require a finite length of time. This time may be evaluated using the resisting functions of Chapter 6 and the dynamic procedures of Chapter 3. This time must be accounted for in determining the window contribution to the blast pressures acting on the wall.

2-15.4.3 Interior Front Wall Loads.

The average pressure acting on the interior face of the front wall will initially build up in a similar manner as the average pressure on the exterior back wall of a closed structure. However, vortices are located all around the interior edges of all openings in the front wall. The effect of these vortices, which tend to reduce the blast load, has been neglected.

The shock front entering through the opening in the front wall travels along the interior face of the front wall, thereby subjecting the wall to incident pressures. When the front reaches the side wall, it is reflected back. The length of wall loaded by this reflected wave is a function of the wave length, L_w. The average pressure acting on the wall is determined assuming a single opening of area A_o located at the center of the wall. In the case of multiple openings, a single opening equal to the combined area of all openings is located in the center of the front wall.

The idealized pressure-time blast load acting on the interior face of the front wall is shown in Figure 2-201a (+). The time at which the shock front arrives at the exterior surface of the front wall is taken as zero ($T_o = 0$). The blast load acting on the wall begins at time T_1. This time represents the time it takes for the shock front to enter the structure through the opening A_o. The pressure buildup is linear from time T_1 to a maximum pressure P_{max} at time T_2, and then it decays linearly to zero at time T_3.

The maximum average pressure P_{max} acting on the interior face of the front wall varies as a function of the incident pressure P_{so} and the wavelength L_w corresponding to that pressure, and the geometry of the wall. Figure 2-203 through Figure 2-206 give the maximum pressure P_{max} acting on front walls having width to height ratios (W/H) equal to 3/4, 3/2, 3 and 6, respectively.

The idealized times T_1, T_2 and T_3 are also obtained from plots of front walls having width to height ratios W/H equal to 3/4, 3/2, 3 and 6. The arrival time T_1 of the load is given in Figure 2-207 (+/+) and Figure 2-208 (+/+) as a function of the incident pressure acting on the exterior surface of the front wall P_{so} for various opening to wall area ratios A_o/A_w. The rise time of the load, T_2 - T_1 is given in Figure 2-209 (+/+) and Figure 2-210 (+/+) as a function of P_{so} and various wave length to width of front ratios L_w/W. Finally, the duration of the load T_3 - T_1 is given in Figure 2-211 (+/+) and Figure 2-212 (+/+) again as a function of P_{so} and L_w/W. The times T_2 and T_3 are obtained from subtracting T_1 from the rise time and duration, respectively.

Failure of the cover sealing openings in a building (windows, doors) will affect the onset of the blast load acting on the interior surface of the front wall. Due to the time required to cause failure of the covers, the onset of the interior pressures may not be in phase with the onset of the exterior blast load. Therefore, care must be taken to arrive at a combined loading for the structural element.

2-15.4.4 Interior Side Wall and Roof Loads.

The blast pressures entering the interior of the building through the opening in the front wall (multiple openings are combined to form a single opening) must travel along the interior face of the front wall before arriving at the side wall. The incident pressures arriving at the side wall are increased due to reflection off the wall itself. The front expands and travels across the side wall until it reaches the back wall. It is then reflected off the back wall, and the reflected wave travels back across the side wall towards the front wall. The length of side wall loaded by this reflected wave is a function of the wave length L_w.

The idealized pressure-time blast load acting on the interior face of the side wall and roof is shown on Figure 2-201b (+). The same assumption is made for the side wall and roof as for the interior front wall. That is, the time at which the shock front arrives at the front wall of the structure is taken as zero ($T_o = 0$). The time T_1 represents the time it takes the shock front to travel from the opening across the interior face of the front wall to the side wall (or roof). The pressure build up is linear from time T_1 to a maximum pressure P_{max} at time T_2, remains constant until time T_3 and decays linearly to zero at time T_4. This idealized curve applies to both the side walls and roof. The structure configuration parameters as given in Figure 2-200 (+) apply for side wall loadings. However, to determine the roof loading, the structure must be rotated 90 degrees so that the roof takes the position of a side wall. The width and height of the structure must be interchanged. All other parameters are not affected.

The maximum average pressure P_{max} acting on the interior face of the side wall (or roof) varies as a function of the incident pressure P_{so} acting on the exterior face of the front wall, the wavelength L_w corresponding to P_{so}, and the geometry of the structure. Since a large number of plots would be required to describe P_{max} for the blast and geometric parameters involved, an equation has been developed. The value of P_{max} is given by:

$$P_{max} = K/(L_w/L) \qquad 2\text{-}15$$

For $6 \geq W/H \leq 3/2$

$$K = \{ A + [B \times (L_w/L)^C] \} \times D \times E \times P_{so}^{1.025} \qquad 2\text{-}16$$

where

$$A = [0.002\ (W/H)^{1.4467}] - 0.0213 \qquad 2\text{-}17$$

$$B = 2.2075 - [1.902\ (W/H)^{-0.085}] \qquad 2\text{-}18$$

$$C = 1.231 + [0.0008\ (W/H)^{2.678}] \qquad 2\text{-}19$$

$$D = [2.573\ (L/H)^{-0.444}] - 0.3911 \qquad 2\text{-}20$$

$$E = 0.4221 + [1.241\ (A_o/A_w)^{0.367}] \qquad 2\text{-}21$$

For $W/H = 3/4$

$$K = A \times B \times C^E \times F^H \times P_{so}^{0.9718} \qquad 2\text{-}22$$

where

$$A = [0.5422\ (L_w/L)^{1.2944}] - 0.001829 \qquad 2\text{-}23$$

$$B = [0.654 + 2.616\ (A_o/A_w) - 4.928\ (A_o/A_w)^2]\cdot[2.209\ (L/H)^{-0.3451} - 0.739] \qquad 2\text{-}24$$

$$C = 0.829 + 0.104\ (L_w/L)^{1.6} + [0.00124 + 0.00414\ (L_w/L)^{3.334}]\ [L/H]^D \qquad 2\text{-}25$$

$$D = 2.579 - 0.0534\ (L_w/L)^{3.891} \qquad 2\text{-}26$$

$$E = 999\ (A_o/A_w)^{9.964} \qquad 2\text{-}27$$

$$F = 1.468 - 1.6627\ (A_o/A_w)^{0.7801} + [1.8692 - 1.1735\ (A_o/A_w)^{-0.2226}]\ [L_w/L]^G \qquad 2\text{-}28$$

$$G = 0.2979\ (A_o/A_w)^{-1.4872} - 0.8351 \qquad 2\text{-}29$$

$$H = (5.425 \times 10^{-4}) + (1.001 \times 10^{-9})\ (L/H)^{9.965} \qquad 2\text{-}30$$

For 3/2 > W/H > 3/4, graphical interpolation is required to determine P_{max}. Several values of P_{max} are determined from Equation 2-15 for values of W/H equal to 3/4, 3/2, and preferably two values greater than 3/2. A plot of P_{max} versus W/H is prepared and the value of P_{max} is read for the required W/H.

The idealized times T_1 and T_2 are determined from Figure 2-213 (+/+). These times are presented as a function of the incident pressure P_{so} arriving at the exterior of the building and the width to height ratio W/H of the front wall. Since the distance that the shock front must travel across the front wall is taken from the center of the opening, times T_1 and T_2 are not a function of the area of the opening. This assumption will not result in significant errors since the openings considered are comparatively small.

The idealized times T_3 and T_4 are determined from Figure 2-214 through Figure 2-229. Each figure is prepared for a given structure configuration defined by the length to height ratio of the side wall L/H and the width to height ratio of the front wall W/H. The times T_3 and T_4 are given on each figure as a function of the incident pressure P_{so} and various values of the wave length to side wall length ratio L_w/L. As explained above, these times are not a function of the area of the opening. For ease of reference, these figures are listed in Table 2-4 (+) for the various L/H and W/H ratios provided. In most cases, interpolation will be required to obtain the correct values of T_3 and T_4 for the given structure configuration.

2-15.4.5 Interior Back Wall.

The blast pressures entering the interior of the building through the opening in the front wall must travel the full length of the building before arriving at the back wall. The incident pressure arriving at the back wall is essentially uniform over the wall. This pressure is immediately increased to the normal reflected pressure when it strikes the back wall.

The idealized pressure-time blast load acting on the interior face of the back wall is shown in Figure 2-201c (+). Again, the time at which the shock front arrives at the front wall of the structure is taken as zero (T_o = 0). The time T_1 represents the time it takes the shock front to travel from the opening to the back wall. The pressure buildup is instantaneous to P_{RIB} due to the normal reflection of the shock front and then decays to zero at time T_2. This loading is similar to the loading of an exterior front wall except that clearing is not possible.

The maximum average pressure P_{RIB} acting on the back wall is obtained from Figure 2-230 (+/+) and Figure 2-231 (+/+). Each figure is prepared for a given value of L/H. The ratio of the maximum average pressure on the back wall to the incident pressure P_{RIB}/P_{so} is given as a function of P_{so} for various values of A_o/A_w. Interpolation between figures may be necessary for a given structural configuration.

The idealized time T_1 is determined from Figure 2-232 (+/+) and Figure 2-233 (+/+). Each figure is prepared for a given value of the width to height ratio of the wall W/H. The time T_1 is given as a function of the incident pressure P_{so} for various values of the wall length to height ratio L/H and the ratio of the opening area to the wall area A_o/A_w. The duration of the load T_2-T_1 is determined from Figure 2-234 (+). The time is given as a function of the incident pressure P_{so} for various values of A_o/A_w. Since the back wall is located at the greatest distance from the front wall, the area of the opening has a significant effect on these times and must be considered.

2-15.5 Pressure Buildup in Structures.

2-15.5.1 General.

The procedures in Section 2-15.4 are for determining the net effects of shock loads entering openings in structures from windows or doors which are not designed to withstand the applied blast loads. In certain cases, structures may have closures which are designed to resist the blast loading, but have very small openings due to vents and ducts, which will not withstand the blast. In this case, the small opening will not allow the shock front to develop inside the structure. However, the structure experiences an increase in its ambient pressure (a "filling" pressure) in a time that is a function of the structure volume, area of the openings, and applied exterior pressure and duration. Since personnel exhibit a tolerance limit to such pressure increases, a method of determining the average pressure inside the structure is needed. It should be noted that the interior pressures immediately adjacent to the openings will be higher than the average pressure.

2-15.5.2 Method of Calculation.

The following procedure is applicable for structures with small area-volume ratios and applied blast pressures less than 150 psi. The change in pressure δP_i inside the structure within a time interval δt is a function of the pressure difference at the openings, P-P_i, and the area-volume ratio, A_o/V_o:

$$\delta P_i = C_L \, (A_o / V_o) \, \delta t \qquad 2\text{-}31$$

where

C_L = *leakage pressure coefficient and a function of the pressure difference* $P\text{-}P_i$ *and is obtained from Figure 2-235* (+)
P = *applied exterior pressure*
P_i = *interior pressure*
δP_i = *interior pressure increment*
A_o = *area of openings*
V_o = *structure volume*
δt = *time increment*

The interior pressure-time curve is calculated as follows:

(1) Determine the pressure-time history of the applied blast pressures P acting on the surface surrounding the opening as presented in Section 2-15.3.

(2) Divide the duration t_o of the applied pressure into n equal intervals (δt), each interval being approximately $t_o/10$ to $t_o/20$, and determine the pressures at the end of each interval.

(3) Compute the pressure differential $P\text{-}P_i$ for each time interval, determine the corresponding value of C_L from Figure 2-235 (+), and calculate δP_i from Equation 2-31 using the proper values of A_o/V_o and δt. Add δP_i to P_i for the interval being considered to obtain the new value of P_i for the next interval.

(4) Repeat for each interval using the proper values of P and P_i. When $P\text{-}P_i$ becomes negative during the analysis, the value of C_L must also be taken as negative.

The above procedure is most easily accomplished by using a tabular arrangement for the required computations. An illustrative example is presented in Appendix 2A.

Figure 2-1 Blast Loading Categories

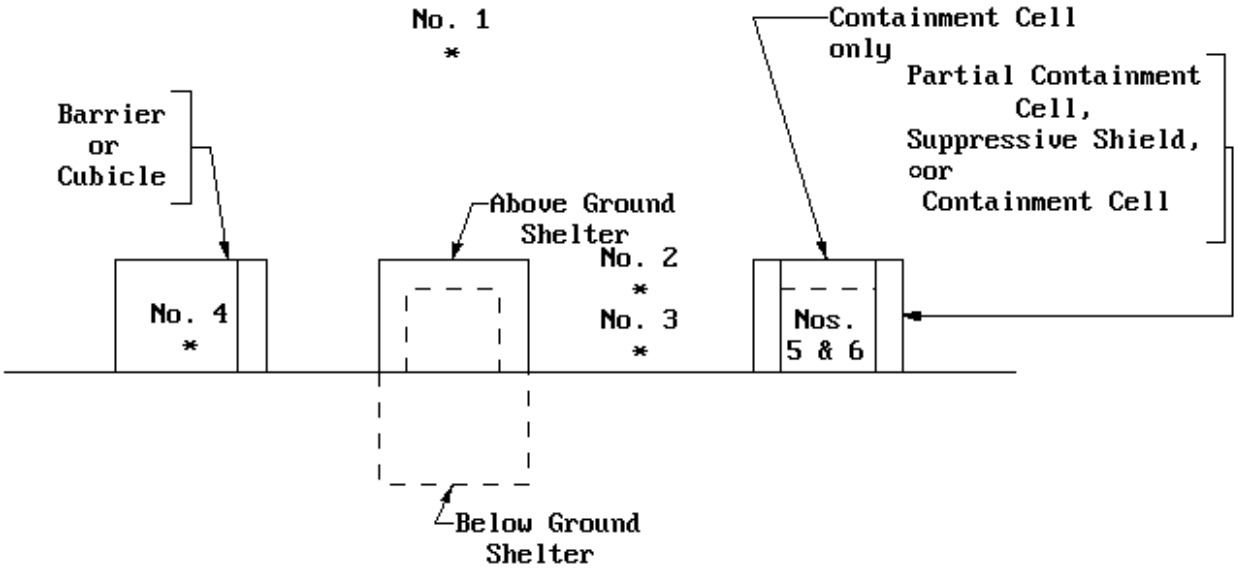

BLAST LOADING CATEGORIES			
CHARGE CONFINEMENT	CATEGORY	PRESSURE LOADS	PROTECTIVE STRUCTURE
Unconfined Explosions	1. Free Air Burst 2. Air Burst 3. Surface Burst	a. Unreflected b. Reflected b. Reflected	Shelter
Confined Explosions	4. Fully Vented	c. Internal Shock d. Leakage	Cubicle
	5. Partially Confined	c. Internal Shock e. Internal Gas d. Leakage	Partial Containment Cell or Suppressive Shield
	6. Fully Confined	c. Internal Shock e. Internal Gas	Full Containment Cell

Figure 2-2 Free-Field Pressure-Time Variation

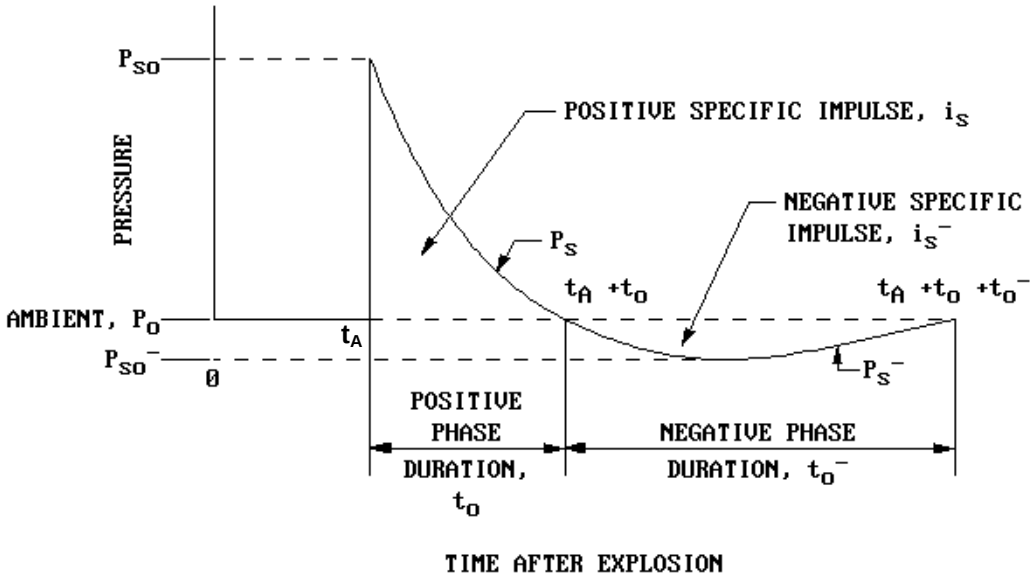

Figure 2-3 Peak Incident Pressure versus Peak Dynamic Pressure, Density of Air Behind the Shock Front, and Particle Velocity

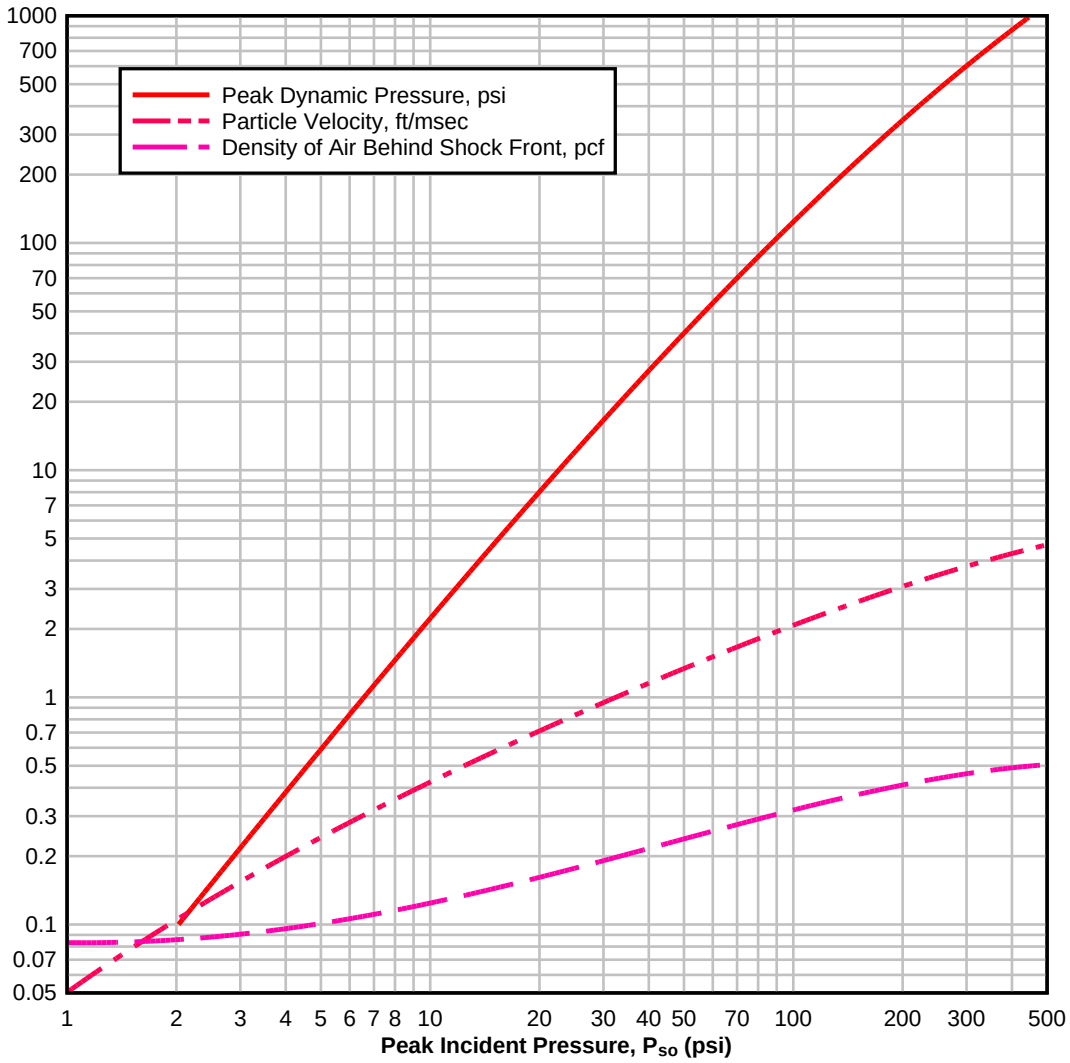

Figure 2-4 Free-Air Burst Blast Environment

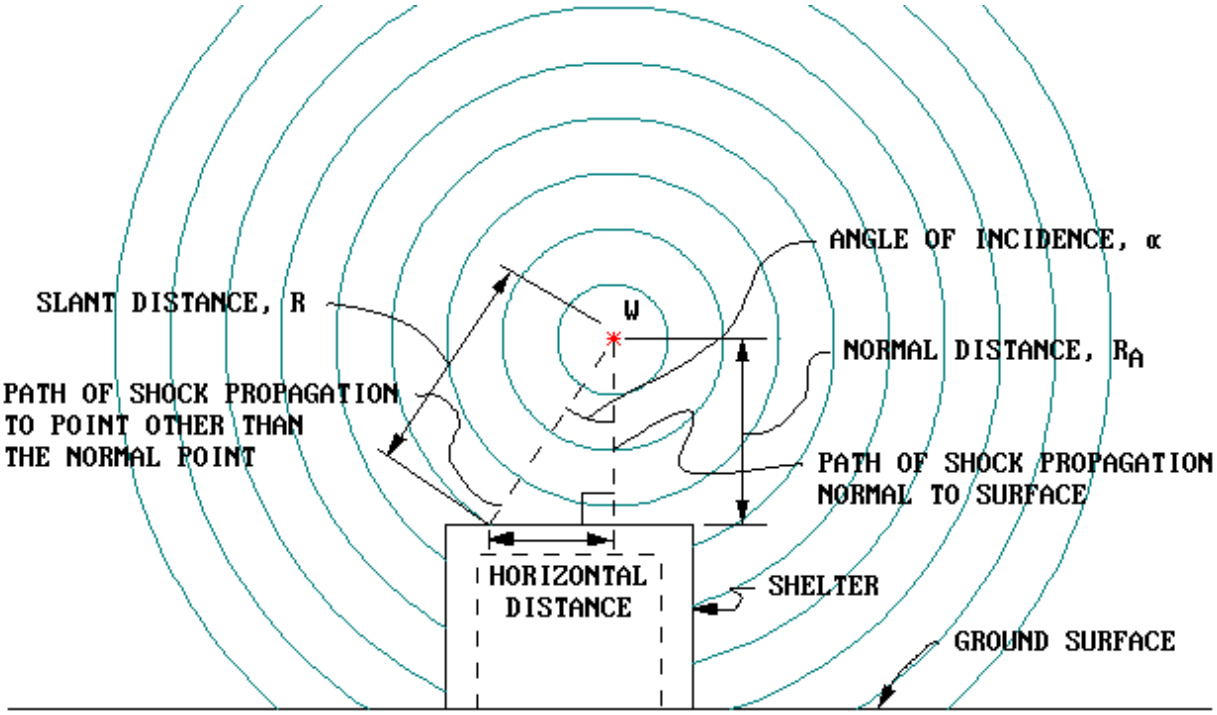

Figure 2-5 Pressure-Time Variation for a Free-Air Burst

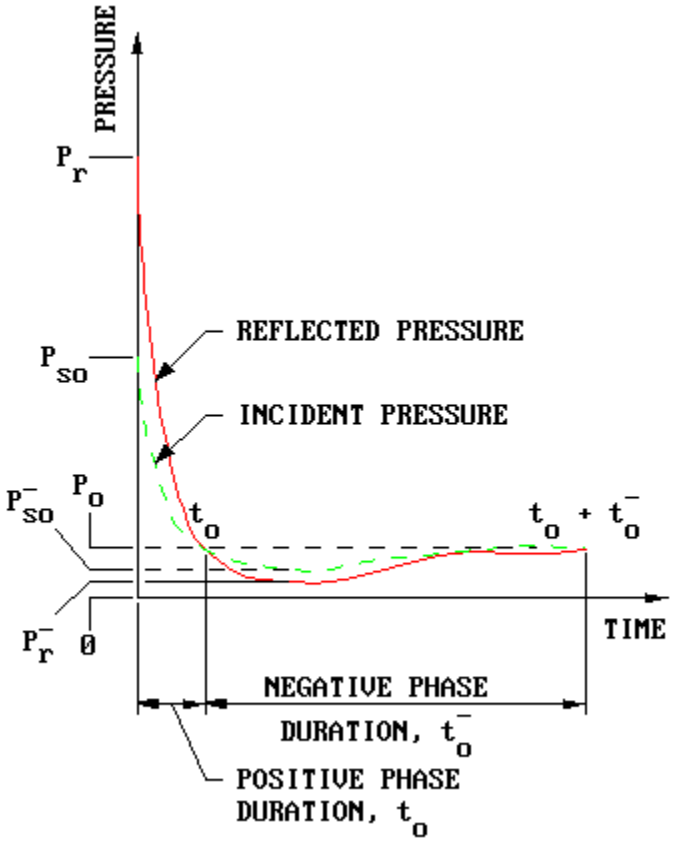

Figure 2-6 Peak Incident Pressure versus the Ratio of Normal Reflected Pressure/Incident Pressure for a Free-Air Burst

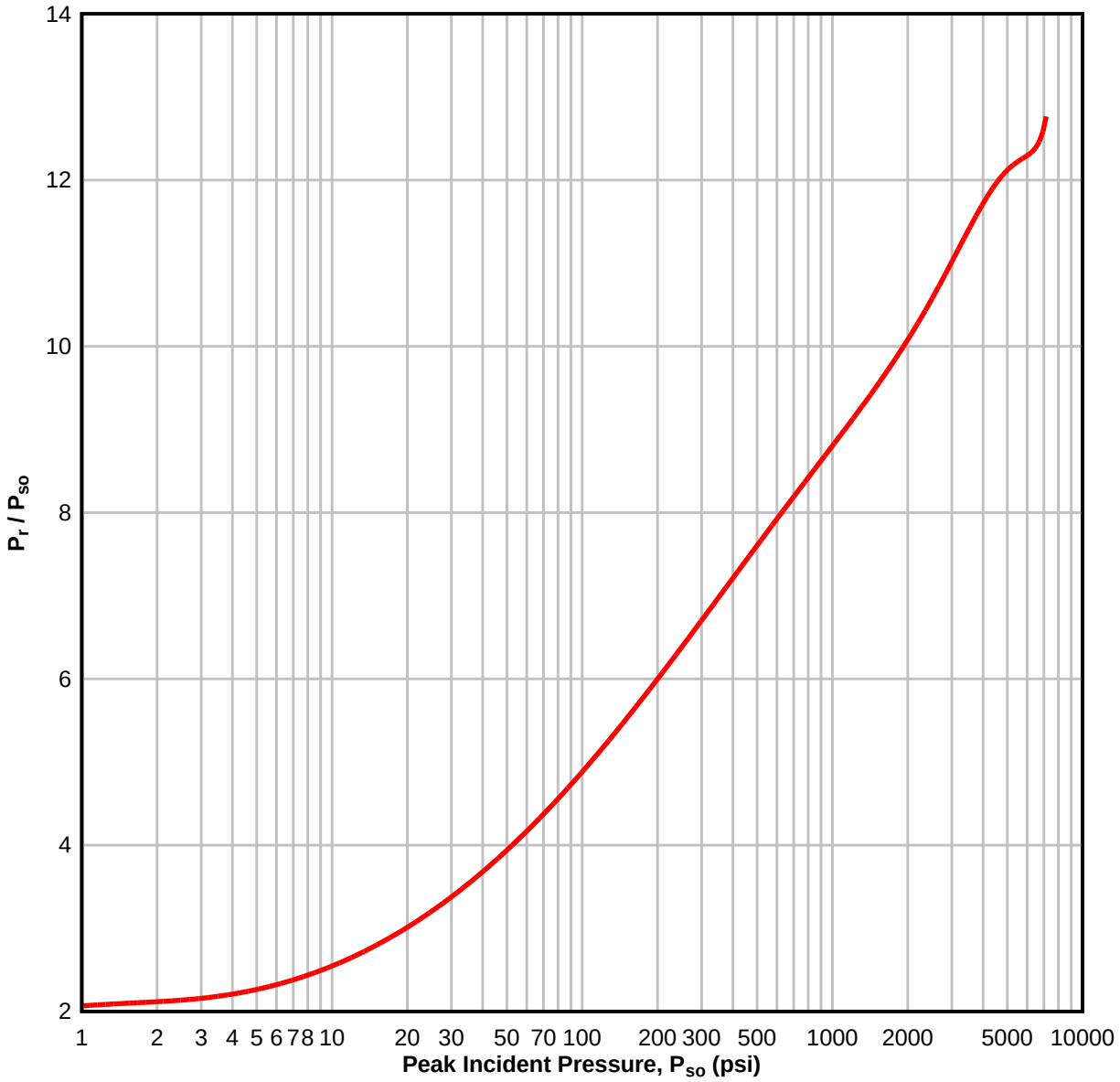

Figure 2-7 Positive Phase Shock Wave Parameters for a Spherical TNT Explosion in Free Air at Sea Level

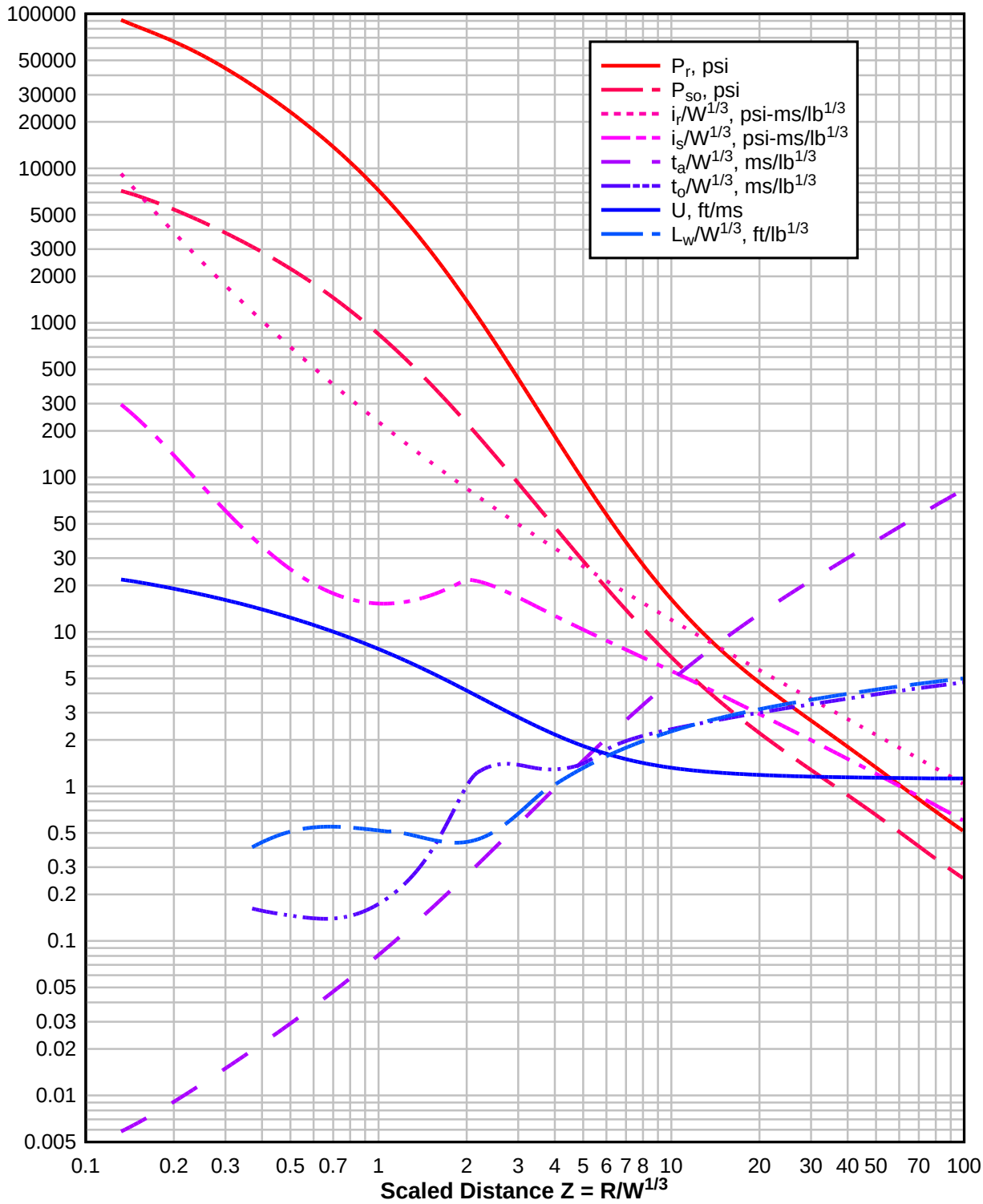

Figure 2-8 Negative Phase Shock Wave Parameters for a Spherical TNT Explosion in Free Air at Sea Level

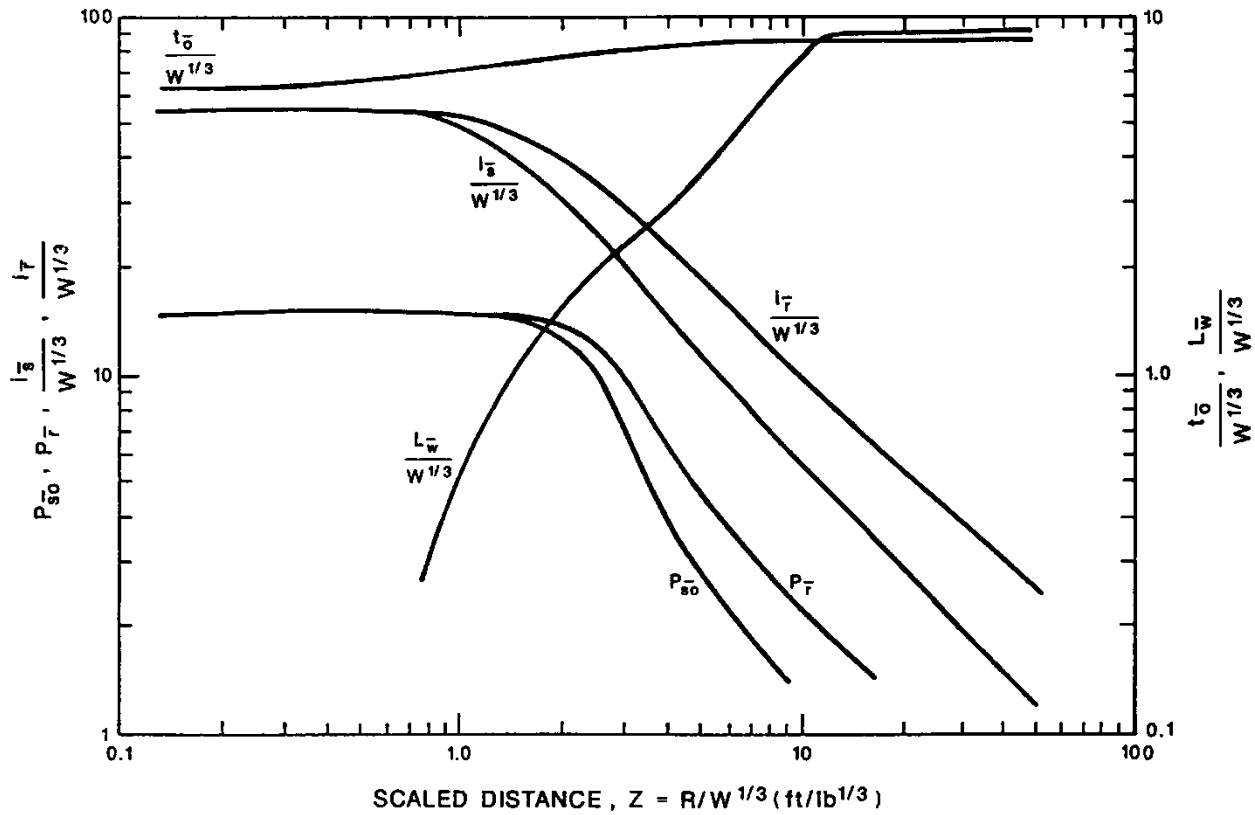

Figure 2-9 Variation of Reflected Pressure as a Function of Angle of Incidence

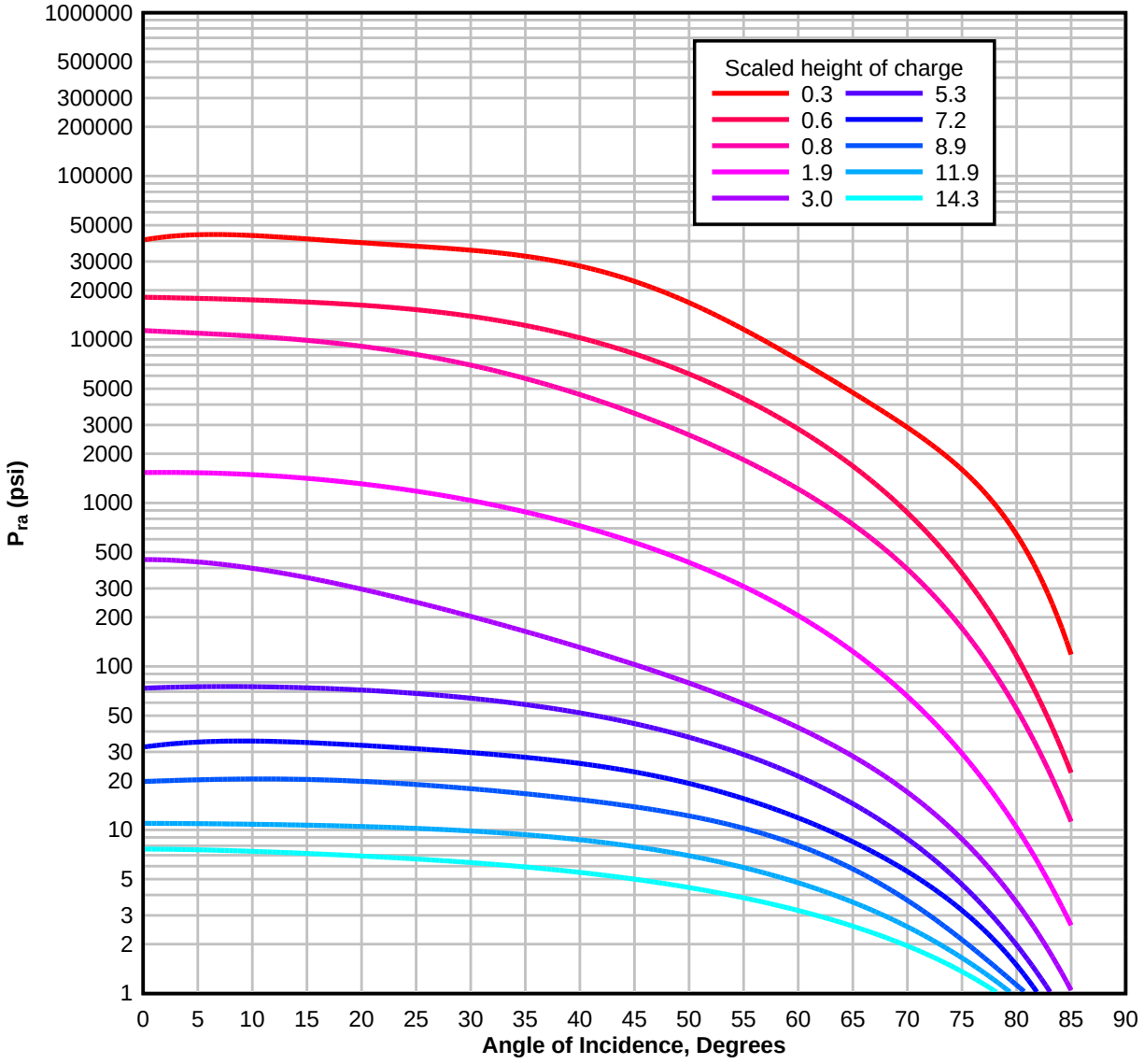

Figure 2-10 Variation of Scaled Reflected Impulse as a Function of Angle of Incidence

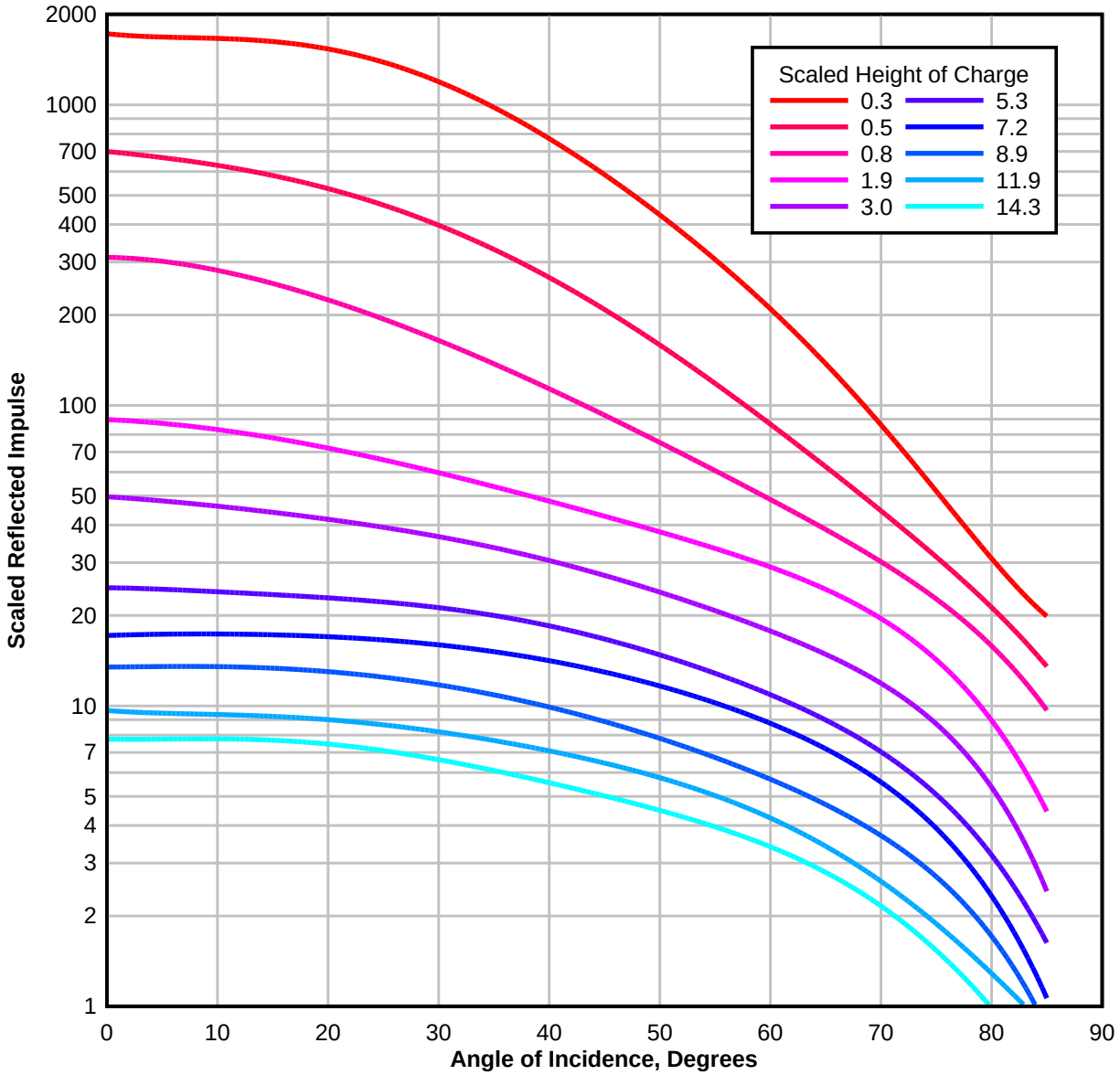

Figure 2-11 Air Burst Blast Environment

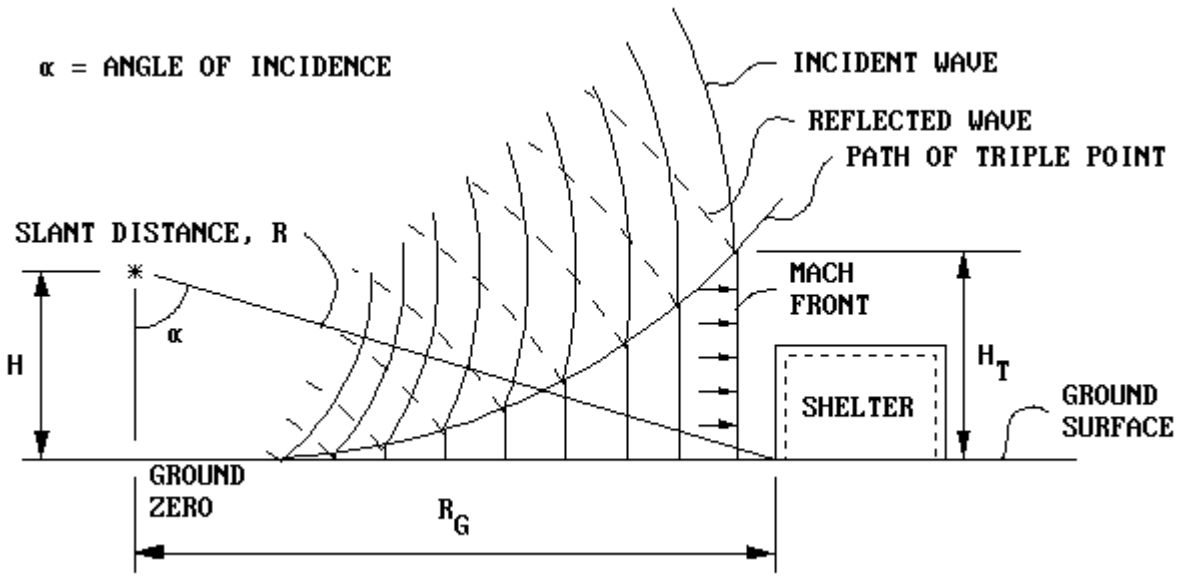

Figure 2-12 Pressure-Time Variation for Air Burst

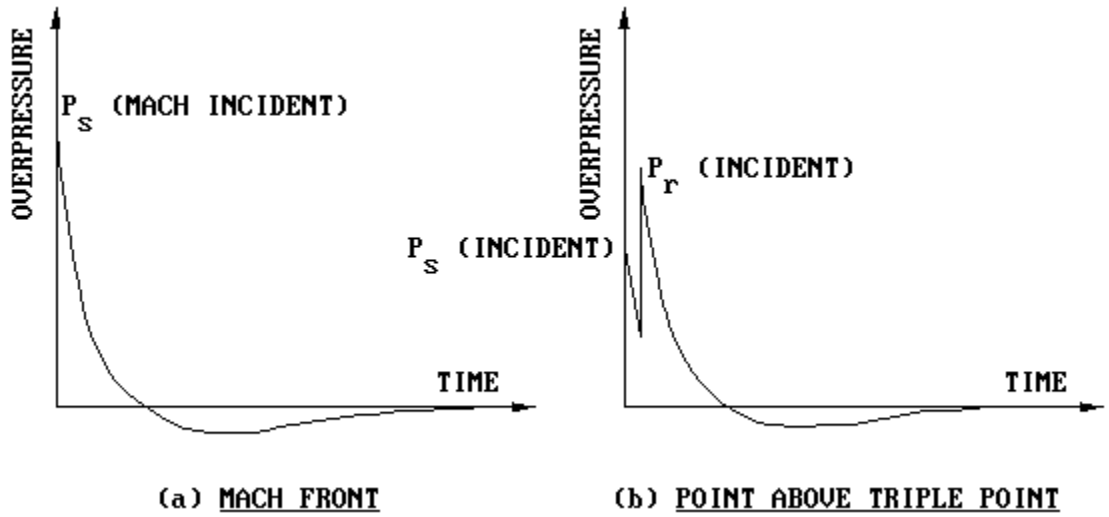

Figure 2-13 Scaled Height of Triple Point

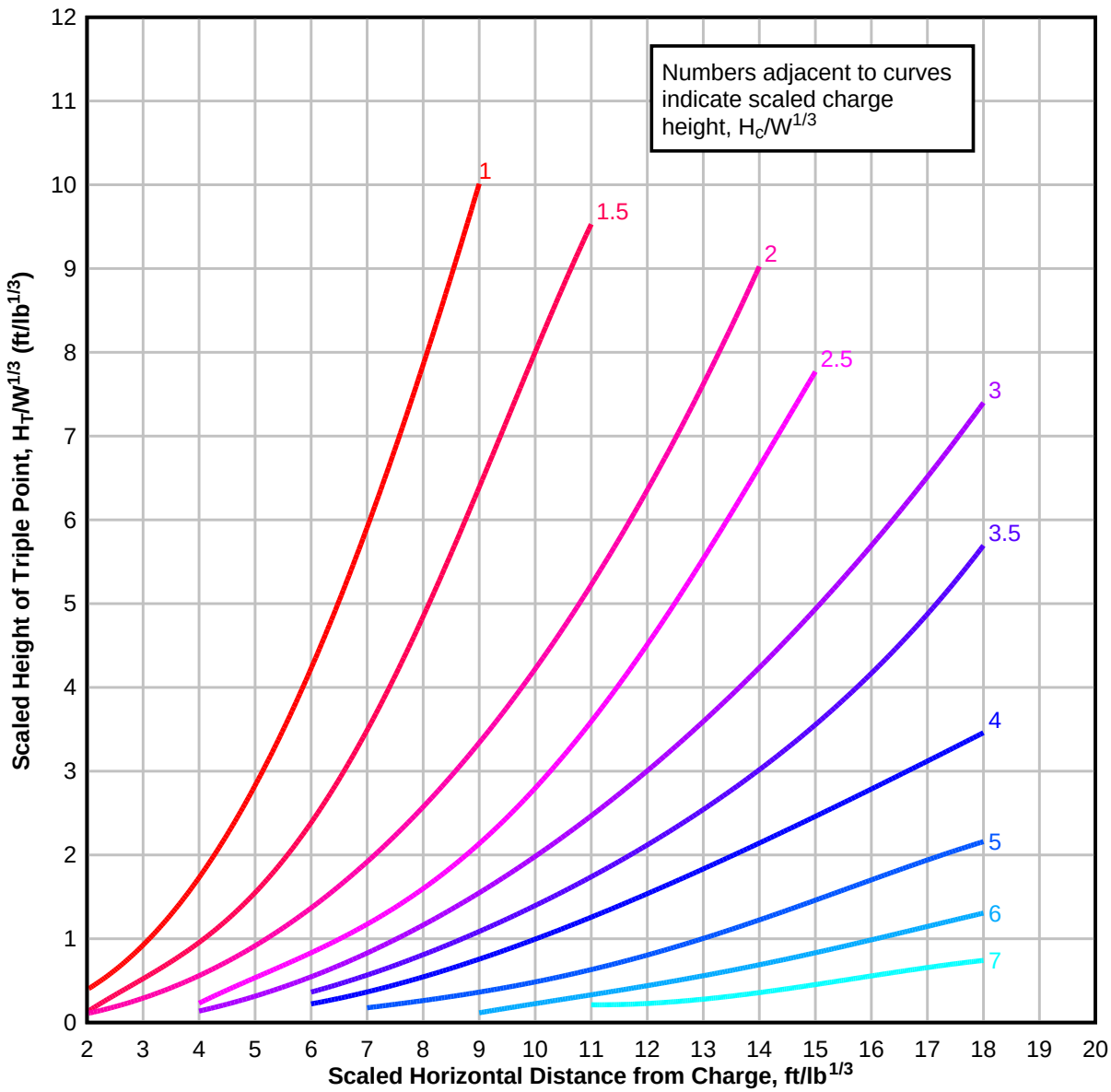

Figure 2-14 Surface Burst Blast Environment

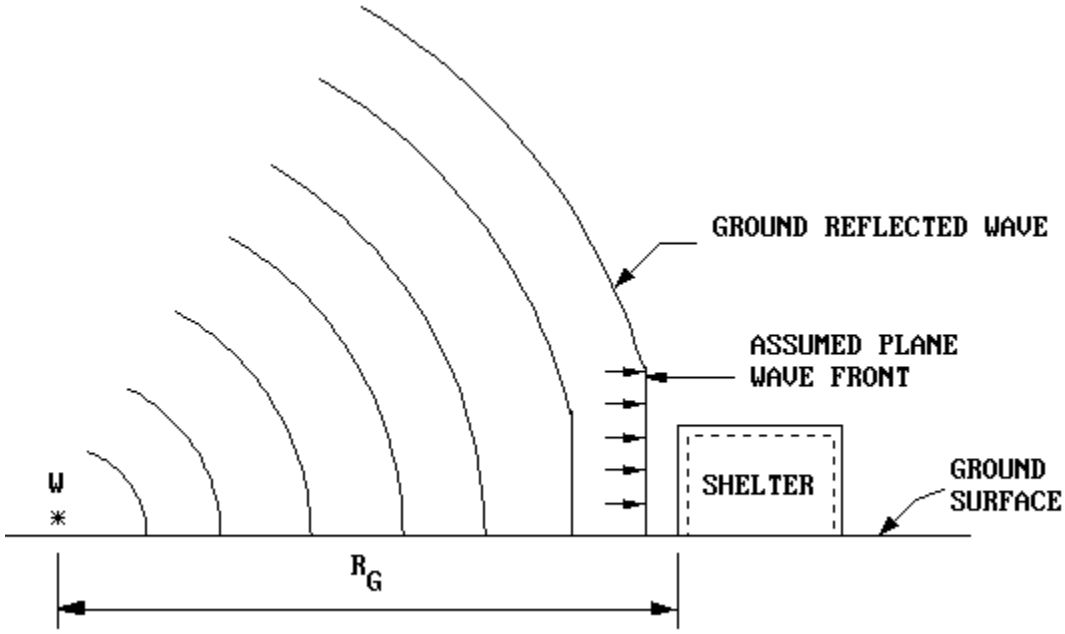

Figure 2-15 Positive Phase Shock Wave Parameters for a Hemispherical TNT Explosion on the Surface at Sea Level

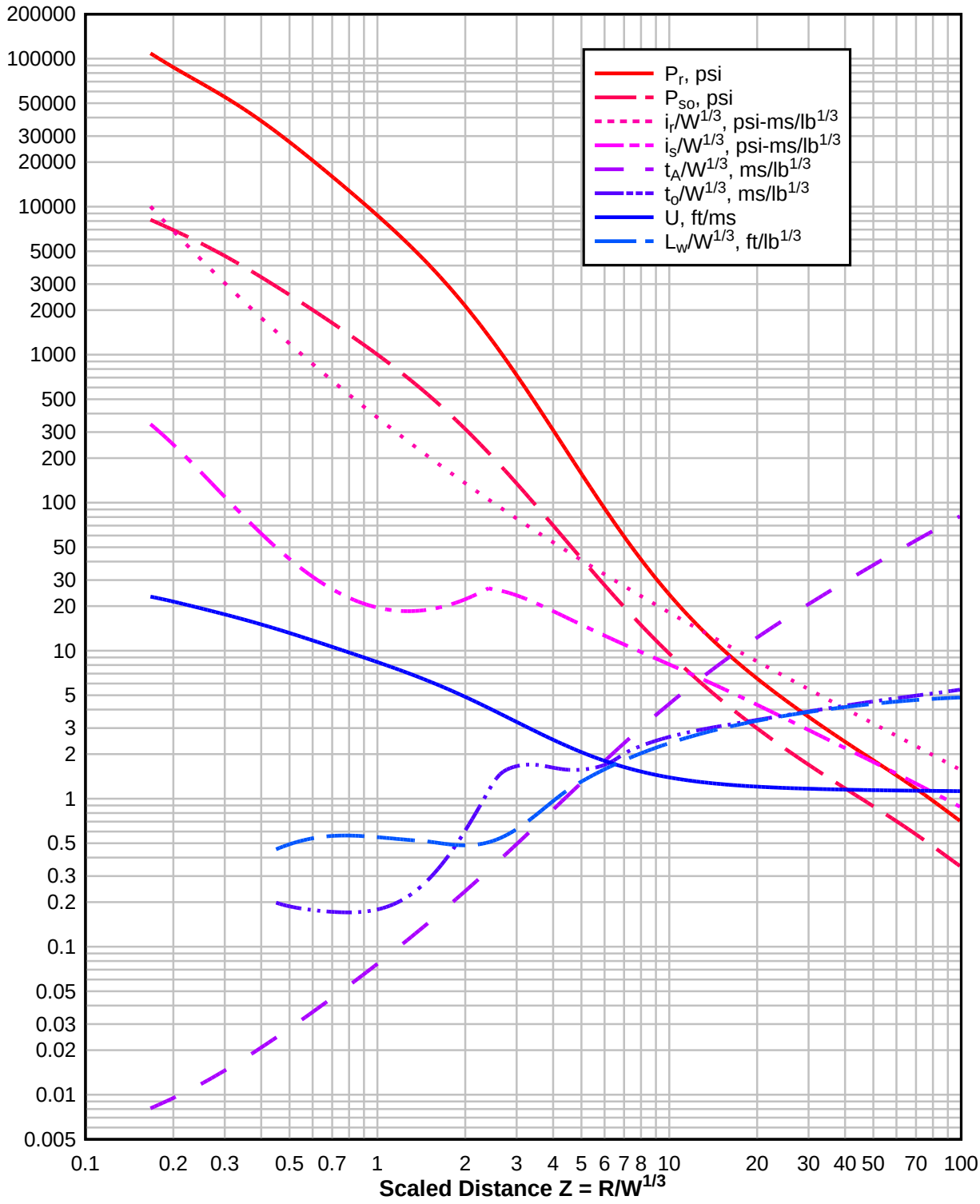

Figure 2-16 Negative Phase Shock Wave Parameters for a Hemispherical TNT Explosion on the Surface at Sea Level

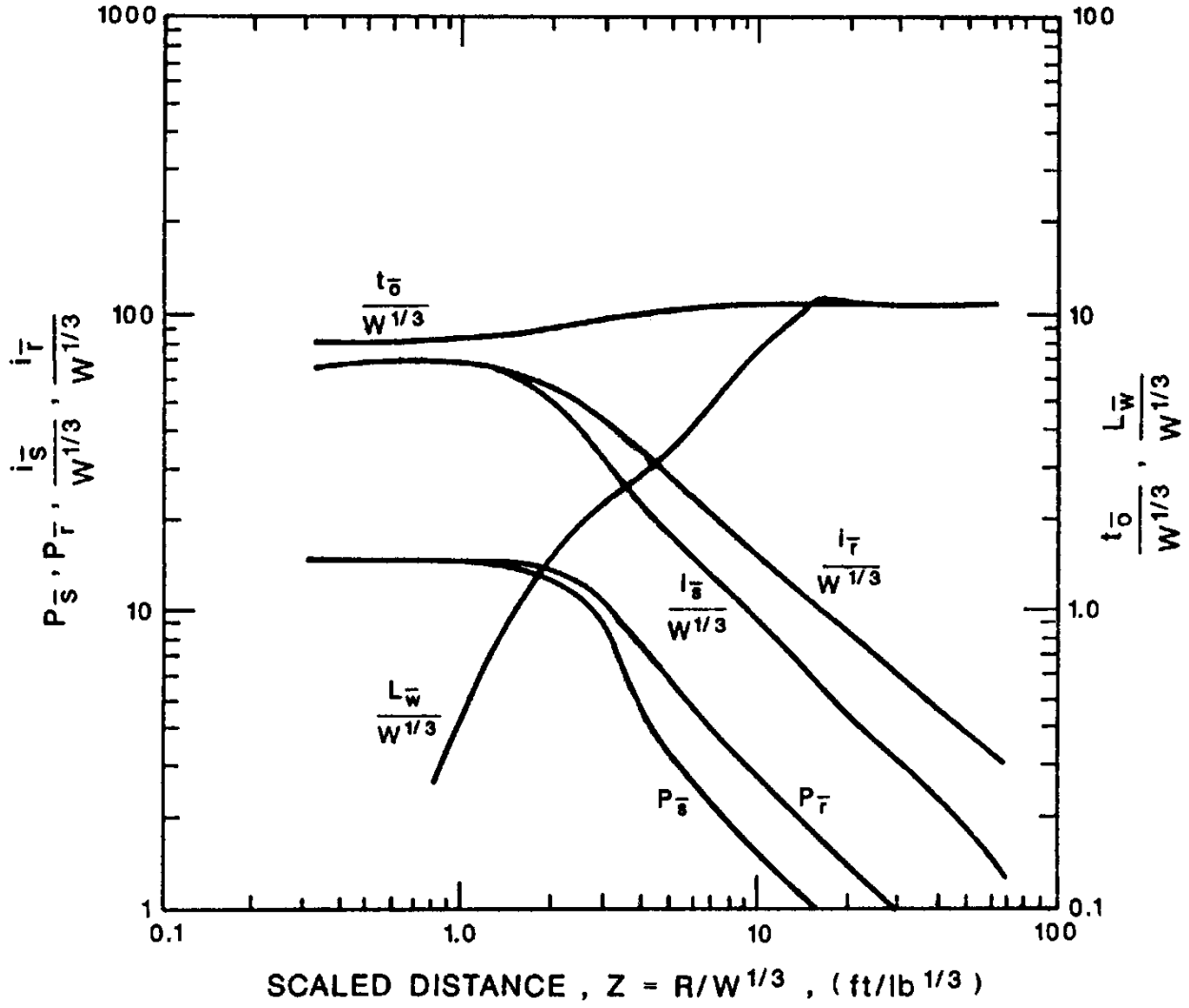

Figure 2-17 Explosive Shapes

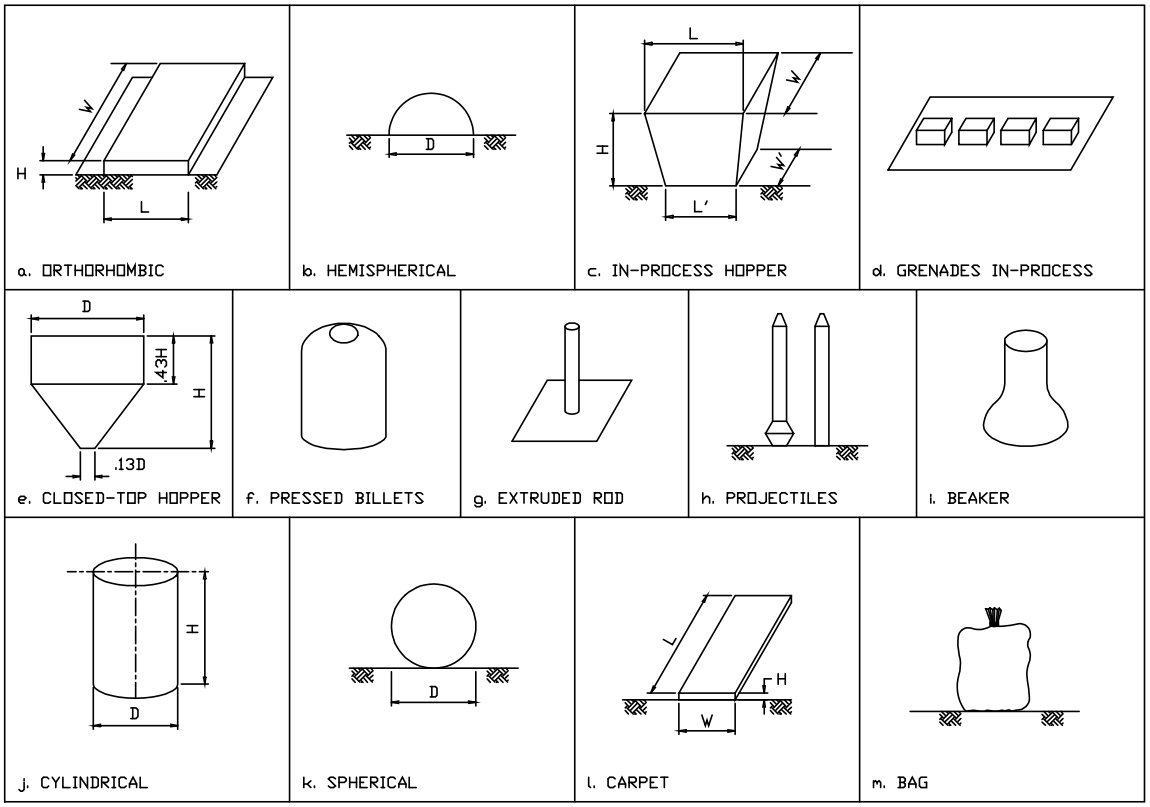

Figure 2-18 Peak Positive Incident Pressure and Scaled Impulse for an Explosion on the Surface at Sea Level, Composition A-3 and A-5

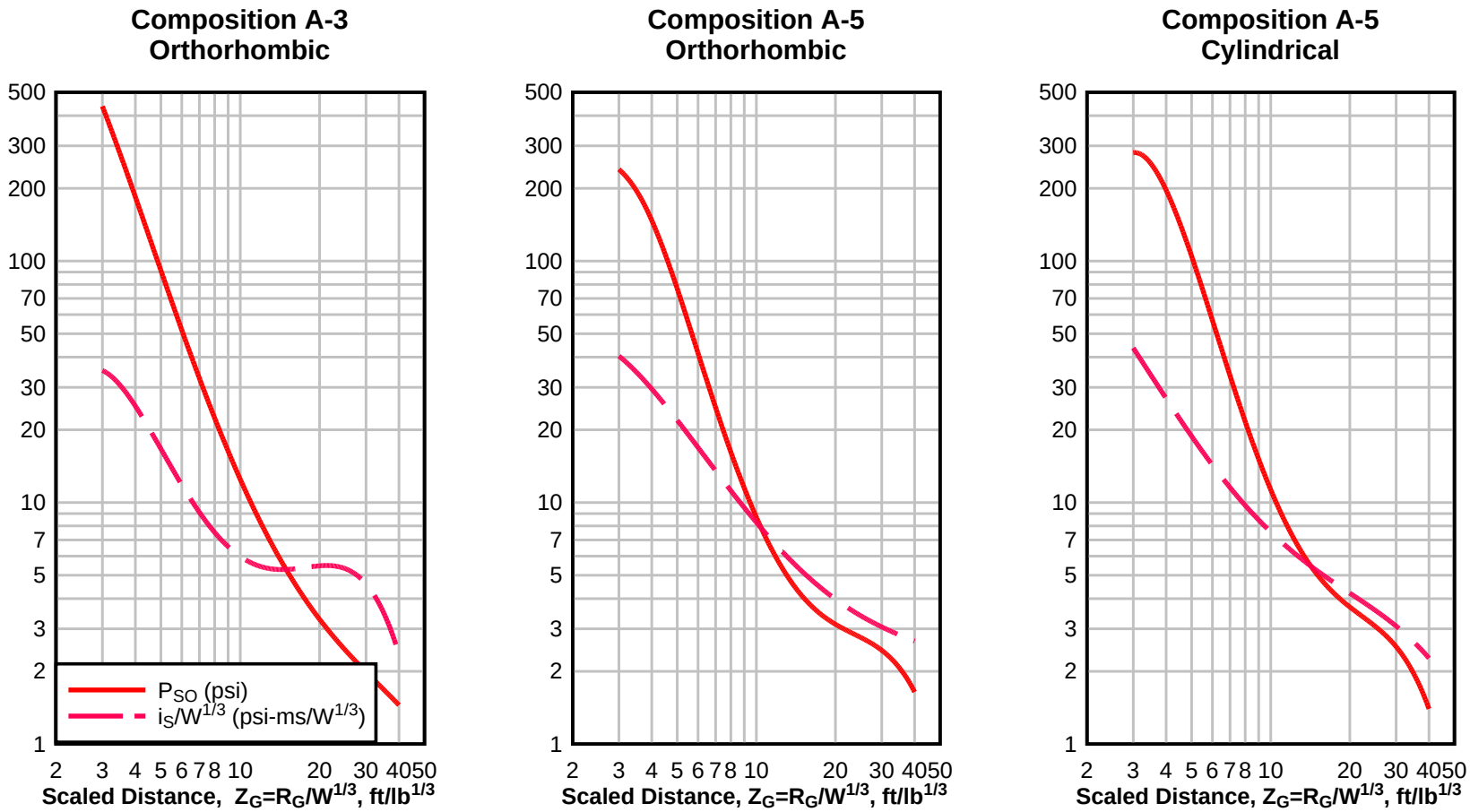

Figure 2-19 Peak Positive Incident Pressure and Scaled Impulse for an Explosion on the Surface at Sea Level, Composition B

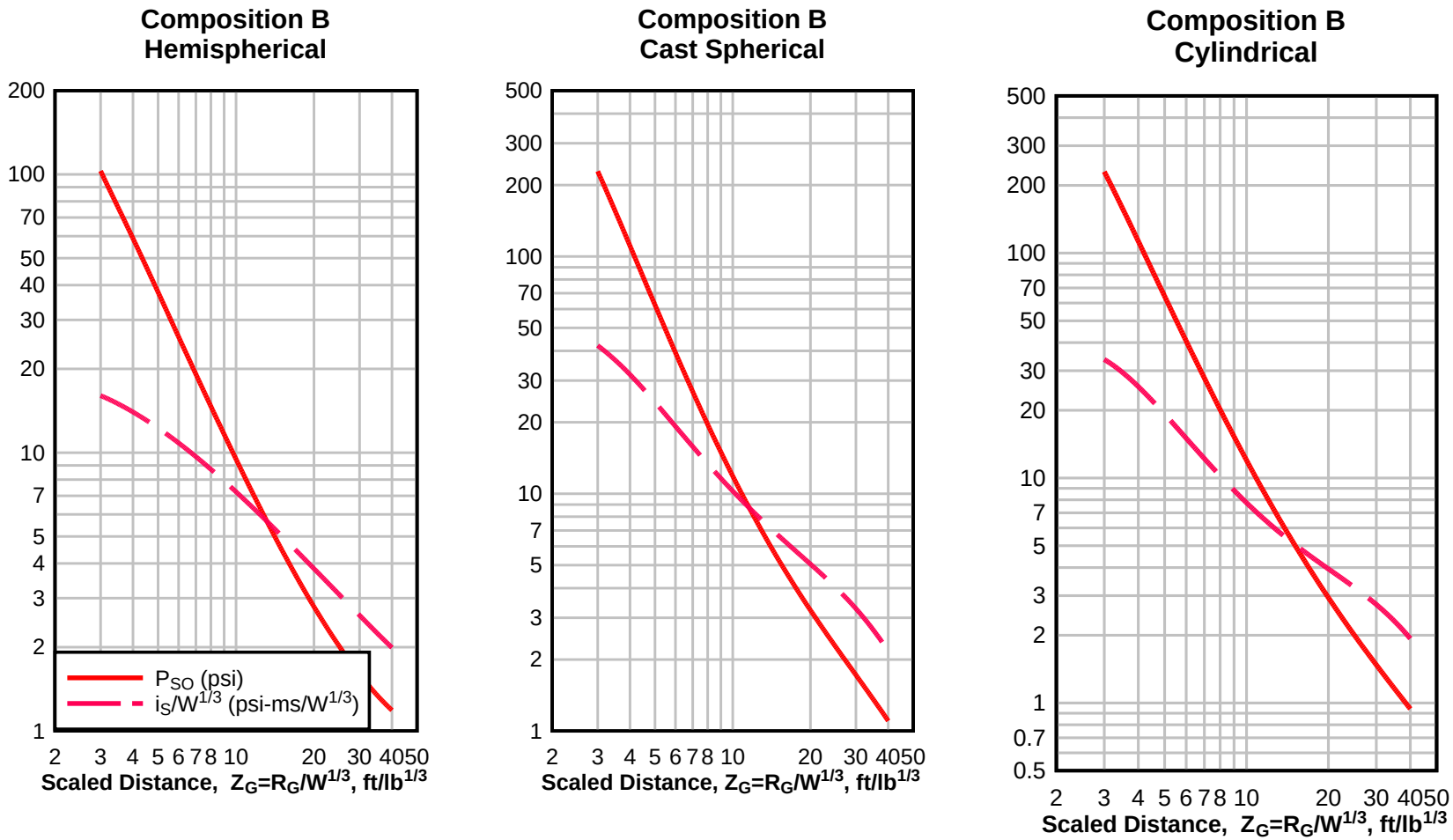

Figure 2-20 Peak Positive Incident Pressure and Scaled Impulse for an Explosion on the Surface at Sea Level, Composition C-4 and Guanidine Nitrate

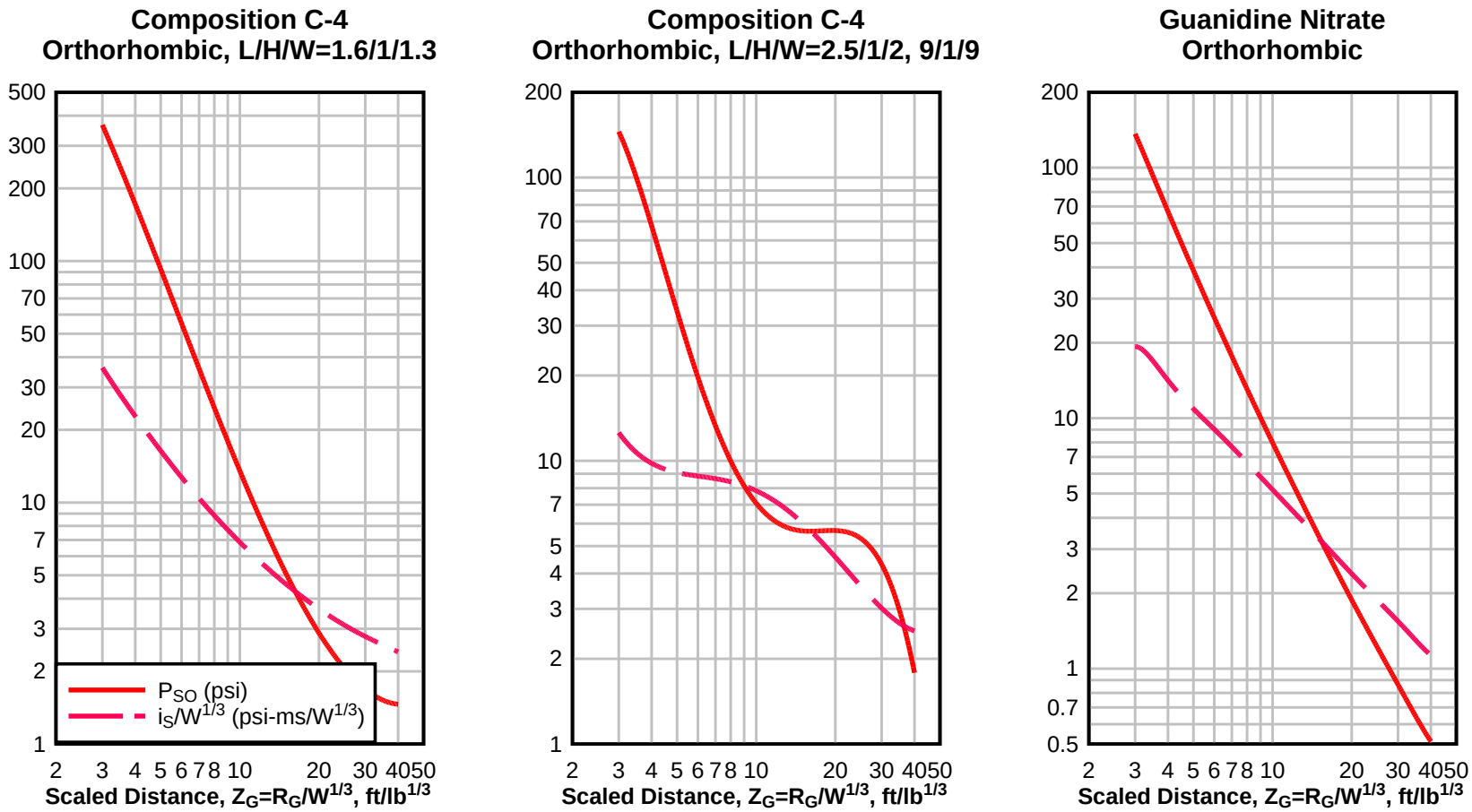

Figure 2-21 Peak Positive Incident Pressure and Scaled Impulse for an Explosion on the Surface at Sea Level, Cyclotol 70/30 and 64 M42 Grenades

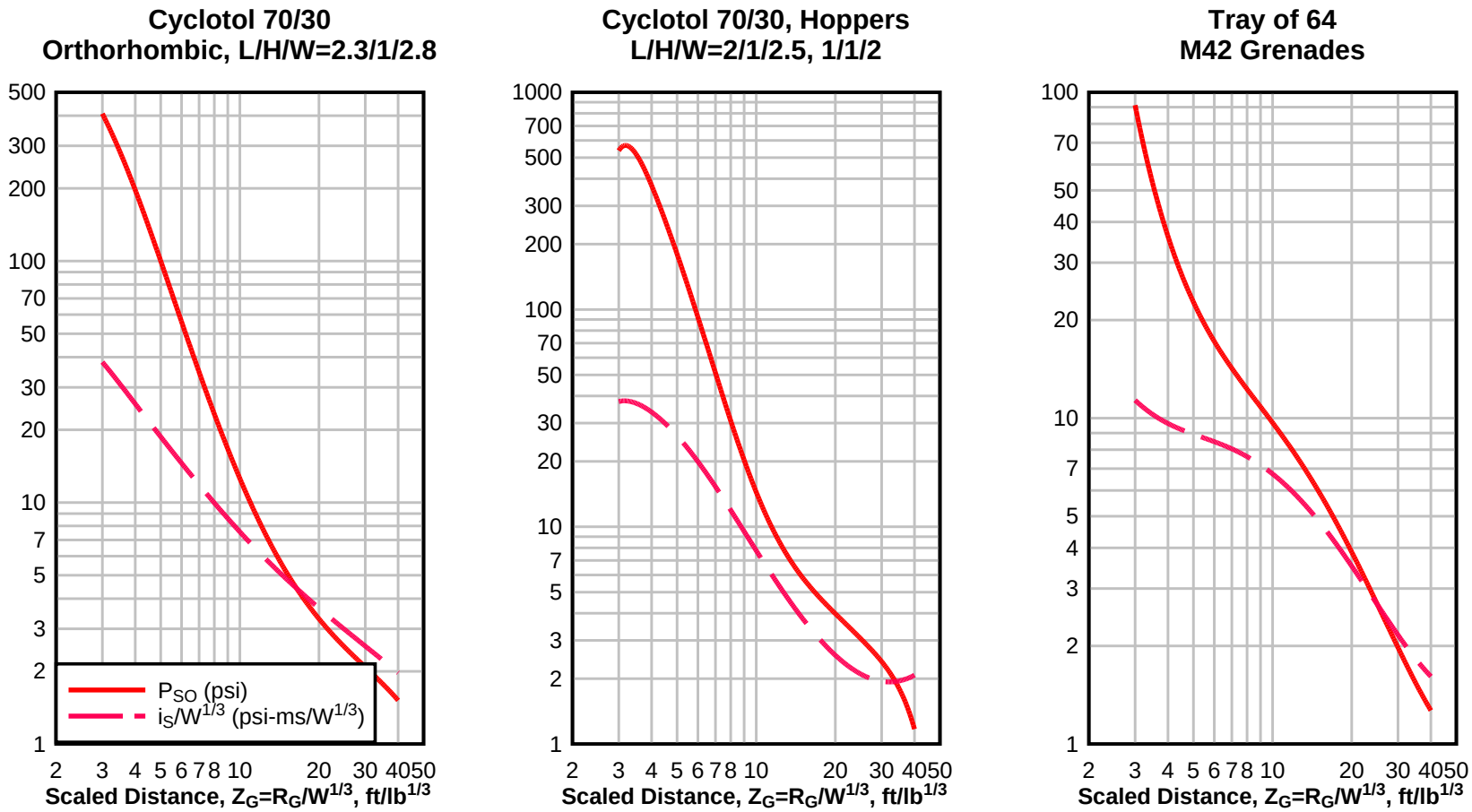

Figure 2-22 Peak Positive Incident Pressure and Scaled Impulse for an Explosion on the Surface at Sea Level, HMX and M483 155mm ICM Projectile

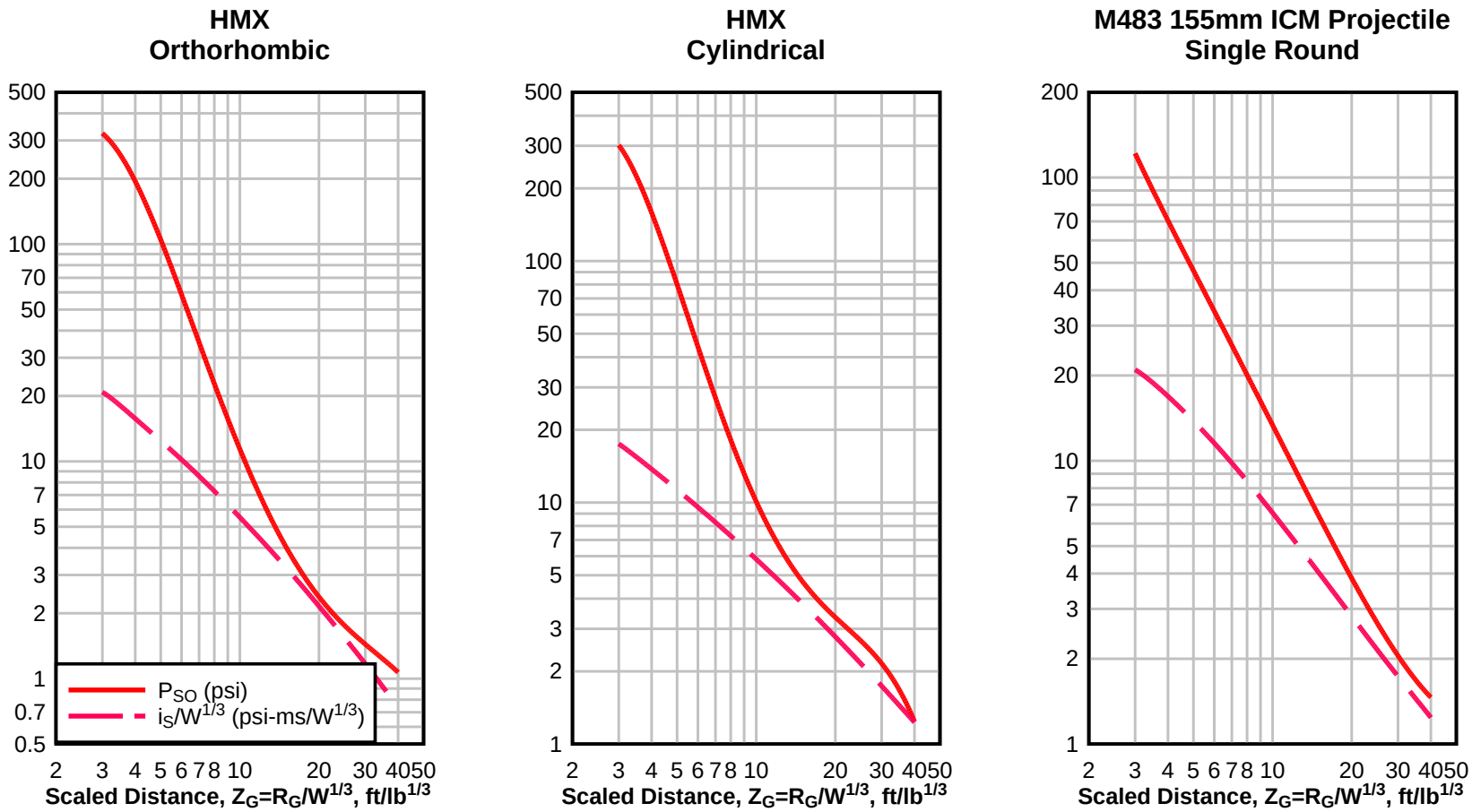

Figure 2-23 Peak Positive Incident Pressure and Scaled Impulse for an Explosion on the Surface at Sea Level, Lead Azide (dextrinated) and Lead Styphnate

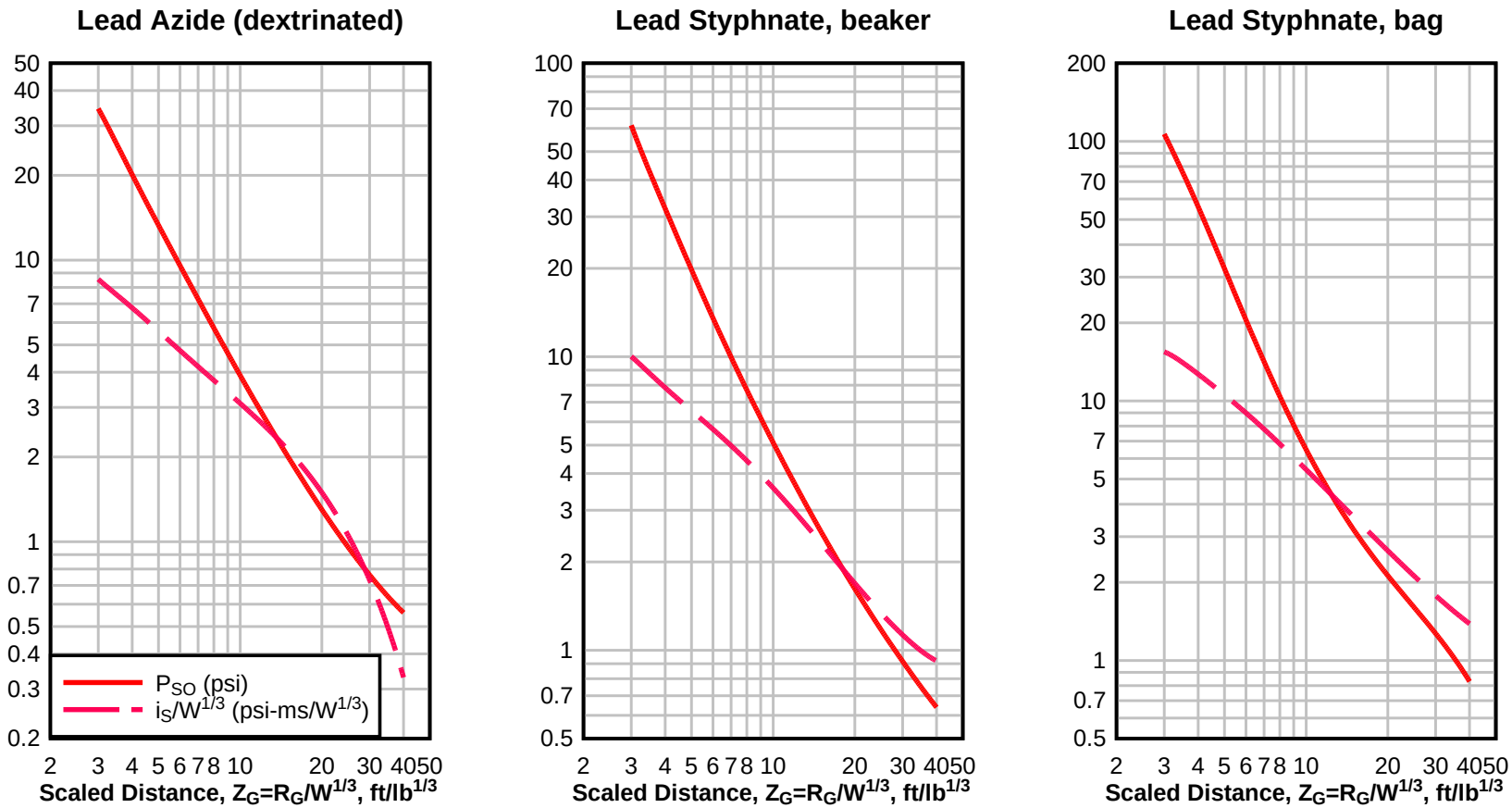

Figure 2-24 Peak Positive Incident Pressure and Scaled Impulse for an Explosion on the Surface at Sea Level, LX-14

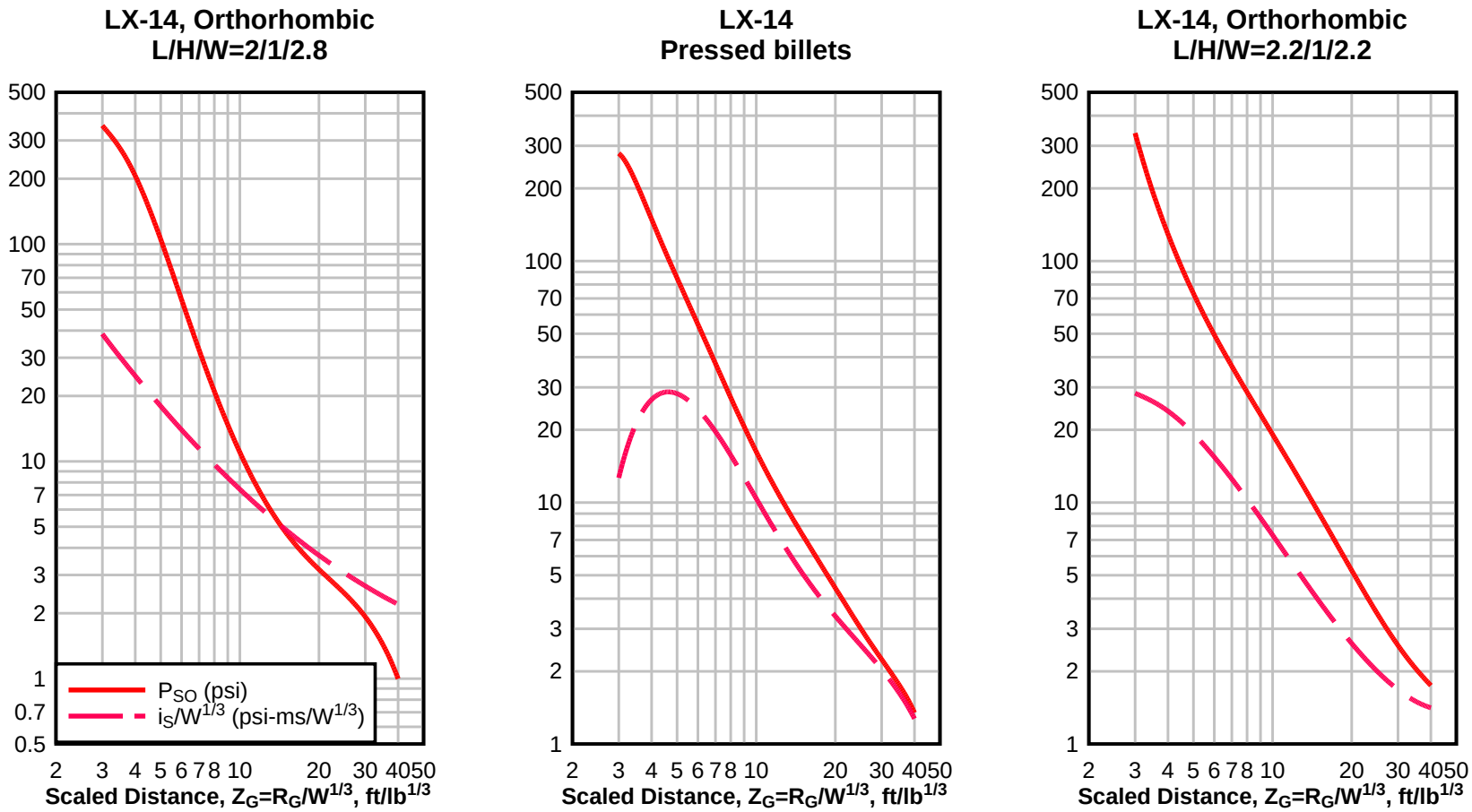

Figure 2-25 Peak Positive Incident Pressure and Scaled Impulse for an Explosion on the Surface at Sea Level, Octol 75/25 and M718/741 RAAM

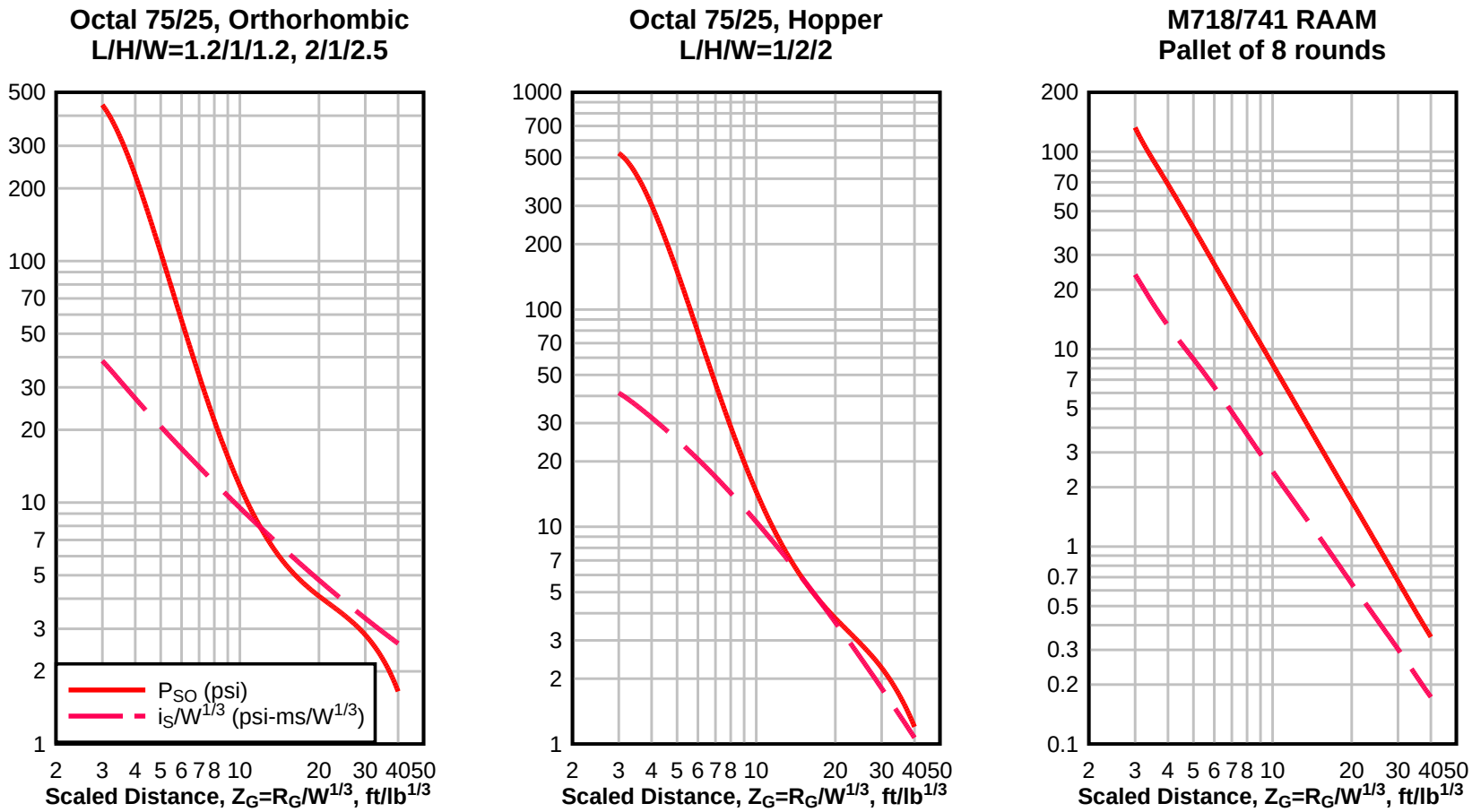

Figure 2-26 Peak Positive Incident Pressure and Scaled Impulse for an Explosion on the Surface at Sea Level, Nitrocellulose

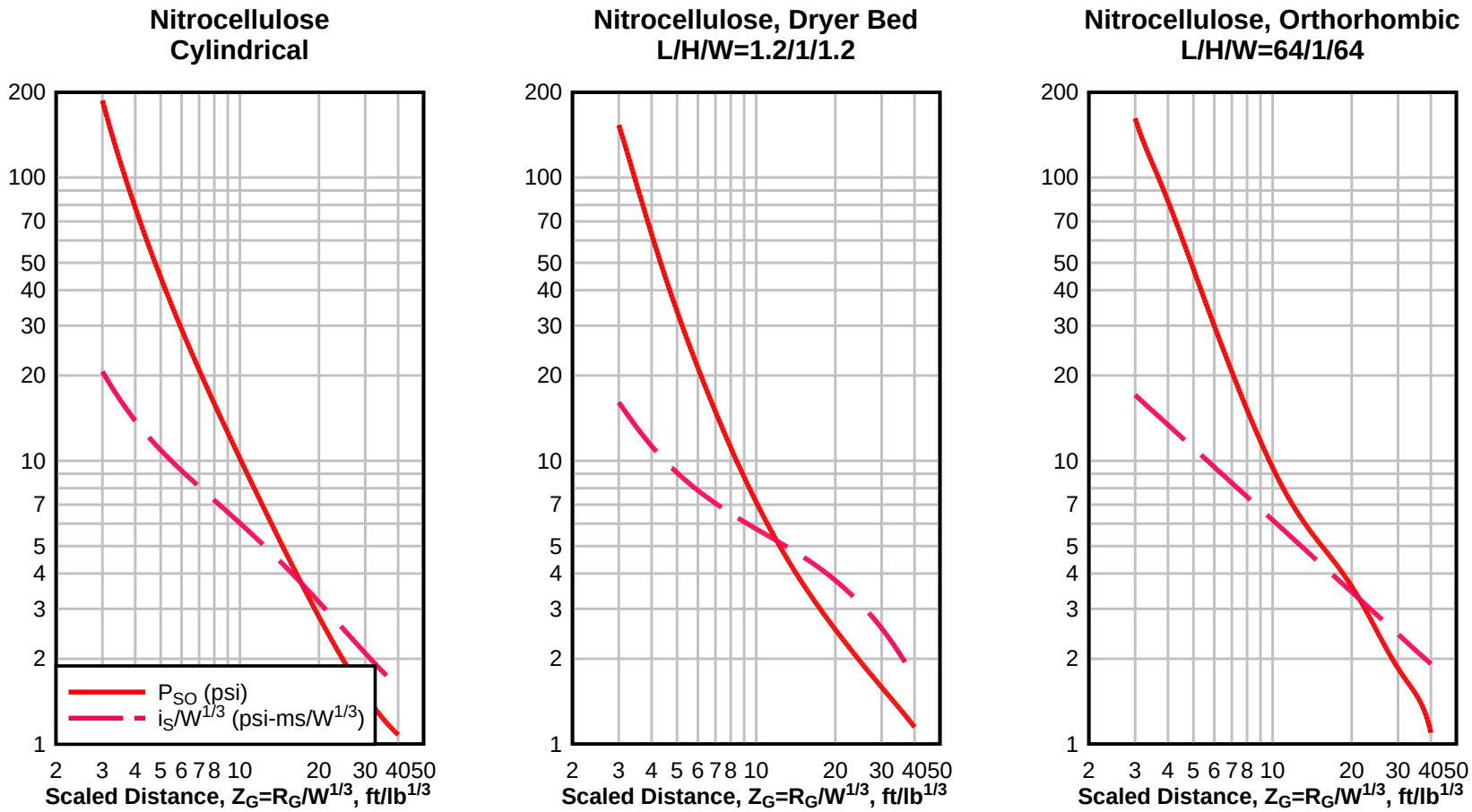

Figure 2-27 Peak Positive Incident Pressure and Scaled Impulse for an Explosion on the Surface at Sea Level, Nitroglycerine and PBXC-203

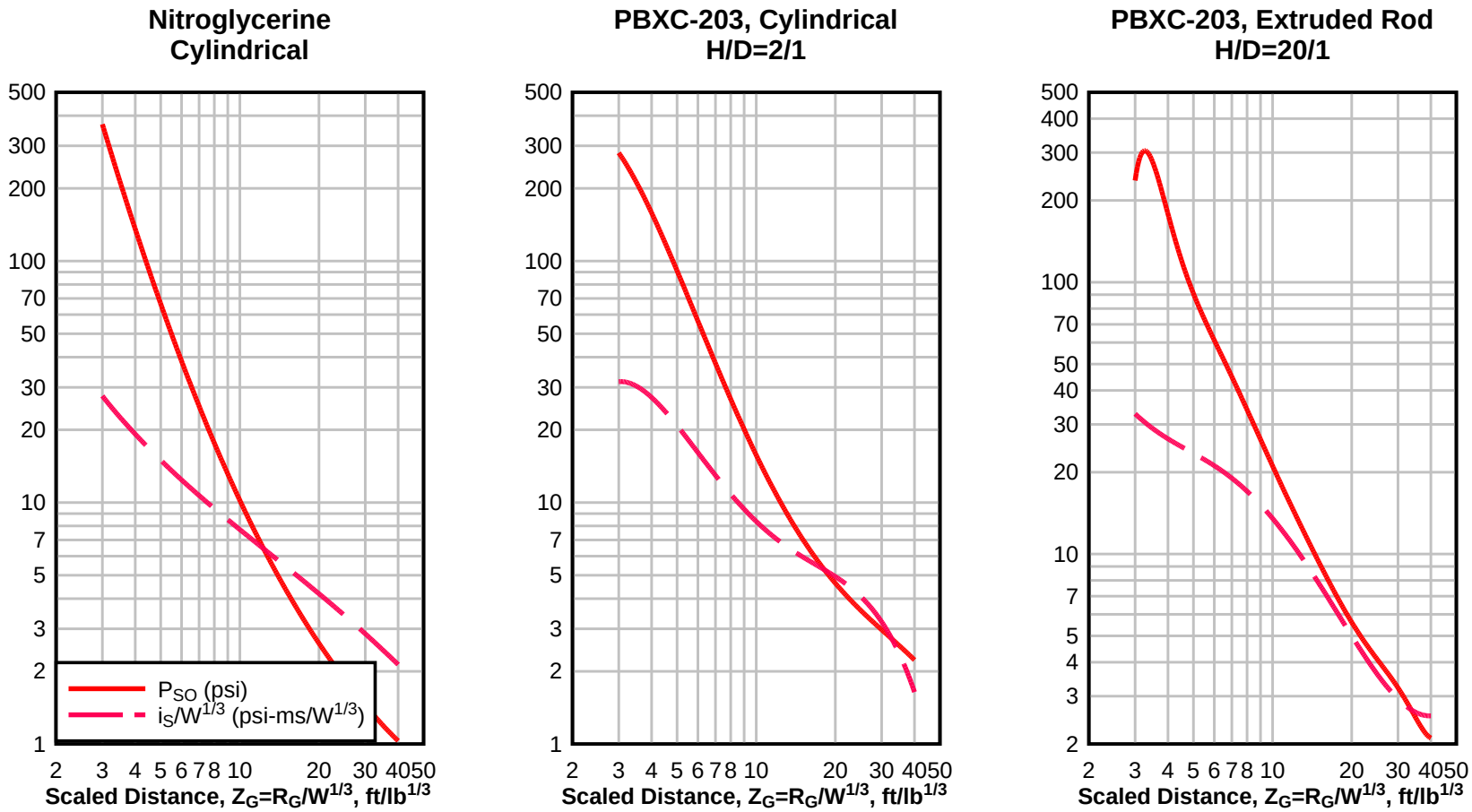

Figure 2-28 Peak Positive Incident Pressure and Scaled Impulse for an Explosion on the Surface at Sea Level, RDX Slurry and RDX 98/2

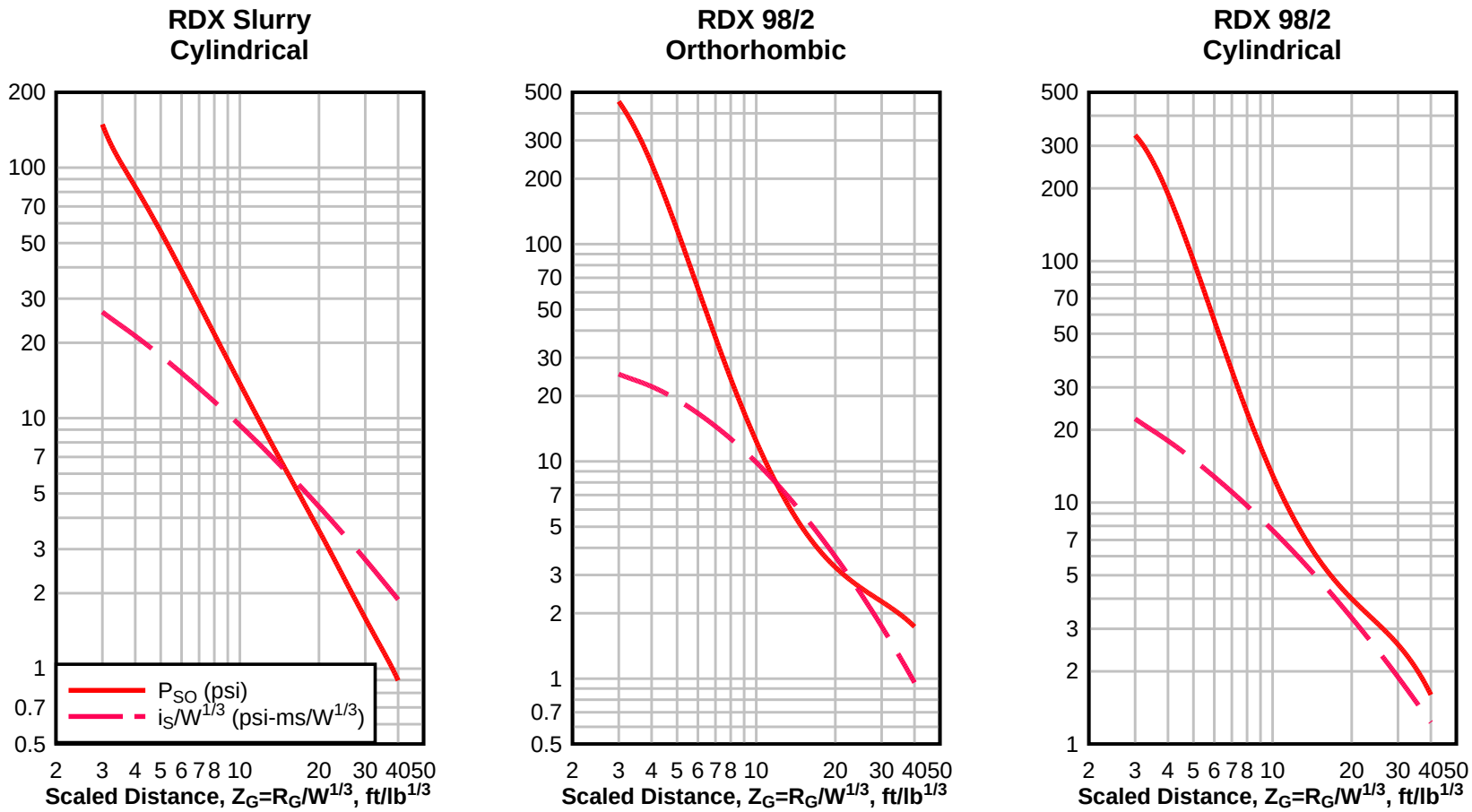

Figure 2-29 Peak Positive Incident Pressure and Scaled Impulse for an Explosion on the Surface at Sea Level, TNT

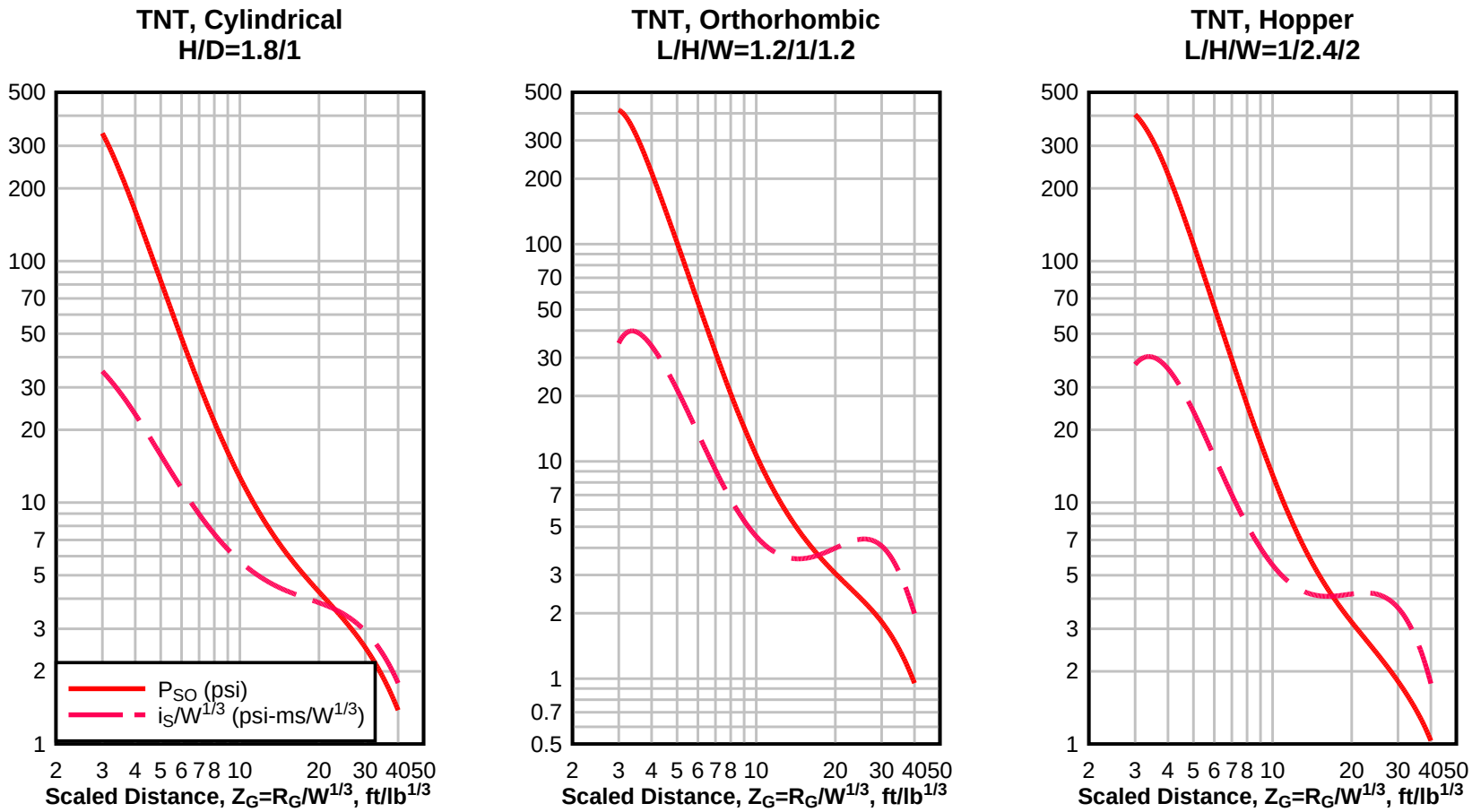

Figure 2-30 Peak Positive Incident Pressure and Scaled Impulse for an Explosion on the Surface at Sea Level, Tetracene and Nitroguanidine

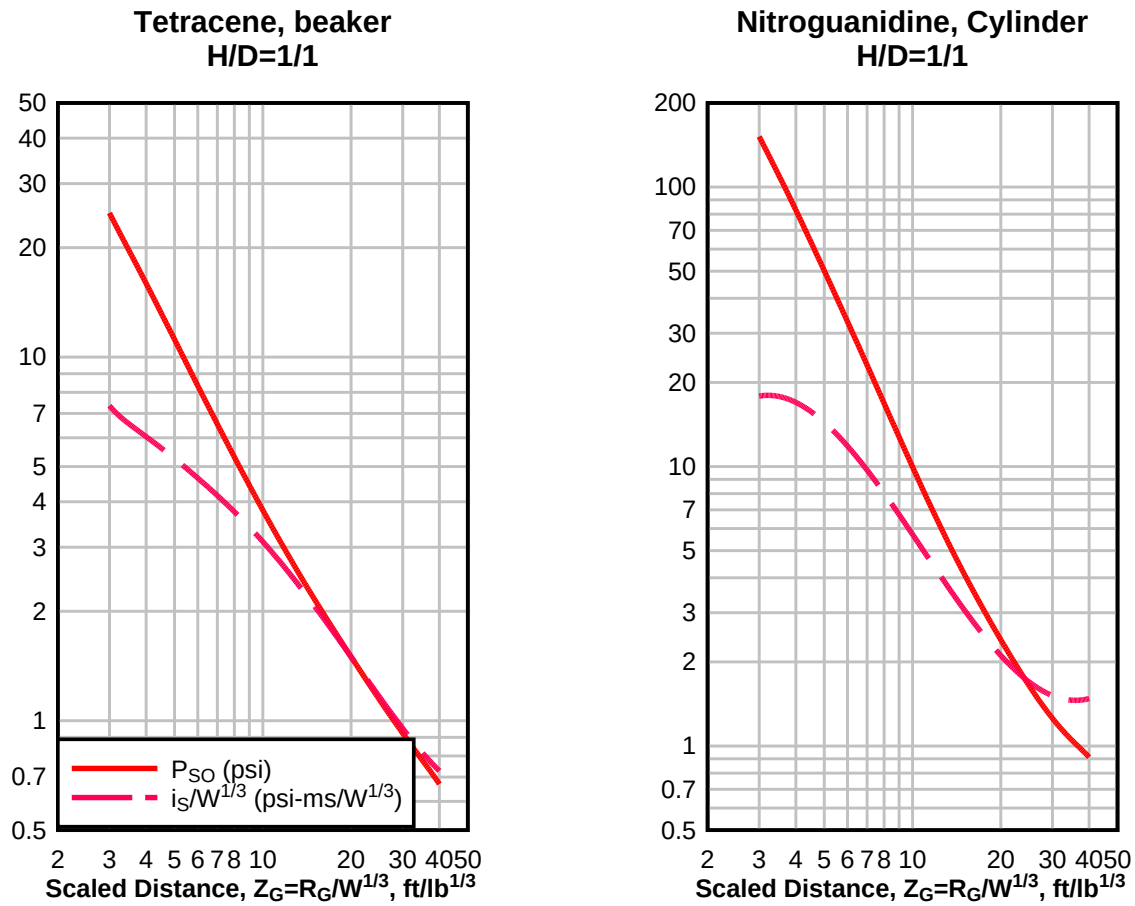

Figure 2-31 Peak Positive Incident Pressure and Scaled Impulse for an Explosion on the Surface at Sea Level, Benite Propellant and Black Powder

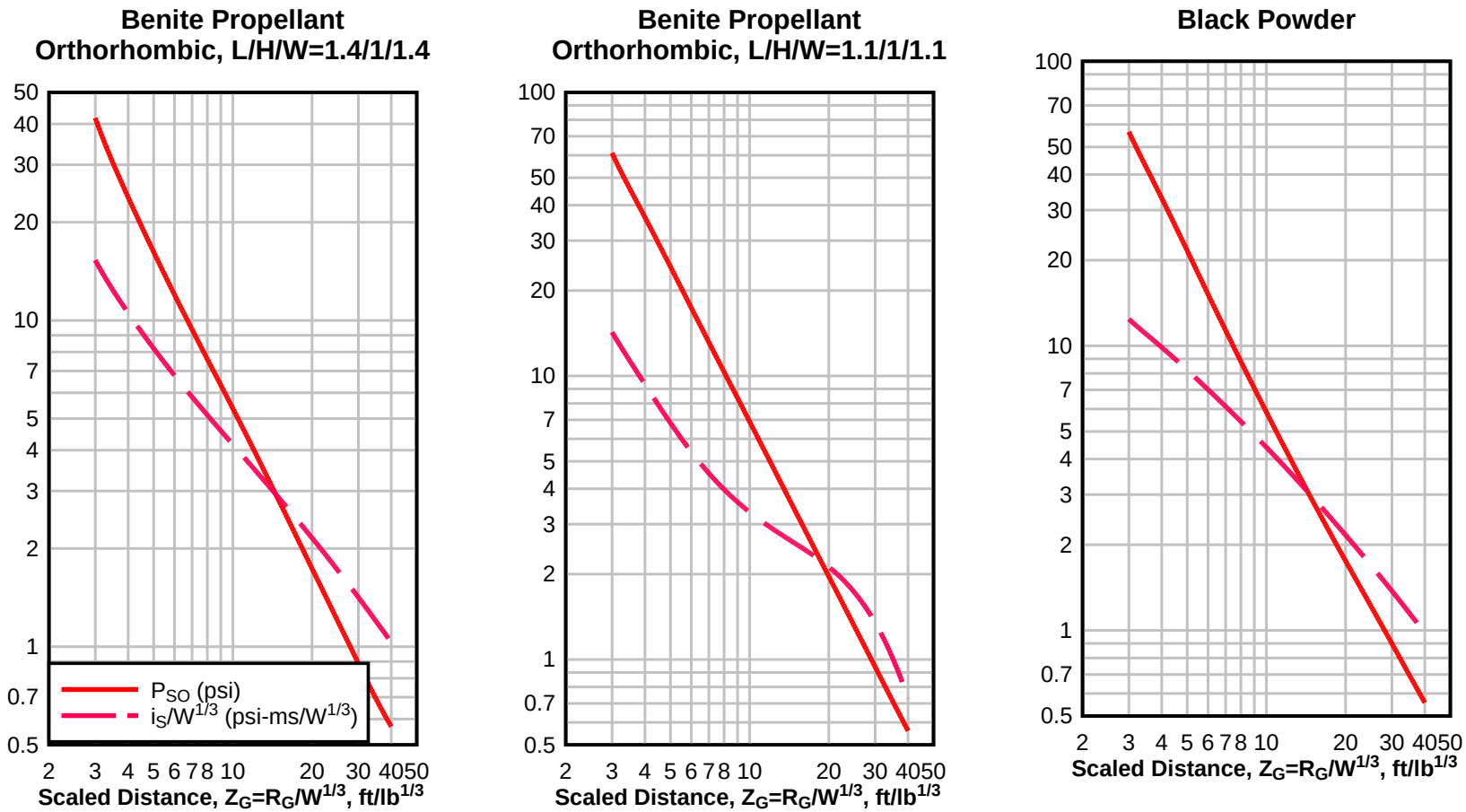

Figure 2-32 Peak Positive Incident Pressure and Scaled Impulse for an Explosion on the Surface at Sea Level, BS-NACO Propellant

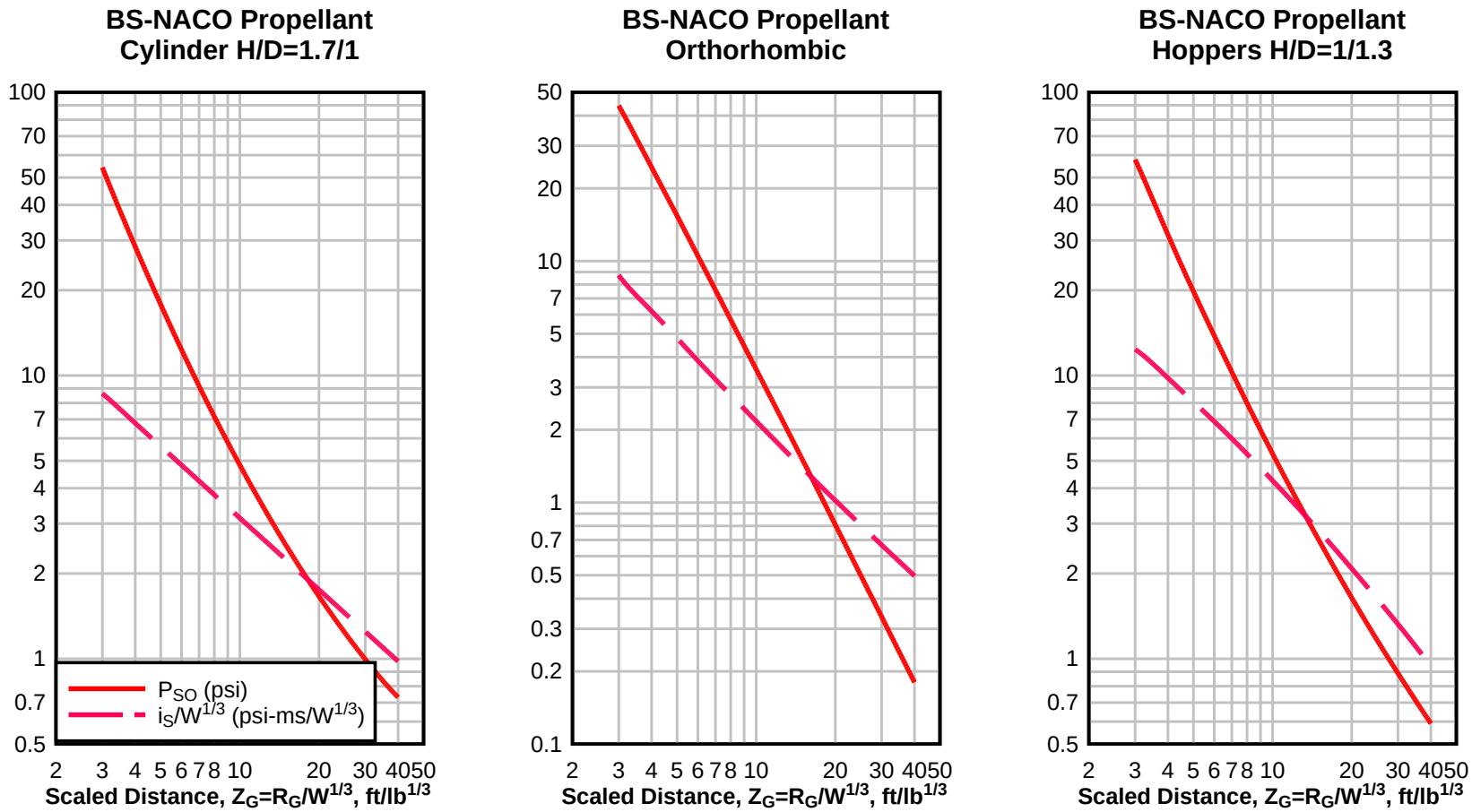

Figure 2-33 Peak Positive Incident Pressure and Scaled Impulse for an Explosion on the Surface at Sea Level, DIGL-RP I5420, I5421, and I5422 Propellants

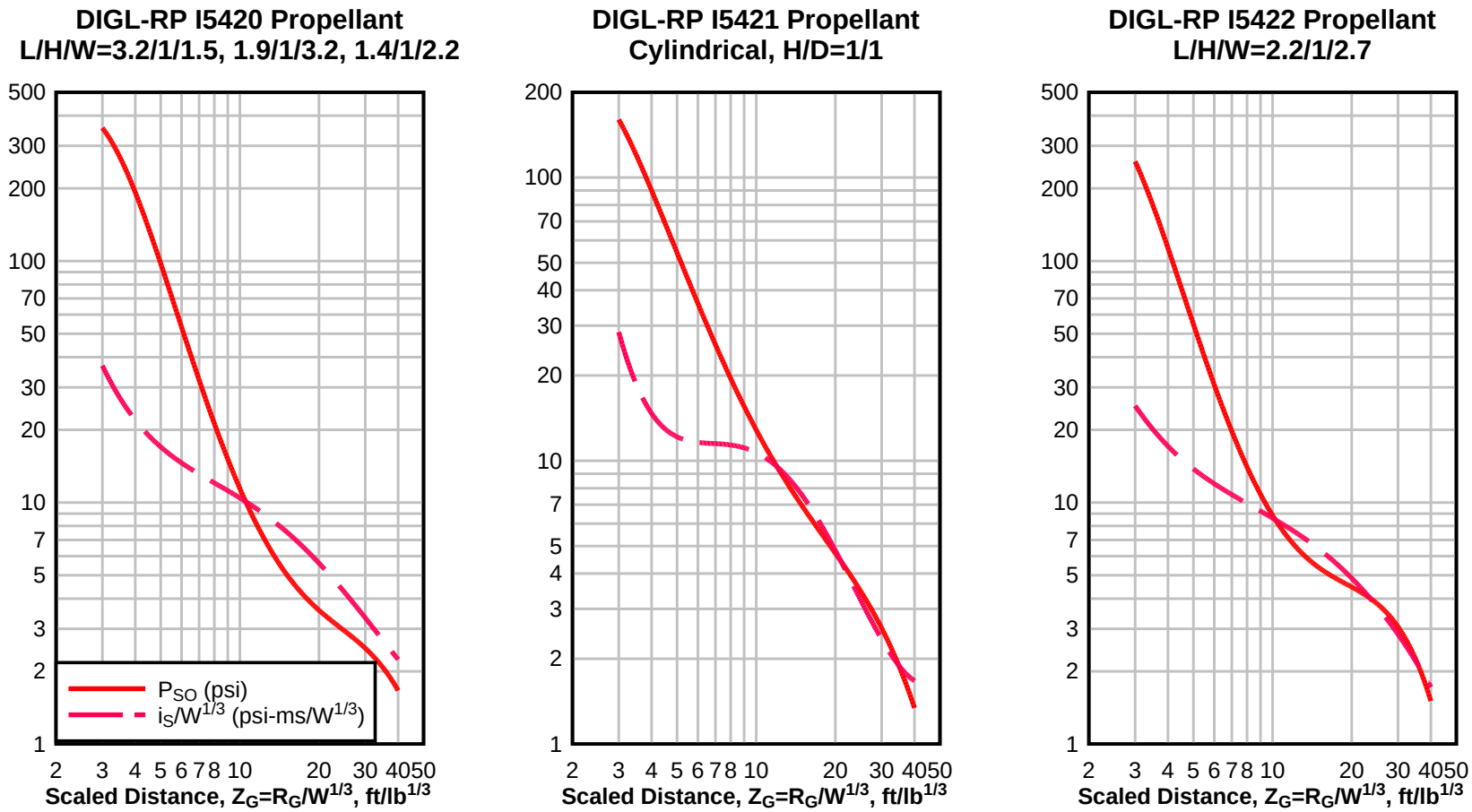

Figure 2-34 Peak Positive Incident Pressure and Scaled Impulse for an Explosion on the Surface at Sea Level, MI and M26 EI Propellants

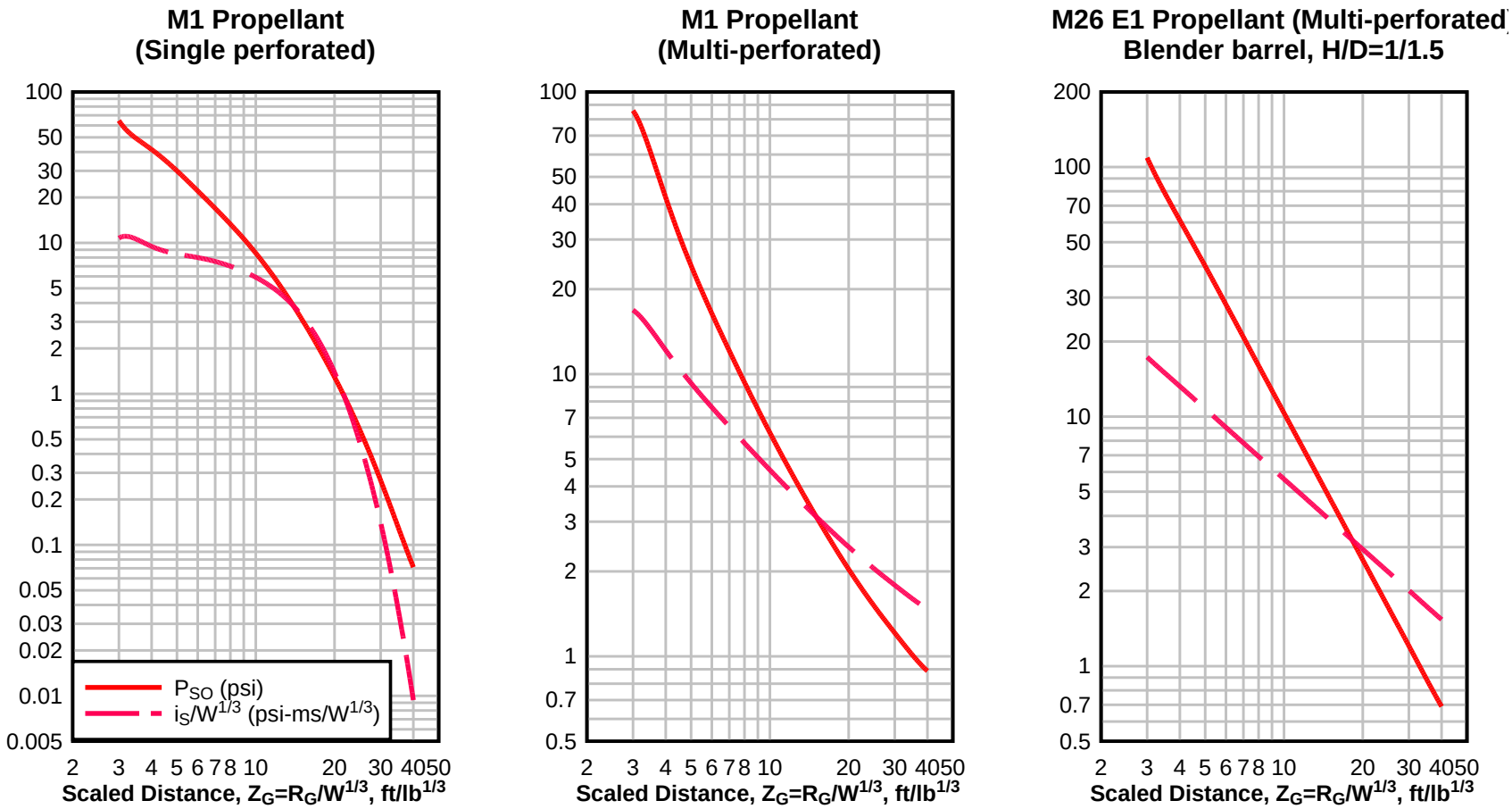

Figure 2-35 Peak Positive Incident Pressure and Scaled Impulse for an Explosion on the Surface at Sea Level, M26 EI Propellant

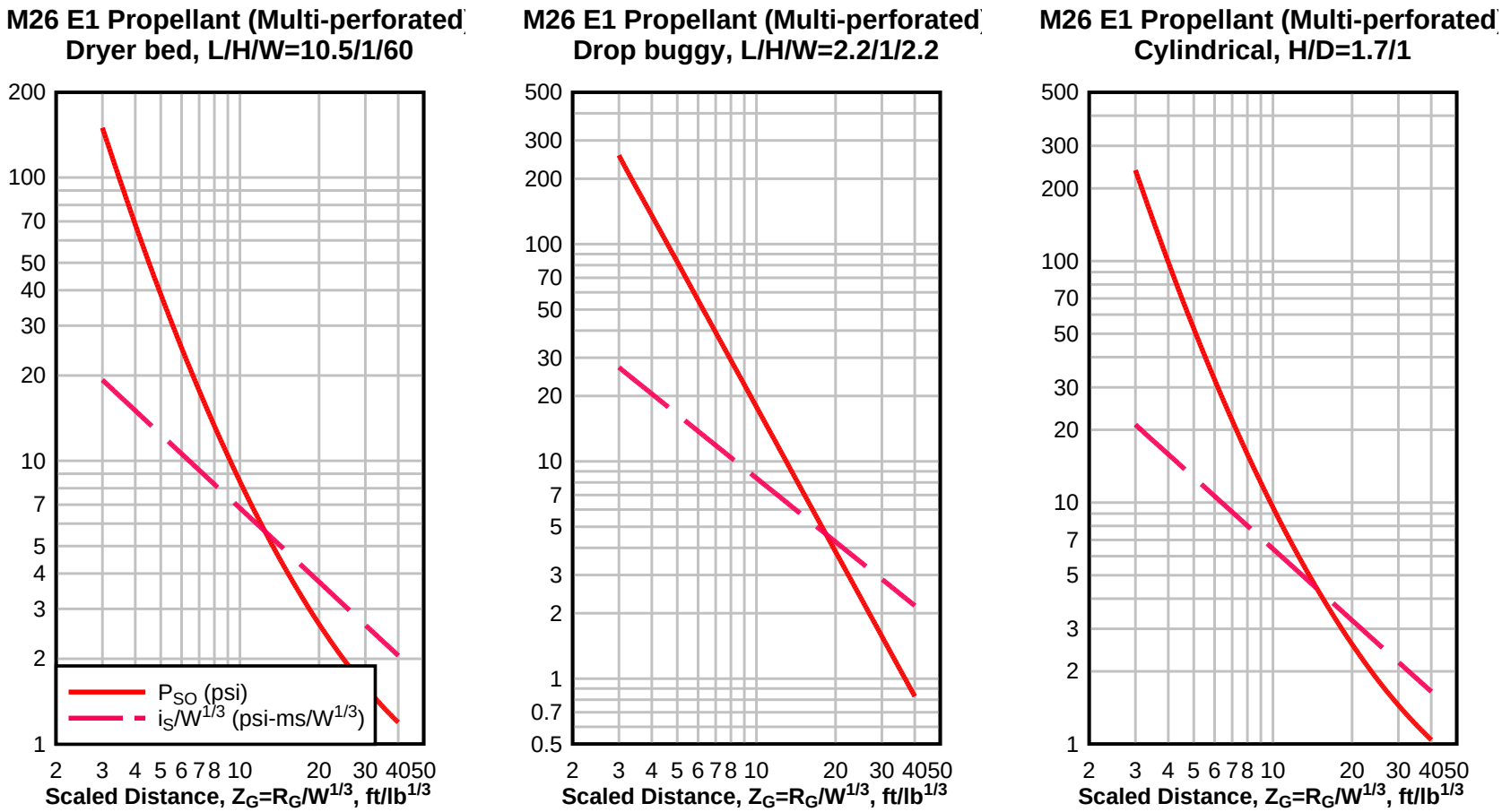

Figure 2-36 Peak Positive Incident Pressure and Scaled Impulse for an Explosion on the Surface at Sea Level, M30 AI Propellant

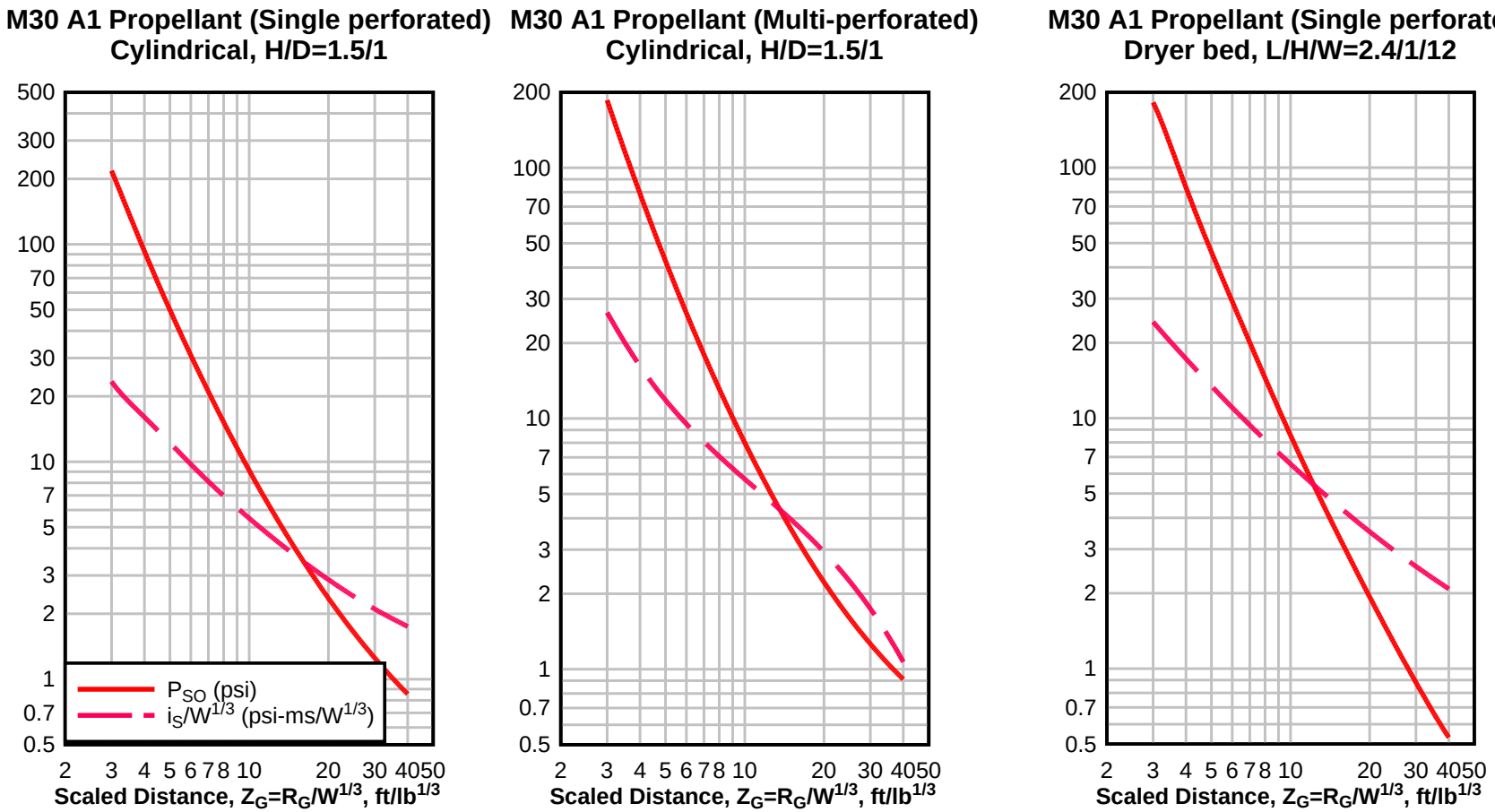

Figure 2-37 Peak Positive Incident Pressure and Scaled Impulse for an Explosion on the Surface at Sea Level, M30 Al Propellant and M31 Al El Slotted Stick Propellant

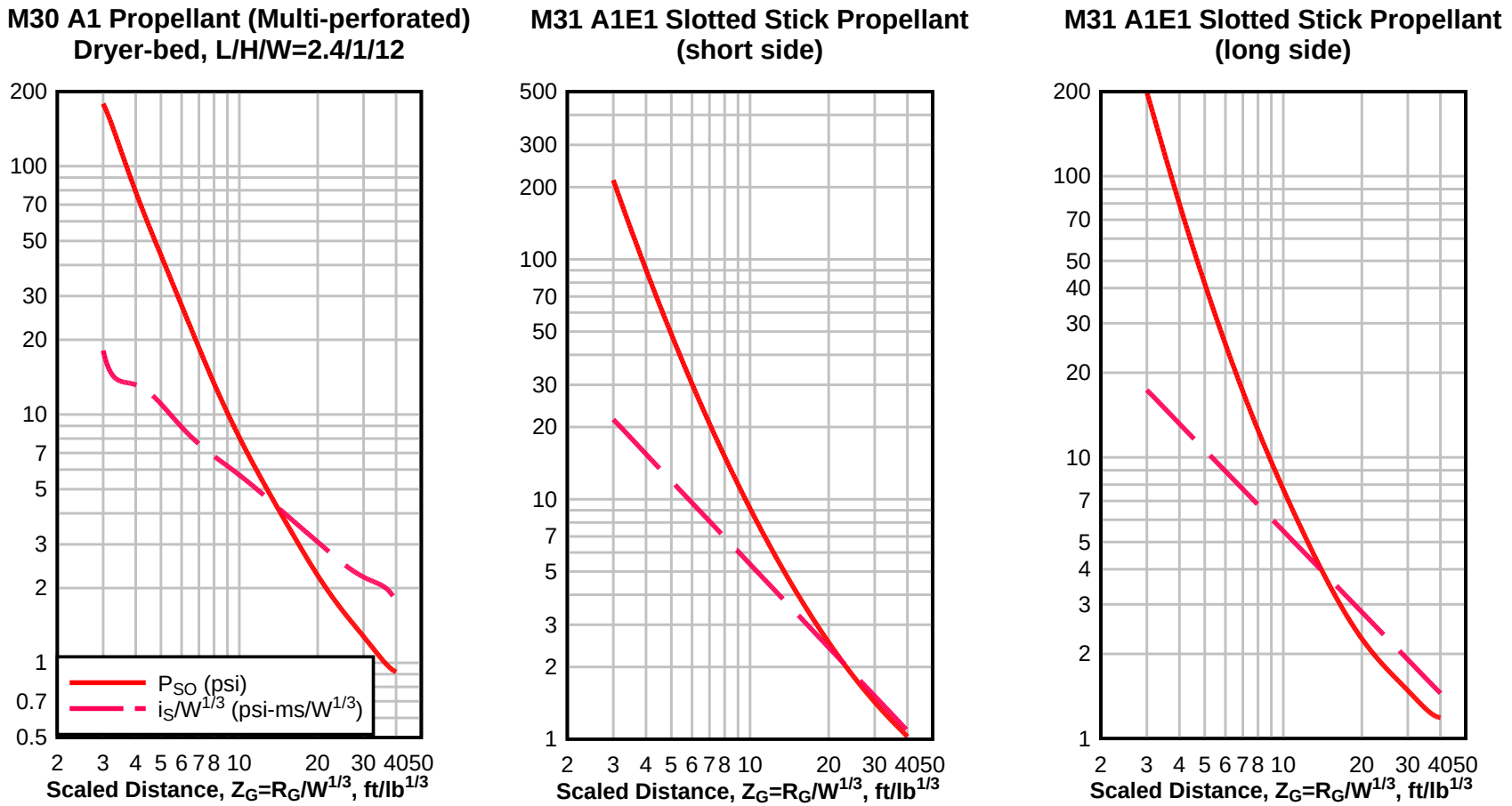

Figure 2-38 Peak Positive Incident Pressure and Scaled Impulse for an Explosion on the Surface at Sea Level, M31AIEI Slotted Stick Propellant and N5 Propellant

M3IAIEI Slotted Stick Propellant Orthorhombic (Short Side)

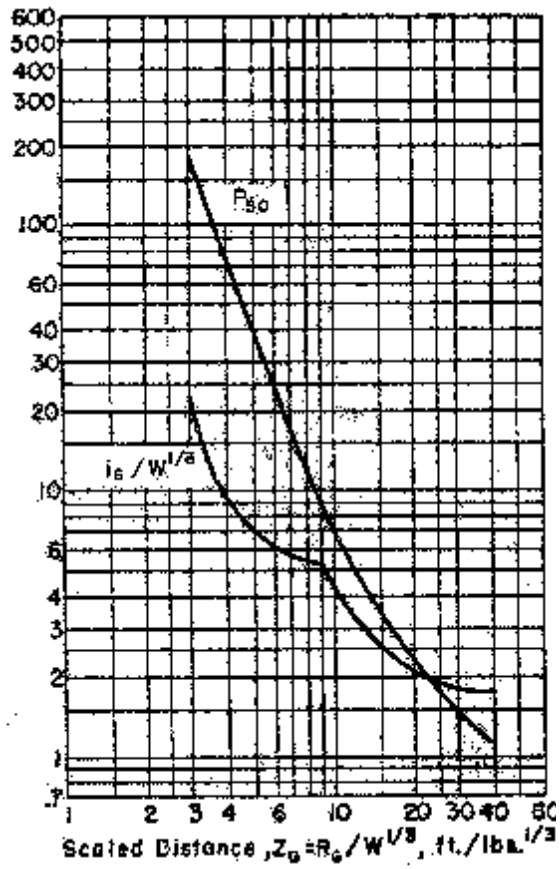

M3IAIEI Slotted Stick Propellant Orthorhombic (Long Side)

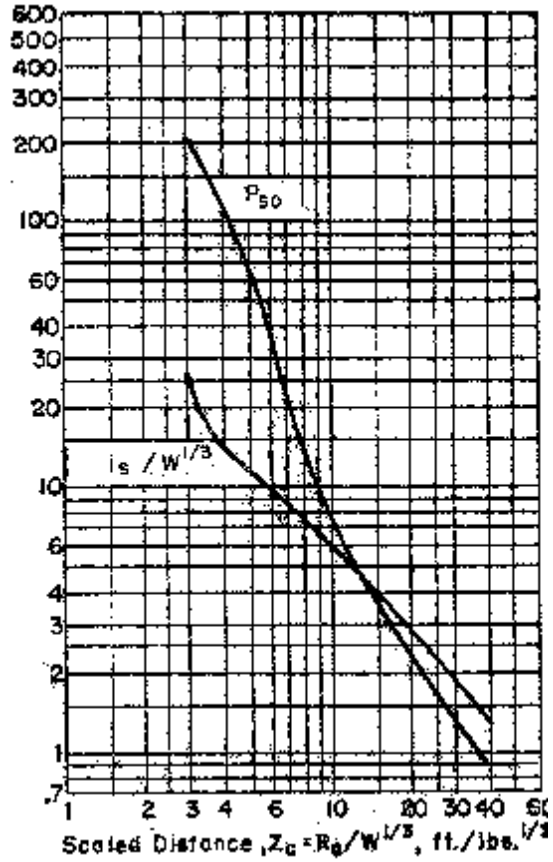

N5 Propellant, Shipping containers H/D=1.5/1

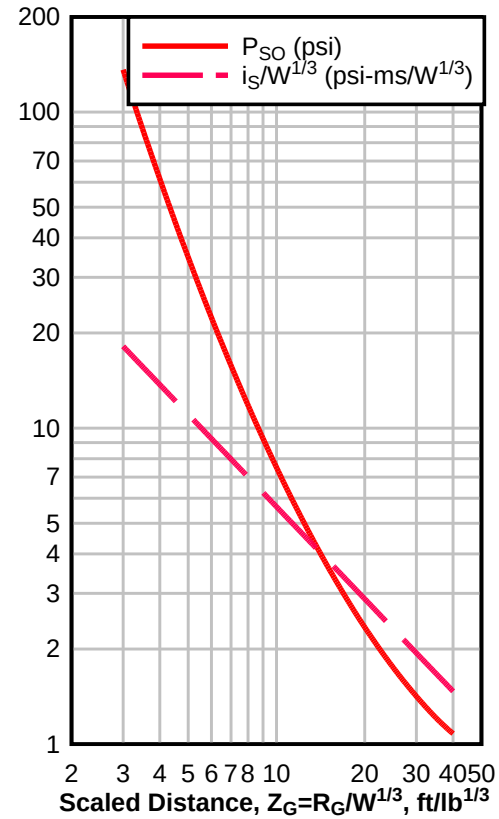

Figure 2-39 Peak Positive Incident Pressure and Scaled Impulse for an Explosion on the Surface at Sea Level, N5 Propellant

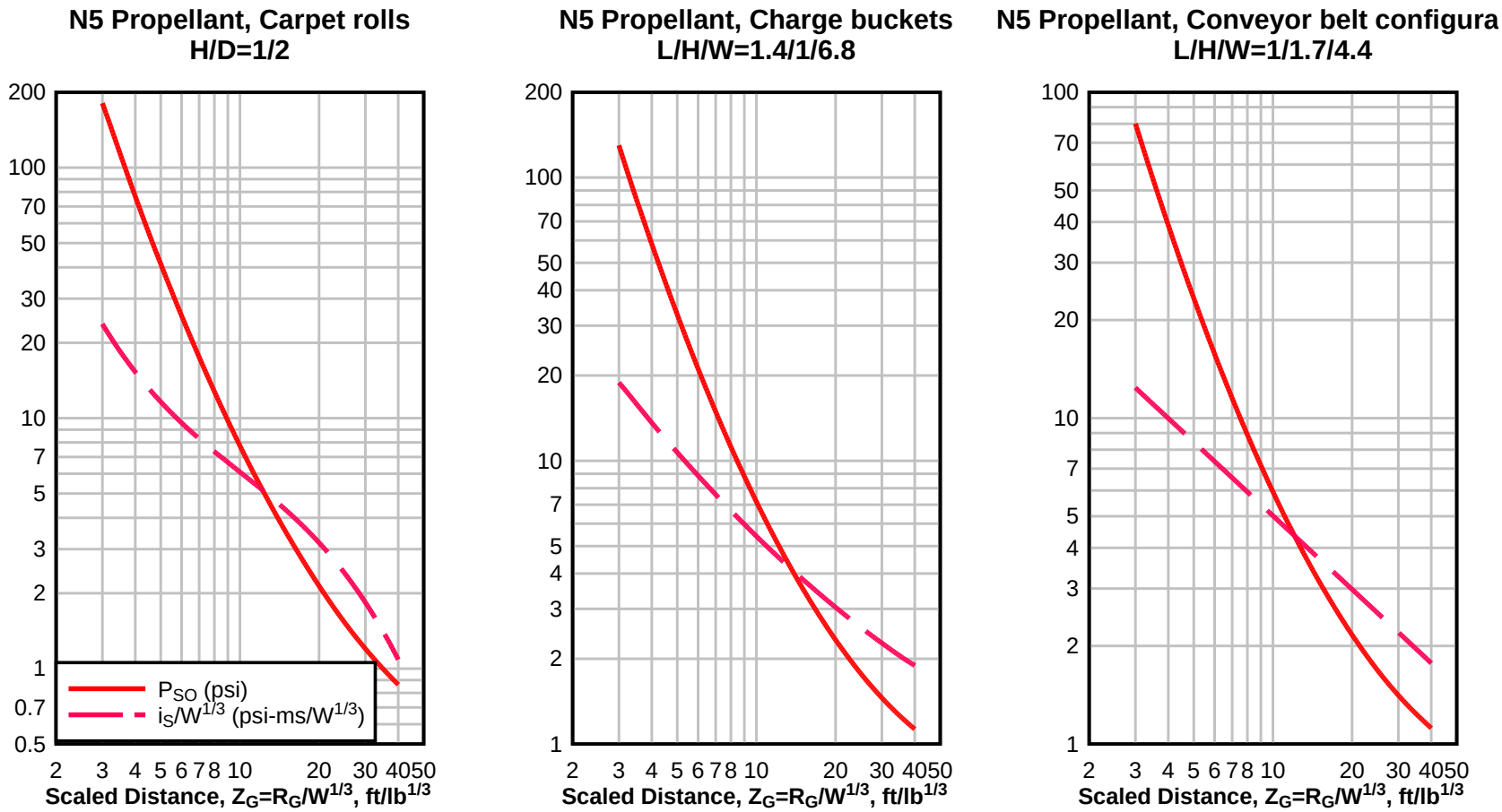

Figure 2-40 Peak Positive Incident Pressure and Scaled Impulse for an Explosion on the Surface at Sea Level, M6 Propellant

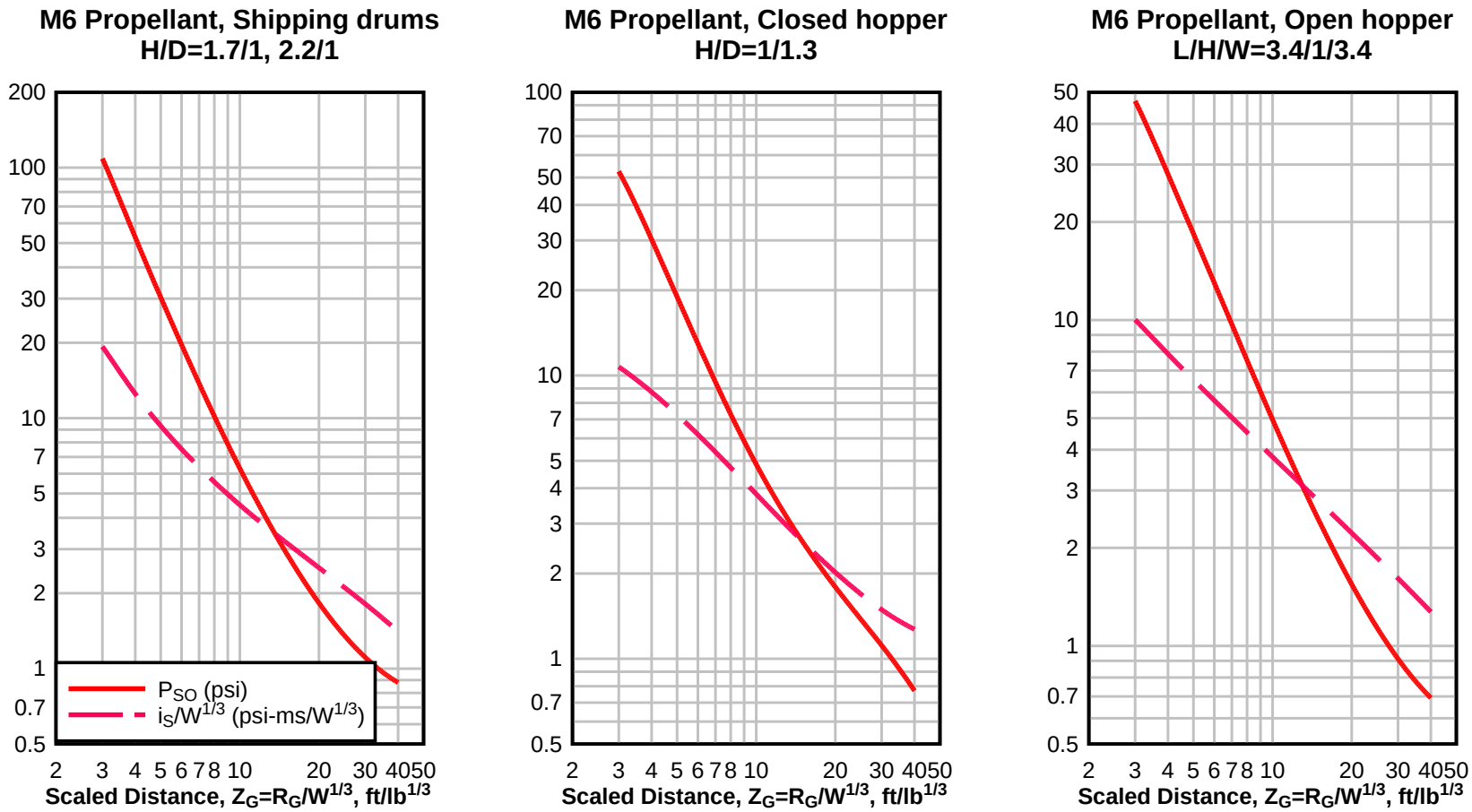

Figure 2-41 Peak Positive Incident Pressure and Scaled Impulse for an Explosion on the Surface at Sea Level, 2.75in Rocket Grain and WC844 Ball Powder

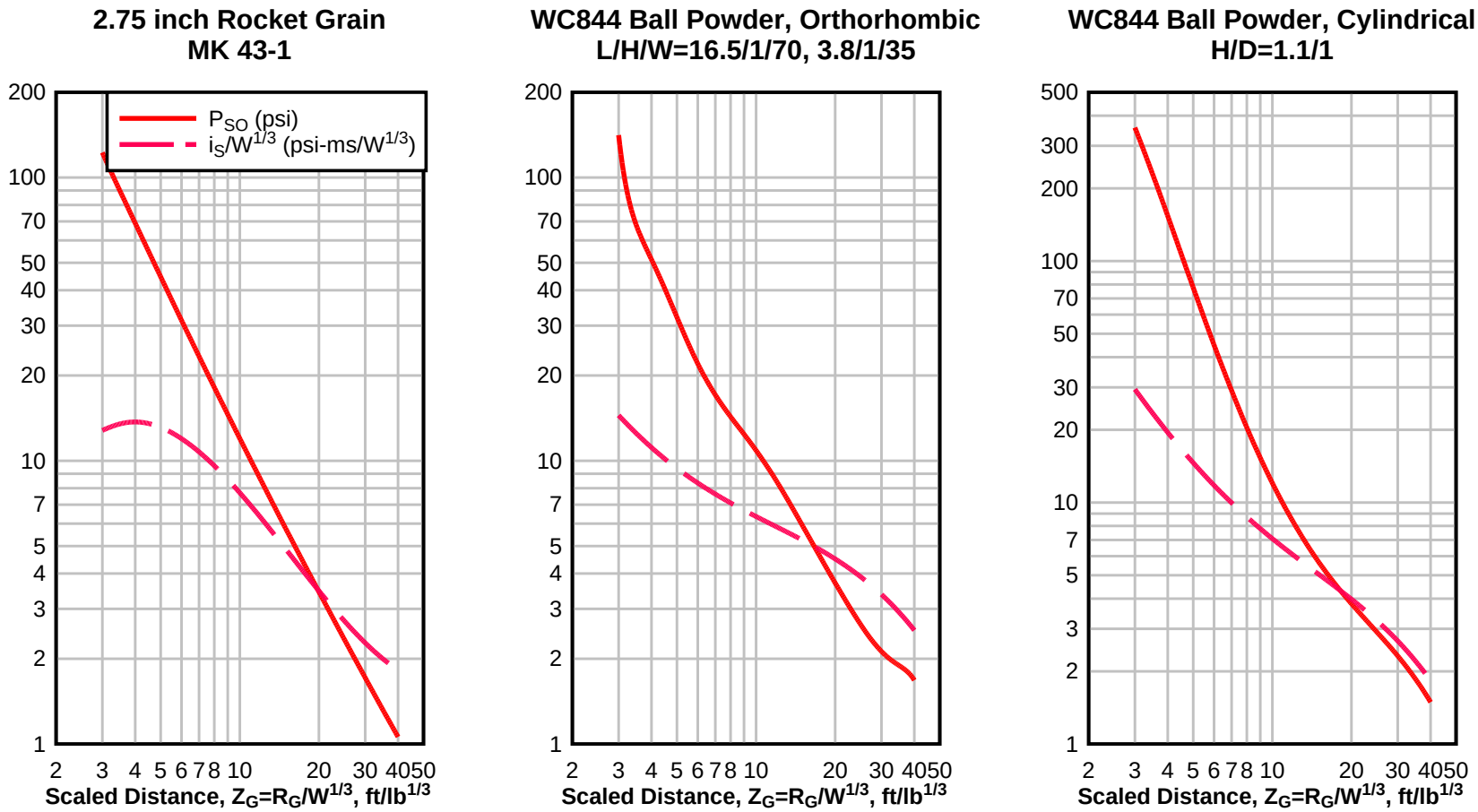

Figure 2-42 Peak Positive Incident Pressure and Scaled Impulse for an Explosion on the Surface at Sea Level, XM37 RAP Propellant

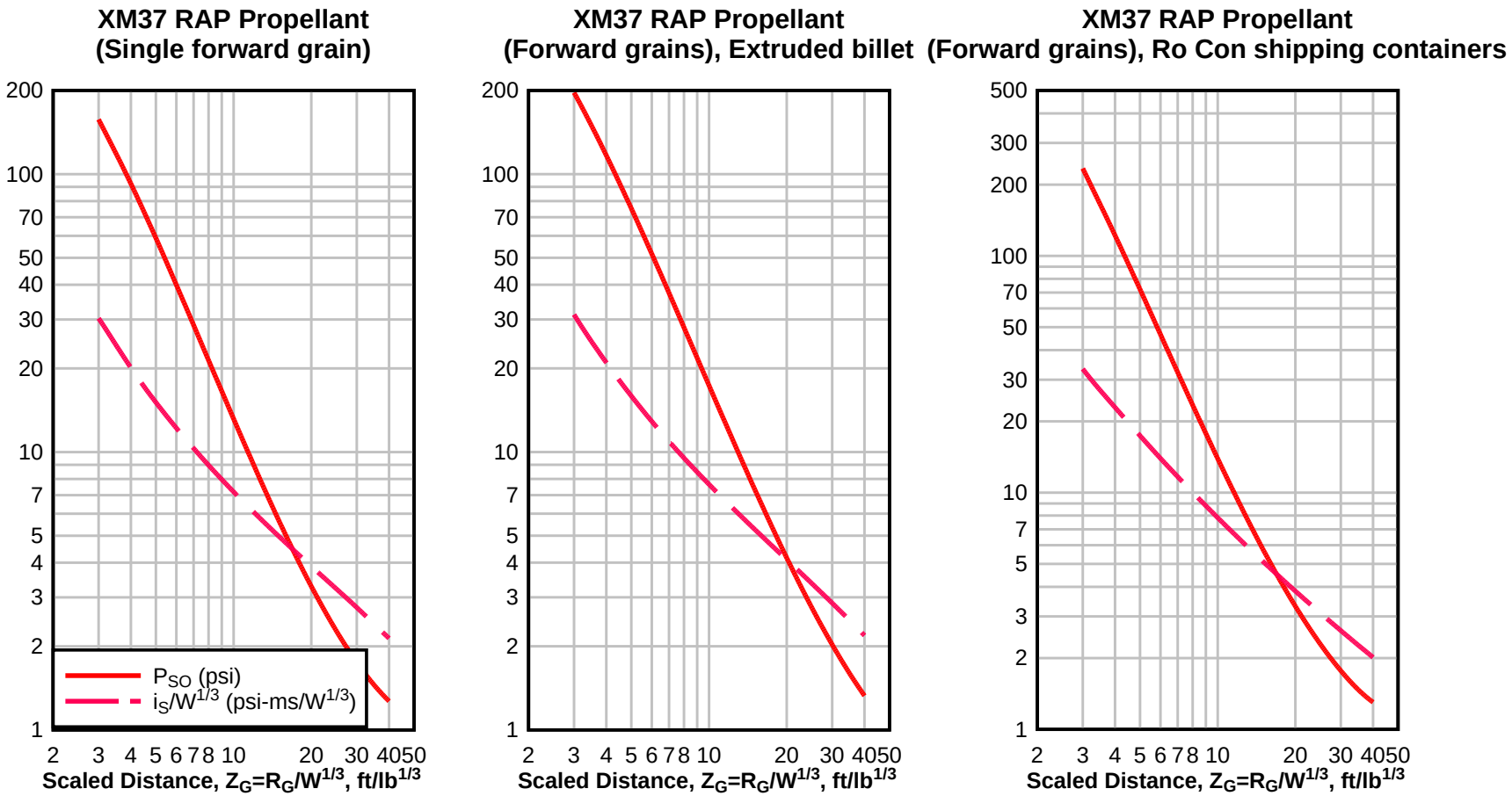

Figure 2-43 Peak Positive Incident Pressure and Scaled Impulse for an Explosion on the Surface at Sea Level, XM37 RAP Propellant, continued

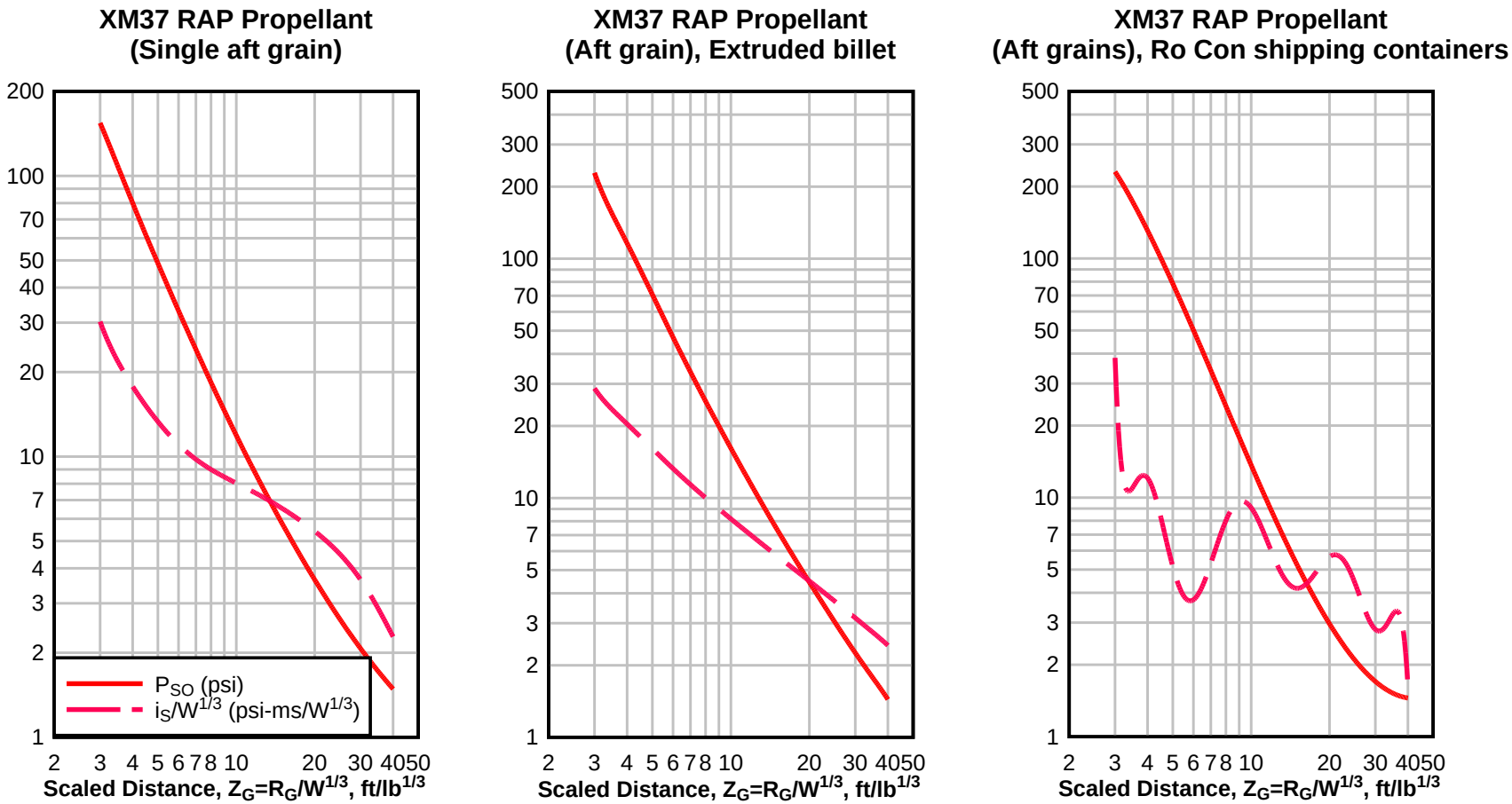

Figure 2-44 Peak Positive Incident Pressure and Scaled Impulse for an Explosion on the Surface at Sea Level, JA-2 (L5460) Propellant and M10 Propellant

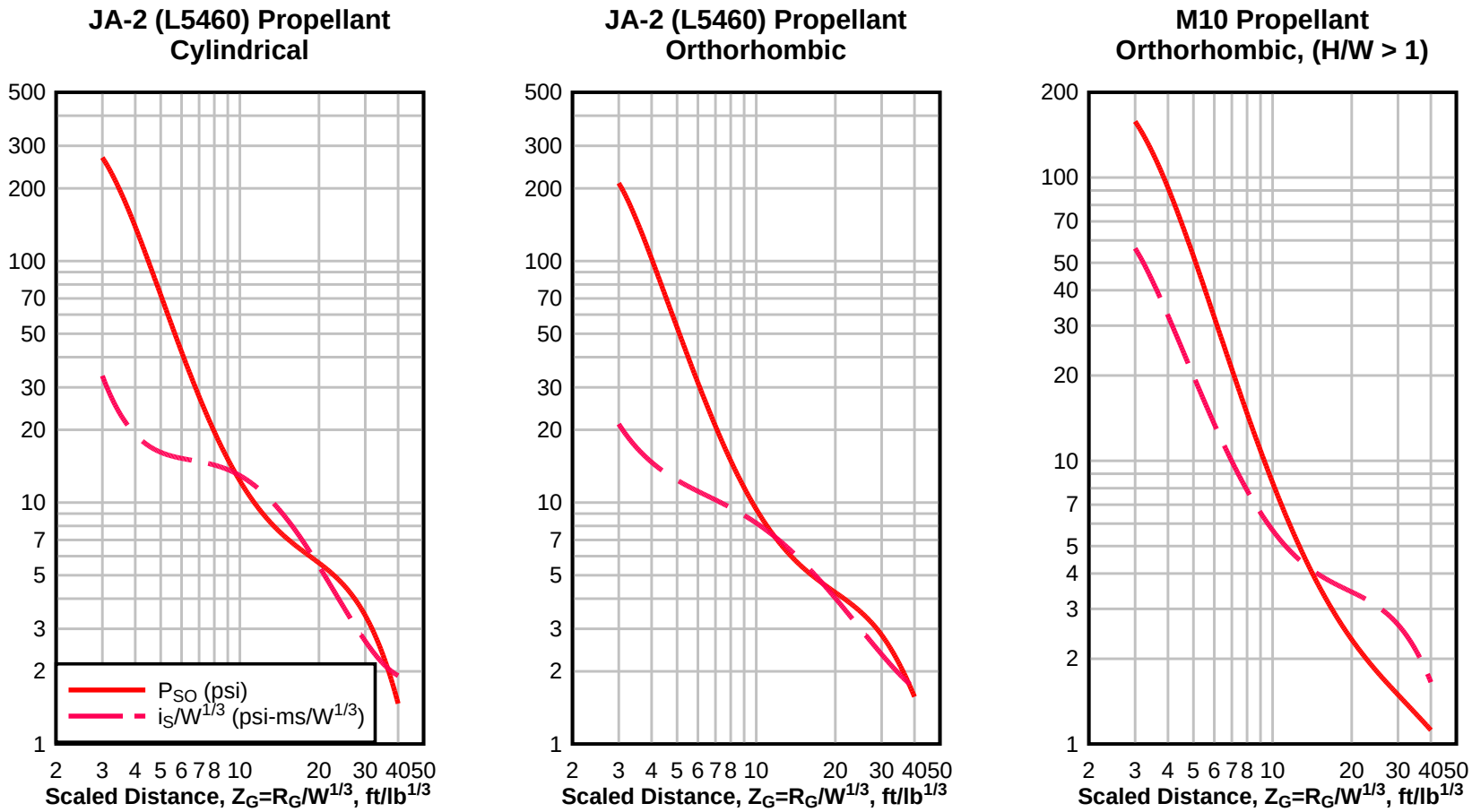

Figure 2-45 Peak Positive Incident Pressure and Scaled Impulse for an Explosion on the Surface at Sea Level, M10 Propellant and 105mm M314-A3

M10 Propellant Orthorhombic, (H/W < 1)

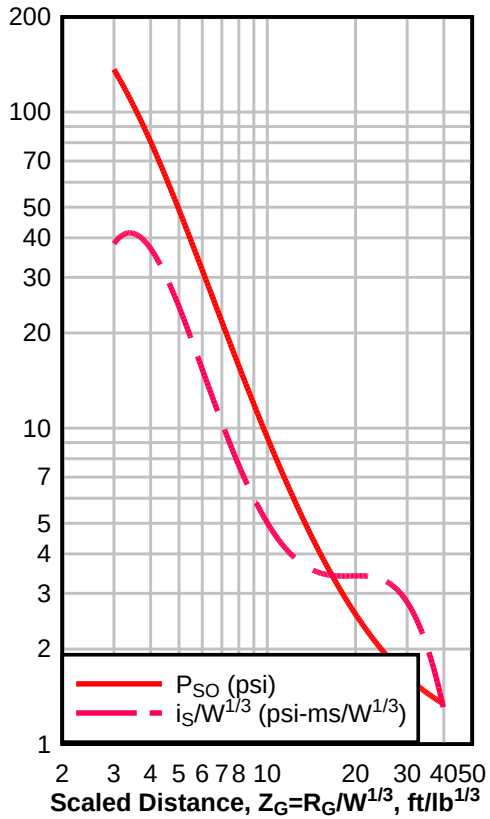

105mm M314-A3 Illuminated Composition Cylindrical

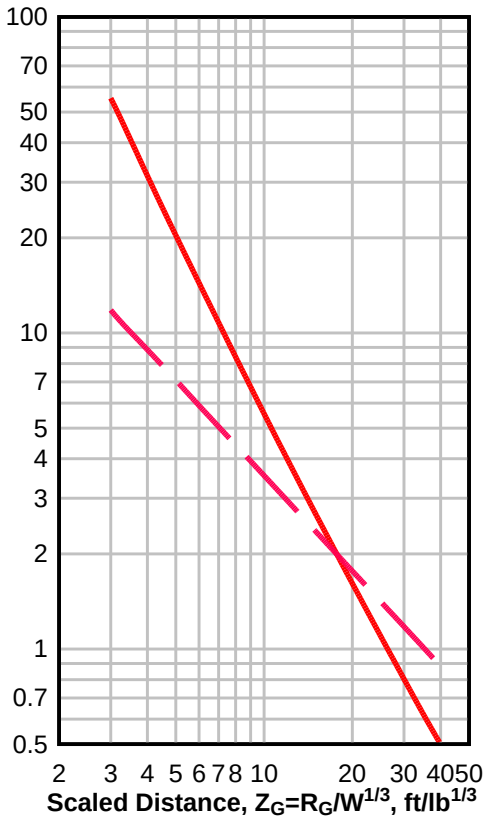

105mm M314-A3 Illuminated Composition (Cylindrical)

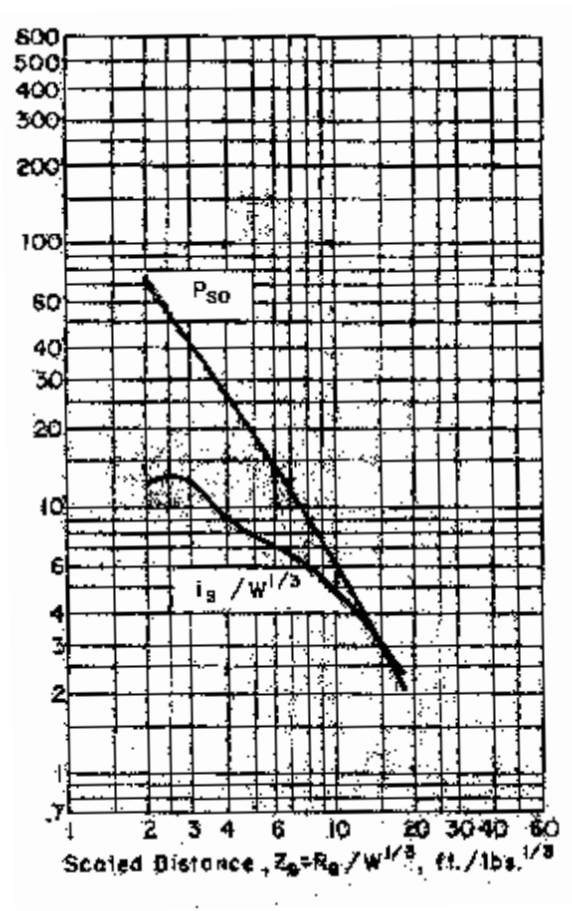

Figure 2-46 Peak Positive Incident Pressure and Scaled Impulse for an Explosion on the Surface at Sea Level, I559 Igniter Mixture and I560 Subigniter Mixture

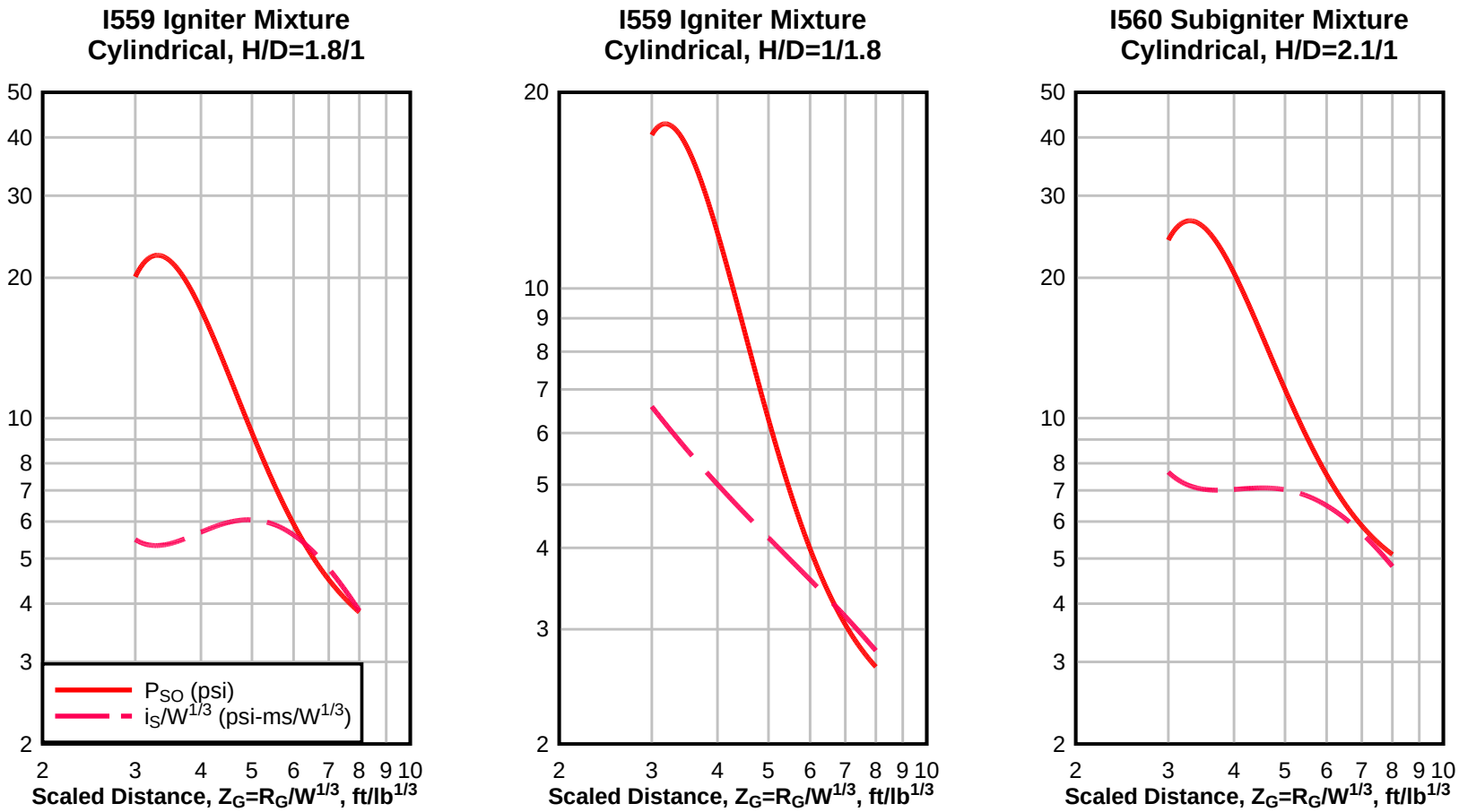

Figure 2-47 Peak Positive Incident Pressure and Scaled Impulse for an Explosion on the Surface at Sea Level, I560 Subigniter Mixture and R284 Tracer Mixture

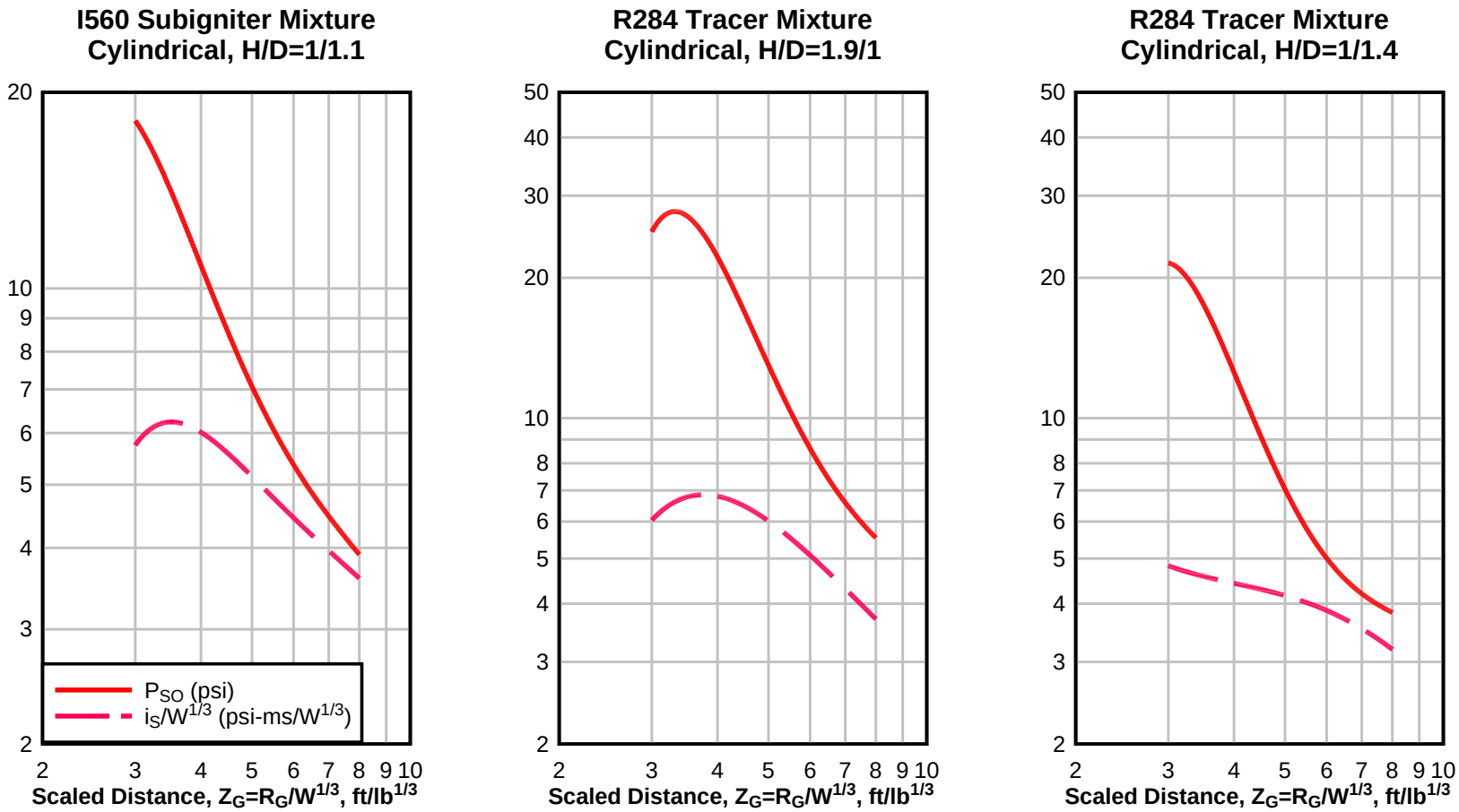

Figure 2-48 Peak Positive Incident Pressure and Scaled Impulse for an Explosion on the Surface at Sea Level, M314-A3 First Fire Composition and M49-A1 Trip Flare Composition

M314-A3 First Fire Composition Orthorhombic

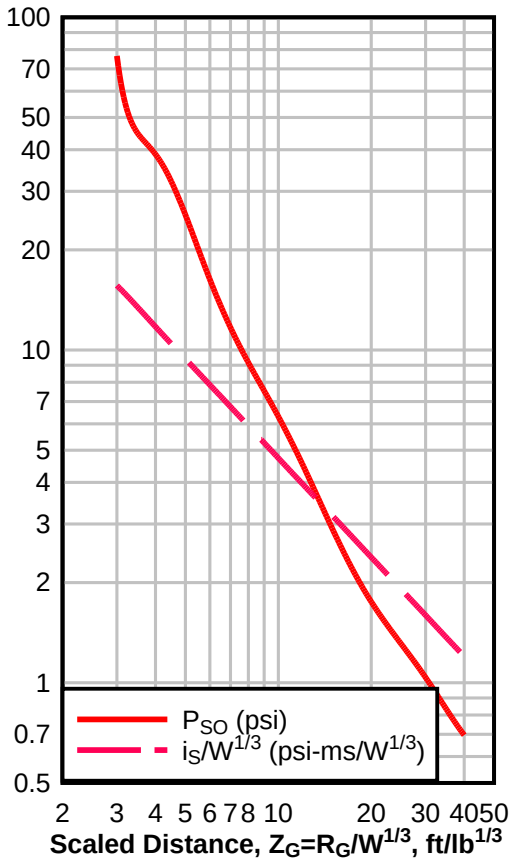

M314-A3 First Fire Composition Cylindrical

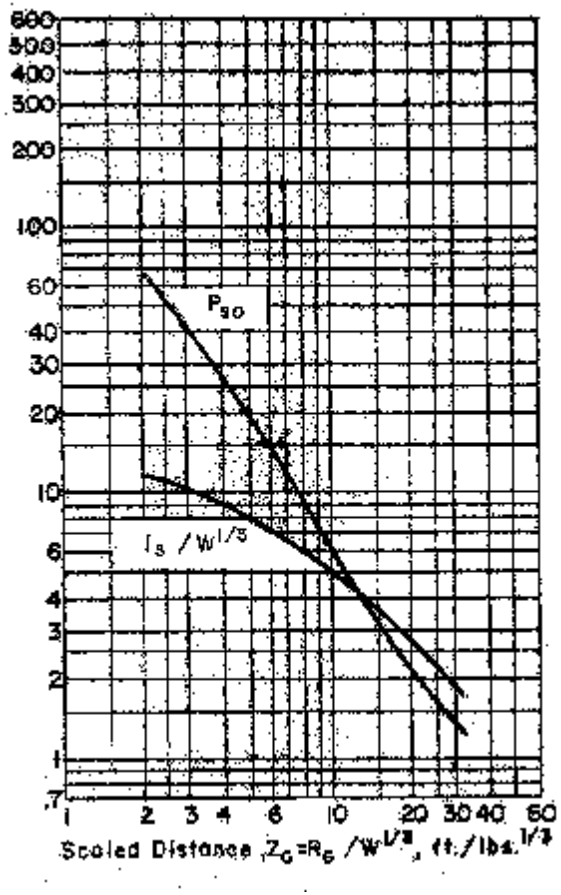

M49-A1 Trip Flare Composition Cylindrical (H/D=1/1.4)

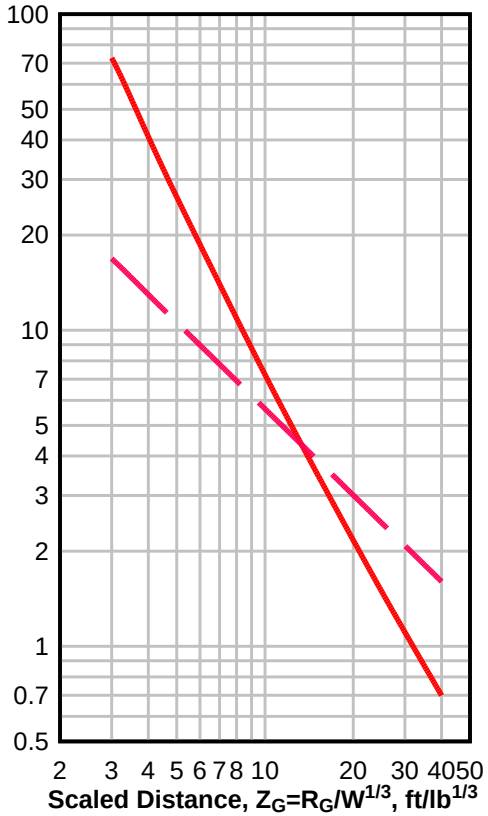

Figure 2-49 Peak Positive Incident Pressure and Scaled Impulse for an Explosion on the Surface at Sea Level, M49-A1 Trip Flare Composition

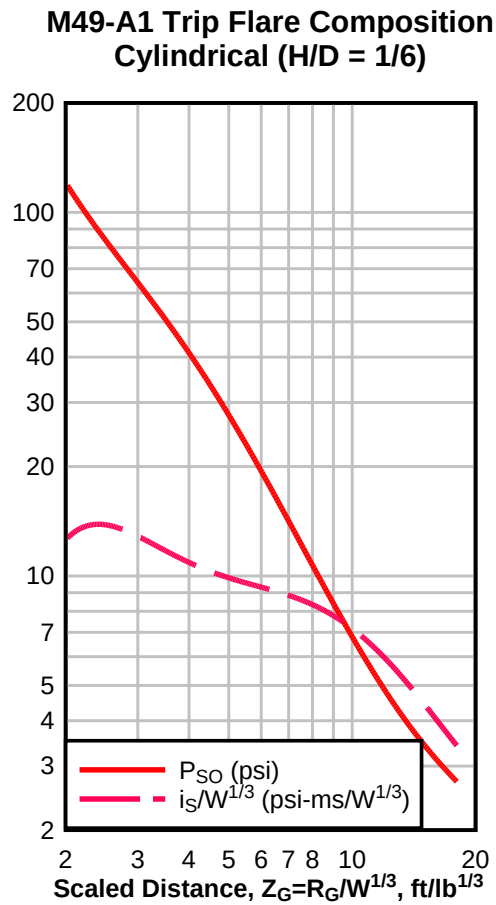

Figure 2-50 Confined Explosion Structures

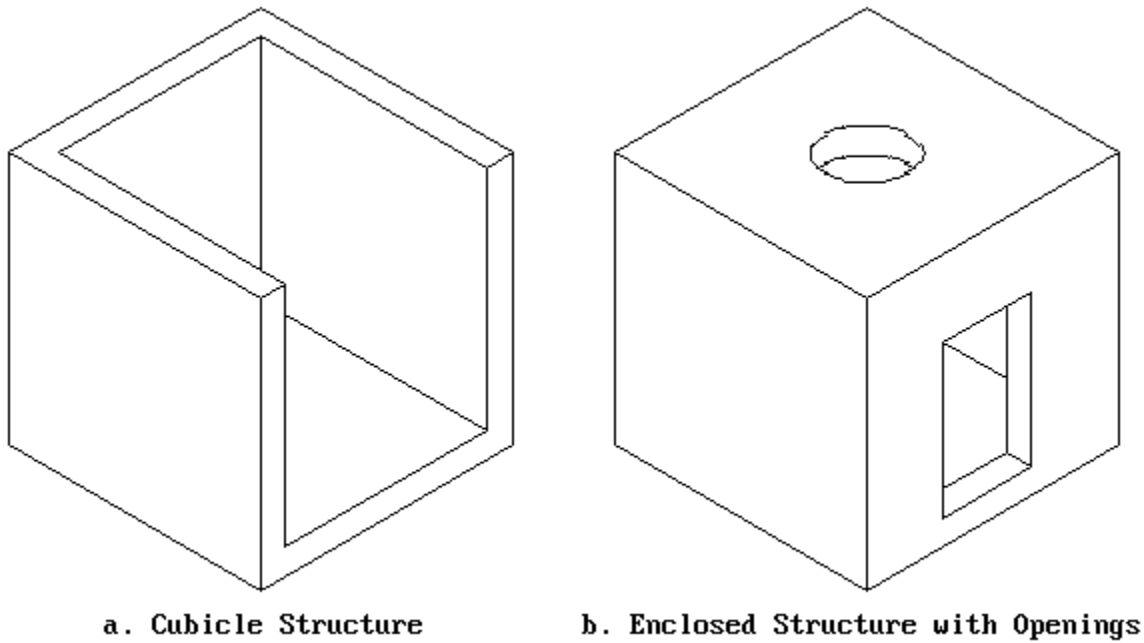

Figure 2-51 Barrier and Cubicle Configurations and Parameters

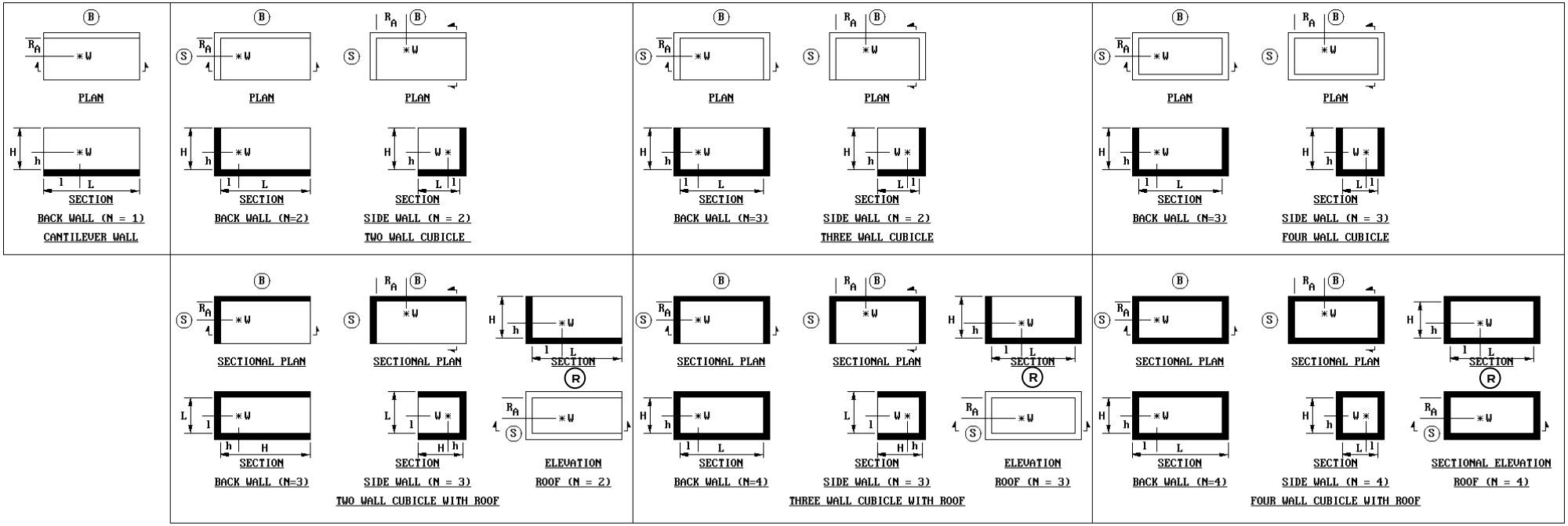

Notes:

1. B denotes Back Wall, S denotes Side Wall and R denotes Roof.
2. Numbers in parenthesis indicate number, N, of reflecting surfaces adjacent to surface in question.
3. h is always measured to the nearest reflecting surface.
4. l is always measured to the nearest reflecting surface except for the cantilever wall where it is measured to the nearest free edge.
5. For values of average peak pressures for barrier and cubicle arrangements shown, see Figures 2-52 to 2-100.
   For respective scaled average impulses, see Figures 2-101 to 2-149.
   For reference list of above Figures for particular values of required parameters in Note 6, see Figure 2-3.
6. Required parameters: N, l/L, h/H, L/H, L/R_A, $Z_A = R_A/W^{1/3}$

Figure 2-52 Average Peak Reflected Pressure (*N* = 1, l/*L* = 0.10, *h*/*H* = 0.10)

Numbers adjacent to curves indicate scaled range (ft/lb$^{1/3}$)

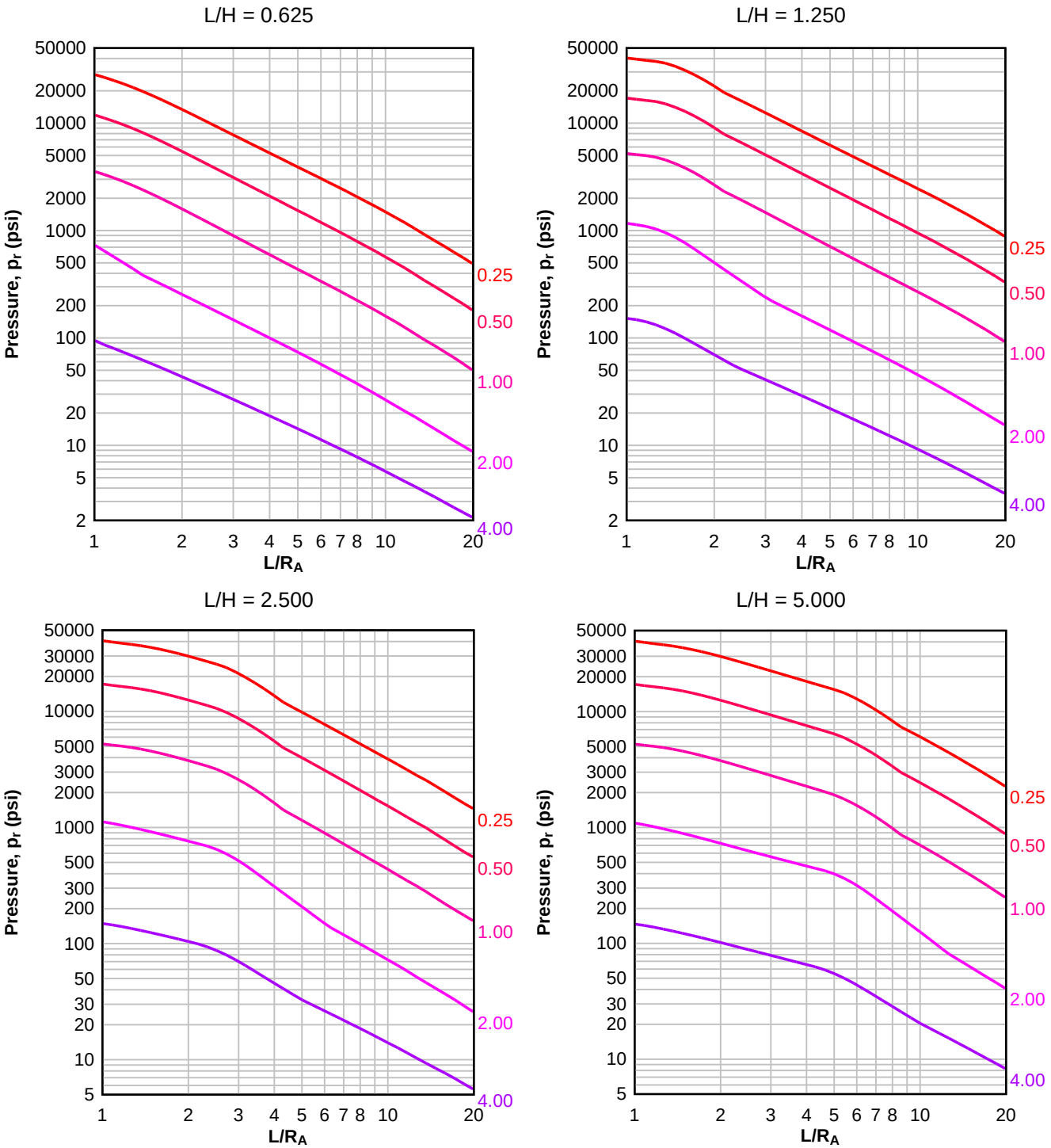

Figure 2-53 Average Peak Reflected Pressure (*N* = 1, l/*L* = 0.25 and 0.75, *h*/*H* = 0.10)

Numbers adjacent to curves indicate scaled range (ft/lb$^{1/3}$)

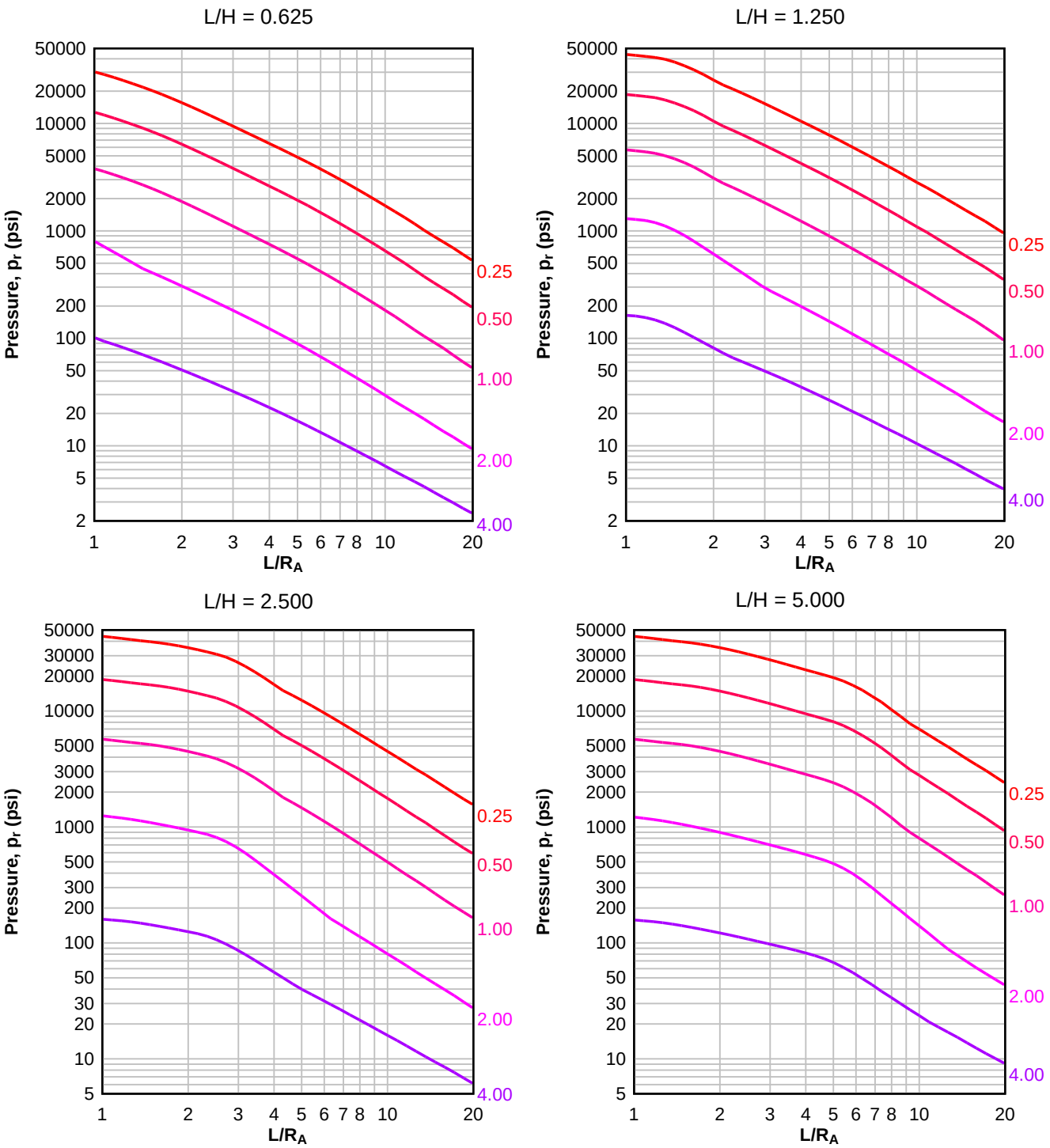

Figure 2-54 Average Peak Reflected Pressure (*N* = 1, l/*L* = 0.50, *h*/*H* = 0.10)

Numbers adjacent to curves indicate scaled range (ft/lb$^{1/3}$)

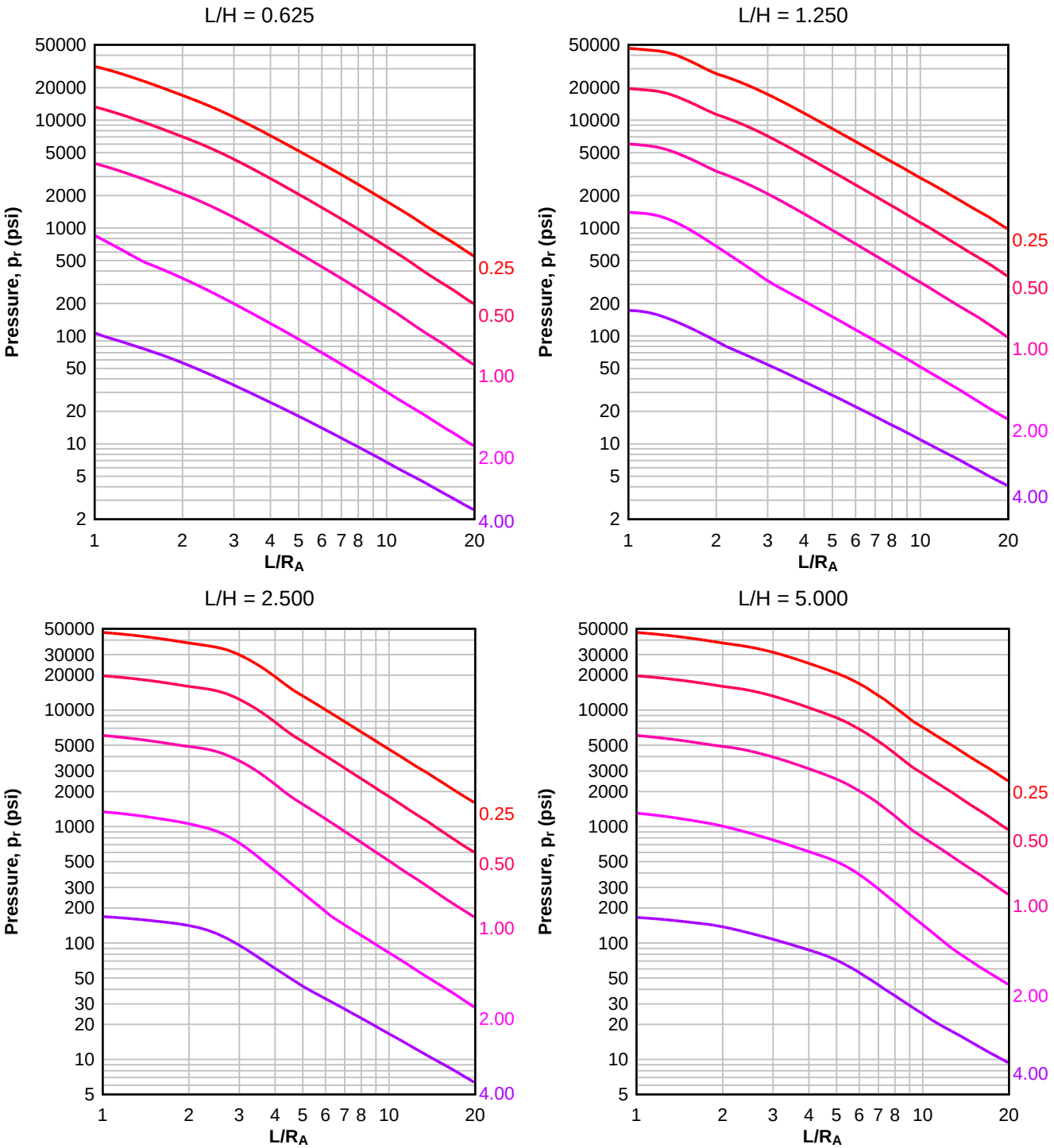

Figure 2-55 Average Peak Reflected Pressure (*N* = 1, *l/L* = 0.10, *h/H* = 0.25)

Numbers adjacent to curves indicate scaled range (ft/lb$^{1/3}$)

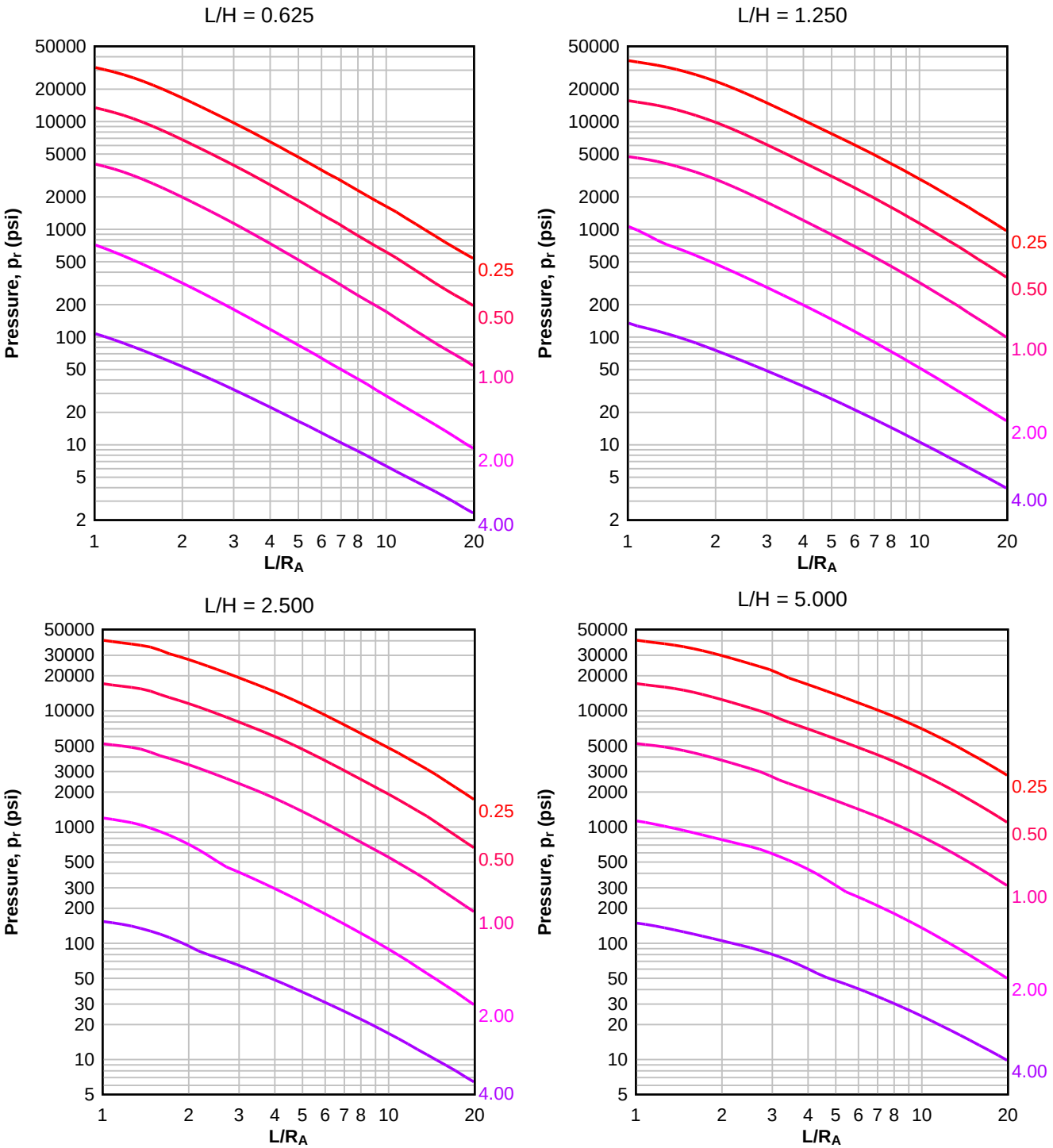

Figure 2-56 Average Peak Reflected Pressure (*N* = 1, *l/L* = 0.25 and 0.75, *h/H* = 0.25)

Numbers adjacent to curves indicate scaled range (ft/lb$^{1/3}$)

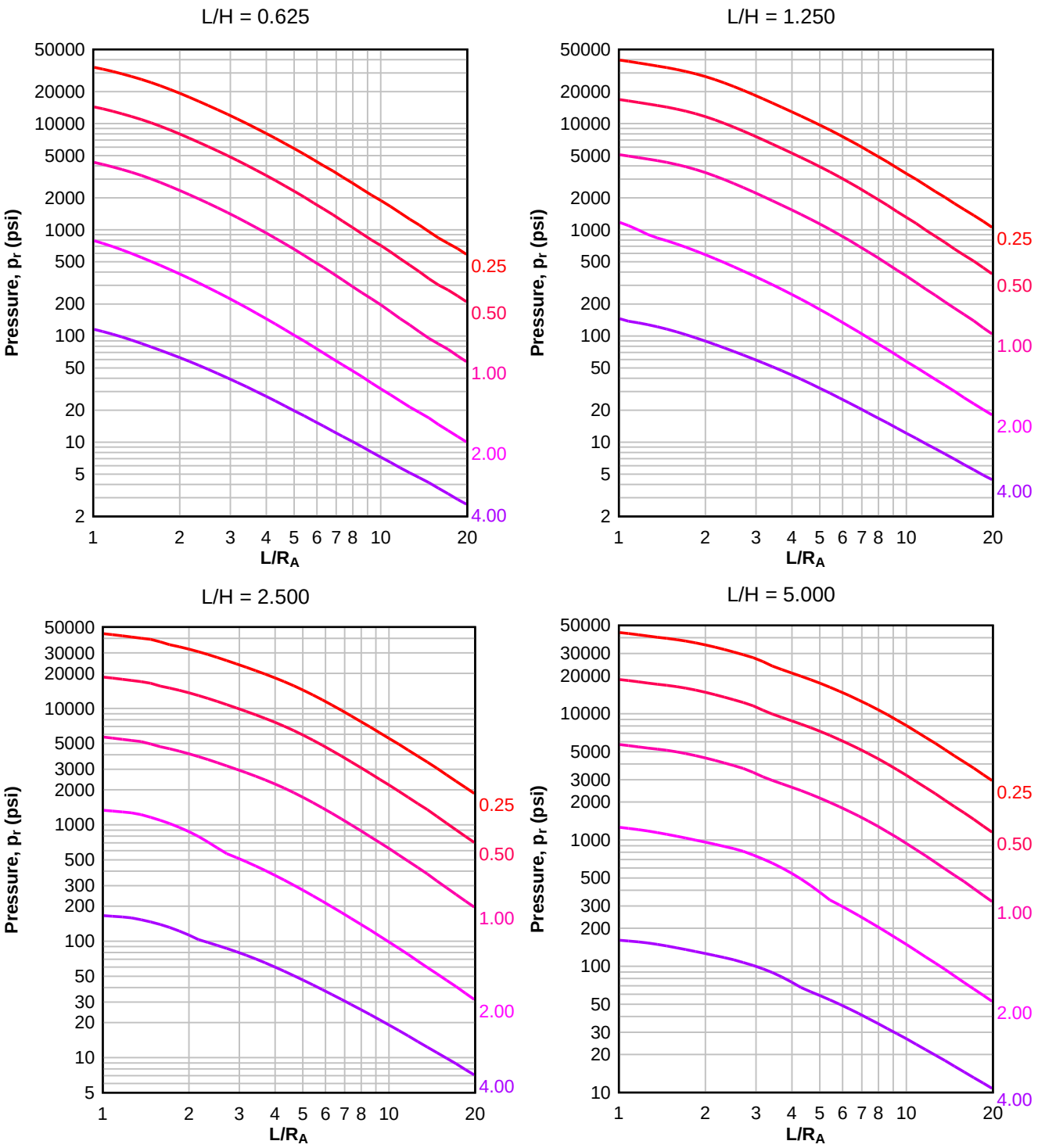

Figure 2-57 Average Peak Reflected Pressure (*N* = 1, *l*/*L* = 0.50, *h*/*H* = 0.25)

Numbers adjacent to curves indicate scaled range (ft/lb$^{1/3}$)

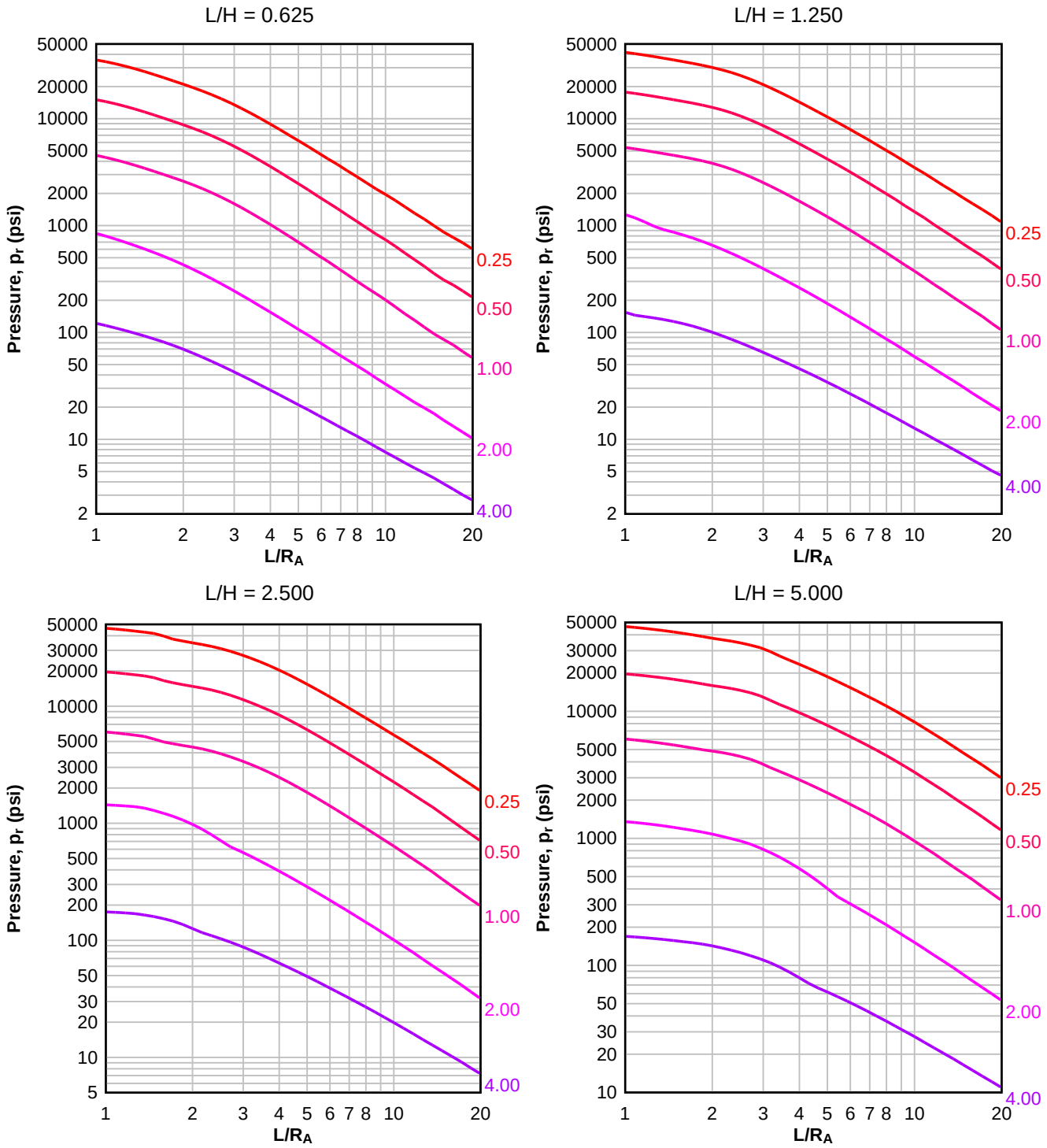

Figure 2-58 Average Peak Reflected Pressure (*N* = 1, *l*/*L* = 0.10, *h*/*H* = 0.50)

Numbers adjacent to curves indicate scaled range (ft/lb$^{1/3}$)

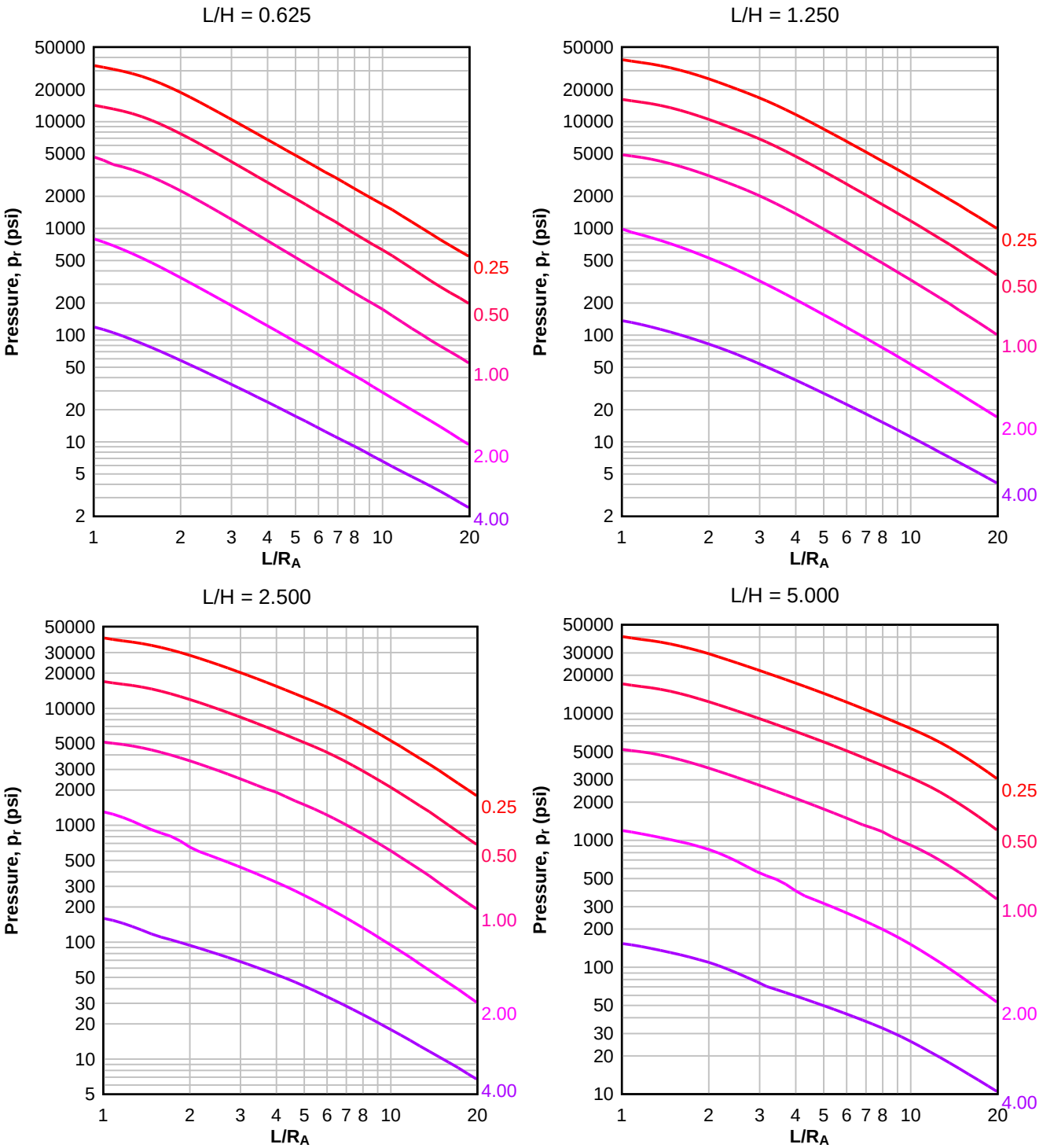

Figure 2-59 Average Peak Reflected Pressure (*N* = 1, *l/L* = 0.25 and 0.75, *h/H* = 0.50)

Numbers adjacent to curves indicate scaled range (ft/lb$^{1/3}$)

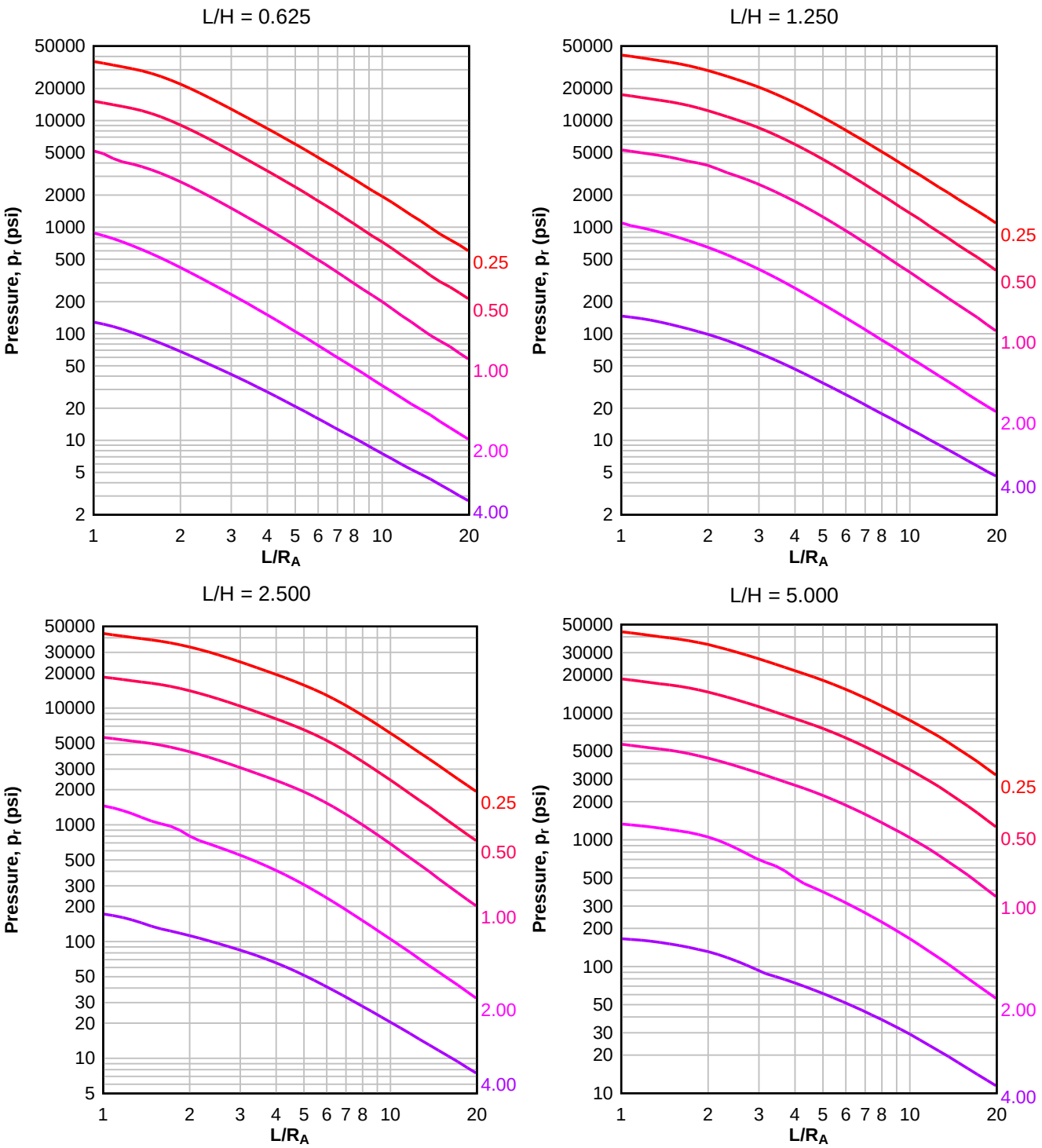

Figure 2-60 Average Peak Reflected Pressure (*N* = 1, *l*/*L* = 0.50, *h*/*H* = 0.50)

Numbers adjacent to curves indicate scaled range (ft/lb$^{1/3}$)

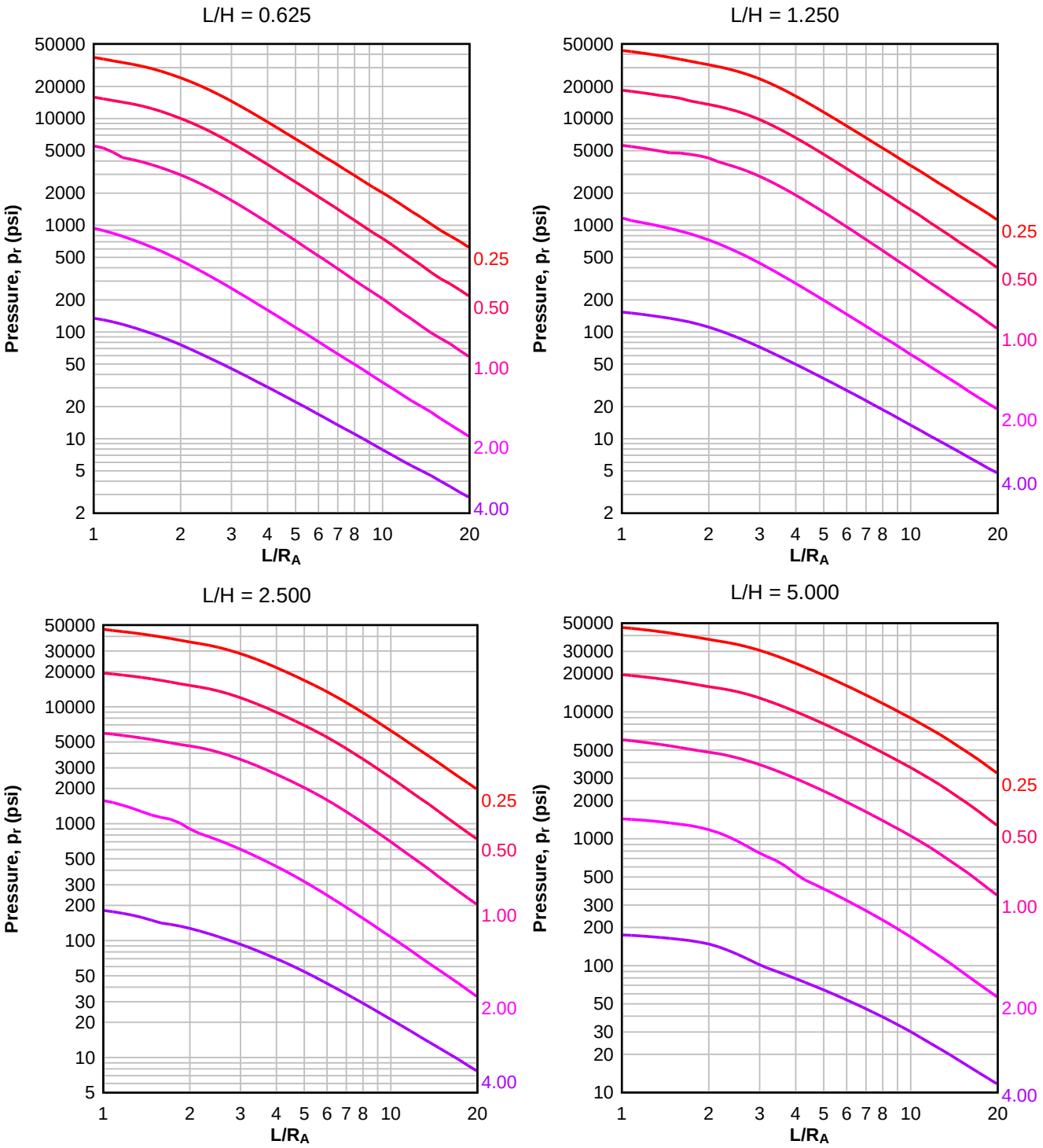

Figure 2-61 Average Peak Reflected Pressure (*N* = 1, *l*/*L* = 0.10, *h*/*H* = 0.75)

Numbers adjacent to curves indicate scaled range (ft/lb$^{1/3}$)

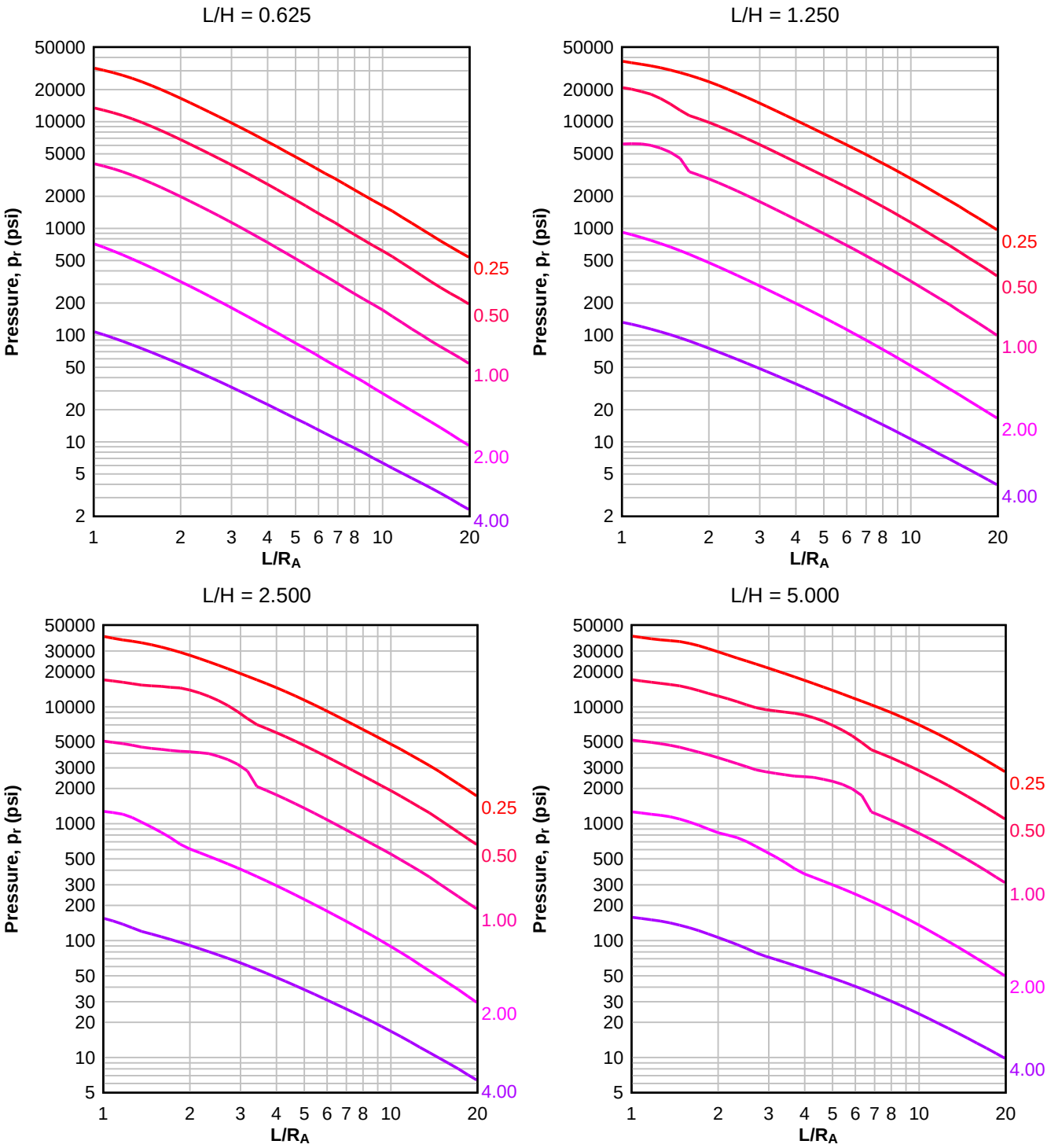

Figure 2-62 Average Peak Reflected Pressure (*N* = 1, *l/L* = 0.25 and 0.75, *h/H* = 0.75)

Numbers adjacent to curves indicate scaled range (ft/lb$^{1/3}$)

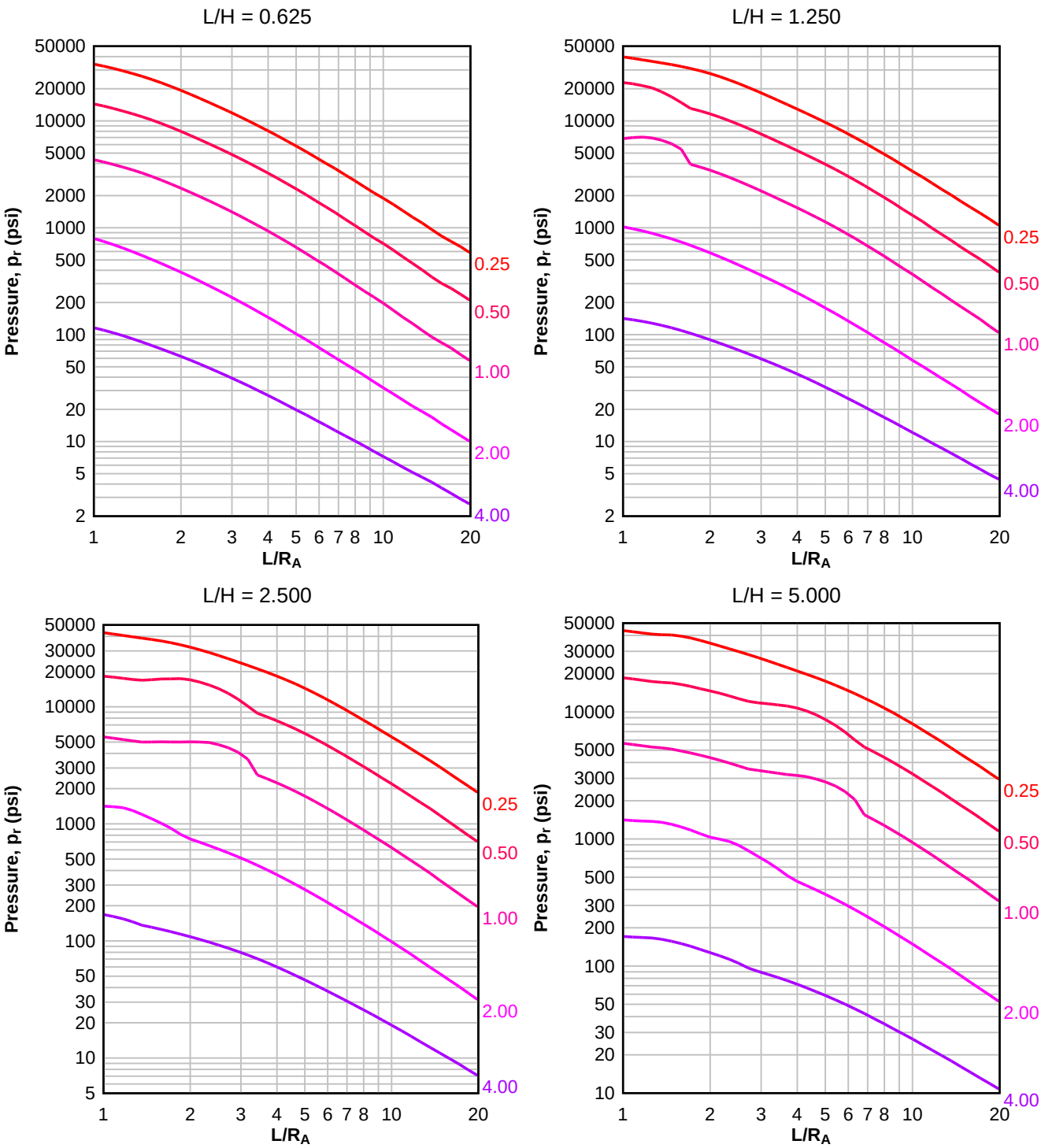

Figure 2-63 Average Peak Reflected Pressure (*N* = 1, *l*/*L* = 0.50, *h*/*H* = 0.75)

Numbers adjacent to curves indicate scaled range (ft/lb$^{1/3}$)

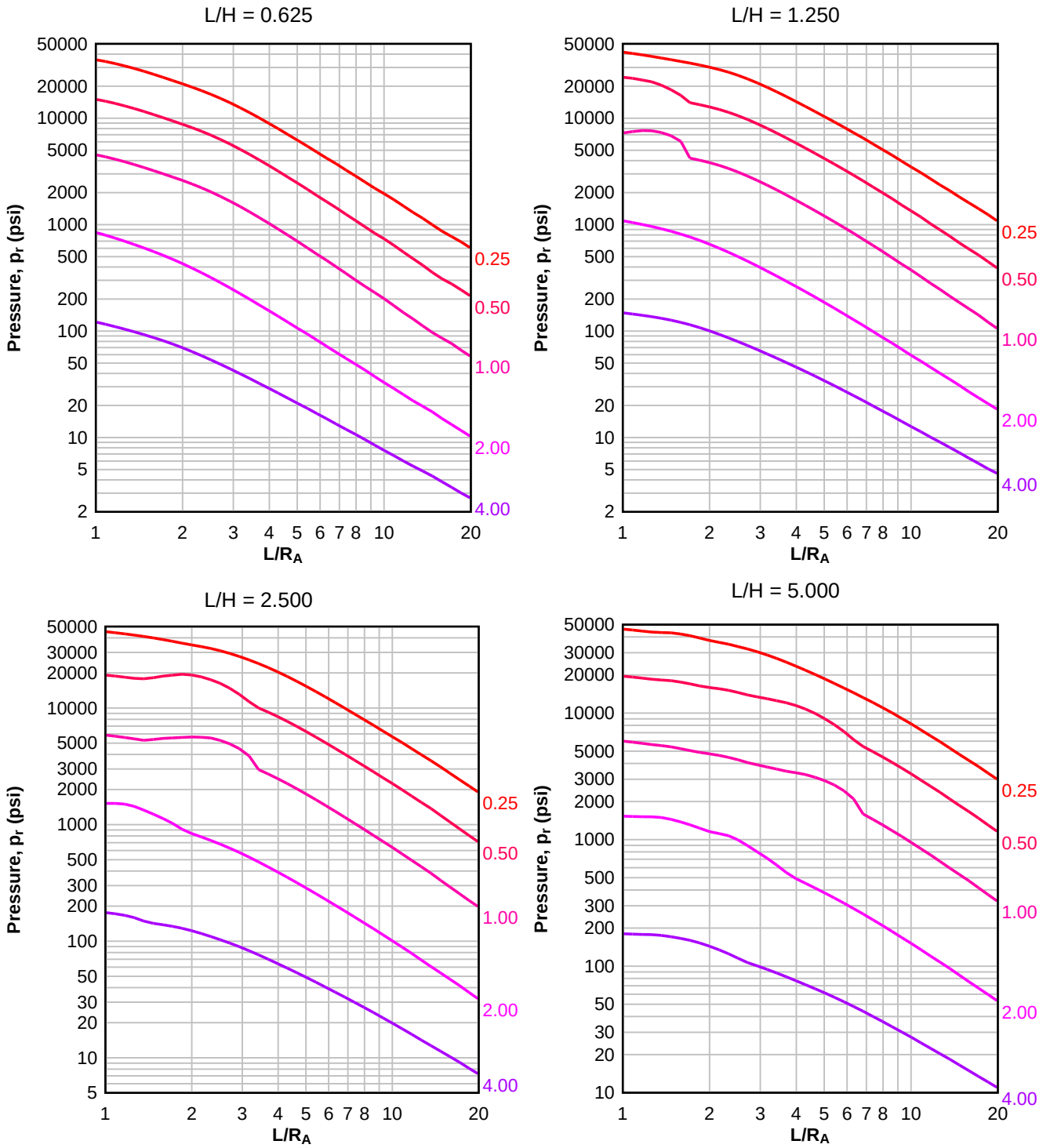

Figure 2-64 Average Peak Reflected Pressure (*N* = 2, *l*/*L* = 0.10, *h*/*H* = 0.10)

Numbers adjacent to curves indicate scaled range (ft/lb$^{1/3}$)

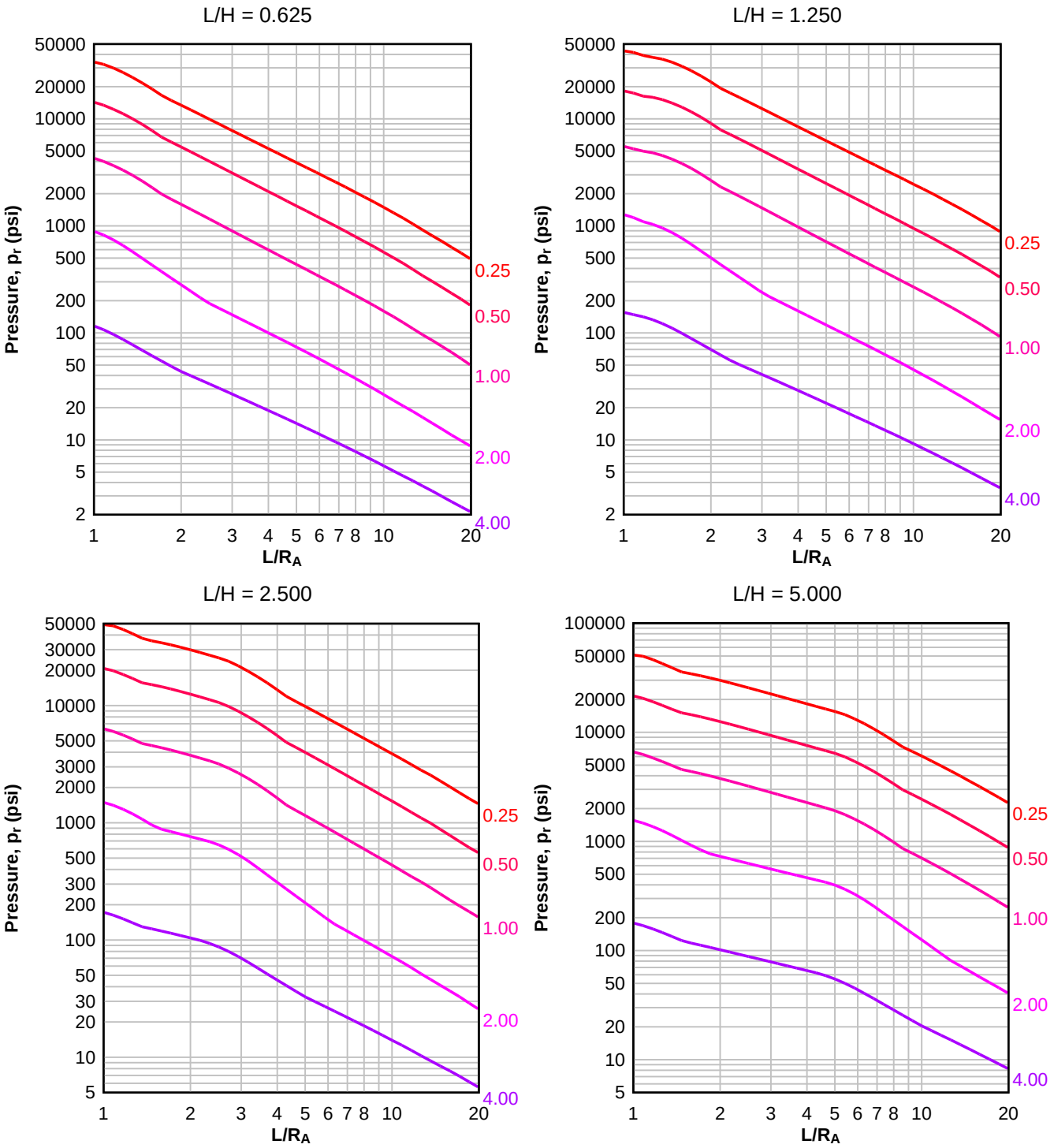

Figure 2-65 Average Peak Reflected Pressure (*N* = 2, *l*/*L* = 0.25, *h*/*H* = 0.10)

Numbers adjacent to curves indicate scaled range (ft/lb$^{1/3}$)

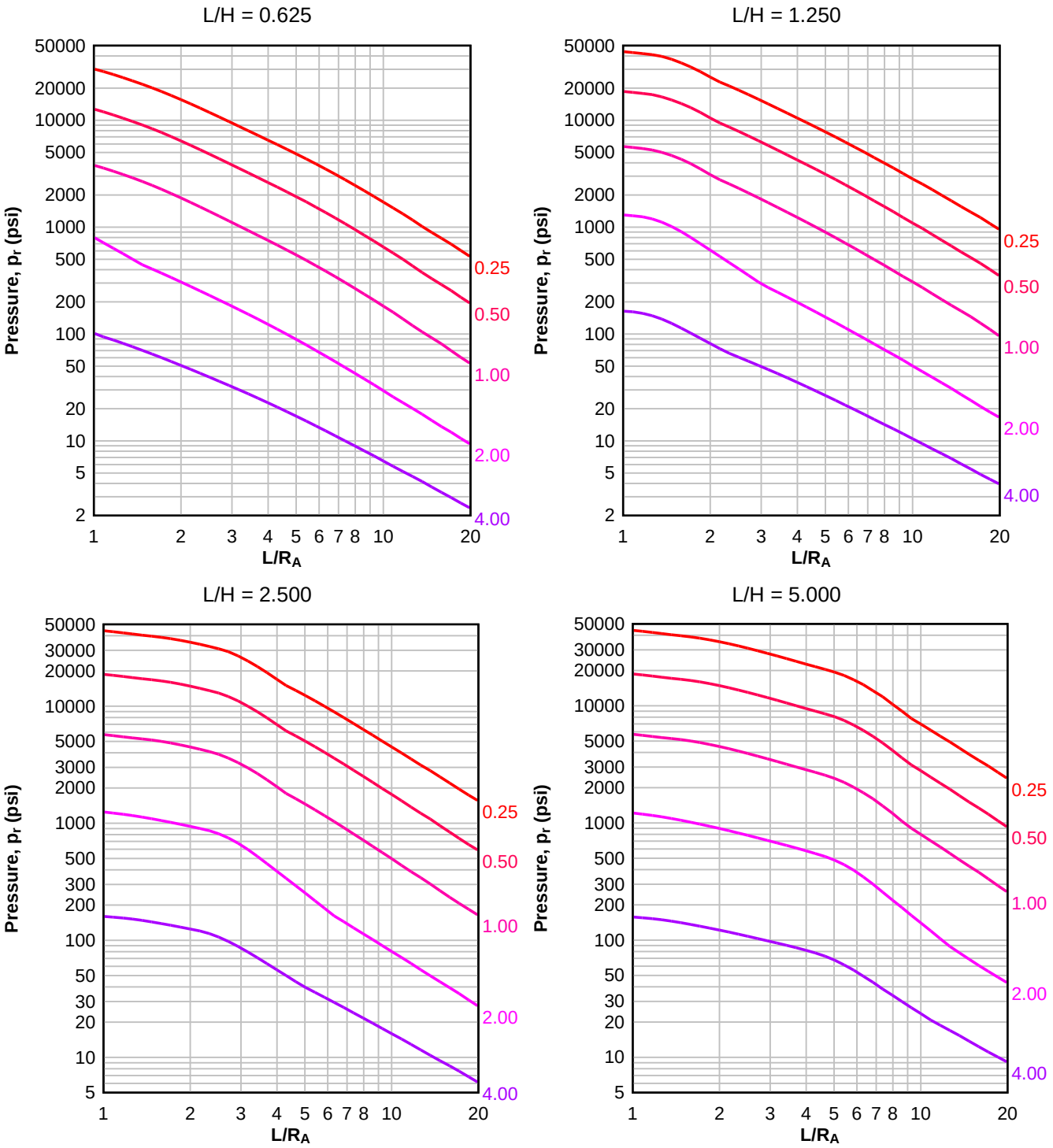

Figure 2-66 Average Peak Reflected Pressure (*N* = 2, *l*/*L* = 0.50, *h*/*H* = 0.10)

Numbers adjacent to curves indicate scaled range (ft/lb$^{1/3}$)

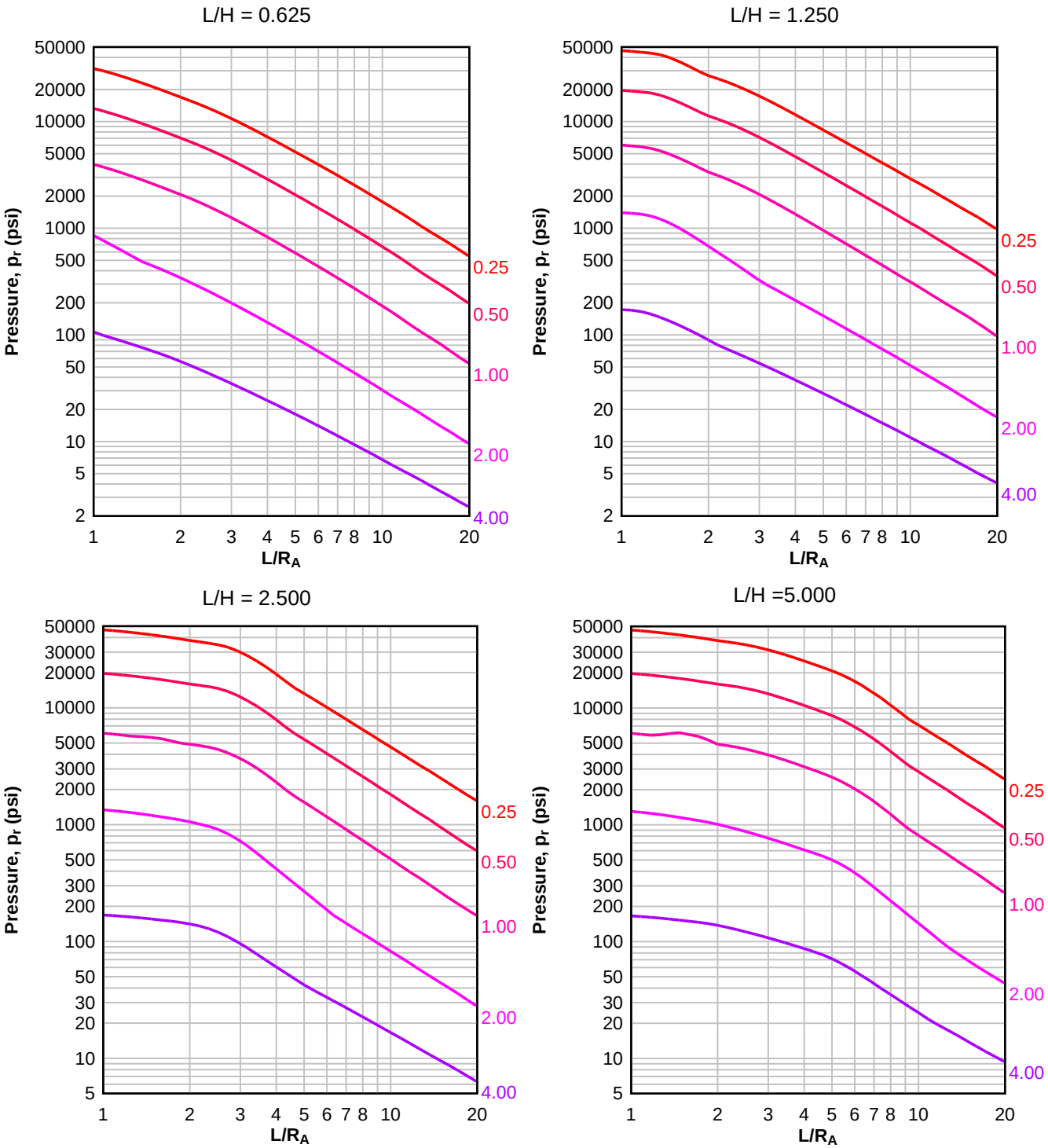

Figure 2-67 Average Peak Reflected Pressure (*N* = 2, *l*/*L* = 0.75, *h*/*H* = 0.10)

Numbers adjacent to curves indicate scaled range (ft/lb$^{1/3}$)

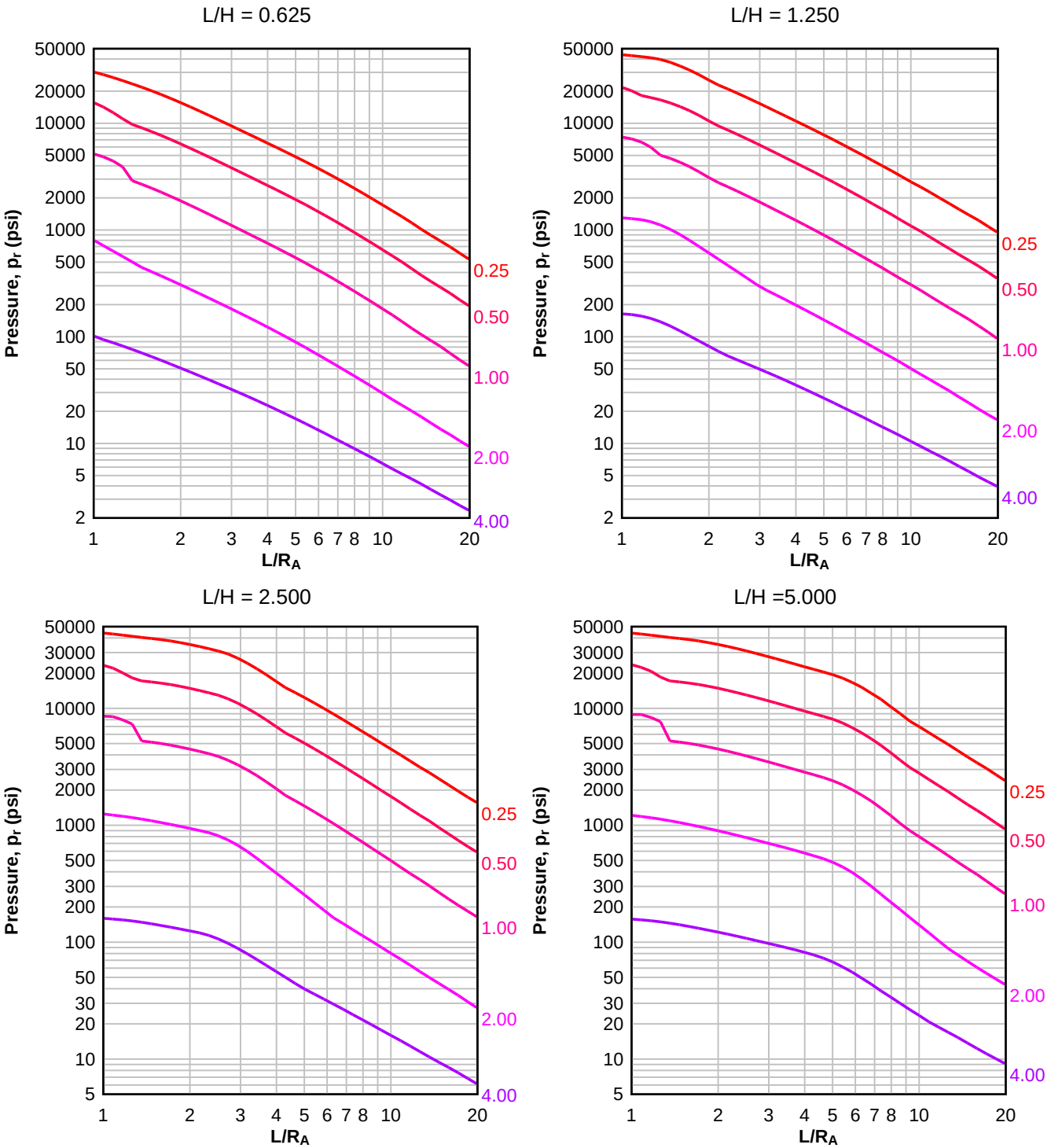

Figure 2-68 Average Peak Reflected Pressure (*N* = 2, *l/L* = 0.10, *h/H* = 0.25)

Numbers adjacent to curves indicate scaled range (ft/lb$^{1/3}$)

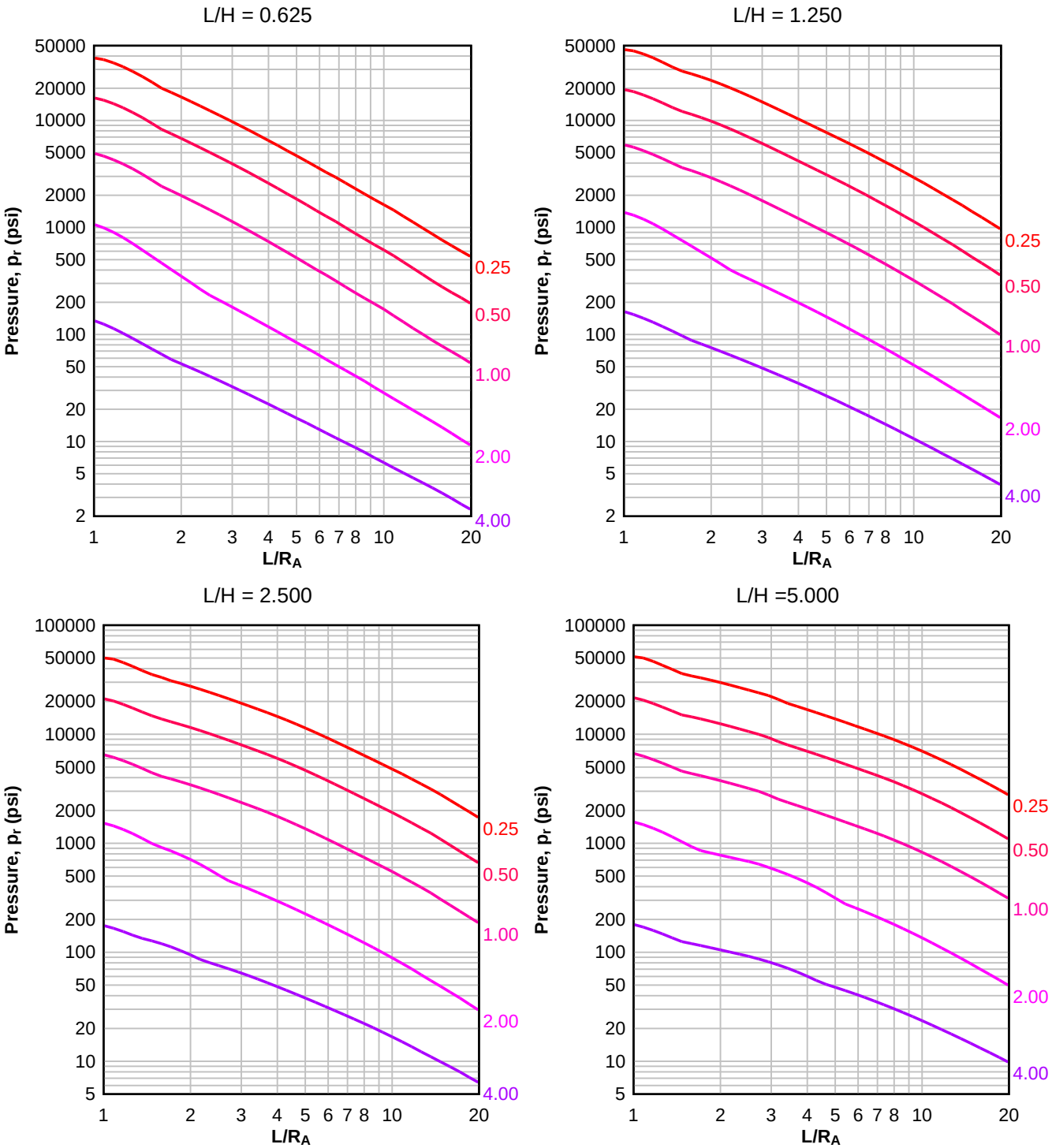

Figure 2-69 Average Peak Reflected Pressure (*N* = 2, *l/L* = 0.25, *h/H* = 0.25)

Numbers adjacent to curves indicate scaled range (ft/lb$^{1/3}$)

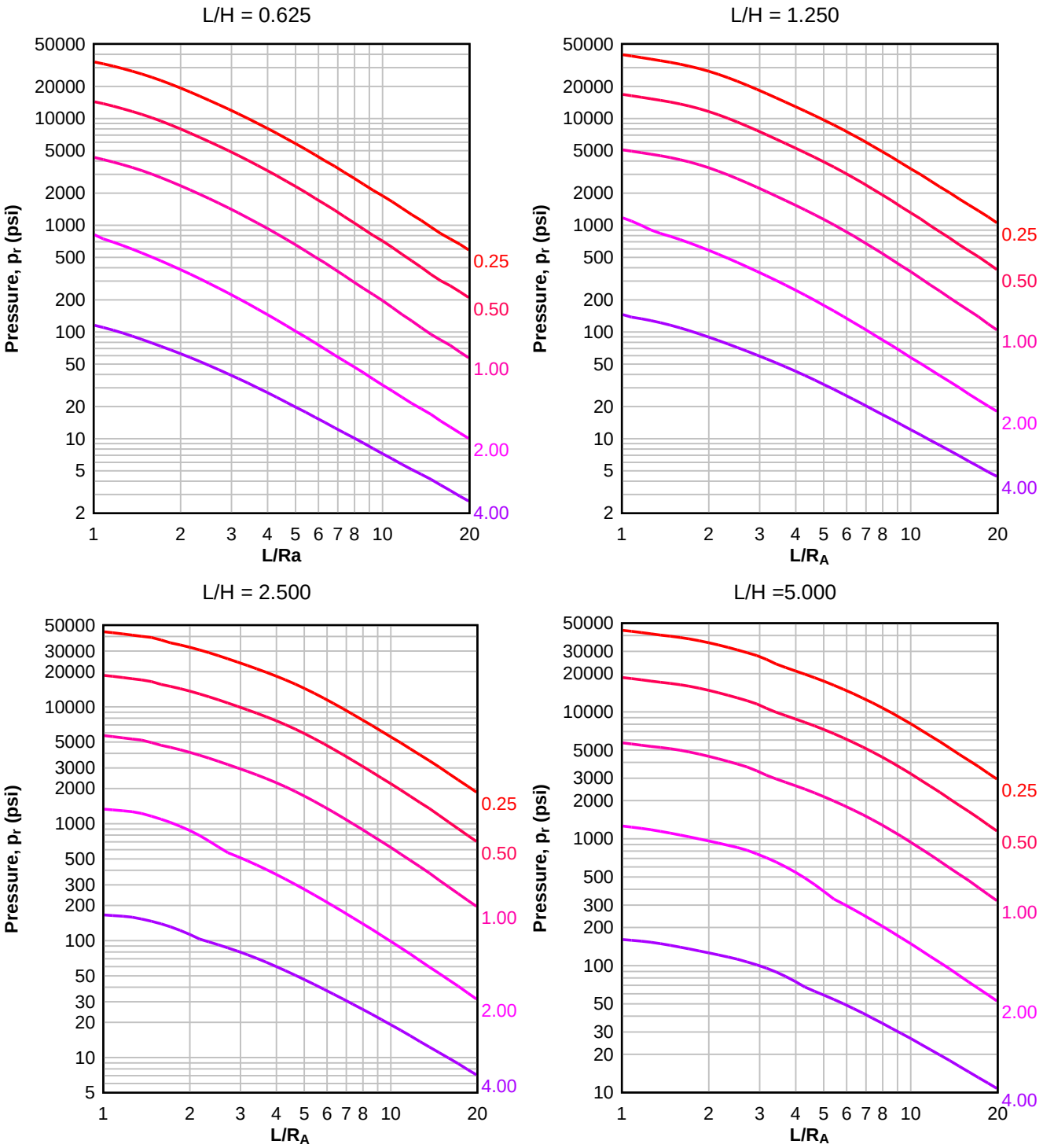

Figure 2-70 Average Peak Reflected Pressure (*N* = 2, *l*/*L* = 0.50, *h*/*H* = 0.25)

Numbers adjacent to curves indicate scaled range (ft/lb$^{1/3}$)

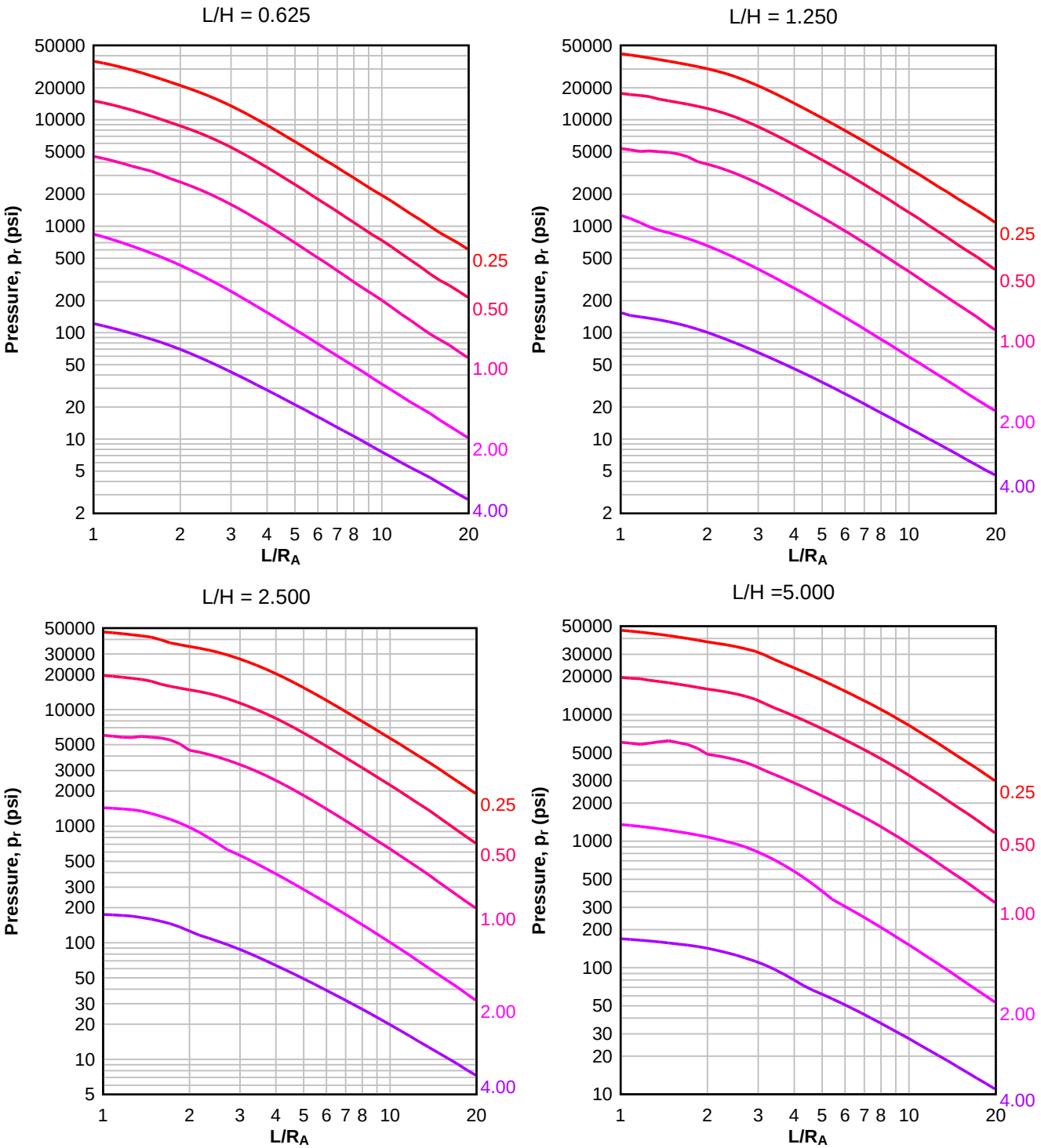

Figure 2-71 Average Peak Reflected Pressure (*N* = 2, *l*/*L* = 0.75, *h*/*H* = 0.25)

Numbers adjacent to curves indicate scaled range (ft/lb$^{1/3}$)

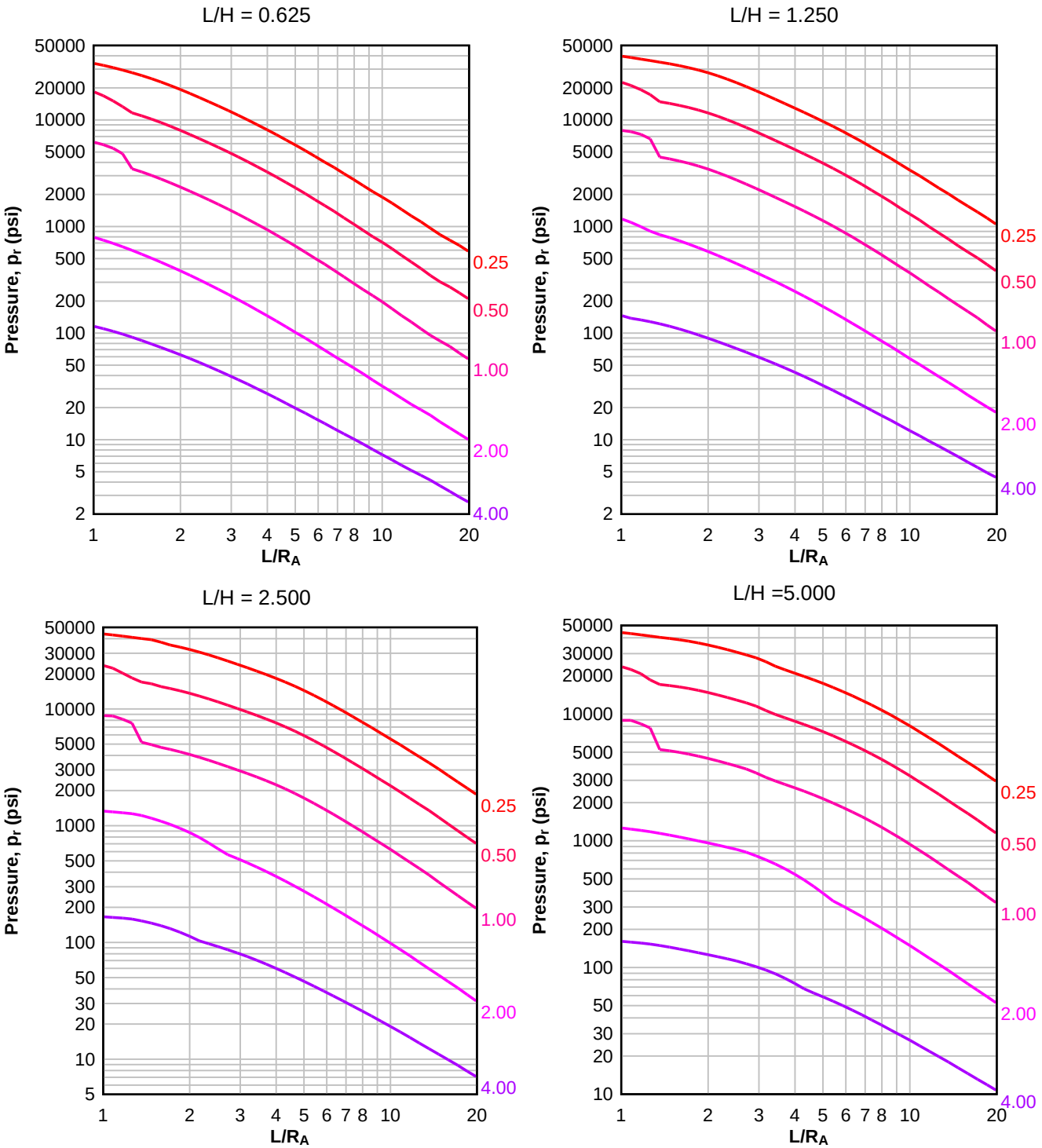

Figure 2-72 Average Peak Reflected Pressure (*N* = 2, *l*/*L* = 0.10, *h*/*H* = 0.50)

Numbers adjacent to curves indicate scaled range (ft/lb$^{1/3}$)

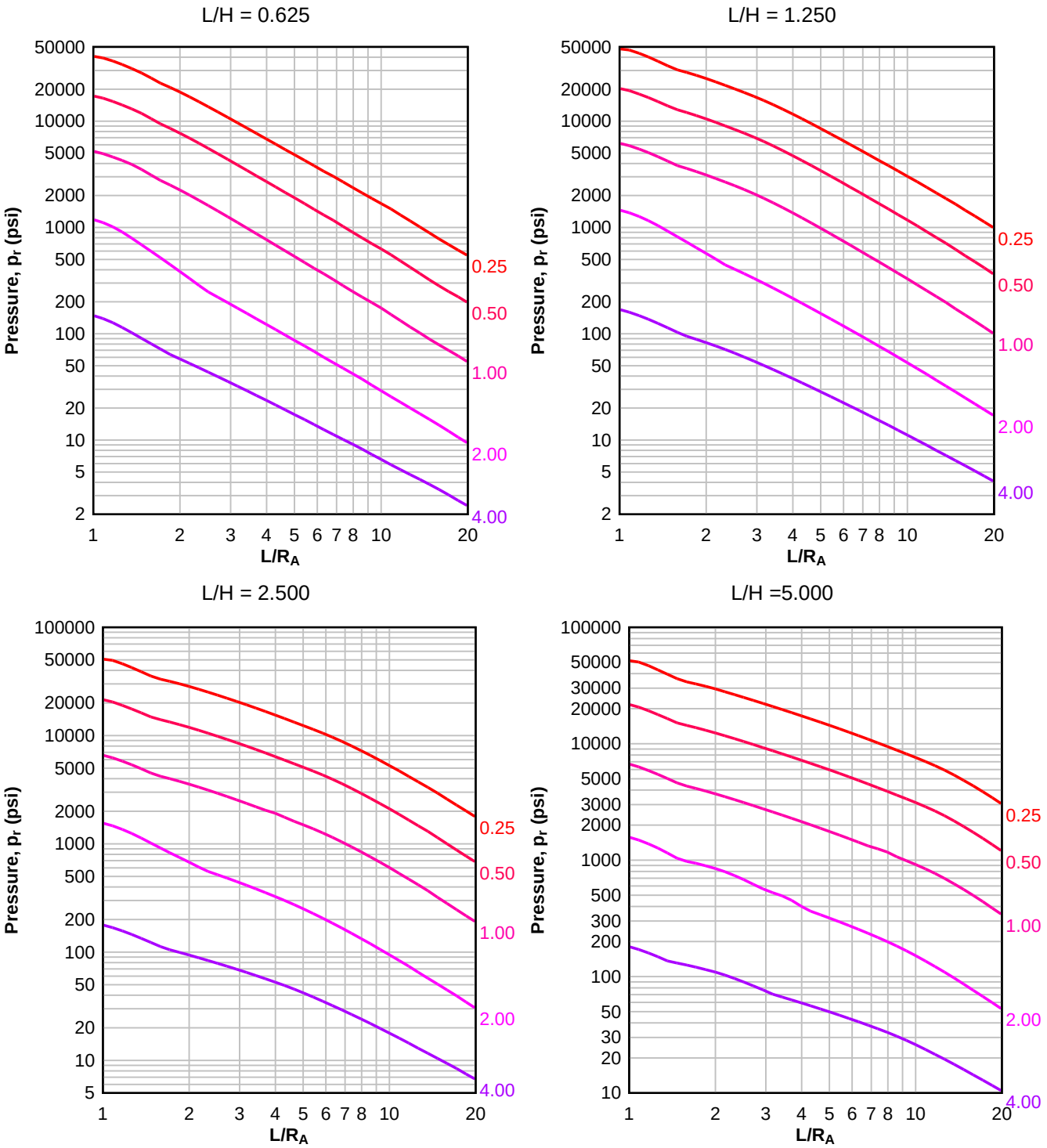

Figure 2-73 Average Peak Reflected Pressure (*N* = 2, *l*/*L* = 0.25, *h*/*H* = 0.50)

Numbers adjacent to curves indicate scaled range (ft/lb$^{1/3}$)

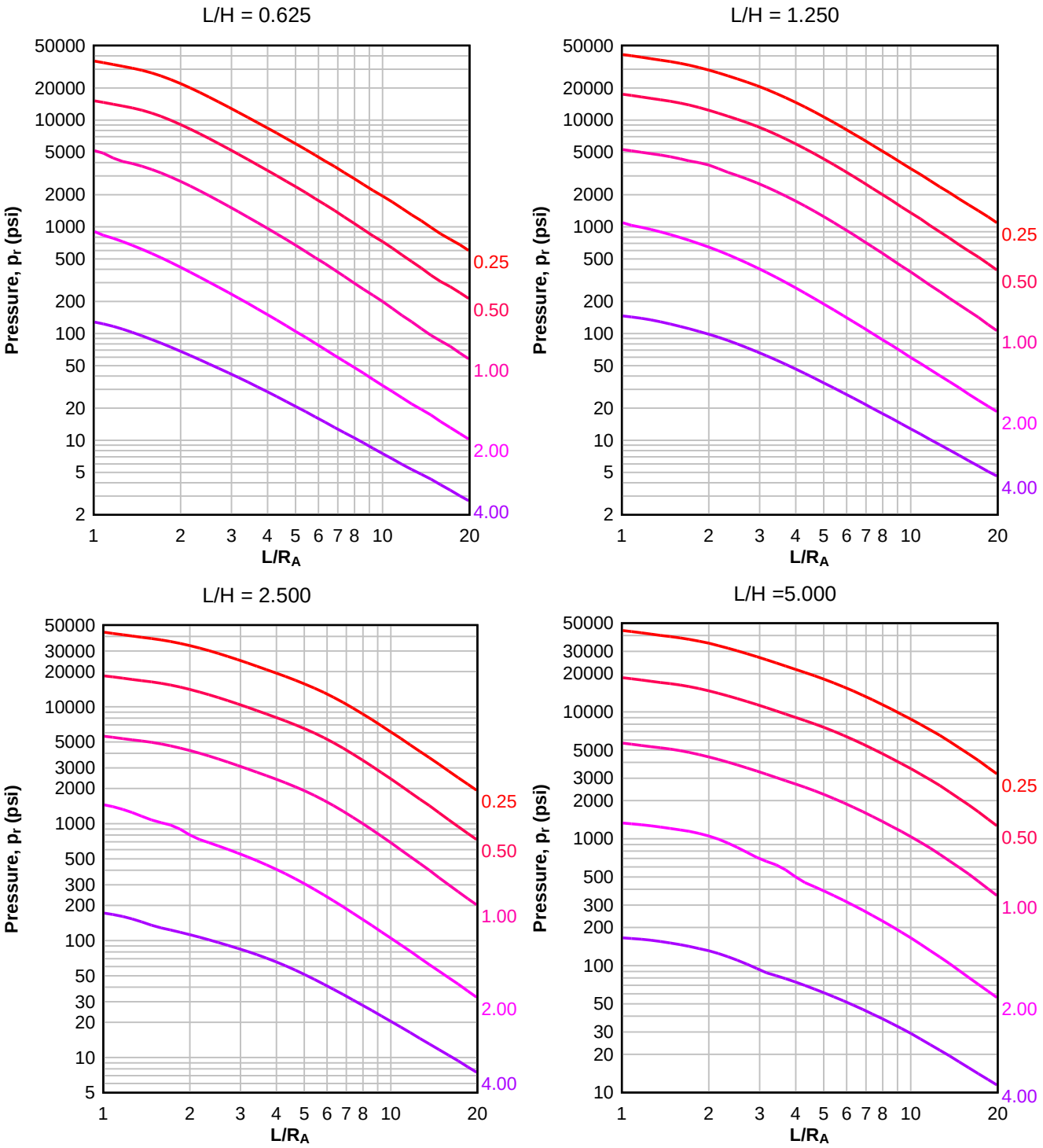

Figure 2-74 Average Peak Reflected Pressure (*N* = 2, *l*/*L* = 0.50, *h*/*H* = 0.50)

Numbers adjacent to curves indicate scaled range (ft/lb$^{1/3}$)

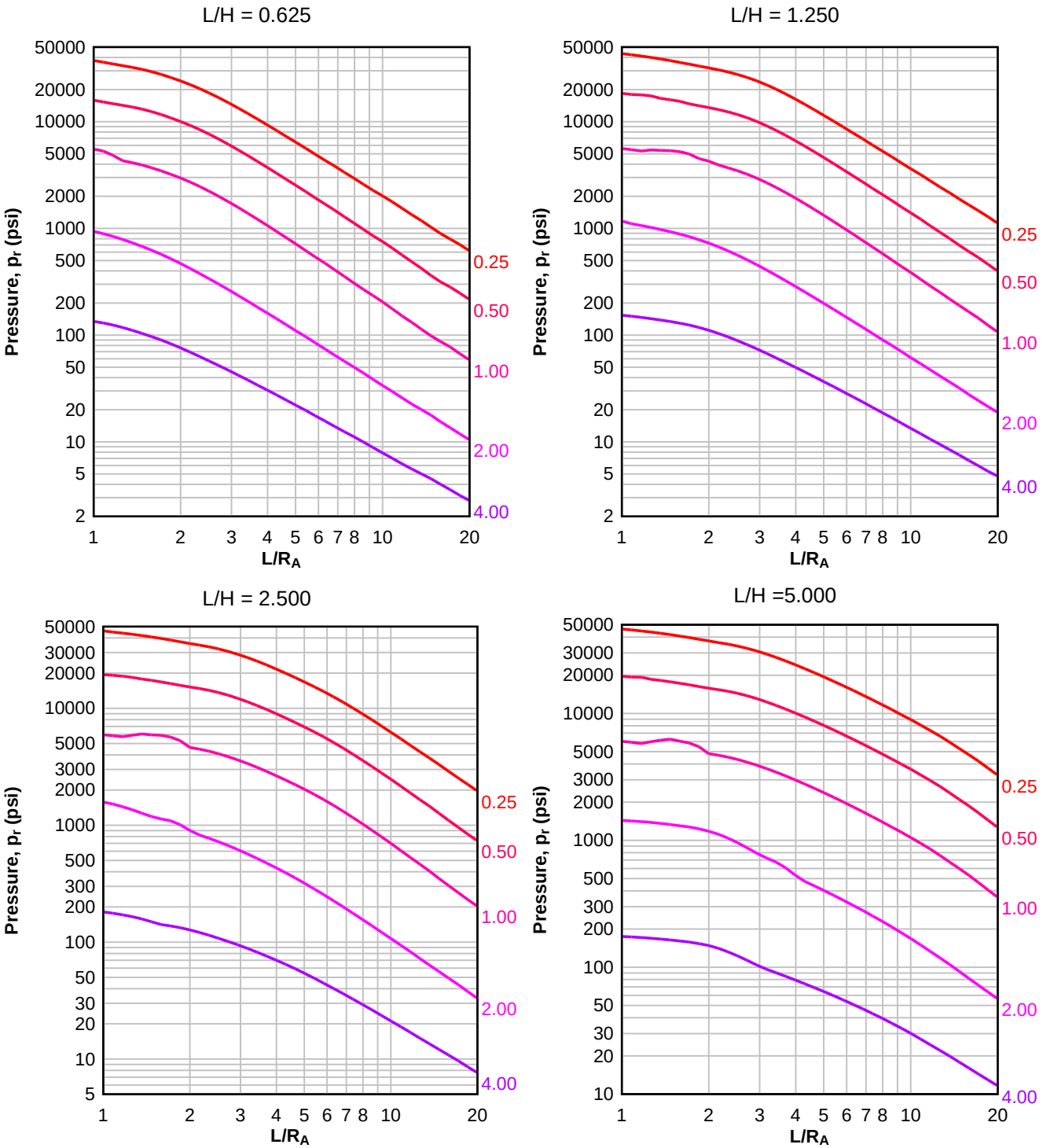

Figure 2-75 Average Peak Reflected Pressure (*N* = 2, *l*/*L* = 0.75, *h*/*H* = 0.50)

Numbers adjacent to curves indicate scaled range (ft/lb$^{1/3}$)

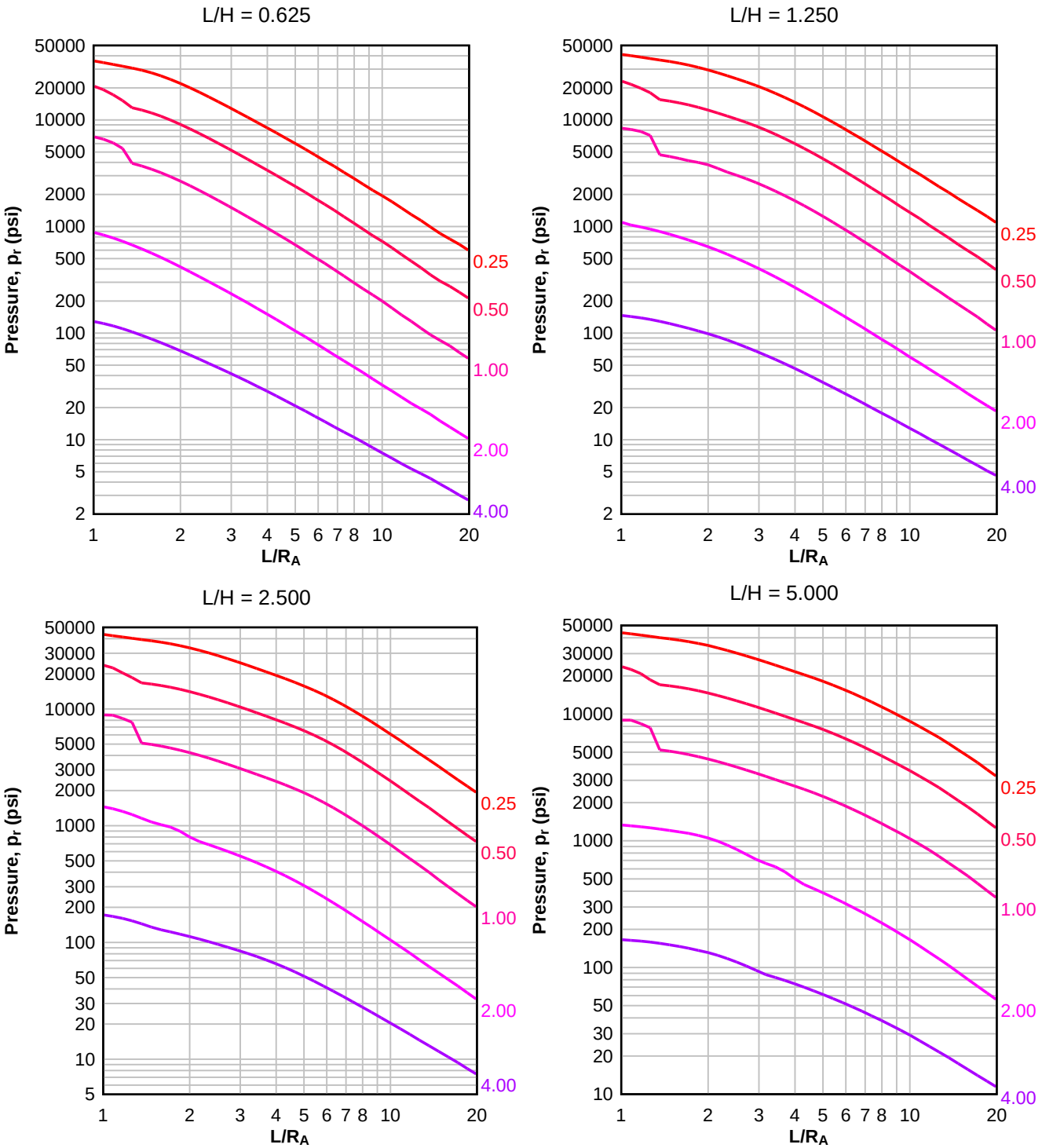

Figure 2-76 Average Peak Reflected Pressure (*N* = 2, *l*/*L* = 0.10, *h*/*H* = 0.75)

Numbers adjacent to curves indicate scaled range (ft/lb$^{1/3}$)

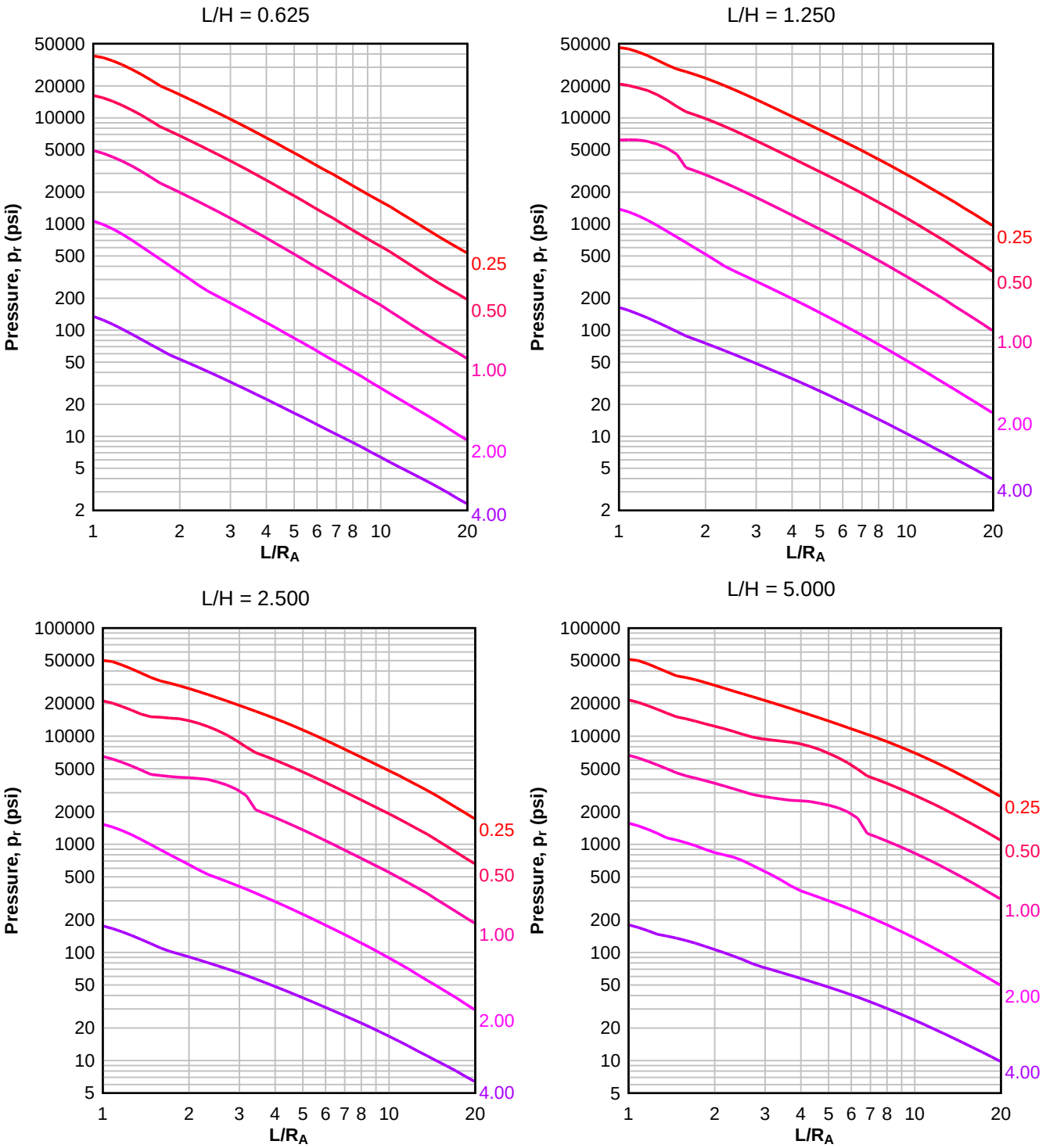

Figure 2-77 Average Peak Reflected Pressure (*N* = 2, *l*/*L* = 0.25, *h*/*H* = 0.75)

Numbers adjacent to curves indicate scaled range (ft/lb$^{1/3}$)

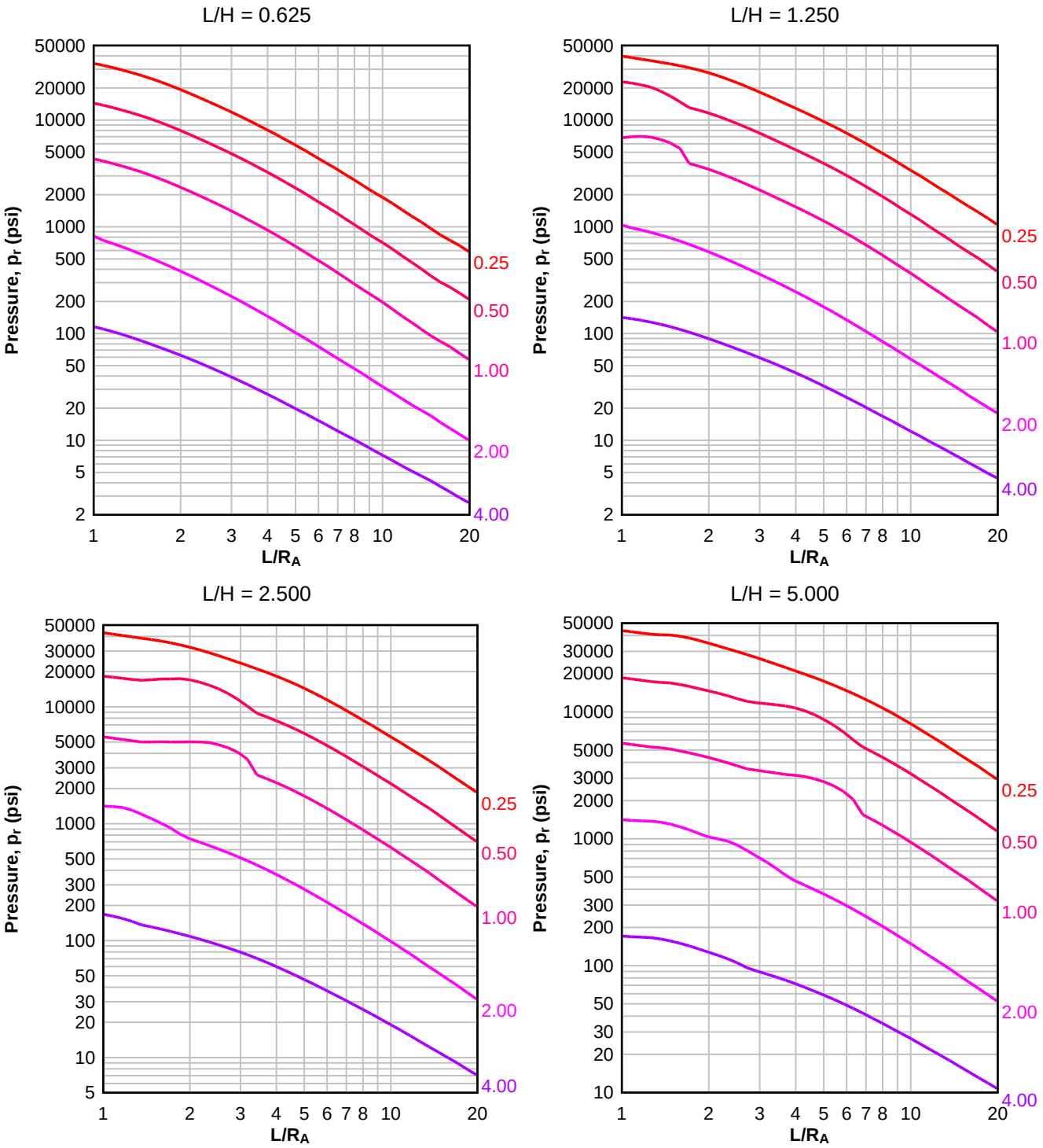

Figure 2-78 Average Peak Reflected Pressure (*N* = 2, *l*/*L* = 0.50, *h*/*H* = 0.75)

Numbers adjacent to curves indicate scaled range (ft/lb$^{1/3}$)

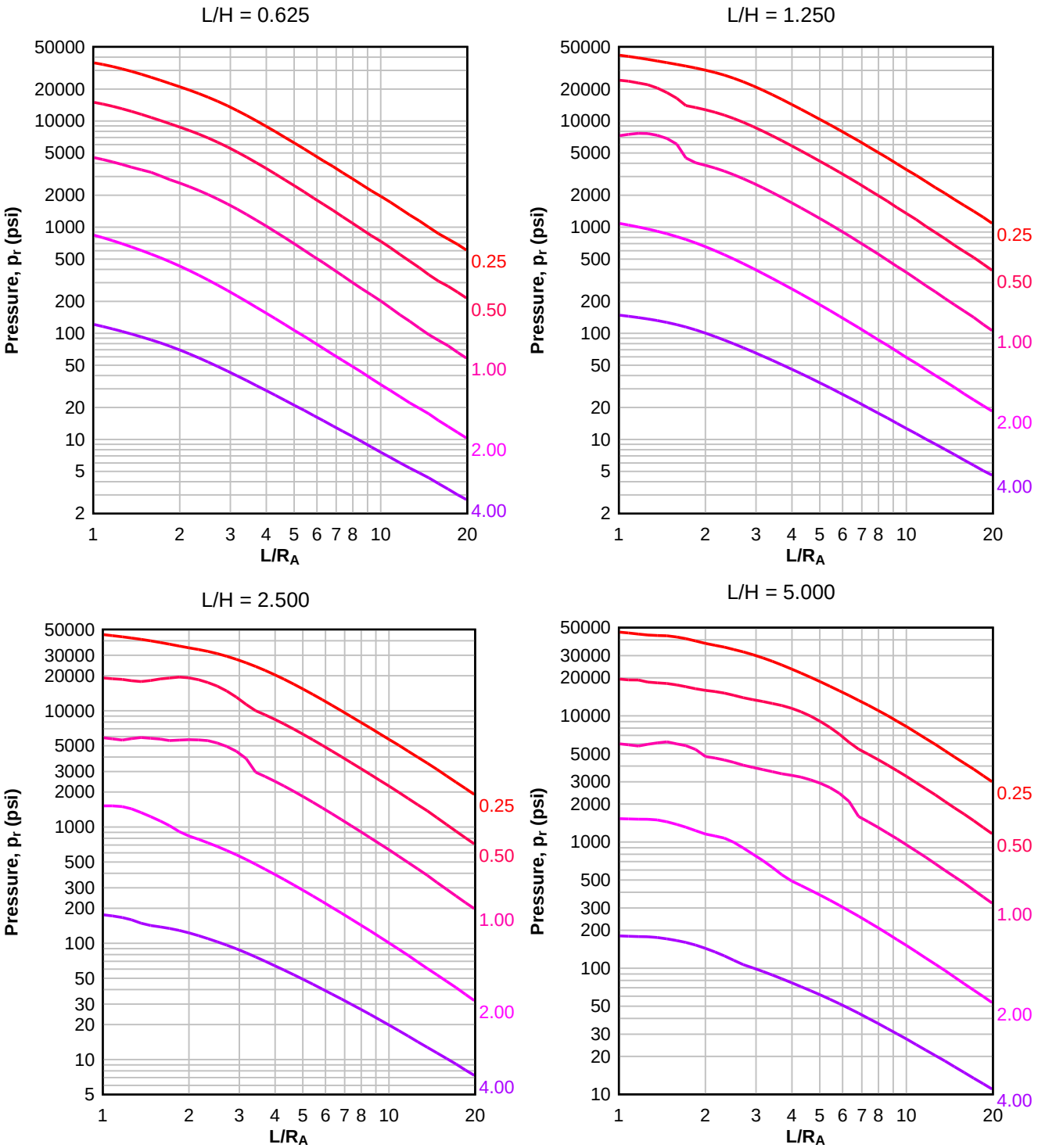

Figure 2-79 Average Peak Reflected Pressure (*N* = 2, *l*/*L* = 0.75, *h*/*H* = 0.75)

Numbers adjacent to curves indicate scaled range (ft/lb$^{1/3}$)

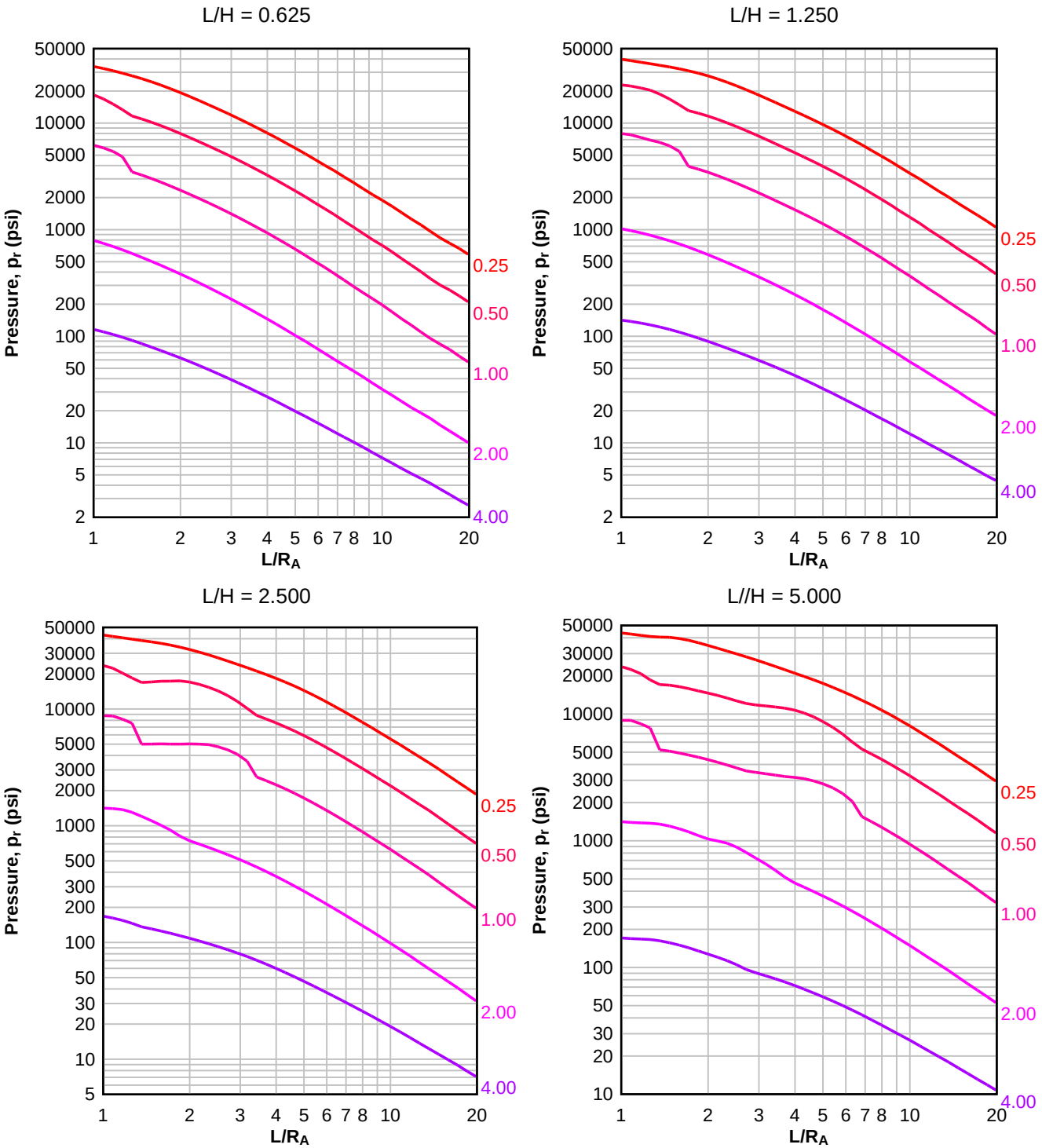

Figure 2-80 Average Peak Reflected Pressure (*N* = 3, *l*/*L* = 0.10, *h*/*H* = 0.10)

Numbers adjacent to curves indicate scaled range (ft/lb$^{1/3}$)

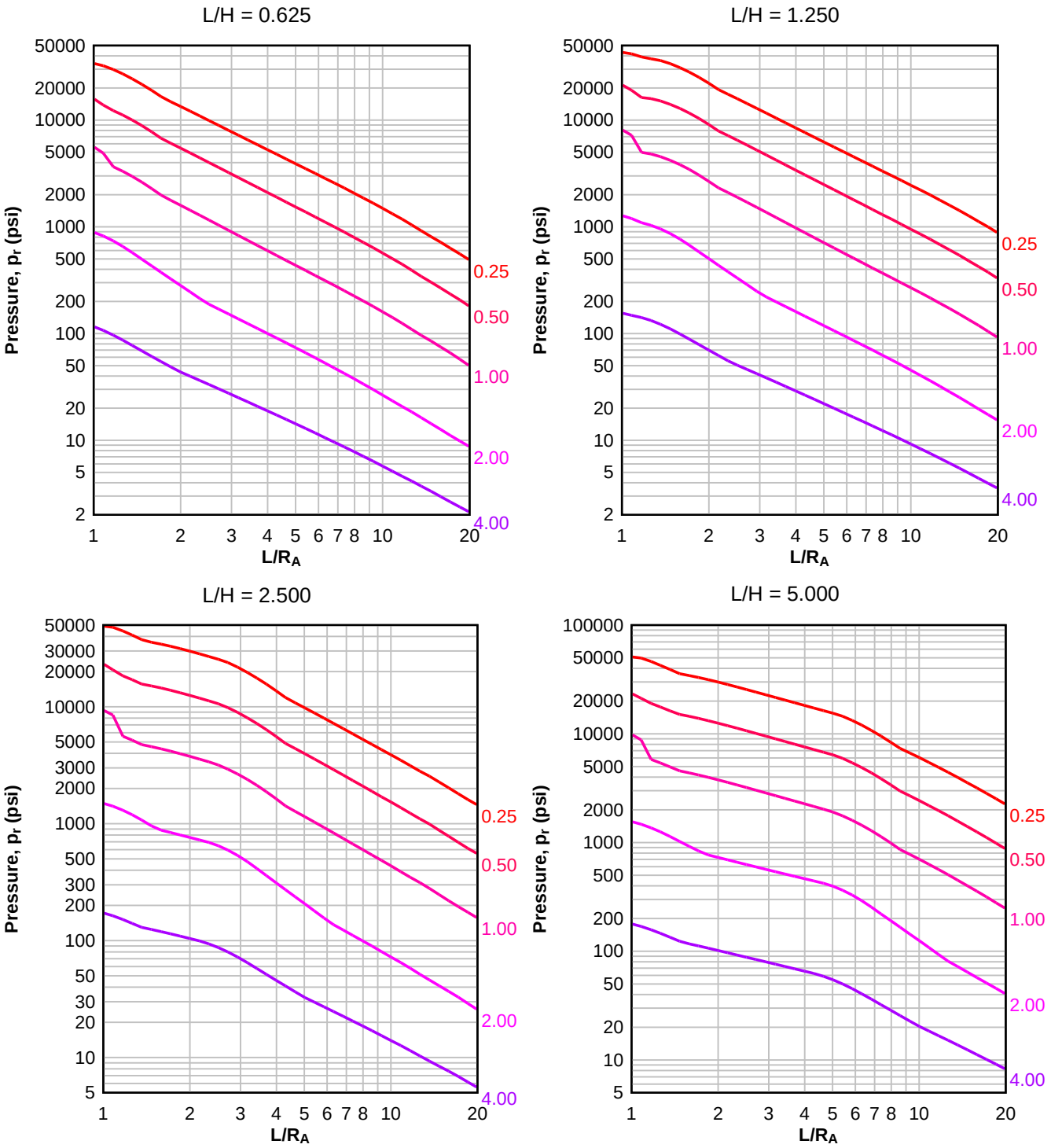

Figure 2-81 Average Peak Reflected Pressure (*N* = 3, *l/L* = 0.25 and 0.75, *h/H* = 0.10)

Numbers adjacent to curves indicate scaled range (ft/lb$^{1/3}$)

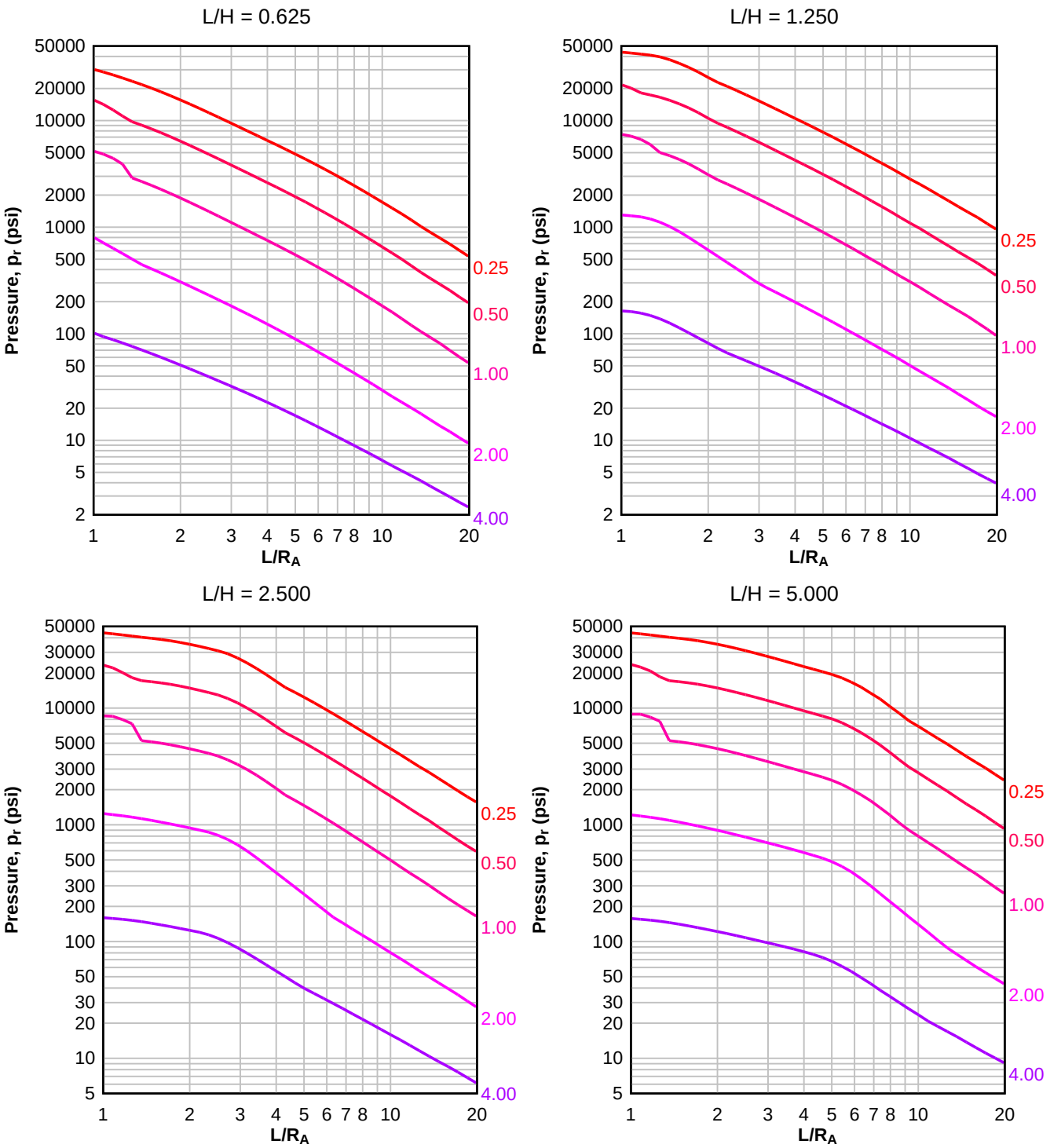

Figure 2-82 Average Peak Reflected Pressure (*N* = 3, *l*/*L* = 0.50, *h*/*H* = 0.10)

Numbers adjacent to curves indicate scaled range (ft/lb$^{1/3}$)

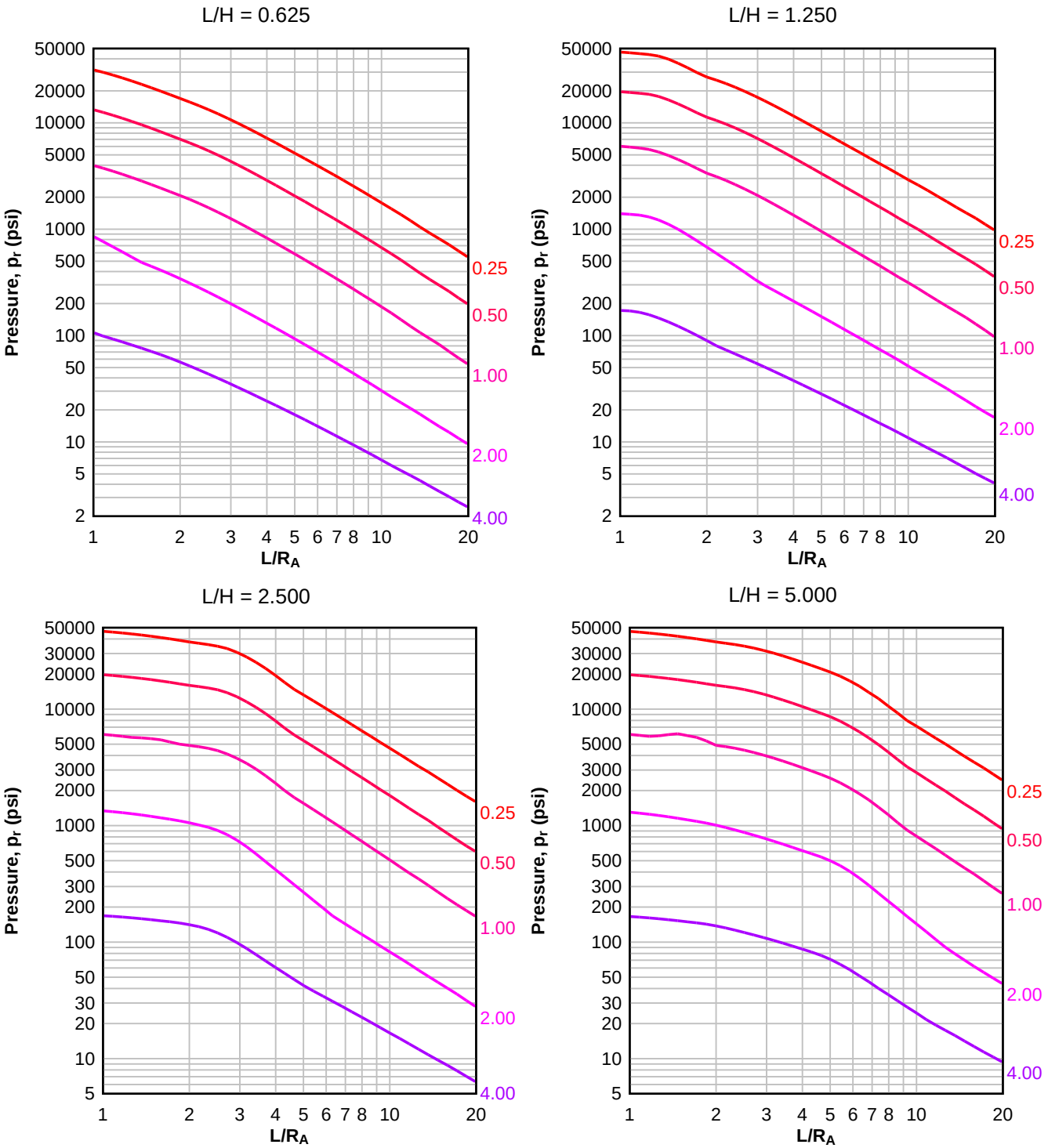

Figure 2-83 Average Peak Reflected Pressure (*N* = 3, *l*/*L* = 0.10, *h*/*H* = 0.25)

Numbers adjacent to curves indicate scaled range (ft/lb$^{1/3}$)

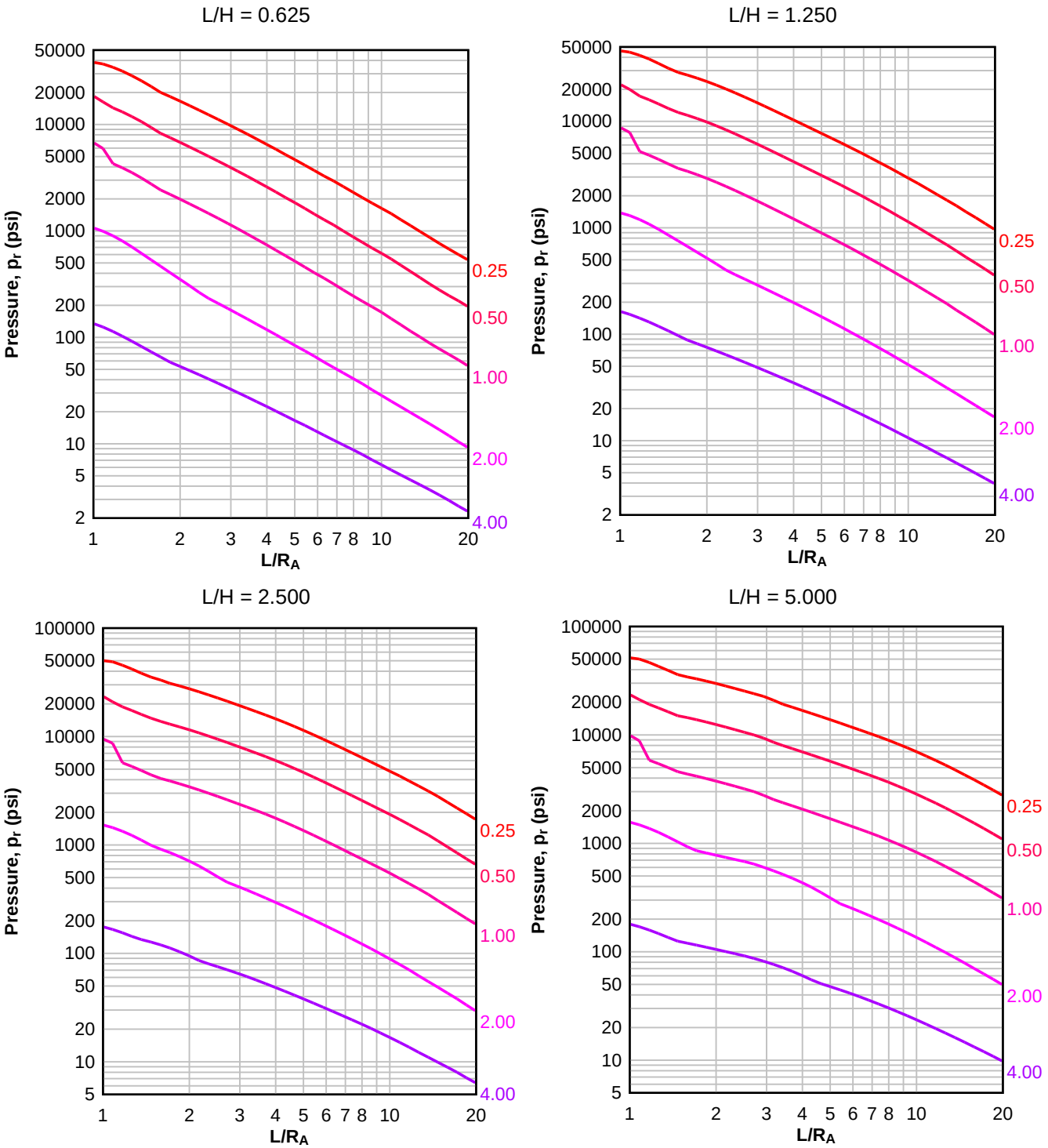

Figure 2-84 Average Peak Reflected Pressure (*N* = 3, *l/L* = 0.25 and 0.75, *h/H* = 0.25)

Numbers adjacent to curves indicate scaled range (ft/lb$^{1/3}$)

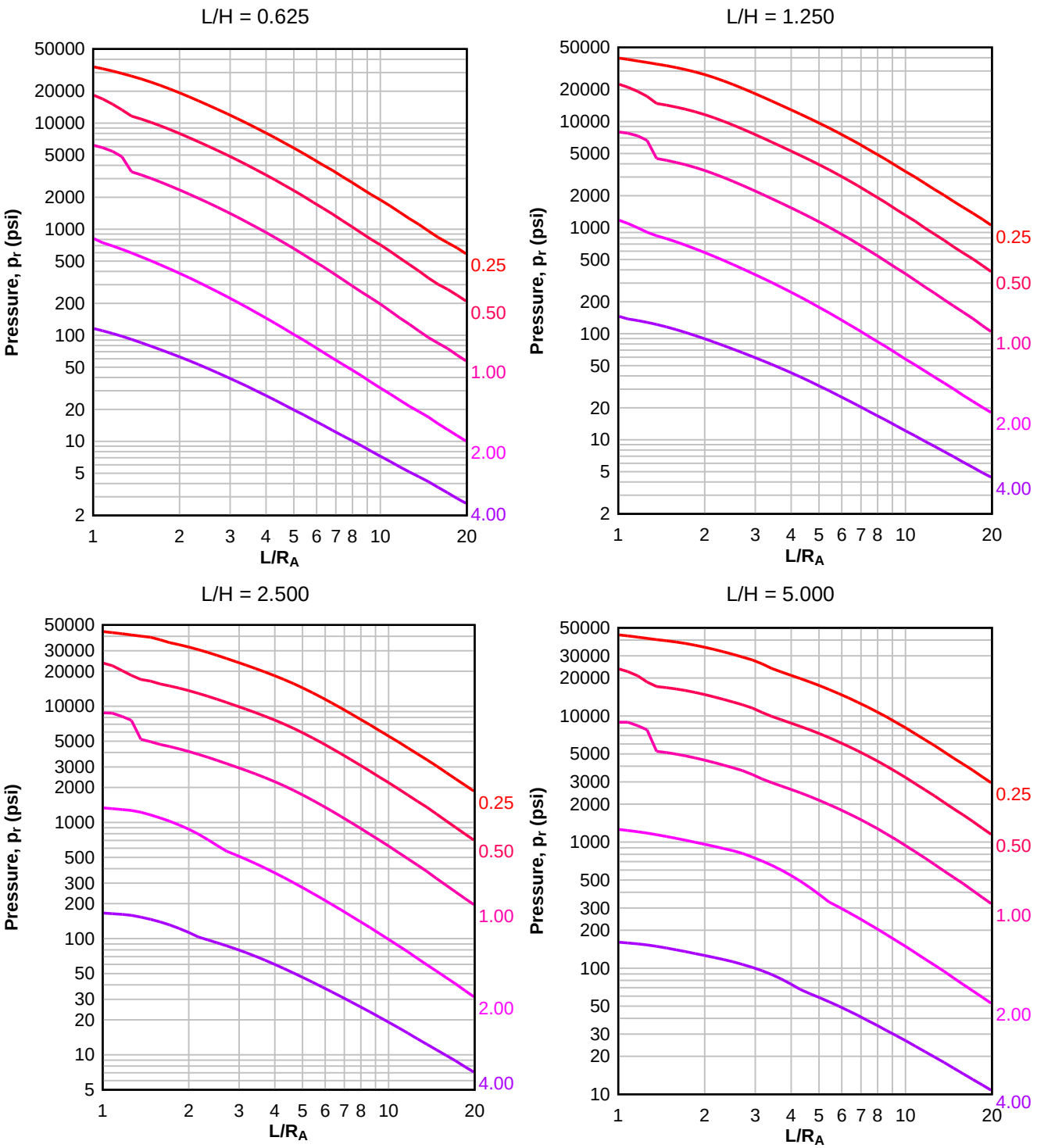

Figure 2-85 Average Peak Reflected Pressure (*N* = 3, *l*/*L* = 0.50, *h*/*H* = 0.25)

Numbers adjacent to curves indicate scaled range (ft/lb$^{1/3}$)

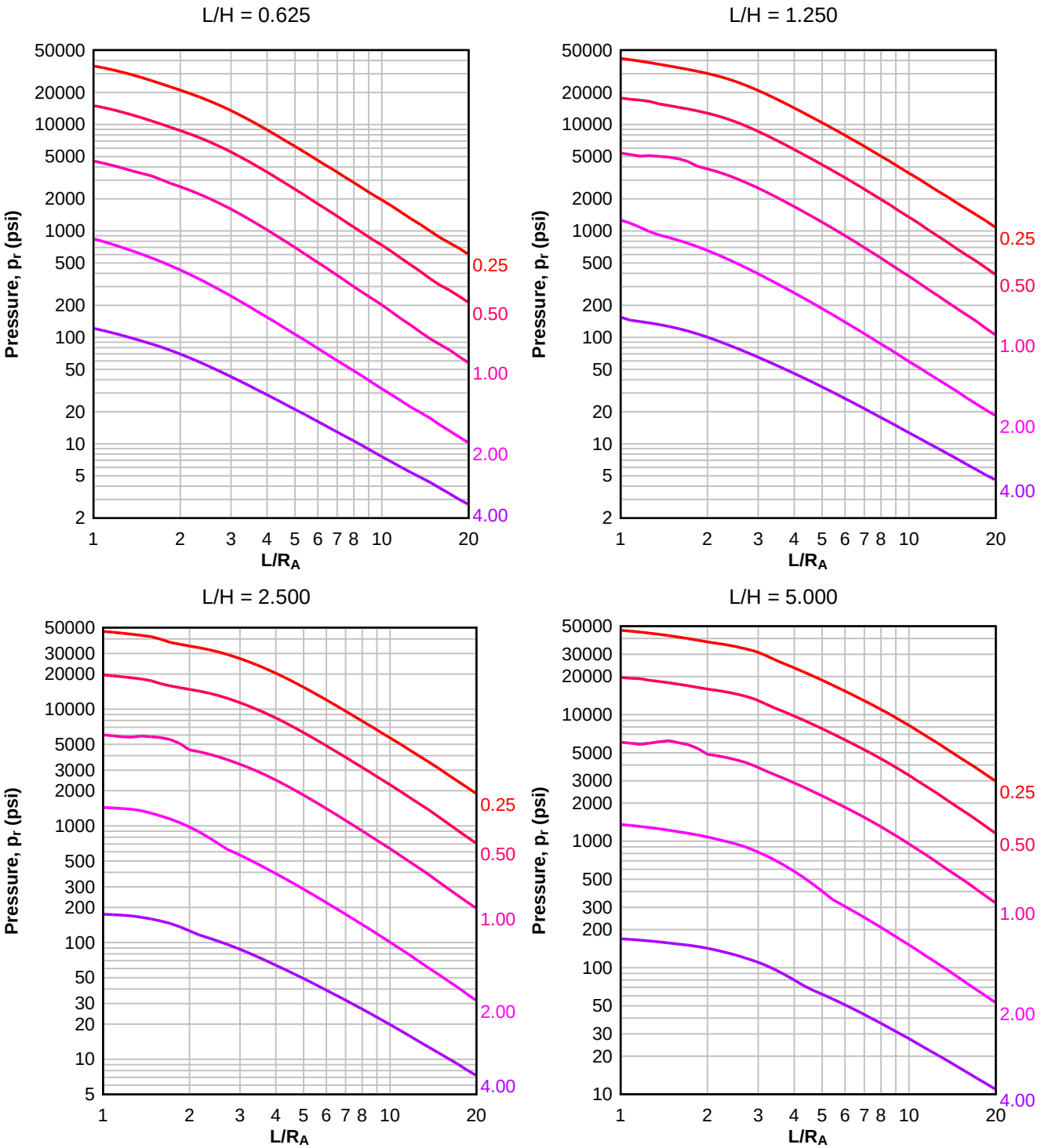

Figure 2-86 Average Peak Reflected Pressure (*N* = 3, *l*/*L* = 0.10, *h*/*H* = 0.50)

Numbers adjacent to curves indicate scaled range (ft/lb$^{1/3}$)

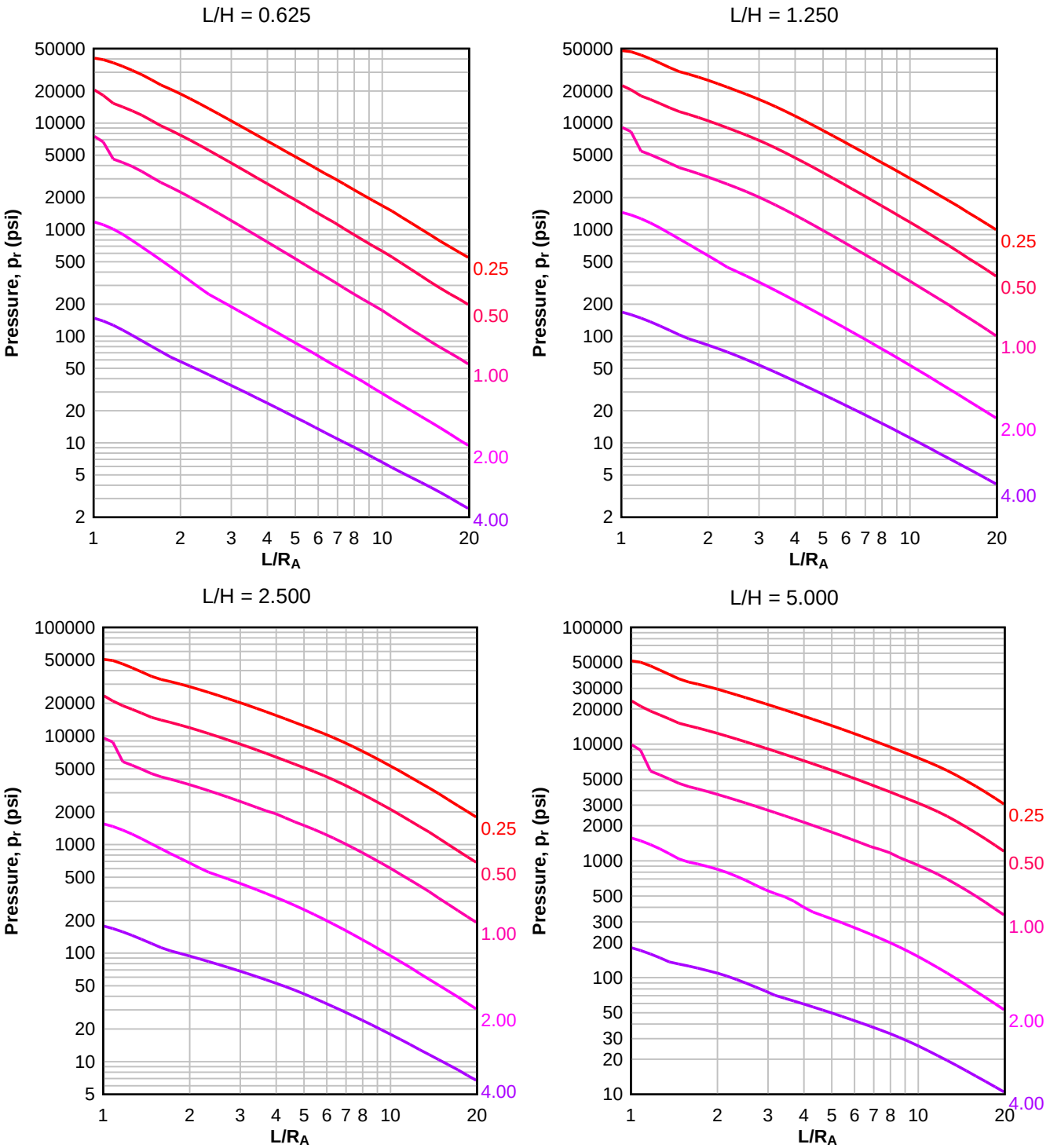

Figure 2-87 Average Peak Reflected Pressure (*N* = 3, *l/L* = 0.25 and 0.75, *h/H* = 0.50)

Numbers adjacent to curves indicate scaled range (ft/lb$^{1/3}$)

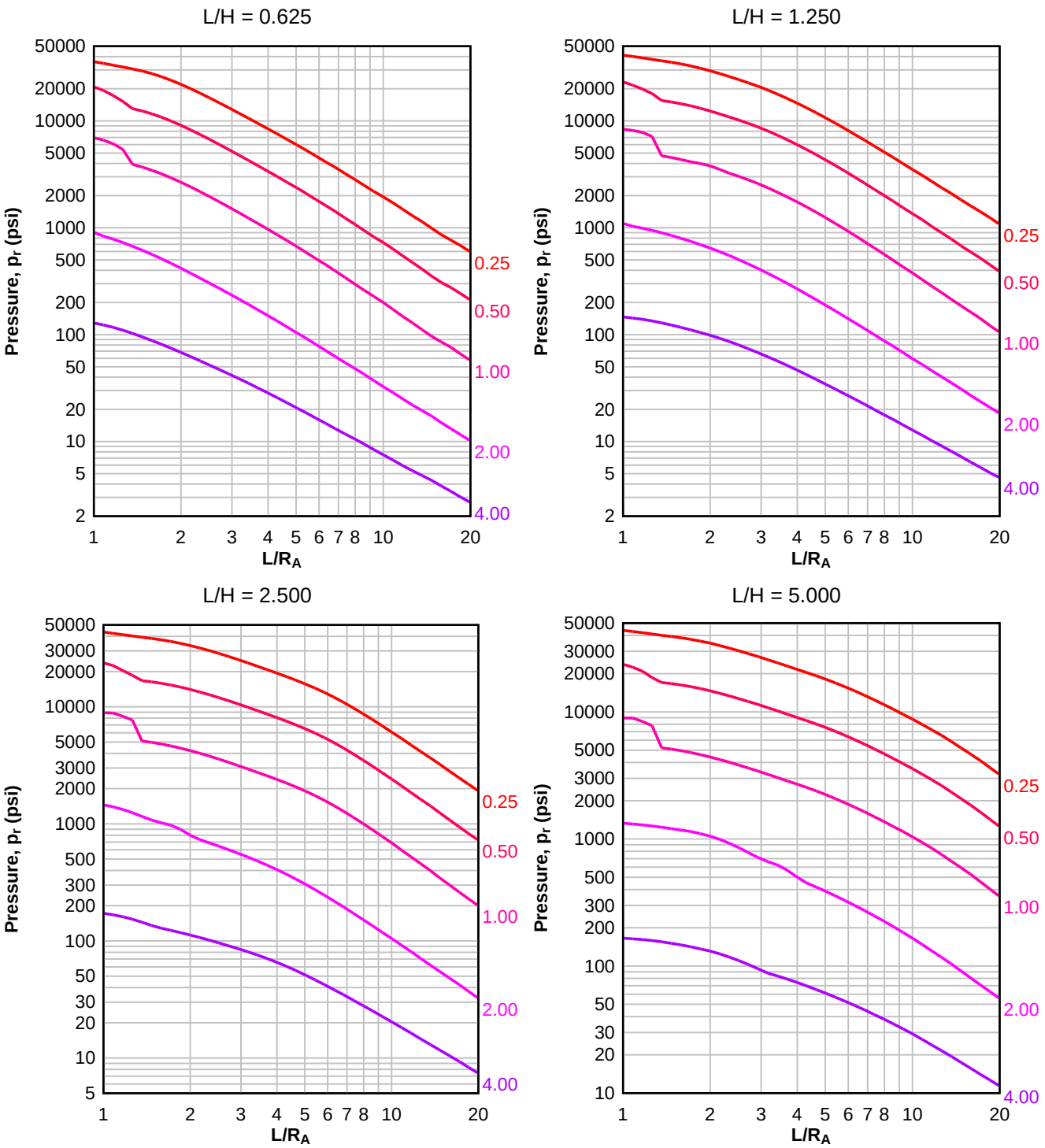

Figure 2-88 Average Peak Reflected Pressure (*N* = 3, *l*/*L* = 0.50, *h*/*H* = 0.50)

Numbers adjacent to curves indicate scaled range (ft/lb$^{1/3}$)

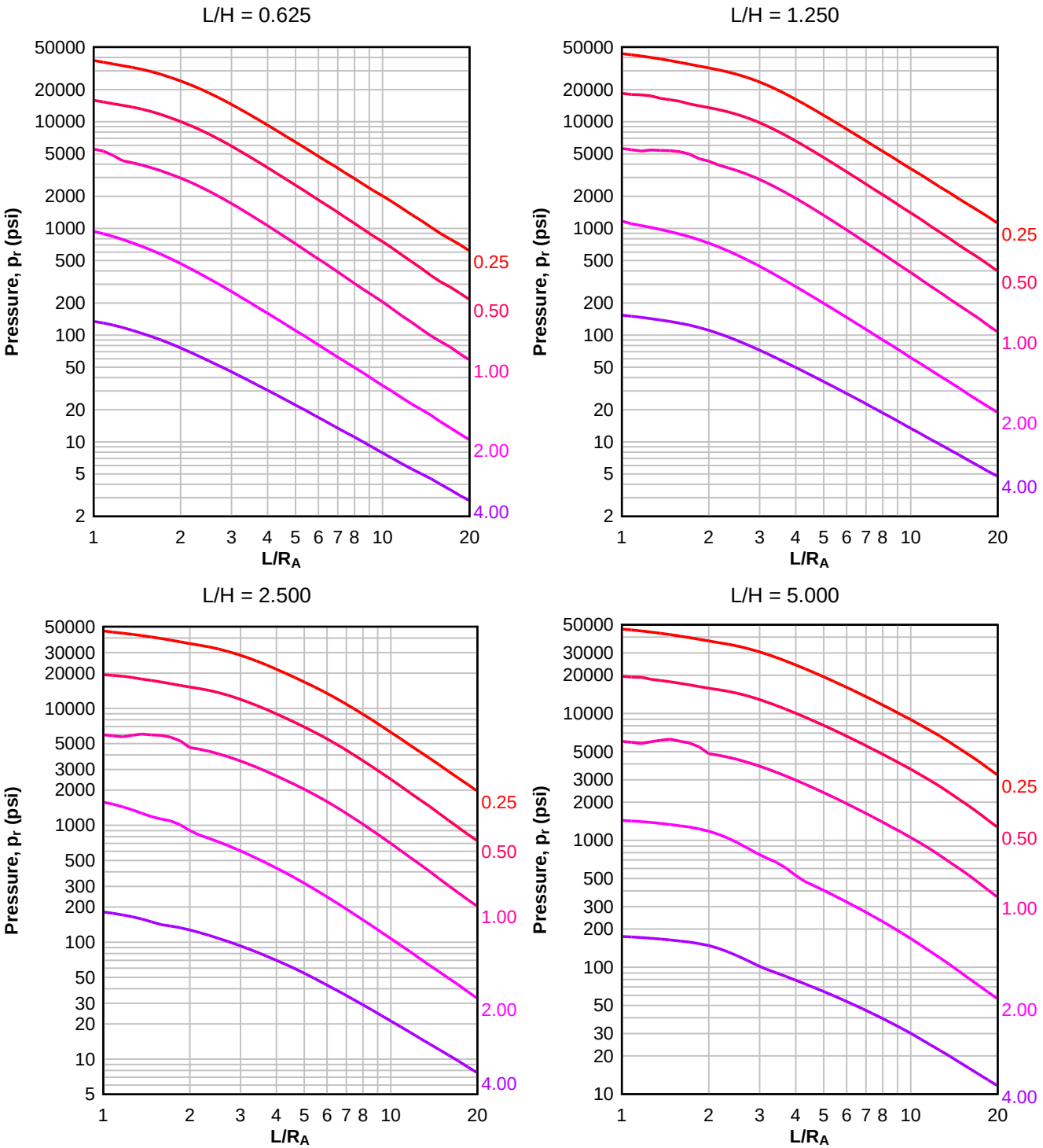

Figure 2-89 Average Peak Reflected Pressure (*N* = 3, *l*/*L* = 0.10, *h*/*H* = 0.75)

Numbers adjacent to curves indicate scaled range (ft/lb$^{1/3}$)

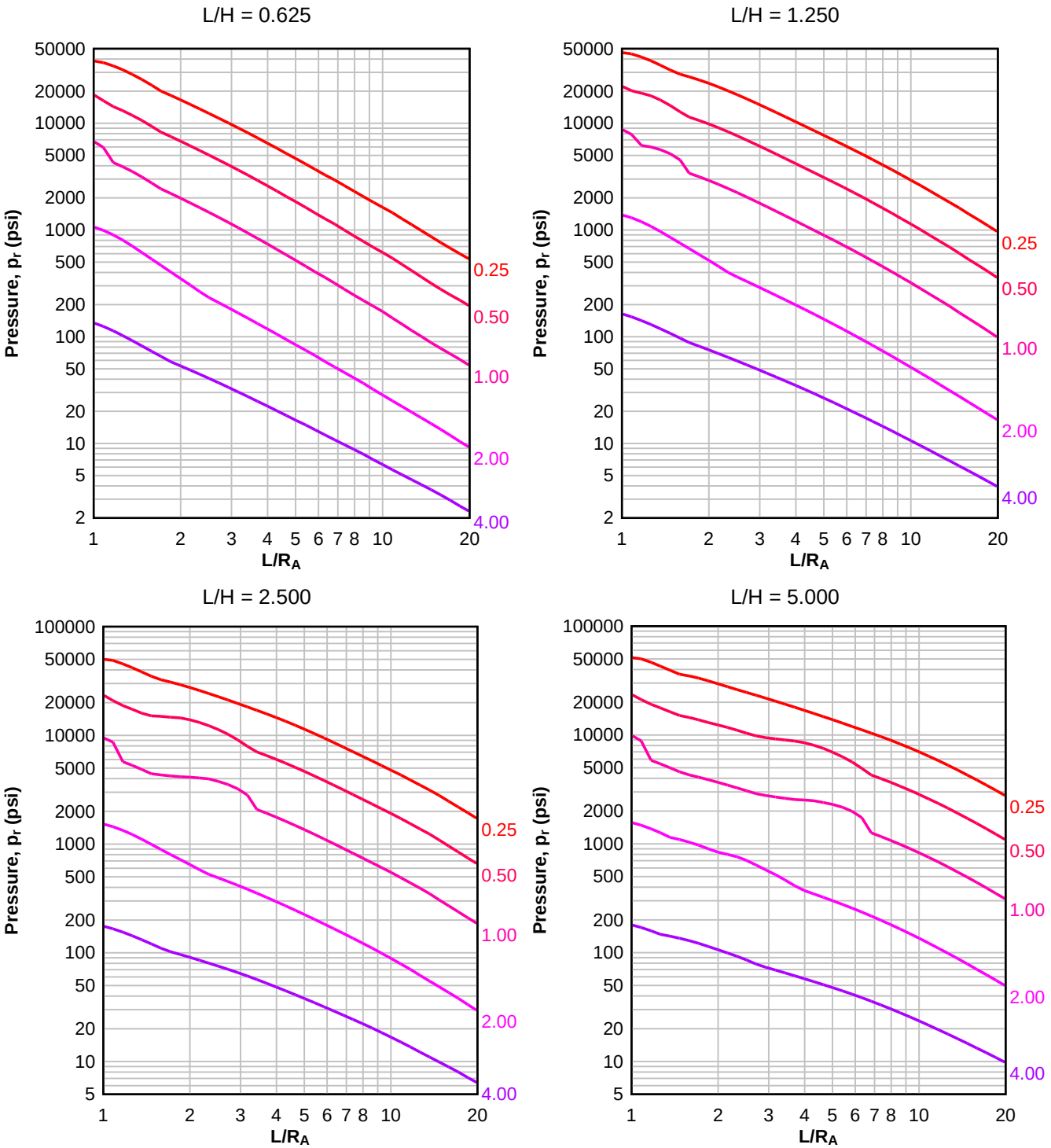

Figure 2-90 Average Peak Reflected Pressure (*N* = 3, *l/L* = 0.25 and 0.75, *h/H* = 0.75)

Numbers adjacent to curves indicate scaled range (ft/lb$^{1/3}$)

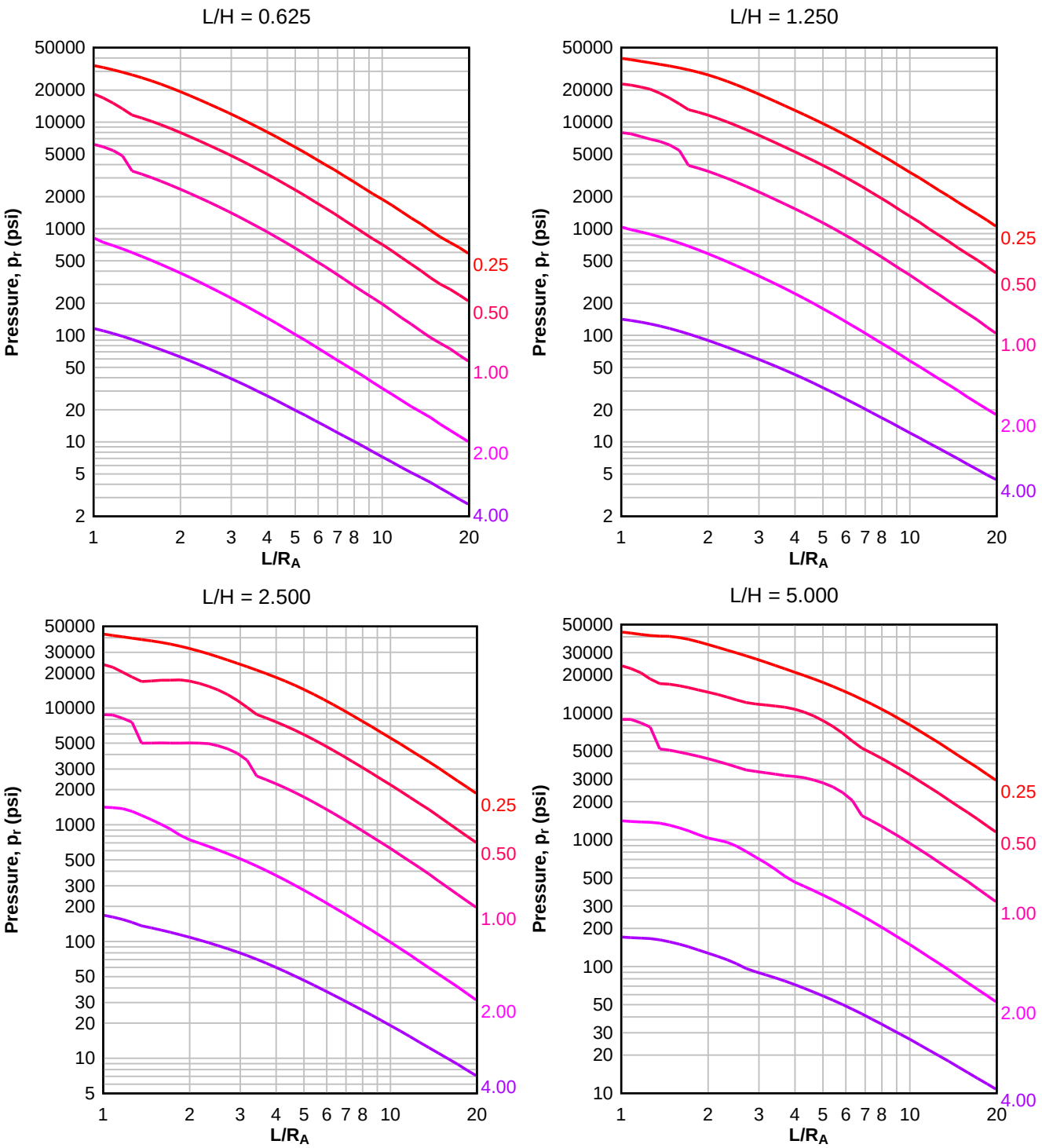

Figure 2-91 Average Peak Reflected Pressure (*N* = 3, *l/L* = 0.50, *h/H* = 0.75)

Numbers adjacent to curves indicate scaled range (ft/lb$^{1/3}$)

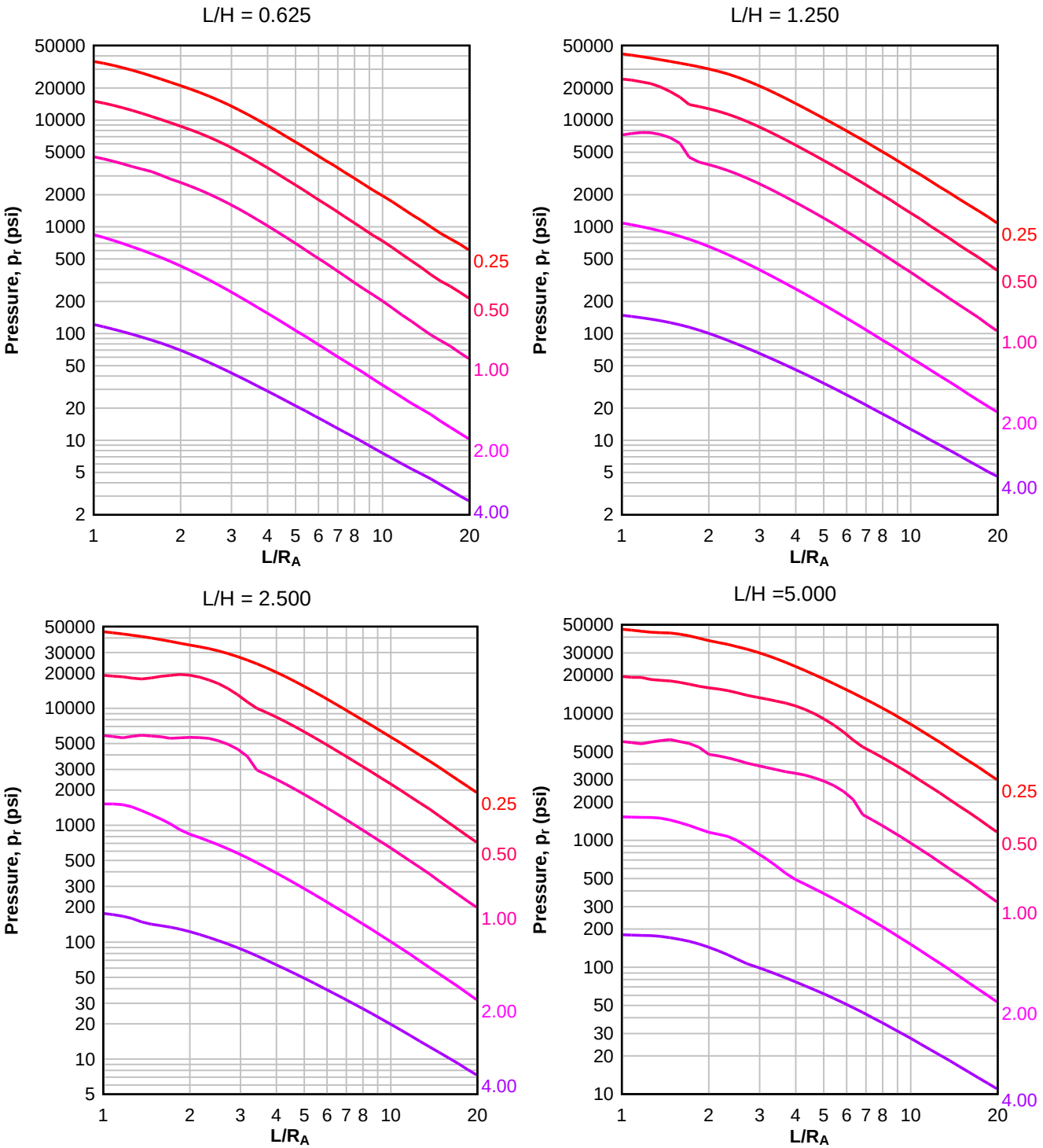

Figure 2-92 Average Peak Reflected Pressure (*N* = 4, *l*/*L* = 0.10, *h*/*H* = 0.10)

Numbers adjacent to curves indicate scaled range (ft/lb$^{1/3}$)

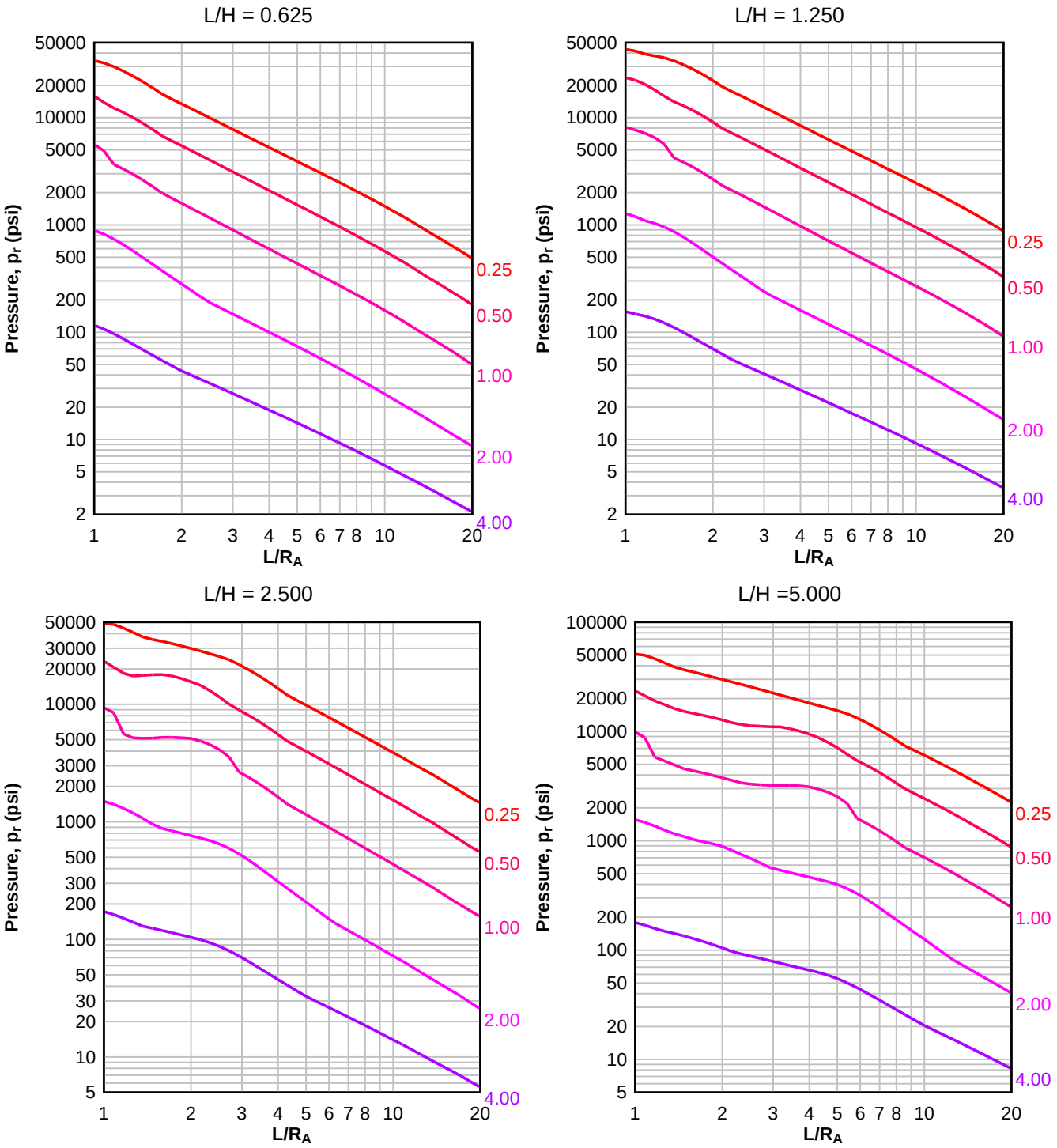

Figure 2-93 Average Peak Reflected Pressure (*N* = 4, *l/L* = 0.25 and 0.75, *h/H* = 0.10)

Numbers adjacent to curves indicate scaled range (ft/lb$^{1/3}$)

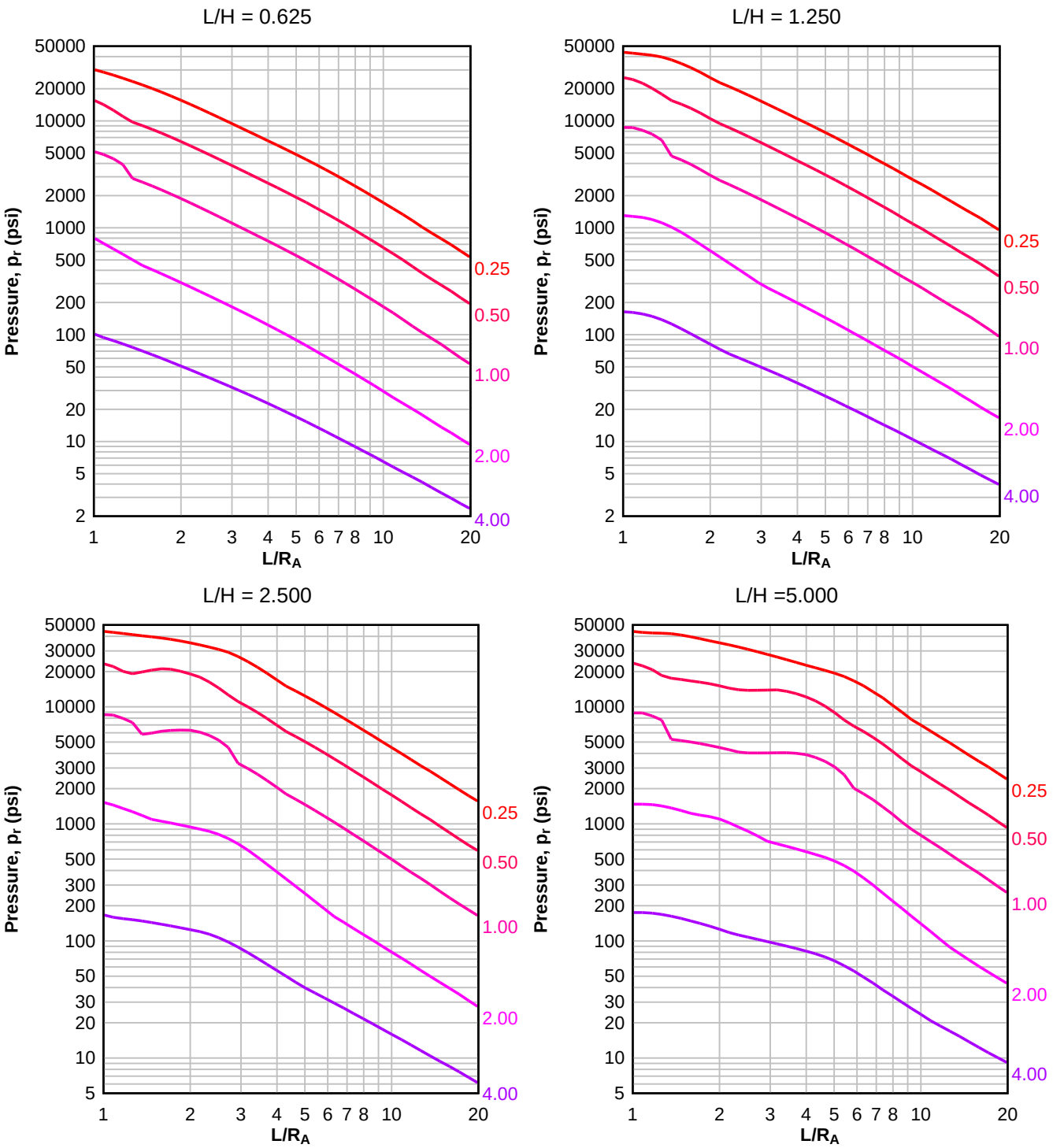

Figure 2-94 Average Peak Reflected Pressure (*N* = 4, *l/L* = 0.50, *h/H* = 0.10)

Numbers adjacent to curves indicate scaled range (ft/lb$^{1/3}$)

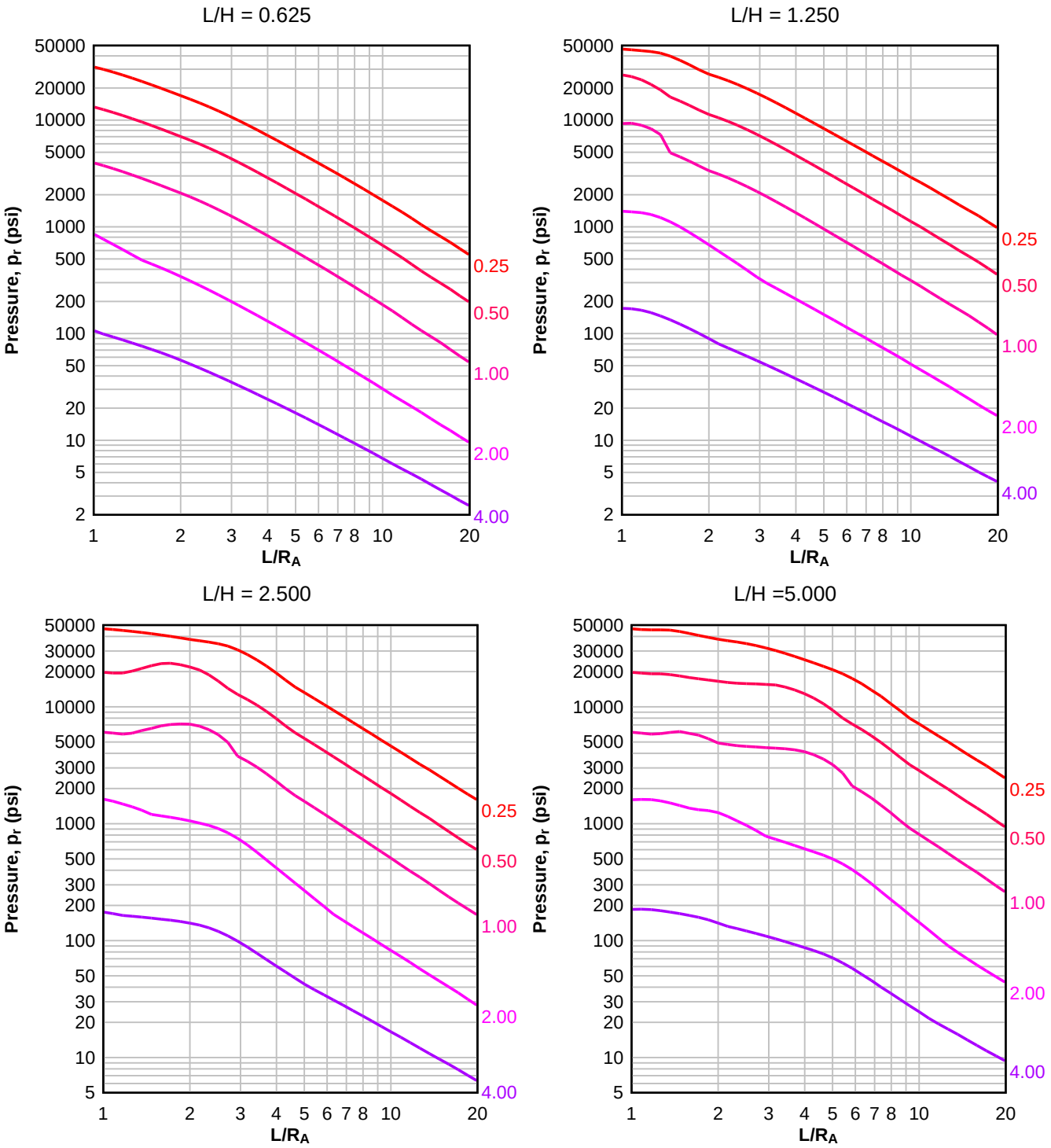

Figure 2-95 Average Peak Reflected Pressure (*N* = 4, *l/L* = 0.10, *h/H* = 0.25 and 0.75)

Numbers adjacent to curves indicate scaled range (ft/lb$^{1/3}$)

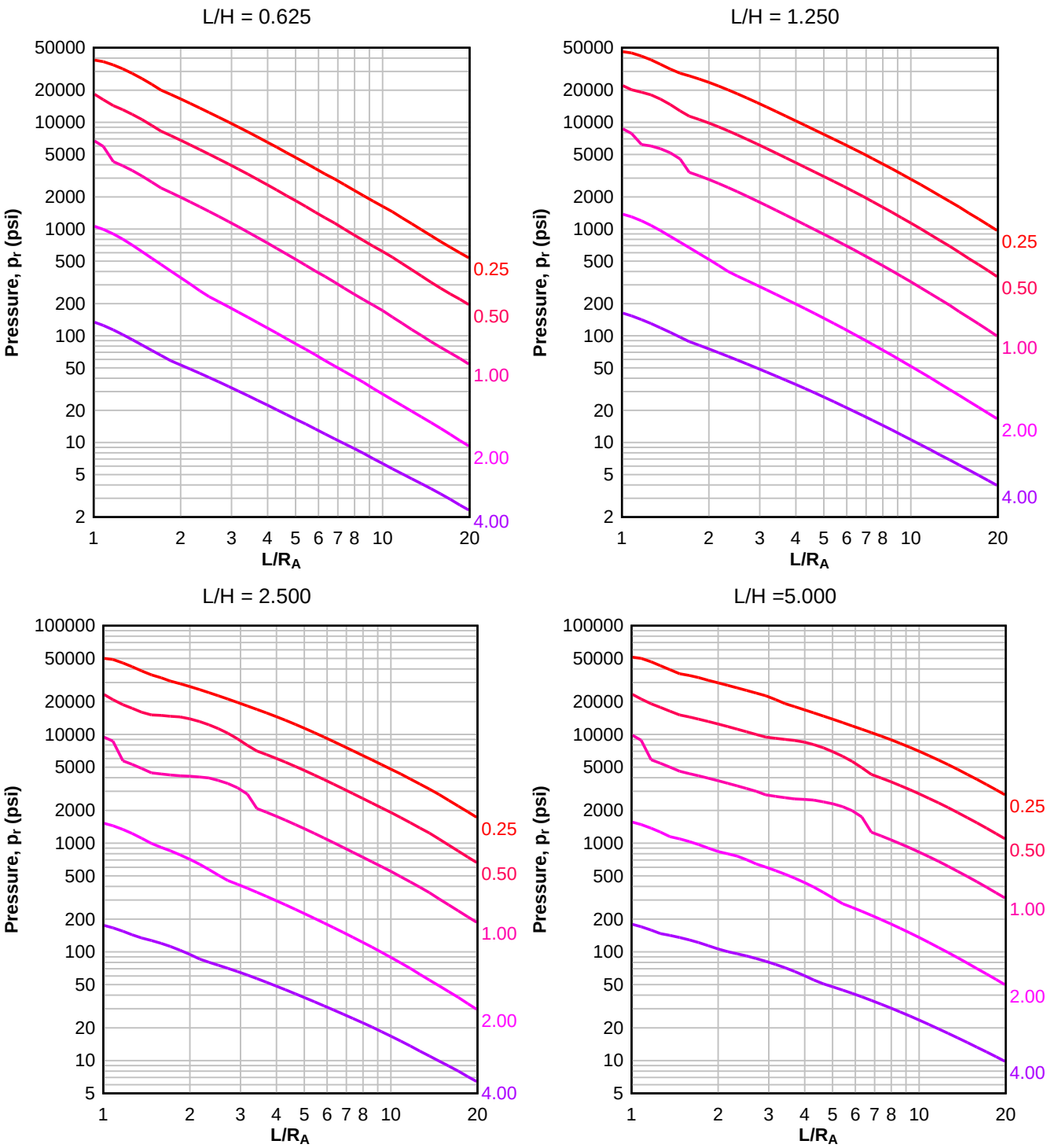

Figure 2-96 Average Peak Reflected Pressure (*N* = 4, *l/L* = 0.25 and 0.75, *h/H* = 0.25 and 0.75)

Numbers adjacent to curves indicate scaled range (ft/lb$^{1/3}$)

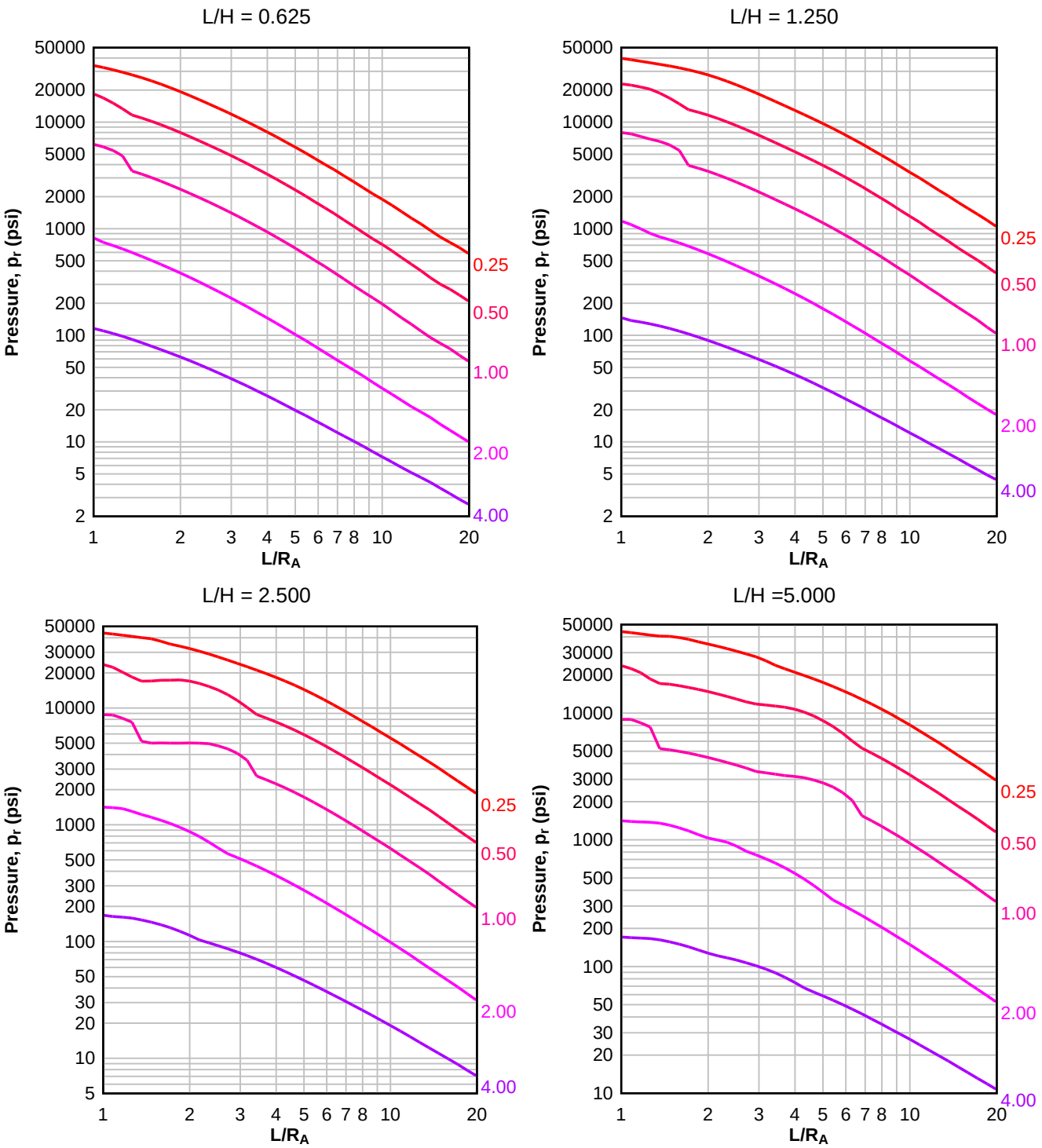

Figure 2-97 Average Peak Reflected Pressure (*N* = 4, *l/L* = 0.50, *h/H* = 0.25 and 0.75)

Numbers adjacent to curves indicate scaled range (ft/lb$^{1/3}$)

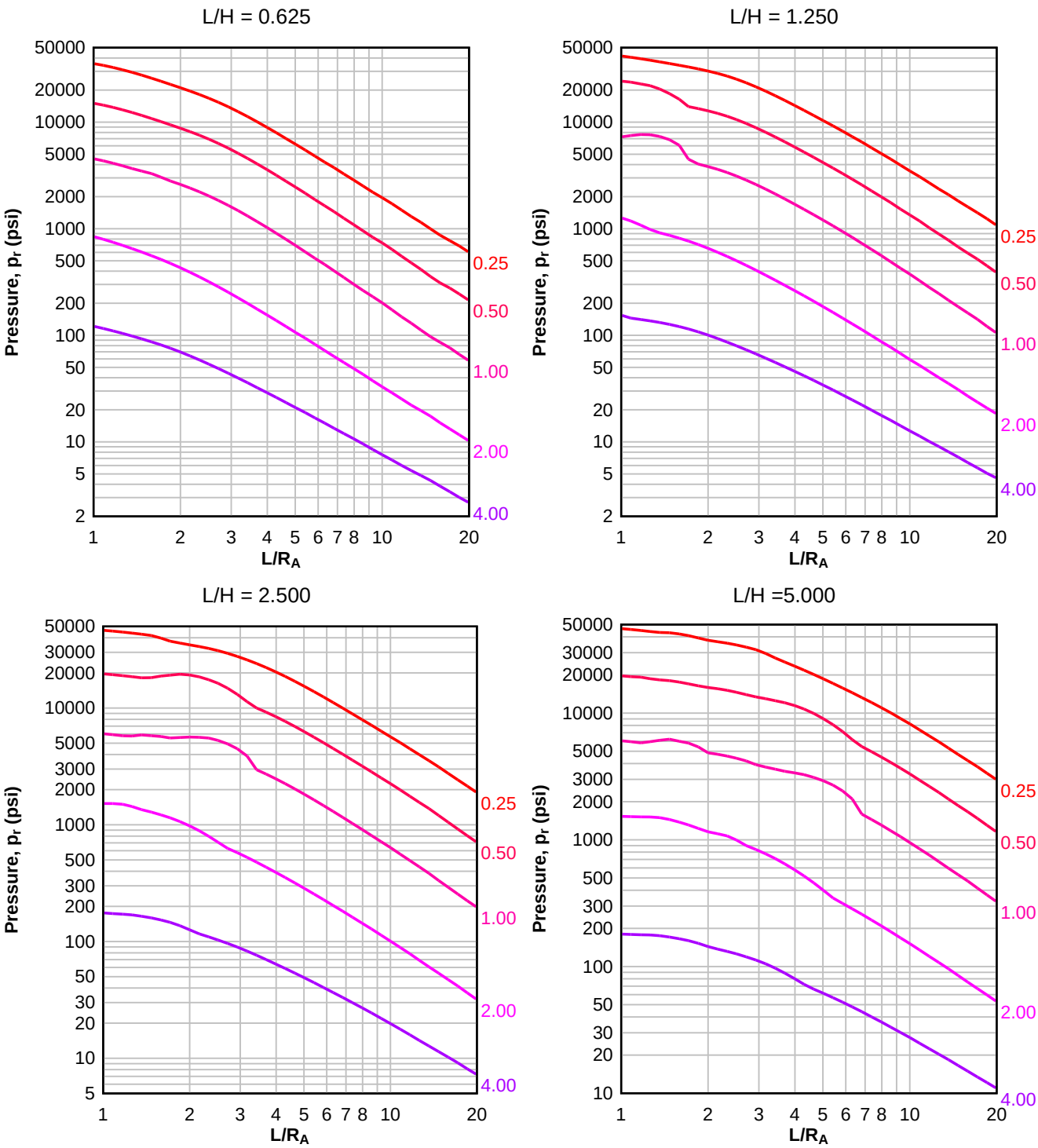

Figure 2-98 Average Peak Reflected Pressure (*N* = 4, *l/L* = 0.10, *h/H* = 0.50)

Numbers adjacent to curves indicate scaled range (ft/lb$^{1/3}$)

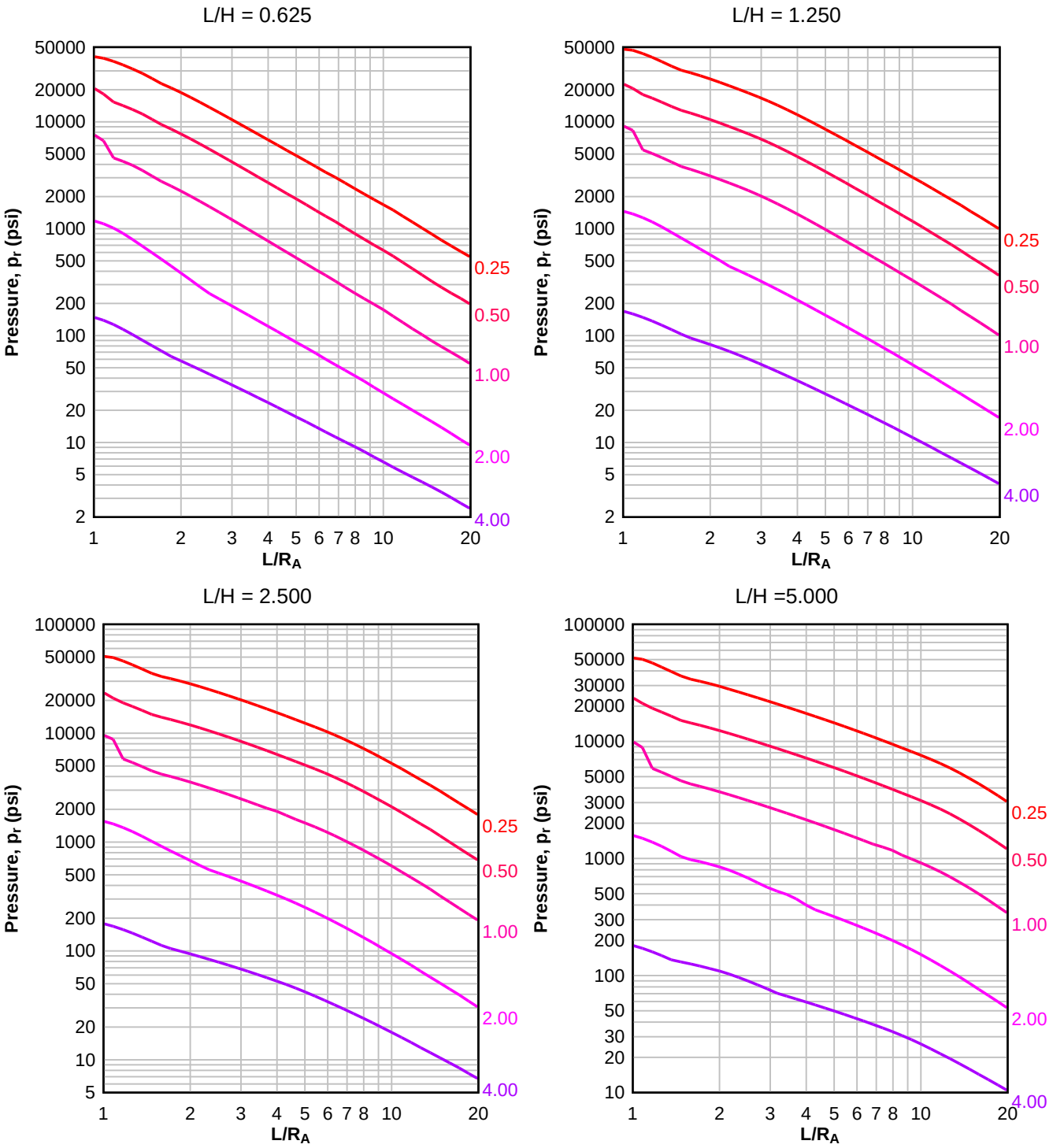

Figure 2-99 Average Peak Reflected Pressure (*N* = 4, *l/L* = 0.25 and 0.75, *h/H* = 0.50)

Numbers adjacent to curves indicate scaled range (ft/lb$^{1/3}$)

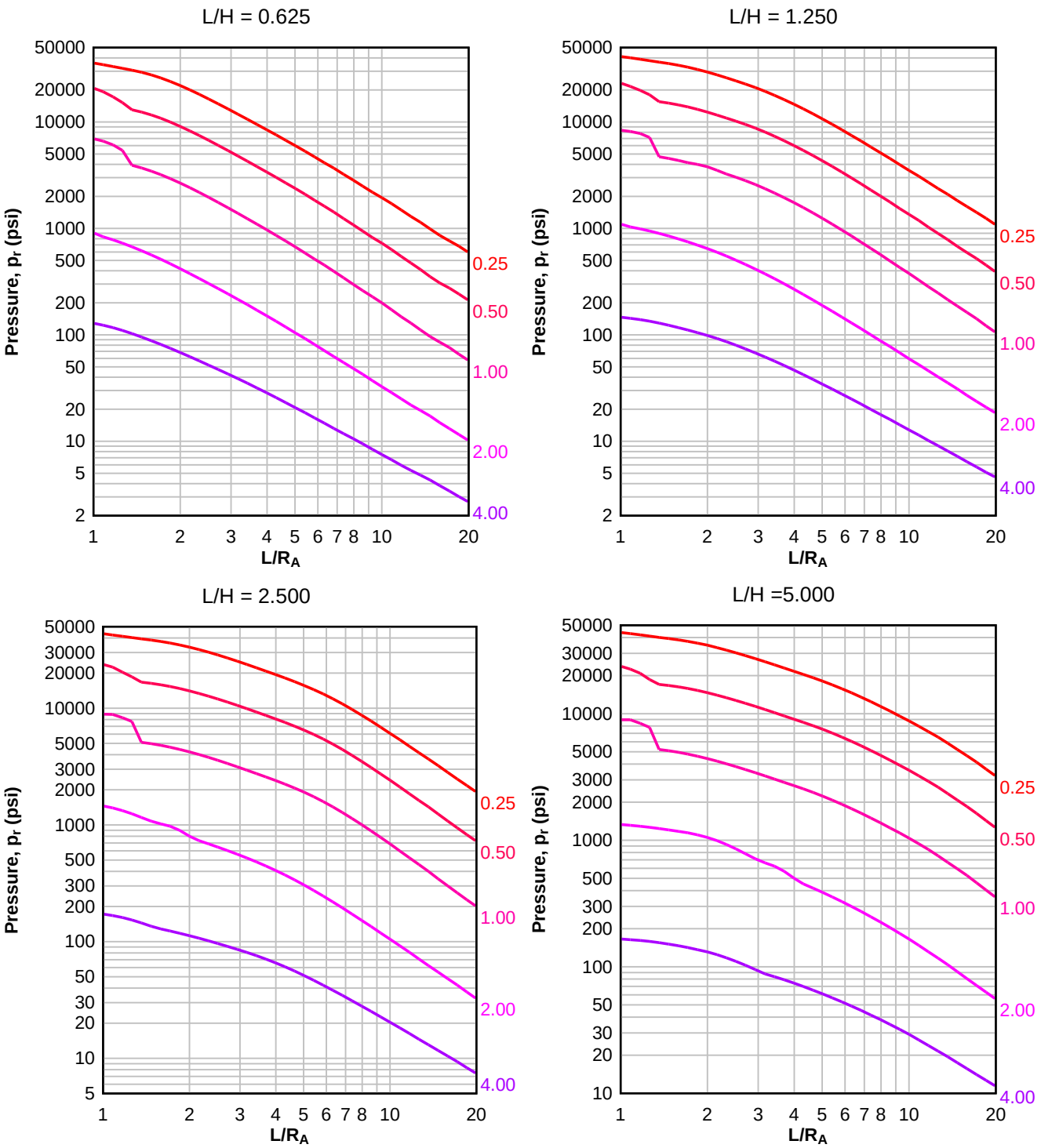

Figure 2-100 Average Peak Reflected Pressure (*N* = 4, *l/L* = 0.50, *h/H* = 0.50)

Numbers adjacent to curves indicate scaled range (ft/lb$^{1/3}$)

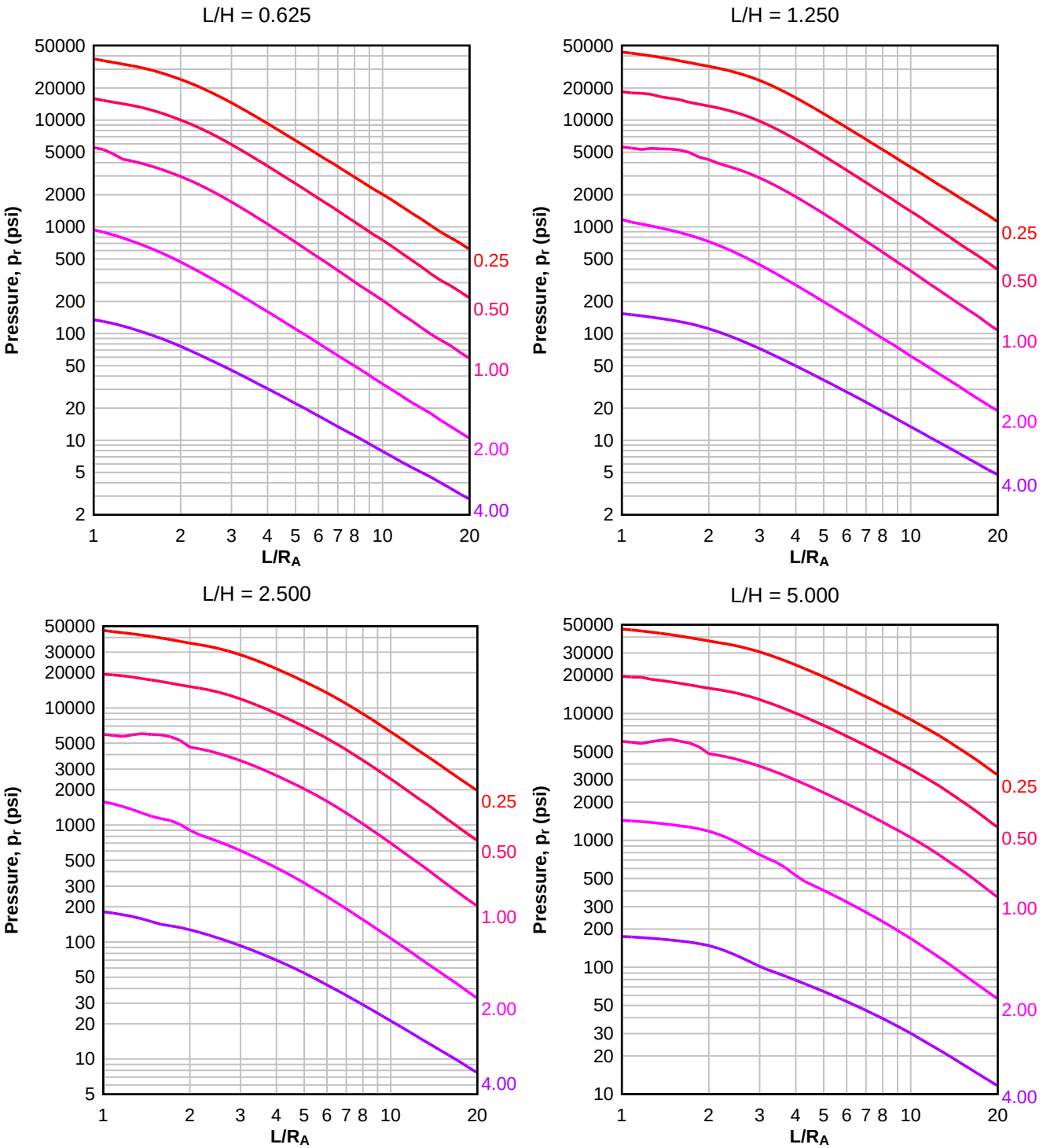

Figure 2-101 Scaled Average Unit Reflected Impulse (*N* = 1, *l*/*L* = 0.10, *h*/*H* = 0.10)

Numbers adjacent to curves indicate scaled range (ft/lb$^{1/3}$)

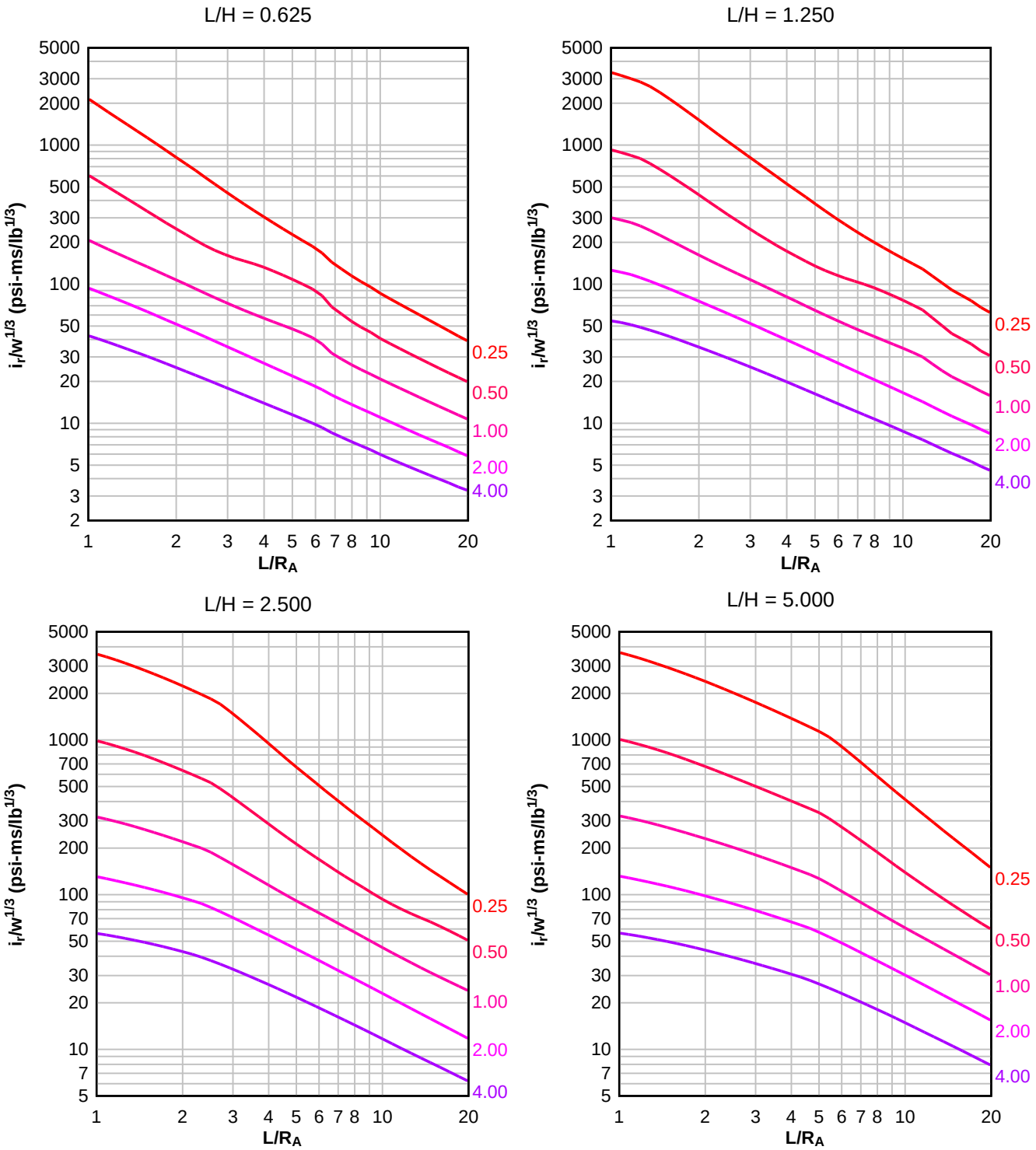

Figure 2-102 Scaled Average Unit Reflected Impulse (*N* = 1, *l/L* = 0.25 and 0.75, *h/H* = 0.10)

Numbers adjacent to curves indicate scaled range (ft/lb$^{1/3}$)

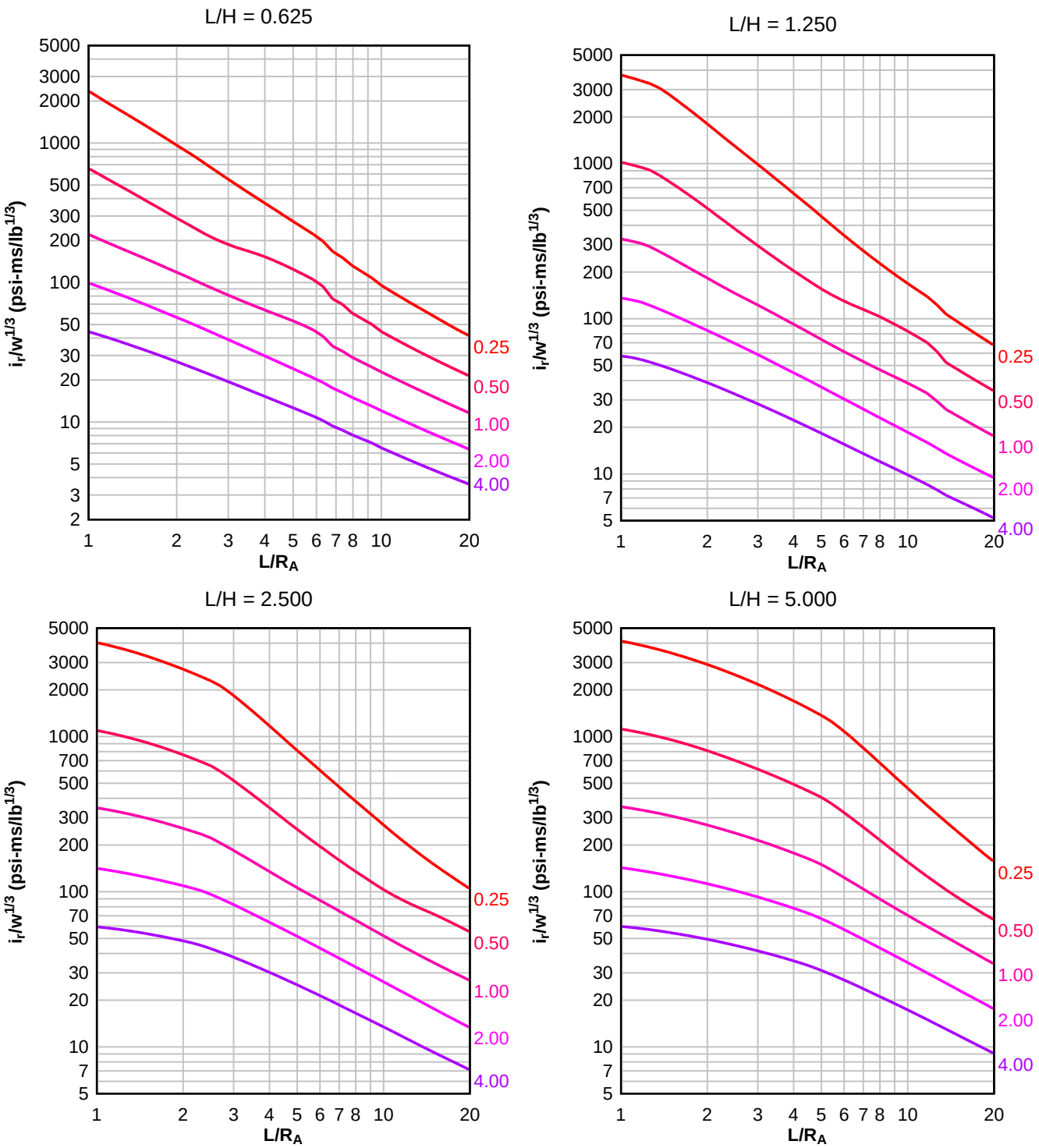

Figure 2-103 Scaled Average Unit Reflected Impulse (*N* = 1, *l/L* = 0.50, *h/H* = 0.10)

Numbers adjacent to curves indicate scaled range (ft/lb$^{1/3}$)

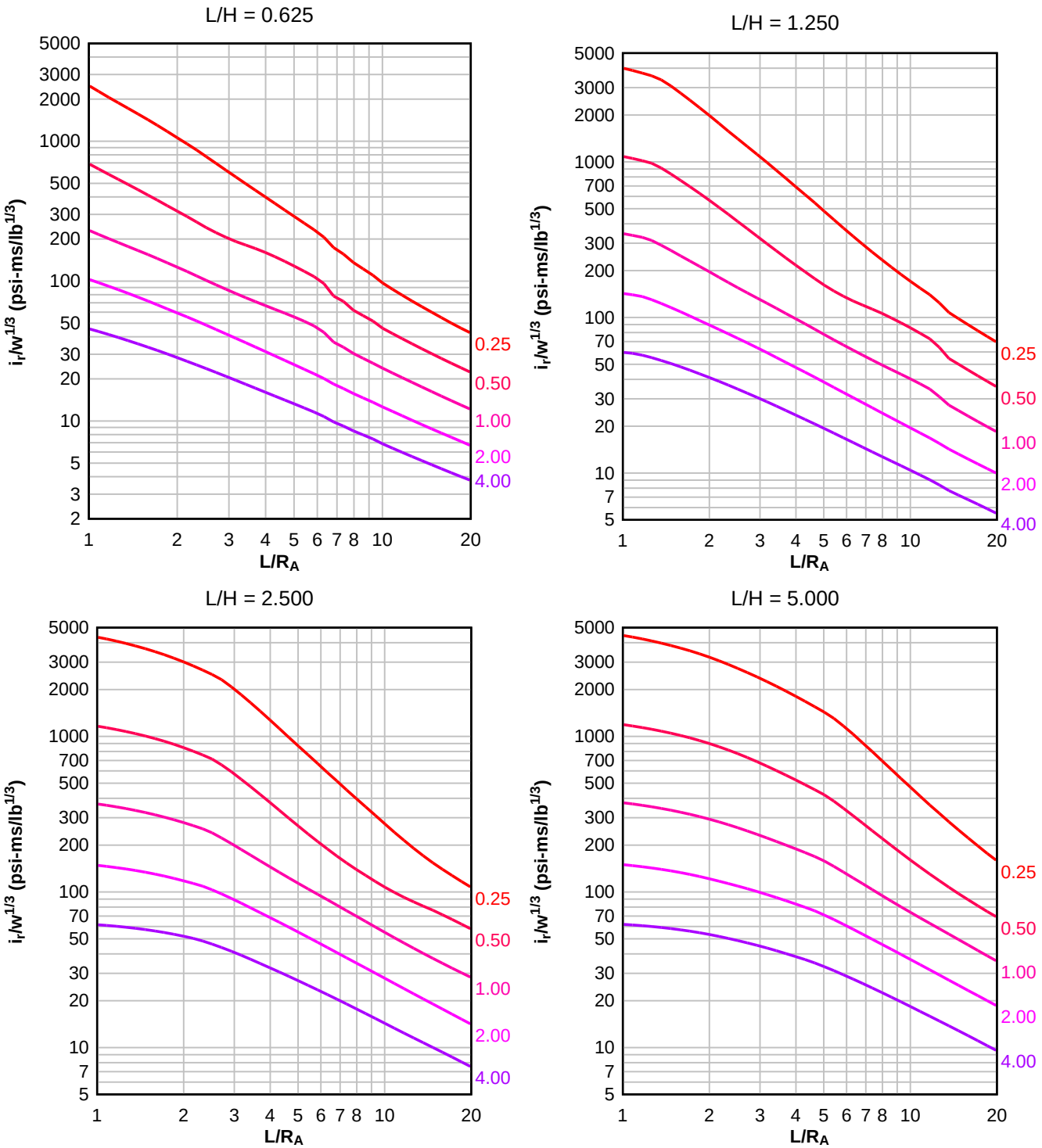

Figure 2-104 Scaled Average Unit Reflected Impulse (*N* = 1, *l/L* = 0.10, *h/H* = 0.25)

Numbers adjacent to curves indicate scaled range (ft/lb$^{1/3}$)

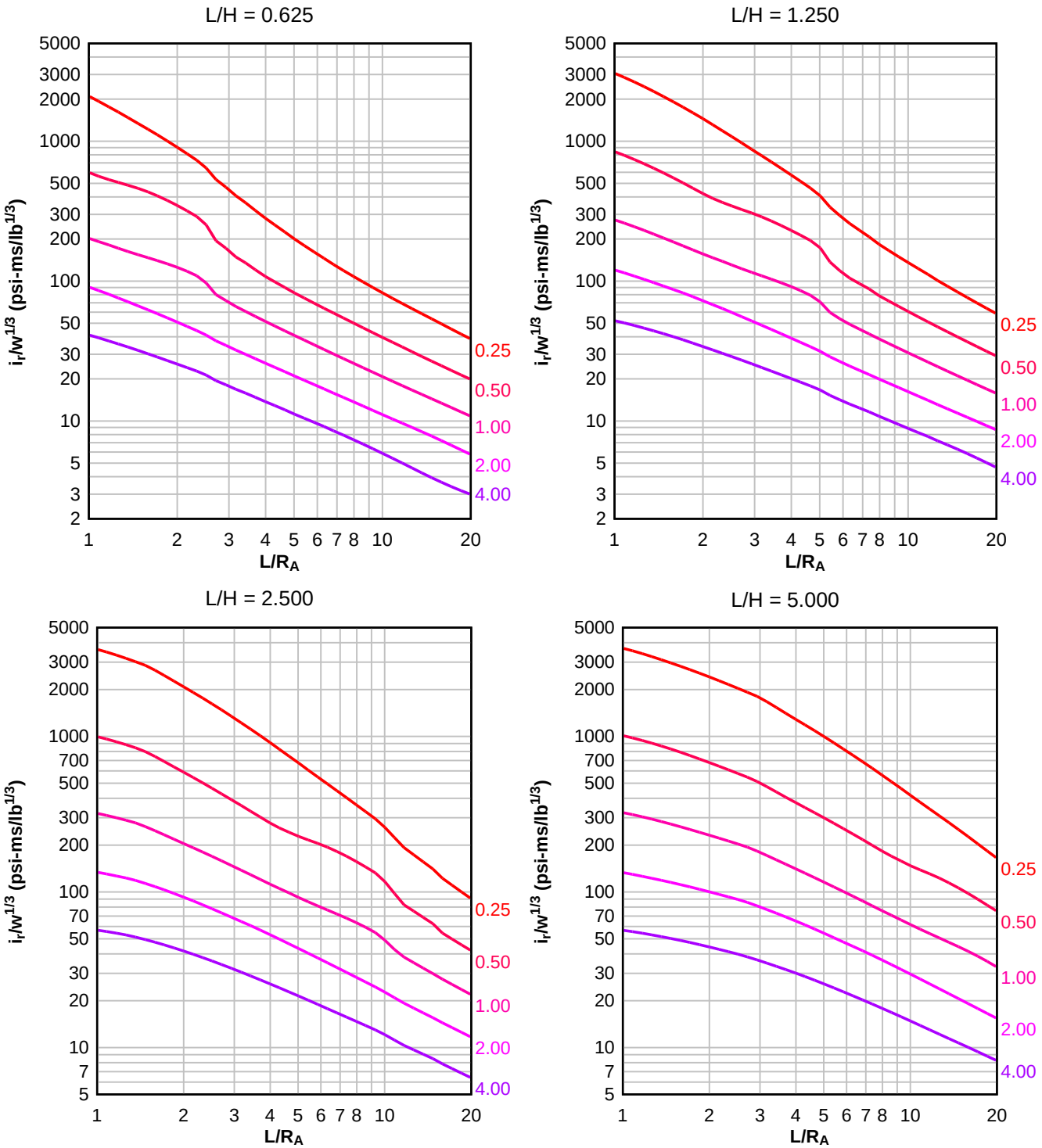

Figure 2-105 Scaled Average Unit Reflected Impulse (*N* = 1, *l/L* = 0.25 and 0.75, *h/H* = 0.25)

Numbers adjacent to curves indicate scaled range (ft/lb$^{1/3}$)

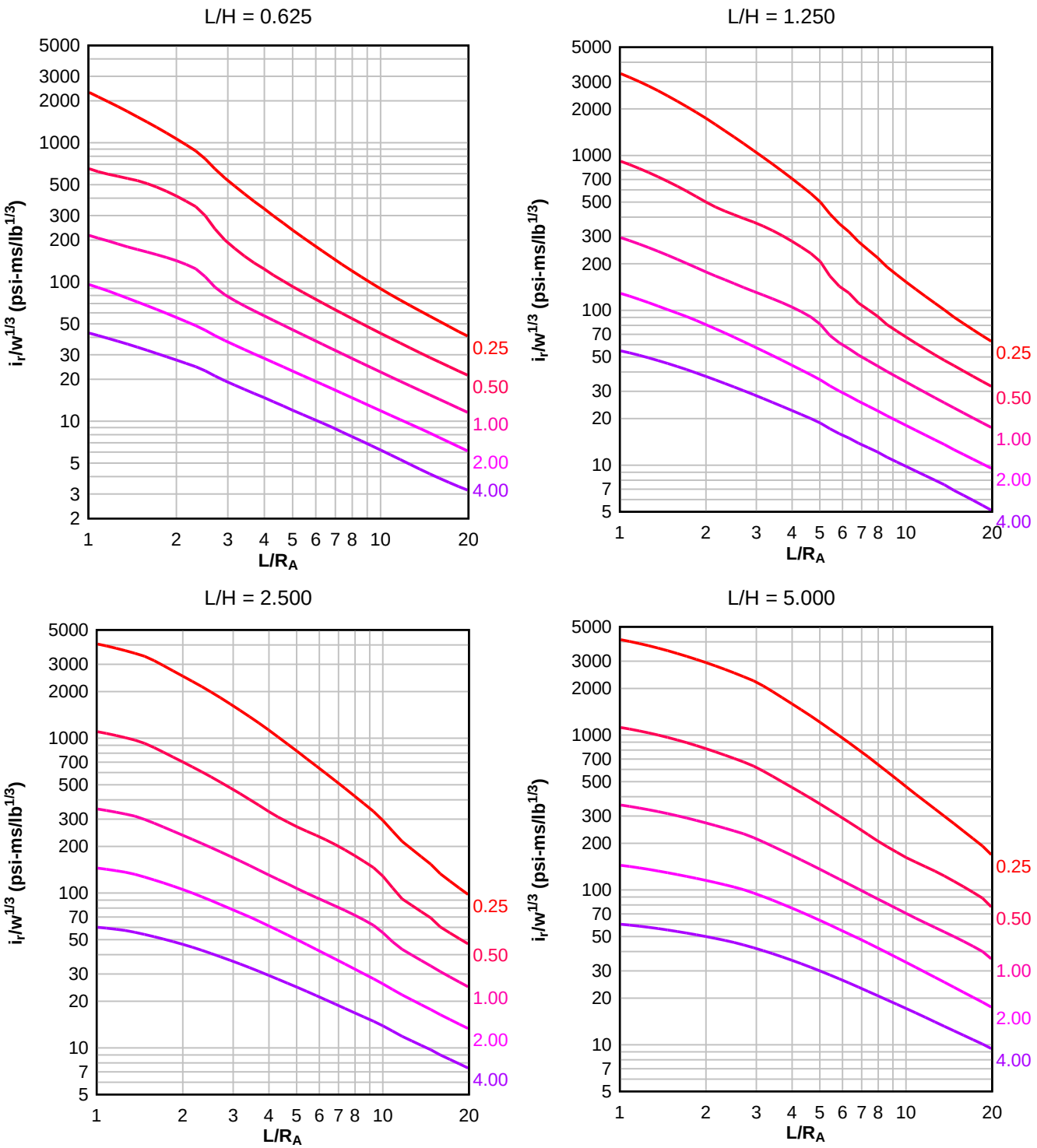

Figure 2-106 Scaled Average Unit Reflected Impulse (*N* = 1, *l/L* = 0.50, *h/H* = 0.25)

Numbers adjacent to curves indicate scaled range (ft/lb$^{1/3}$)

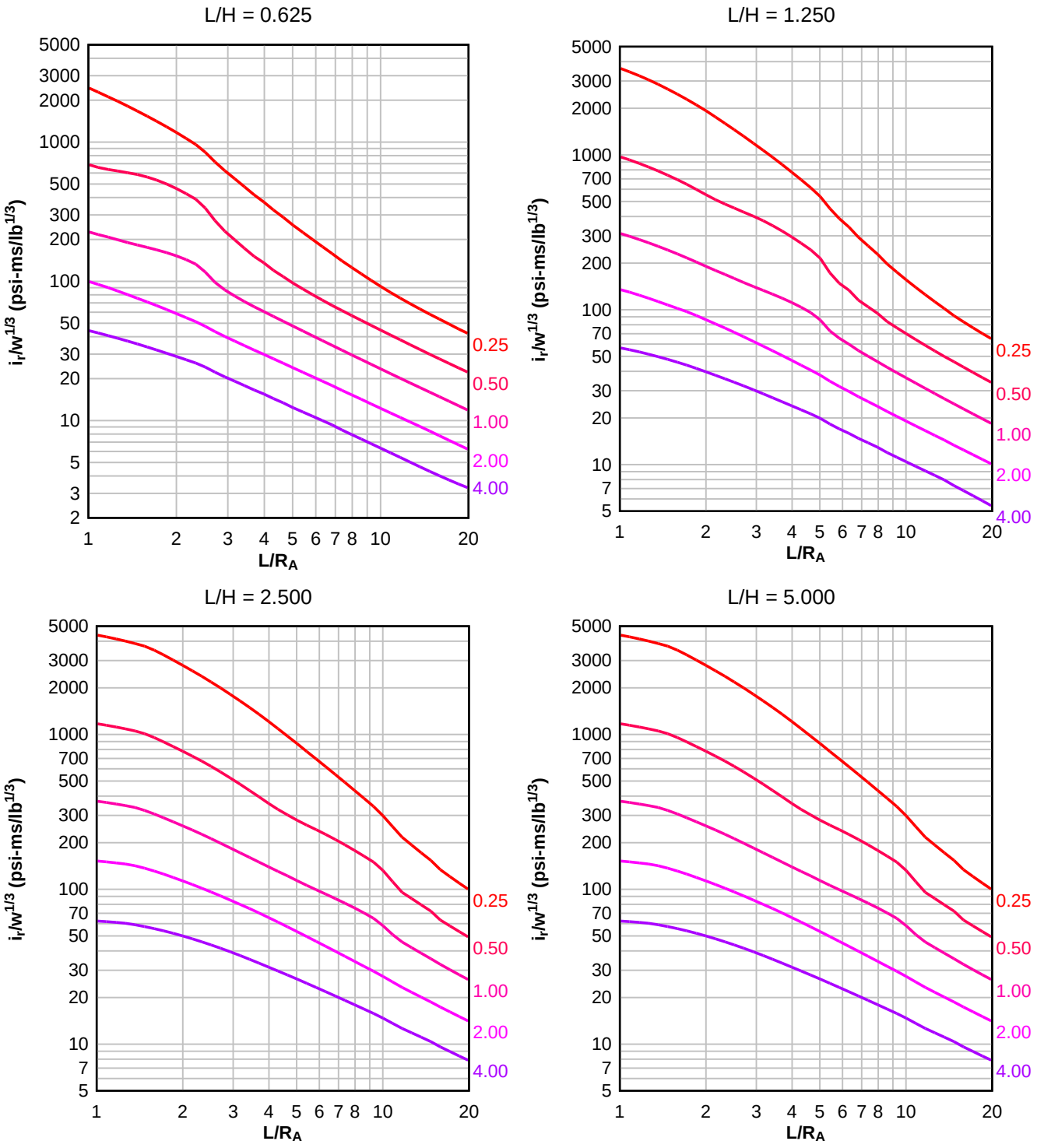

Figure 2-107 Scaled Average Unit Reflected Impulse (*N* = 1, *l/L* = 0.10, *h/H* = 0.50)

Numbers adjacent to curves indicate scaled range (ft/lb$^{1/3}$)

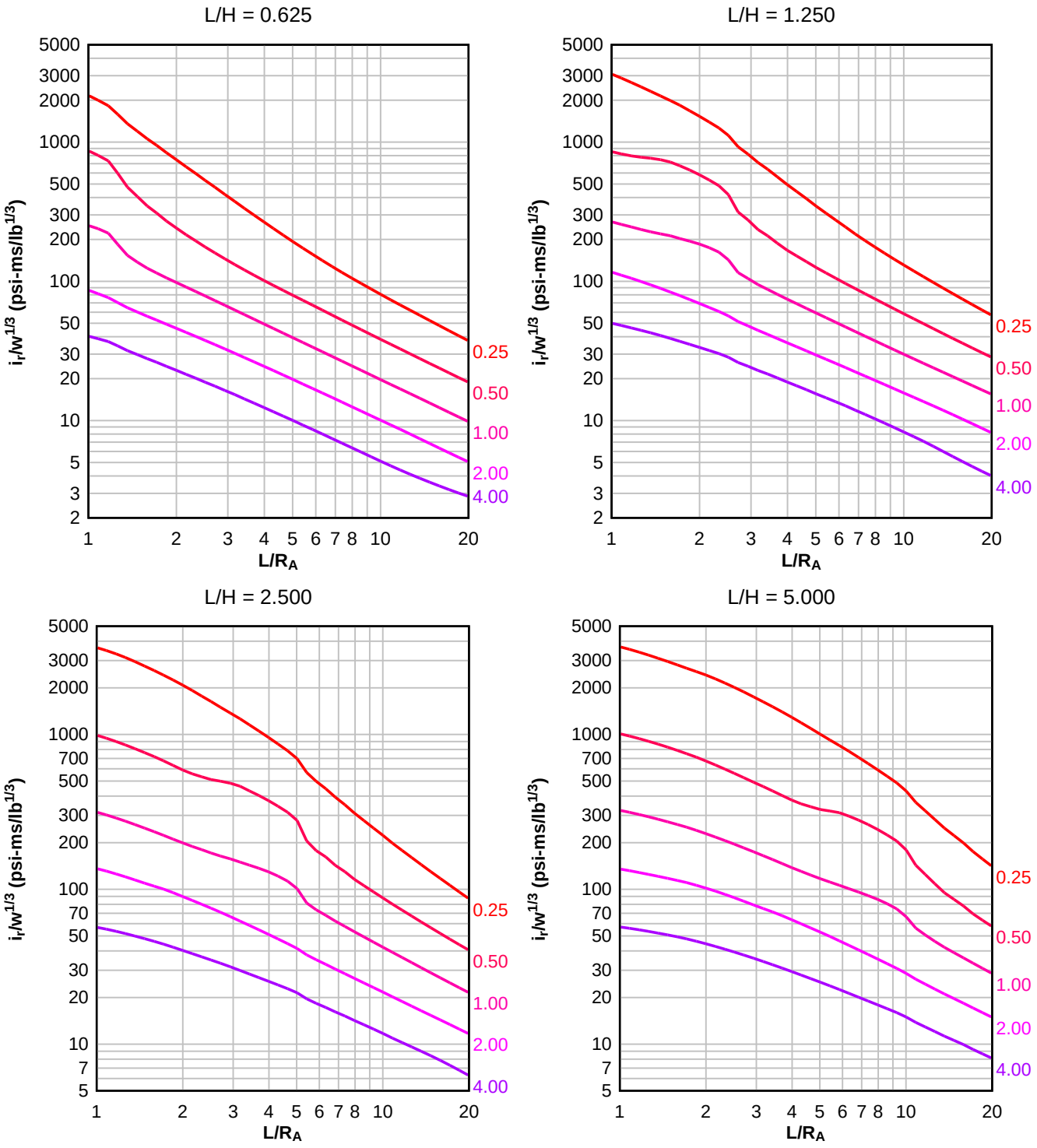

Figure 2-108 Scaled Average Unit Reflected Impulse (*N* = 1, *l/L* = 0.25 and 0.75, *h/H* = 0.50)

Numbers adjacent to curves indicate scaled range (ft/lb$^{1/3}$)

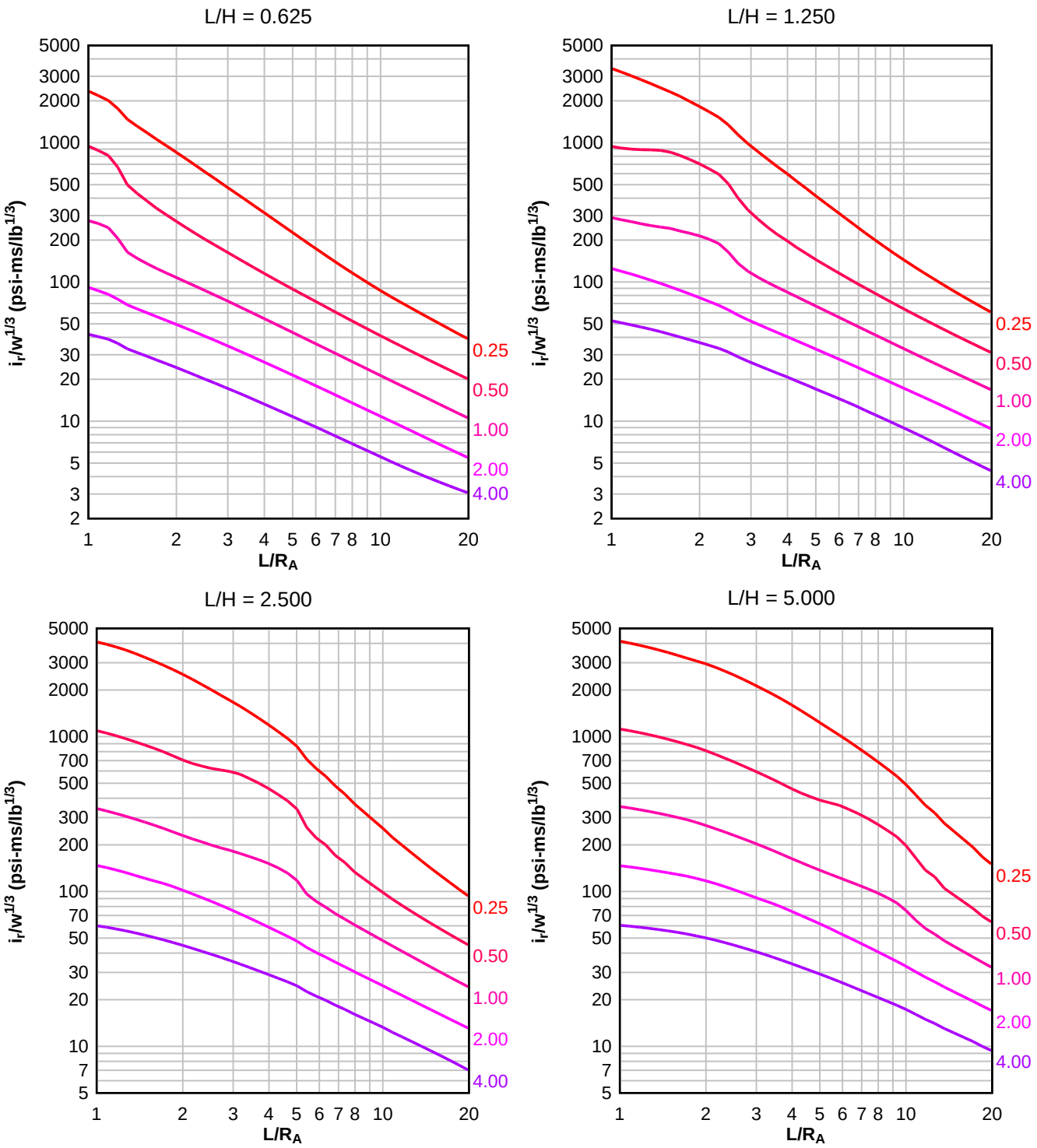

Figure 2-109 Scaled Average Unit Reflected Impulse (*N* = 1, *l/L* = 0.50, *h/H* = 0.50)

Numbers adjacent to curves indicate scaled range (ft/lb$^{1/3}$)

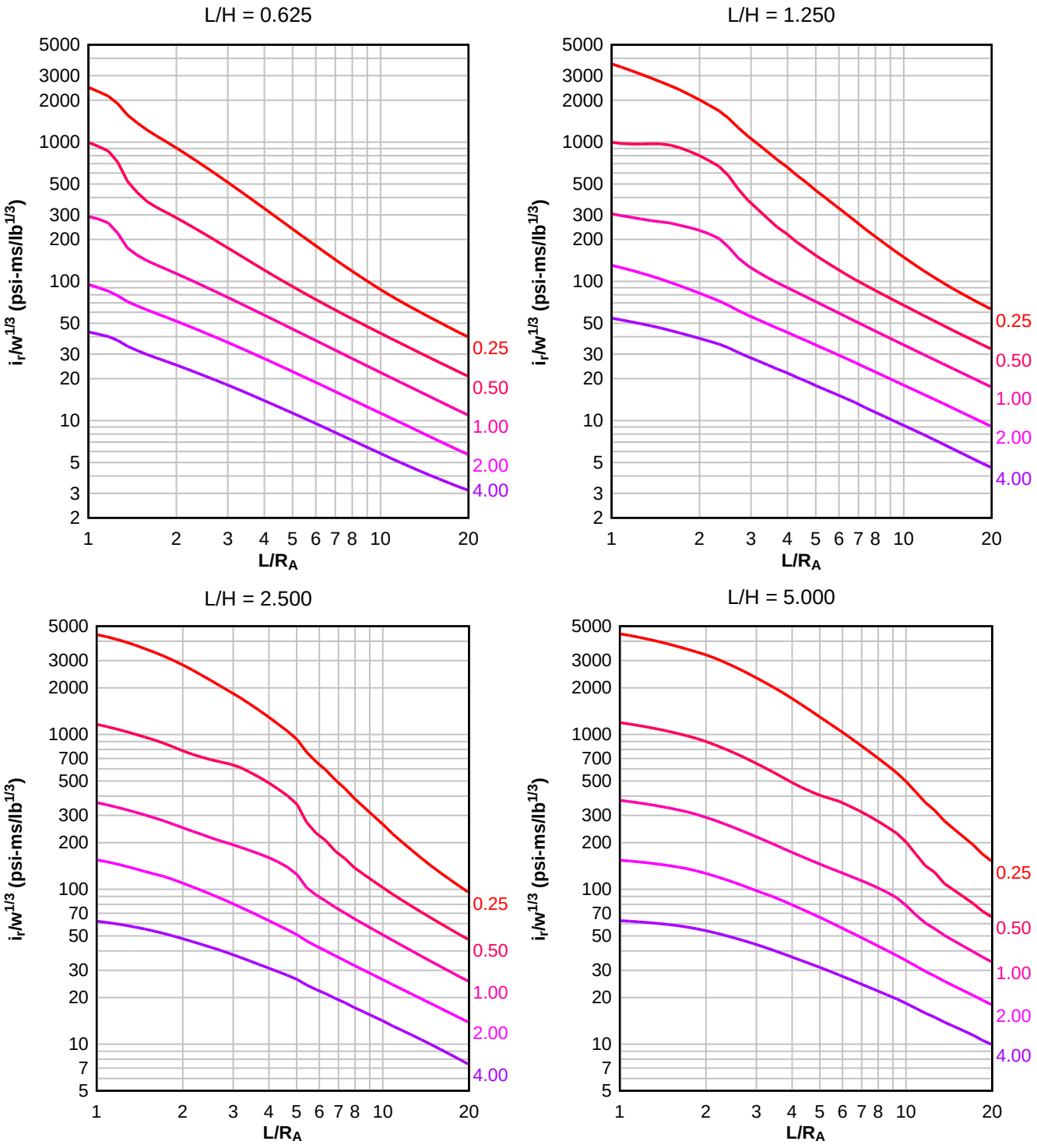

Figure 2-110 Scaled Average Unit Reflected Impulse (*N* = 1, *l*/*L* = 0.10, *h*/*H* = 0.75)

Numbers adjacent to curves indicate scaled range (ft/lb$^{1/3}$)

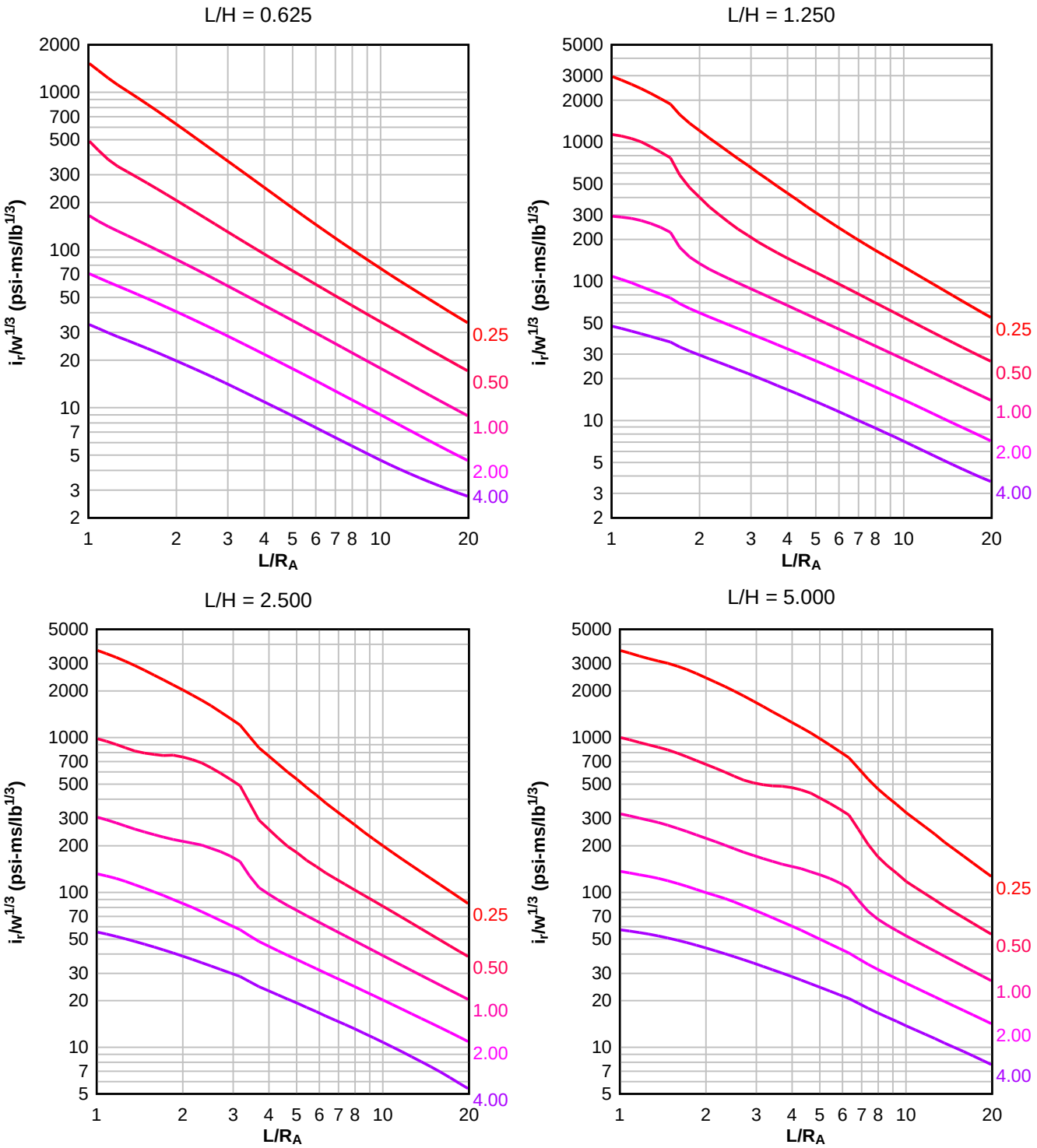

Figure 2-111 Scaled Average Unit Reflected Impulse (*N* = 1, *l/L* = 0.25 and 0.75, *h/H* = 0.75)

Numbers adjacent to curves indicate scaled range (ft/lb$^{1/3}$)

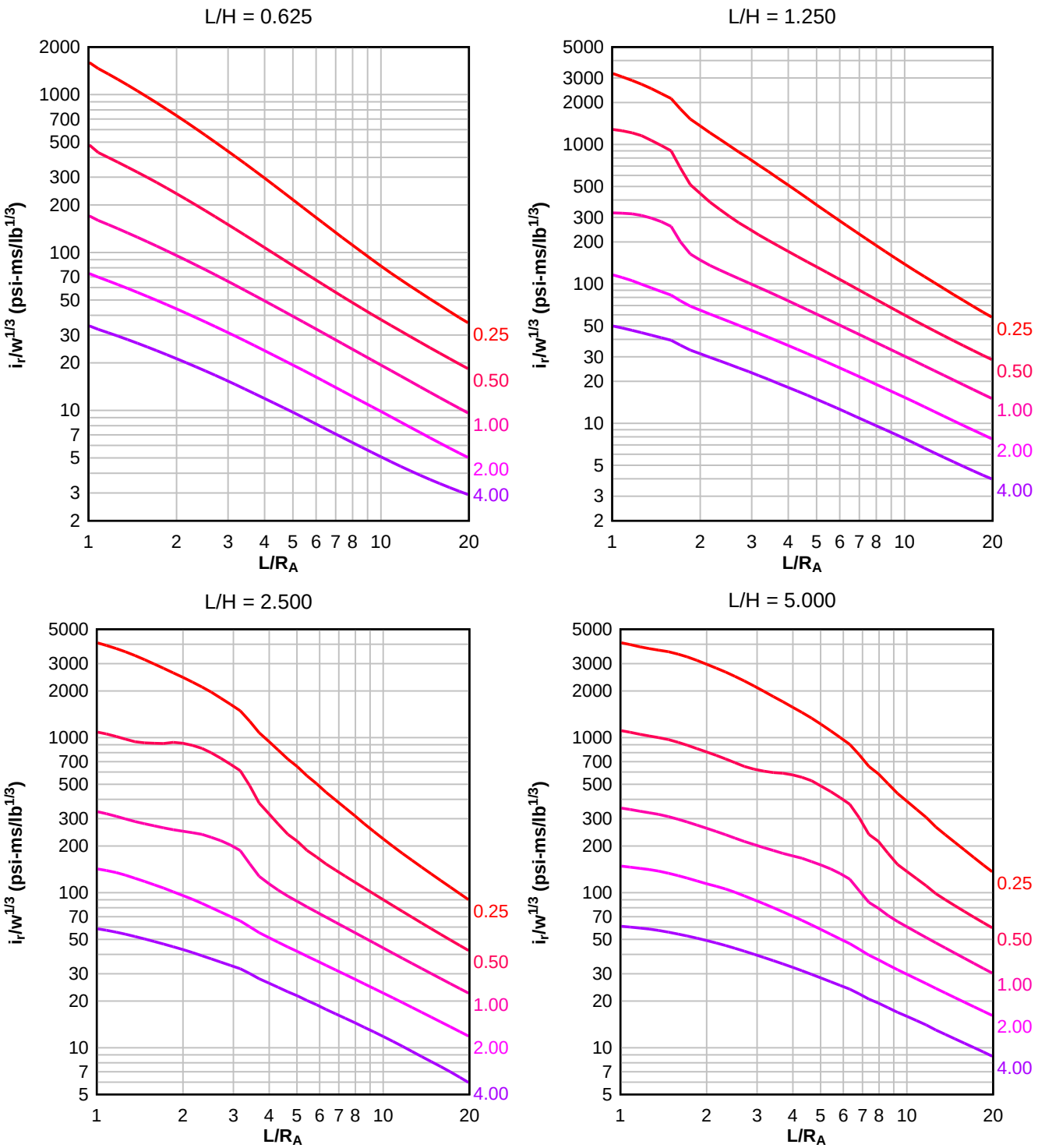

Figure 2-112 Scaled Average Unit Reflected Impulse (*N* = 1, *l/L* = 0.50, *h/H* = 0.75)

Numbers adjacent to curves indicate scaled range (ft/lb$^{1/3}$)

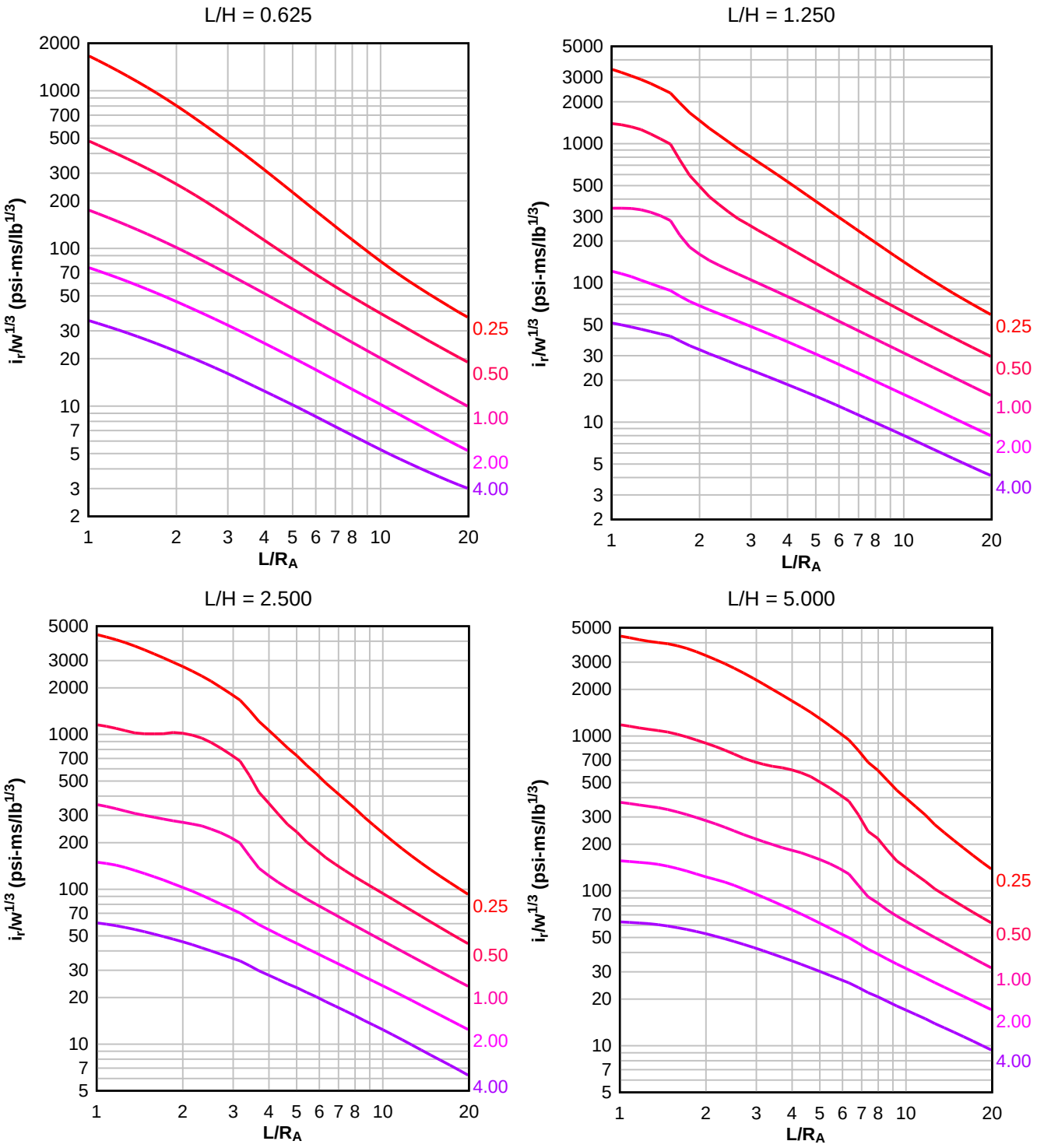

Figure 2-113 Scaled Average Unit Reflected Impulse (*N* = 2, *l*/*L* = 0.10, *h*/*H* = 0.10)

Numbers adjacent to curves indicate scaled range (ft/lb$^{1/3}$)

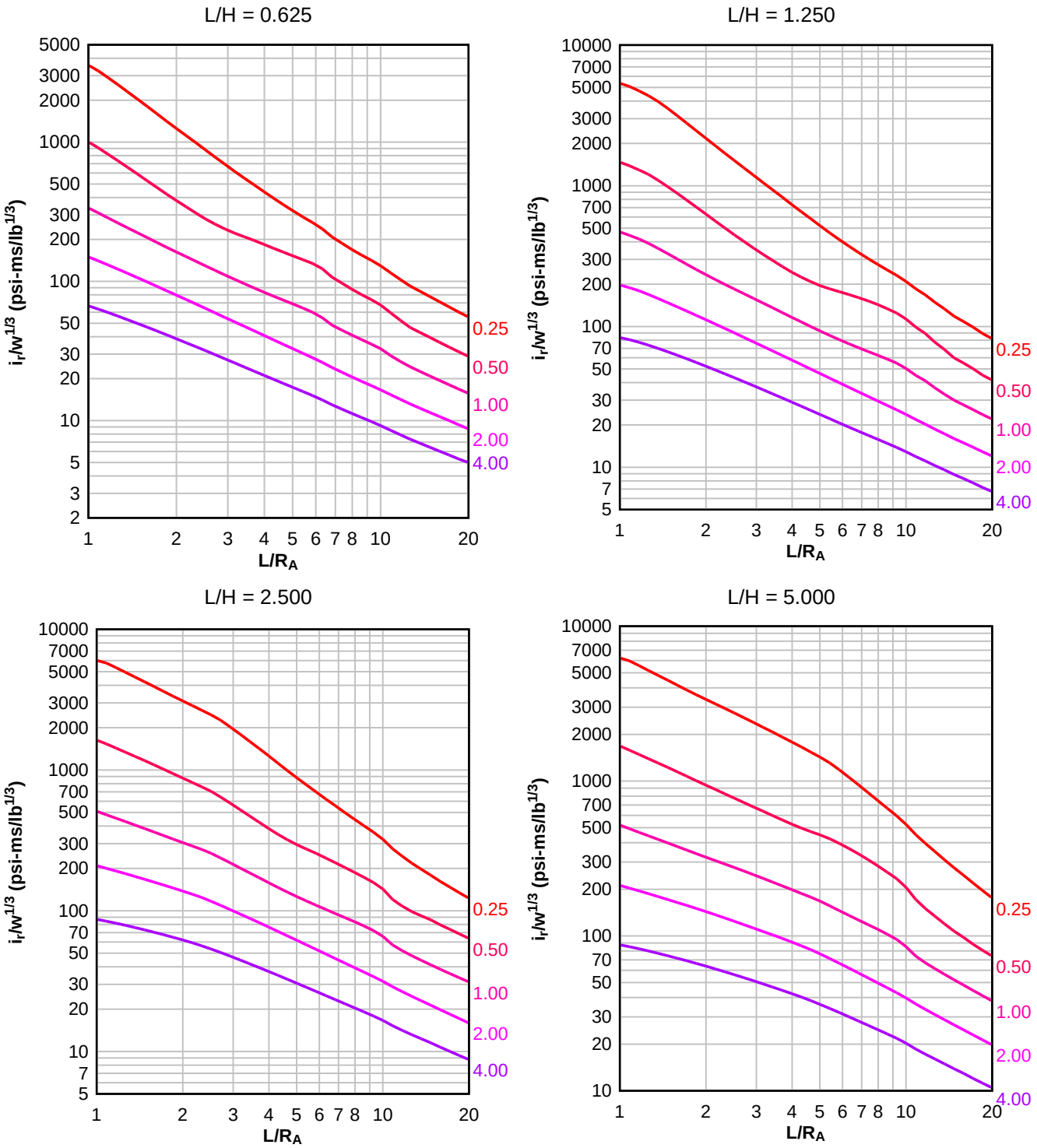

Figure 2-114 Scaled Average Unit Reflected Impulse (*N* = 2, *l/L* = 0.25, *h/H* = 0.10)

Numbers adjacent to curves indicate scaled range (ft/lb$^{1/3}$)

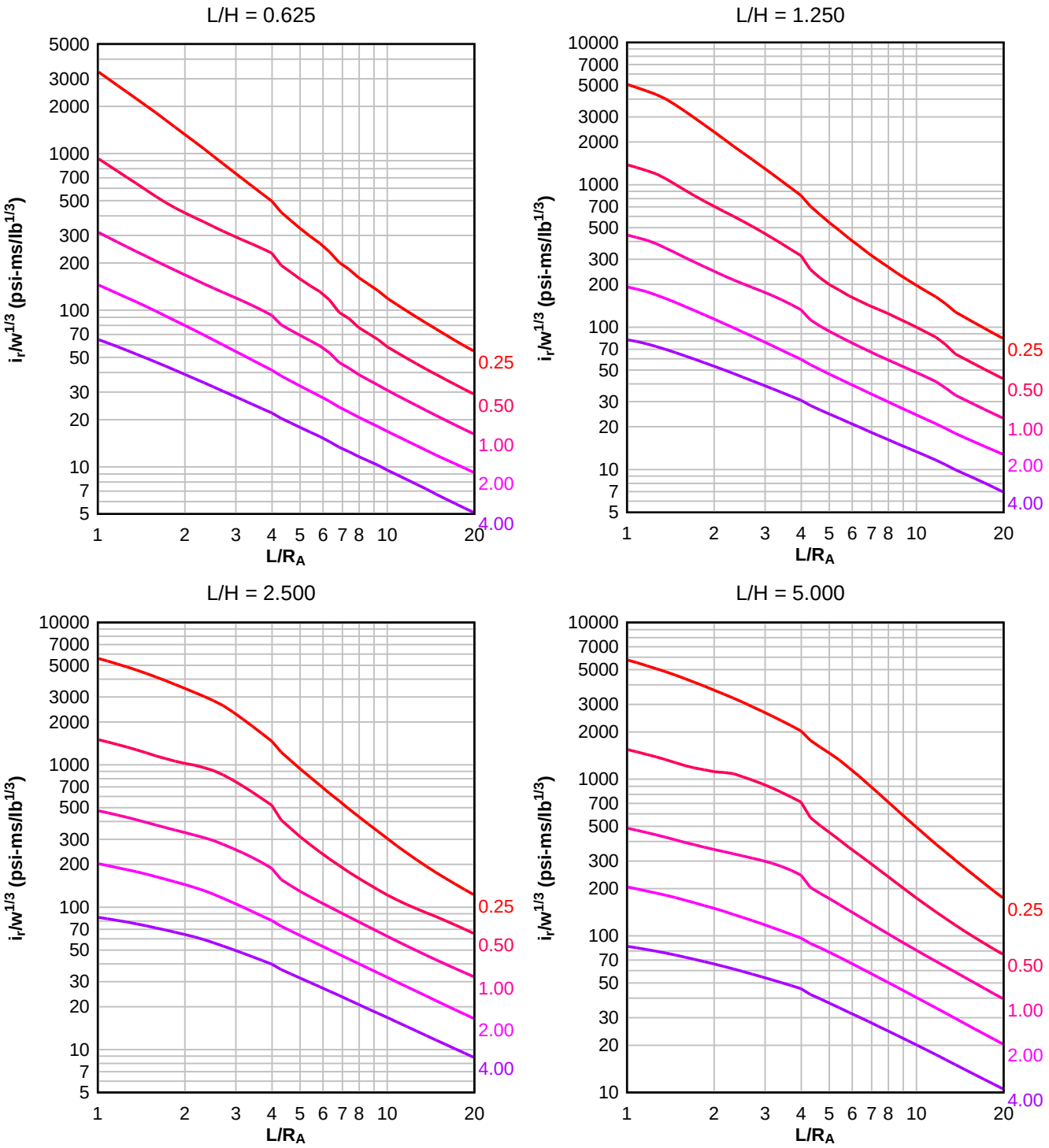

Figure 2-115 Scaled Average Unit Reflected Impulse (*N* = 2, *l/L* = 0.50, *h/H* = 0.10)

Numbers adjacent to curves indicate scaled range (ft/lb$^{1/3}$)

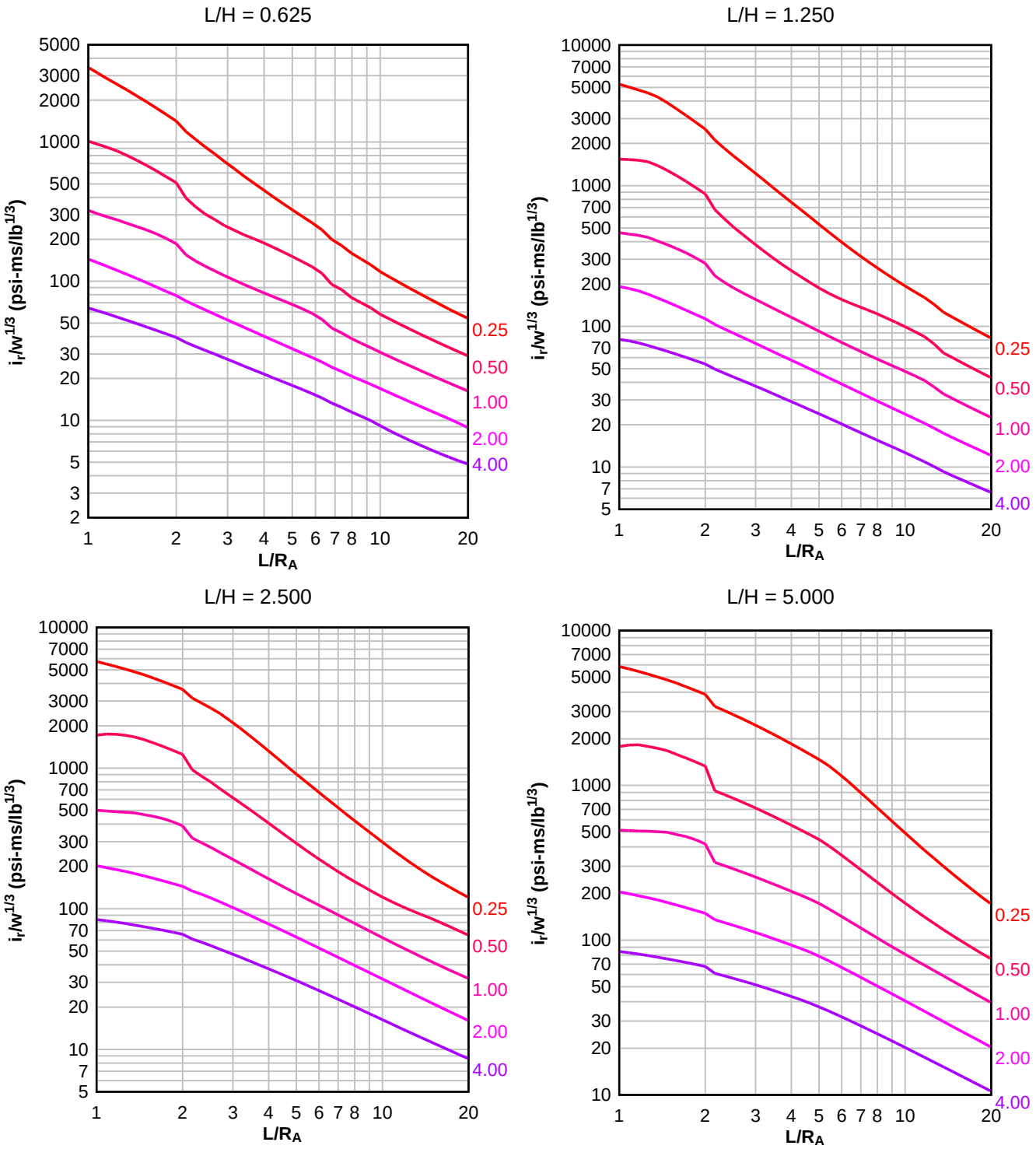

Figure 2-116 Scaled Average Unit Reflected Impulse (*N* = 2, *l/L* = 0.75, *h/H* = 0.10)

Numbers adjacent to curves indicate scaled range (ft/lb$^{1/3}$)

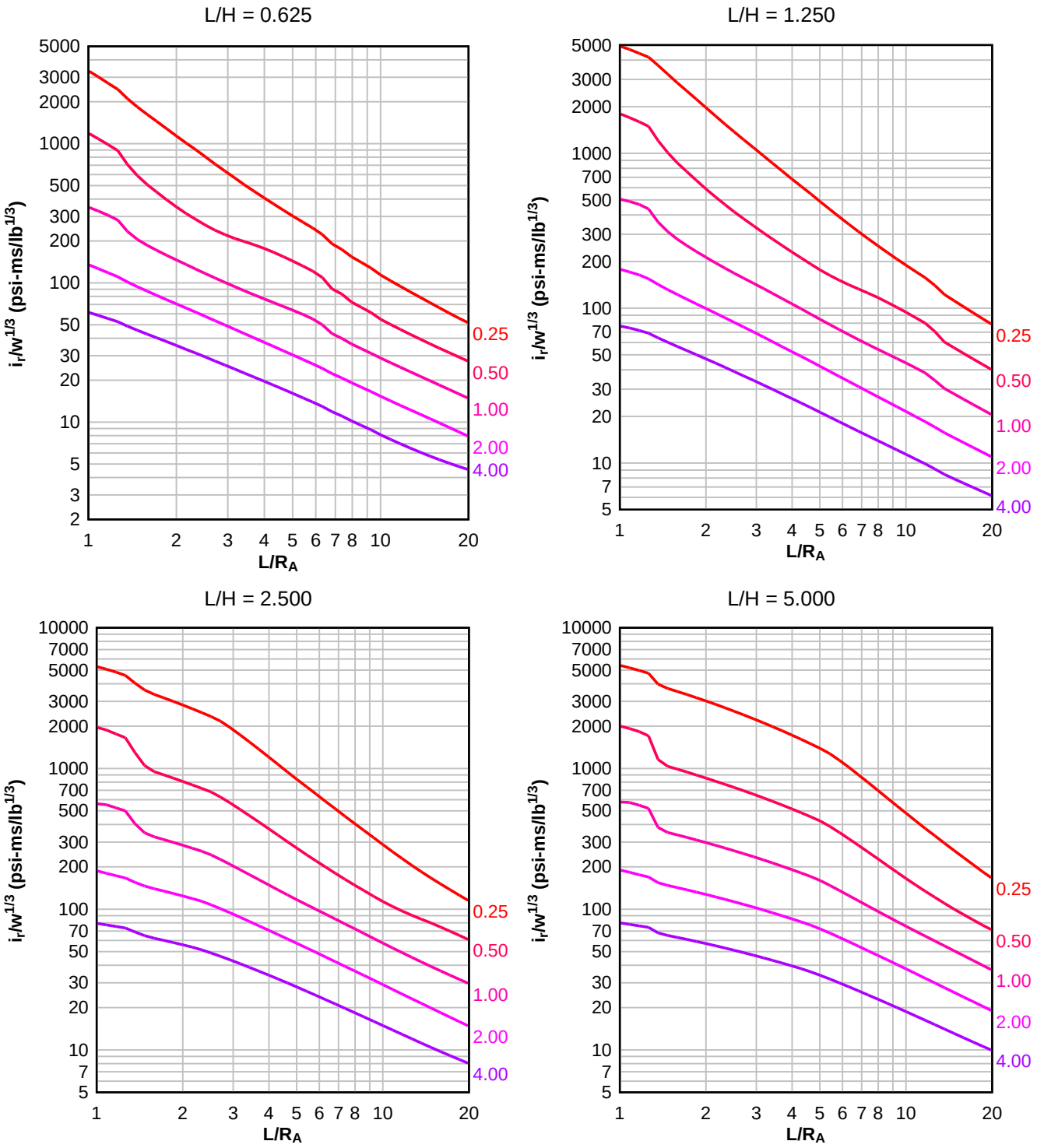

Figure 2-117 Scaled Average Unit Reflected Impulse (*N* = 2, *l*/*L* = 0.10, *h*/*H* = 0.25)

Numbers adjacent to curves indicate scaled range (ft/lb$^{1/3}$)

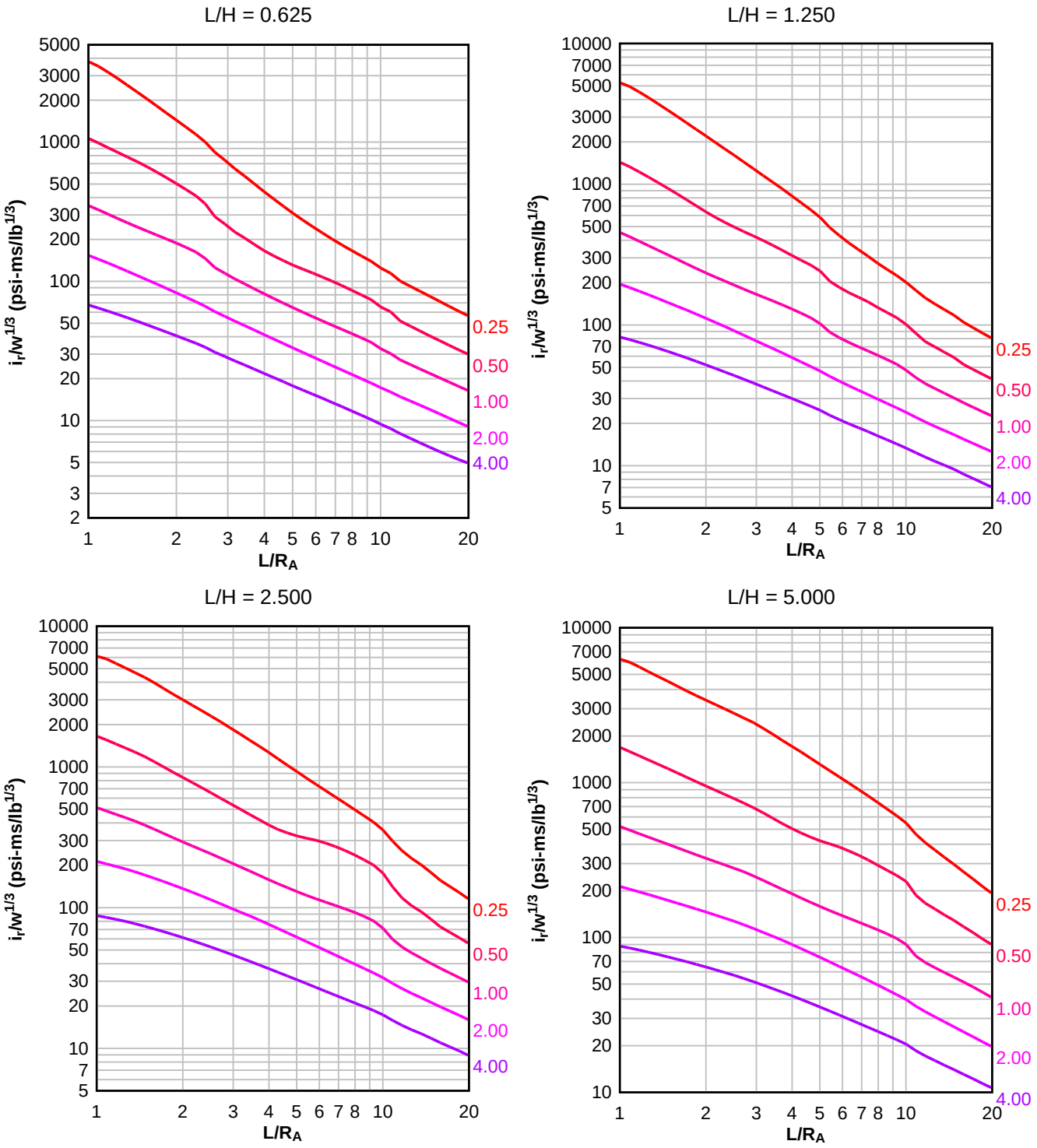

Figure 2-118 Scaled Average Unit Reflected Impulse (*N* = 2, *l/L* = 0.25, *h/H* = 0.25)

Numbers adjacent to curves indicate scaled range (ft/lb$^{1/3}$)

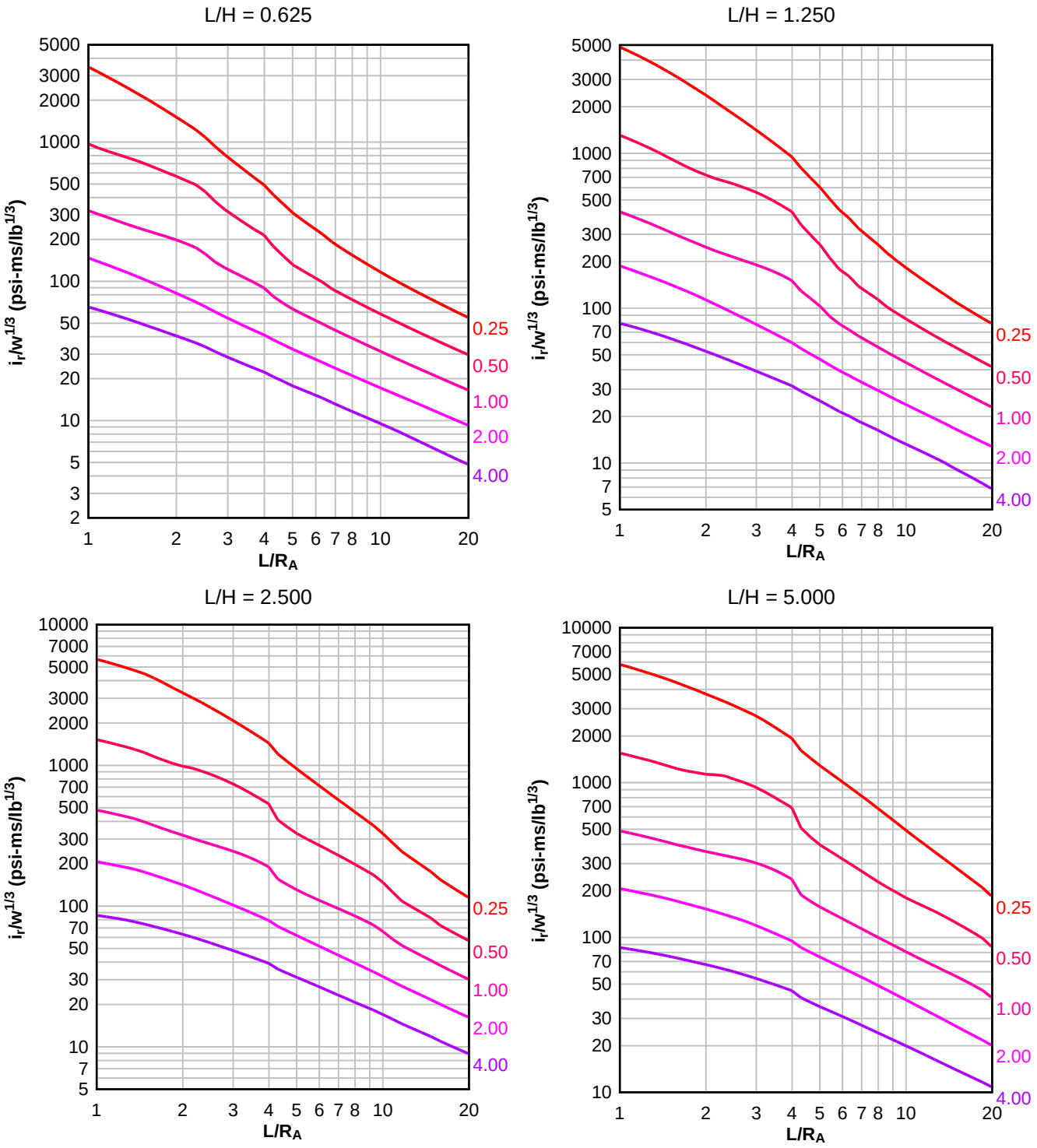

Figure 2-119 Scaled Average Unit Reflected Impulse (*N* = 2, *l*/*L* = 0.50, *h*/*H* = 0.25)

Numbers adjacent to curves indicate scaled range (ft/lb$^{1/3}$)

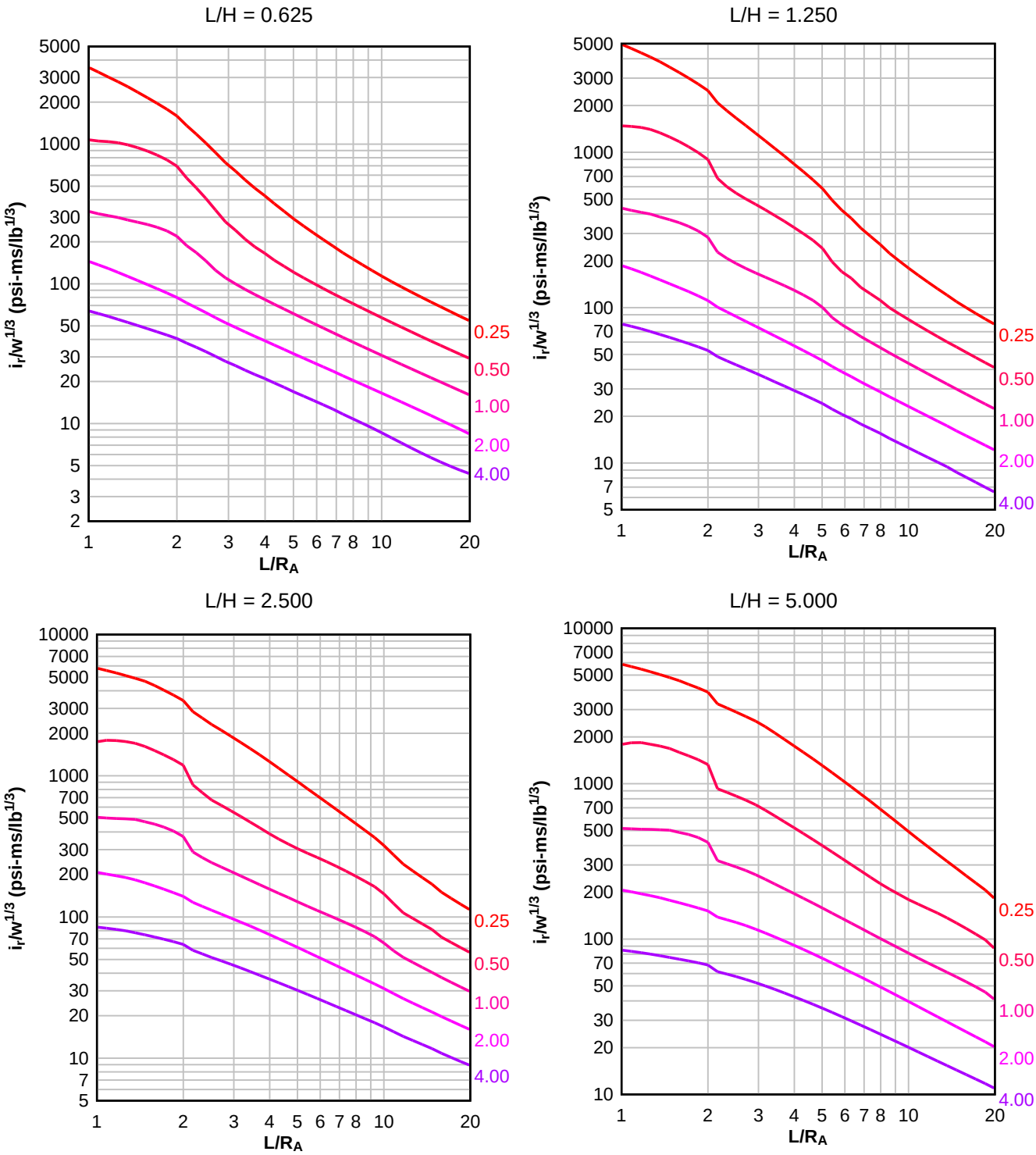

Figure 2-120 Scaled Average Unit Reflected Impulse (*N* = 2, *l/L* = 0.75, *h/H* = 0.25)

Numbers adjacent to curves indicate scaled range (ft/lb$^{1/3}$)

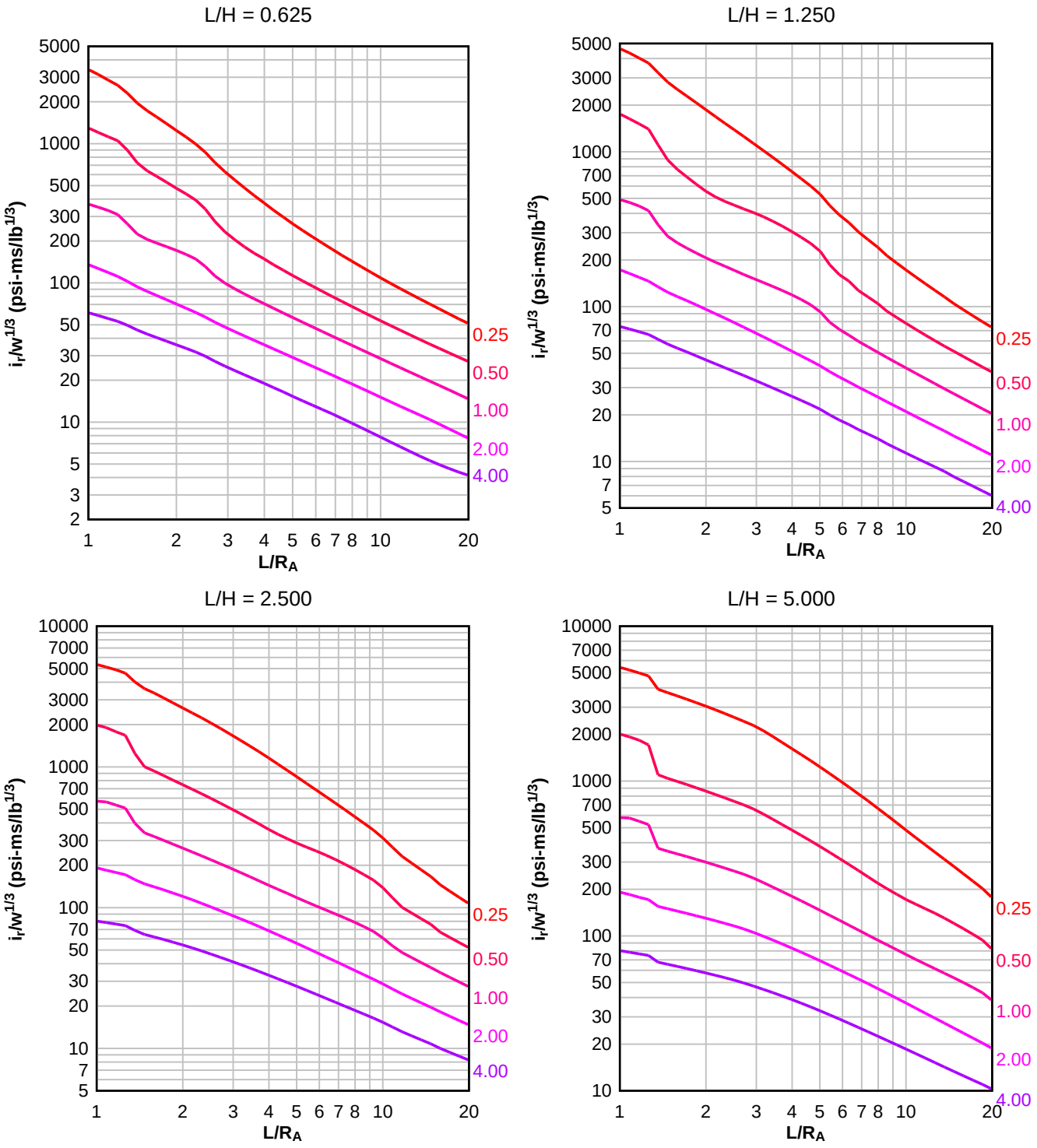

Figure 2-121 Scaled Average Unit Reflected Impulse (*N* = 2, *l*/*L* = 0.10, *h*/*H* = 0.50)

Numbers adjacent to curves indicate scaled range (ft/lb$^{1/3}$)

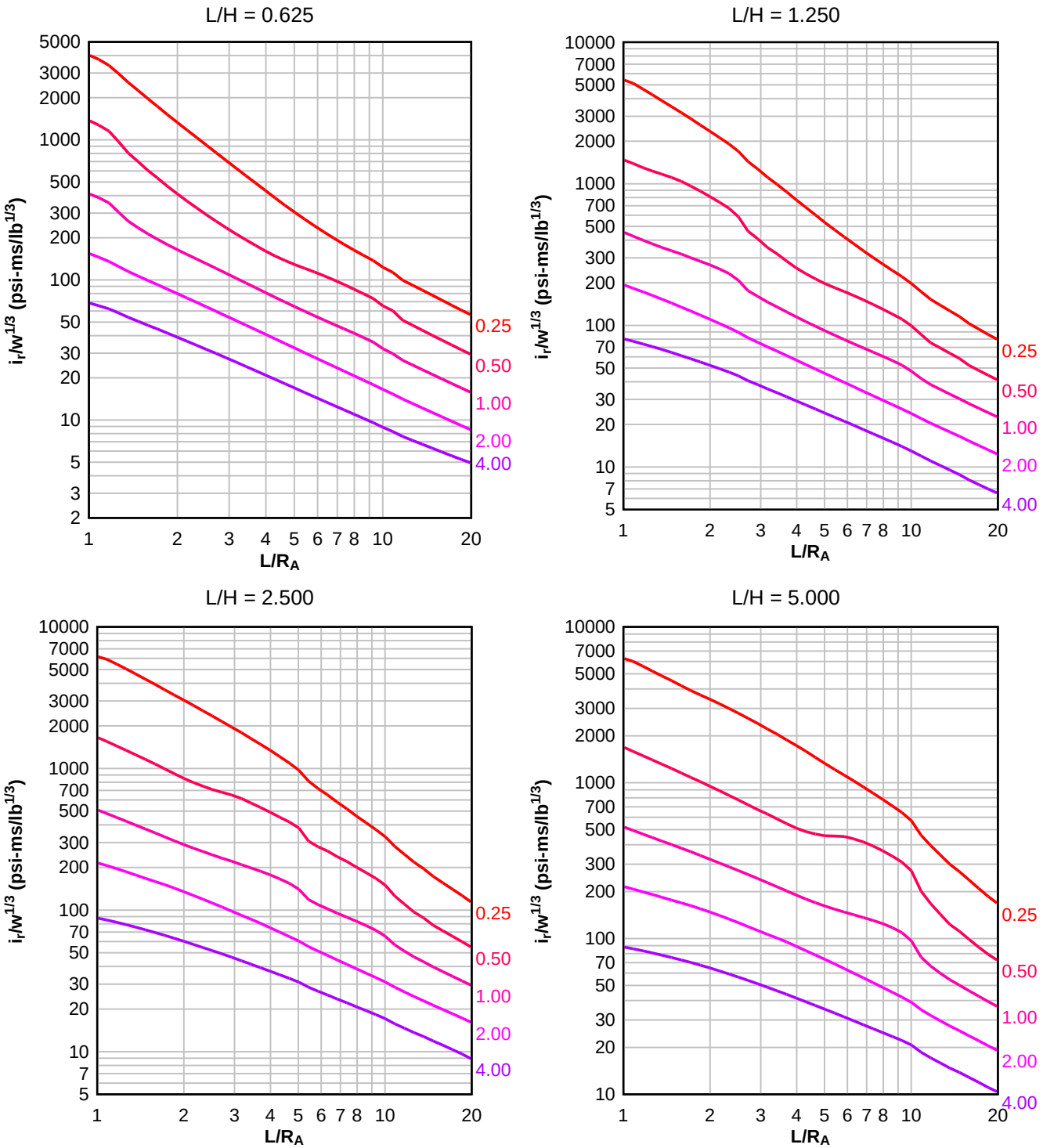

Figure 2-122 Scaled Average Unit Reflected Impulse (*N* = 2, *l/L* = 0.25, *h/H* = 0.50)

Numbers adjacent to curves indicate scaled range (ft/lb$^{1/3}$)

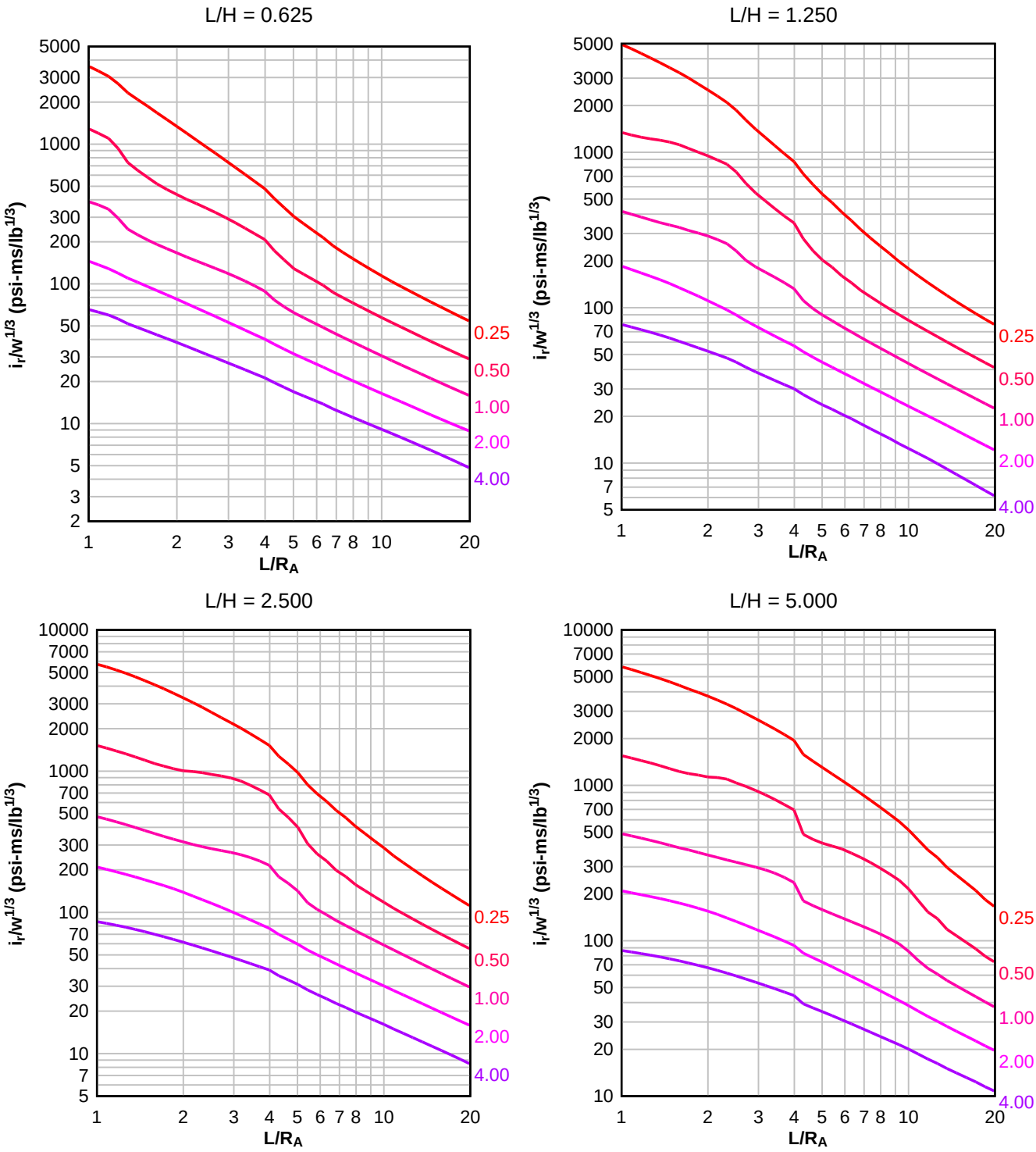

Figure 2-123 Scaled Average Unit Reflected Impulse (*N* = 2, *l/L* = 0.50, *h/H* = 0.50)

Numbers adjacent to curves indicate scaled range (ft/lb$^{1/3}$)

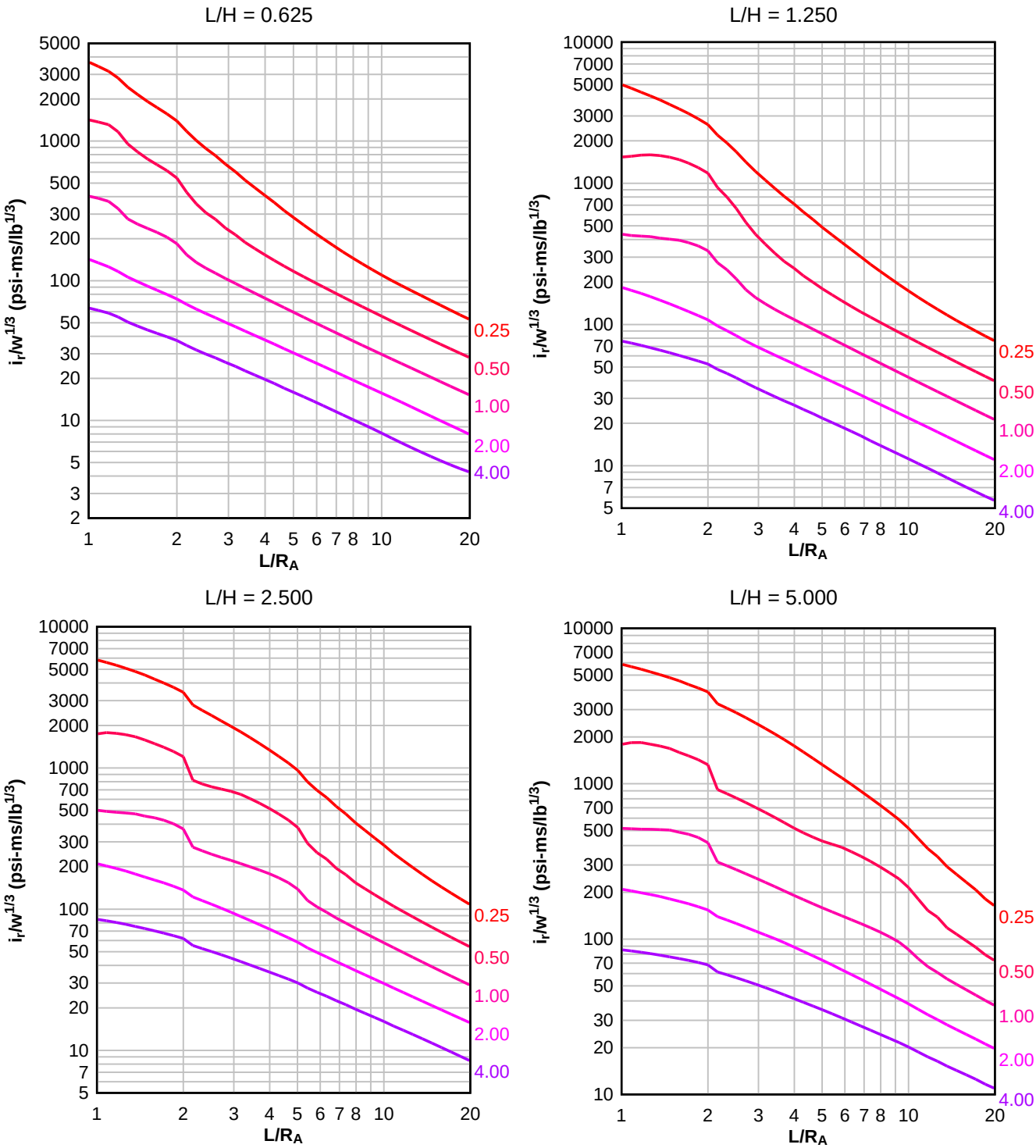

Figure 2-124 Scaled Average Unit Reflected Impulse (*N* = 2, *l/L* = 0.75, *h/H* = 0.50)

Numbers adjacent to curves indicate scaled range (ft/lb$^{1/3}$)

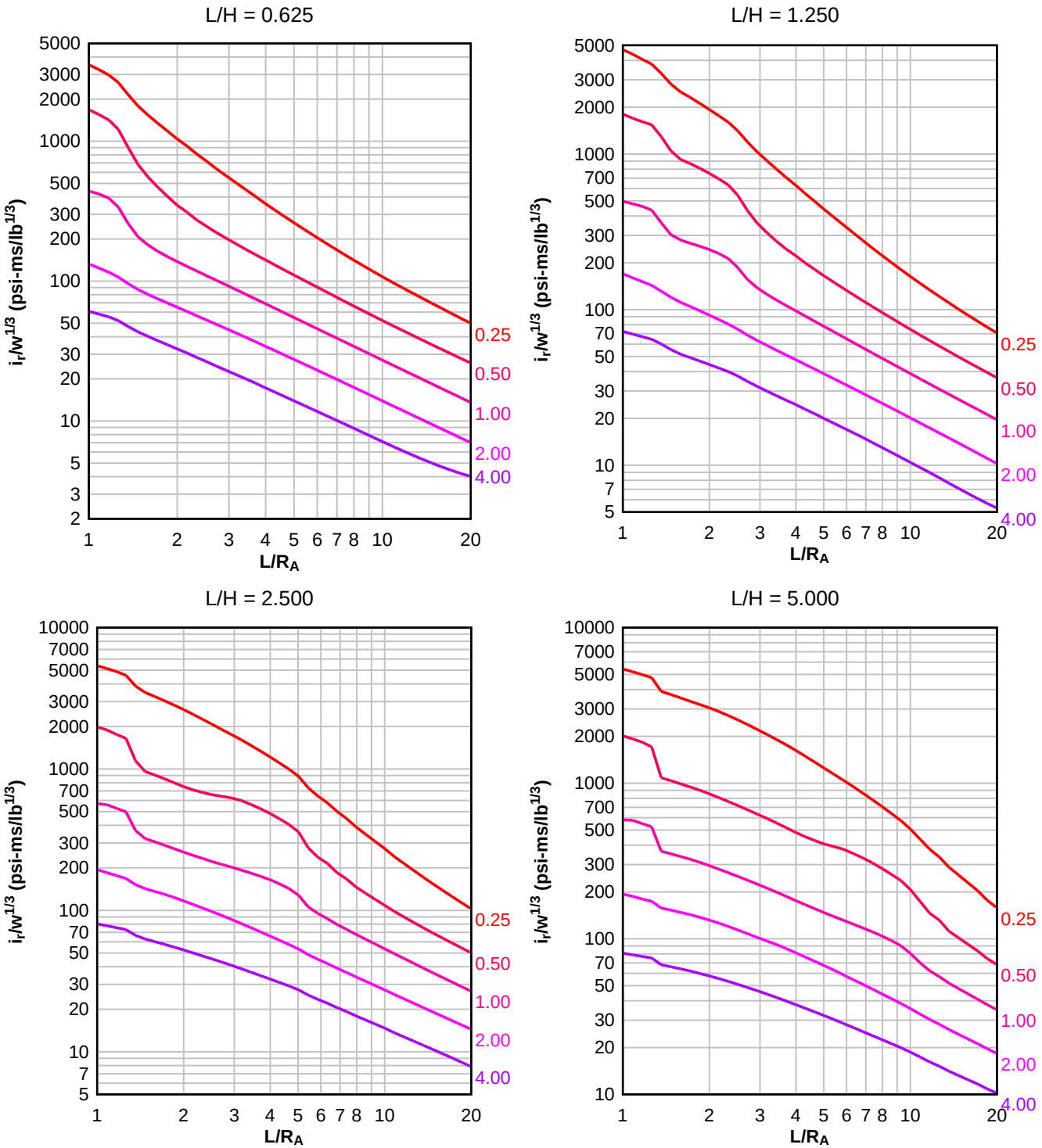

Figure 2-125 Scaled Average Unit Reflected Impulse (*N* = 2, *l*/*L* = 0.10, *h*/*H* = 0.75)

Numbers adjacent to curves indicate scaled range (ft/lb$^{1/3}$)

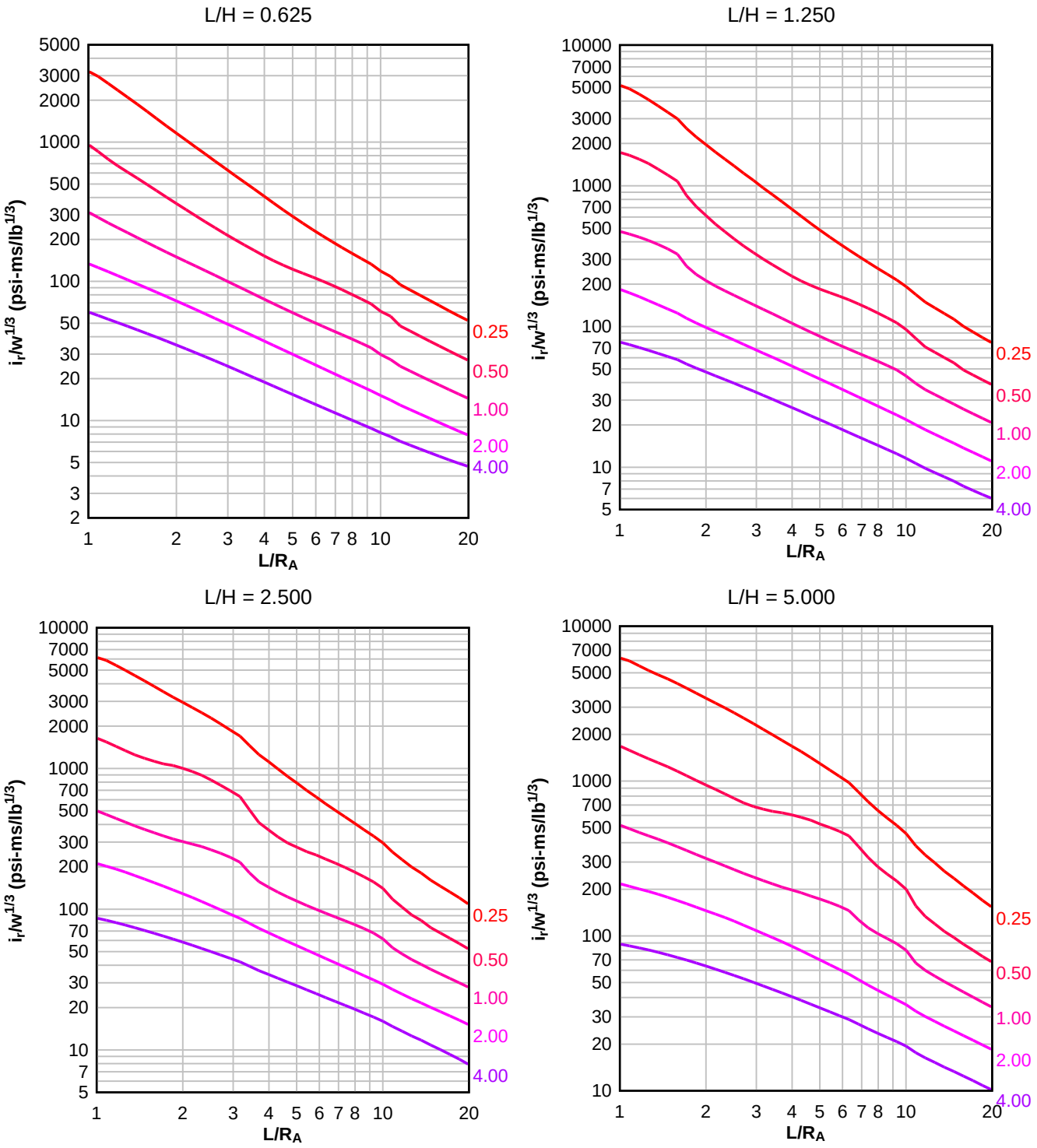

Figure 2-126 Scaled Average Unit Reflected Impulse (*N* = 2, *l/L* = 0.25, *h/H* = 0.75)

Numbers adjacent to curves indicate scaled range (ft/lb$^{1/3}$)

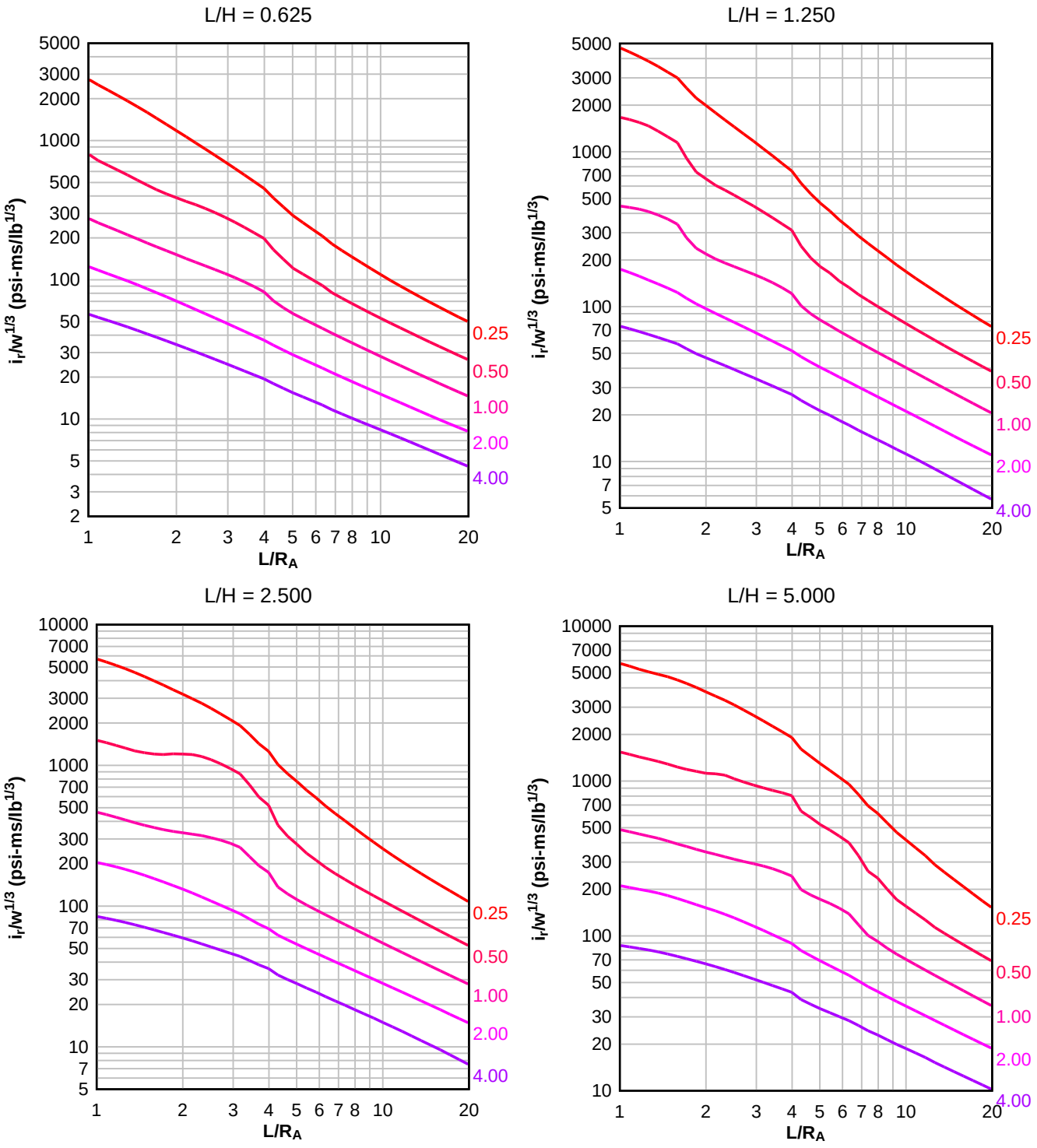

Figure 2-127 Scaled Average Unit Reflected Impulse (*N* = 2, *l*/*L* = 0.50, *h*/*H* = 0.75)

Numbers adjacent to curves indicate scaled range (ft/lb$^{1/3}$)

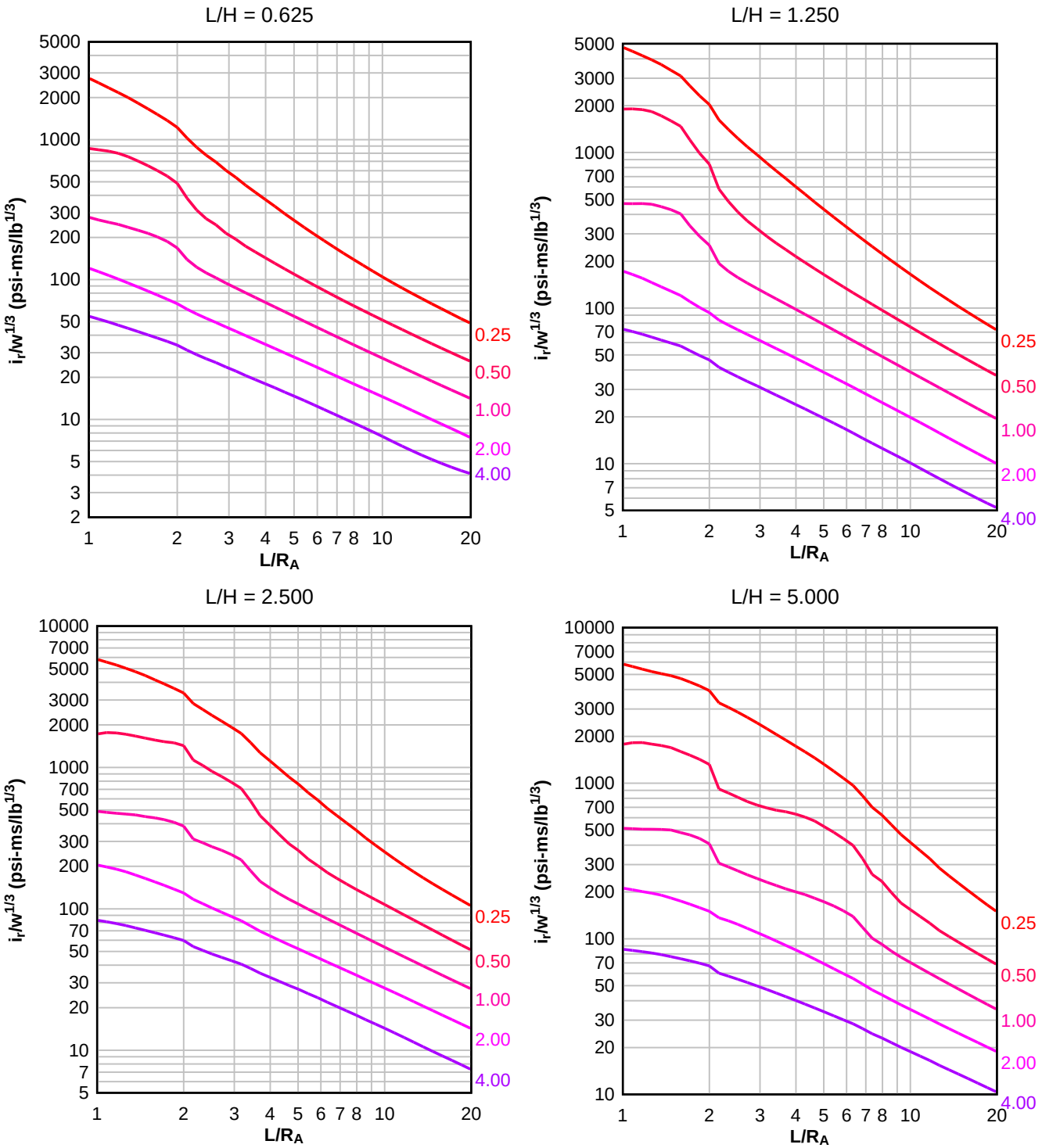

Figure 2-128 Scaled Average Unit Reflected Impulse (*N* = 2, *l/L* = 0.75, *h/H* = 0.75)

Numbers adjacent to curves indicate scaled range (ft/lb$^{1/3}$)

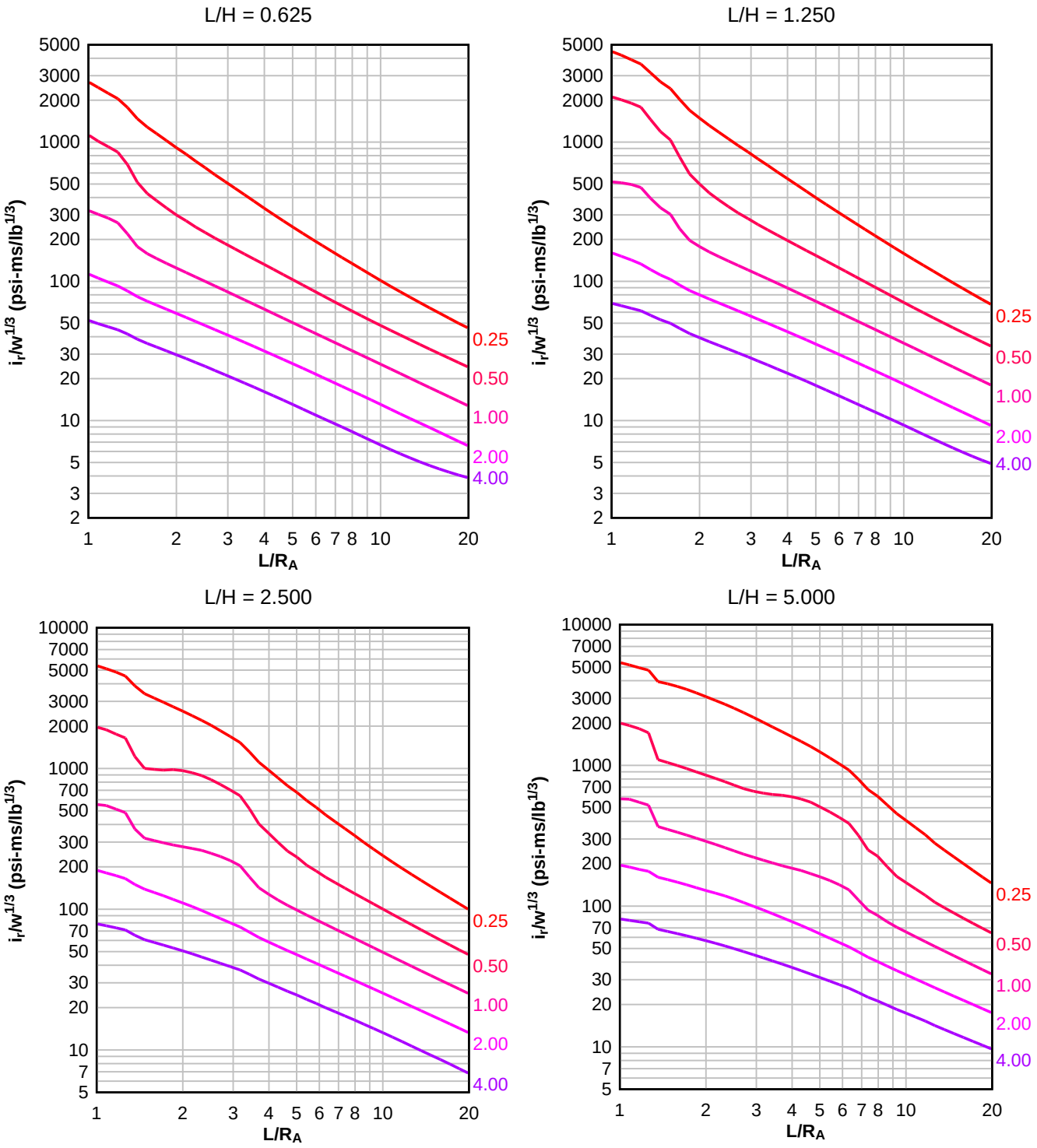

Figure 2-129 Scaled Average Unit Reflected Impulse (*N* = 3, *l/L* = 0.10, *h/H* = 0.10)

Numbers adjacent to curves indicate scaled range (ft/lb$^{1/3}$)

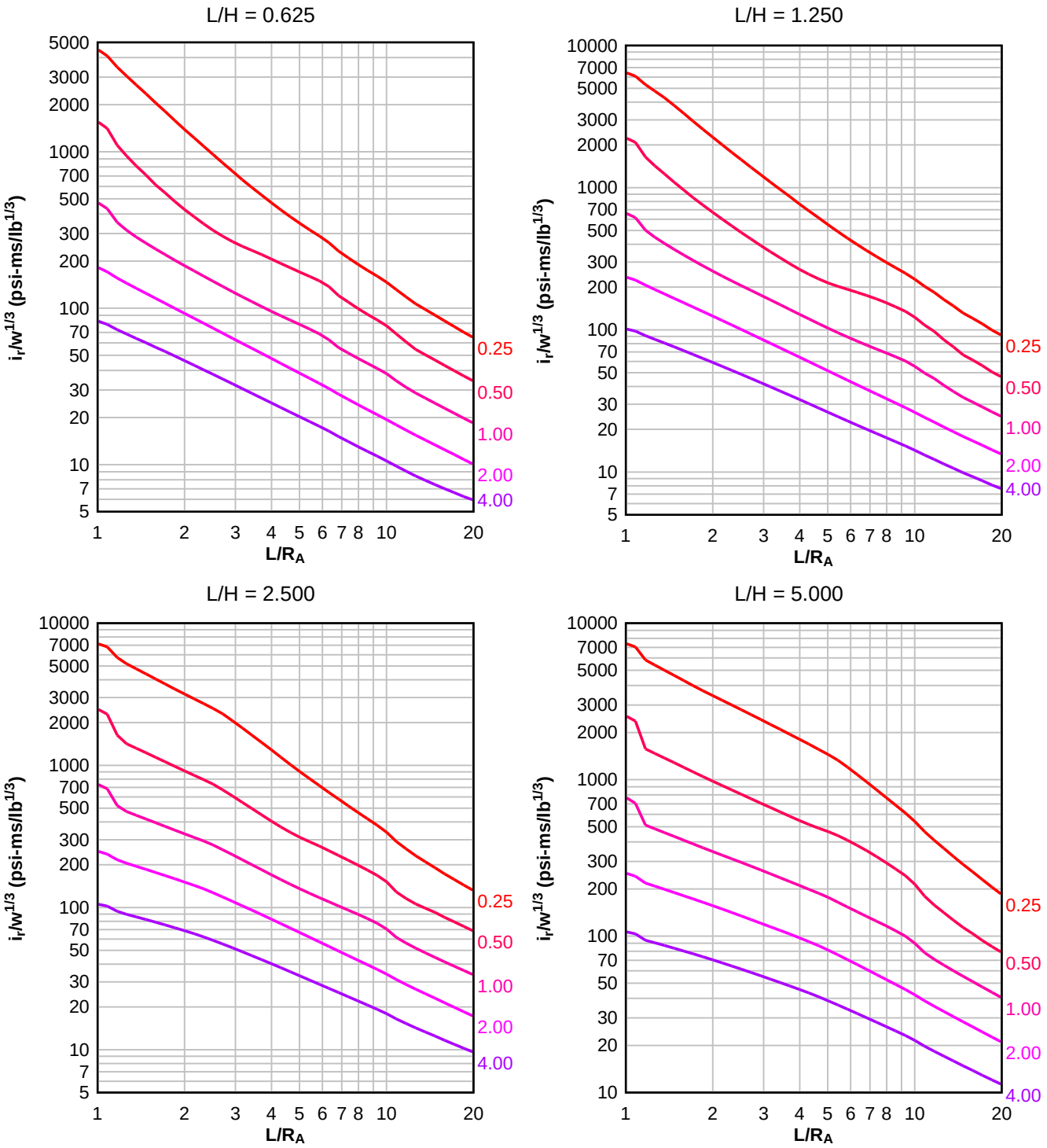

Figure 2-130 Scaled Average Unit Reflected Impulse (*N* = 3, *l/L* = 0.25 and 0.75, *h/H* = 0.10)

Numbers adjacent to curves indicate scaled range (ft/lb$^{1/3}$)

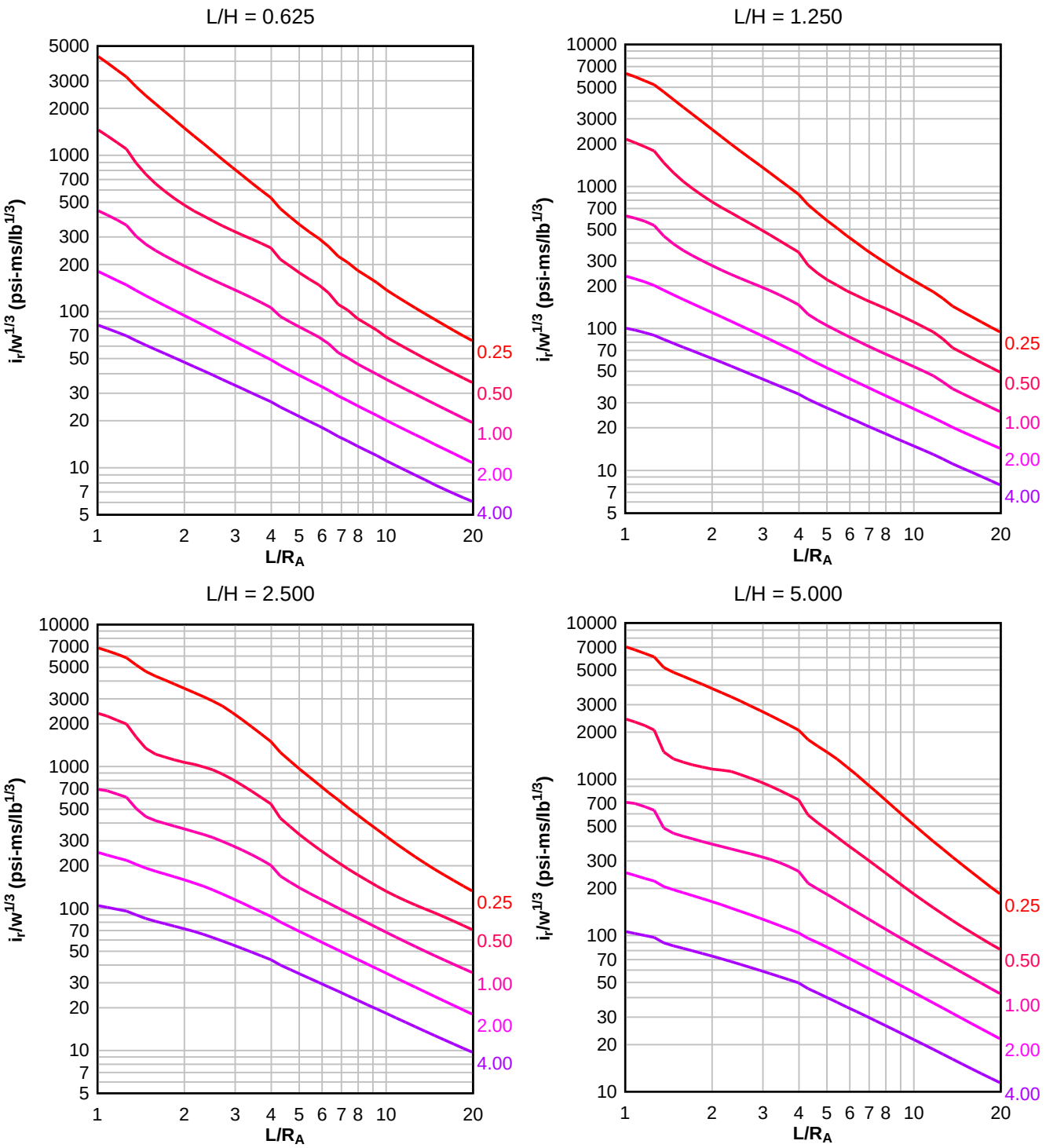

Figure 2-131 Scaled Average Unit Reflected Impulse (*N* = 3, *l/L* = 0.50, *h/H* = 0.10)

Numbers adjacent to curves indicate scaled range (ft/lb$^{1/3}$)

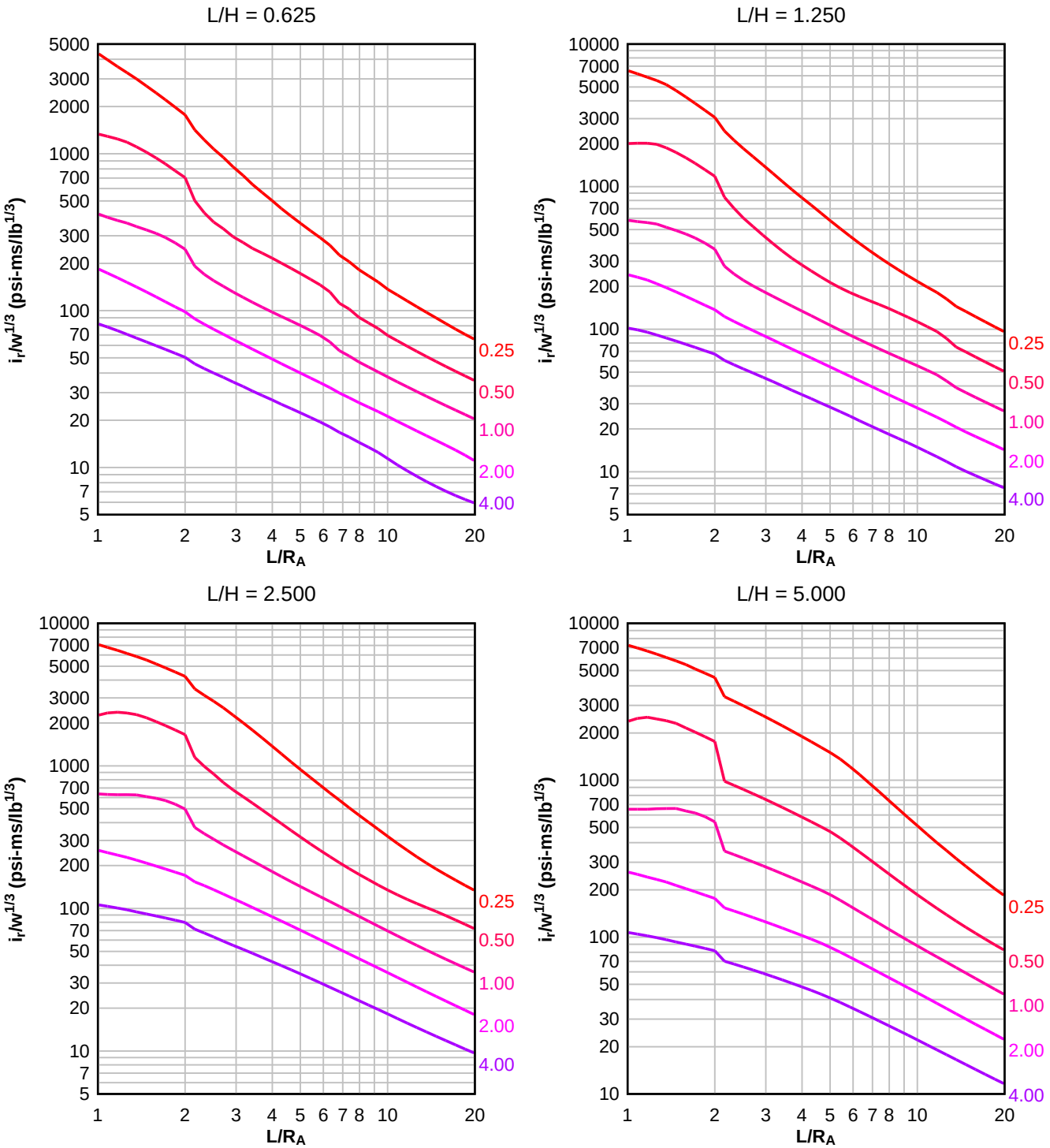

Figure 2-132 Scaled Average Unit Reflected Impulse (*N* = 3, *l/L* = 0.10, *h/H* = 0.25)

Numbers adjacent to curves indicate scaled range (ft/lb$^{1/3}$)

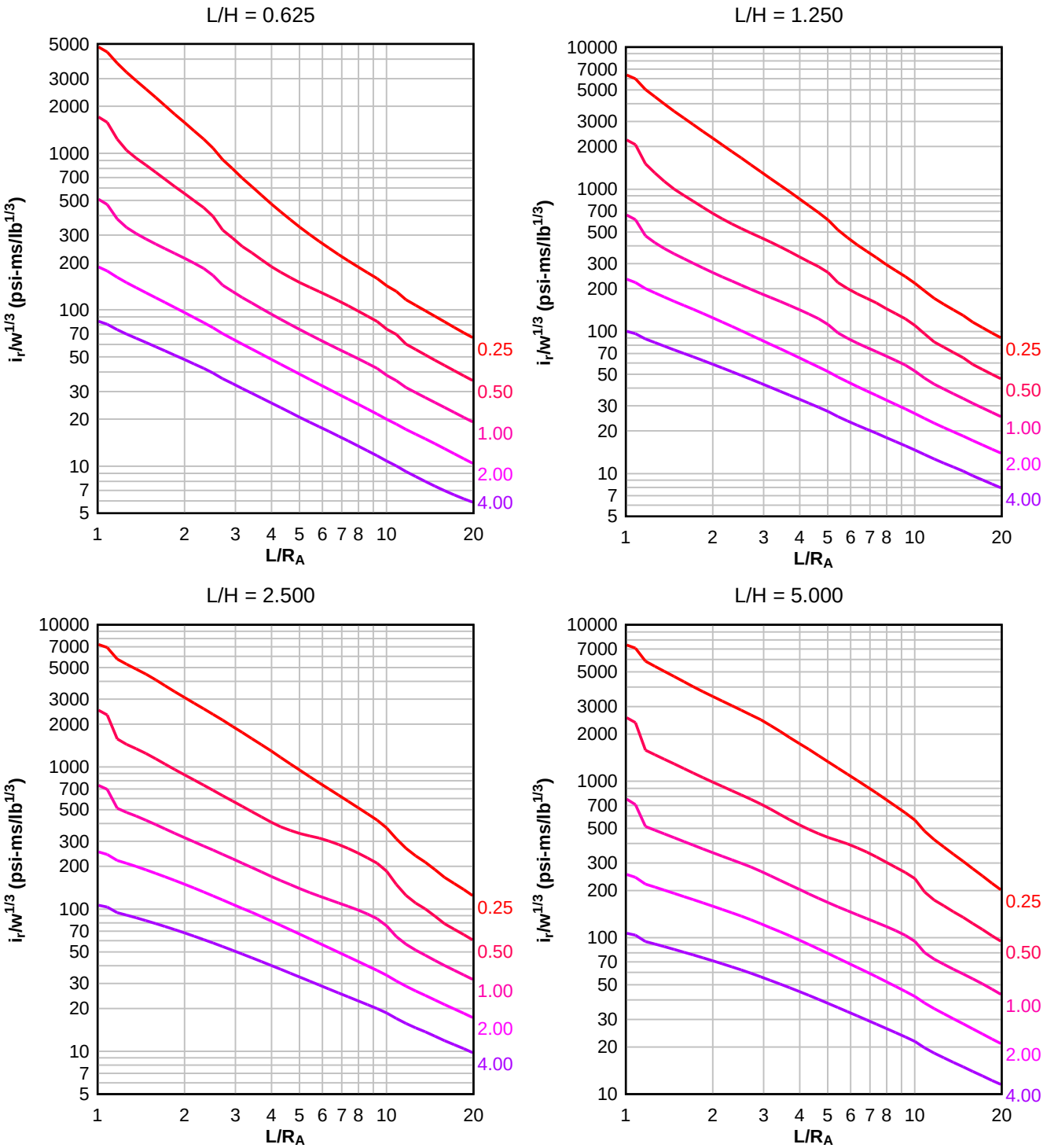

Figure 2-133 Scaled Average Unit Reflected Impulse (*N* = 3, *l/L* = 0.25 and 0.75, *h/H* = 0.25)

Numbers adjacent to curves indicate scaled range (ft/lb$^{1/3}$)

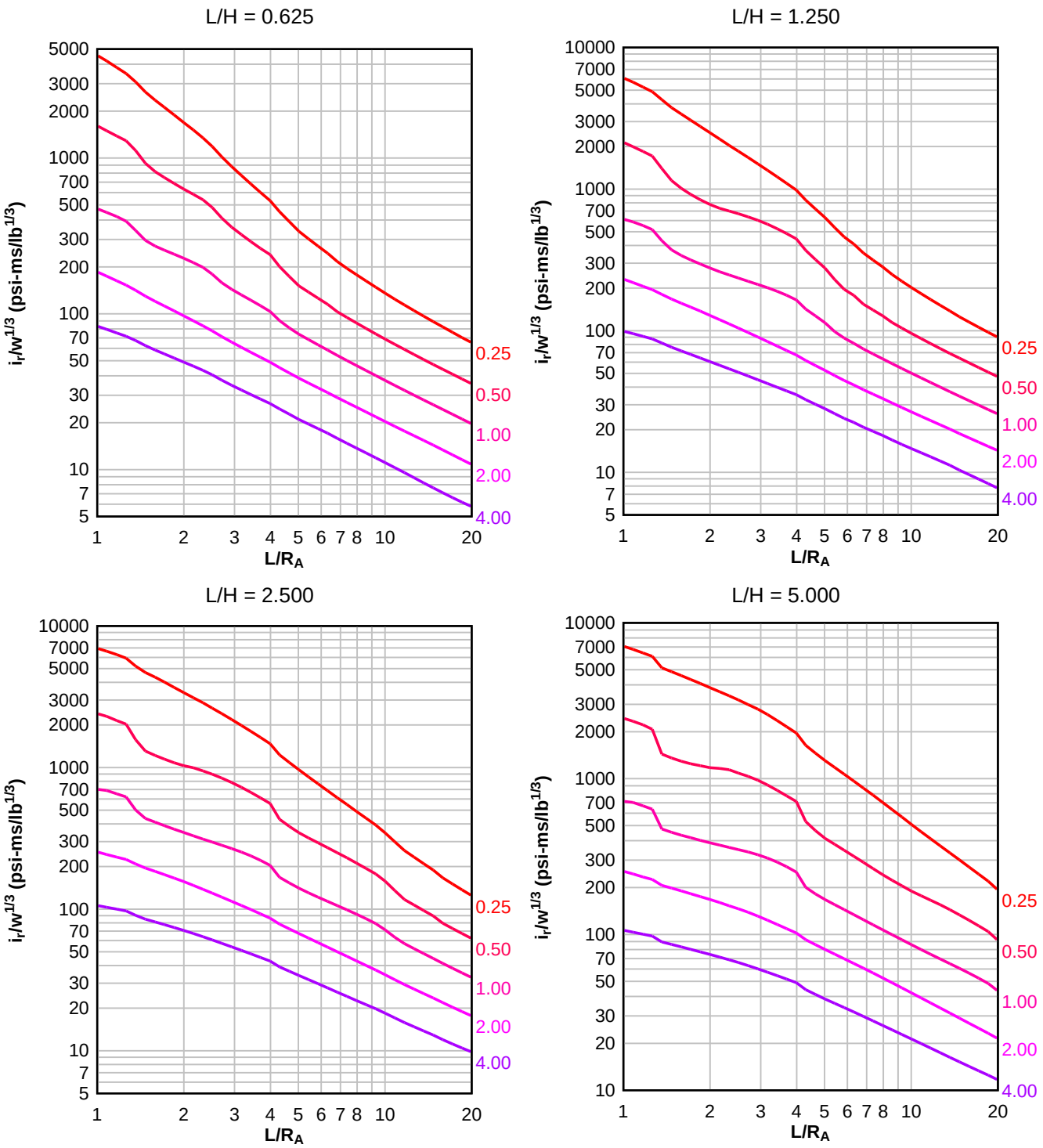

Figure 2-134 Scaled Average Unit Reflected Impulse (*N* = 3, *l/L* = 0.50, *h/H* = 0.25)

Numbers adjacent to curves indicate scaled range (ft/lb$^{1/3}$)

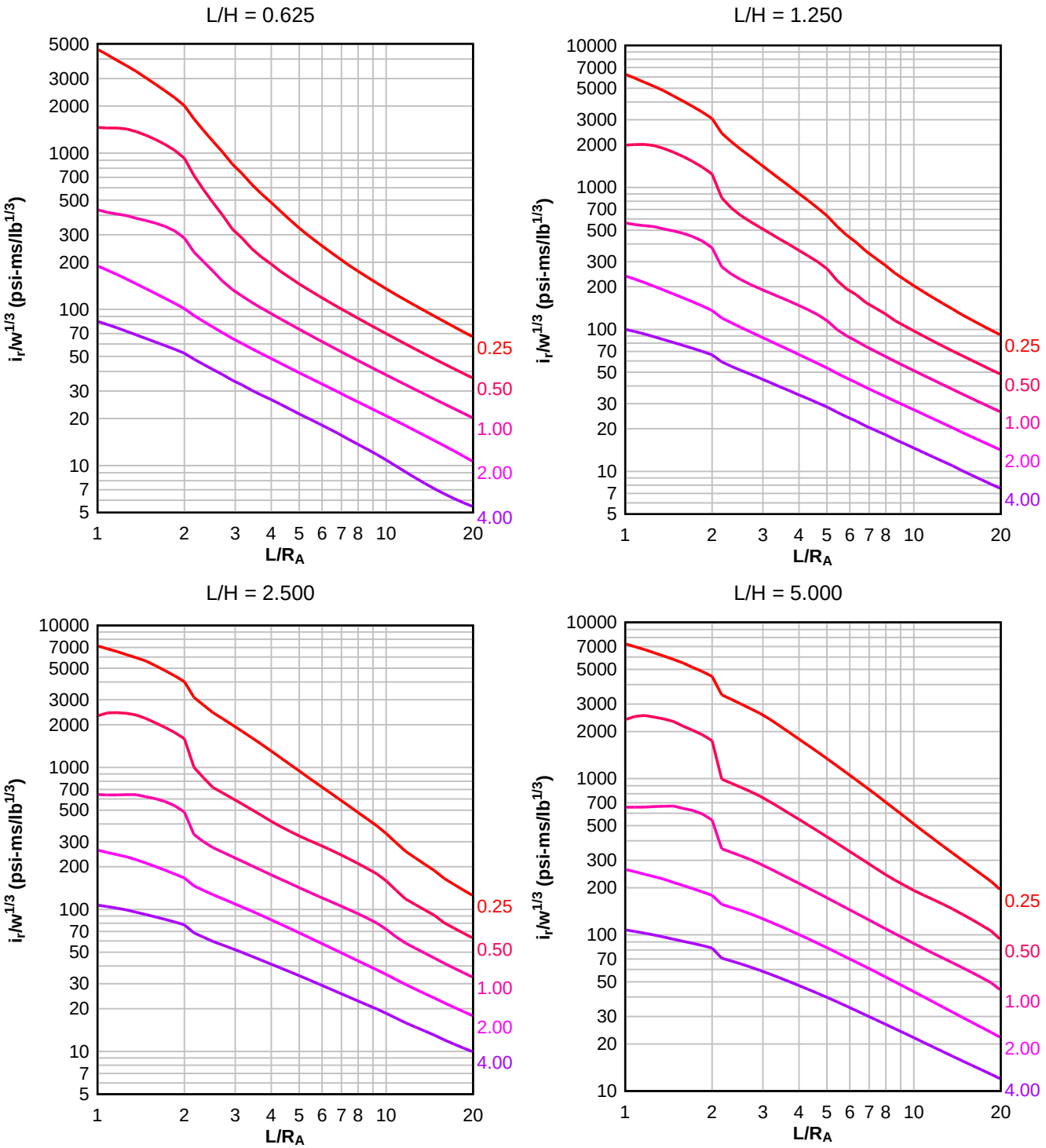

Figure 2-135 Scaled Average Unit Reflected Impulse (*N* = 3, *l/L* = 0.10, *h/H* = 0.50)

Numbers adjacent to curves indicate scaled range (ft/lb$^{1/3}$)

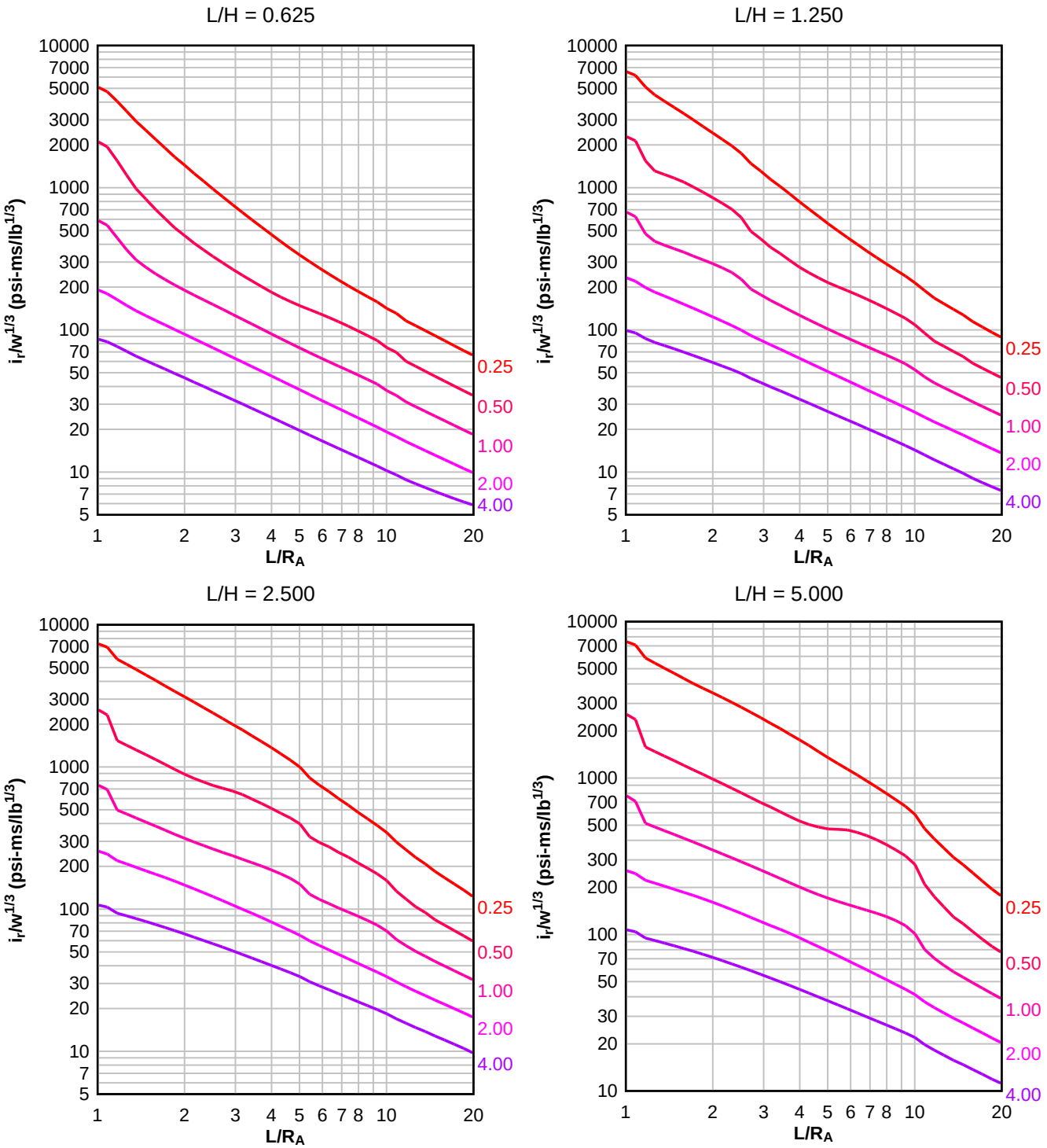

Figure 2-136 Scaled Average Unit Reflected Impulse (*N* = 3, *l/L* = 0.25 and 0.75, *h/H* = 0.50)

Numbers adjacent to curves indicate scaled range (ft/lb$^{1/3}$)

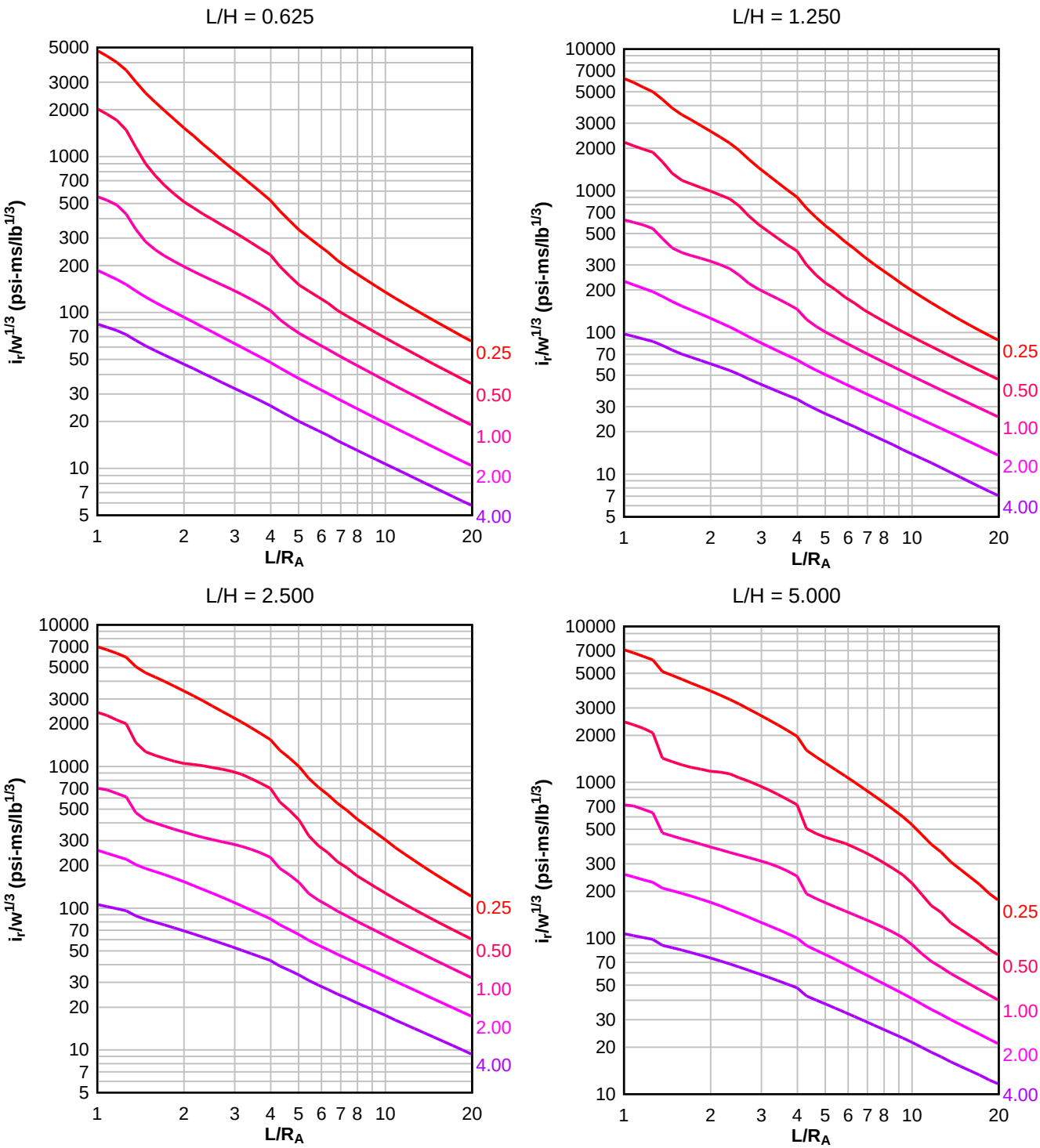

Figure 2-137 Scaled Average Unit Reflected Impulse (*N* = 3, *l/L* = 0.50, *h/H* = 0.50)

Numbers adjacent to curves indicate scaled range (ft/lb$^{1/3}$)

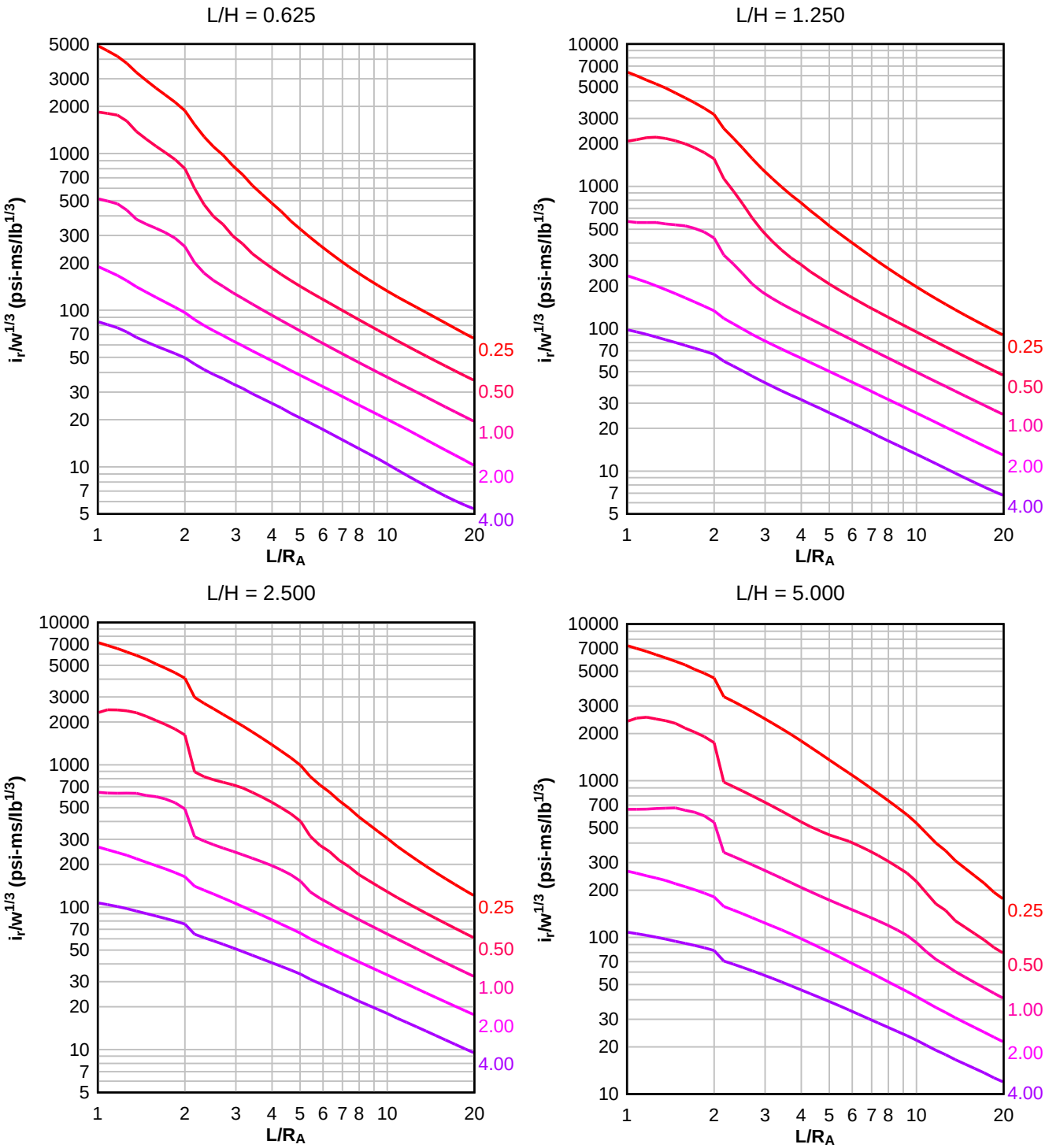

Figure 2-138 Scaled Average Unit Reflected Impulse (*N* = 3, *l/L* = 0.10, *h/H* = 0.75)

Numbers adjacent to curves indicate scaled range (ft/lb$^{1/3}$)

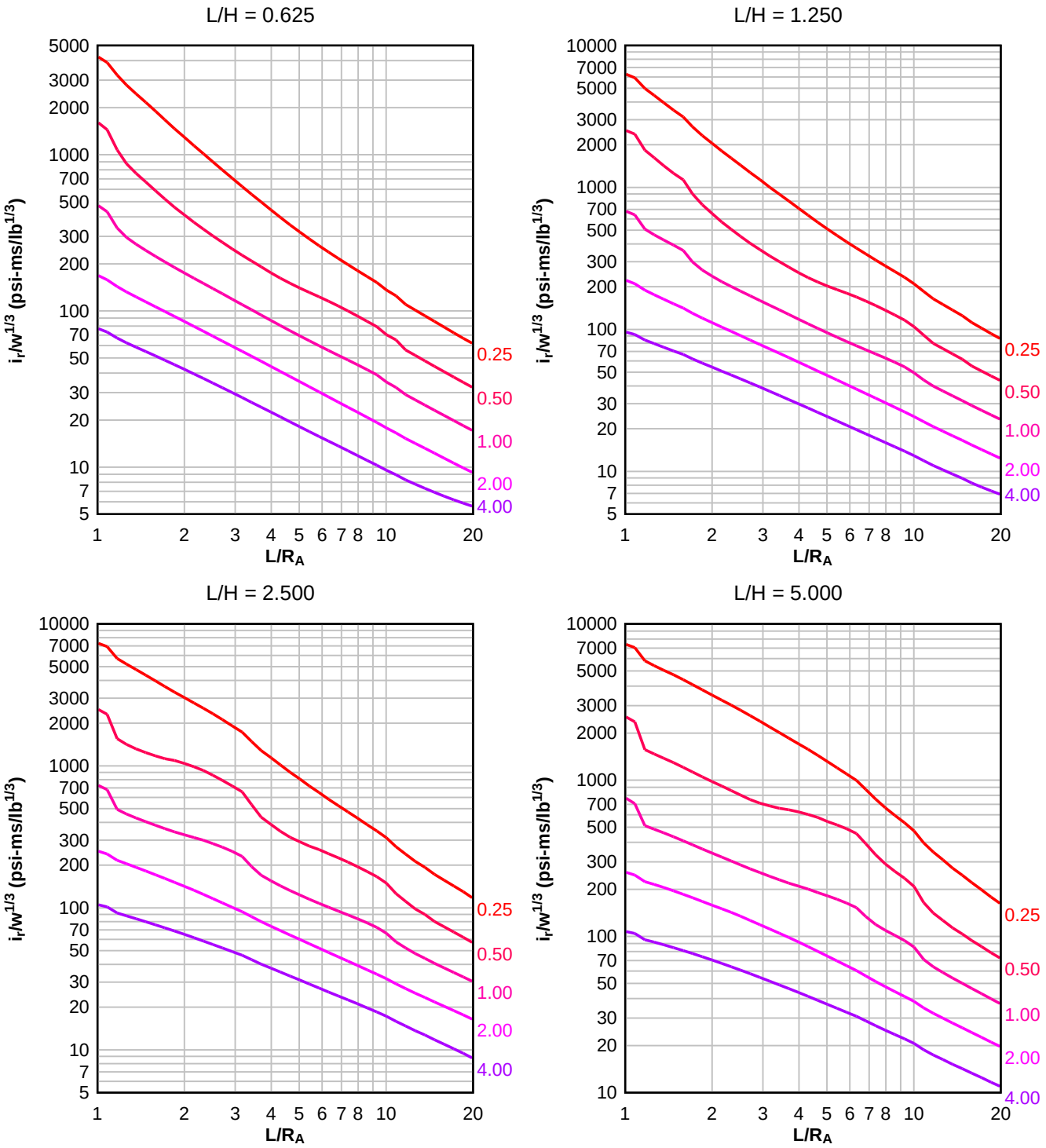

Figure 2-139 Scaled Average Unit Reflected Impulse (*N* = 3, *l/L* = 0.25 and 0.75, *h/H* = 0.75)

Numbers adjacent to curves indicate scaled range (ft/lb$^{1/3}$)

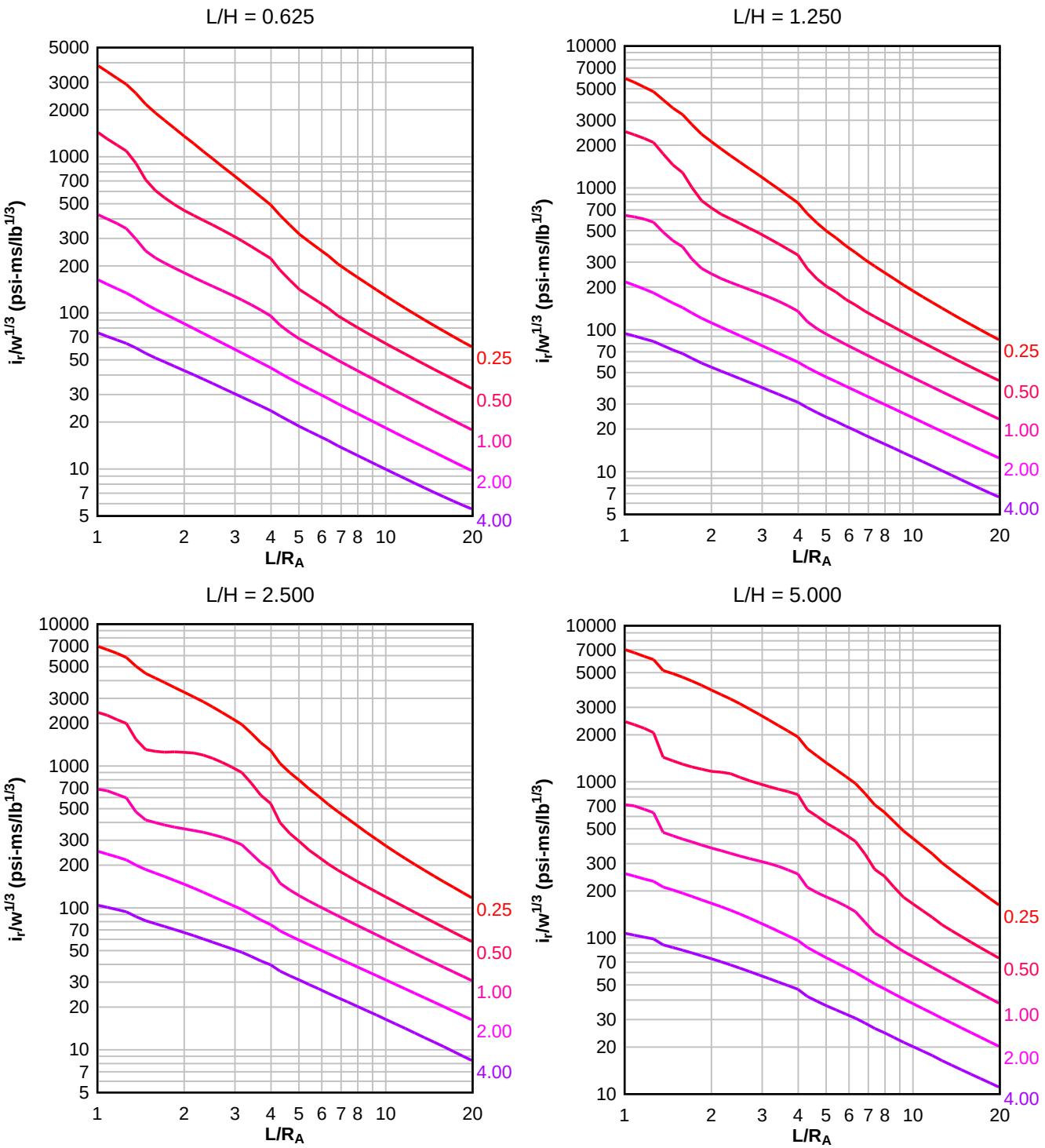

Figure 2-140 Scaled Average Unit Reflected Impulse (*N* = 3, *l/L* = 0.50, *h/H* = 0.75)

Numbers adjacent to curves indicate scaled range (ft/lb$^{1/3}$)

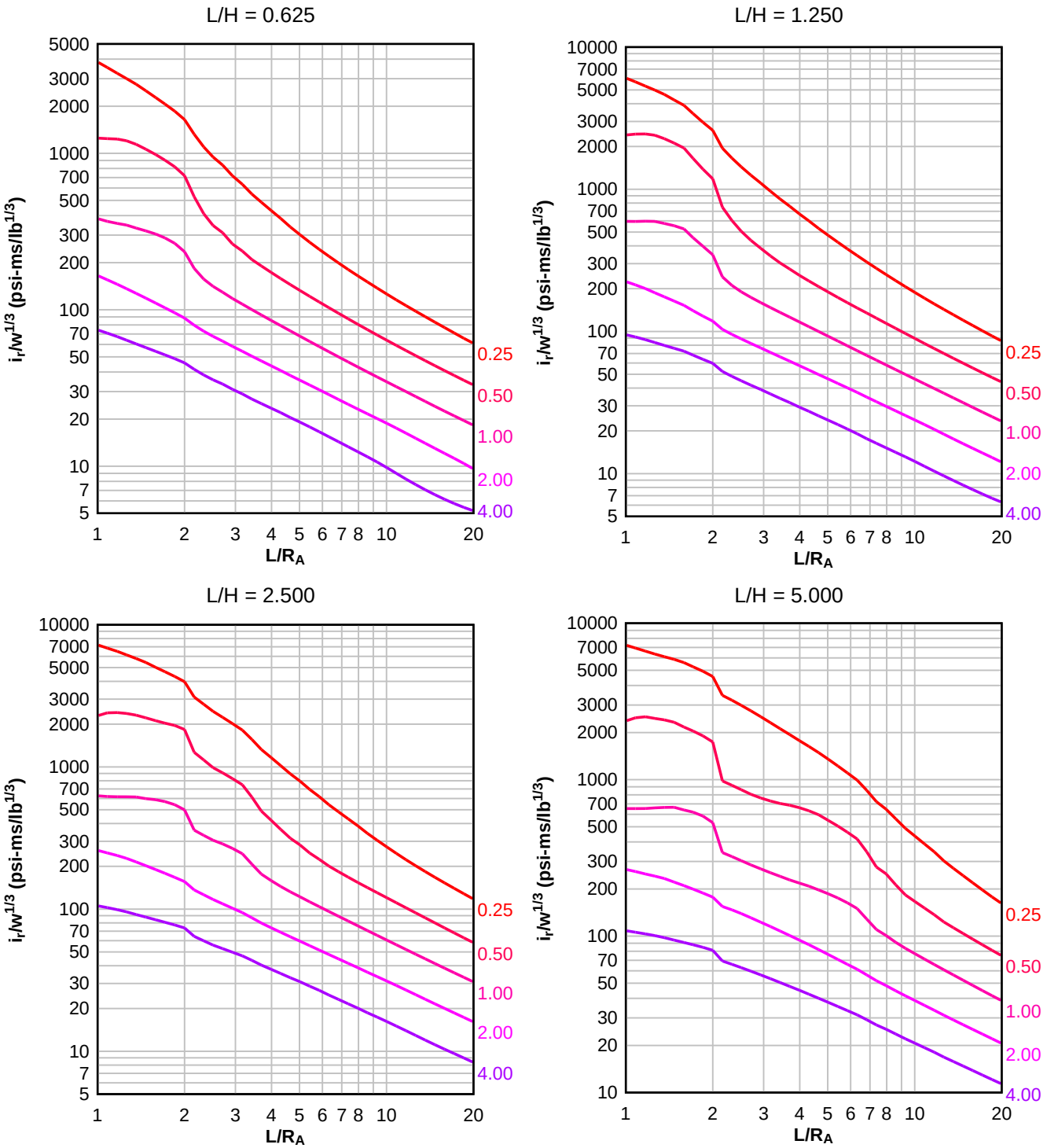

Figure 2-141 Scaled Average Unit Reflected Impulse (*N* = 4, *l*/*L* = 0.10, *h*/*H* = 0.10)

Numbers adjacent to curves indicate scaled range (ft/lb$^{1/3}$)

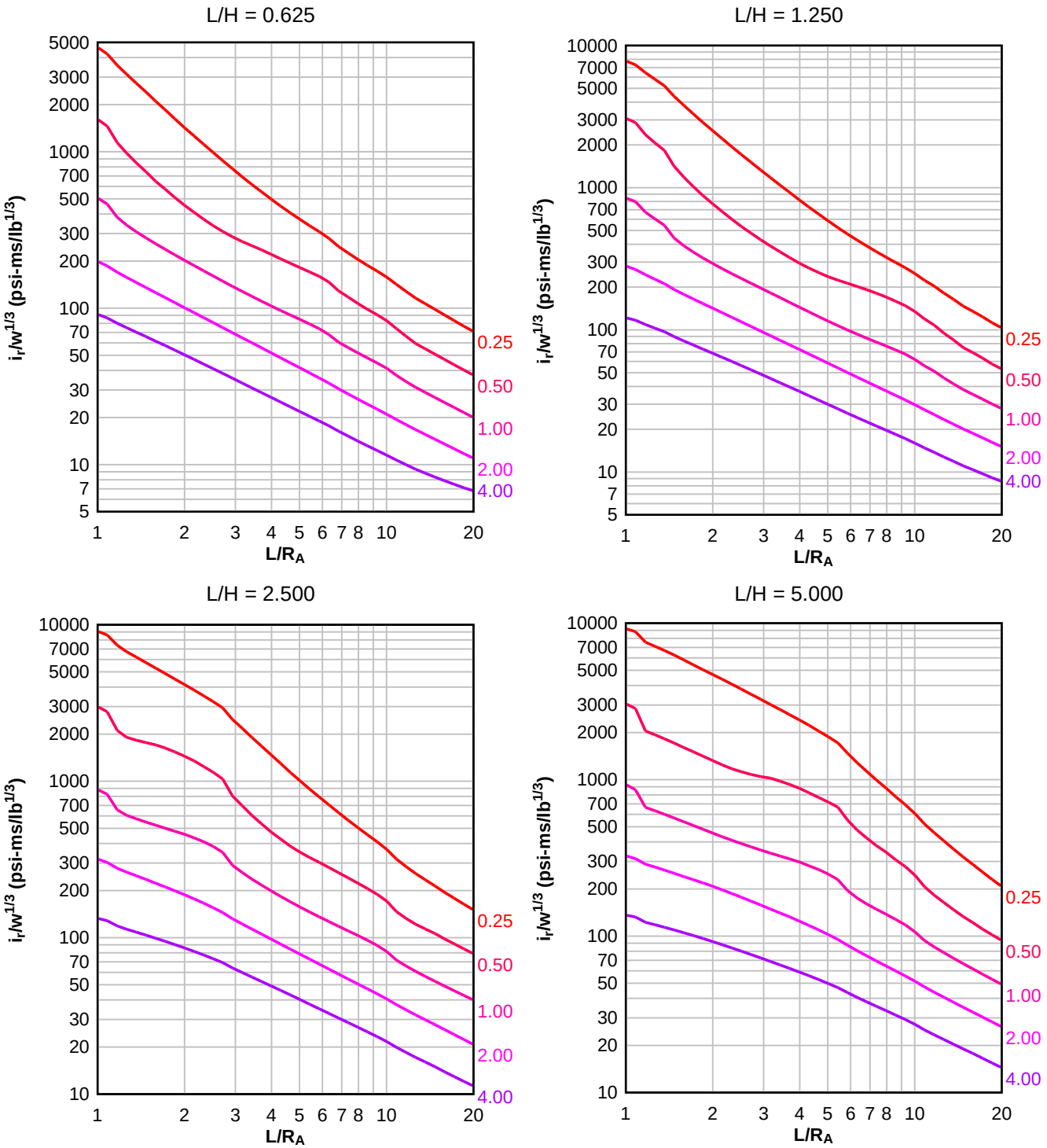

Figure 2-142 Scaled Average Unit Reflected Impulse (*N* = 4, *l/L* = 0.25 and 0.75, *h/H* = 0.10)

Numbers adjacent to curves indicate scaled range (ft/lb$^{1/3}$)

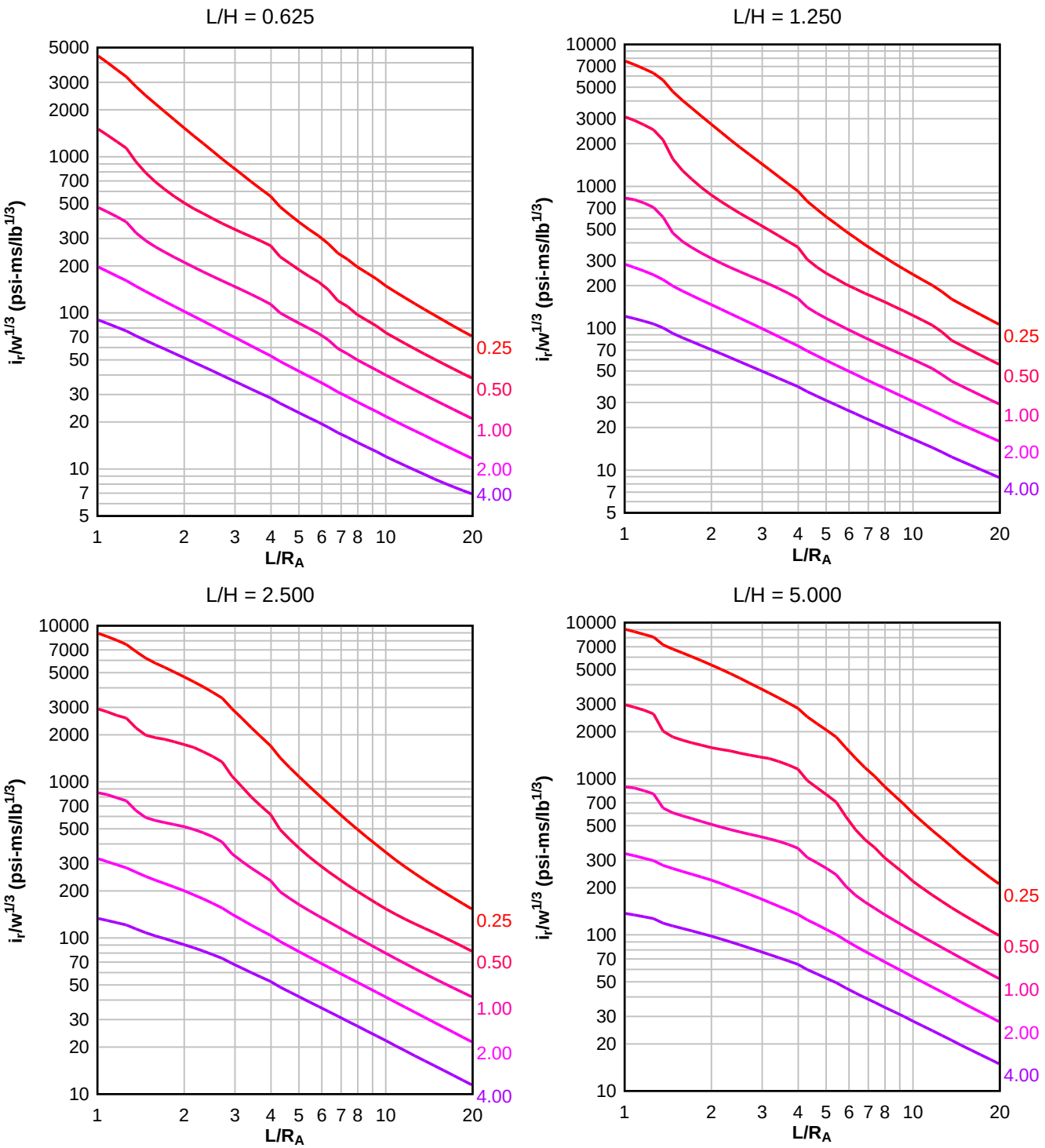

Figure 2-143 Scaled Average Unit Reflected Impulse (*N* = 4, *l*/*L* = 0.50, *h*/*H* = 0.10)

Numbers adjacent to curves indicate scaled range (ft/lb$^{1/3}$)

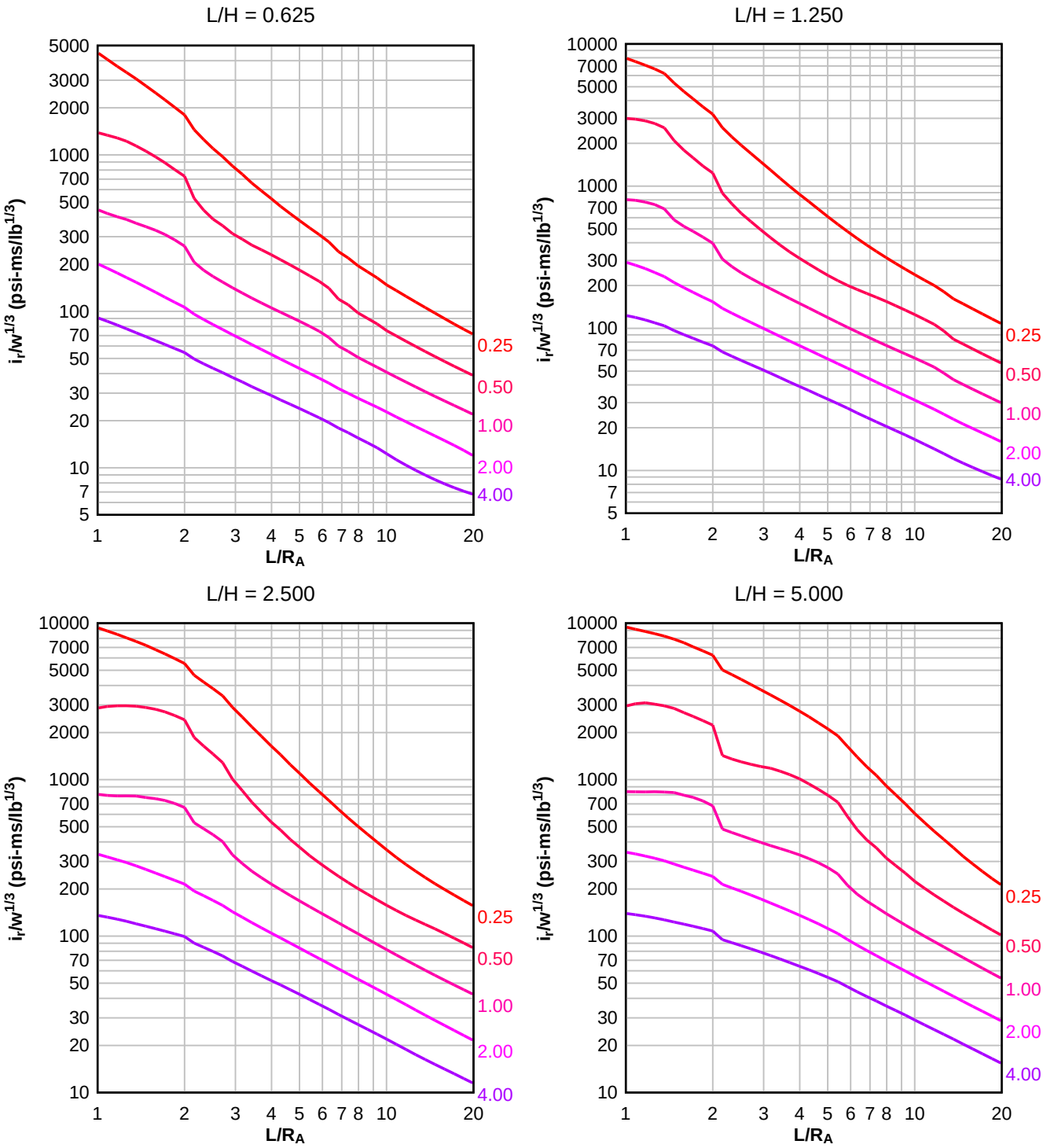

Figure 2-144 Scaled Average Unit Reflected Impulse (*N* = 4, *l/L* = 0.10, *h/H* = 0.25 and 0.75)

Numbers adjacent to curves indicate scaled range (ft/lb$^{1/3}$)

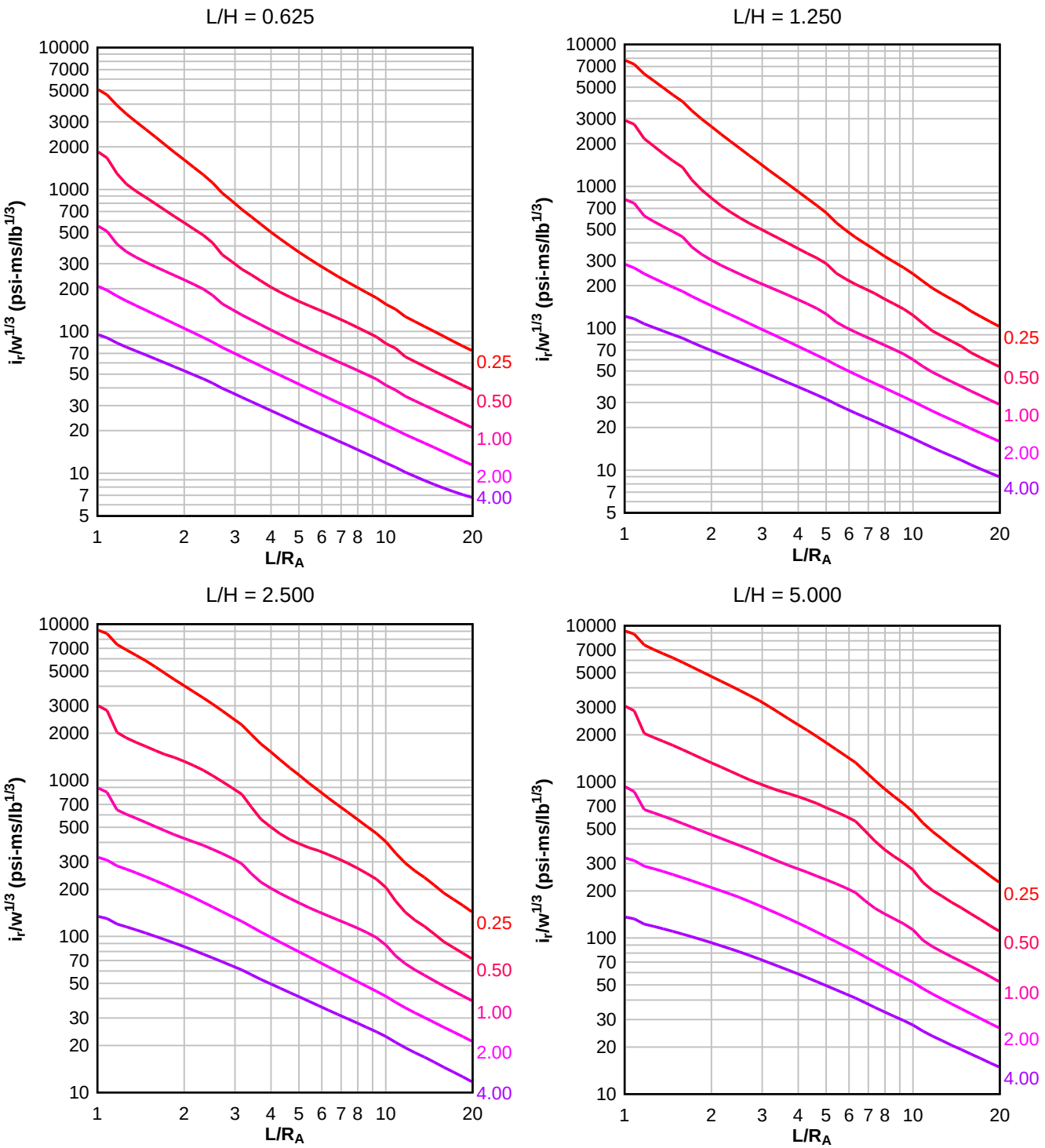

Figure 2-145 Scaled Average Unit Reflected Impulse (*N* = 4, *l/L* = 0.25 and 0.75, *h/H* = 0.25 and 0.75)

Numbers adjacent to curves indicate scaled range (ft/lb$^{1/3}$)

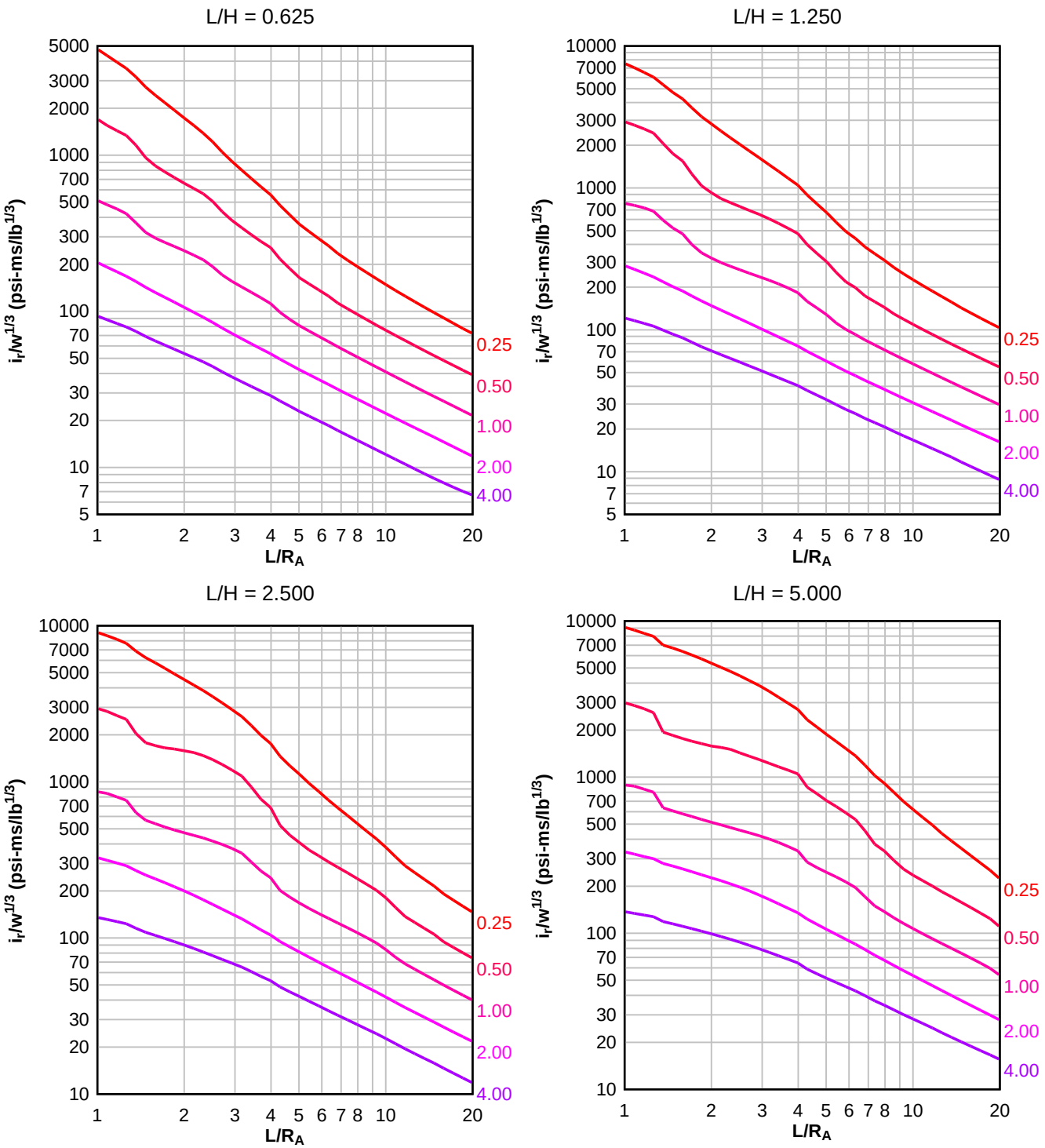

Figure 2-146 Scaled Average Unit Reflected Impulse (*N* = 4, *l/L* = 0.50, *h/H* = 0.25 and 0.75)

Numbers adjacent to curves indicate scaled range (ft/lb$^{1/3}$)

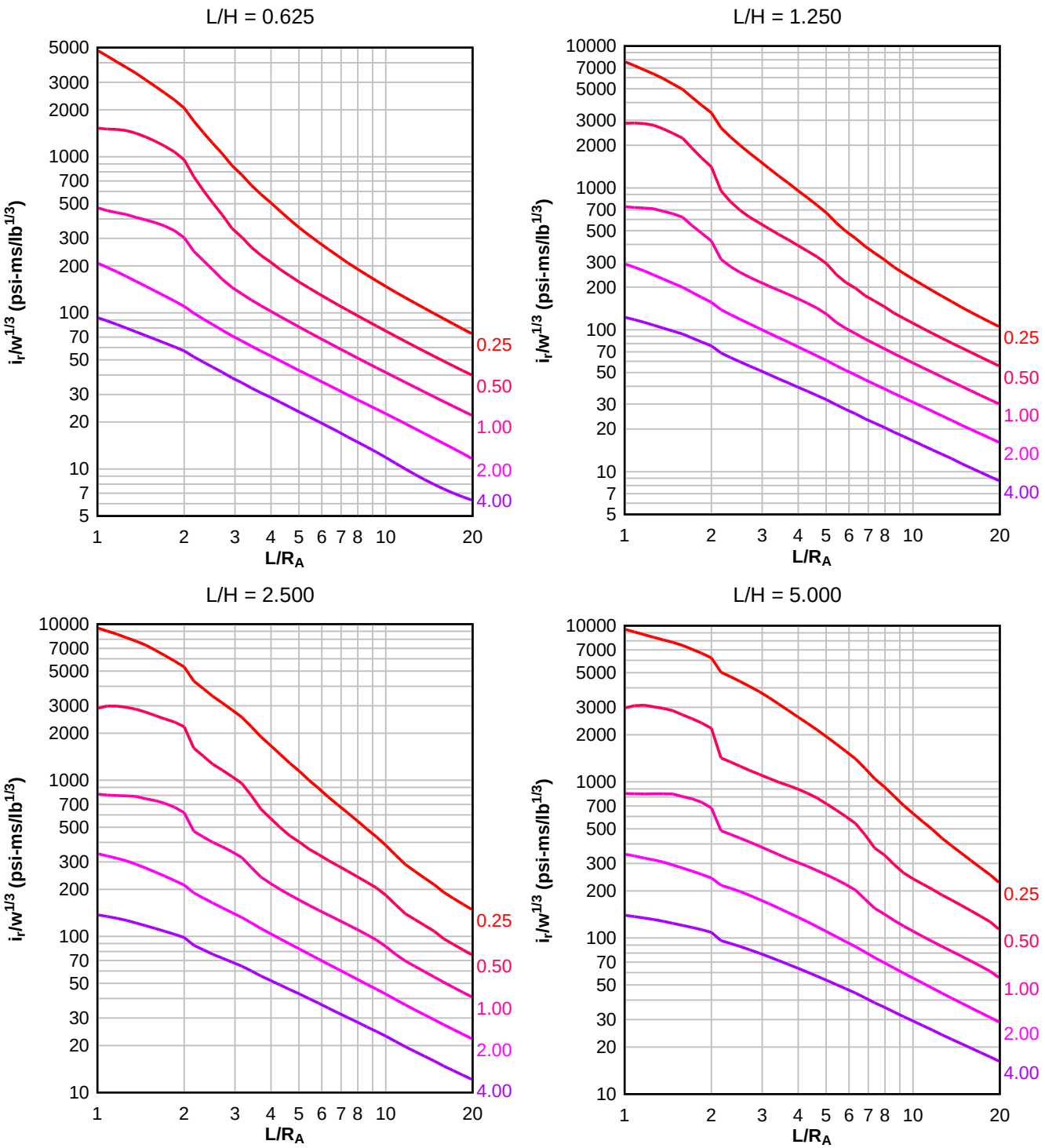

Figure 2-147 Scaled Average Unit Reflected Impulse (*N* = 4, *l*/*L* = 0.10, *h*/*H* = 0.50)

Numbers adjacent to curves indicate scaled range (ft/lb$^{1/3}$)

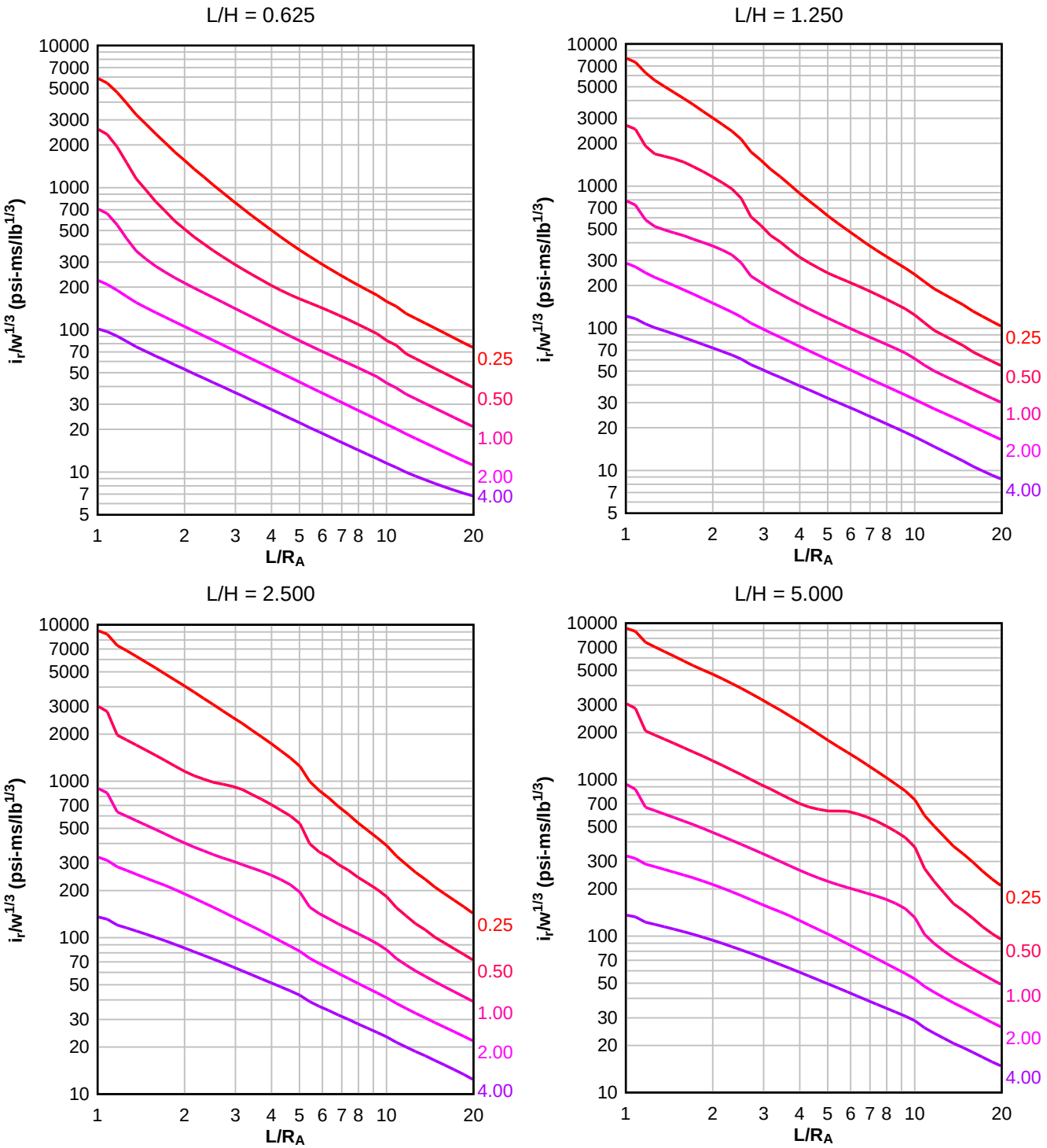

Figure 2-148 Scaled Average Unit Reflected Impulse (*N* = 4, *l/L* = 0.25 and 0.75, *h/H* = 0.50)

Numbers adjacent to curves indicate scaled range (ft/lb$^{1/3}$)

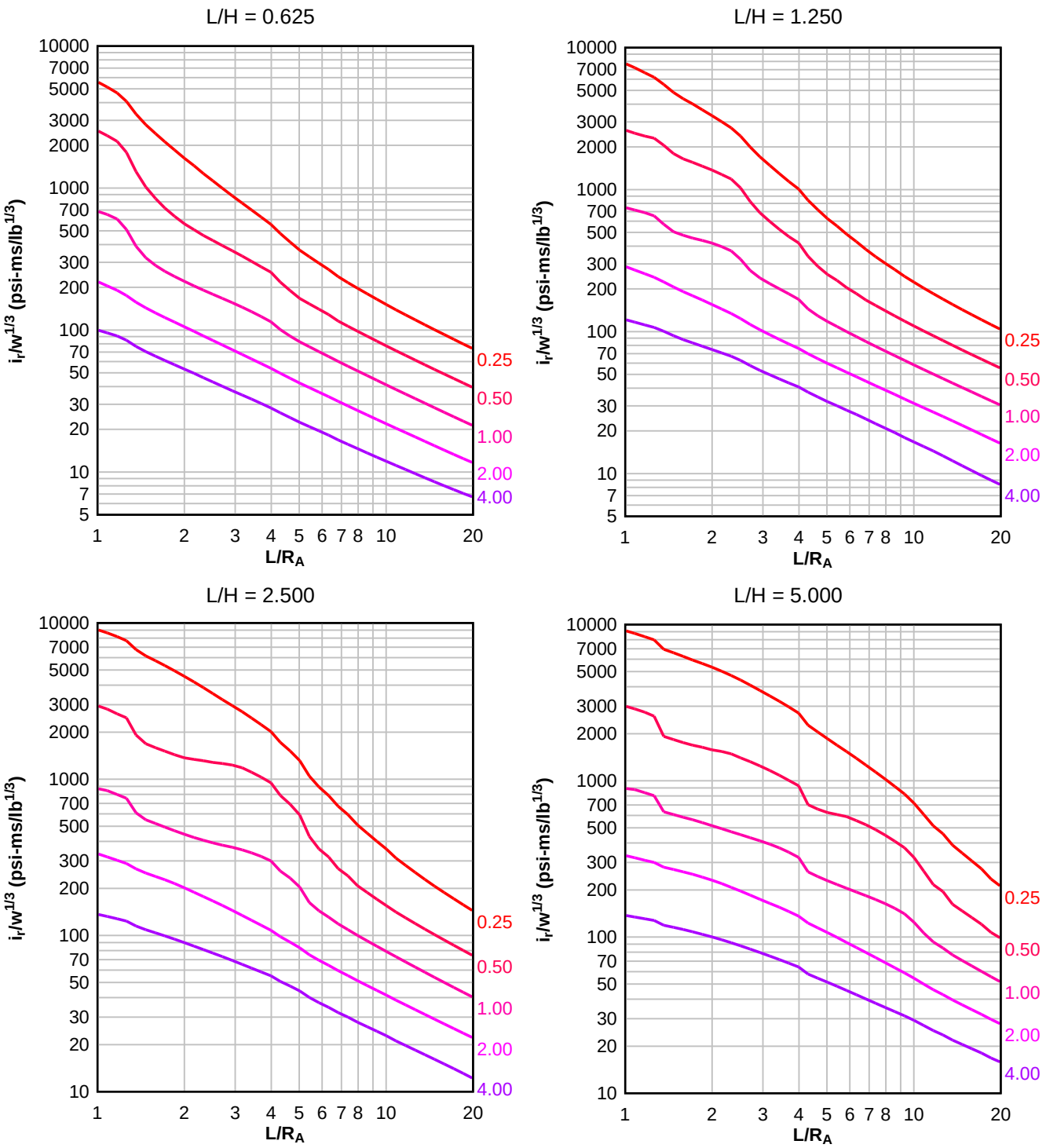

Figure 2-149 Scaled Average Unit Reflected Impulse (*N* = 4, *l/L* = 0.50, *h/H* = 0.50)

Numbers adjacent to curves indicate scaled range (ft/lb$^{1/3}$)

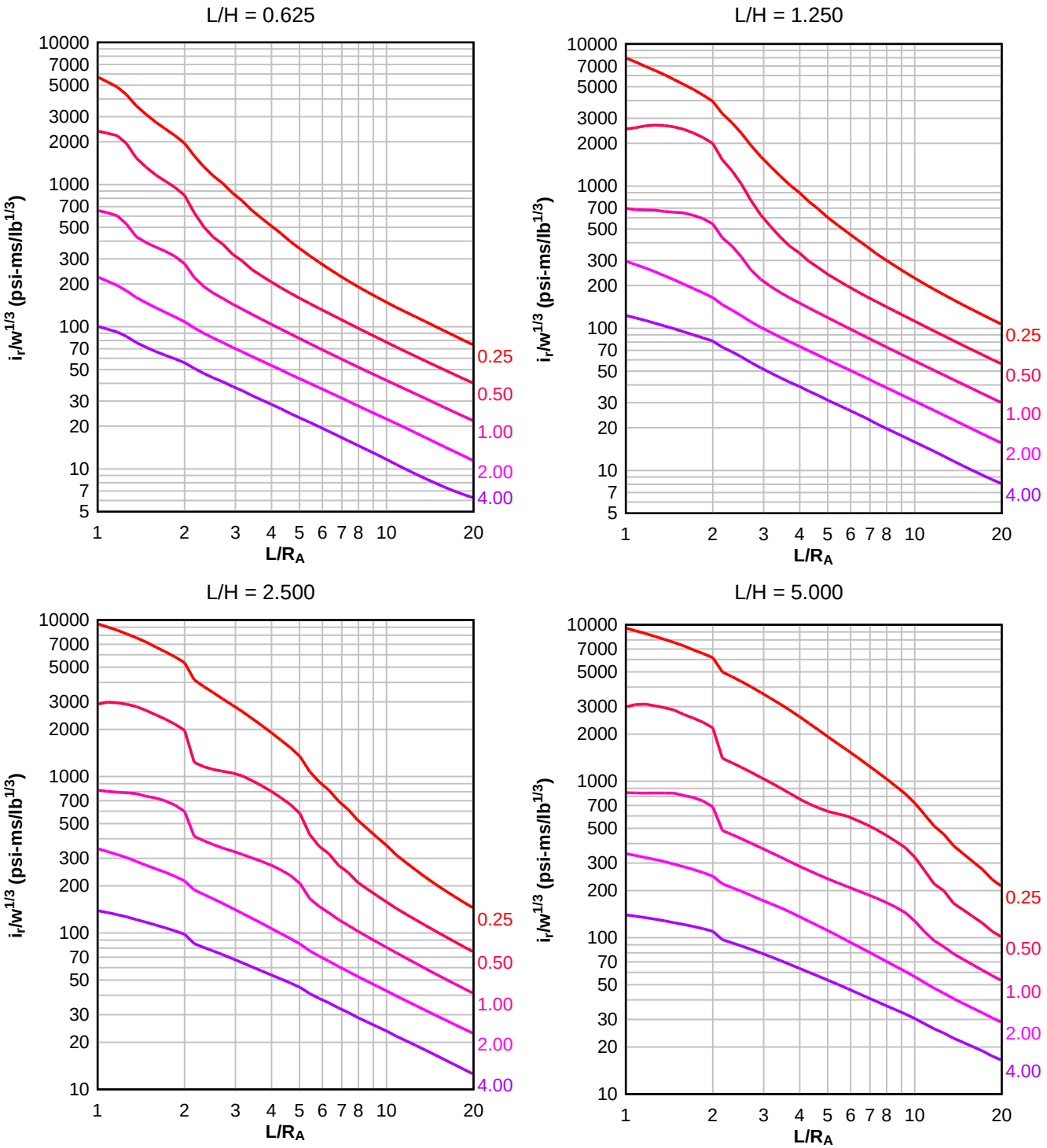

Figure 2-150 Reflection Factor for Shock Loads on Frangible Elements

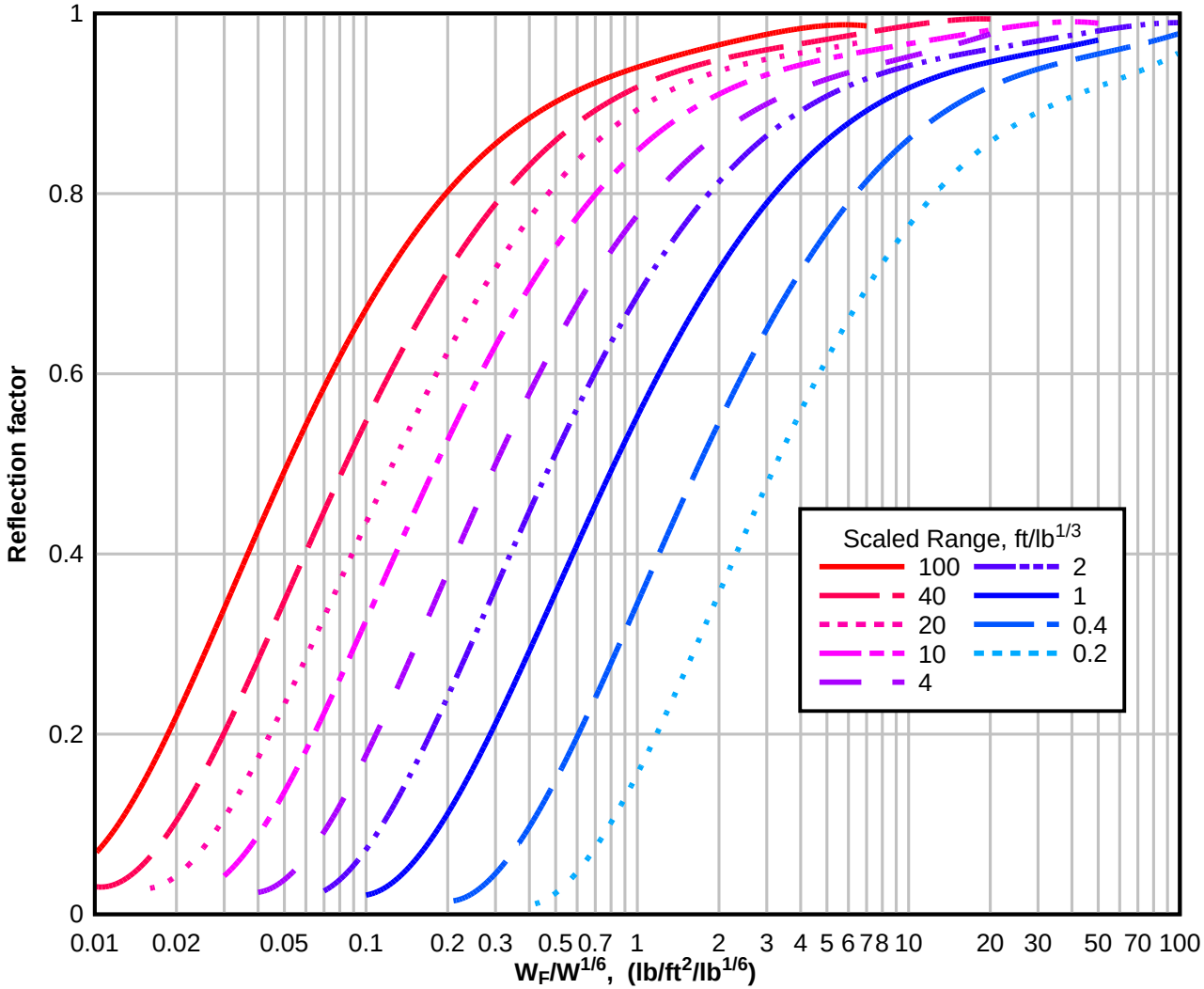

Figure 2-151 Pressure-Time Variation for a Partially Vented Explosion

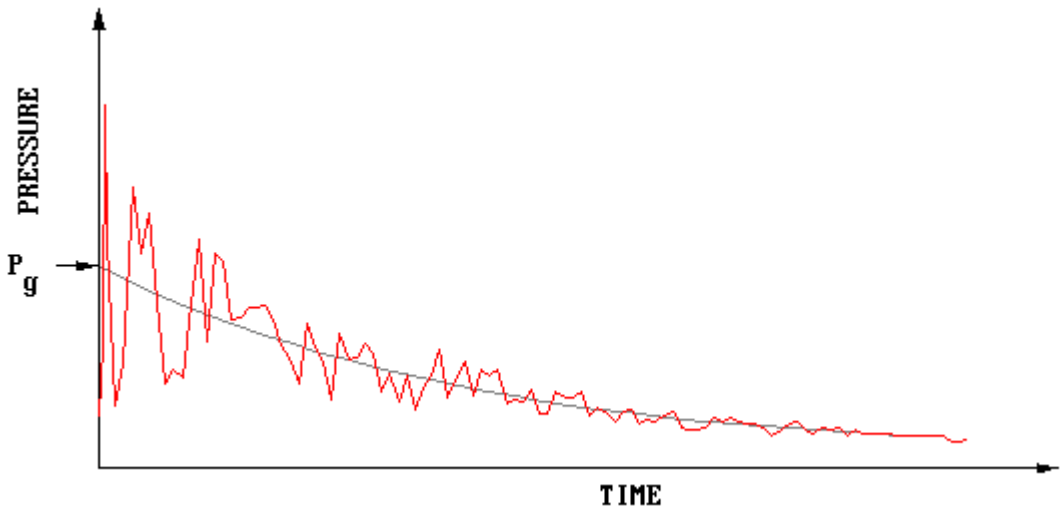

\1\

Figure 2-152 Peak Gas Pressure Produced by a TNT Detonation in a Partially Contained Chamber

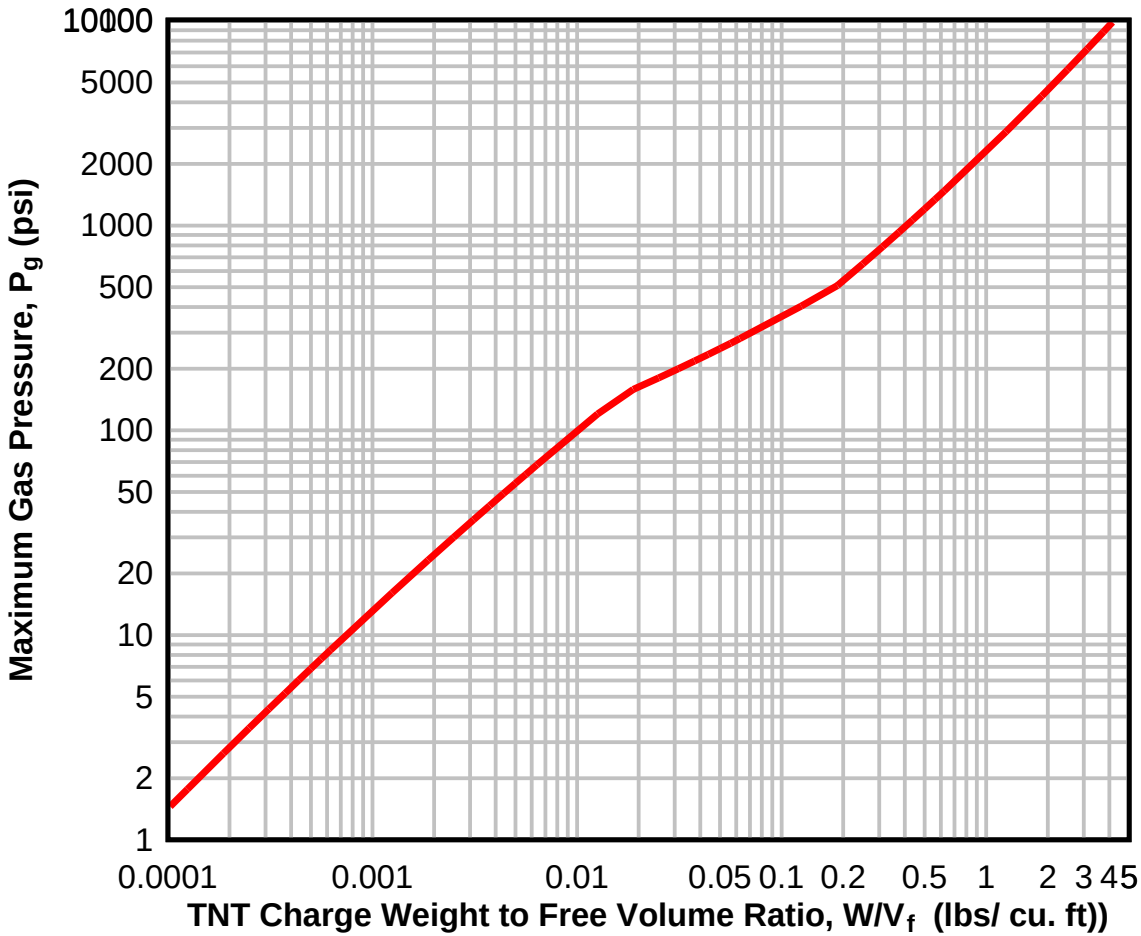

/1/

Figure 2-153 Scaled Gas Impulse (W/V_f = 0.002, $i_r/W^{1/3}$ = 20)

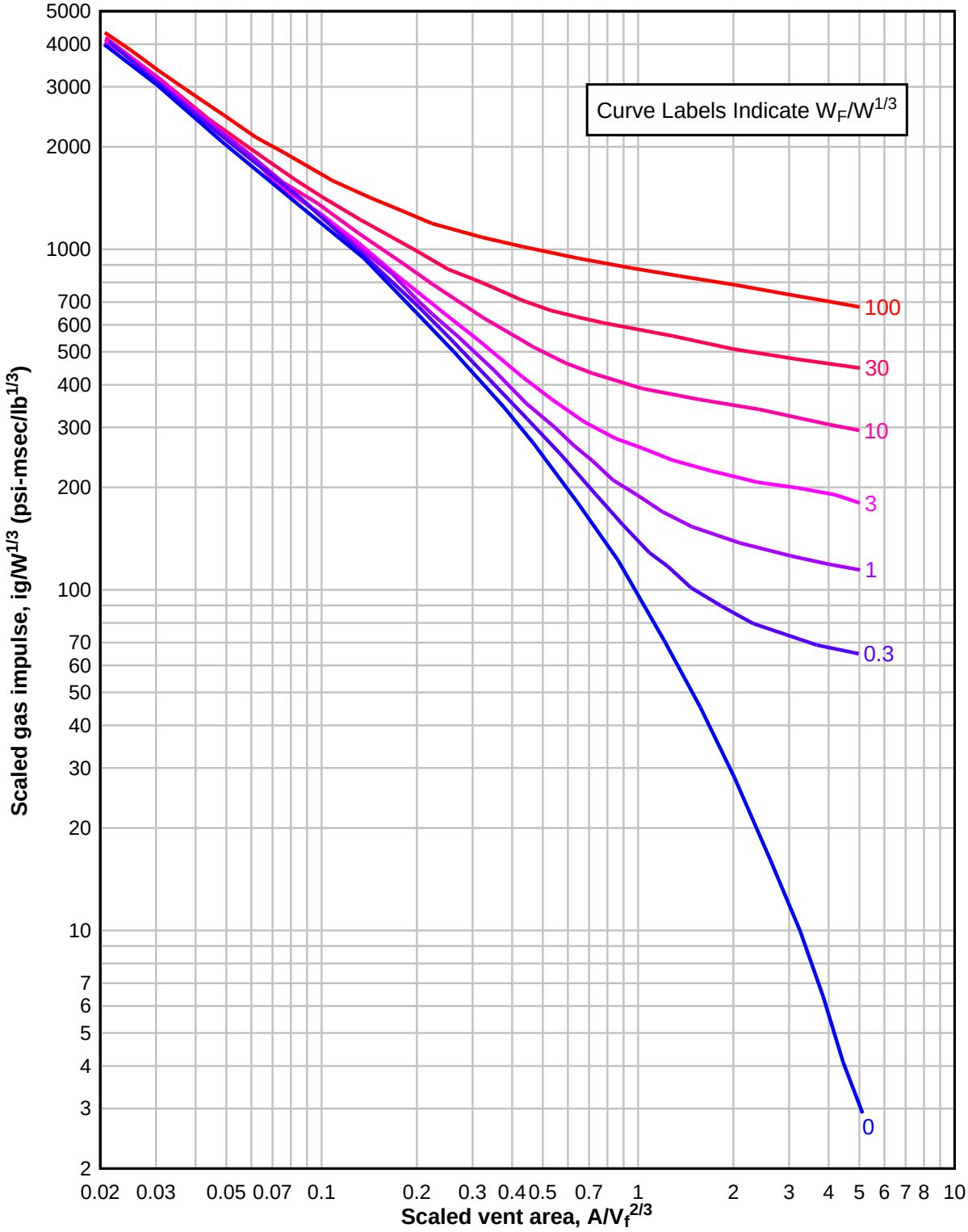

Figure 2-154 Scaled Gas Impulse (W/V_f = 0.002, $i_r/W^{1/3}$ = 100)

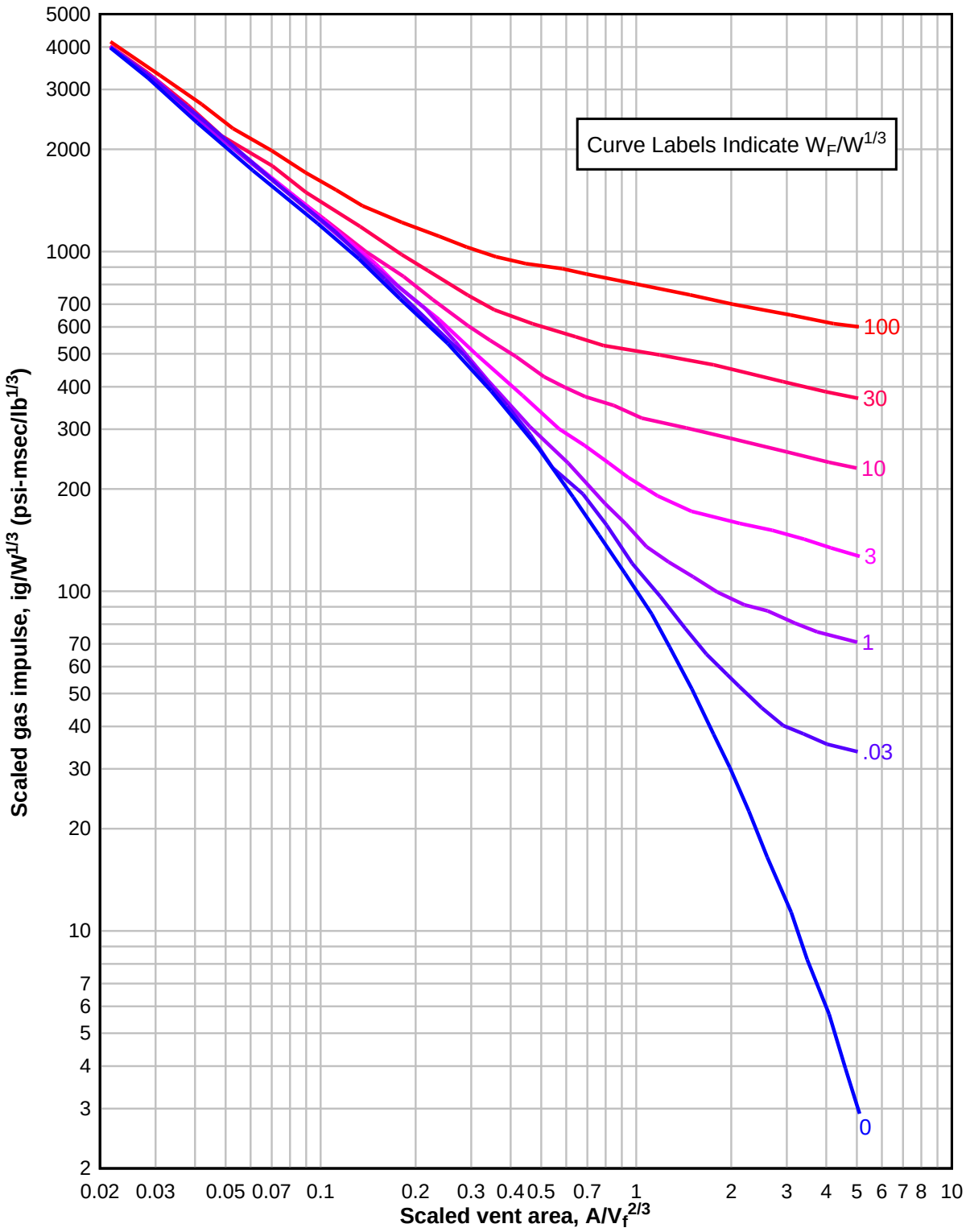

Figure 2-155 Scaled Gas Impulse (W/V_f = 0.002, $i_r/W^{1/3}$ = 600)

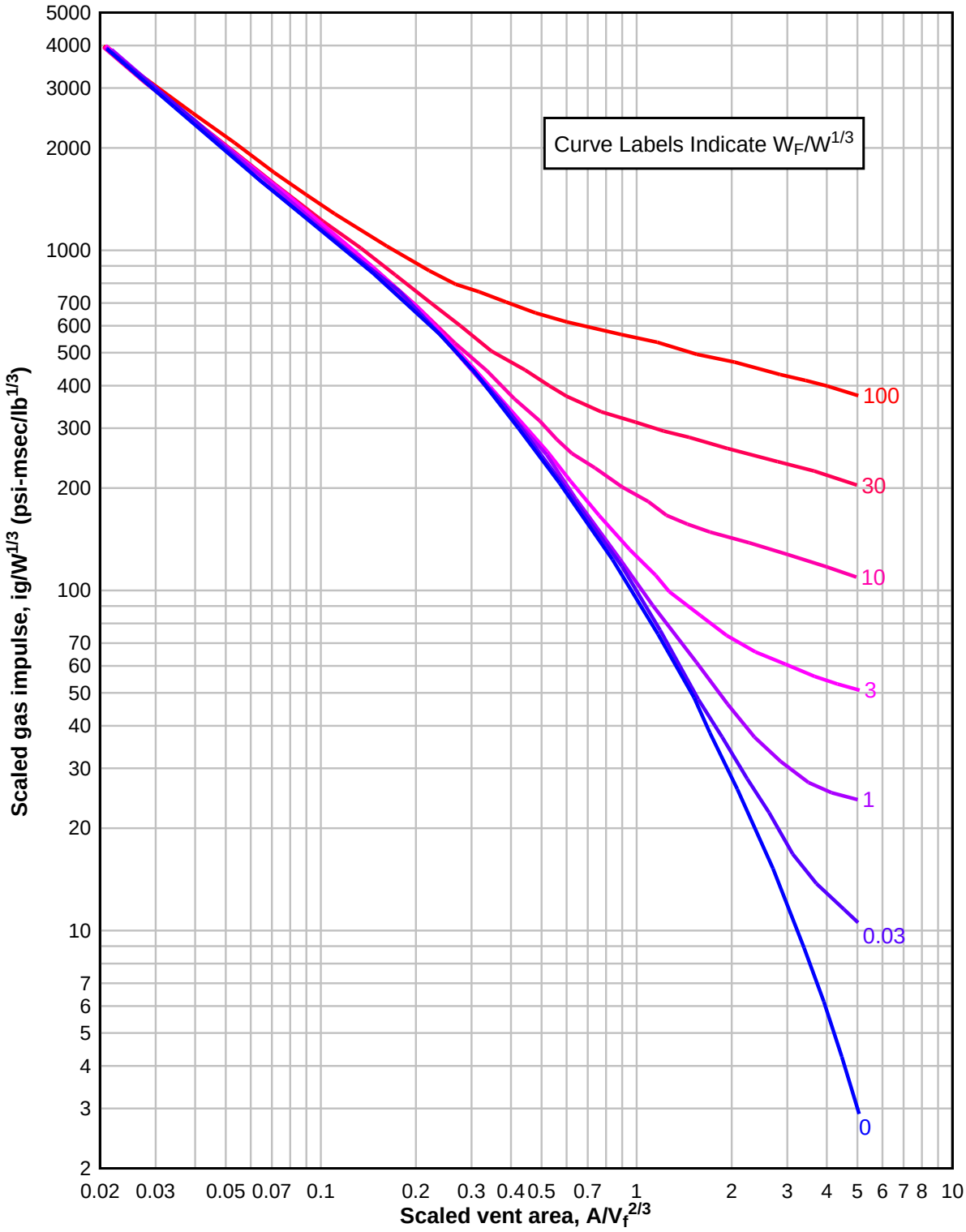

Figure 2-156 Scaled Gas Impulse (W/V_f = 0.015, $i_r/W^{1/3}$ = 20)

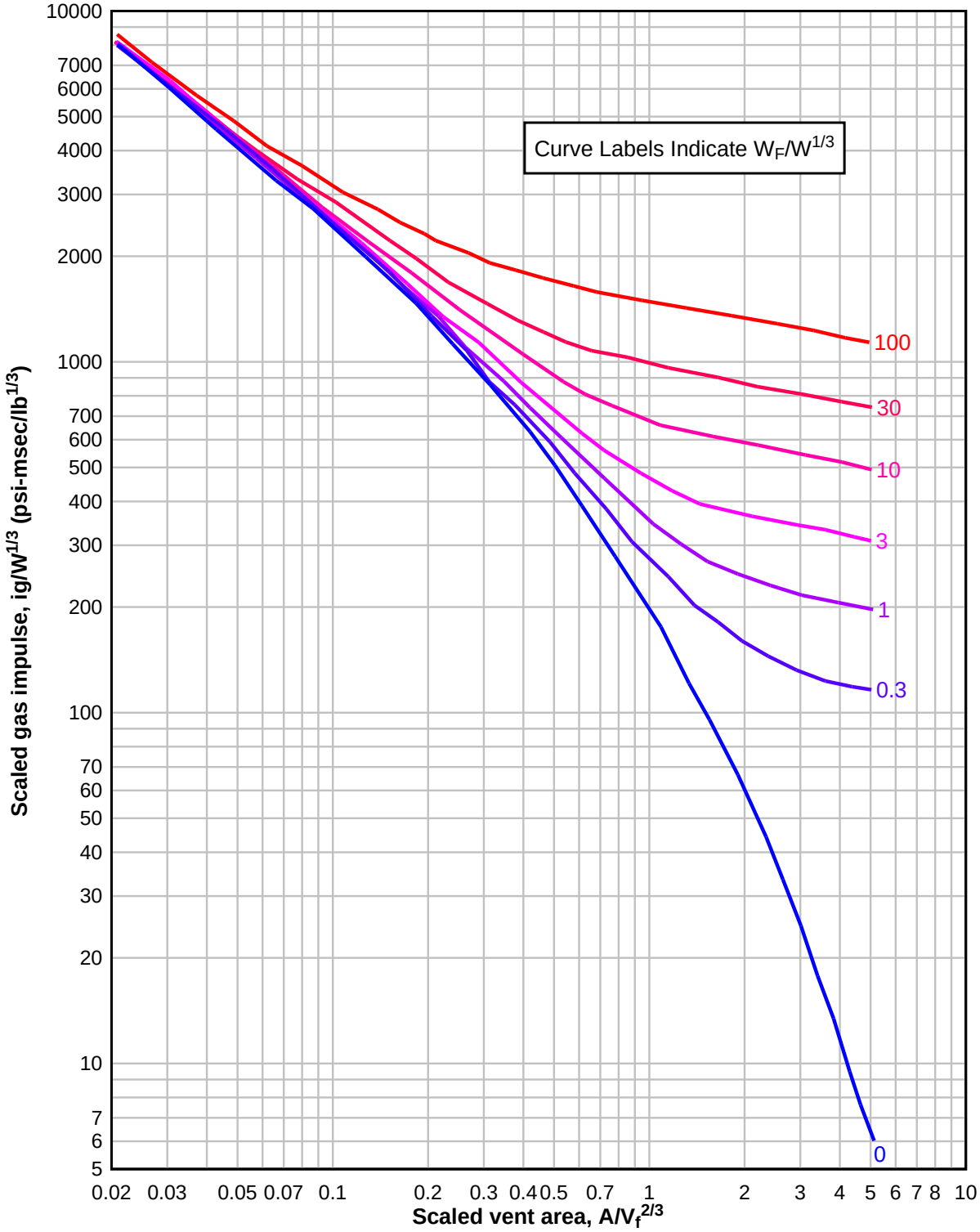

Figure 2-157 Scaled Gas Impulse (W/V_f = 0.015, $i_r/W^{1/3}$ = 100)

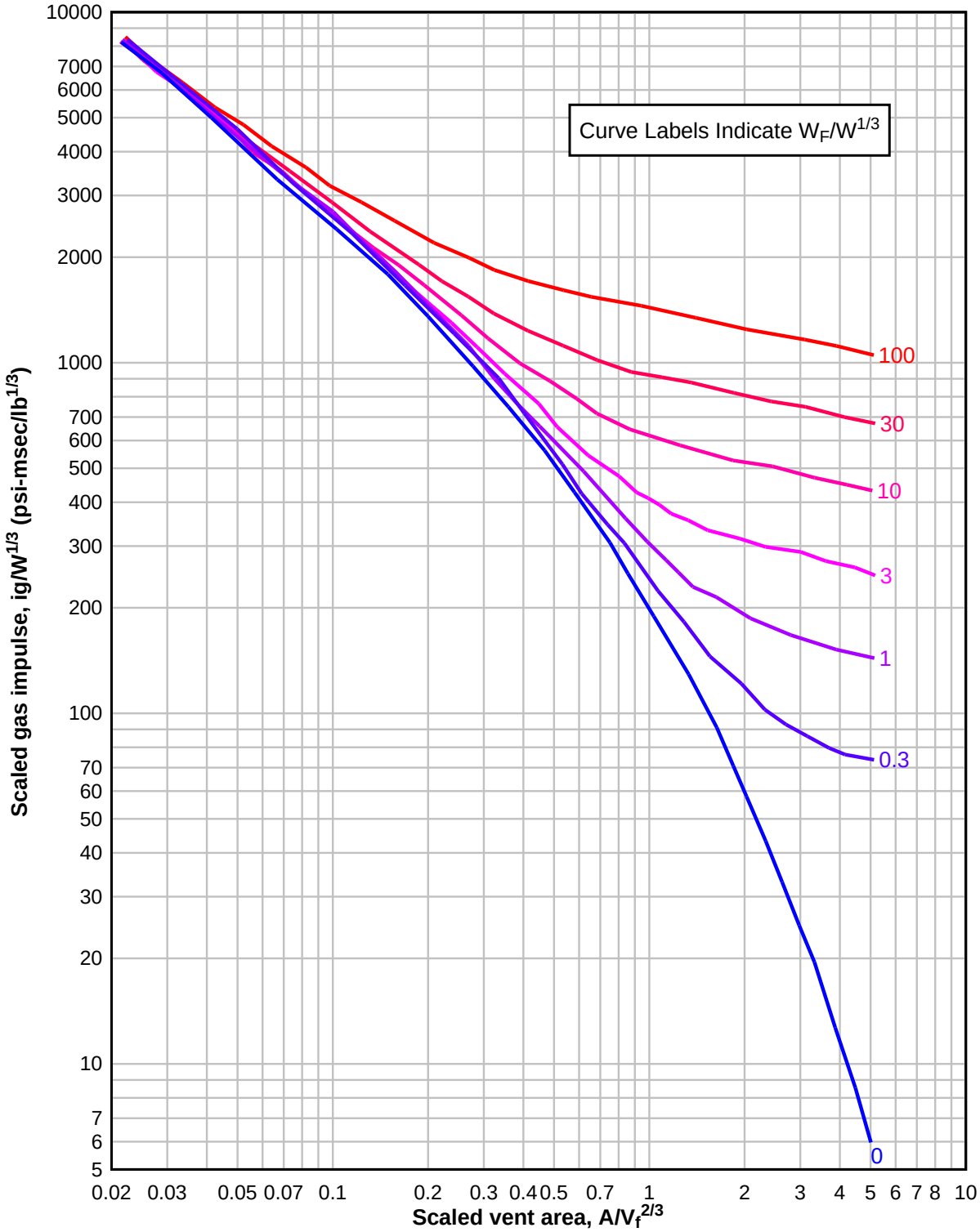

Figure 2-158 Scaled Gas Impulse (W/V_f = 0.015, $i_r/W^{1/3}$ = 600)

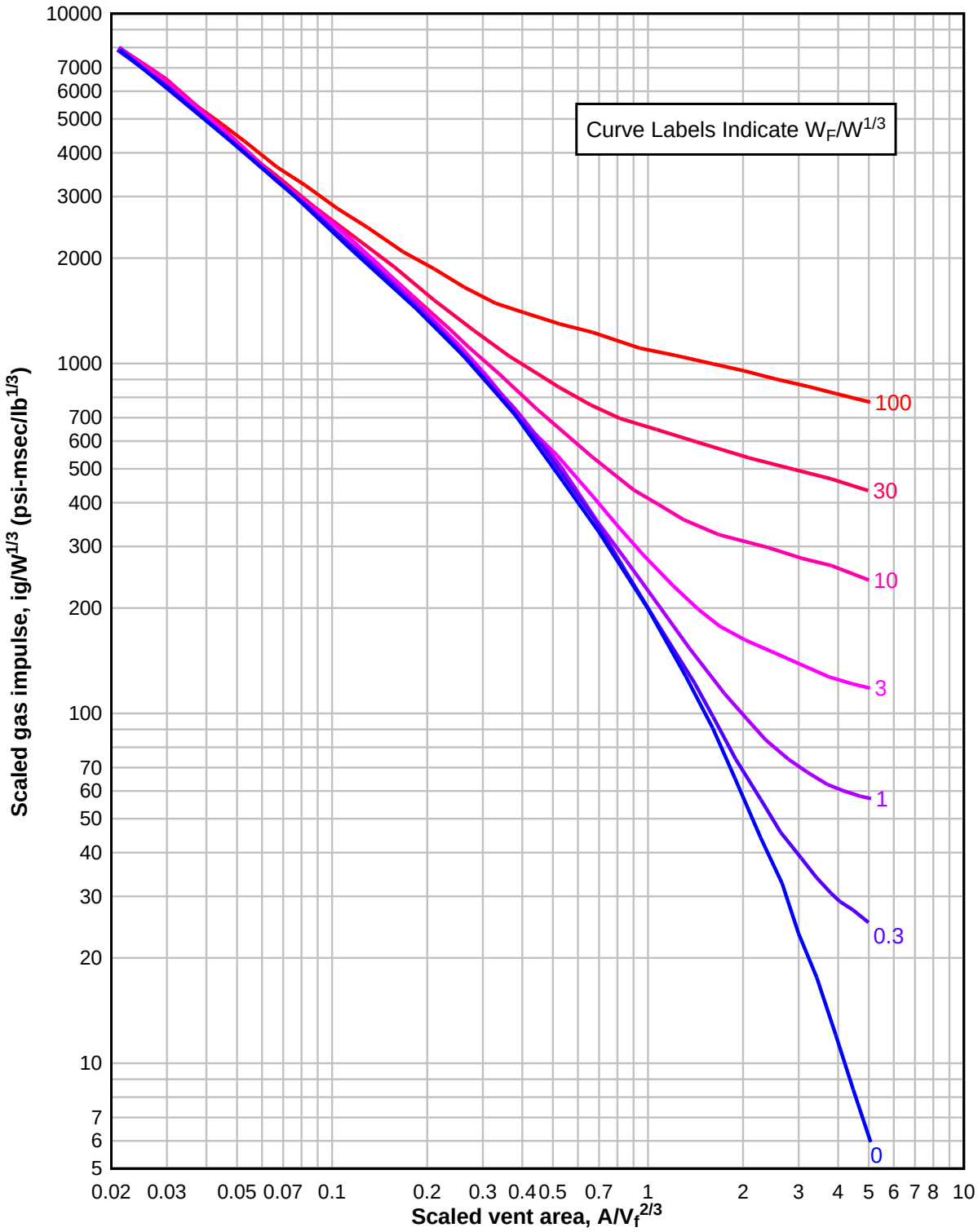

Figure 2-159 Scaled Gas Impulse (W/V_f = 0.15, $i_r/W^{1/3}$ = 20)

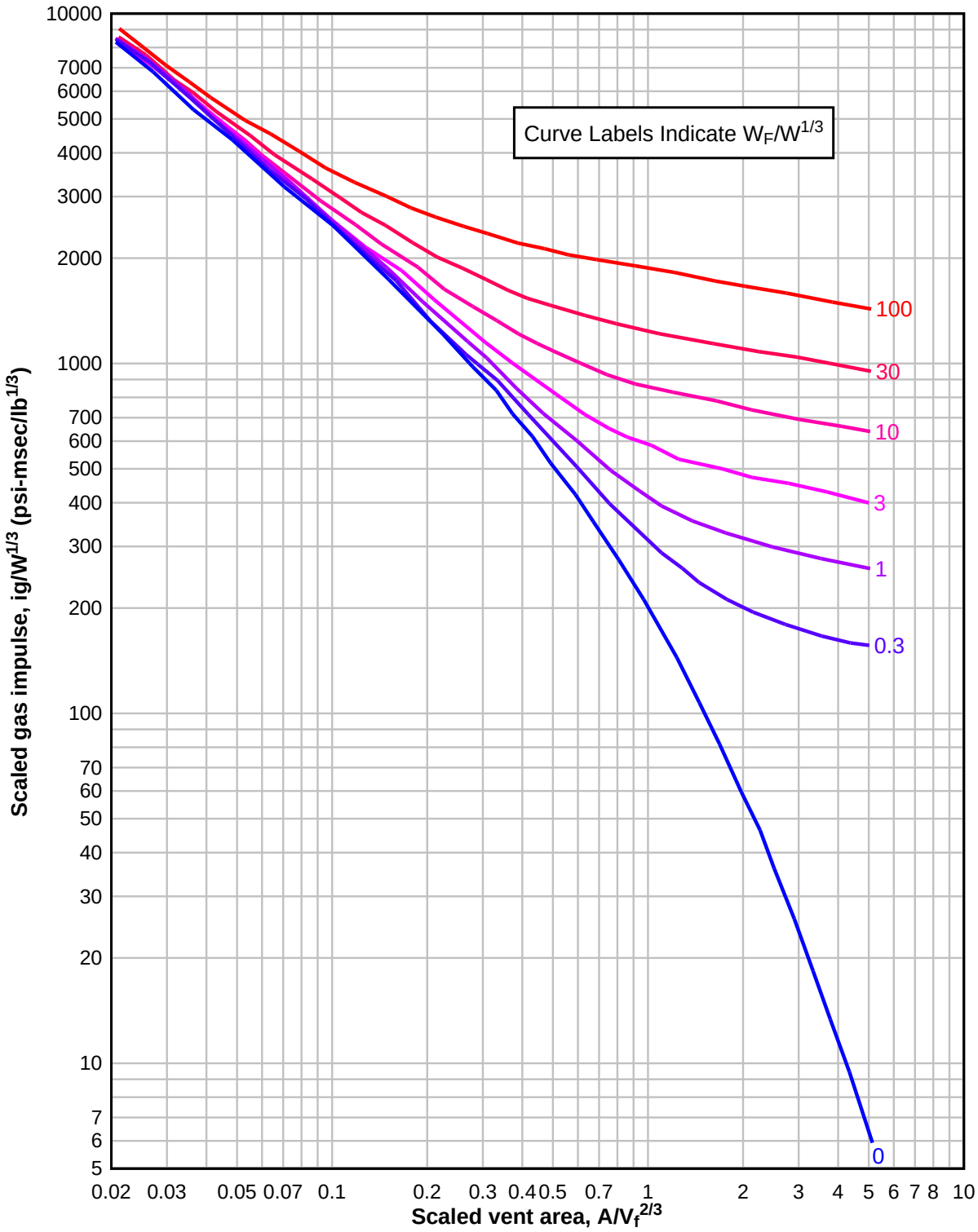

Figure 2-160 Scaled Gas Impulse (W/V_f = 0.15, $i_r/W^{1/3}$ = 100)

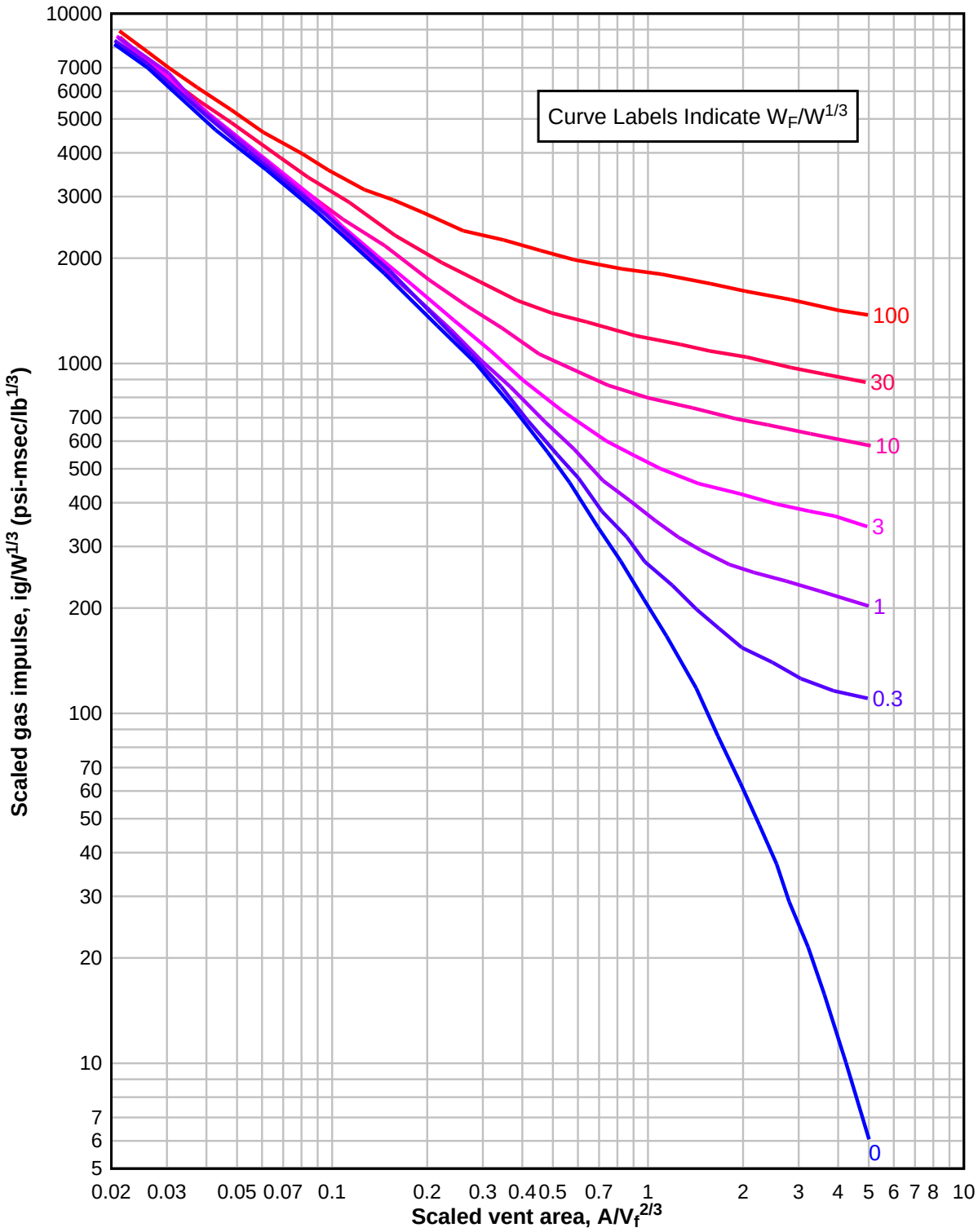

Figure 2-161 Scaled Gas Impulse (W/V_f = 0.15, $i_r/W^{1/3}$ = 600)

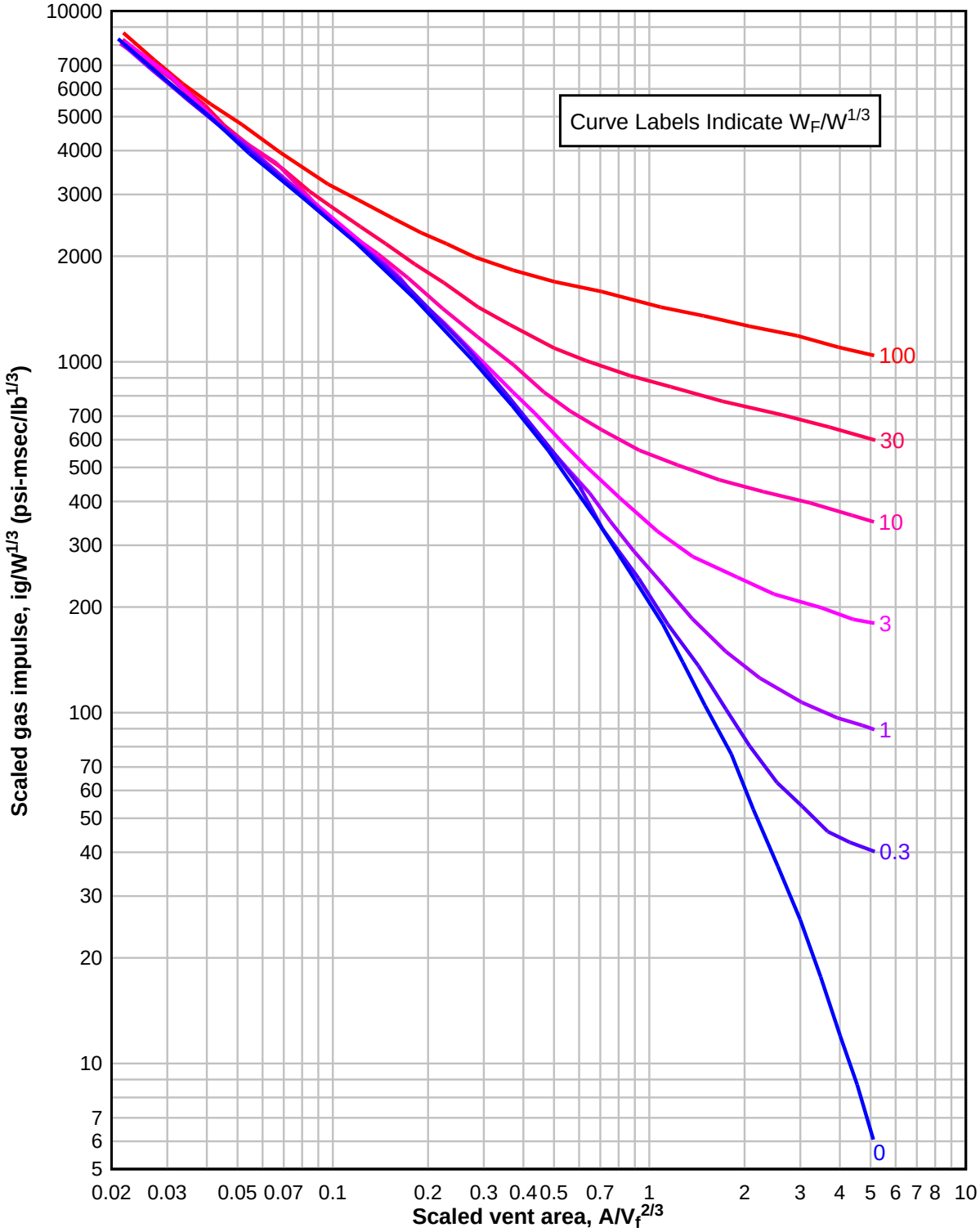

Figure 2-162 Scaled Gas Impulse (W/V_f = 1.0, $i_r/W^{1/3}$ = 100)

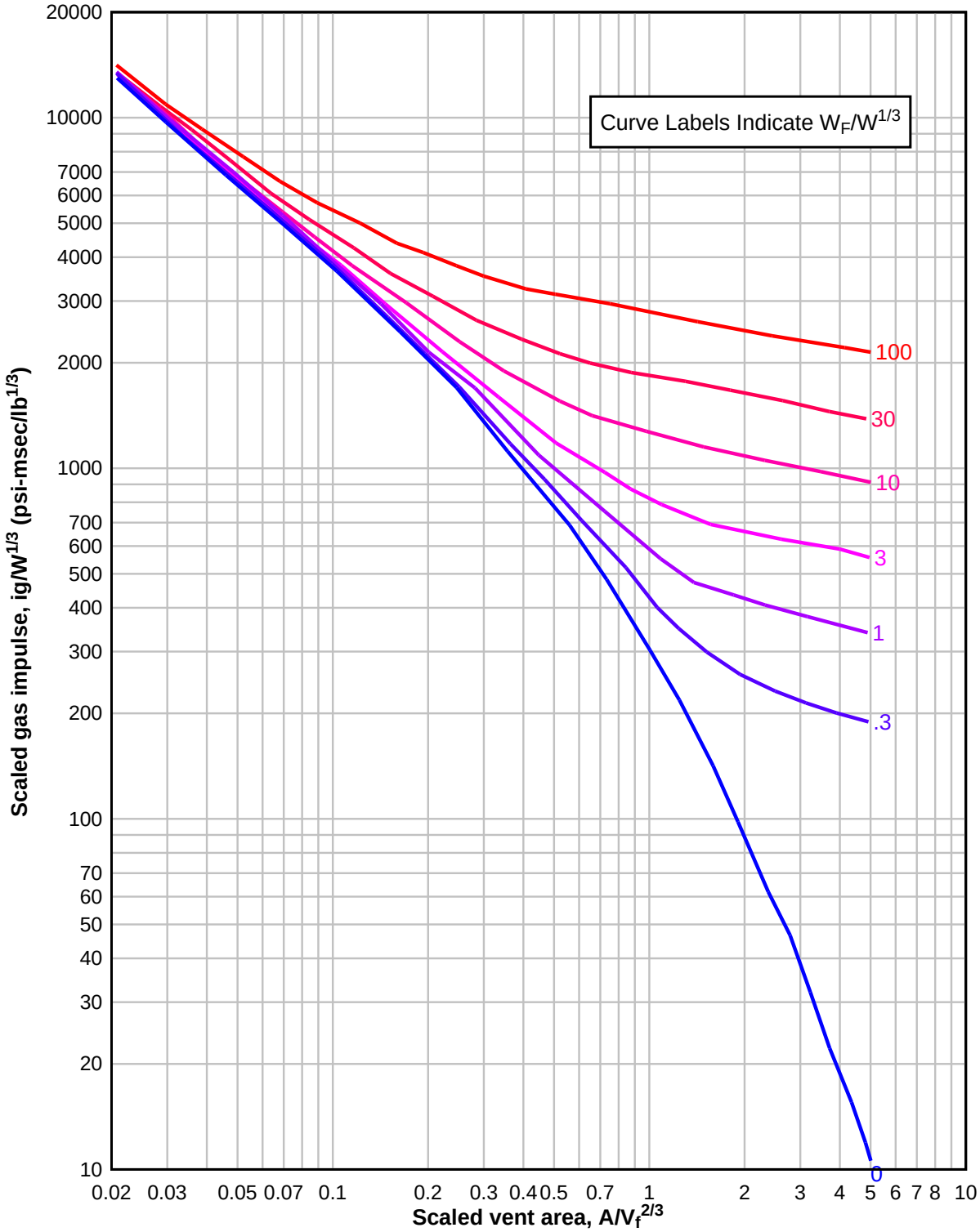

Figure 2-163 Scaled Gas Impulse (W/V_f = 1.0, $i_r/W^{1/3}$ = 600)

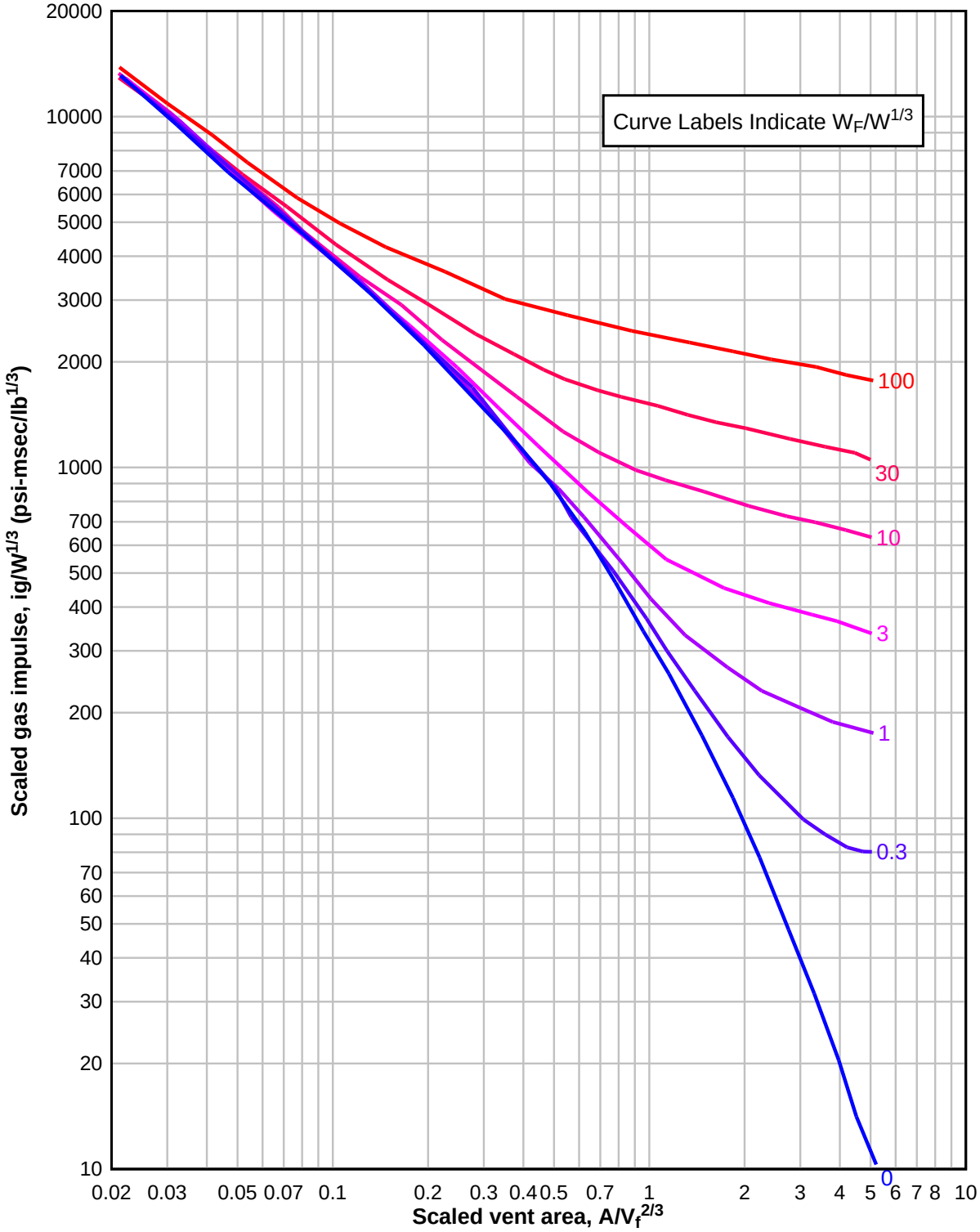

Figure 2-164 Scaled Gas Impulse (W/V_f = 1.0, $i_r/W^{1/3}$ = 2000)

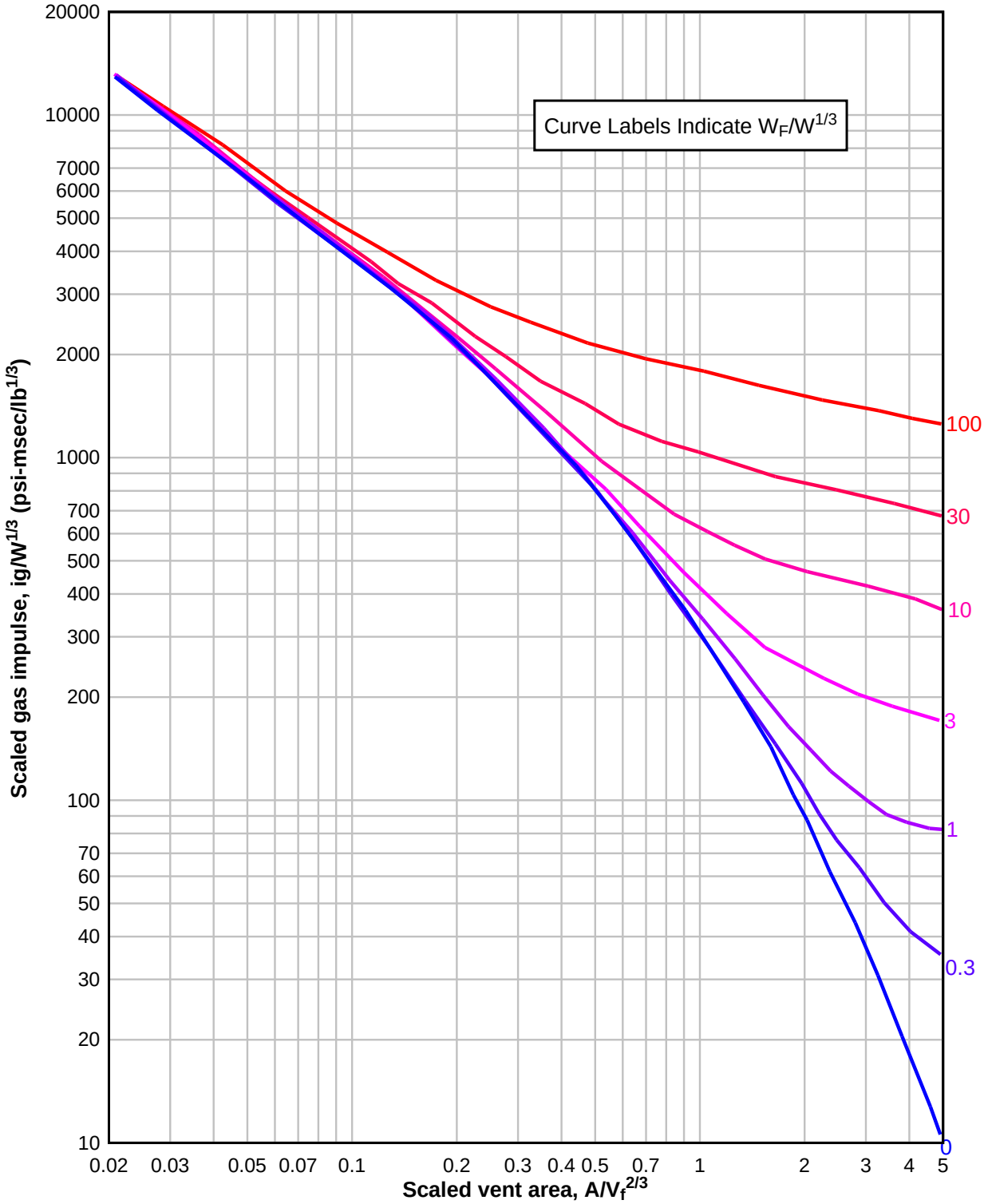

Figure 2-165 Combined Shock and Gas Pressures

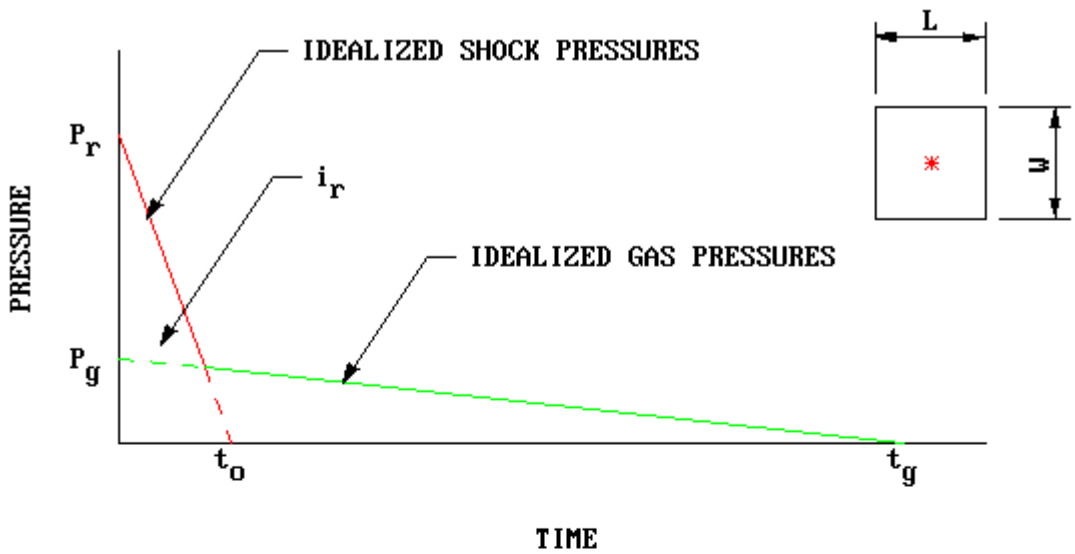

a) SMALL AND/OR SQUARE CHAMBER

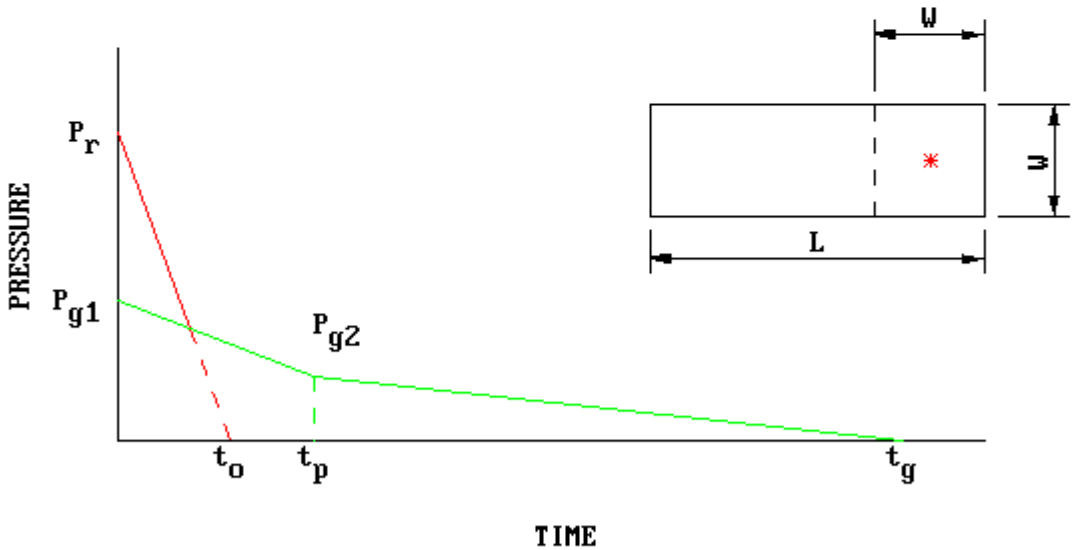

b) LONG RECTANGULAR CHAMBER

Figure 2-166 TNT Conversion Factor for Charges

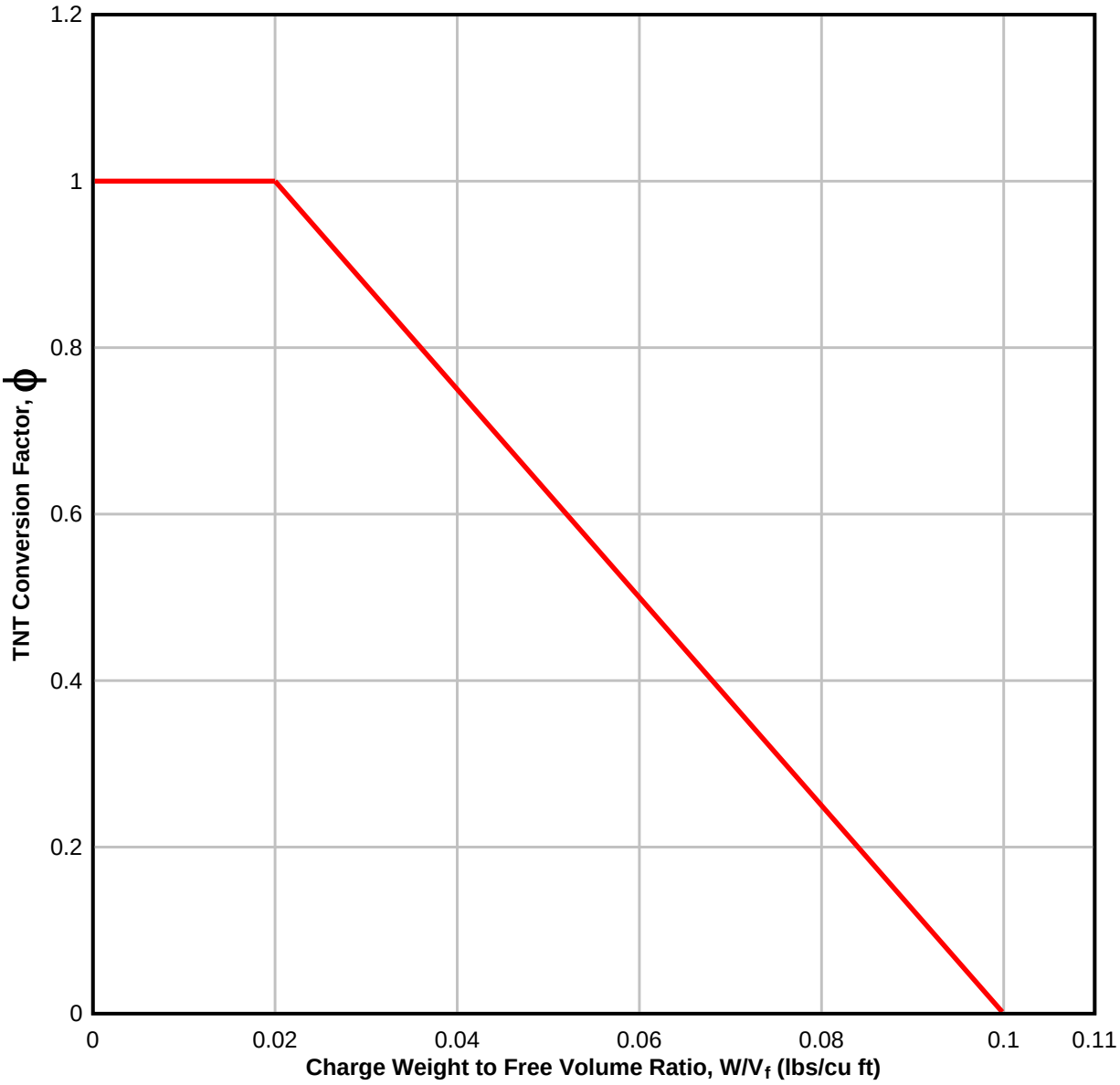

Figure 2-167 Fully Vented Three-Wall Cubicles and Direction of Blast Wave Propagation

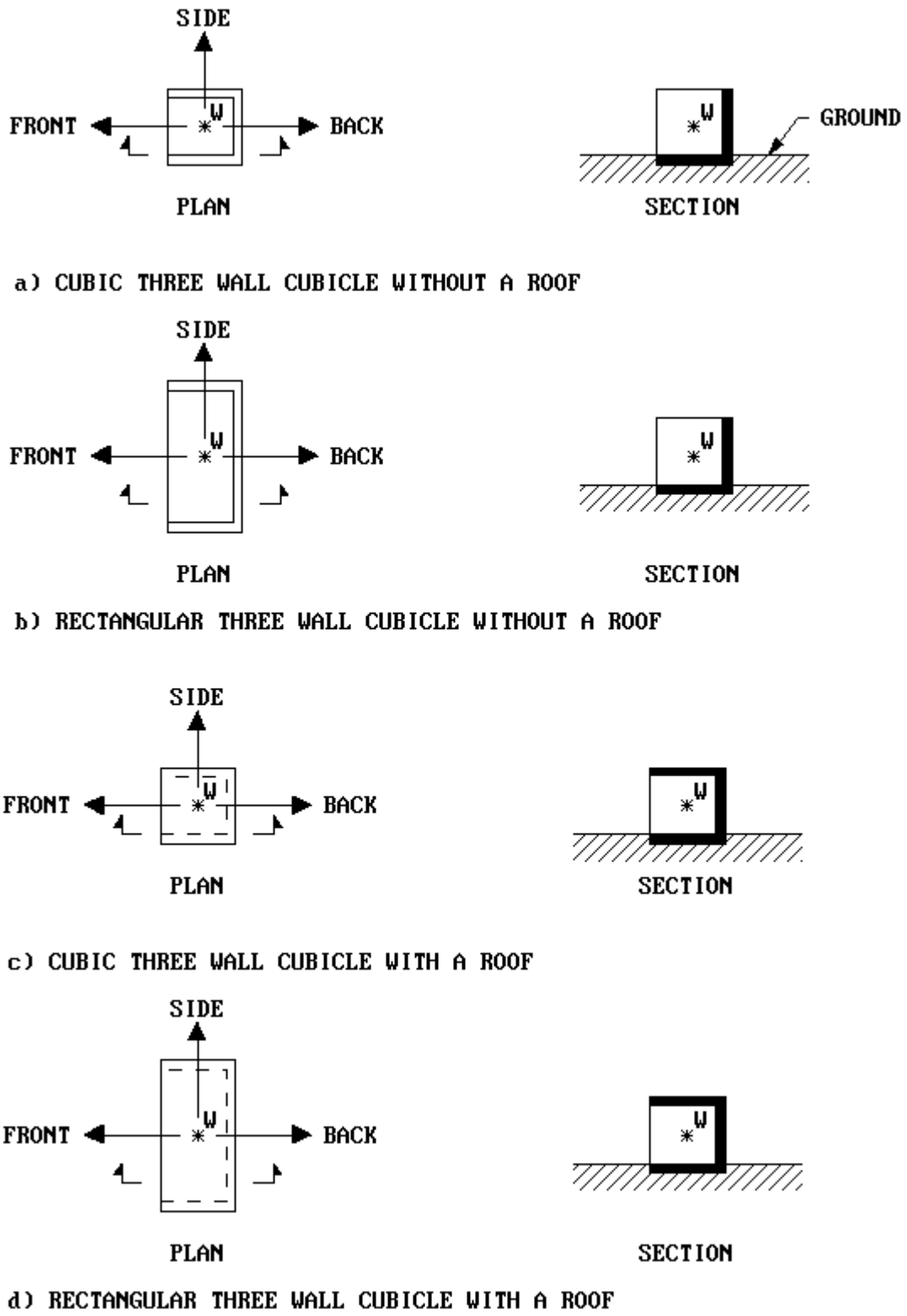

Figure 2-168 Envelope Curves for Peak Positive Pressure Outside Three-Wall Cubicles without a Roof

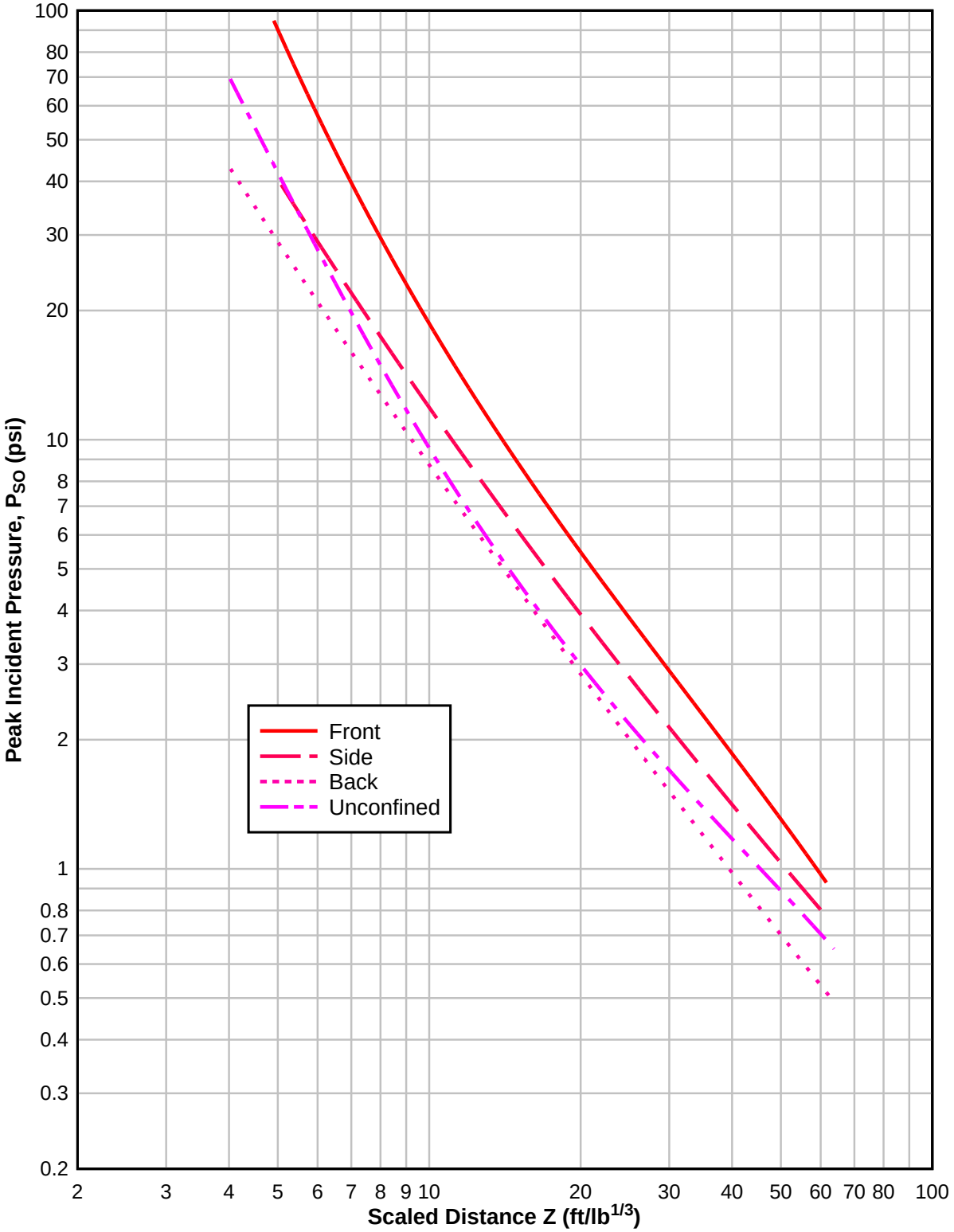

Figure 2-169 Envelope Curves for Peak Positive Pressure Outside Three-Wall Cubicles with a Roof

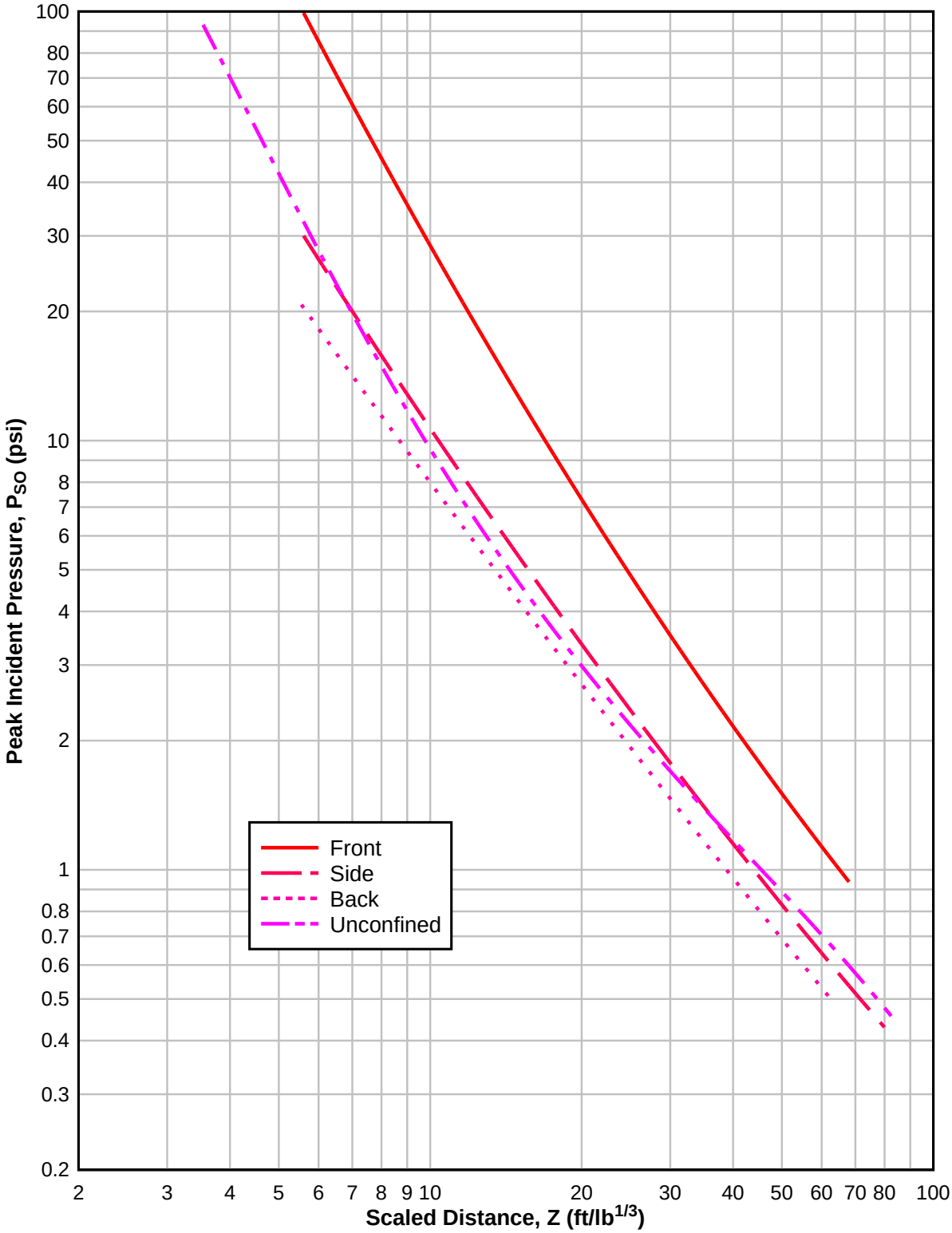

Figure 2-170 Envelope Curves for Maximum Peak Pressure Outside Three-Wall Cubicles

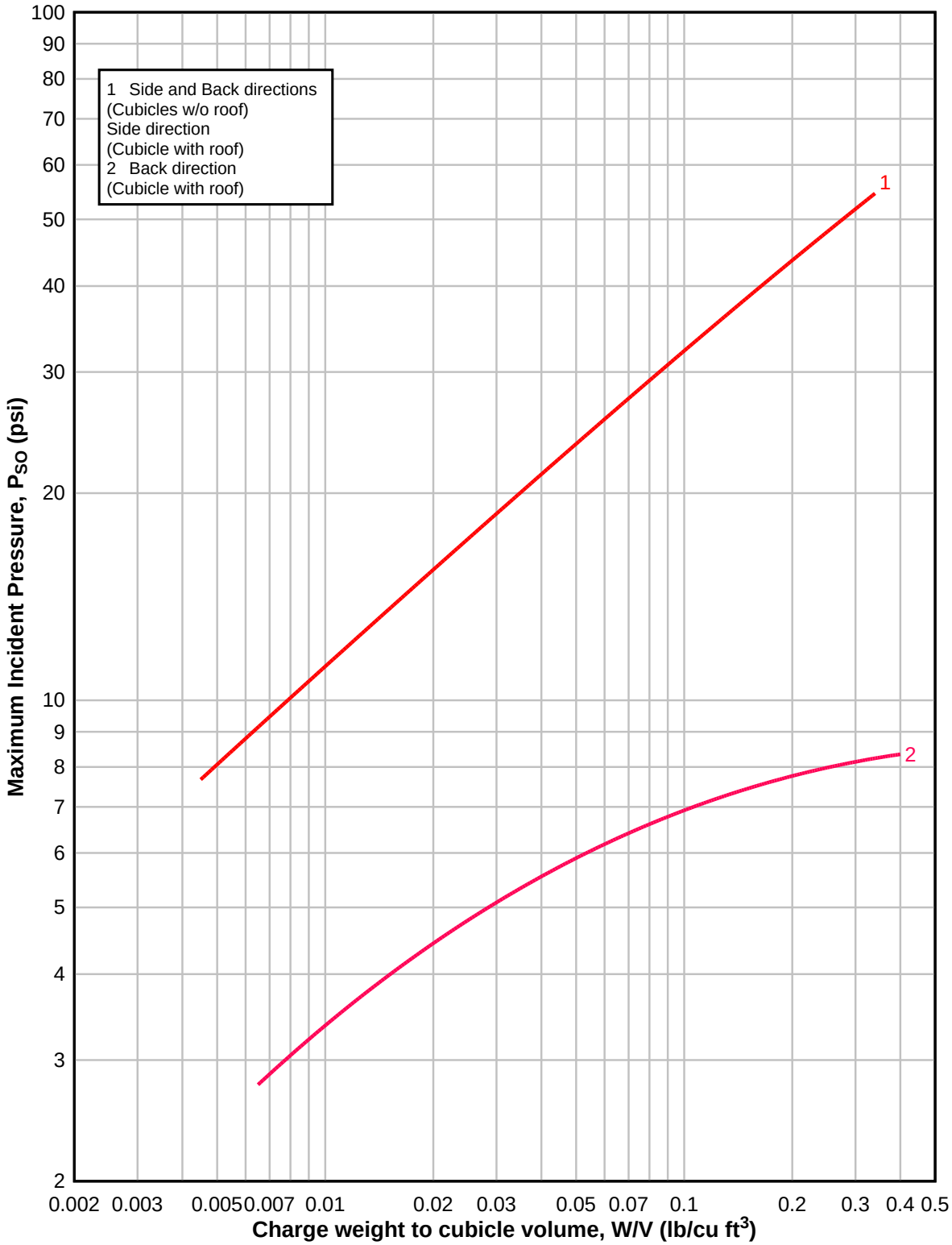

Figure 2-171 Scaled Peak Positive Impulse Out the Open Front of Cubic Three-Wall Cubicle without a Roof

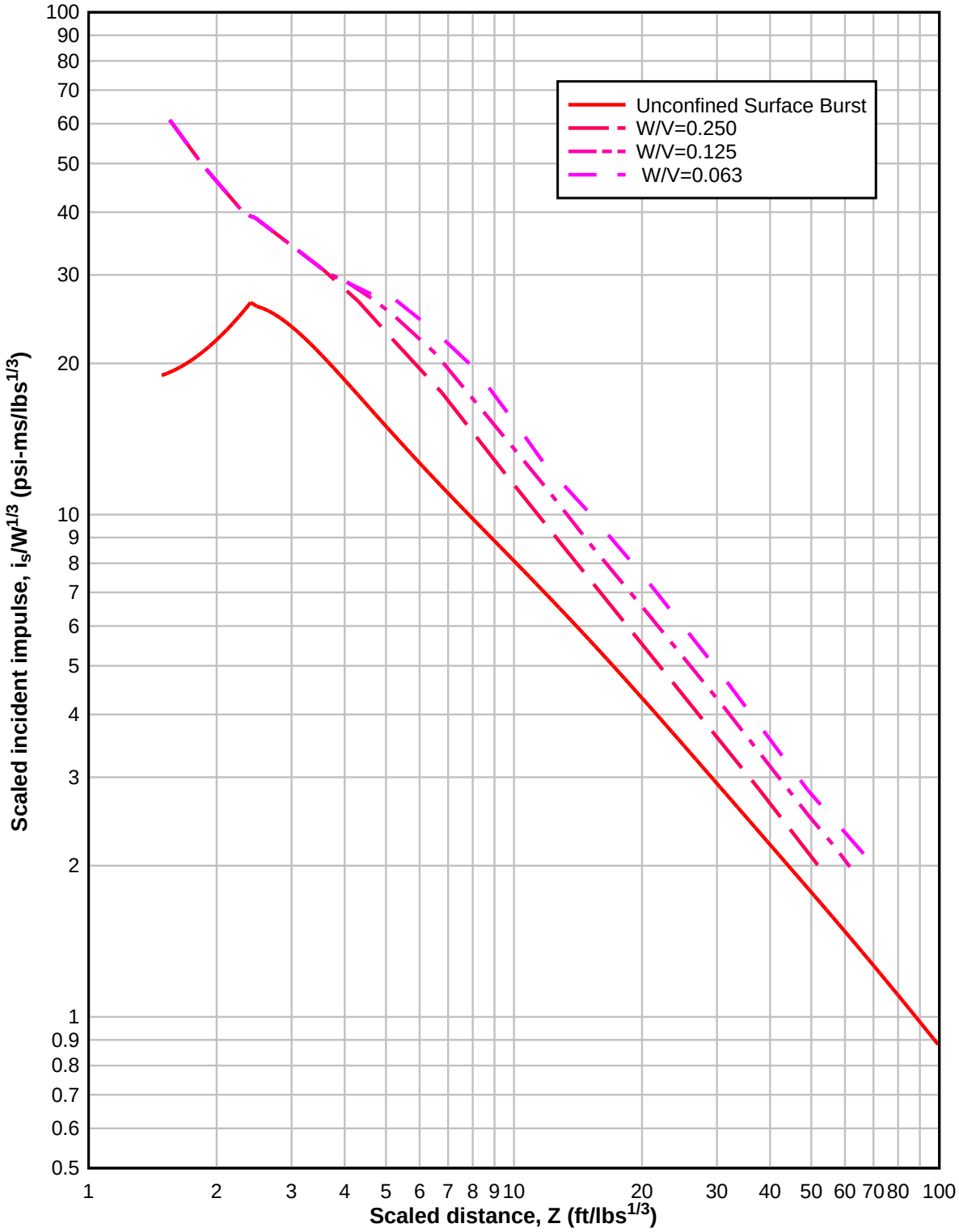

Figure 2-172 Scaled Peak Positive Impulse Out the Open Front of Rectangular Three-Wall Cubicle without a Roof

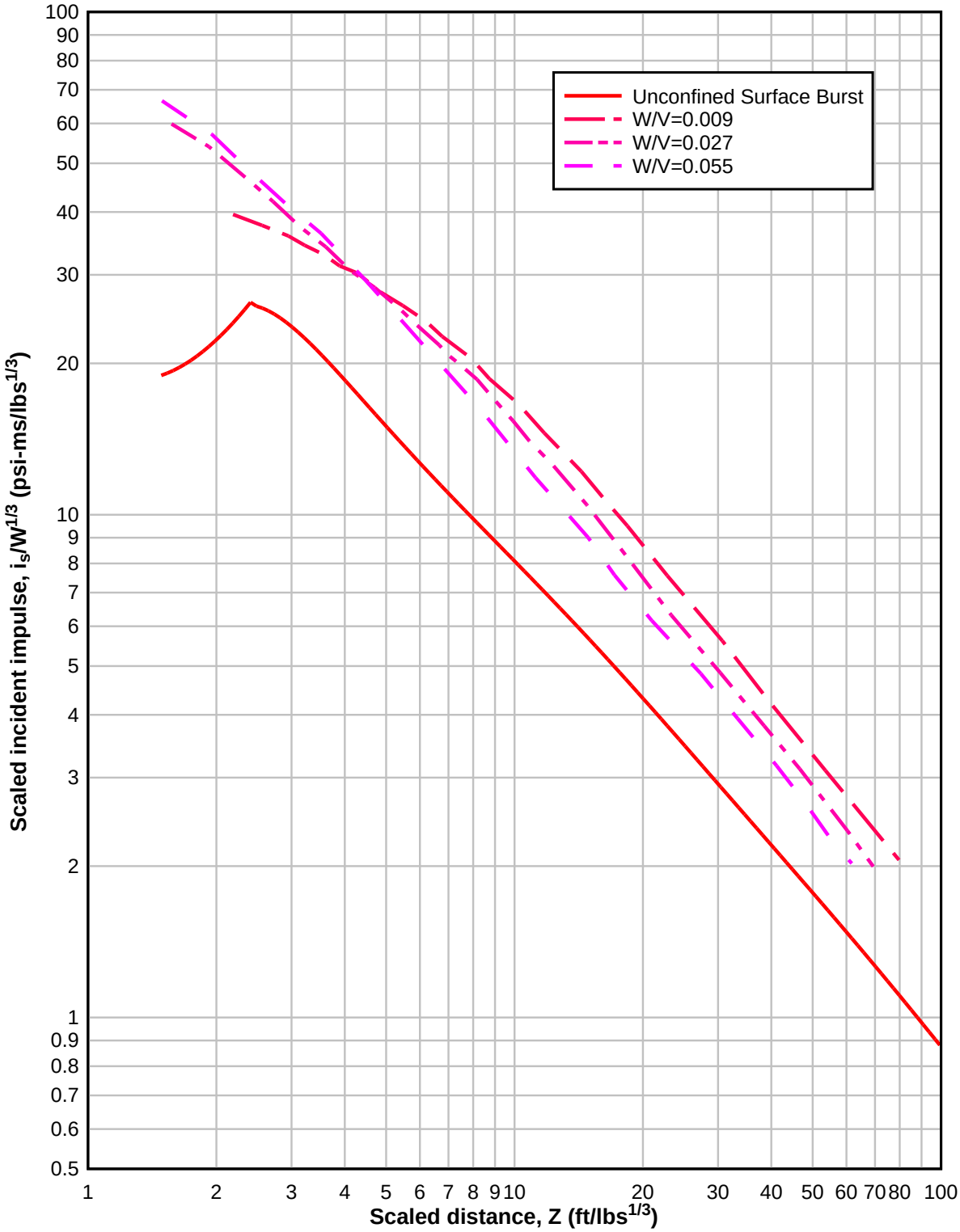

Figure 2-173 Scaled Peak Positive Impulse Behind Sidewall of Cubic Three-Wall Cubicle without a Roof

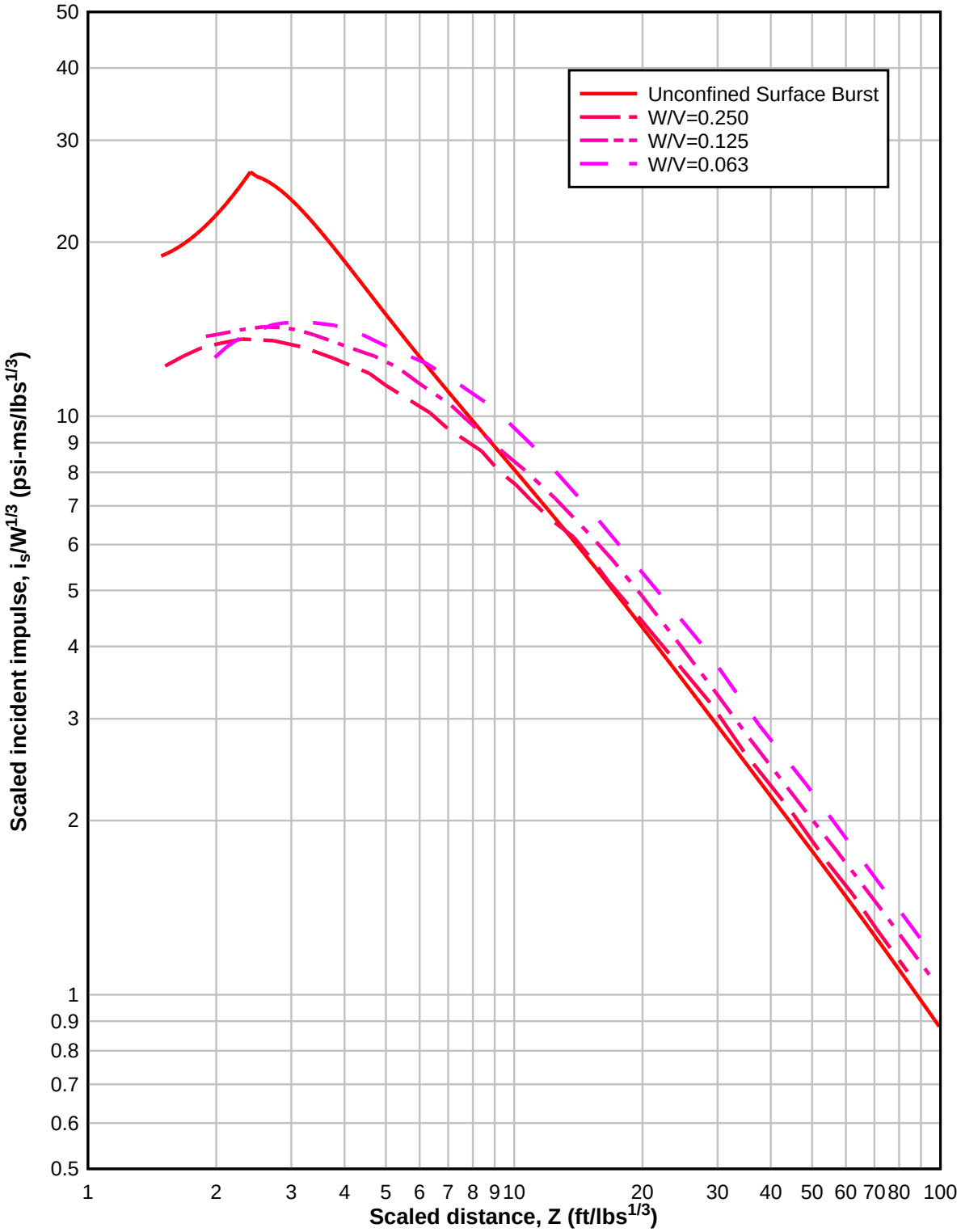

Figure 2-174 Scaled Peak Positive Impulse Behind Sidewall of Rectangular Three-Wall Cubicle without a Roof

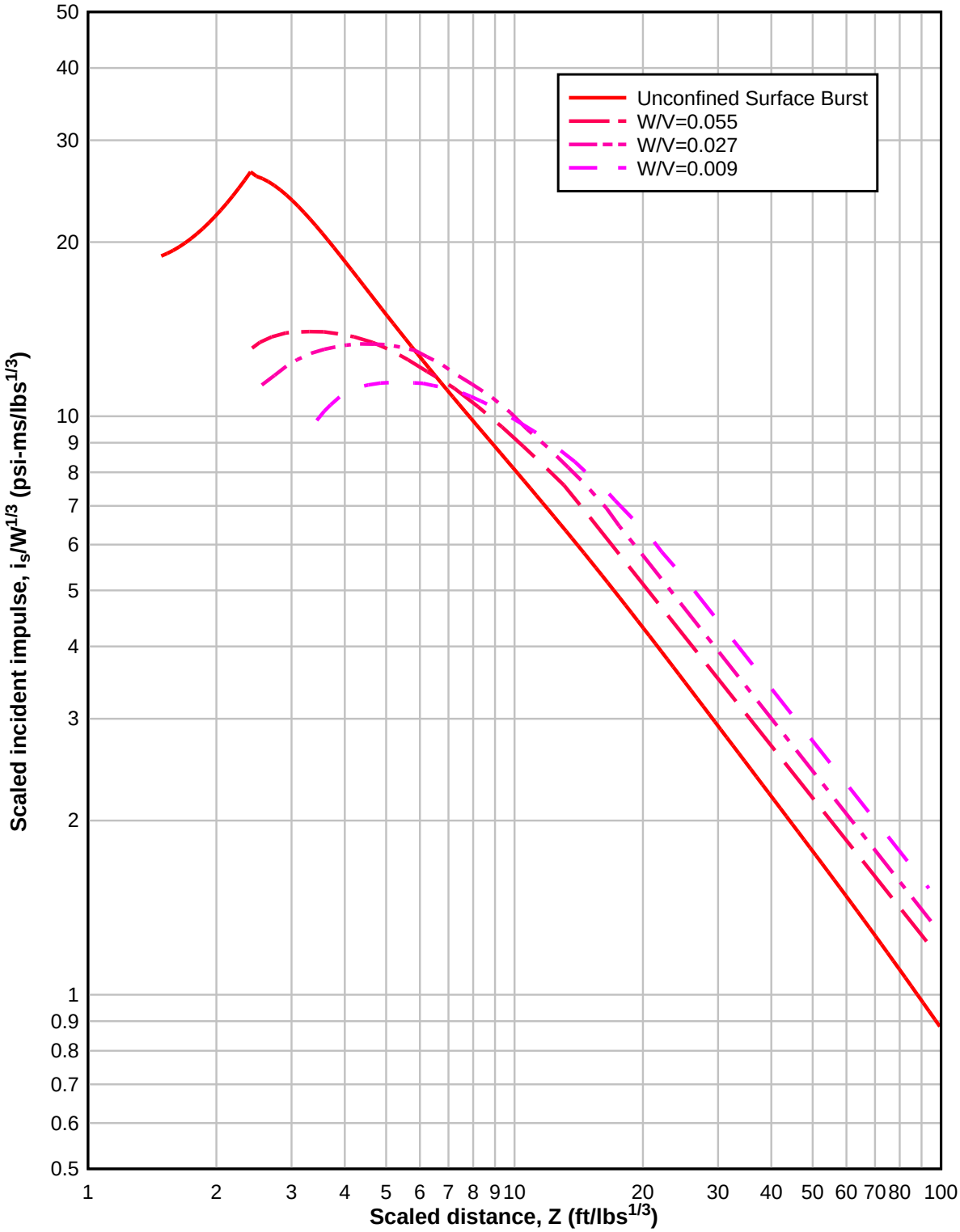

Figure 2-175 Scaled Peak Positive Impulse Behind Backwall of Cubic Three-Wall Cubicle without a Roof

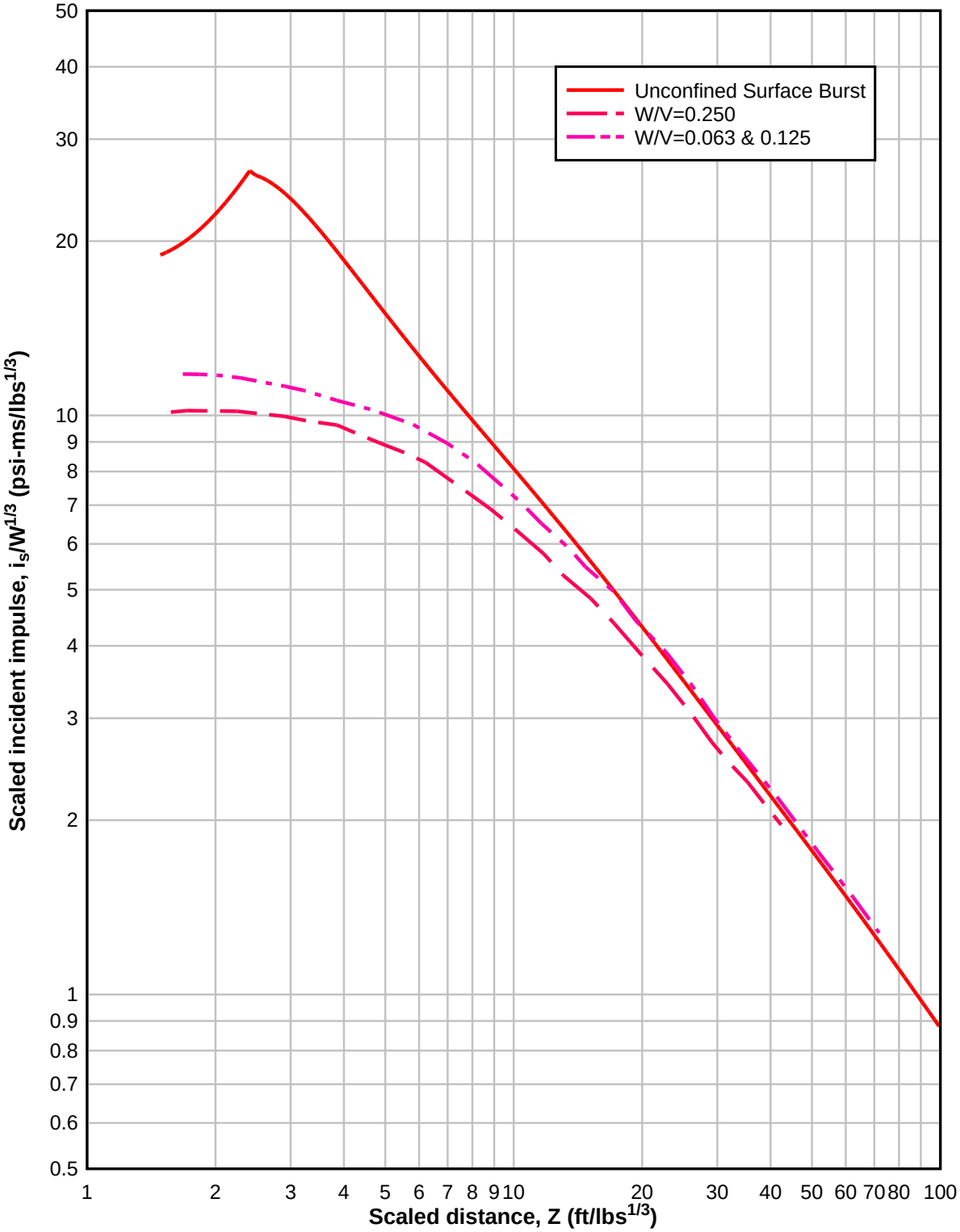

Figure 2-176 Scaled Peak Positive Impulse Behind Backwall of Rectangular Three-Wall Cubicle without a Roof

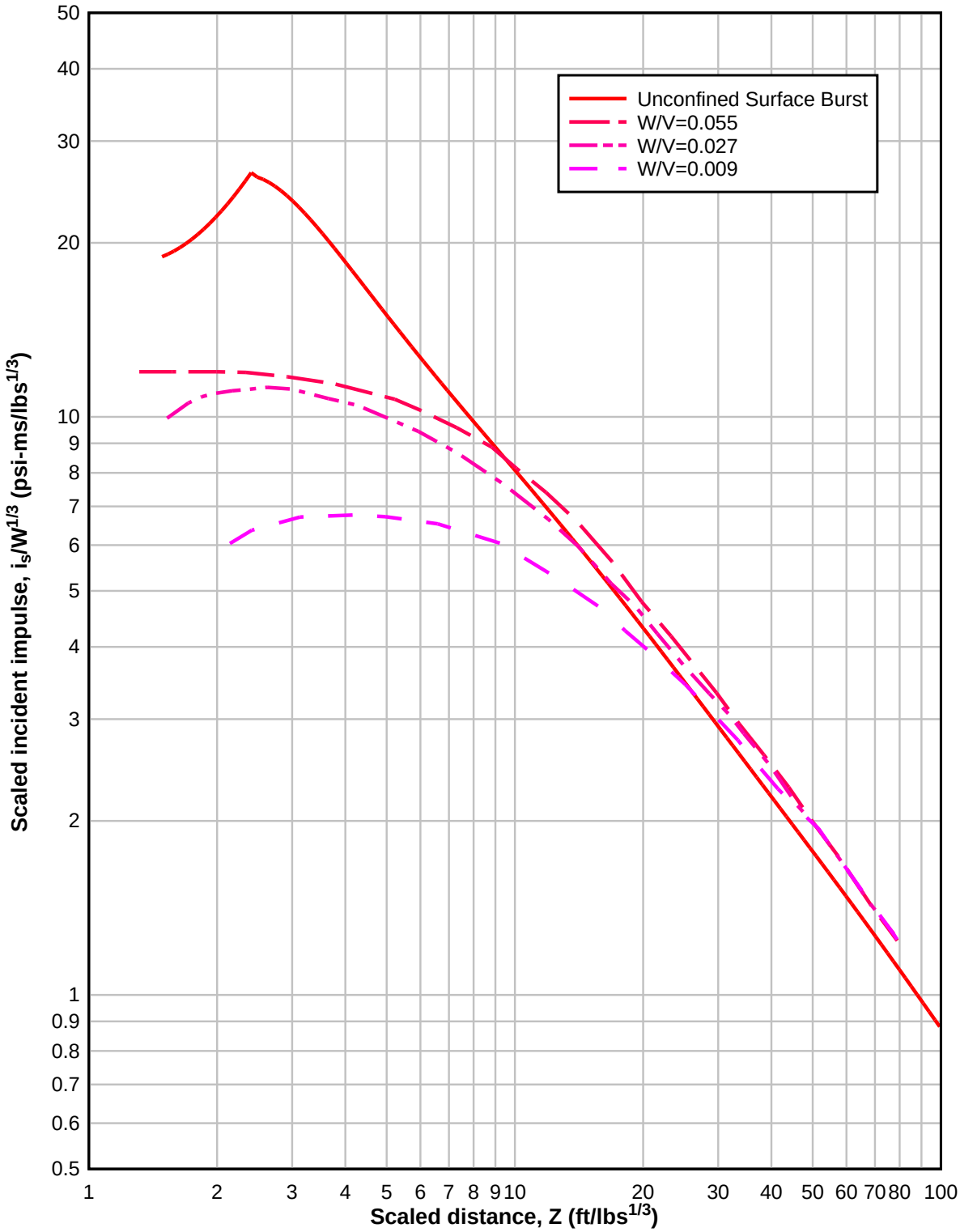

Figure 2-177 Scaled Peak Positive Impulse Out the Open Front of Cubic Three-Wall Cubicle with a Roof

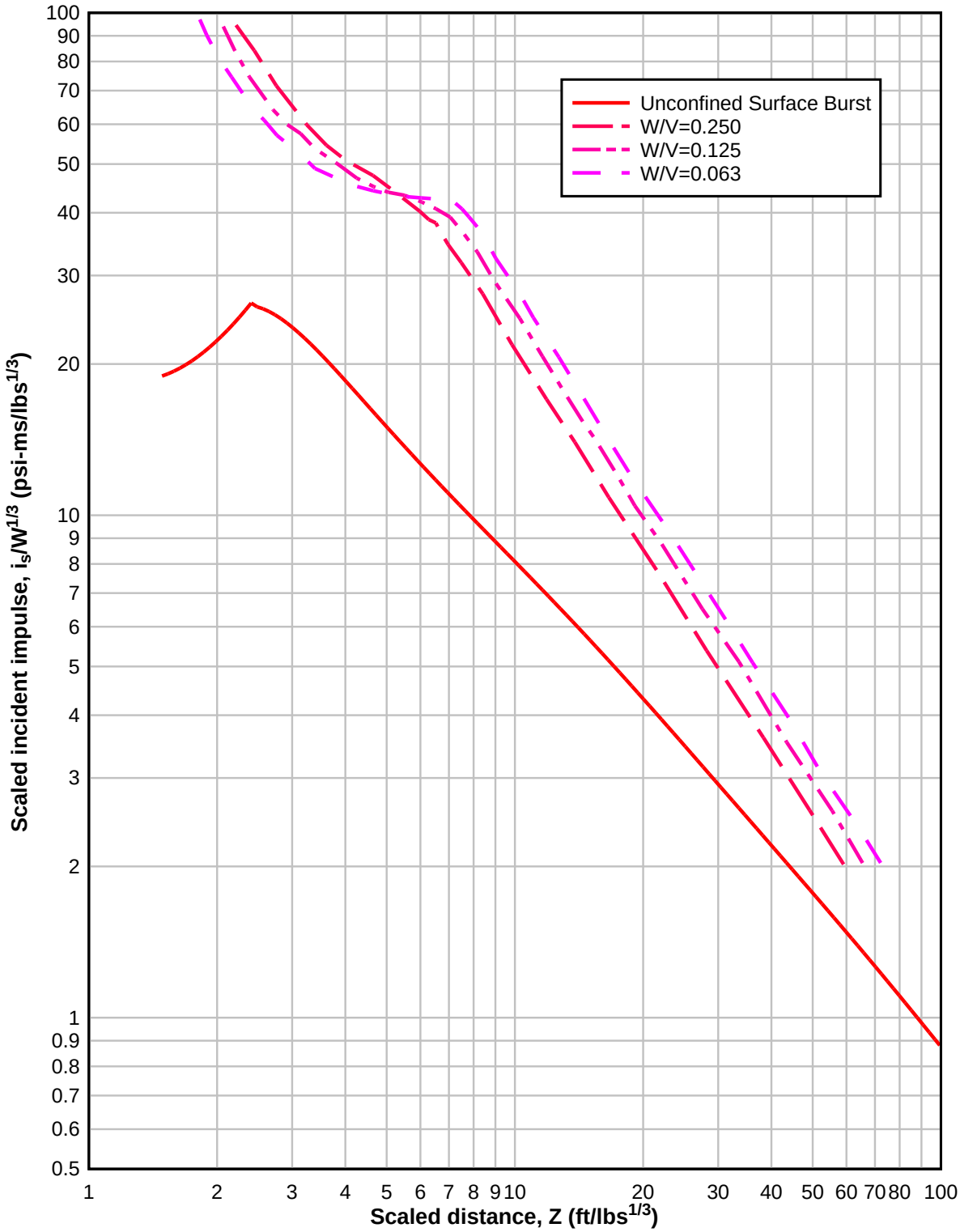

Figure 2-178 Scaled Peak Positive Impulse Out the Open Front of Rectangular Three-Wall Cubicle with a Roof

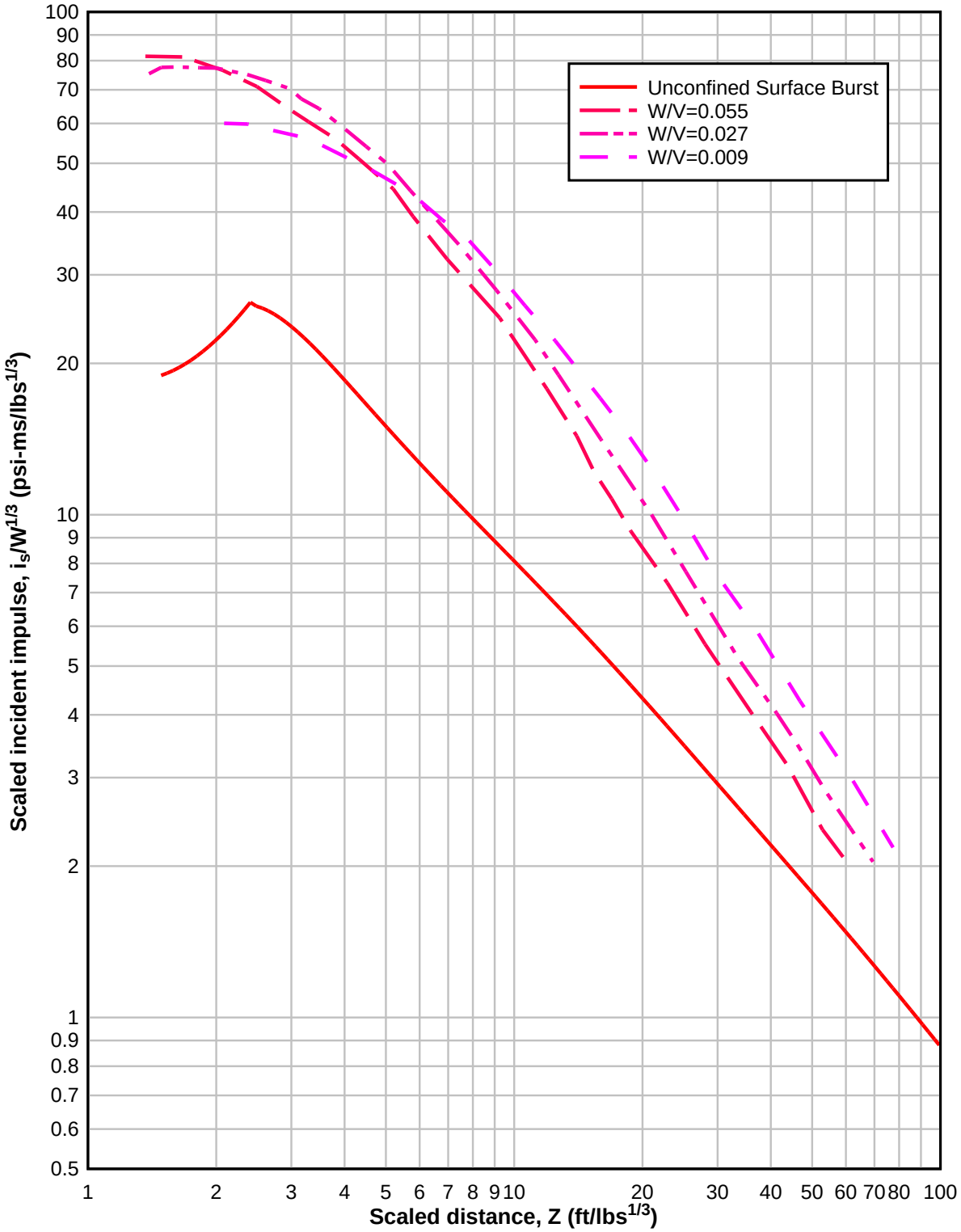

Figure 2-179 Scaled Peak Positive Impulse Behind Sidewall of Cubic Three-Wall Cubicle with a Roof

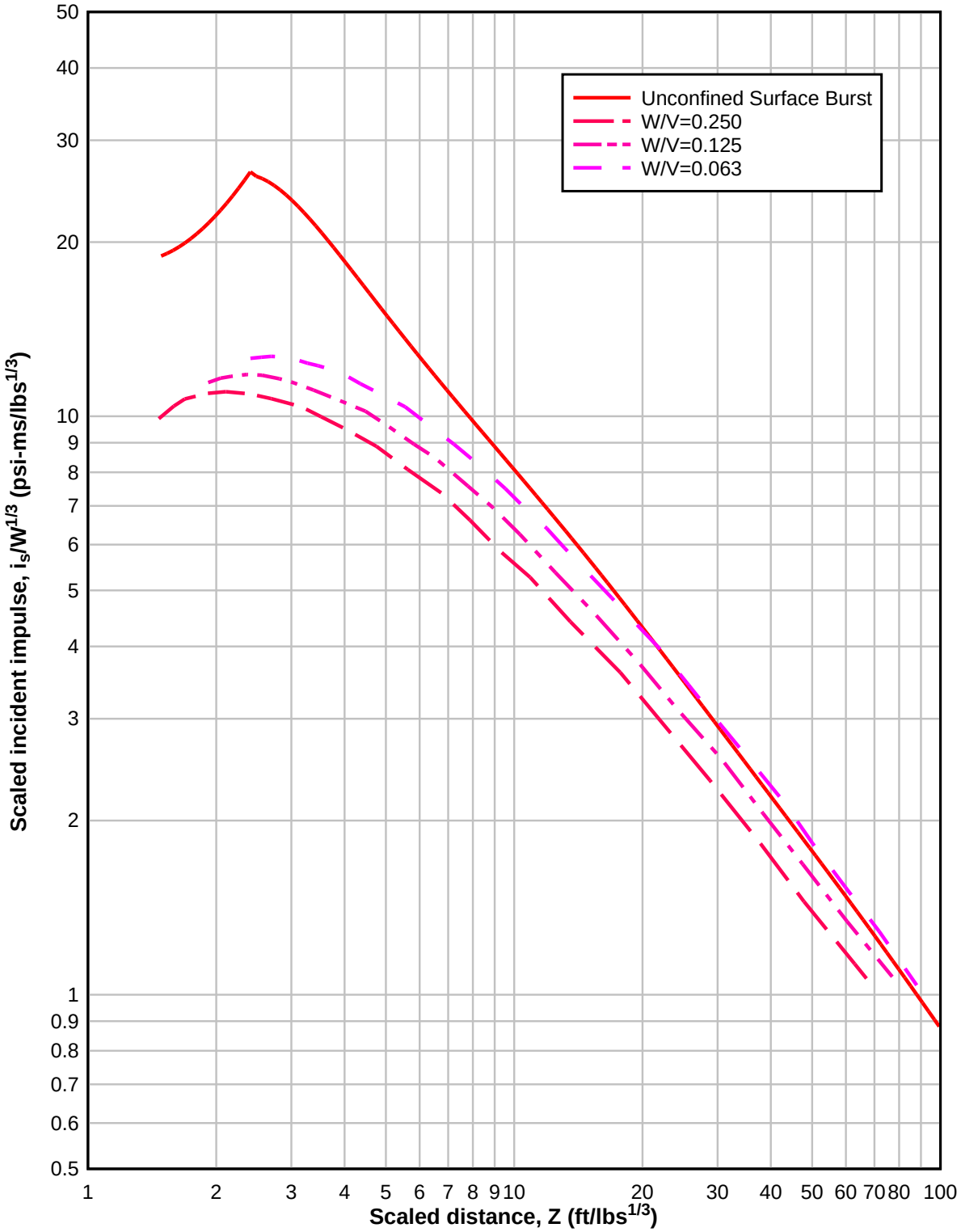

Figure 2-180 Scaled Peak Positive Impulse Behind Sidewall of Rectangular Three-Wall Cubicle with a Roof

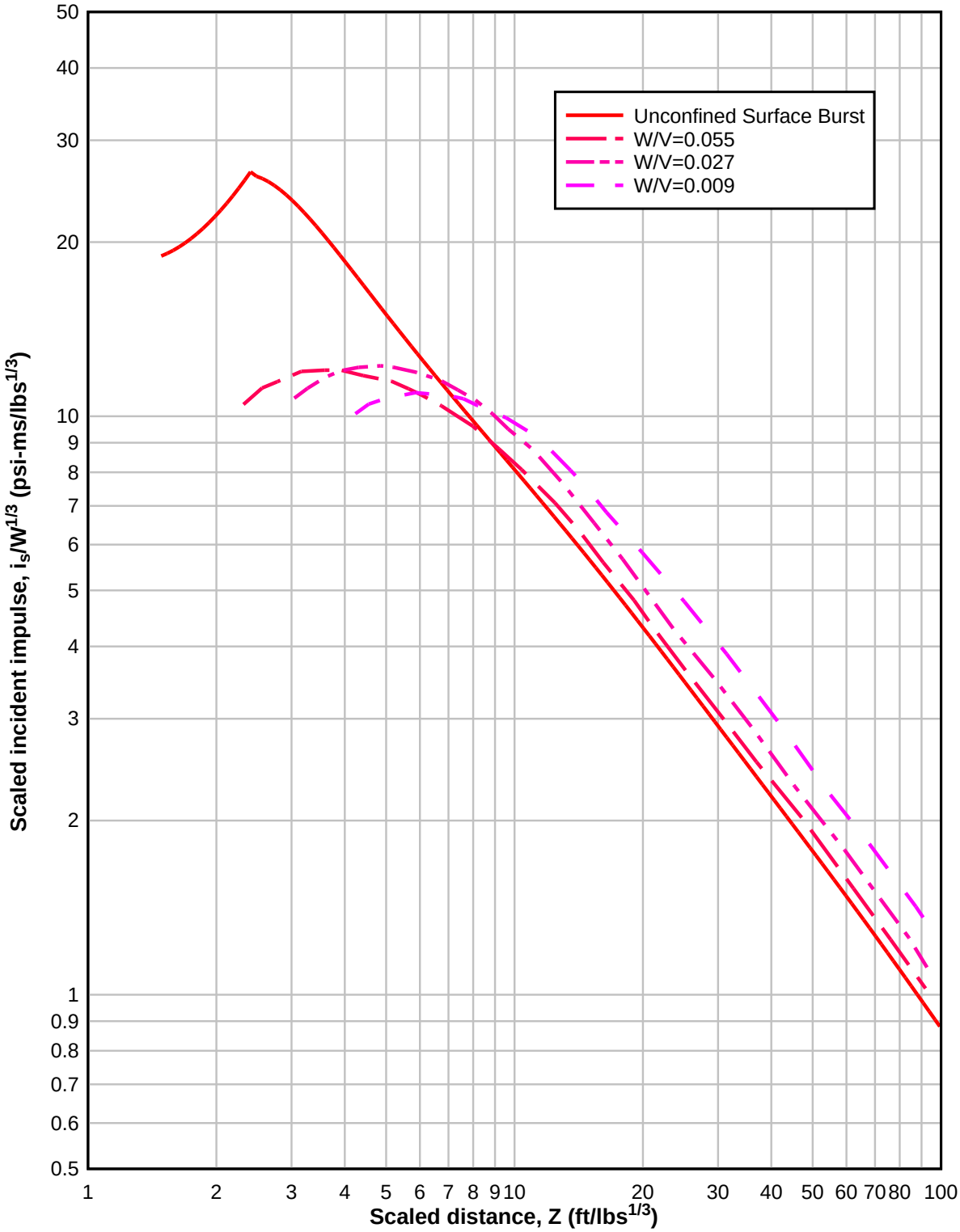

Figure 2-181 Scaled Peak Positive Impulse Behind Backwall of Cubic Three-Wall Cubicle with a Roof

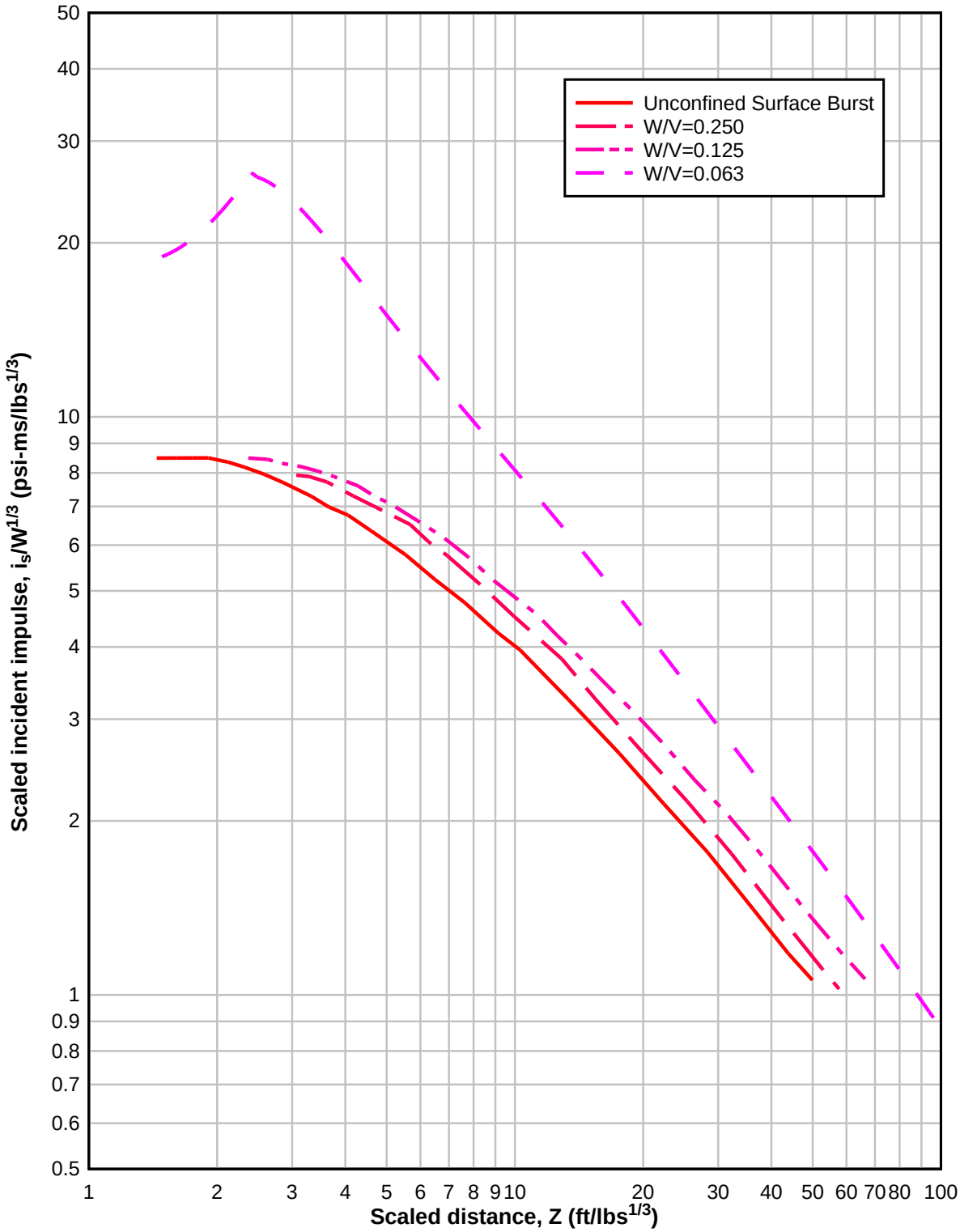

Figure 2-182 Scaled Peak Positive Impulse Behind Backwall of Rectangular Three-Wall Cubicle with a Roof

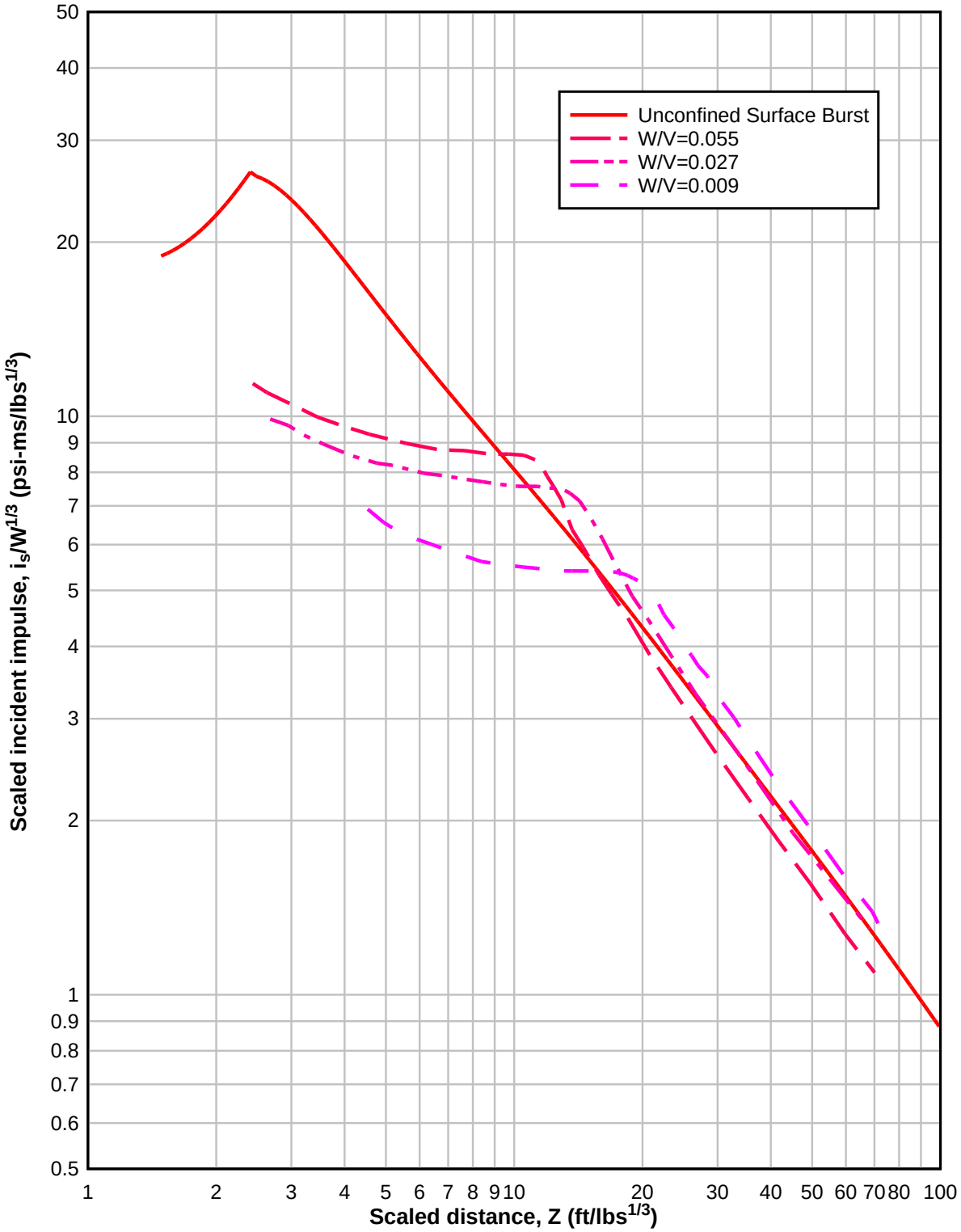

Figure 2-183 Four Wall Cubicle Vented Through its Roof

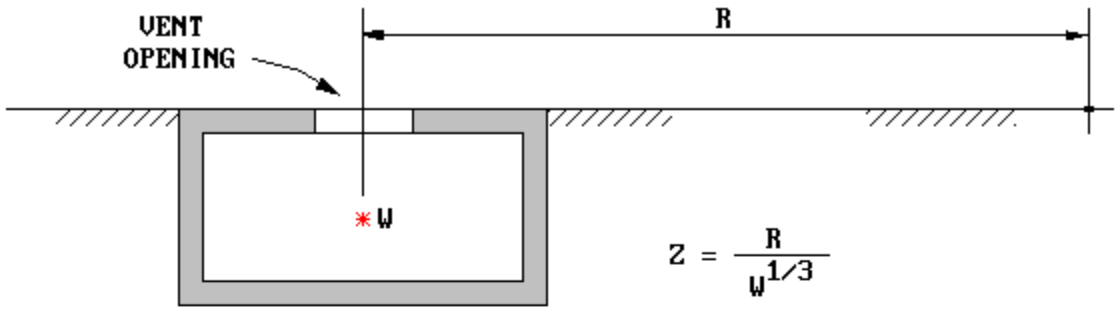

a) BELOW GROUND STRUCTURE WITH ROOF AT GROUND SURFACE

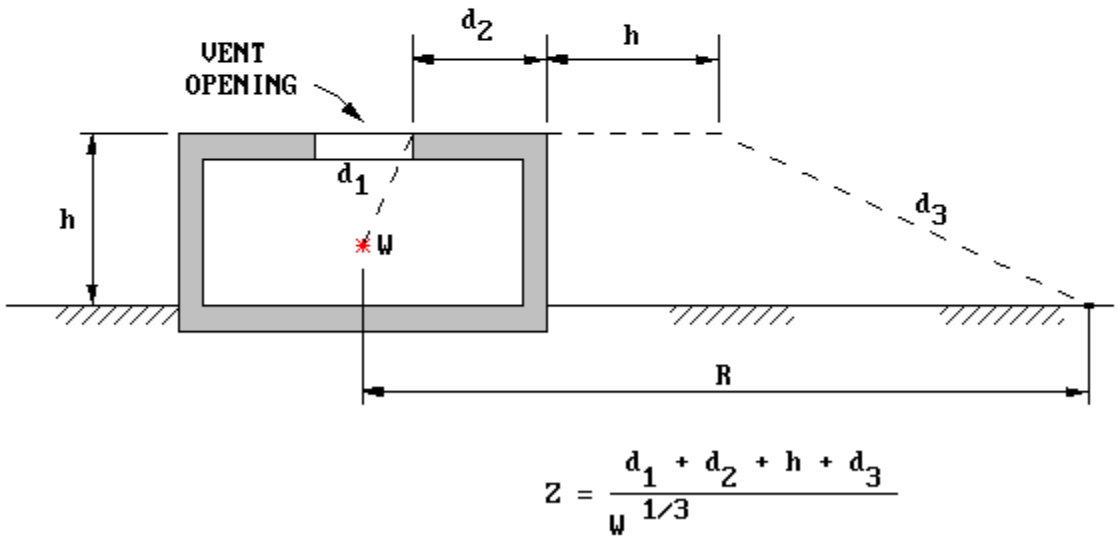

b) ABOVE GROUND STRUCTURE

Figure 2-184 Peak Positive Pressure Outside of a Four-Wall Cubicle Vented Through Its Roof

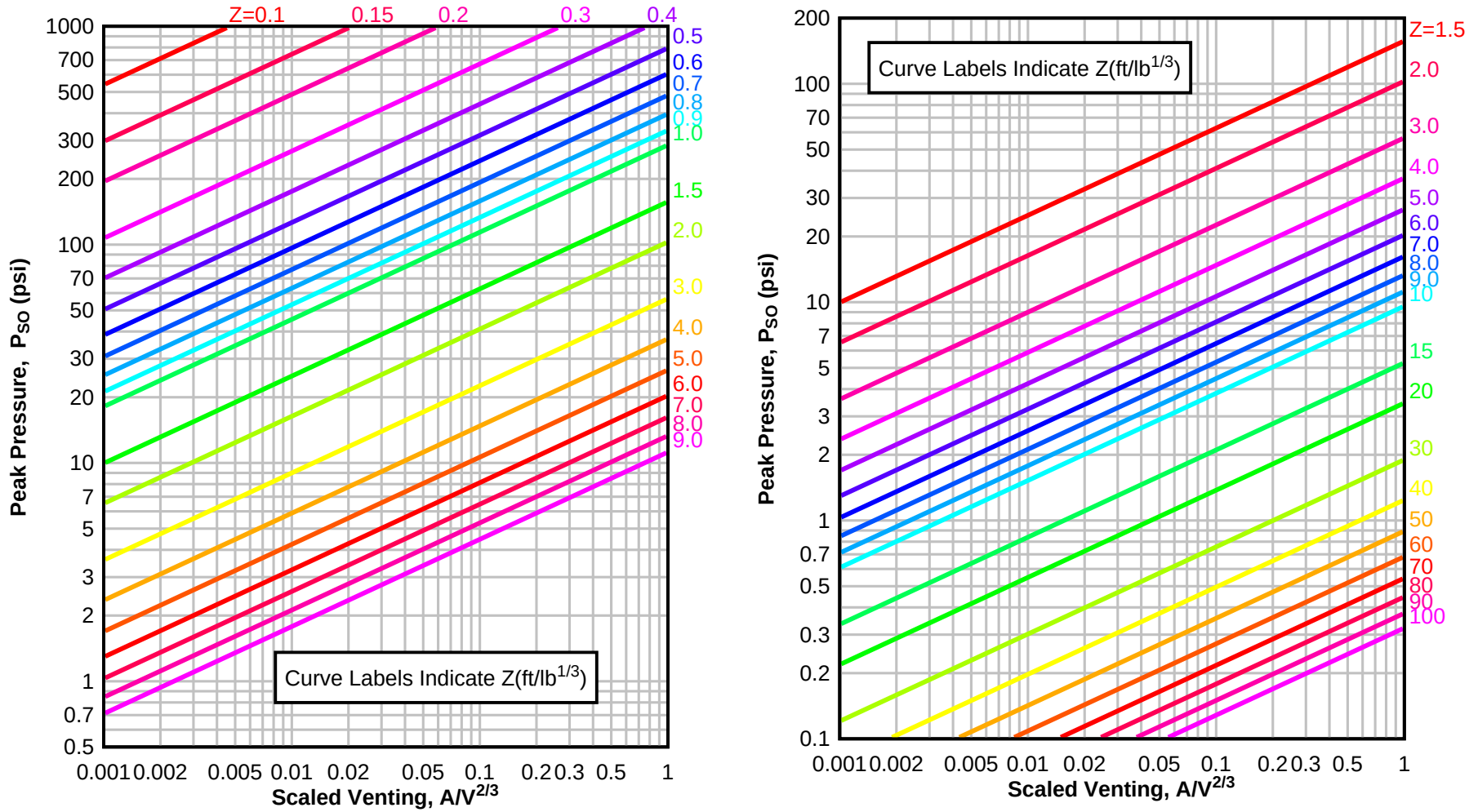

Figure 2-185 Scaled Positive Impulse Outside of a Four-Wall Cubicle Vented Through Its Roof

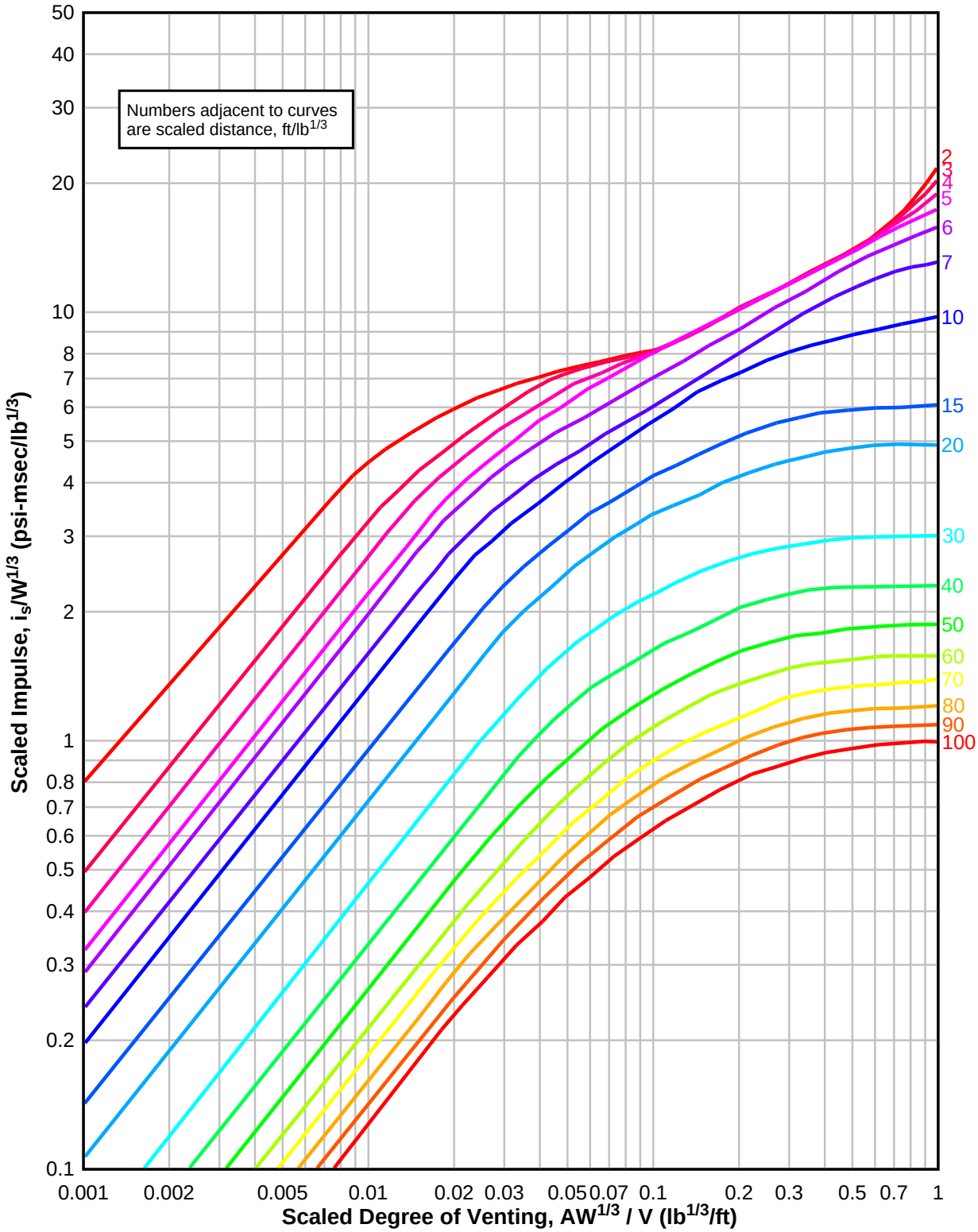

Figure 2-186 Four Wall Cubicle Vented Through a Wall and Direction of Blast Wave Propagation

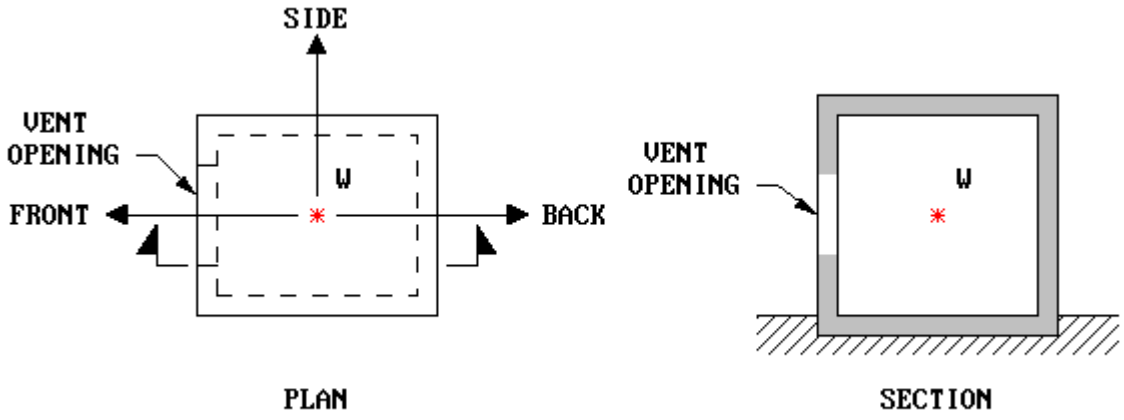

Figure 2-187 Peak Positive Pressure at the Front of a Partially Vented Four-Wall Cubicle

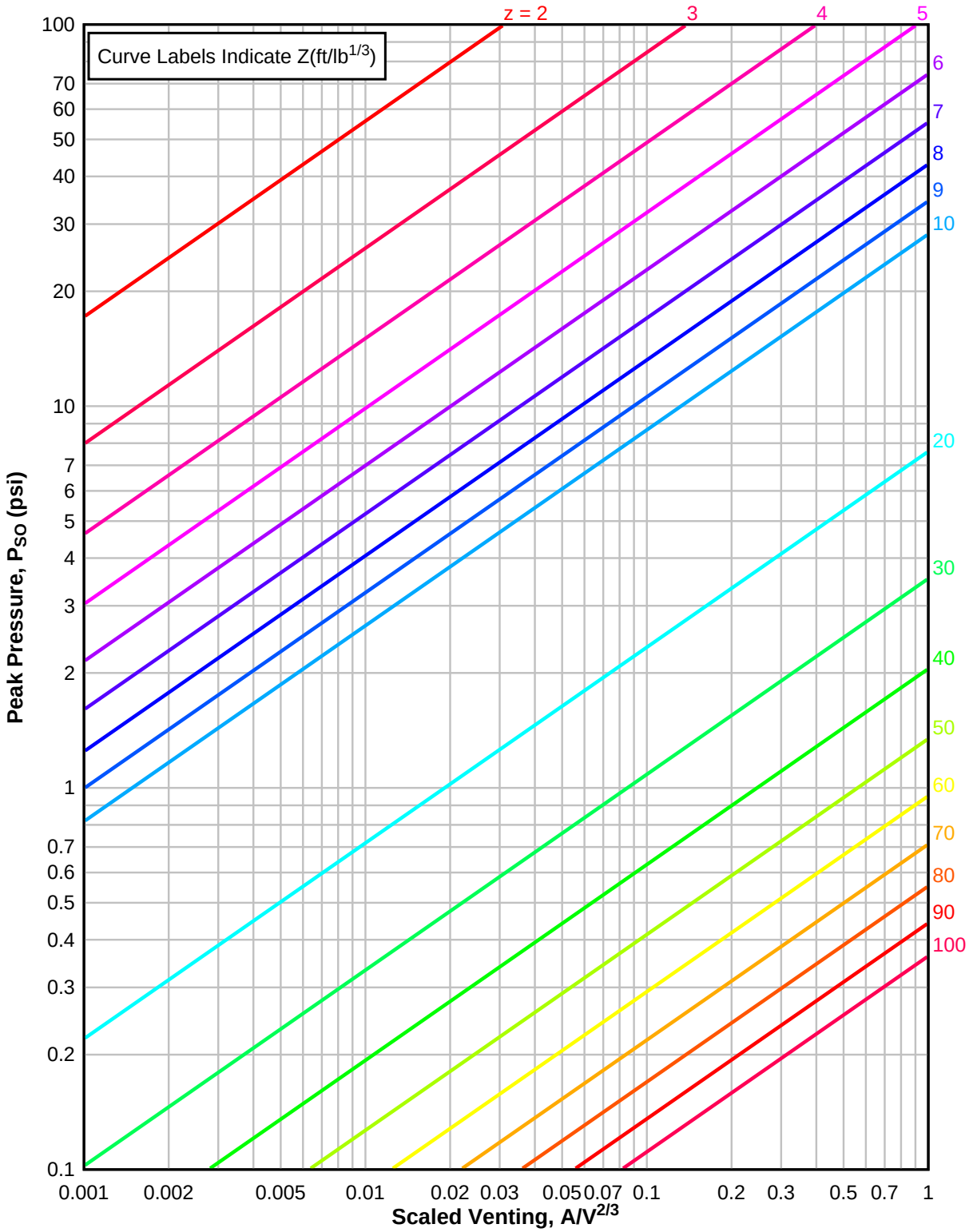

Figure 2-188 Peak Positive Pressure at the Side of a Partially Vented Four-Wall Cubicle

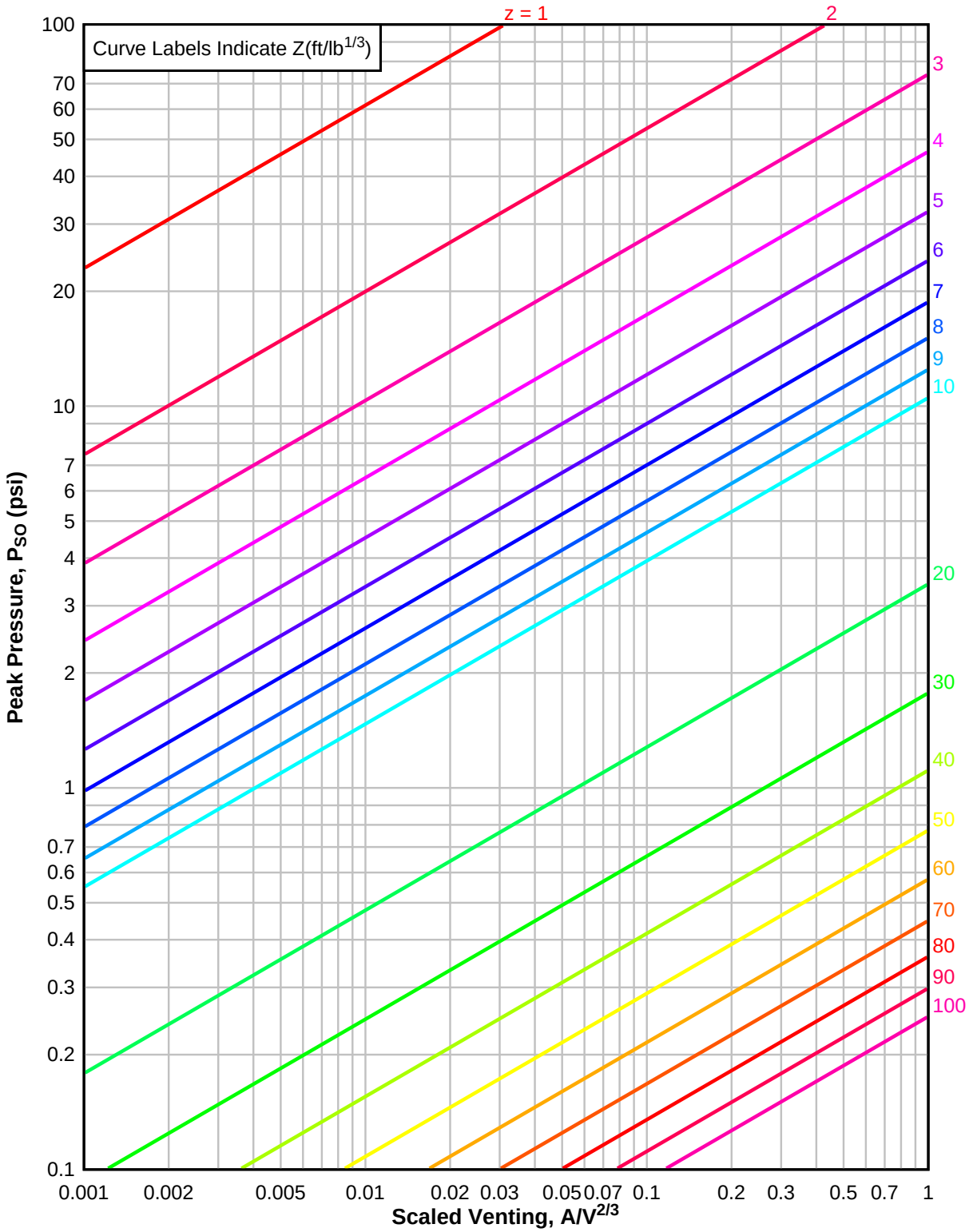

Figure 2-189 Peak Positive Pressure at the Back of a Partially Vented Four-Wall Cubicle

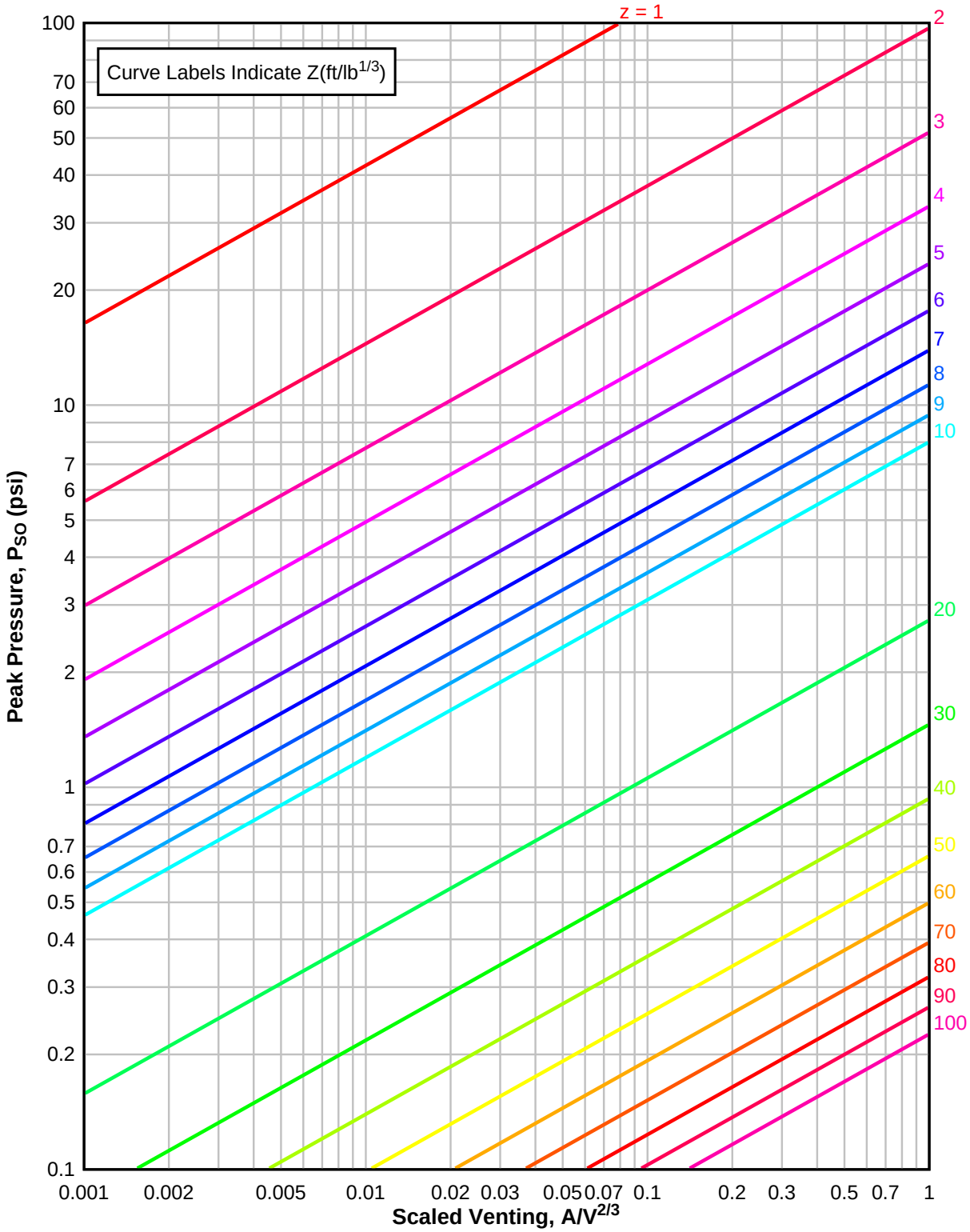

Figure 2-190 Idealized Pressure-Time Variation

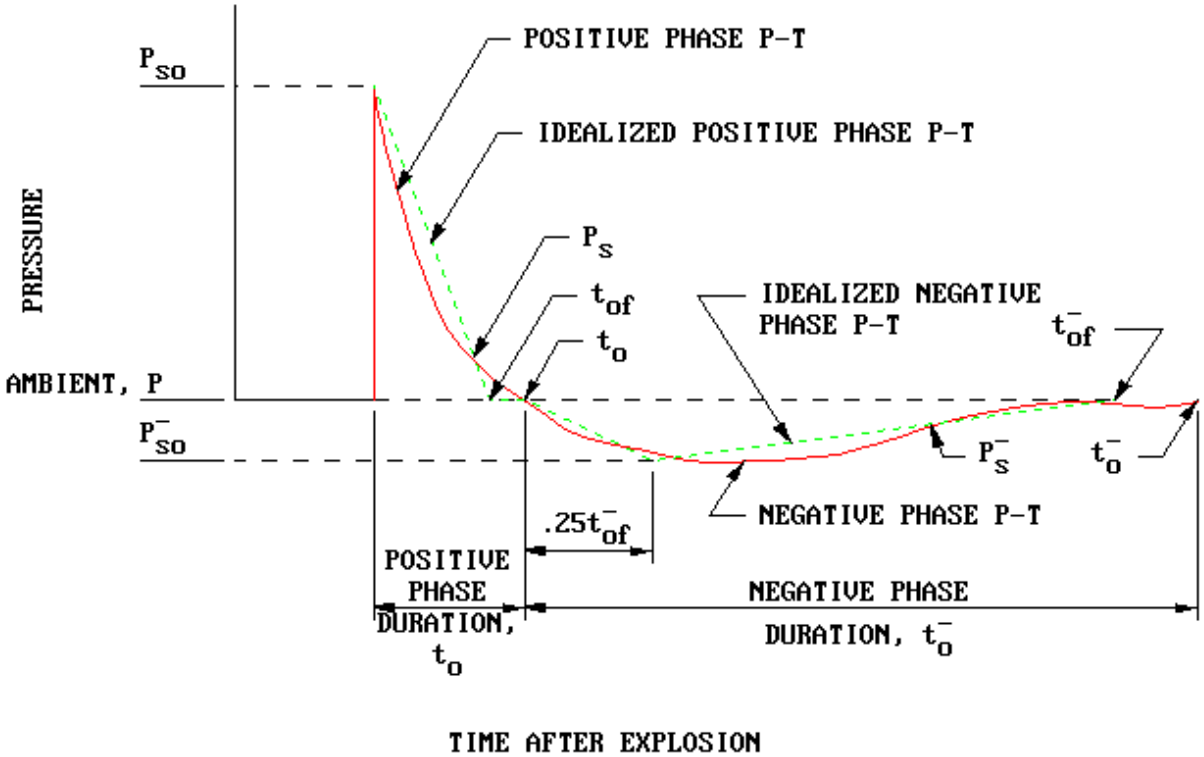

Figure 2-191 Front Wall Loading

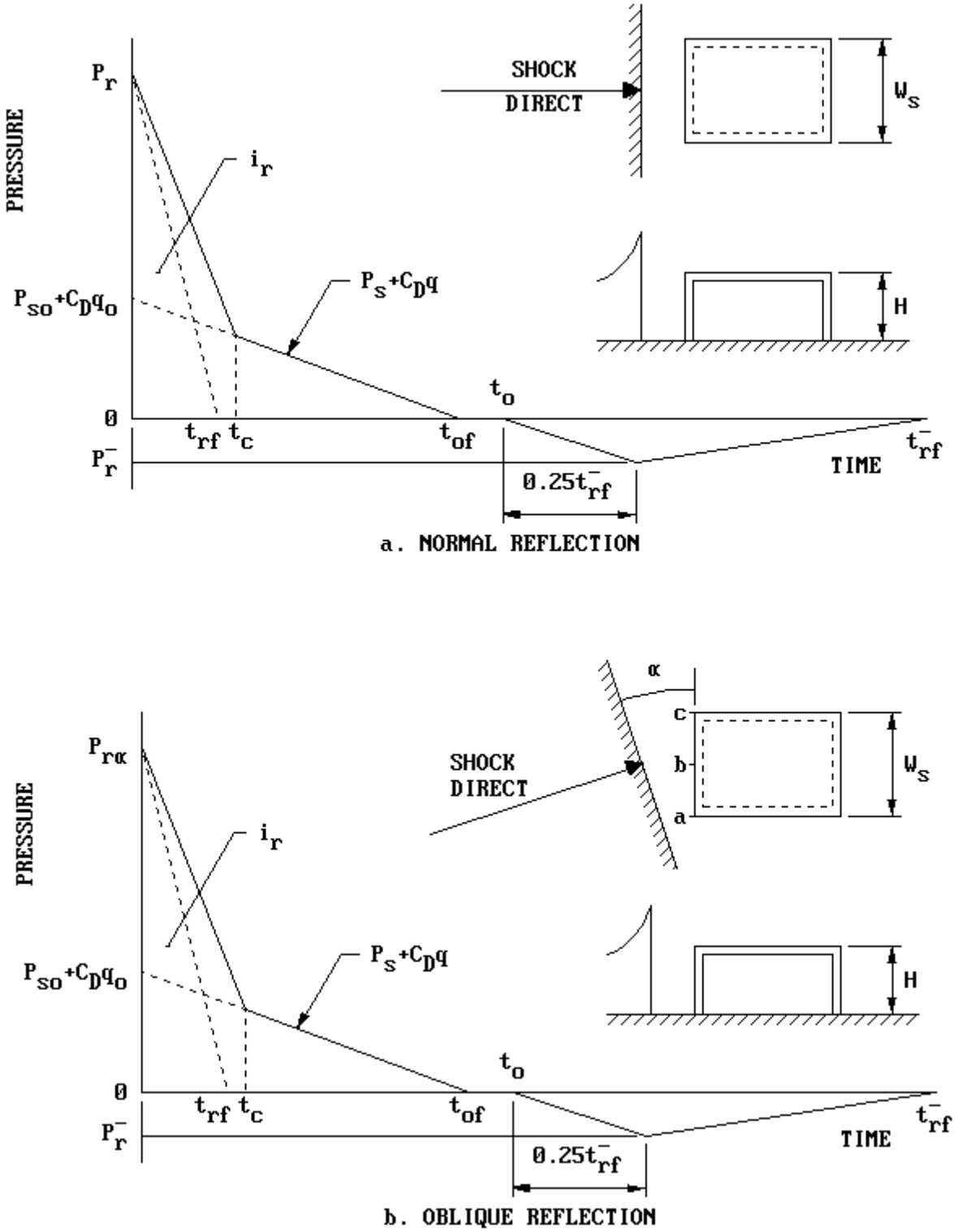

Figure 2-192 Velocity of Sound in Reflected Overpressure Region versus Peak Incident Overpressure

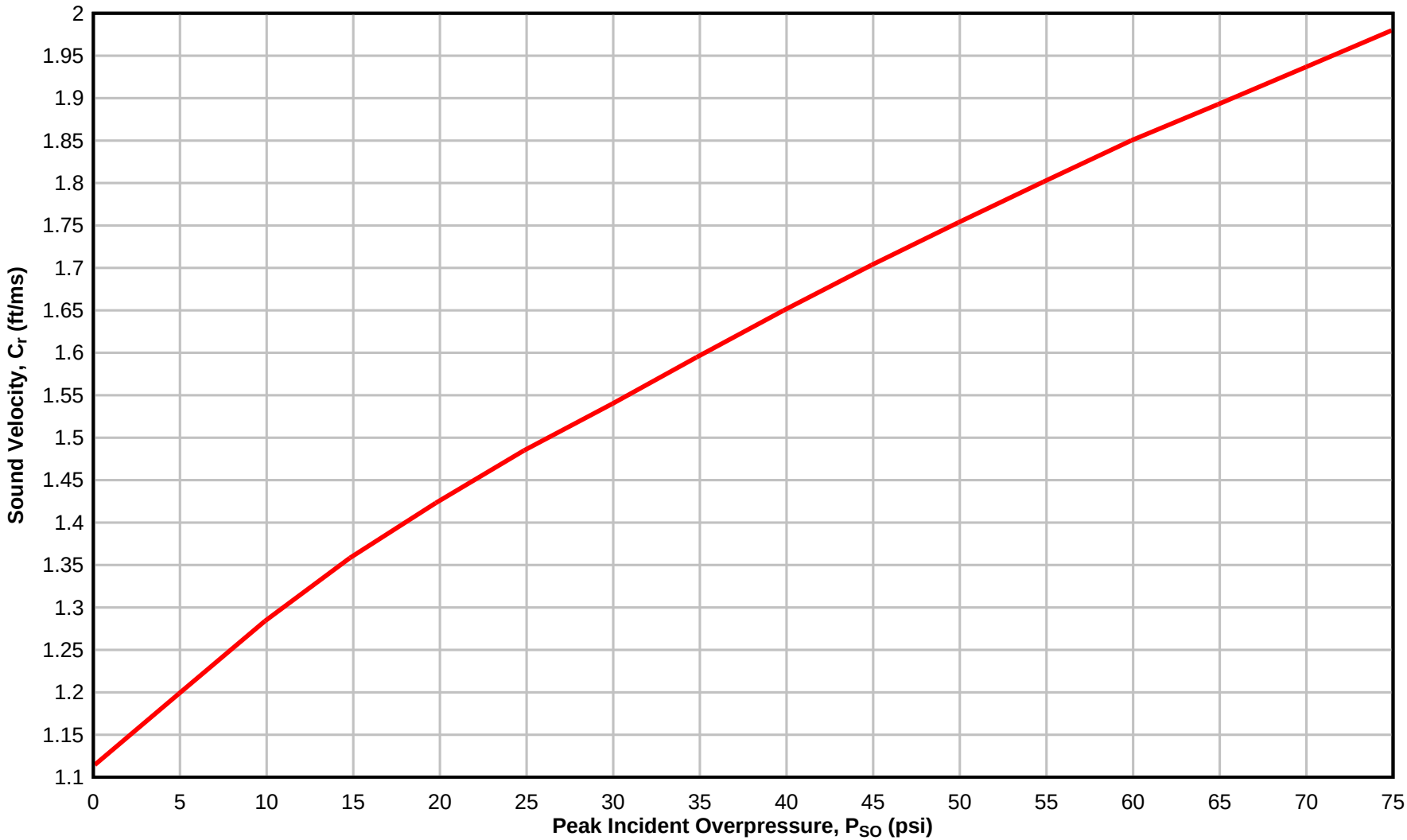

Figure 2-193 Reflected Pressure Coefficient versus Angle of Incidence

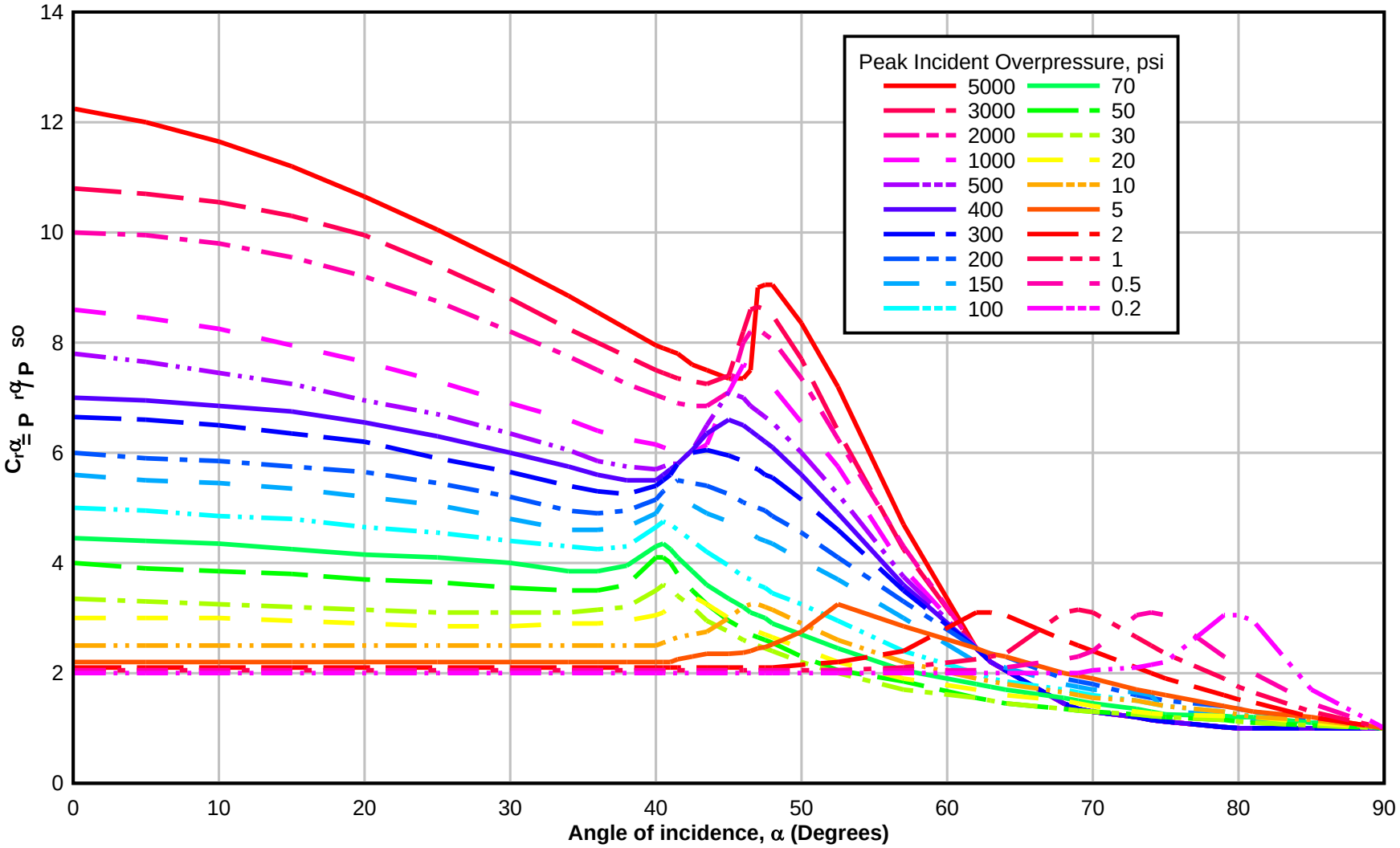

Figure 2-194 (a) Reflected Scaled Impulse versus Angle of Incidence

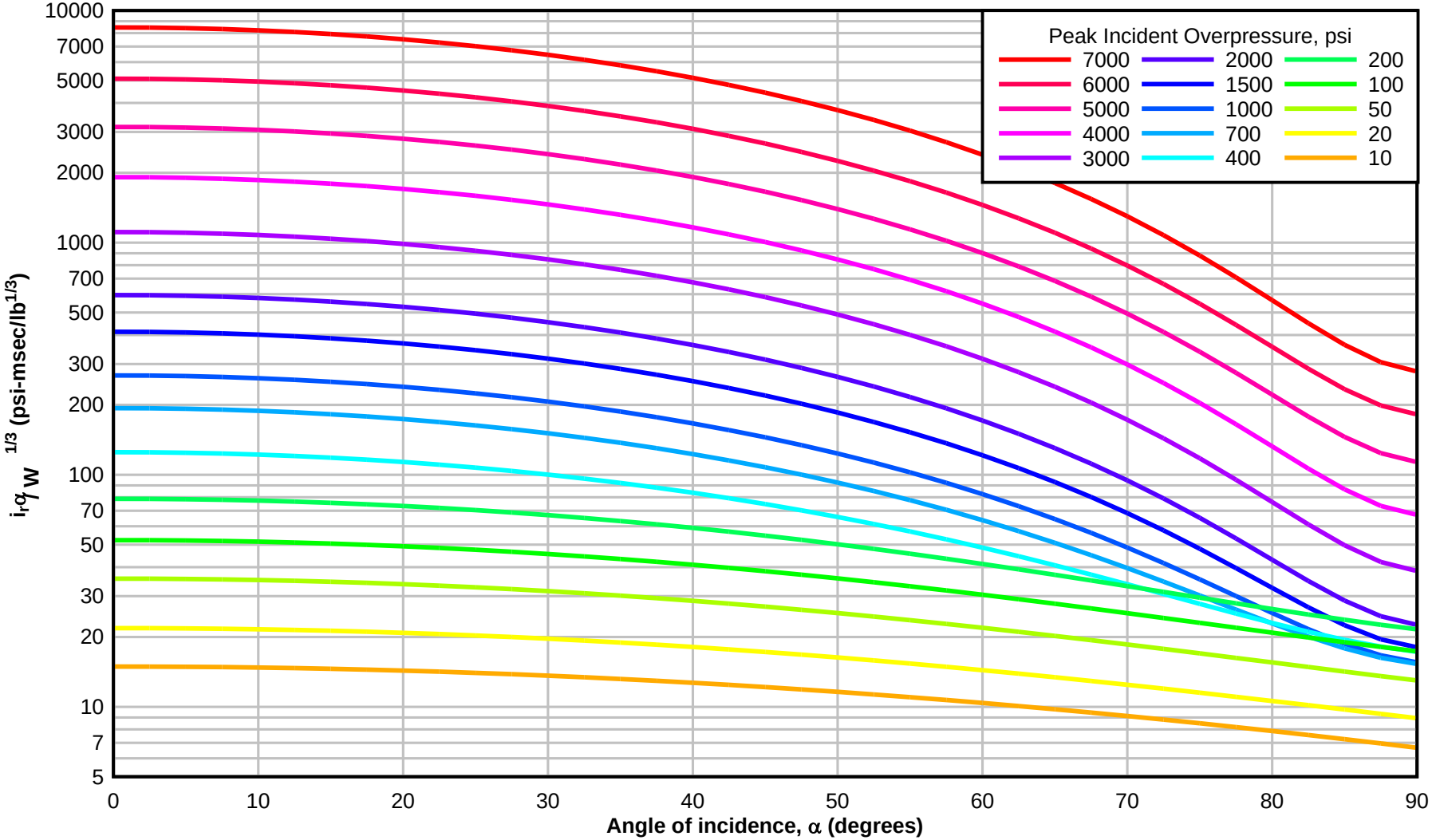

Figure 2-194 (b) Reflected Scaled Impulse versus Angle of Incidence

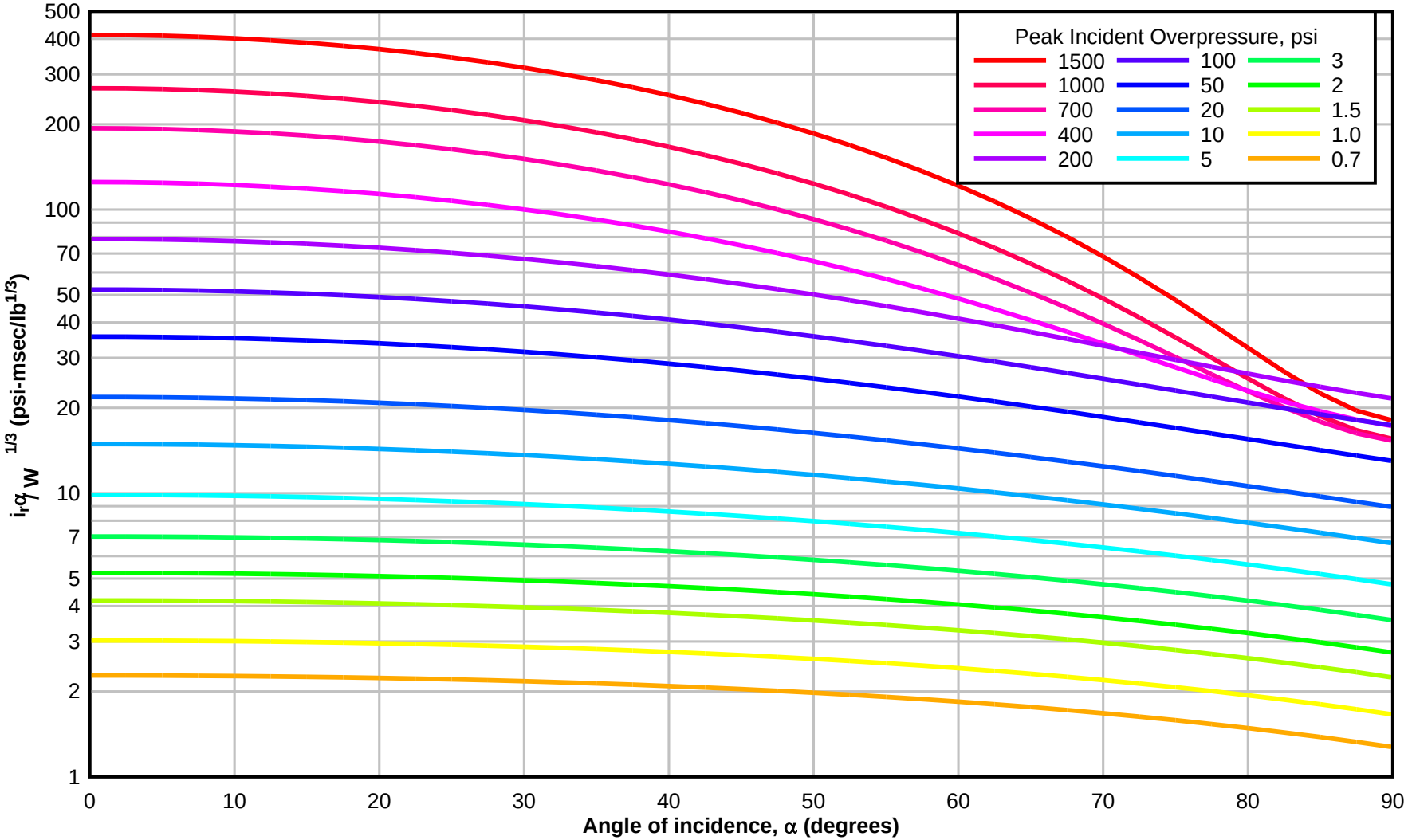

Figure 2-195 Roof and Side Wall Loading

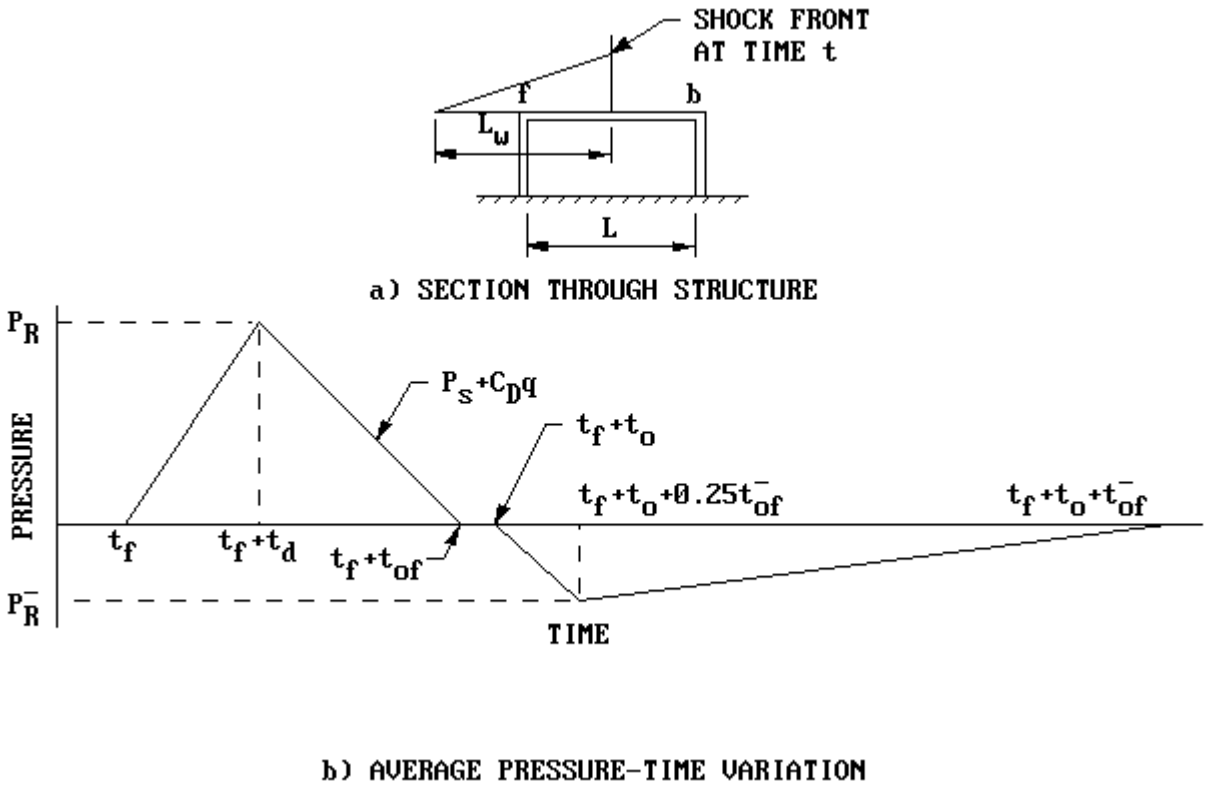

Figure 2-196 Peak Equivalent Uniform Roof Pressures

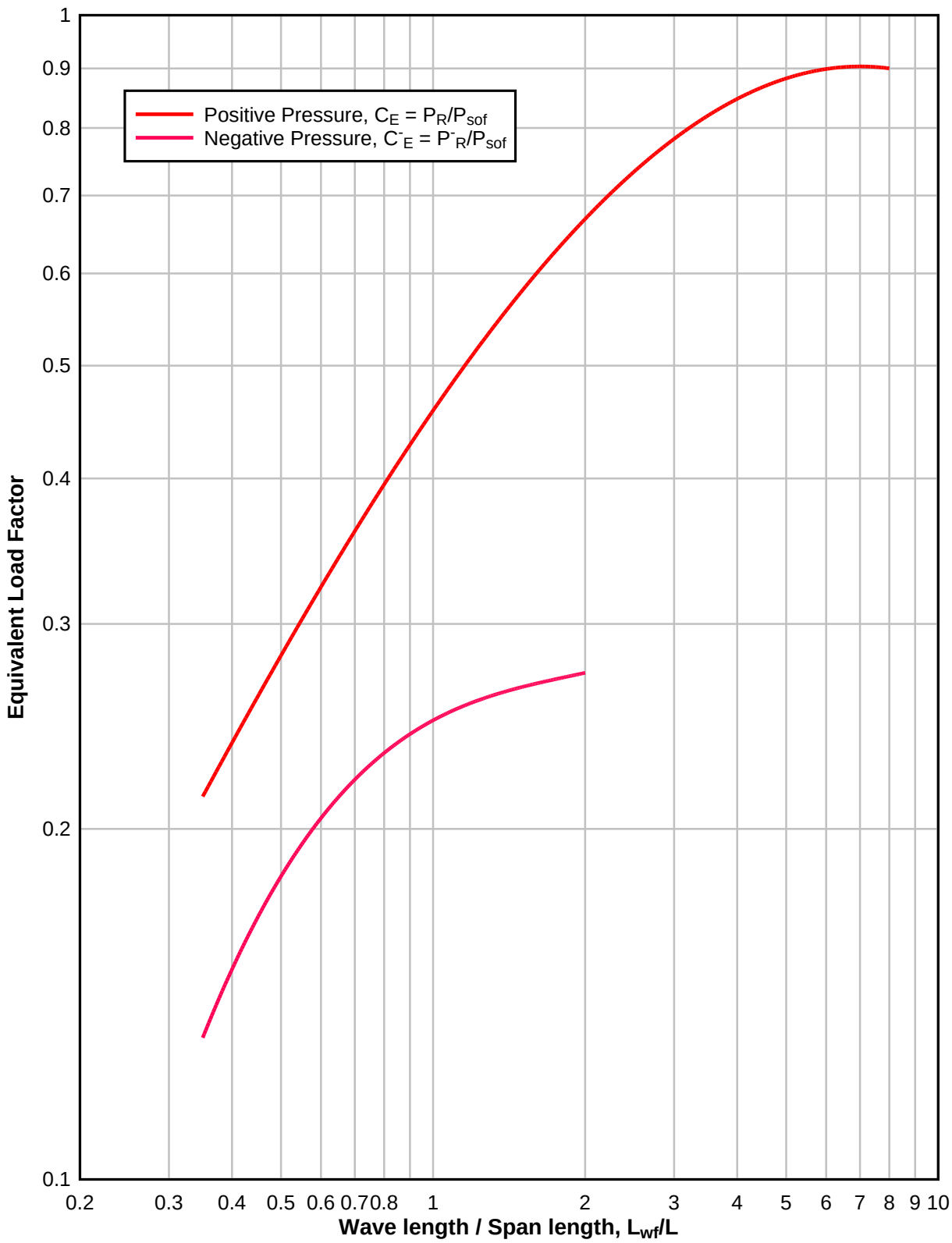

Figure 2-197 Scaled Rise Time of Equivalent Uniform Positive Roof Pressures

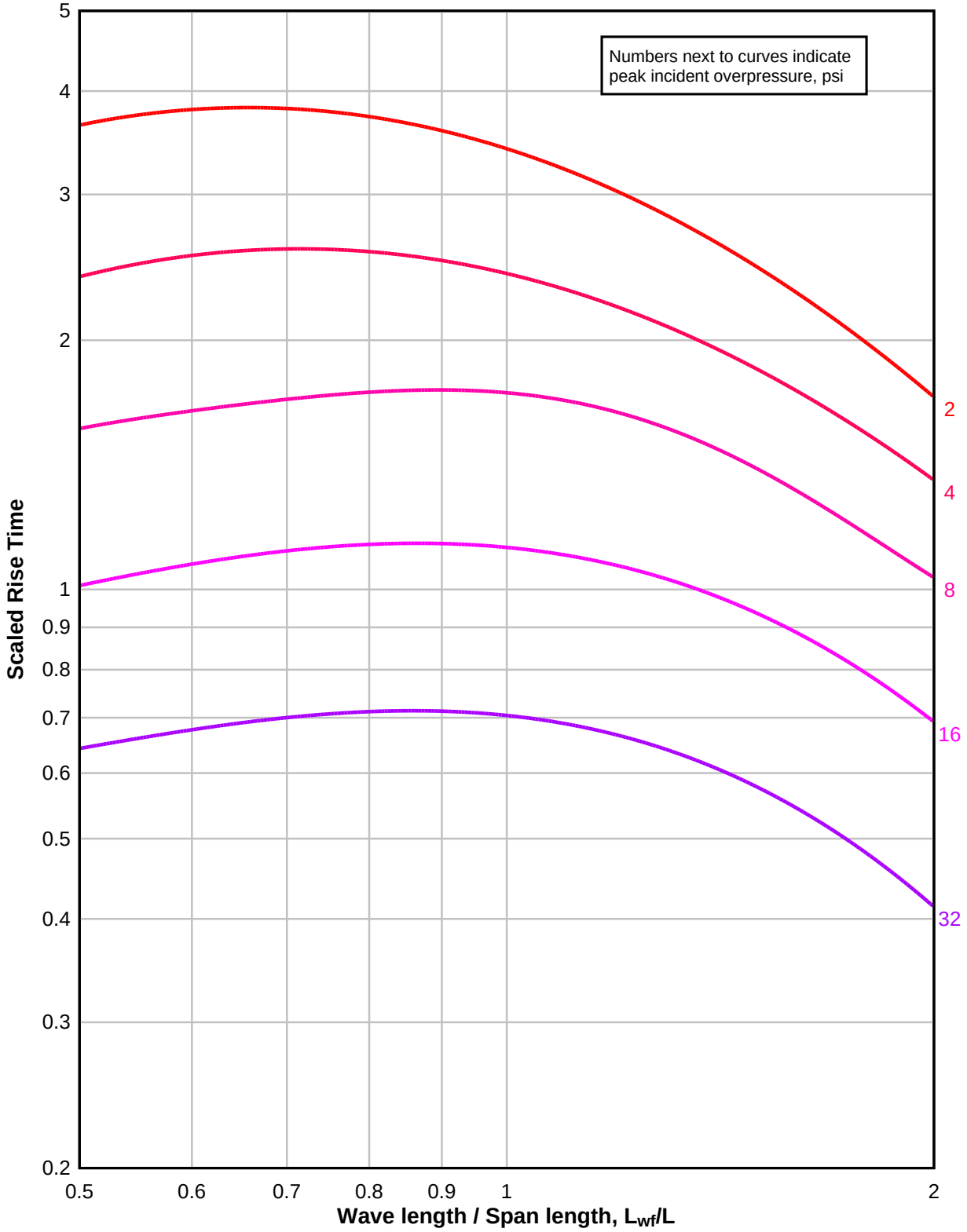

Figure 2-198 Scaled Duration of Equivalent Uniform Roof Pressures

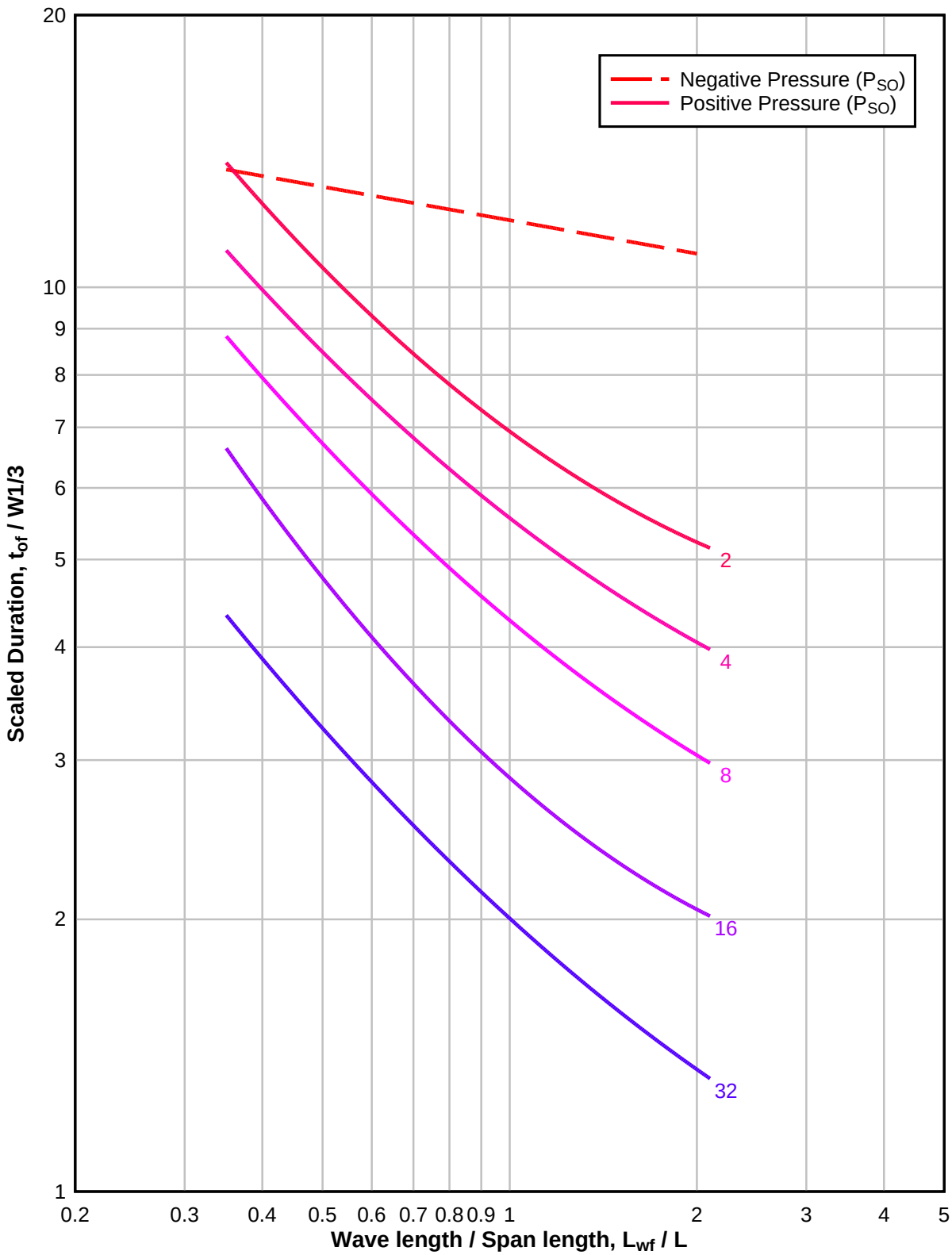

Figure 2-199 Rear Wall Loading

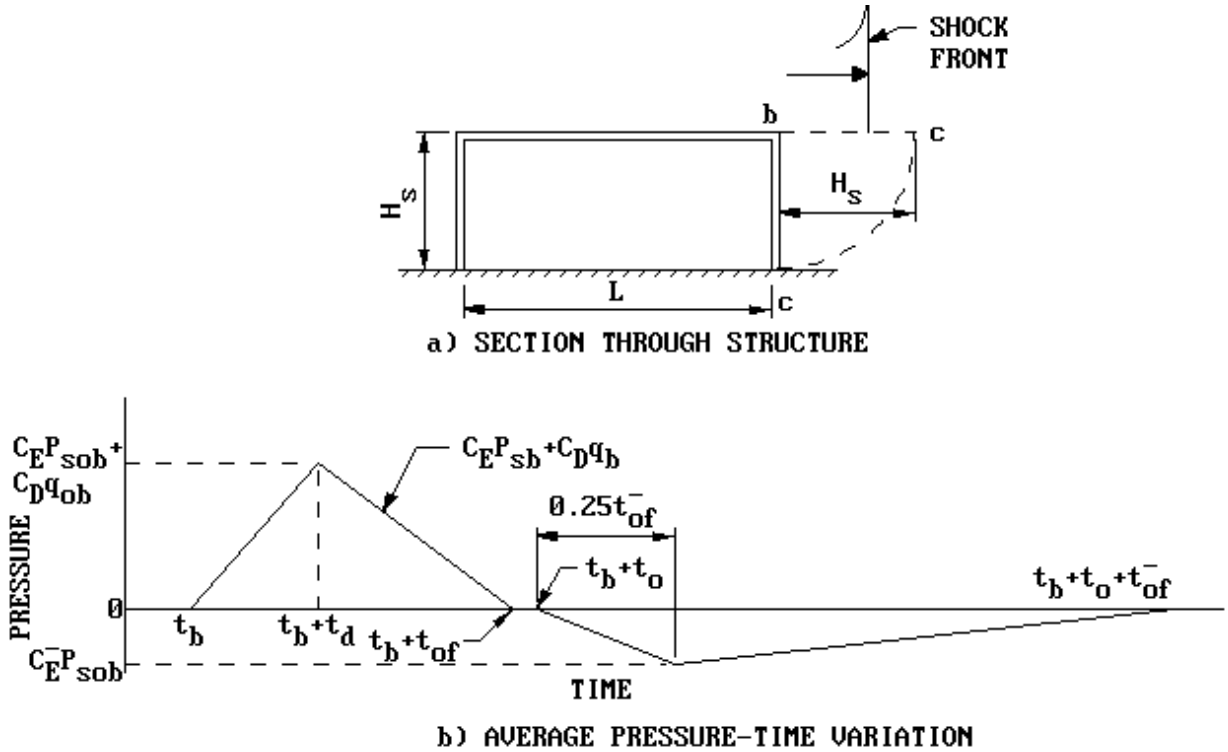

Figure 2-200 Idealized Structure Configuration for Interior Blast Loads

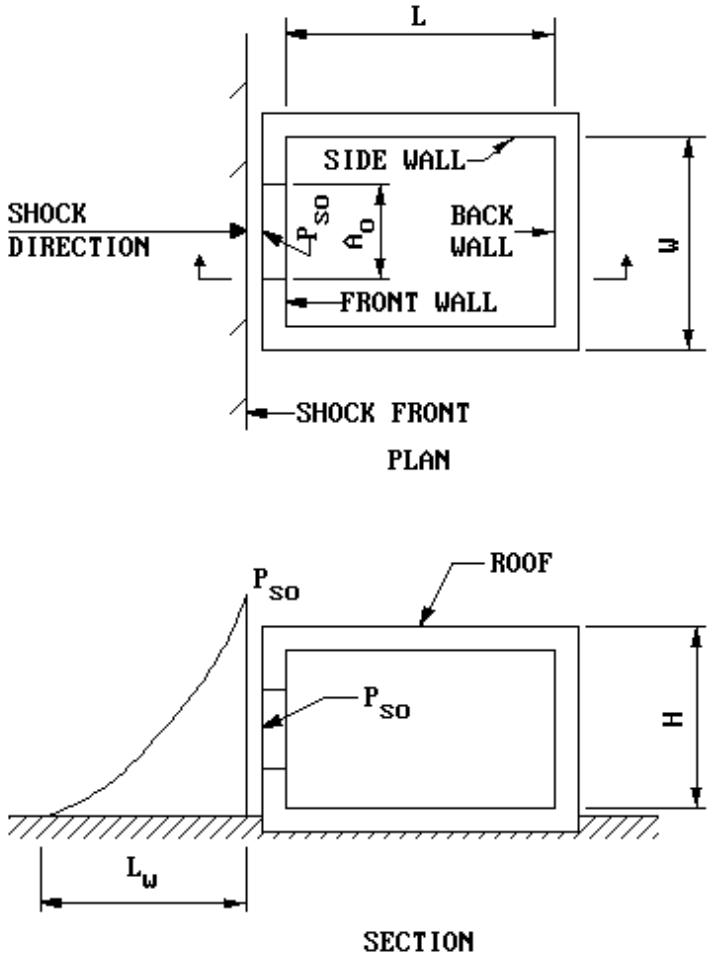

NOMENCLATURE:
L, LENGTH OF SIDE WALL
W, WIDTH OF BACK WALL AND FRONT WALL
H, HEIGHT OF ALL WALLS
A_o, AREA OF OPENING IN FRONT WALL
A_w, AREA OF BACK WALL
L_w, WAVE LENGTH OF SHOCK WAVE OF INCIDENT PRESSURE, P_{so}, AT EXTERIOR FACE OF FRONT WALL

Figure 2-201 Idealized Interior Blast Loads

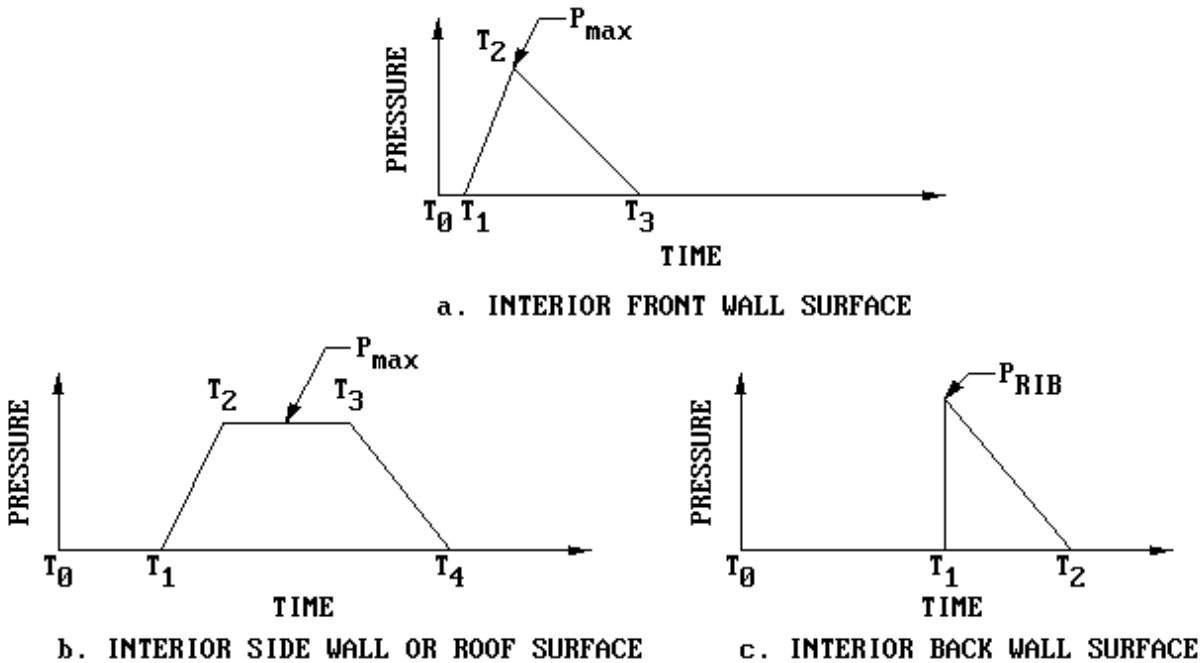

Figure 2-202 Sub-Division of Typical Front Wall with Openings

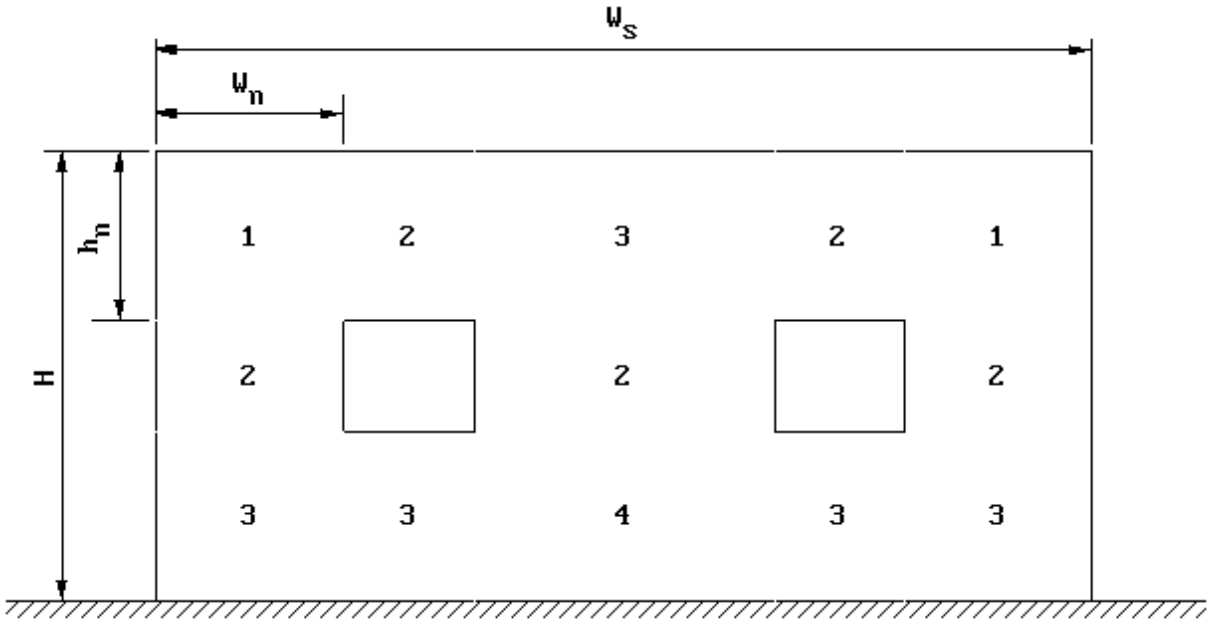

Figure 2-203 Maximum Average Pressure on Interior Face of Front Wall (*W*/*H* = 3/4)

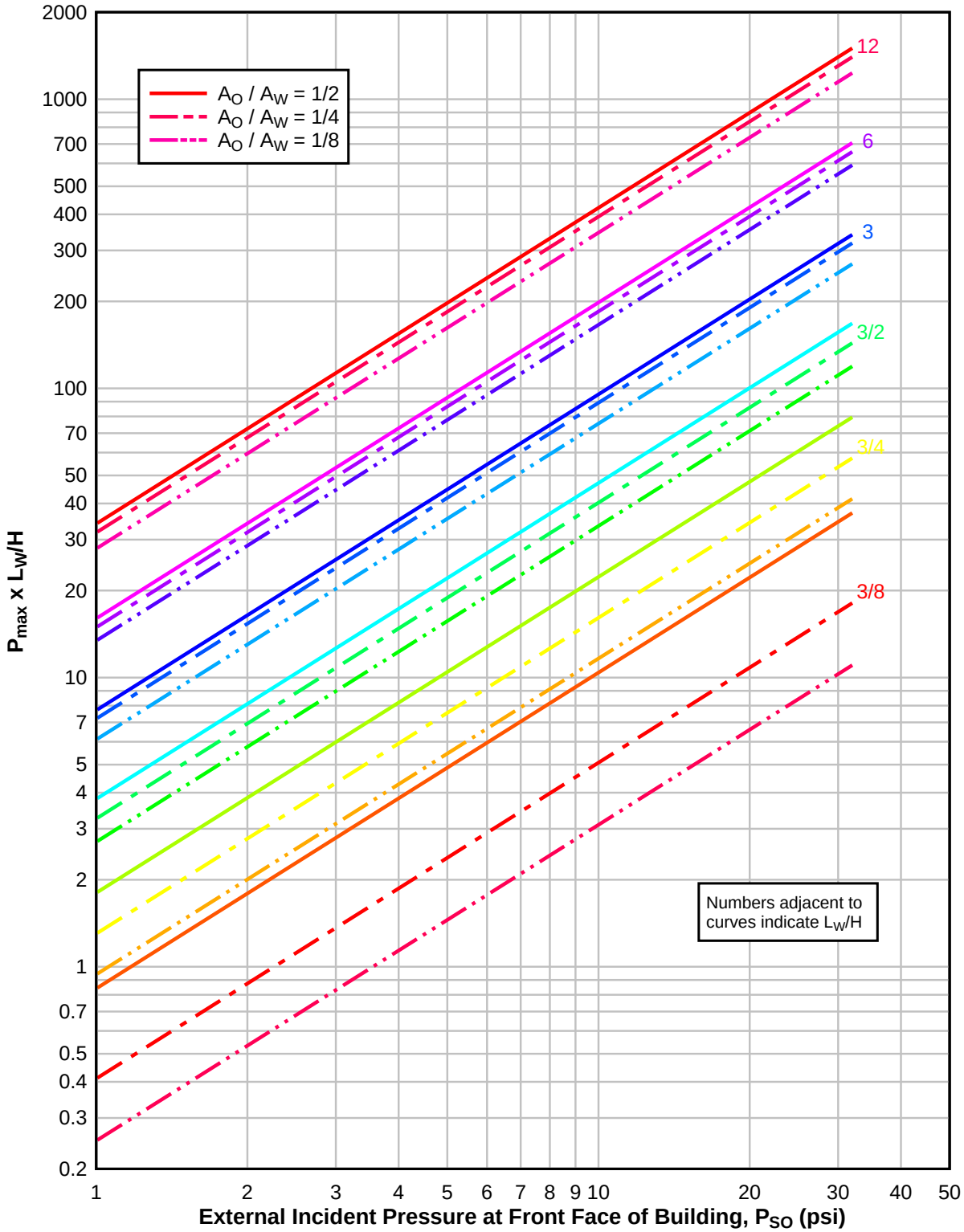

Figure 2-204 Maximum Average Pressure on Interior Face of Front Wall (*W*/*H* = 3/2)

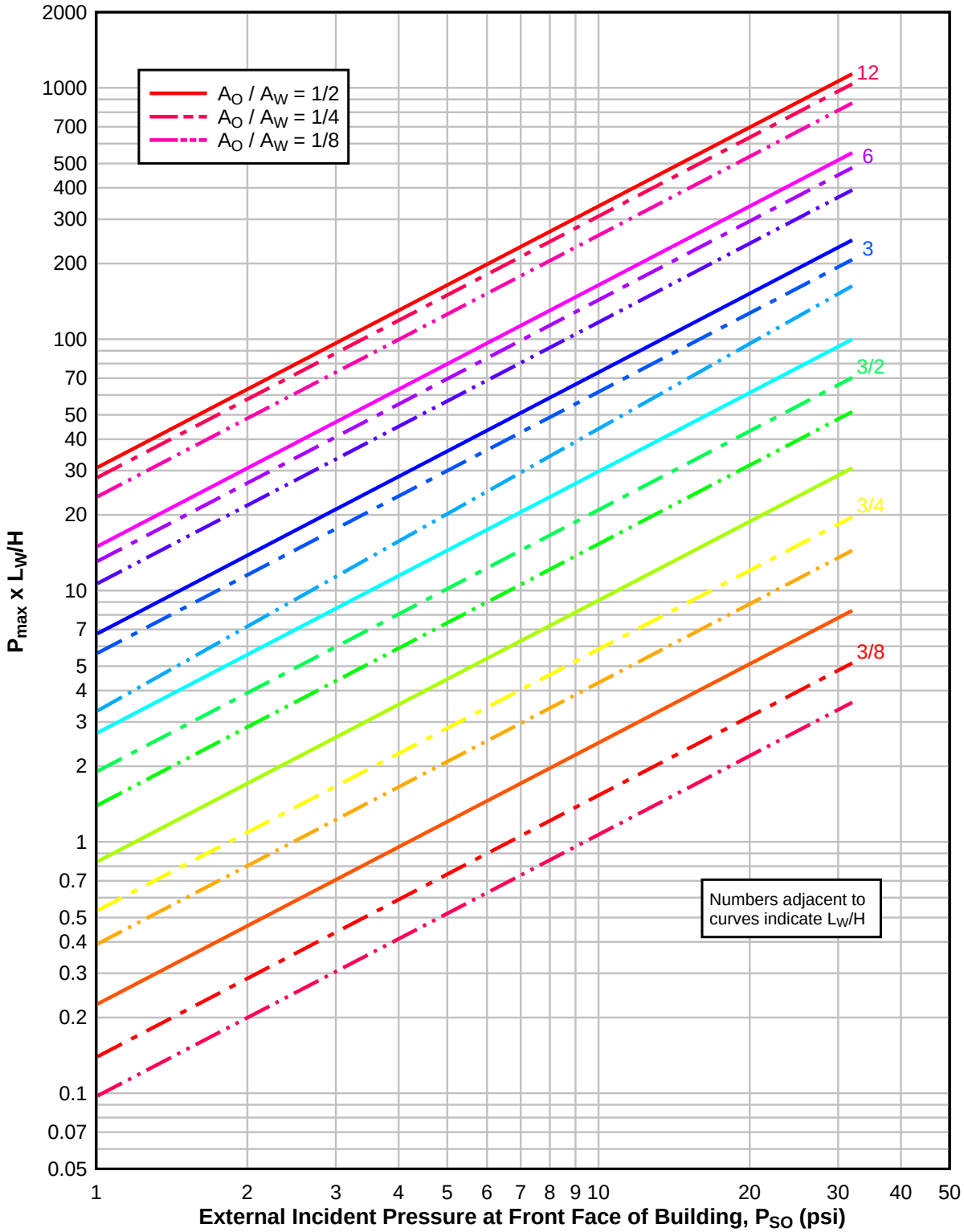

Figure 2-205 Maximum Average Pressure on Interior Face of Front Wall (*W*/*H* = 3)

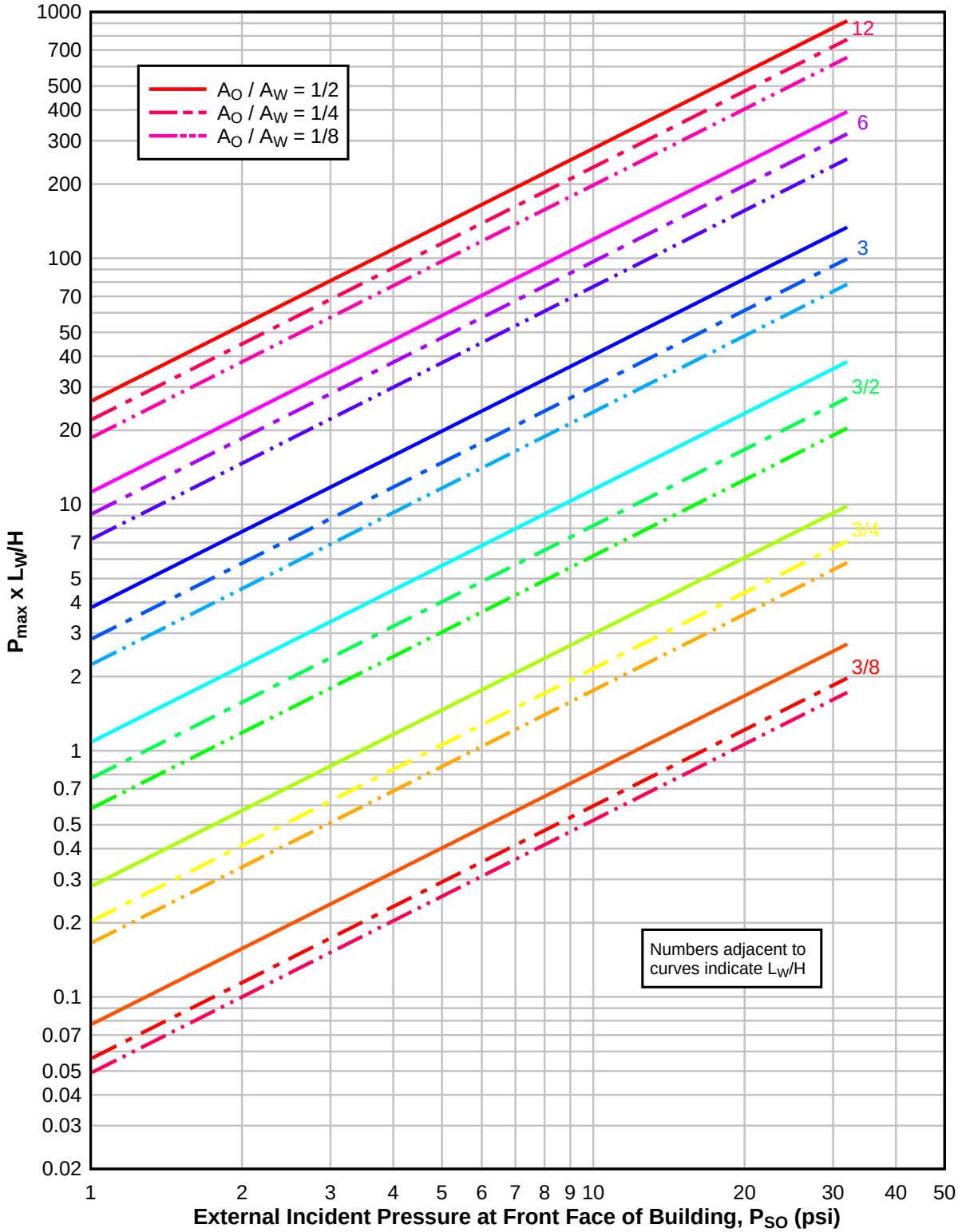

Figure 2-206 Maximum Average Pressure on Interior Face of Front Wall (*W*/*H* = 6)

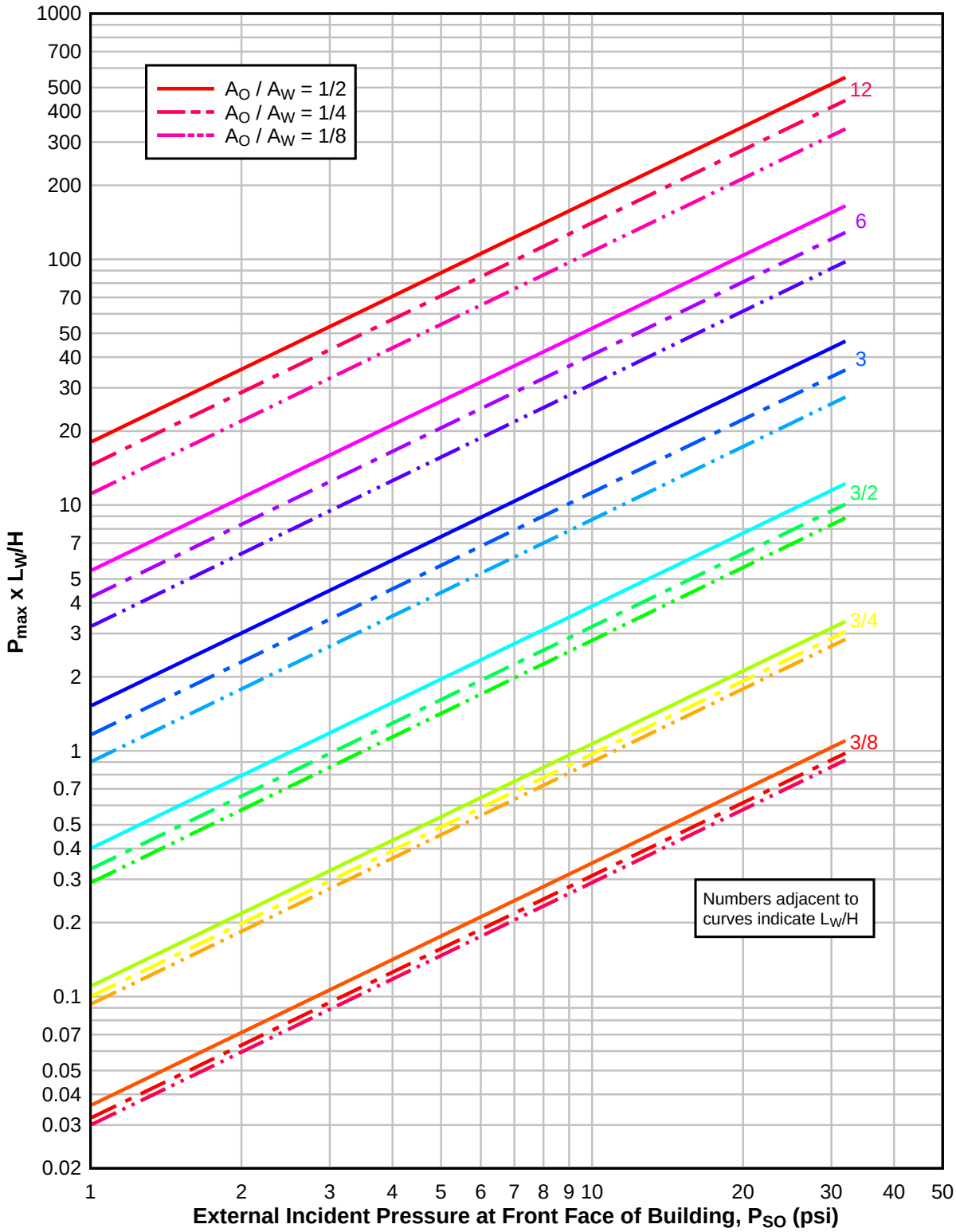

Figure 2-207 Arrival Time, T_1, for Interior Front Wall Blast Load (W/H = 3/4 and 3/2)

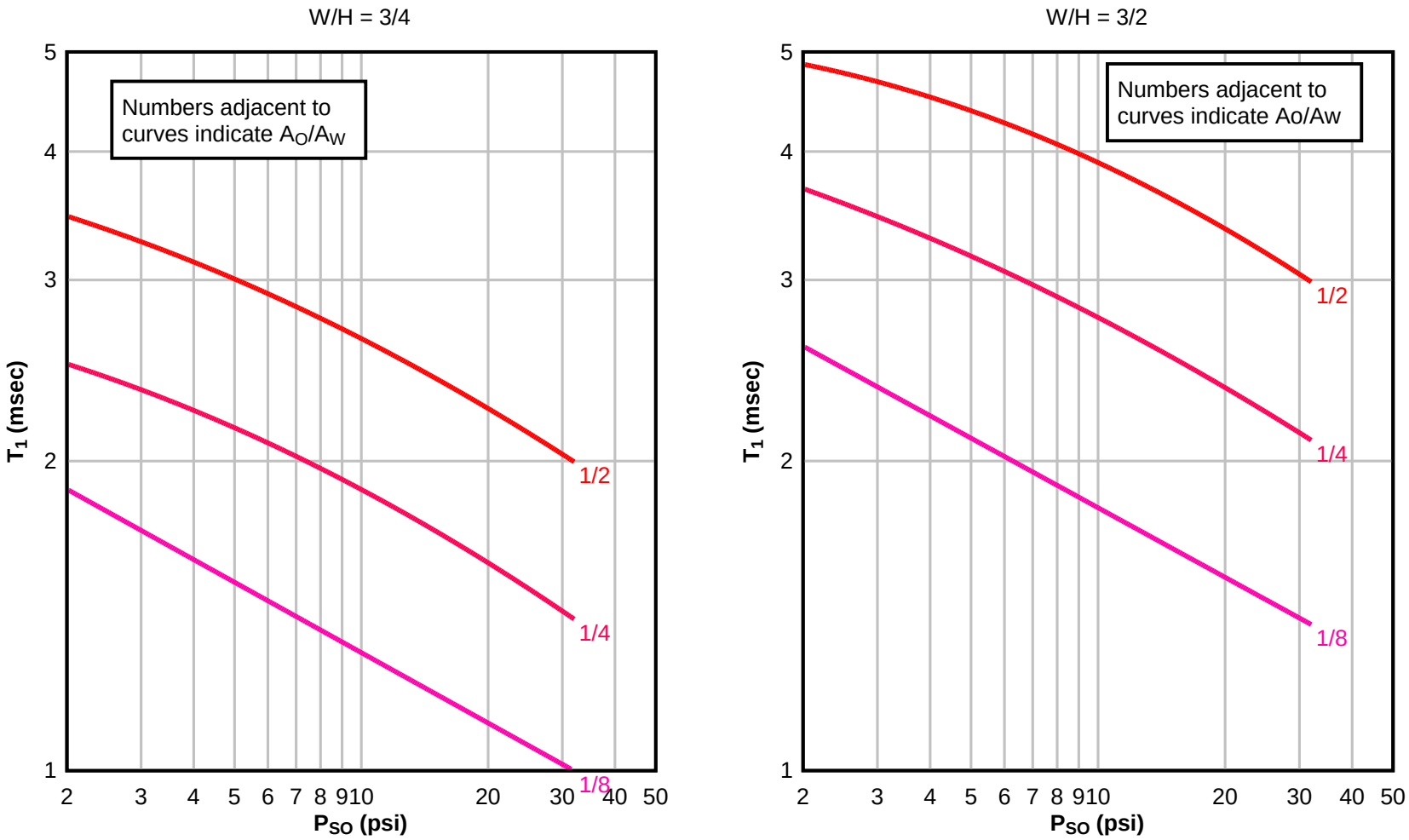

External Incident Pressure at Front Face of Building, P_{so} (psi)

Figure 2-208 Arrival Time, T_1, for Interior Front Wall Blast Load (W/H = 3 and 6)

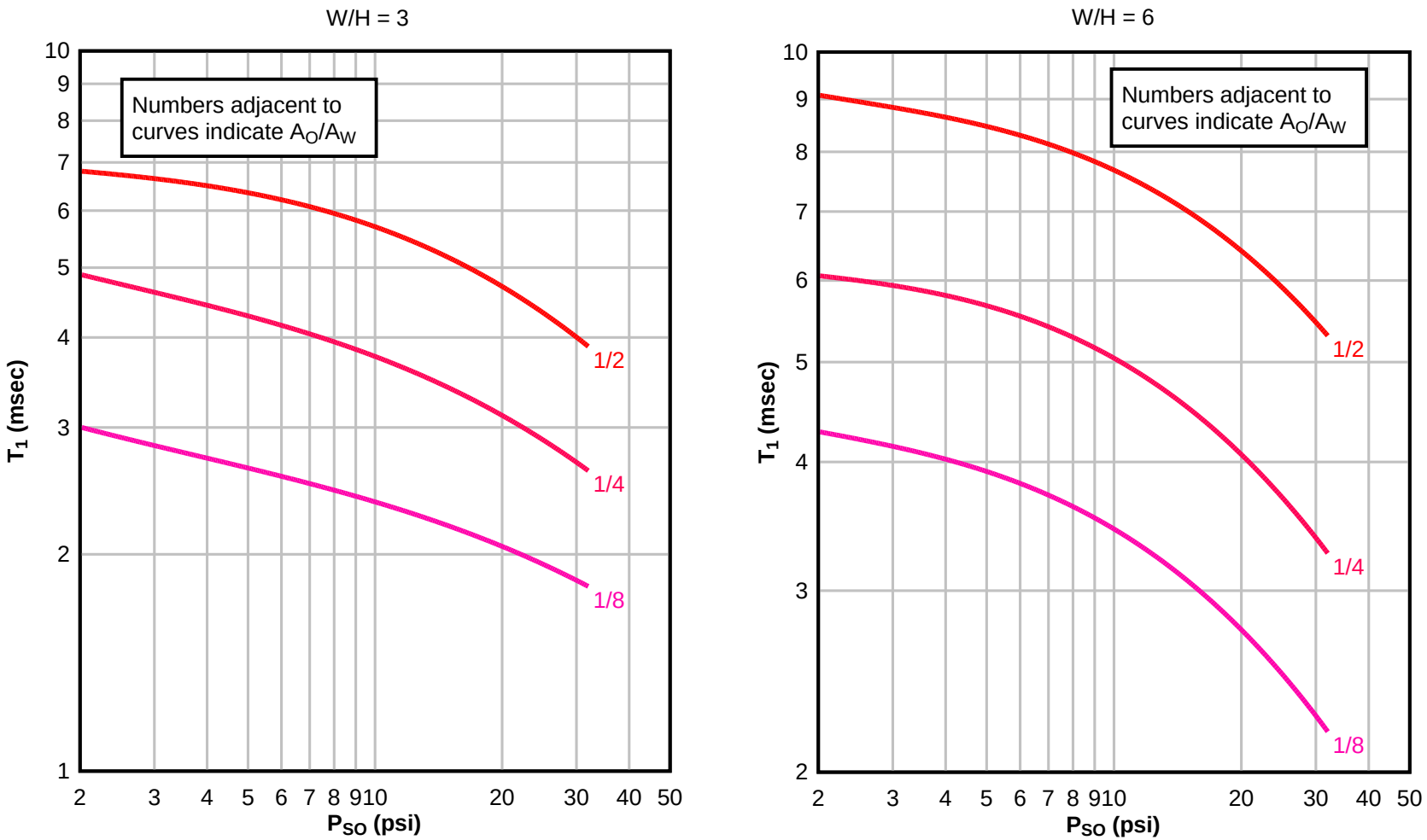

External Incident Pressure at Front Face of Building, P_{so} (psi)

Figure 2-209 Idealized Rise Time, T_2 - T_1, for Interior Front Wall Blast Load (W/H = 3/4 and 3/2)

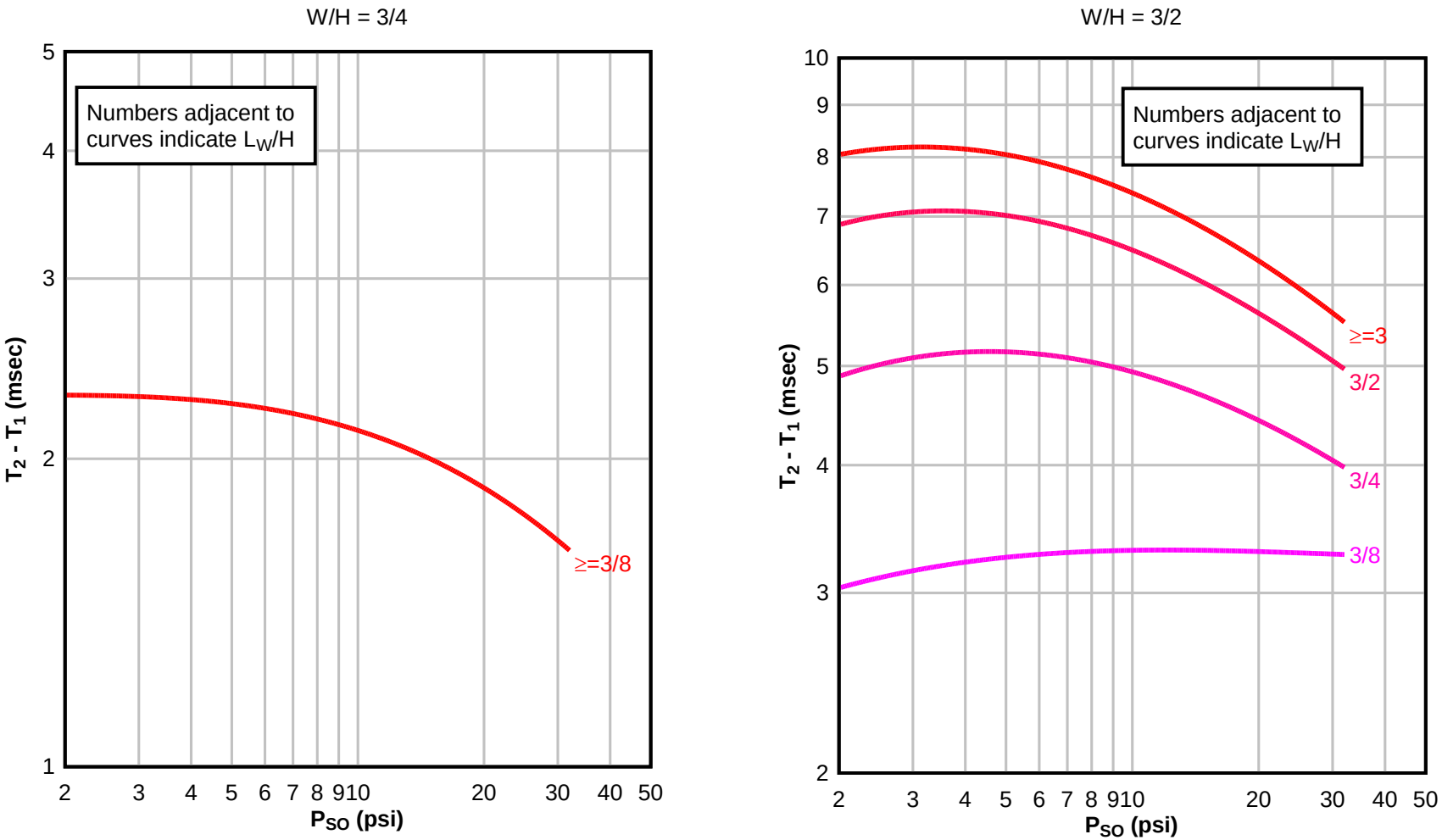

External Incident Pressure at Front Face of Building, P_{so} (psi)

Figure 2-210 Idealized Rise Time, T_2 - T_1, for Interior Front Wall Blast Load (W/H = 3 and 6)

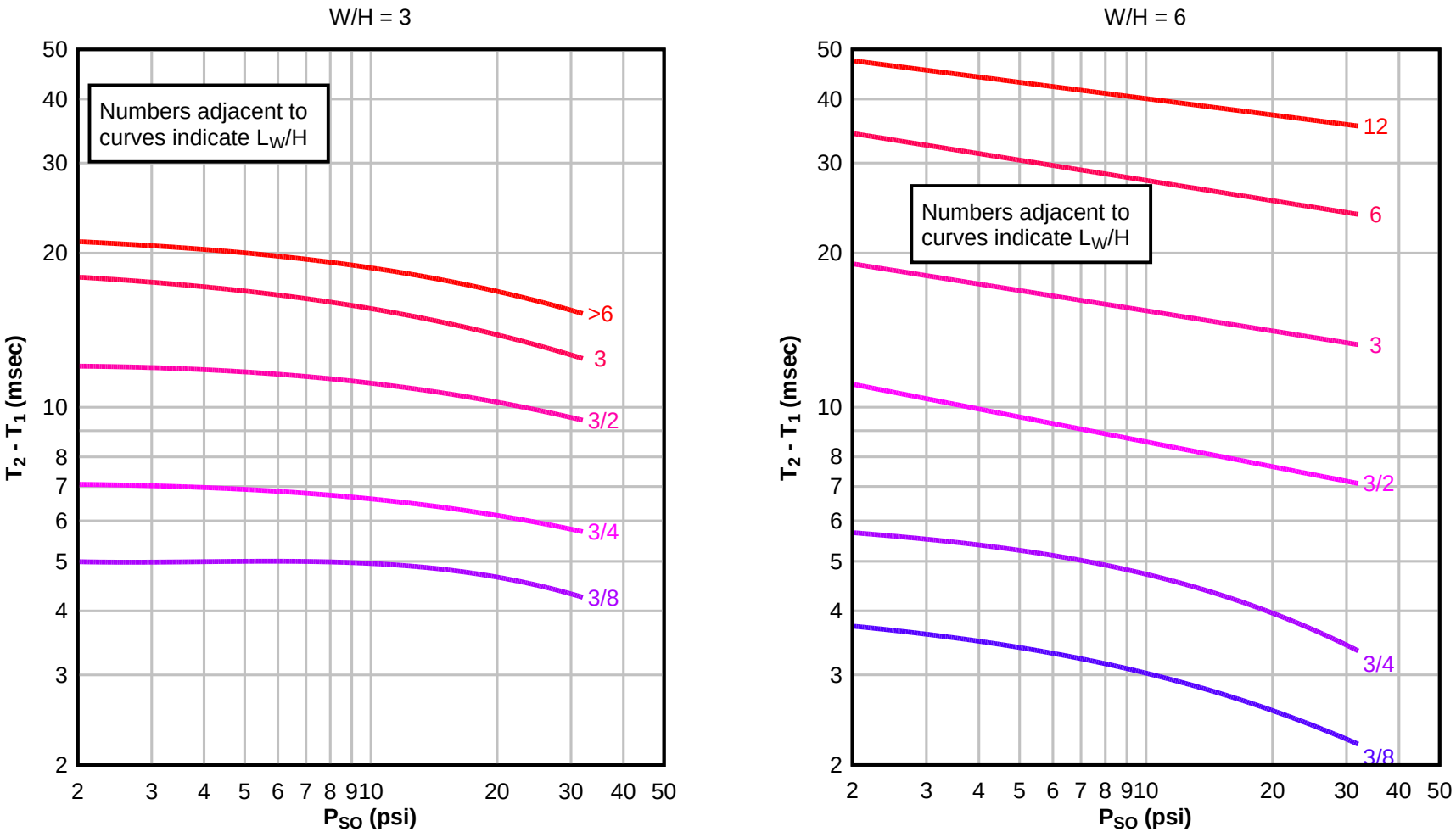

External Incident Pressure at Front Face of Building, P_{so} (psi)

Figure 2-211 Idealized Duration, T_3 - T_1, for Interior Front Wall Blast Load (W/H = 3/4 and 3/2)

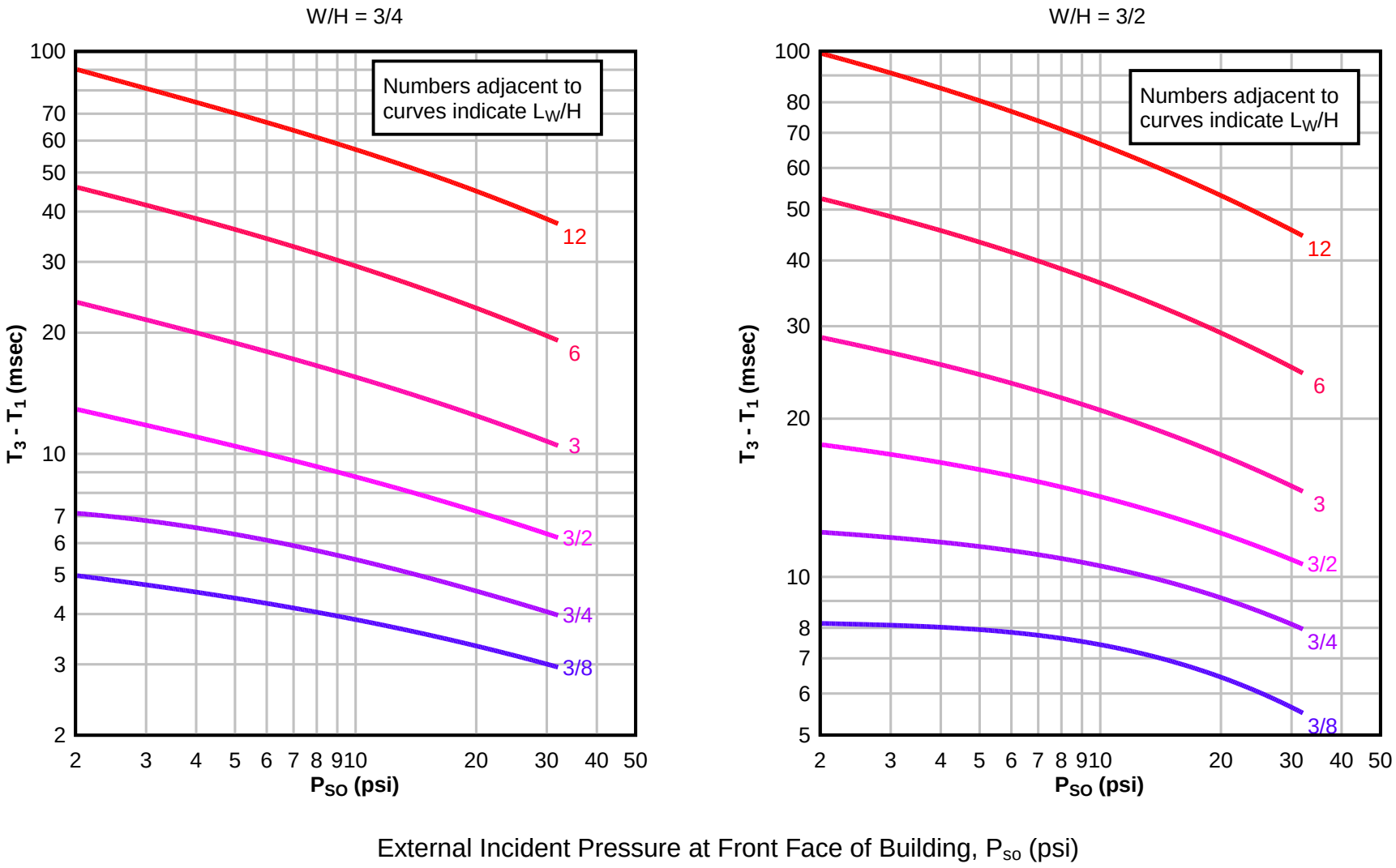

External Incident Pressure at Front Face of Building, P_{so} (psi)

Figure 2-212 Idealized Duration, T_3 - T_1, for Interior Front Wall Blast Load (W/H = 3 and 6)

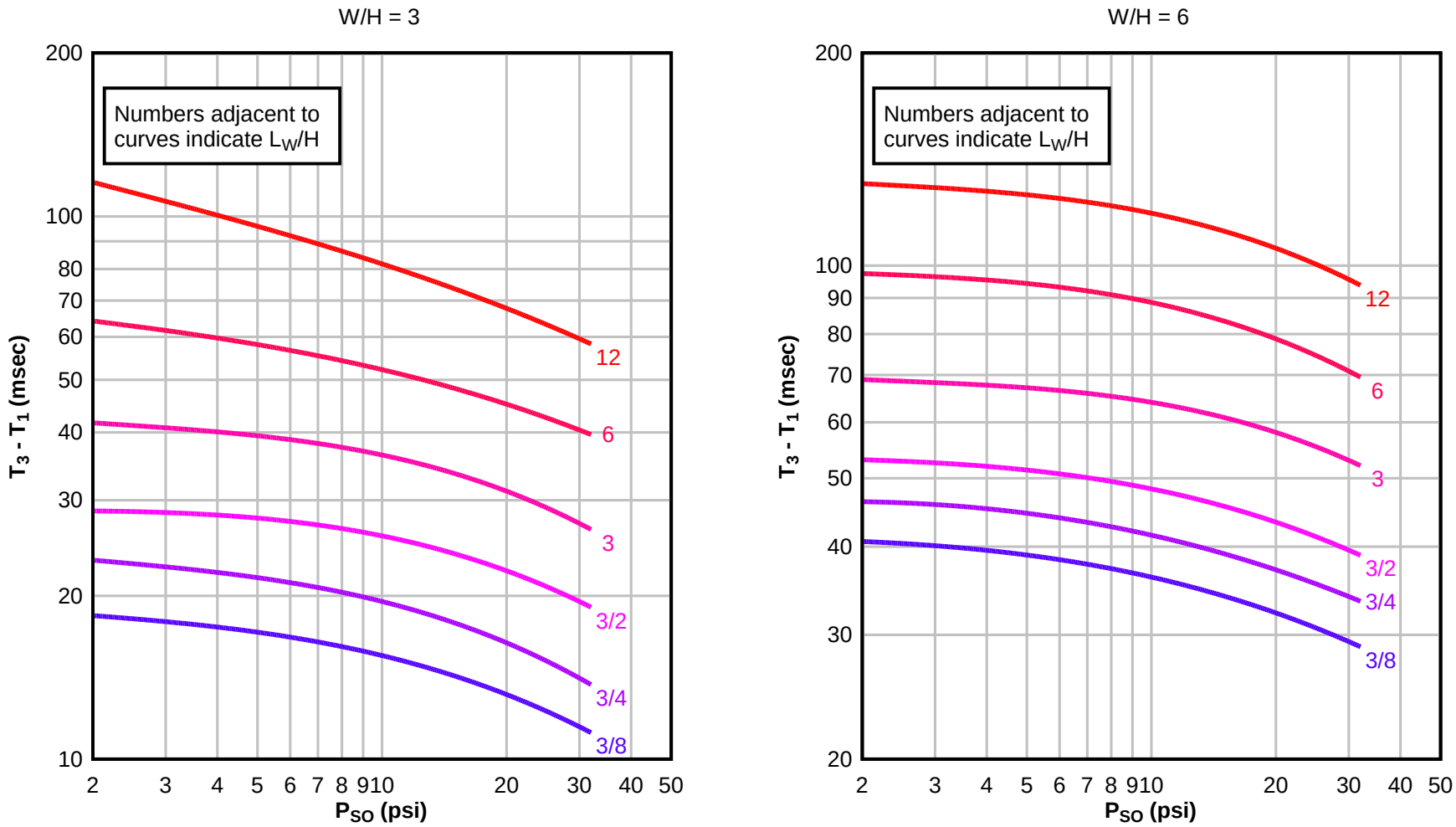

External Incident Pressure at Front Face of Building, P_{so} (psi)

Figure 2-213 Idealized Times T_1 and T_2 for Interior Side Wall Blast Load

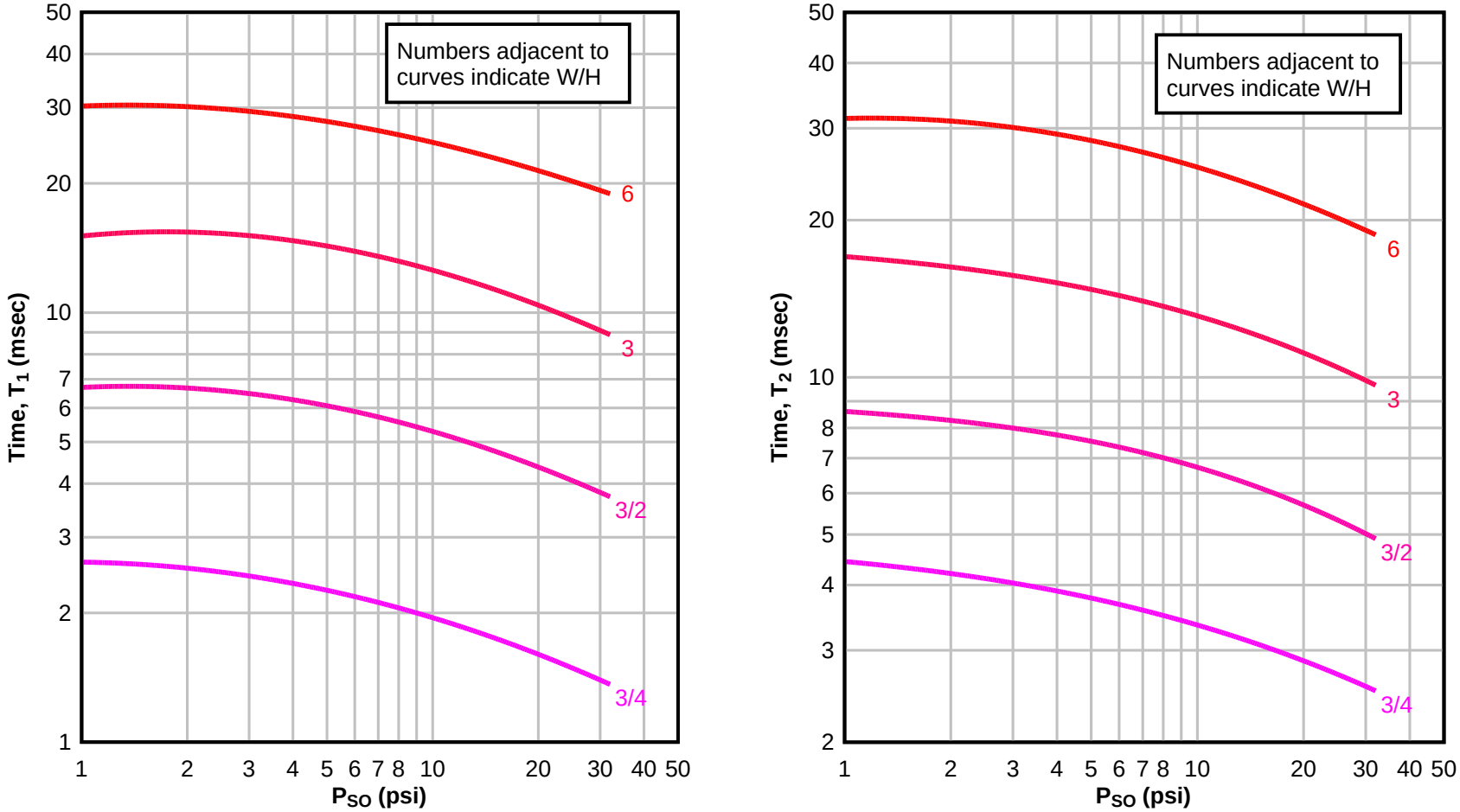

External Incident Pressure at Front Face of Building, P_{so} (psi)

Figure 2-214 Idealized Times T_3 and T_4 for Interior Side Wall Blast Load (L/H = 1, W/H = 3/4)

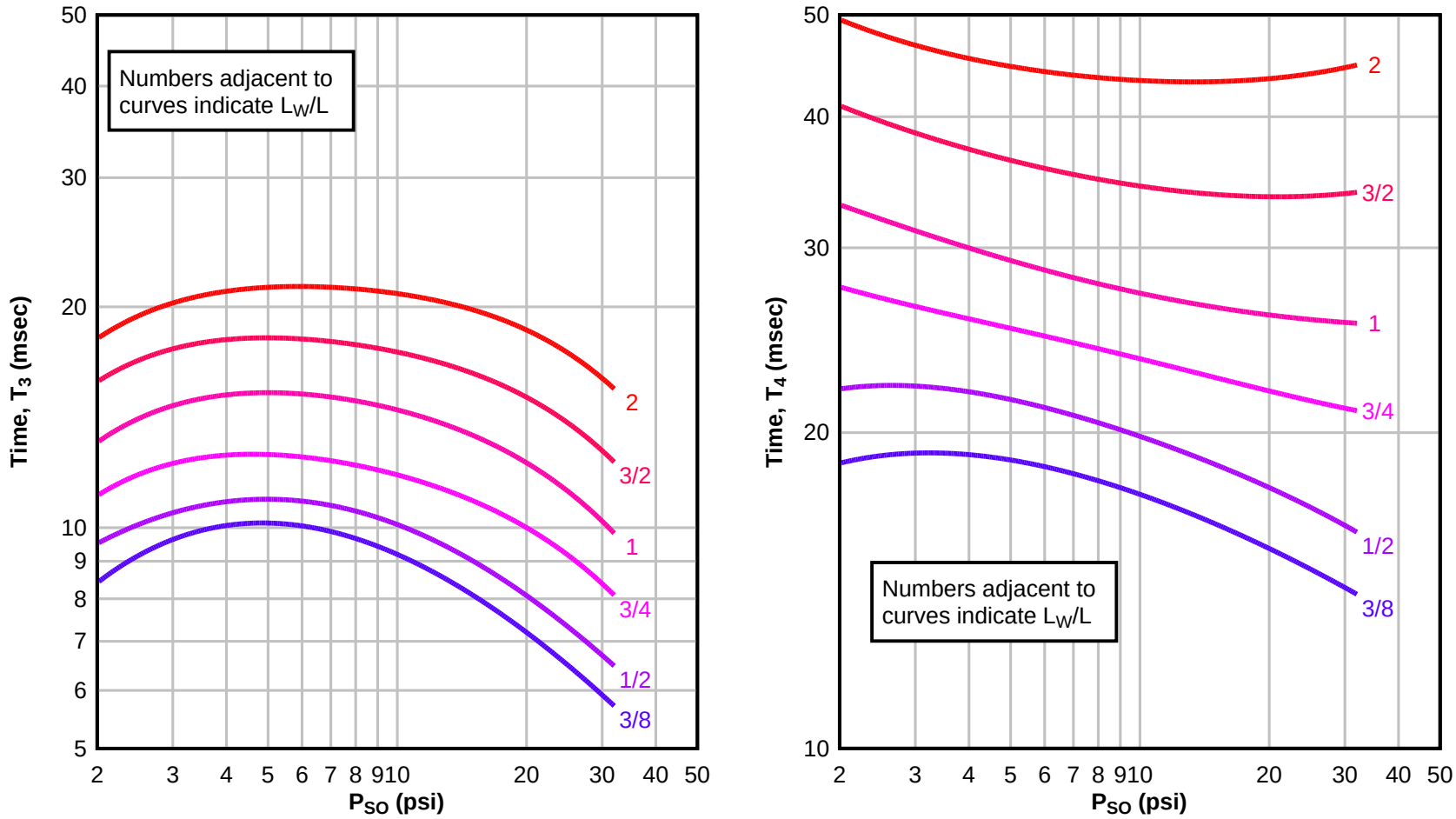

External Incident Pressure at Front Face of Building, P_{so} (psi)

Figure 2-215 Idealized Times T_3 and T_4 for Interior Side Wall Blast Load (L/H = 1, W/H = 3/2)

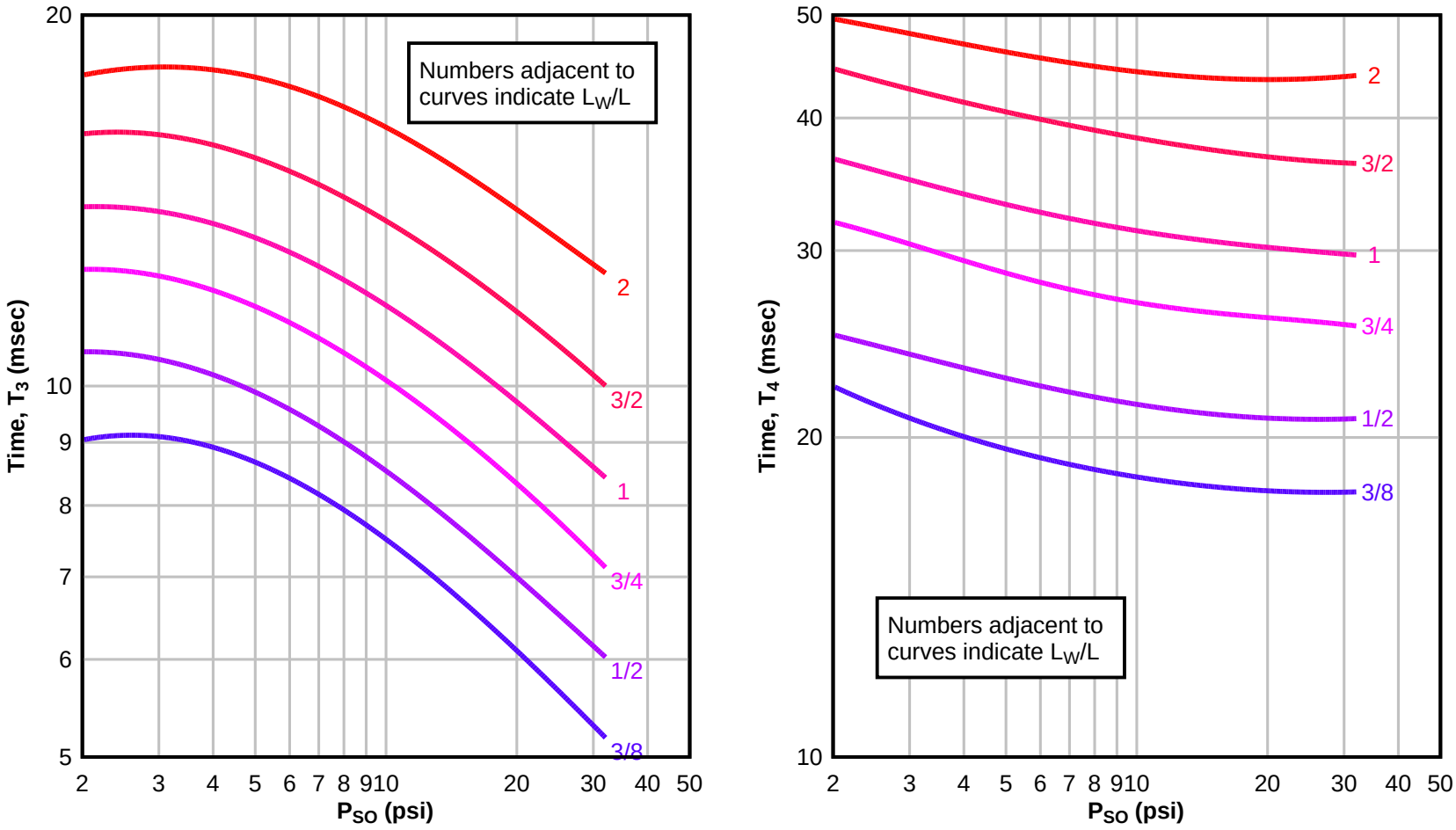

External Incident Pressure at Front Face of Building, P_{so} (psi)

Figure 2-216 Idealized Times T_3 and T_4 for Interior Side Wall Blast Load (L/H = 1, W/H = 3)

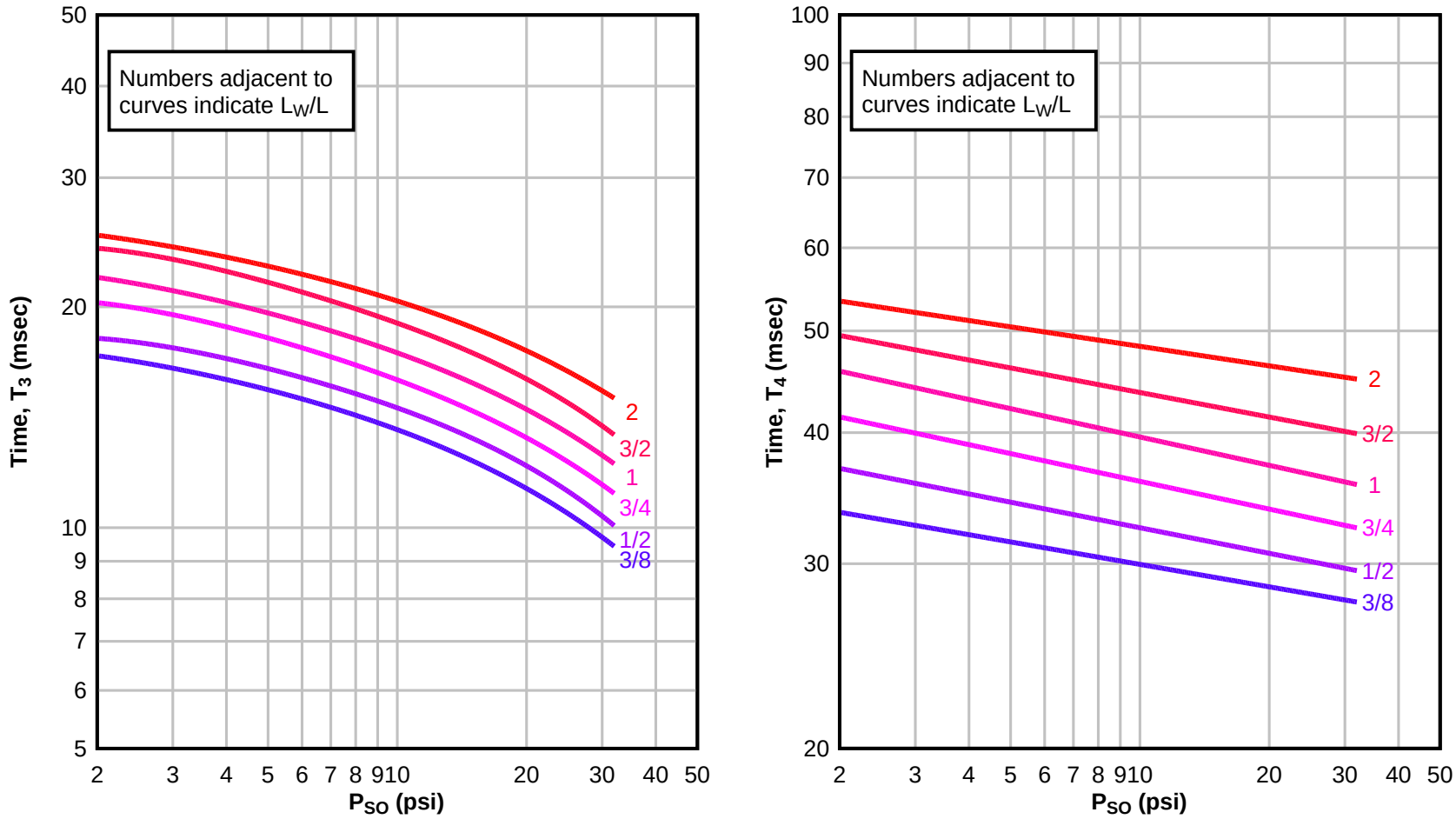

External Incident Pressure at Front Face of Building, P_{so} (psi)

Figure 2-217 Idealized Times T_3 and T_4 for Interior Side Wall Blast Load (L/H = 1, W/H = 6)

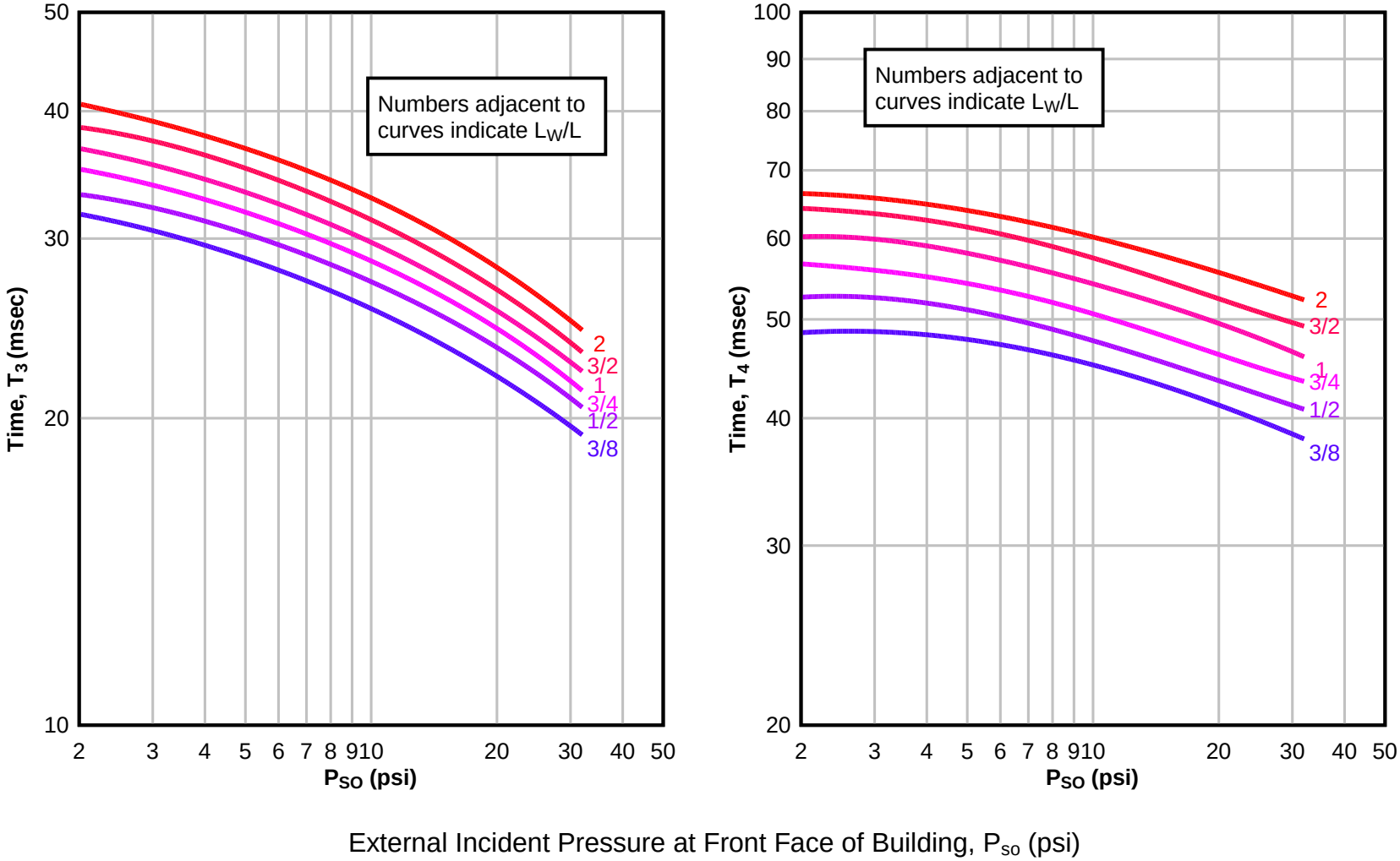

External Incident Pressure at Front Face of Building, P_{so} (psi)

Figure 2-218 Idealized Times T_3 and T_4 for Interior Side Wall Blast Load (L/H = 2, W/H = 3/4)

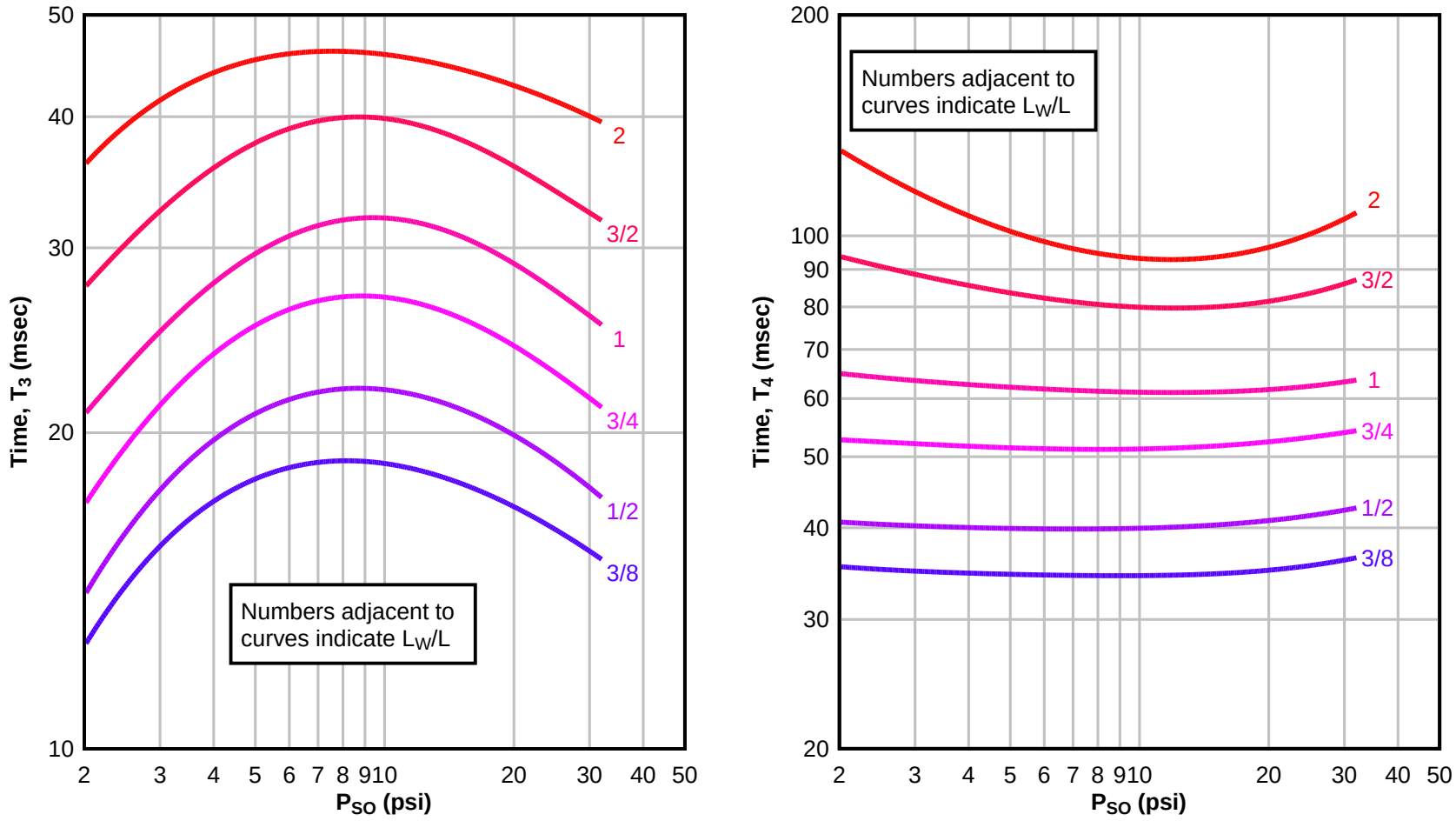

External Incident Pressure at Front Face of Building, P_{so} (psi)

Figure 2-219 Idealized Times T_3 and T_4 for Interior Side Wall Blast Load (L/H = 2, W/H = 3/2)

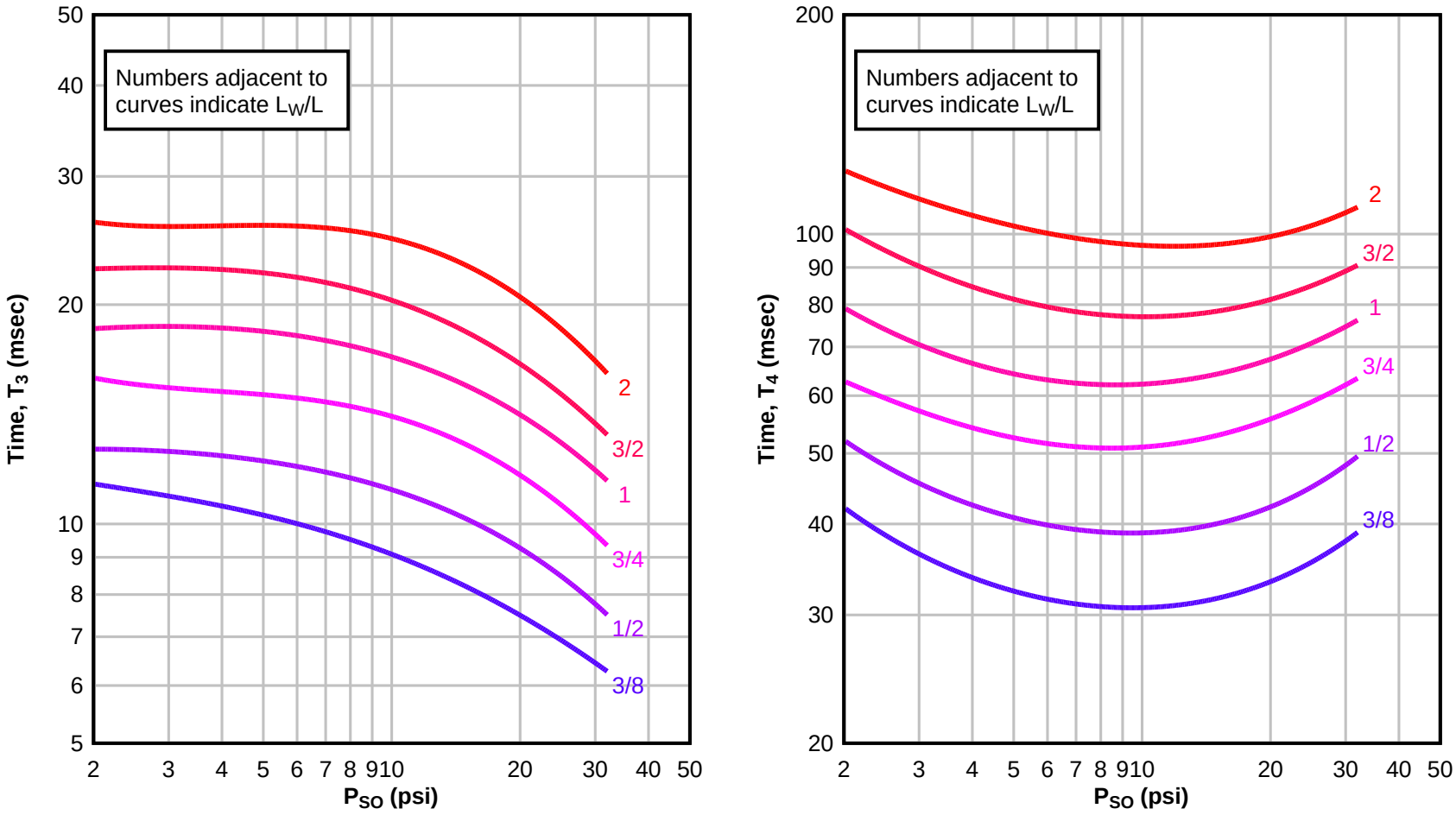

External Incident Pressure at Front Face of Building, P_{so} (psi)

Figure 2-220 Idealized Times T_3 and T_4 for Interior Side Wall Blast Load (L/H = 2, W/H = 3)

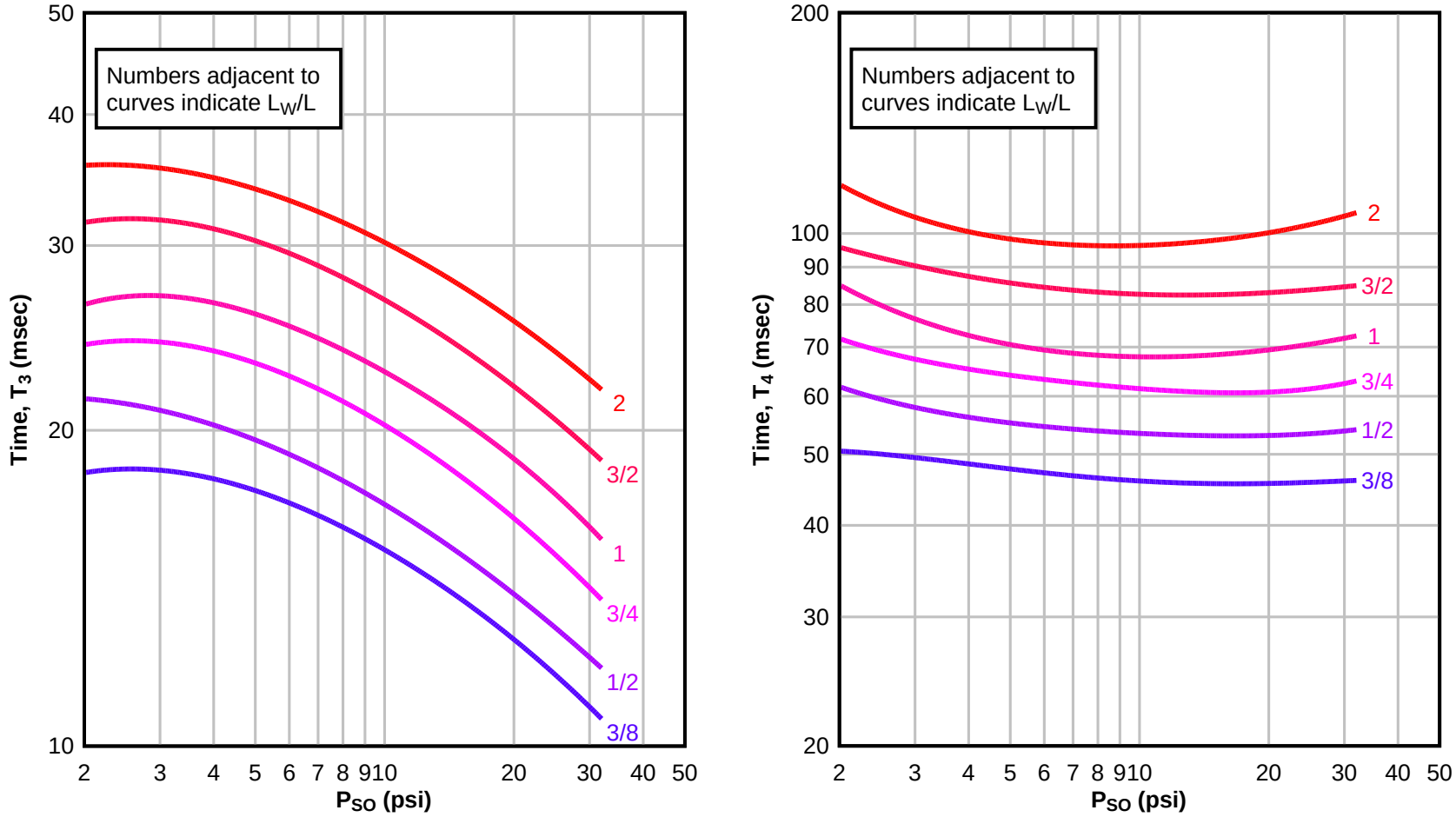

External Incident Pressure at Front Face of Building, P_{so} (psi)

Figure 2-221 Idealized Times T_3 and T_4 for Interior Side Wall Blast Load (L/H = 2, W/H = 6)

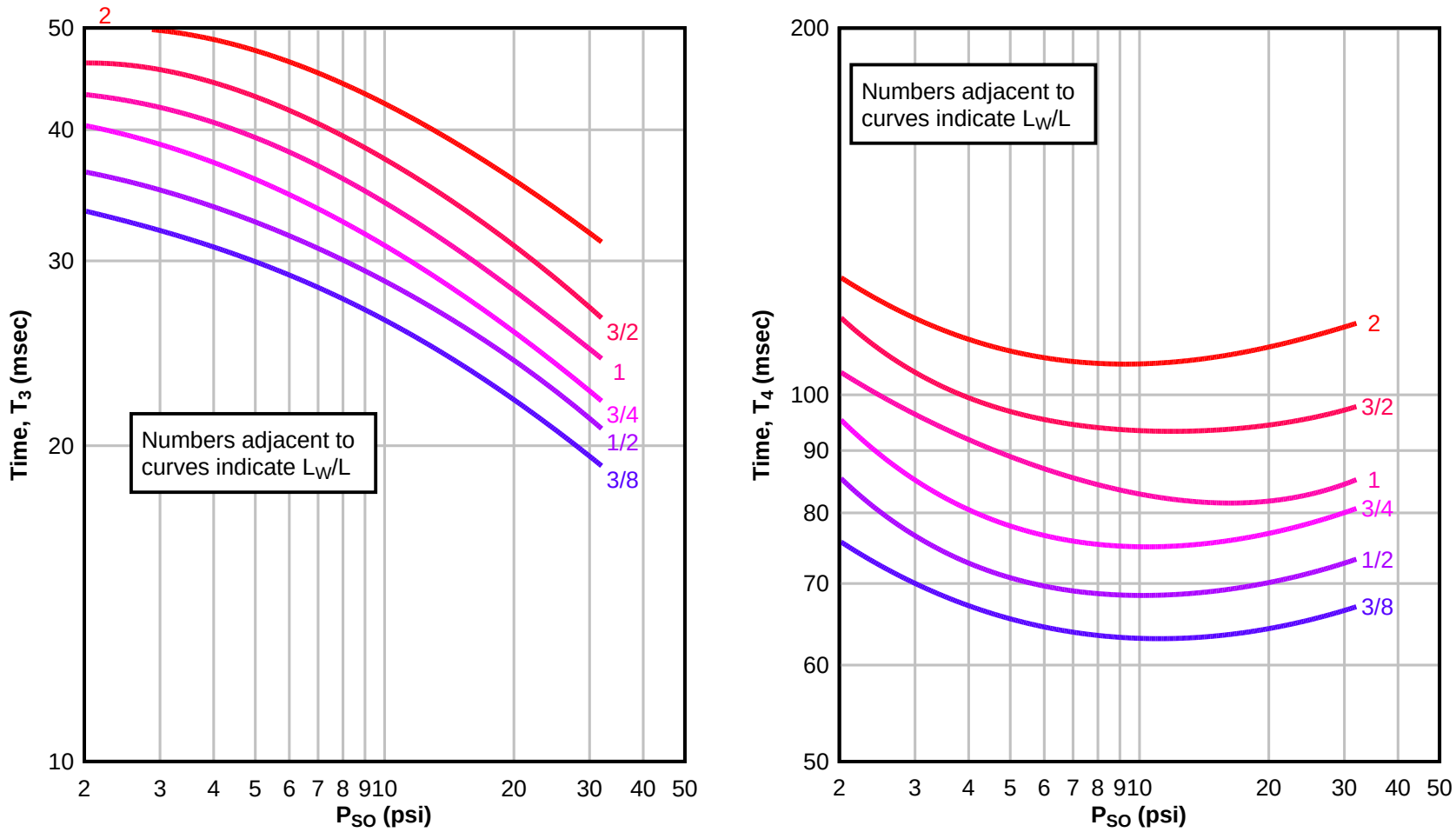

External Incident Pressure at Front Face of Building, P_{so} (psi)

Figure 2-222 Idealized Times T_3 and T_4 for Interior Side Wall Blast Load (L/H = 4, W/H = 3/4)

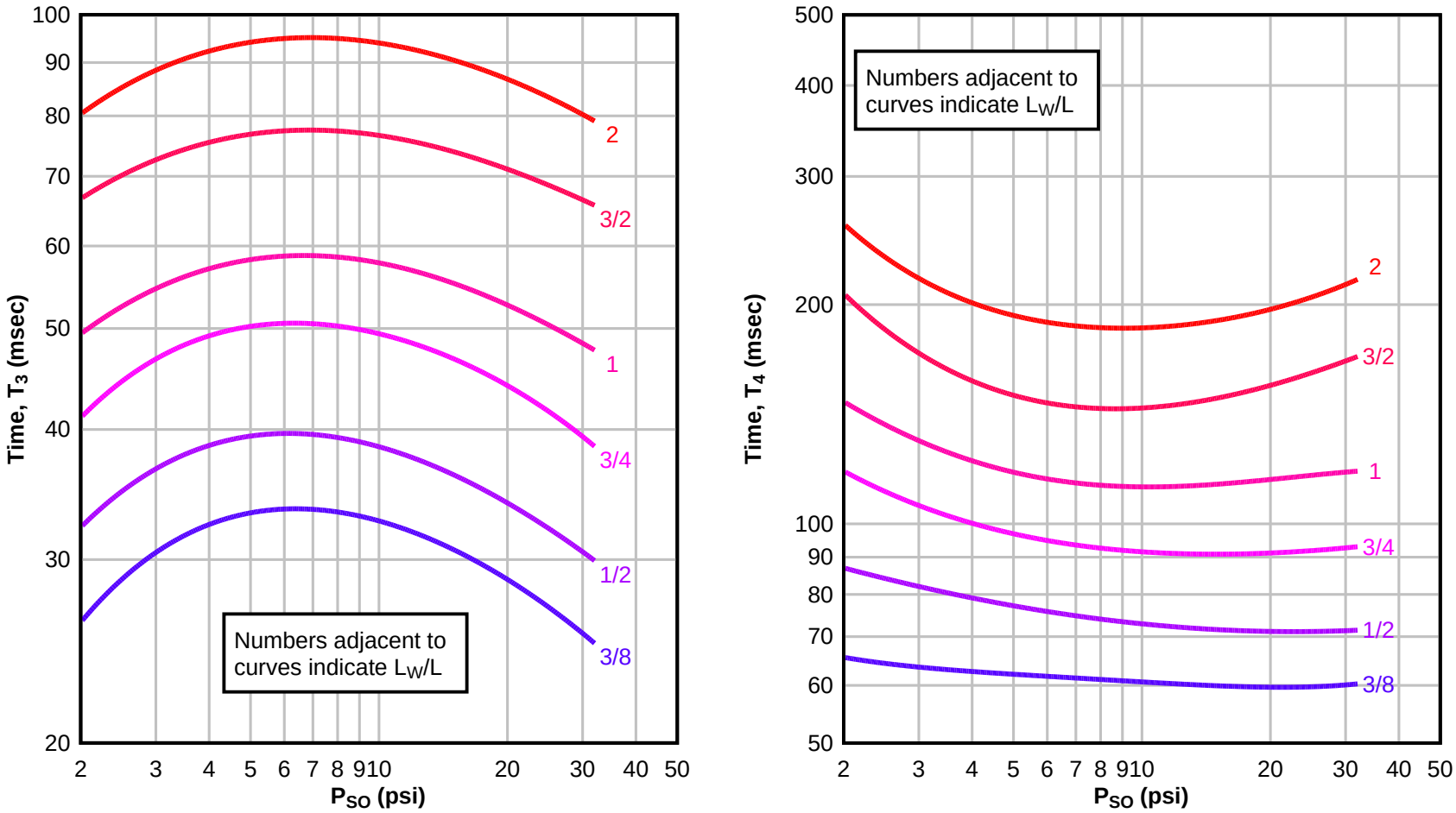

External Incident Pressure at Front Face of Building, P_{so} (psi)

Figure 2-223 Idealized Times T_3 and T_4 for Interior Side Wall Blast Load (L/H = 4, W/H = 3/2)

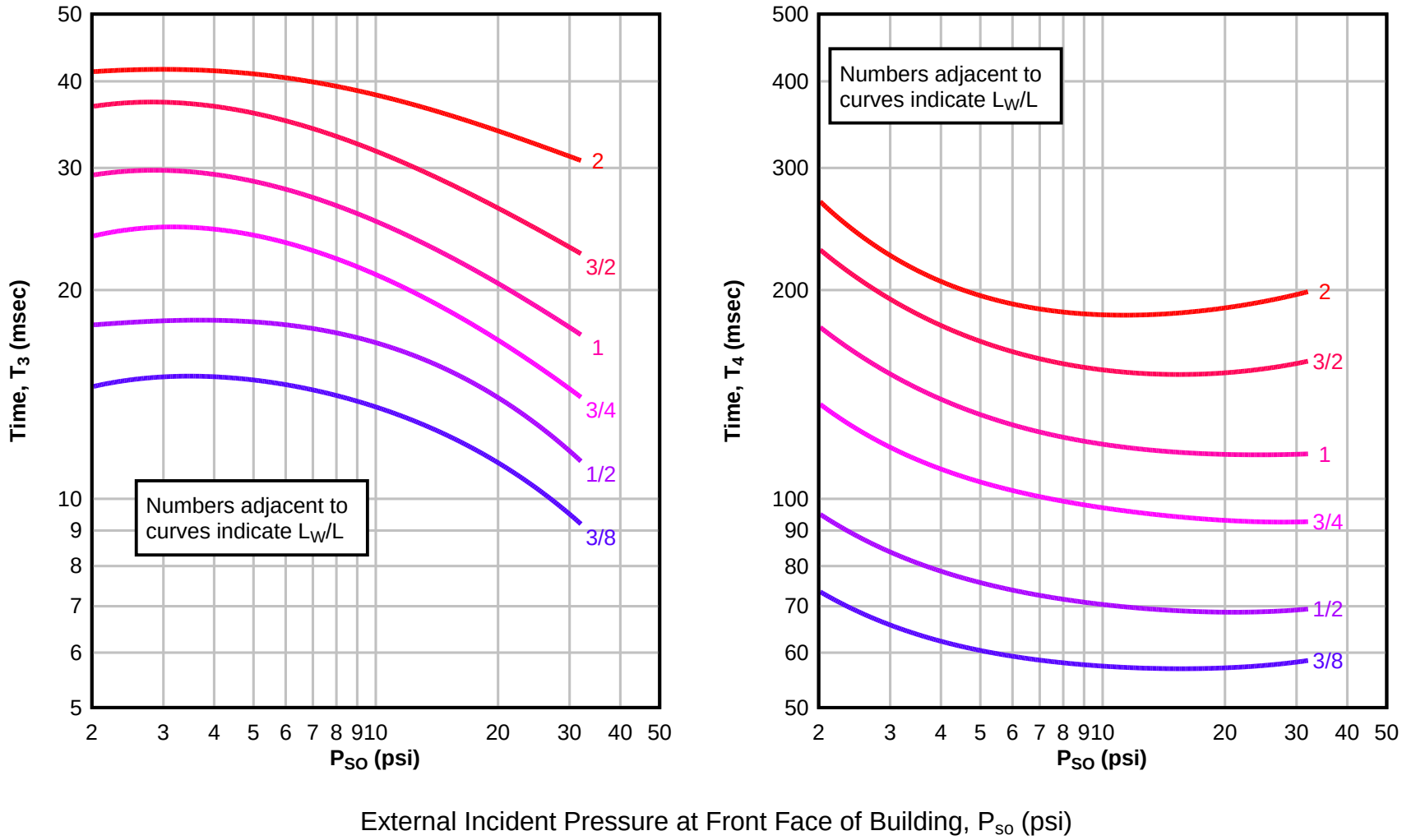

External Incident Pressure at Front Face of Building, P_{so} (psi)

Figure 2-224 Idealized Times T_3 and T_4 for Interior Side Wall Blast Load (L/H = 4, W/H = 3)

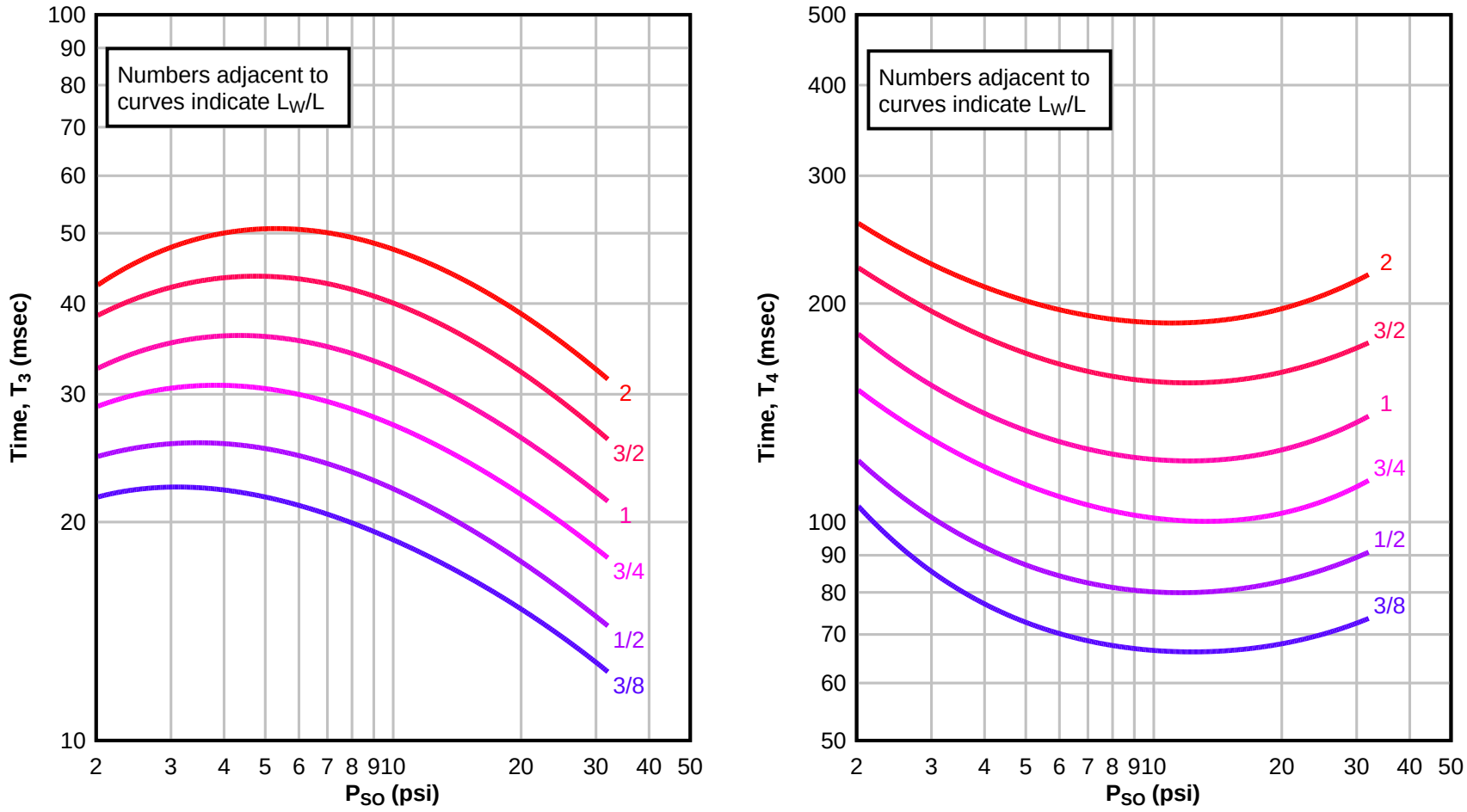

External Incident Pressure at Front Face of Building, P_{so} (psi)

Figure 2-225 Idealized Times T_3 and T_4 for Interior Side Wall Blast Load (L/H = 4, W/H = 6)

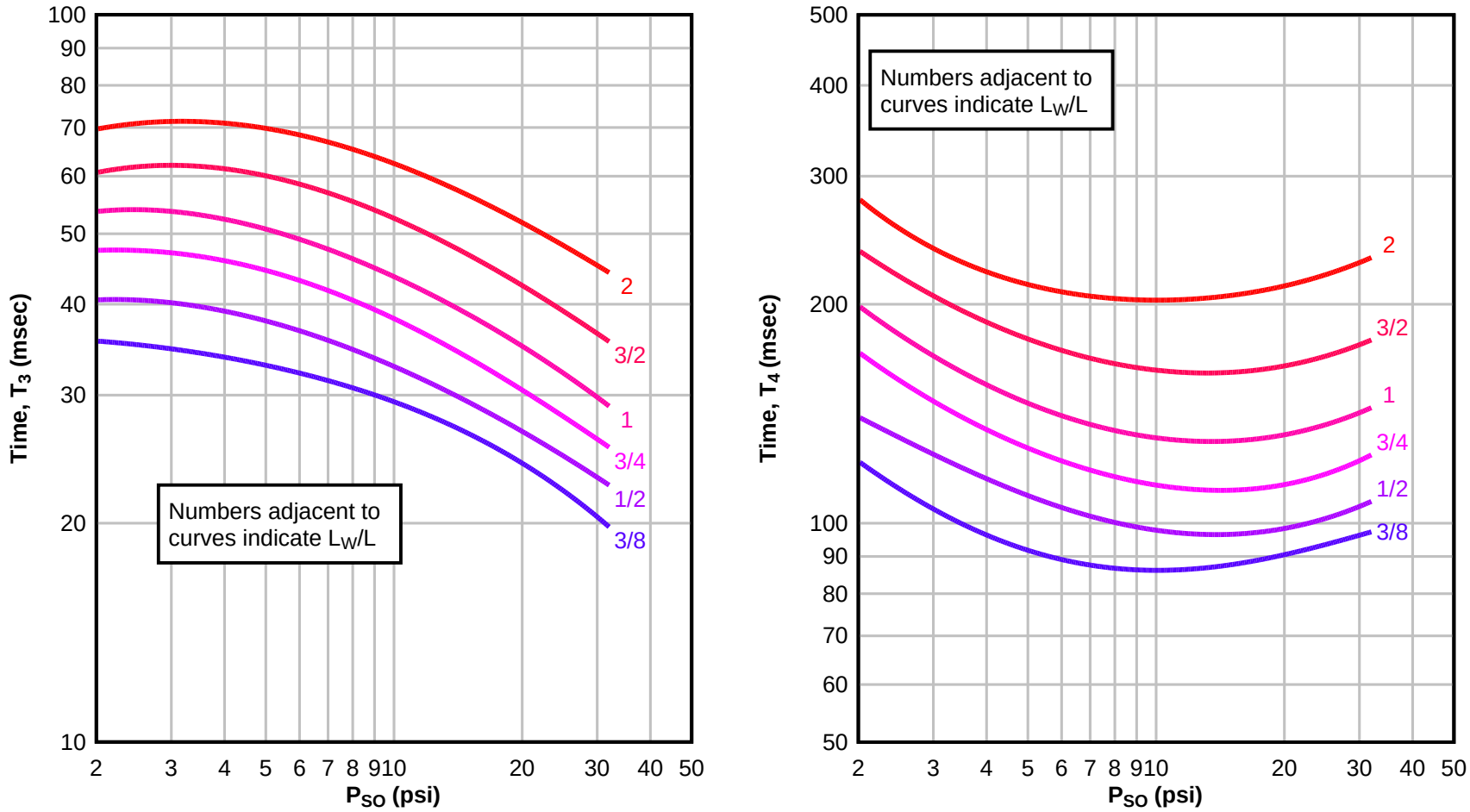

External Incident Pressure at Front Face of Building, P_{so} (psi)

Figure 2-226 Idealized Times T_3 and T_4 for Interior Side Wall Blast Load (L/H = 8, W/H = 3/4)

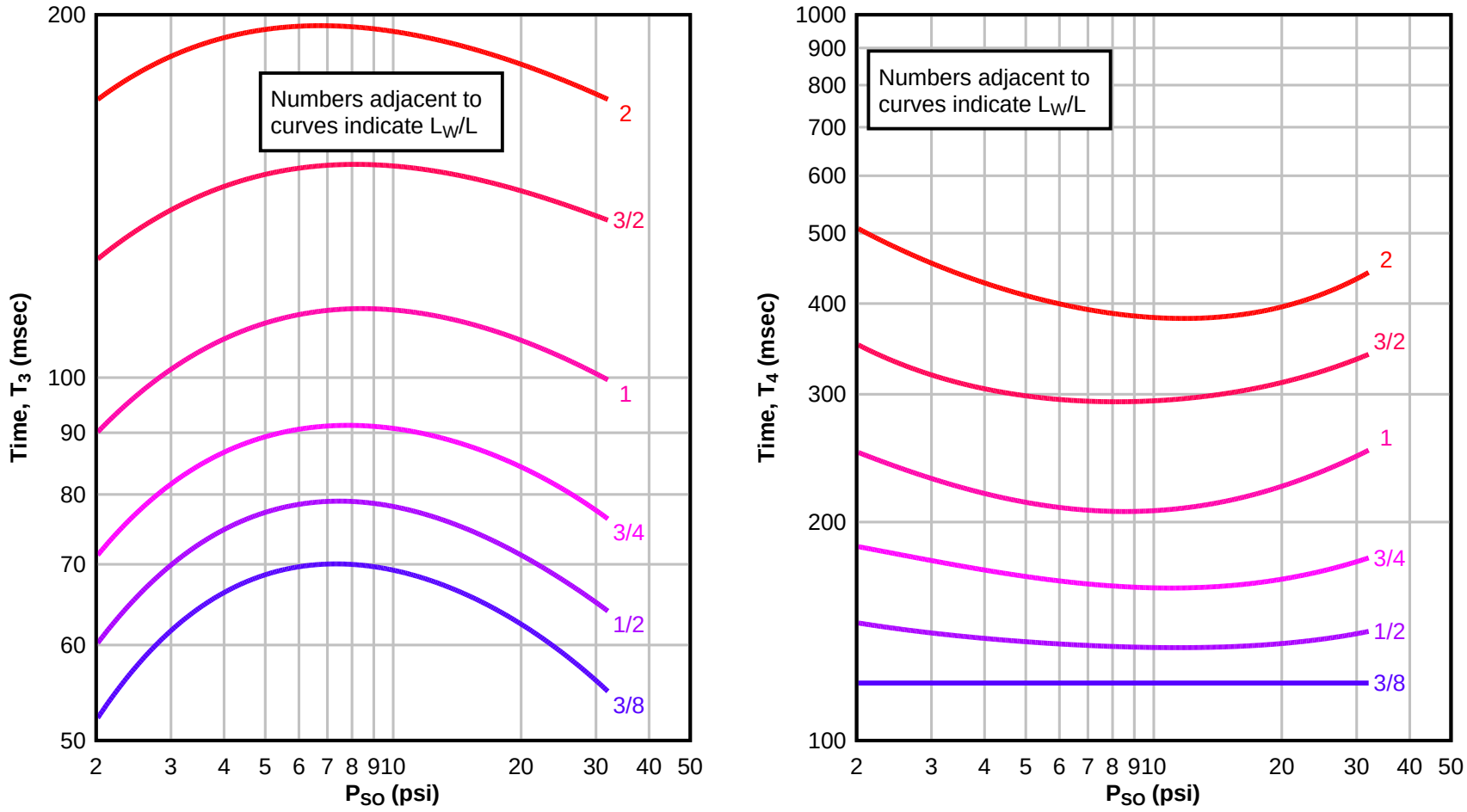

External Incident Pressure at Front Face of Building, P_{so} (psi)

Figure 2-227 Idealized Times T_3 and T_4 for Interior Side Wall Blast Load (L/H = 8, W/H = 3/2)

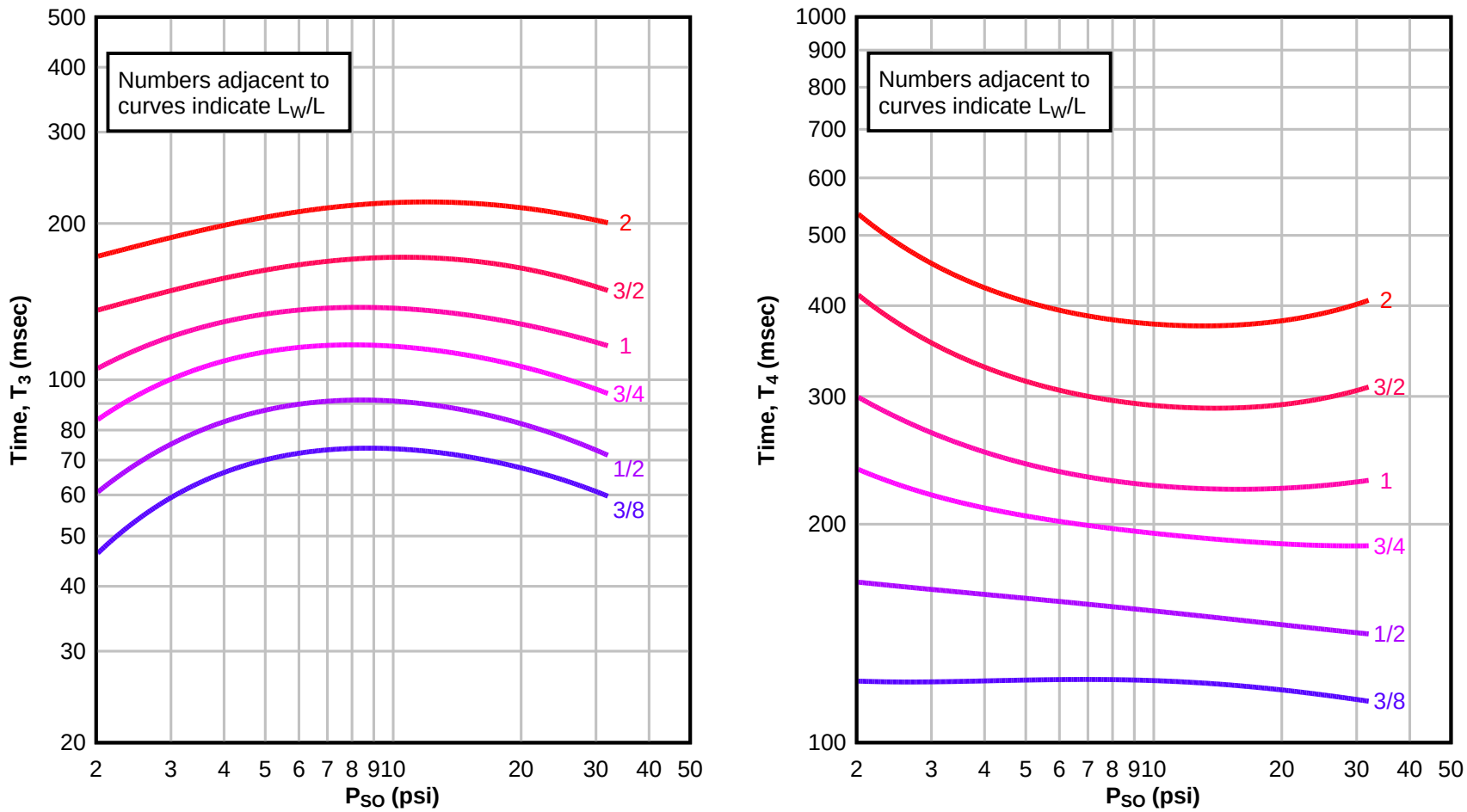

External Incident Pressure at Front Face of Building, P_{so} (psi)

Figure 2-228 Idealized Times T_3 and T_4 for Interior Side Wall Blast Load (L/H = 8, W/H = 3)

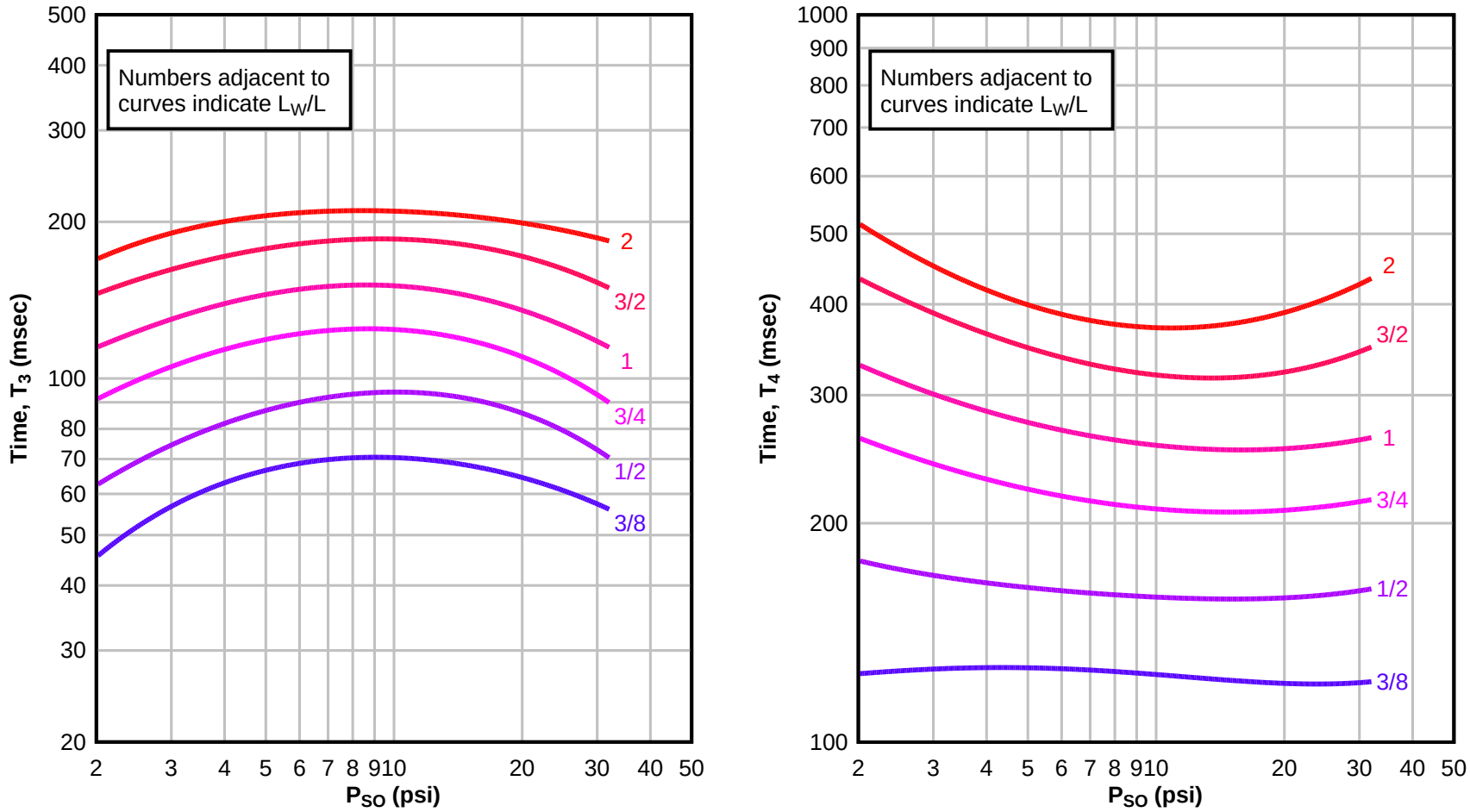

External Incident Pressure at Front Face of Building, P_{so} (psi)

Figure 2-229 Idealized Times T_3 and T_4 for Interior Side Wall Blast Load (L/H = 8, W/H = 6)

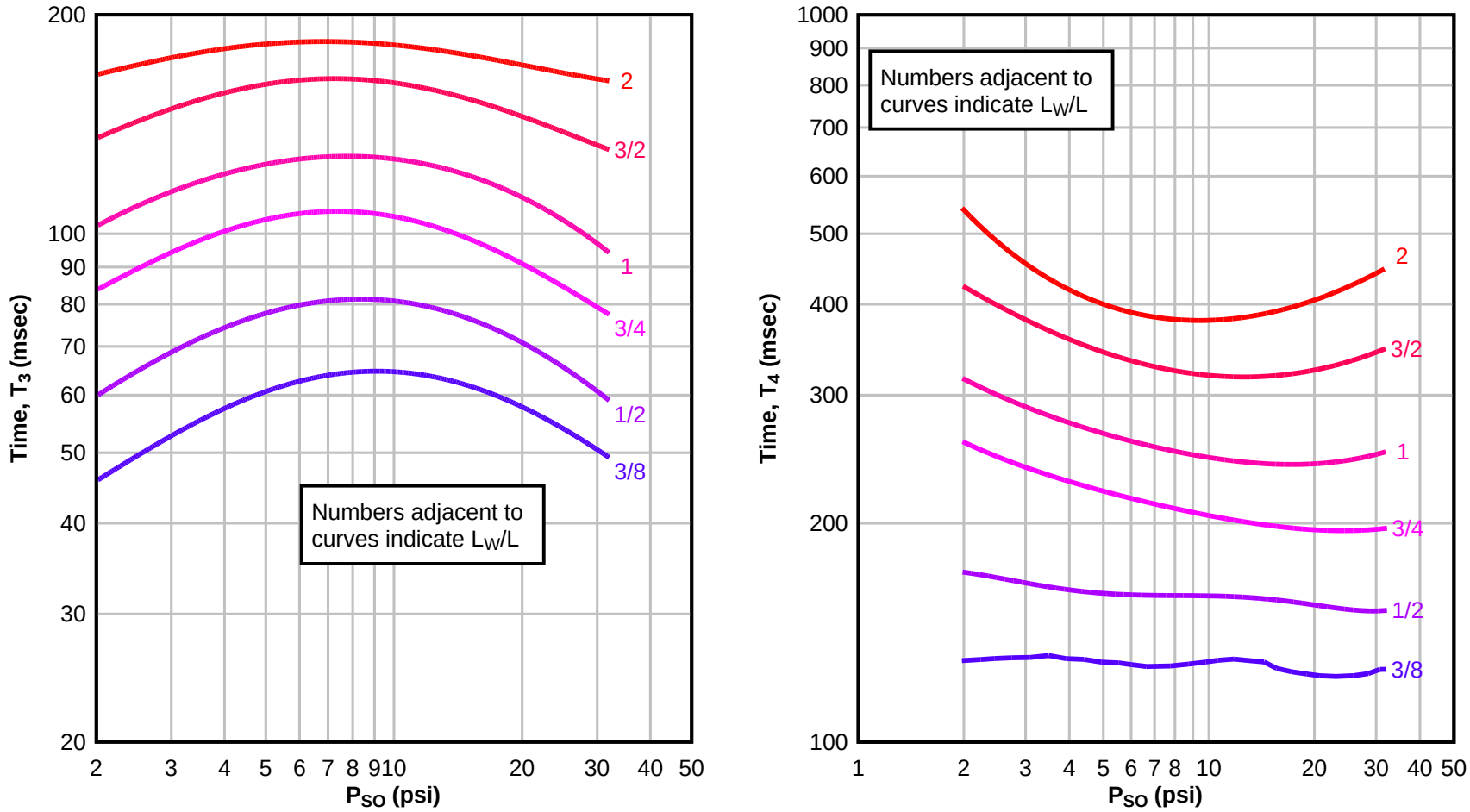

External Incident Pressure at Front Face of Building, P_{so} (psi)

Figure 2-230 Idealized Pressure Coefficient for Back Wall Interior Blast Load (*L/H* = 1 and 2)

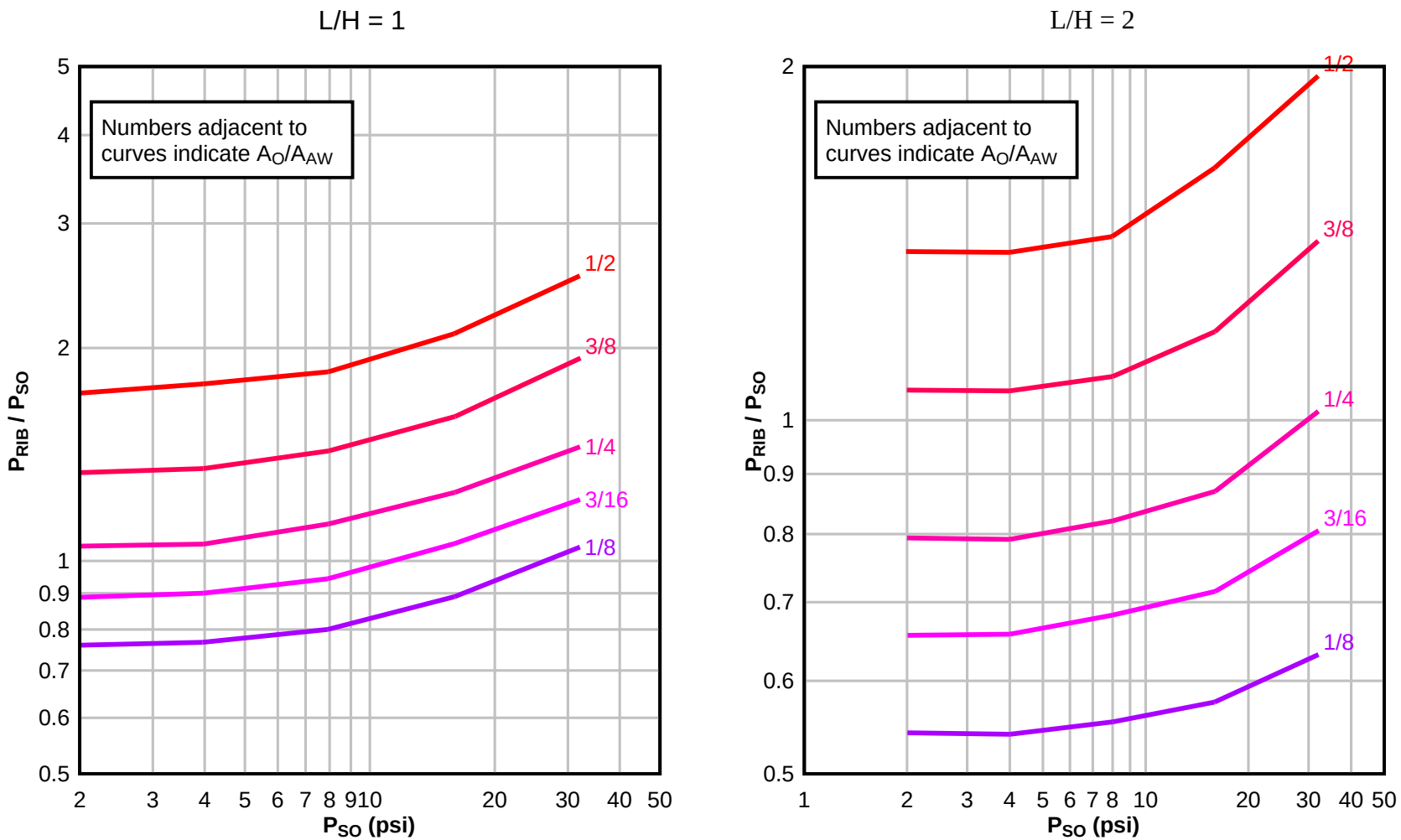

External Incident Pressure at Front Face of Building, P_{so} (psi)

Figure 2-231 Idealized Pressure Coefficient for Back Wall Interior Blast Load (*L/H* = 4 and 8)

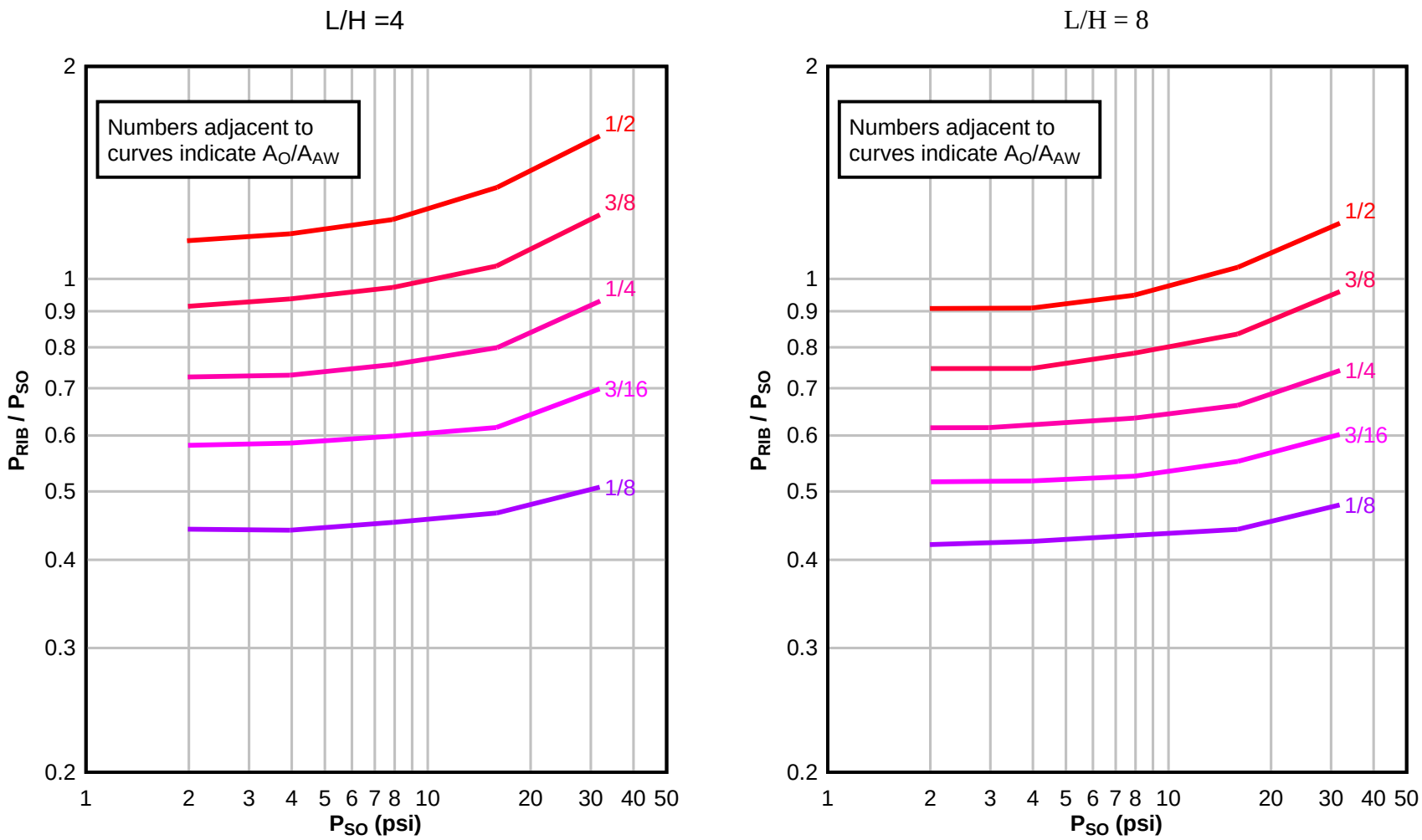

External Incident Pressure at Front Face of Building, P_{so} (psi)

Figure 2-232 Arrival Time, T_1, for Interior Back Wall Blast Load (W/H = 3/4 and 3/2)

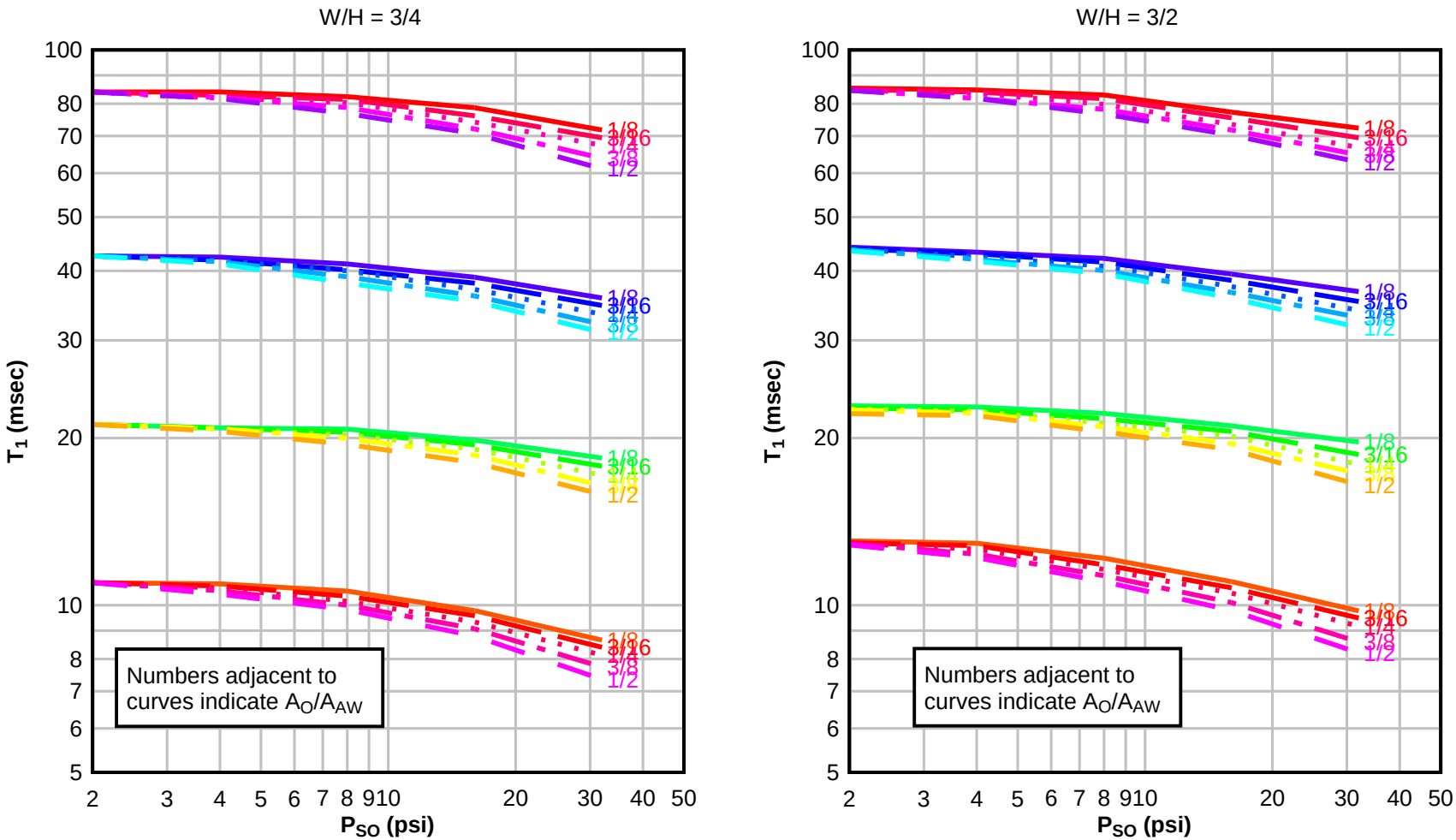

External Incident Pressure at Front Face of Building, P_{so} (psi)

Figure 2-233 Arrival Time, T_1, for Interior Back Wall Blast Load (W/H = 3 and 6)

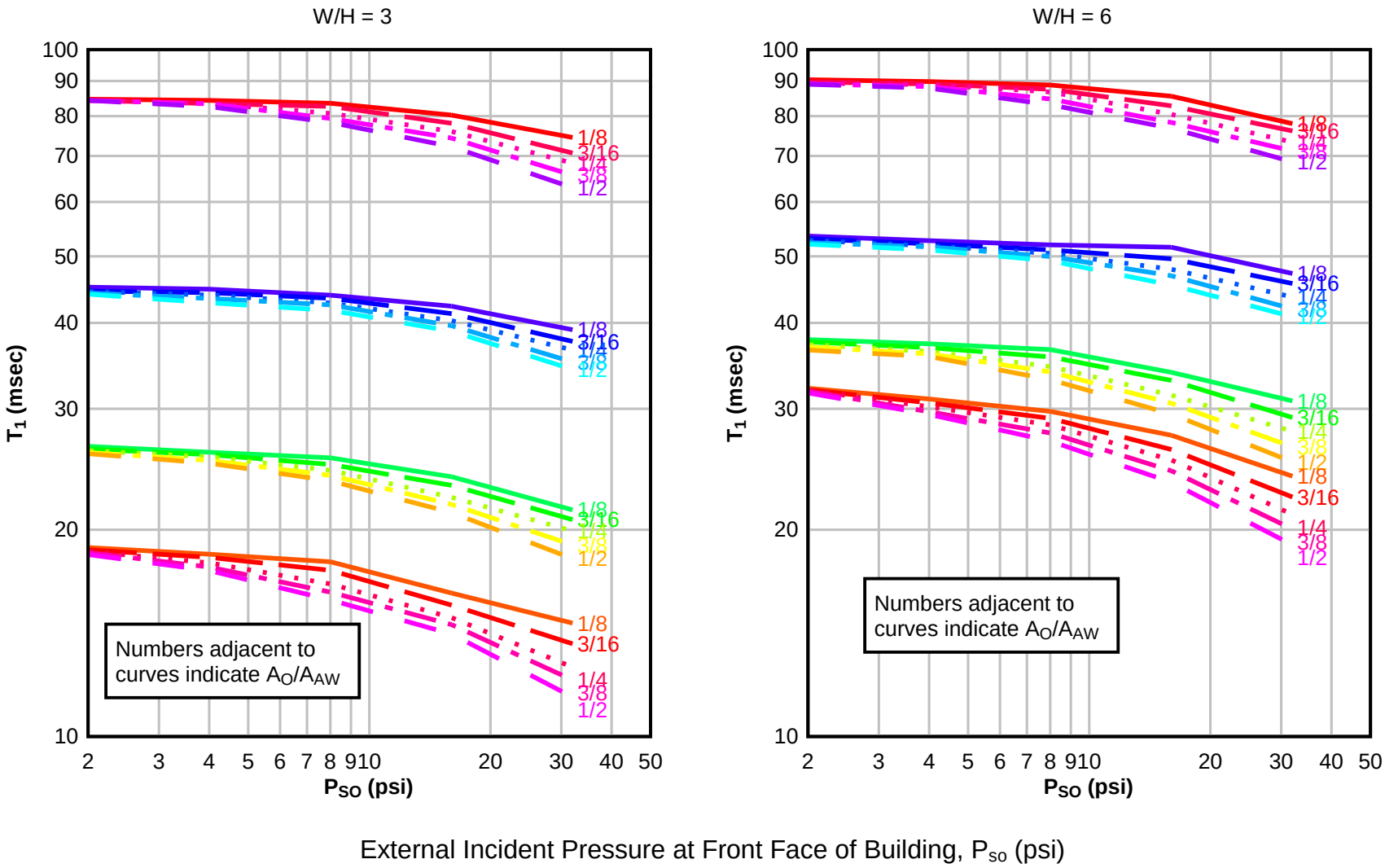

Figure 2-234 Idealized Time $T_2 - T_1$ for Interior Back Wall Blast Load

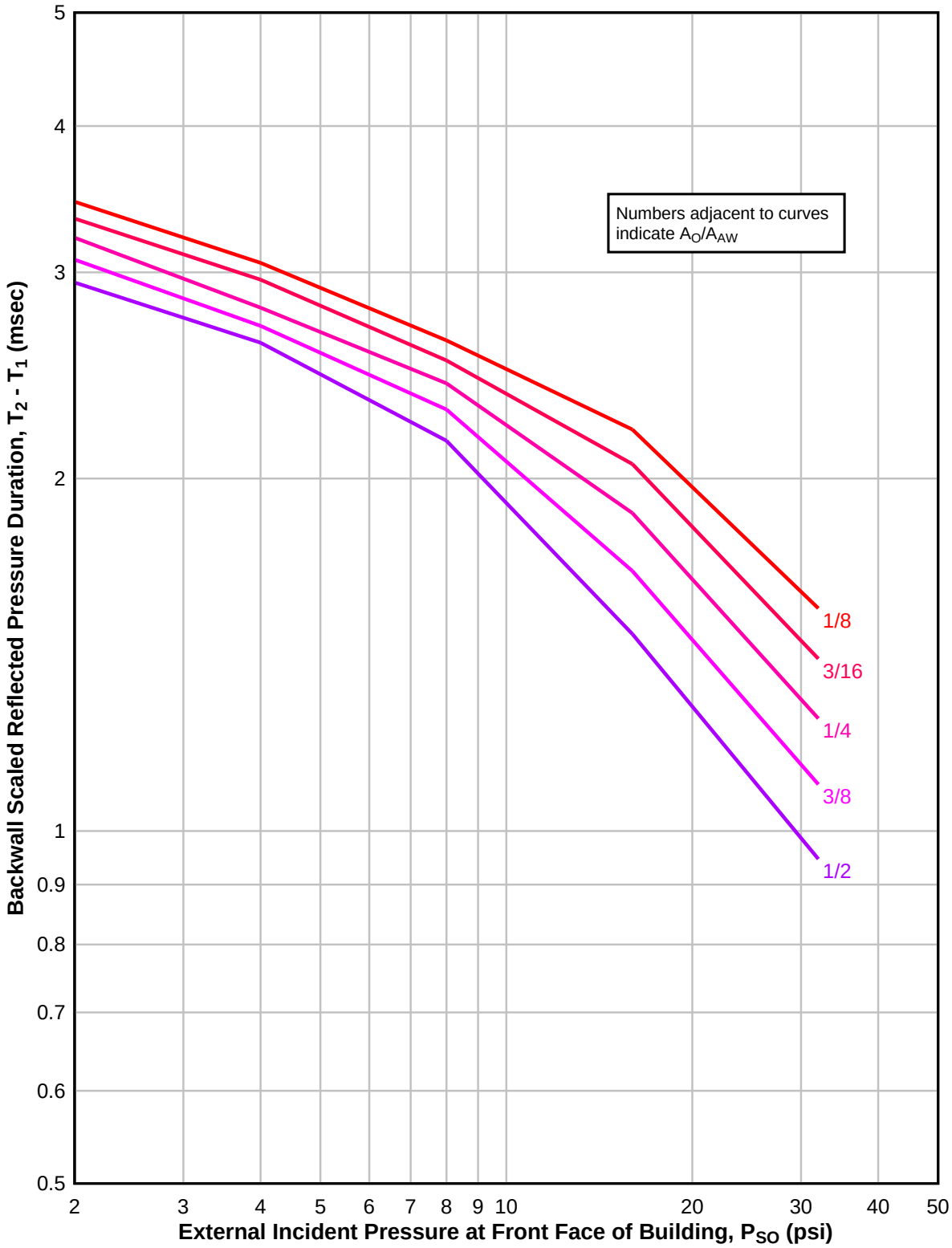

Figure 2-235 Leakage Pressure Coefficient versus Pressure Differential

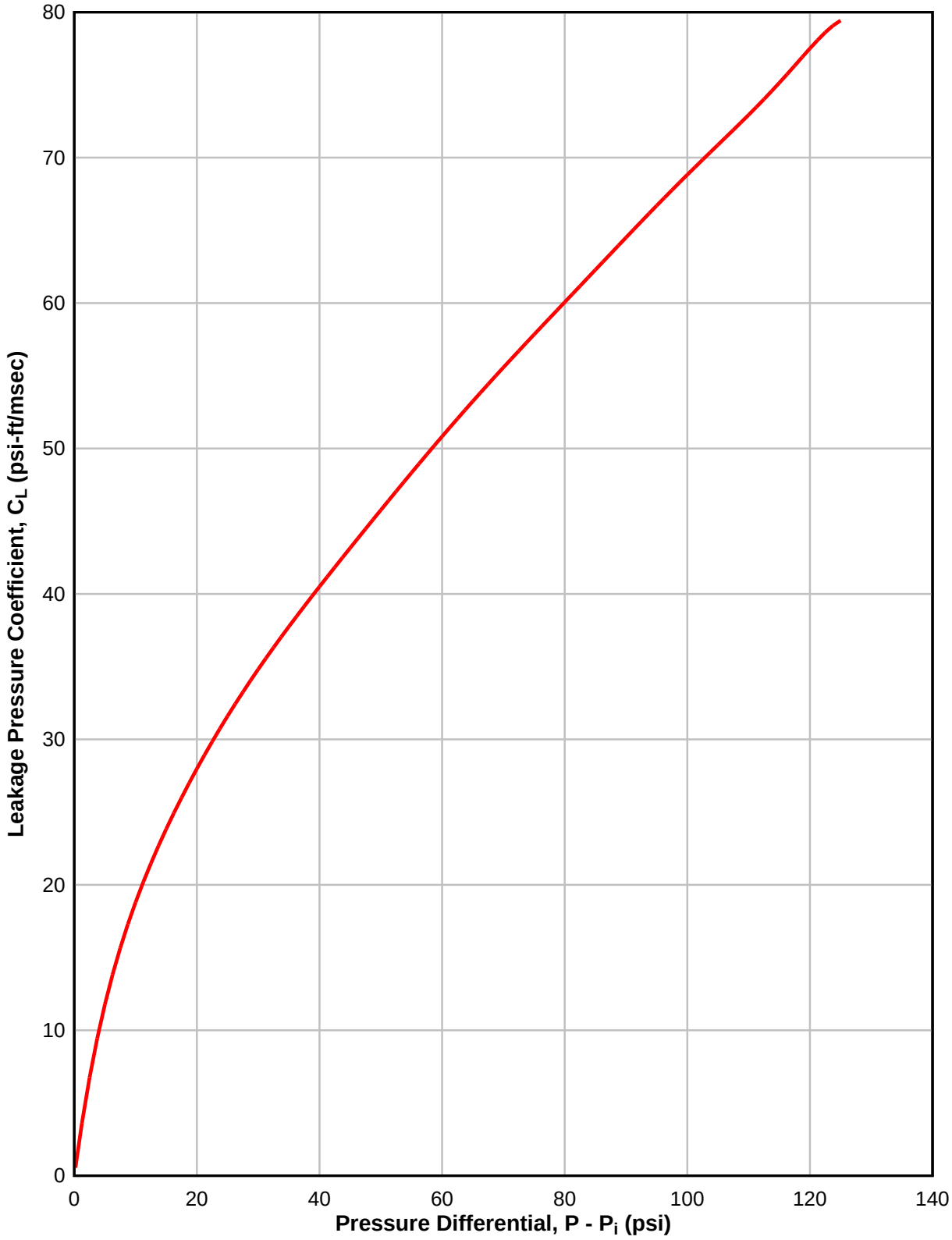

Table 2-1 Heat of Detonation and Heat of Combustion

Explosive Name	Symbol	Heat of Detonation (ft-lb/lb)	Heat of Combustion (ft-lb/lb)
Baratol	-	1.04 E+06	
Boracitol	-	5.59 E+06	
	BTF	2.37 E+06	
Composition B	Comp B	2.15 E+06	3.91 E+06
Composition C-4	Comp C-4	2.22 E+06	
Cyclotol 75/25	-	2.20 E+06	3.68 E+06
	DATB/DATNB	1.76 E+06	4.08 E+06
	DIPAM	1.89 E+06	
	DNPA	1.48 E+06	
	EDNP	1.72 E+06	
	FEFO	2.03 E+06	
	HMX	2.27 E+06	3.31 E+06
	HNAB	2.06 E+06	
	HNS	1.99 E+06	
	LX-01	2.41 E+06	
	LX-02-1	1.99 E+06	
	LX-04	1.99 E+06	
	LX-07	2.08 E+06	
	LX-08	2.77 E+06	
	LX-09-0	2.24 E+06	
	LX-10-0	2.17 E+06	
	LX-11	1.72 E+06	
	LX-14	2.20 E+06	
	NG	2.22 E+06	2.26 E+06
	NQ	1.49 E+06	2.79 E+06
Octol 70/30	-	2.20 E+06	3.81 E+06
	PBX-9007	2.18 E+06	
	PBX-9010	2.06 E+06	
	PBX-9011	2.14 E+06	
	PBX-9205	2.04 E+06	
	PBX-9404	2.18 E+06	
	PBX-9407	2.24 E+06	3.31 E+06
	PBX-9501	2.22 E+06	
Pentolite 50/50	-	2.14 E+06	
	PETN	2.31 E+06	2.70 E+06
	RDX	2.27 E+06	3.20 E+06
	TETRYL	2.11 E+06	4.08 E+06
	TNETB	2.34 E+06	
	TNT	1.97 E+06	5.05 E+06

Table 2-2 List of Illustrations of Peak Incident Pressure and Impulse Produced By Surface Detonation of Various Explosives

MATERIAL	FIGURE	DENSITY RANGE	SHAPE	CONFIGURATIONS				REMARKS
				L/H/W	*L/L'*	*W/W'*	*H/D*	
Composition A-3	2-18a (+)	1.59 to 1.91	2-17a (+)	2.0/1.0/2.5 2.4/1.0/2.9 1.8/1.0/2.6	-	-	-	1) 91% RDX, 9% WAX 2) Fiberboard shipping containers
Composition A-5	2-18b (+)	1.67 to 1.72	2-17a	2.5/1.0/2.0	-	-	-	1) 98.5% RDX, 1.5 ± 0.5% Stearic Acid 2) Fiberboard shipping containers
	2-18c (+)	1.67 to 1.72	2-17j	-	-	-	1.7/1.0	
Composition B	2-19a (+)	1.65	2-17b	-	-	-	1.0/2.0	1) Mixture of RDX and TNT (60/40 percent, respectively) with 1% WAX added
	2-19b (+)	1.65	2-17k	-	-	-	1.0/1.0	
	2-19c (+)	1.65	2-17j	-	-	-	1.0/1.0	
Composition C-4	2-20a (+)	1.52 to 1.61	2-17a	1.6/1.0/1.3	-	-	-	1) 91% RDX, 9% plasticizer (nonexplosive) 2) Fiberboard shipping container and M112 extruded demolition blocks (Figure 2-20a (+)) 3) Dryer bed configuration (Figure 2-20b (+))
	2-20c (+)	1.52 to 1.61	2-17a	2.5/1.0/2.0	-	-	-	
				9.0/1.0/9.0	-	-	-	
Guanidine Nitrate	2-20c (+)	0.72	2-17a	1.0/1.0/1.0	-	-	-	1) Bulk powder form 2) Tested in simulated storage bin configurations
Cyclotol 70/30	2-21a (+)	1.71	2-17a	2.3/1.0/2.8	-	-	-	1) Type II, Class A 2) Used primarily as a munition filler 3) Fiberboard shipping containers and hopper
	2-21b (+)	1.71	2-17c	2.0/1.0/2.5	1.2/1.0	2.5/1.0	-	
				1.0/2.0/2.0	-	-	-	
M42 Grenades	2-21c (+)	-	2-17d	-	-	-	1.0/1.0	1) Each grenade is filled with .066 lb. of Composition A5 explosive 2) A plywood tray filled with 64 M42 grenades
HMX	2-22a (+)	1.87	2-17a	2.0/1.0/3.0	-	-	-	1) Plywood orthorhombic container 2) Fiberboard cylindrical container 3) Wetted with isopropyl alcohol
	2-22b (+)	1.87	2-17j	-	-	-	1.0/1.2	
M483 Projectile Single Round	2-22c (+)	-	2-17h	-	-	-	4.0/1.0	1) A single full up M483 was placed vertically with the nose pointed downward
Lead Azide	2-23a (+)	-	2-17i	-	-	-	-	1) Wet dextrinated 2) Conductive rubber beaker/bag
Lead Styphnate	2-23b (+)	-	2-17i	-	-	-	-	1) Conductive rubber beaker 2) Test wet and dry state
	2-23c (+)	-	2-17m	-	-	-	-	

Table 2-2 List of Illustrations of Peak Incident Pressure and Impulse Produced By Surface Detonation of Various Explosives, Continued

MATERIAL	FIGURE	DENSITY RANGE	SHAPE	CONFIGURATIONS				REMARKS
				L/H/W	*L/L'*	*W/W'*	*H/D*	
LX-14	2-24a (+)	-	2-17a (+)	2.8/1.0/2.8	-	-	-	1) 95.5% HMX, 4.5% estane 2) Aluminum orthorhomic container 3) Pressed billets
	2-24b (+)	-	2-17f	-	-	-	2.0/1.0	
	2-24c (+)	-	2-17a	2.2/1.0/2.2	-	-	-	
Octol 75/25	2-25a (+)	-	2-17a	1.2/1.0/1.2	-	-	-	1) 75% HMX, 25% TNT 2) Received in flake form 3) Fiberboard shipping container 4) Plywood truncated prism
				2.0/1.0/2.5	-	-	-	
	2-25b (+)	-	2-17c	1.0/2.0/2.0	1.2/1.0	2.5/1.0	-	
M718/741 RAAM Projectile	2-25c (+)	-	2-17h	-	-	-	2.0/1.0	1) Pallet of eight projectiles
Nitrocellulose	2-26a (+)	-	2-17j	-	-	-	1.3/1.0	1) Dehydrated nitrocellulose (13.5% nitrogen) MIL-N-244A, Grade C 2) Standard shipping containers(Figure 2-26a,b (+/+)) 3) Dryerbed (Figure 2-26c (+))
	2-26b (+)	-	2-17a	1.2/1.0/1.2	-	-	-	
	2-26c (+)	-	2-17a	64.0/1.0/64.0	-	-	-	
Nitroglycerine	2-27a (+)	-	2-17i	-	-	-	1.0/1.0	1) Liquid high explosive in polymethylpentene plastic laboratory beakers
PBXC-203	2-27b (+)	1.6 ± 0.5	2-17j	-	-	-	2.0/1.0	1) Granular molding powder 2) Nominal composition by weight of 91% RDX and 9% ethylenevinyl acetate copolymer (EVA) 3) Cylindrical fiberboard container 4) Single, double, and triple extruded rods in varying lengths
	2-27c (+)	1.6 ± 0.5	2-17g	-	-	-	20.0/1.0	
RDX Slurry	2-28a (+)	-	2-17j	-	-	-	3.7/1.0	1) Mixture consisted of RDX in a solution of 60% acetic acid, 32% water and 2% nitric acid 2) Encased in polyethylene container
				-	-	-	2.4/1.0	
RDX 98/2	2-28b (+)	-	2-17a	1.7/1.0/2.6	-	-	-	1) High explosive received wet with isopropyl alcohol 2) Plywood orthorhombic Nutsche container 3) Fiberboard shipping containers
	2-28c (+)	-	2-17j	-	-	-	1.2/1.0	
				-	-	-	0.9/1.0	

Table 2-2 List of Illustrations of Peak Incident Pressure and Impulse Produced By Surface Detonation of Various Explosives, Continued

MATERIAL	FIGURE	DENSITY RANGE	SHAPE	CONFIGURATIONS				REMARKS
				L/H/W	*L/L'*	*W/W'*	*H/D*	
TNT (Flake)	2-29a (+)	-	2-17j (+)	-	-	-	1.8/1.0	1) Flake TNT bulk form 2) Fiberboard cylindrical container 3) Orthorhombic fiberboard container 4) Hopper constructed from plywood
	2-29b (+)	-	2-17a	1.2/1.0/1.2	-	-	-	
	2-29c (+)	-	2-17c	1.0/2.4/2.0	1.25/1.0	2.5/1.0	-	
Tetracene	2-30a (+)	-	2-17i	-	-	-	1.0/1.0	1) A primary explosive, was detonated in beakers in a dry state and in a wet state in storage bags
Nitroguanidine	2-30b (+)	-	2-17j	-	-	-	1.0/1.0	1) Aluminum storage bin 2) Bulk form
Benite Propellant	2-31a (+)	-	2-17a	1.4/1.0/1.4	-	-	-	1) 40% nitrocellulose, 44.3% potassium nitrate, 6.3% sulfur, 9.4% charcoal and 0.5% ethyl centralite 2) Container made of wood and fiberboard
	2-31b (+)	-	2-17a	1.1/1.0/1.1	-	-	-	
Black Powder	2-31c (+)	-	-	1.0/1.0/1.0	-	-	-	1) Class I, 4 by 8; Class 6, 20 by MIL-P-223B Grade A1, 4 by 8, Grade A3, 12 by 16; Grade A-3a 2) Tested in loose powder form 3) Storage bins and tote bins boxes were constructed from plywood
BS-NACO Propellant	2-32a (+)	-	2-17j	-	-	-	1.7/1.0	1) Multi perforated 2) Tested in cardboard drums (Figure 2-32a (+)), full-sized metal shipping containers (Figure 2-32b (+)) and aluminum hoppers (Figure 2-32c (+))
	2-32b (+)	-	2-17a	1.6/1.0/2.9	-	-	-	
	2-32c (+)	-	2-17e	-	-	-	1.0/1.3	
DIGL-RP Propellant	2-33a (+)	-	2-17a	3.2/1.0/1.5	-	-	-	1) Composition of nitrocellulose, diethyleneglycol dinitrate, Akantite II Antralite I, magnesium oxide and graphite 2) Plywood containers (I5420 and I5422) 3) Cylindrical fiberboard container (I5421)
				1.9/1.0/3.2	-	-	-	
				1.4/1.0/2.2	-	-	-	
	2-33b (+)	-	2-17j	-	-	-	1.0/1.0	
	2-33c (+)	-	2-17a	2.2/1.0/2.7	-	-	-	

Table 2-2 List of Illustrations of Peak Incident Pressure and Impulse Produced By Surface Detonation of Various Explosives, Continued

MATERIAL	FIGURE	DENSITY RANGE	SHAPE	CONFIGURATIONS				REMARKS
				L/H/W	*L/L'*	*W/W'*	*H/D*	
M1 Propellant	2-34a (+)	-	2-17j (+)	-	-	-	1.7/1.0	1) 84.2%, 13.15% *N* nitrocellulose, 9.9% dinitrotoluene, 4.9% dibutylphthalate and 1.0% diphenylamine 2) Cylindrical drums, open hopper, closed feed hopper
	2-34b (+)	-	2-17j	-	-	-	1.7/1.0	
	2-34a	-	2-17c	3.5/1.0/3.5	7.0/1.0	7.0/1.0	-	
	2-34a	-	2-17e	-	-	-	1.0/1.3	
	2-34b	-	2-17c	3.4/1.0/3.4	9.0/1.0	9.0/1.0	-	
	2-34b	-	2-17e	-	-	-	1.0/1.3	
M26 E1	2-34c (+)		2-17j	-	-	-	1.0/1.5	1) Multi perforated propellant 2) Cylindrical fiberboard shipping containers, dryer bed configurations constructed from plywood, cylindrical container constructed from stainless steel (Figure 2-35c (+))
	2-35a (+)		2-17a	10.5/1.0/60.0	-	-	-	
	2-35b (+)		2-17a	2.2/1.0/2.2	-	-	-	
	2-35c (+)		2-17j	-	-	-	1.7/1.0	
M30 A1	2-36a (+)	-	2-17j	-	-	-	1.5/1.0	1) Propellant single perforated and multi perforated 2) Cylindrical shipping drums and orthorhombic simulated dryers
	2-36b (+)	-	2-17j	-	-	-	1.5/1.0	
	2-36c (+)	-	2-17a	2.4/1.0/12.0	-	-	-	
	2-37a (+)	-	2-17a	2.4/1.0/12.0	-	-	-	
M31 A1E1	2-37b (+)	-	2-17a	3.1/1.0/1.0	-	-	-	1) Triple-base slotted stick propellant 2) Simulated fiberboard carton 3) Simulated wooden shipping/storage container 4) Short side (L) parallel to shock front, or 5) Long side (W) parallel to shock front
	2-37c (+)	-	2-17a	3.1/1.0/1.0	-	-	-	
	2-38a (+)	-	2-17a	3.8/1.0/2.0	-	-	-	
	2-38b (+)	-	2-17a	3.8/1.0/2.0	-	-	-	
N5 Propellant	2-38c (+)	-	2-17j	-	-	-	1.5/1.0	1) Single base propellant 2) Shipping drums with 10% moisture 3) Carpet rolls cylindrically shaped 4) N5 was loaded into charging buckets and conveyor belt configuration
	2-39a (+)	-	2-17j	-	-	-	1.0/2.0	
							1.0/1.0	
							2.0/1.0	
	2-39b (+)	-	2-17a	1.4/1.0/6.8	-	-	-	
	2-39c (+)	-	2-17a	1.0/1.7/4.4	-	-	-	

Table 2-2 List of Illustrations of Peak Incident Pressure and Impulse Produced By Surface Detonation of Various Explosives, Continued

MATERIAL	FIGURE	DENSITY RANGE	SHAPE	CONFIGURATIONS				REMARKS
				L/H/W	*L/L'*	*W/W'*	*H/D*	
M6 Propellant	2-40a (+)	-	2-17j (+)	-	-	-	1.7/1.0	1) Multi perforated propellant 2) Cylindrical shipping drum 3) Closed and open hoppers
				-	-	-	2.2/1.0	
	2-40b (+)	-	2-17e	-	-	-	1.0/1.3	
	2-40c (+)	-	2-17c	3.4/1.0/3.4	5.8/1.0	5.8/1.0	-	
2.75 in. Rocket Grain MK 43-1	2-41a (+)	-	2-17g	-	-	-	-	1) N5 Propellant 2) Tested in shelves holding one, seven, and nine rocket grains
WC 844 Ball	2-41b (+)	-	2-17a	16.5/1.0/70.0	-	-	-	1) Double base propellant 2) Dryer bed constructed from plywood 3) Cylindrical fiberboard containers
				3.8/1.0/35.0	-	-	-	
	2-41c (+)	-	2-17j	-	-	-	1.1/1.0	
XM37 RAP	2-42a (+)	-	2-17j	-	-	-	1.0/1.3	1) Consist of nitrocellulose 50%, nitroglycerine 36.2%, others 13.8% 2) Forward and aft grains simulated extruded billet, Ro Con shipping drum
	2-42b (+)	-	2-17g	-	-	-	9.0/1.0	
	2-42c (+)	-	2-17a	1.0/1.5/1.0	-	-	-	
	2-43a (+)	-	2-17j	-	-	-	1.0/1.6	
	2-43b (+)	-	2-17g	-	-	-	10.0/1.0	
	2-43c (+)	-	2-17a	1.2/1.0/1.2	-	-	-	
JA-2 (L5460)	2-44a (+)	-	2-17j	-	-	-	1.0/1.0	1) Double base propellant 2) 60% nitrocellulose, 24.6% diethylene glycol dinitrate, 15.4% others 3) Fiberboard cylindrical container 4) Orthorhombic fiberboard container
	2-44b (+)	-	2-17a	10.0/1.0/10.0	-	-	-	
				5.0/1.0/5.0	-	-	-	
				2.5/1.0/2.5	-	-	-	
M10 Propellant	2-44c (+)	-	2-17a	1.0/2.7/1.5	-	-	-	1) 98% nitrocellulose (13.5% N), 1% potassium sulfate and 1% dipheylamine 2) Single perforated 3) Fiberboard box, metal lined wooden boxes, orthorhombic stainless steel vented container
				1.0/1.6/1.1	-	-	-	
	2-45a (+)	-	2-17a	2.1/1.0/1.3	-	-	-	
				1.5/1.0/1.2	-	-	-	

Table 2-2 List of Illustrations of Peak Incident Pressure and Impulse Produced By Surface Detonation of Various Explosives, Continued

MATERIAL	FIGURE	DENSITY RANGE	SHAPE	CONFIGURATIONS				REMARKS
				L/H/W	*L/L'*	*W/W'*	*H/D*	
105mm, M314 A3 Illuminant	2-45b (+)	-	2-17j (+)	-	-	-	1.0/1.4	1) 7.7% Luminac 4116 type A, 56% magnesium, 36% sodium nitrate 2) Fiberboard shipping drums (Figure 2-45b (+)) 3) Simulated steel mixer/muller (Figure 2-45c (+))
	2-45c (+)	-	2-17j	-	-	-	1.0/6.0	
I559 Igniter Mixture	2-46a (+)	-	2-17j	-	-	-	1.8/1.0	1) I136 premix(90% strontiune nitrate and 10% calcium resinute) and a premix (23.3% lead dioxide and 77.7% magnesium) 2) Rubber and aluminum cylinder configurations (Figure 2-46a (+) and Figure 2-46b (+) respectively)
	2-46b (+)	-	2-17j	-	-	-	1.0/1.8	
I560 Subigniter Mixture	2-46c (+)	-	2-17j	-	-	-	2.1/1.0	1) Magnesium/strontium nitrate/strontium peroxide/polyvinyl chloride 27.5/27.5/30/15% by weight respectively 2) Rubber (Figure 2-46c (+)) and aluminum (Figure 2-47a (+)) cylinder configurations
	2-47a (+)	-	2-17j	-	-	-	1.0/1.1	
R284 Tracer Mixture	2-47b (+)	-	2-17j	-	-	-	1.9/1.0	1) Strintium nitrate/polyvinyl chloride/(50/100 mesh) magnesium in 53.7/18.1/28.2% by weight, respectively 2) Rubber (Figure 2-47b (+)) and aluminum (Figure 2-47c (+)) cylinder configurations
	2-47c (+)	-	2-17j	-	-	-	1.0/1.4	
M314-A3 First Fire Composition	2-48a (+)	-	2-17a	1.0/1.17/1.0	-	-	-	1) 50% barium nitrate, 5% laminac Type B, 20% silicon, 15% zirconium hydrate, 10% tetranitro carbozole 2) Cardboard box (Figure 2-48a (+)) simulated mix/muller (Figure 2-48b (+))
	2-48b (+)	-	2-17j	-	-	-	1.0/1.8	
M49A1 Trip Flare Composition	2-48c (+)	-	2-17j	-	-	-	1.0/1.4	1) Magnesium 36%, sodium nitrate 54%, binder 10% 2) Shipping drum fiberboard (Figure 2-48c (+)), simulated steel mixer/muller (Figure 2-49a (+))
	2-49a (+)	-	2-17j	-	-	-	1.0/6.0	

Table 2-3 List of Illustrations for Average Peak Reflected Pressure and Scaled Average Unit Reflected Impulse

h/H	l/L	Average Peak Reflected Pressure				Scaled Average Unit Reflected Impulse			
		Number of Adjacent Reflecting Surfaces							
		One	Two	Three	Four	One	Two	Three	Four
0.10	0.10	2-52	2-64	2-80	2-92	2-101	2-113	2-129	2-141
	0.25	2-53	2-65	2-81	2-93	2-102	2-114	2-130	2-142
	0.50	2-54	2-66	2-82	2-94	2-103	2-115	2-131	2-143
	0.75	2-53	2-67	2-81	2-93	2-102	2-116	2-130	2-142
0.25	0.10	2-55	2-68	2-83	2-95	2-104	2-117	2-132	2-144
	0.25	2-56	2-69	2-84	2-96	2-105	2-118	2-133	2-145
	0.50	2-57	2-70	2-85	2-97	2-106	2-119	2-134	2-146
	0.75	2-56	2-71	2-84	2-96	2-105	2-120	2-133	2-145
0.50	0.10	2-58	2-72	2-86	2-98	2-107	2-121	2-135	2-147
	0.25	2-59	2-73	2-87	2-99	2-108	2-122	2-136	2-148
	0.50	2-60	2-74	2-88	2-100	2-109	2-123	2-137	2-149
	0.75	2-59	2-75	2-87	2-99	2-108	2-124	2-136	2-148
0.75	0.10	2-61	2-76	2-89	2-95	2-110	2-125	2-138	2-144
	0.25	2-62	2-77	2-90	2-96	2-111	2-126	2-139	2-145
	0.50	2-63	2-78	2-91	2-97	2-112	2-127	2-140	2-146
	0.75	2-62	2-79	2-90	2-96	2-111	2-128	2-139	2-145

Table 2-4 List of Illustrations for Interior Side Wall Idealized Times T_3 and T_4

L/H	*W/H*			
	3/4	3/2	3	6
1	2-214	2-215	2-216	2-217
2	2-218	2-219	2-220	2-221
4	2-222	2-223	2-224	2-225
8	2-226	2-227	2-228	2-229

PRIMARY AND SECONDARY FRAGMENTS

2-16 GENERAL.

Previous sections in this chapter have discussed explosive accident predictions in reference to studies of blast waves and their effects. Significant damage from accidental explosions can also be caused by the impact of fragments or objects which were generated during the explosions and hurled against structures or other receivers at high speed.

Fragments resulting from accidental explosions can be divided into two categories. The term “primary fragment” denotes a fragment from a casing, which is a container of an explosive source, or a fragment from an object in intimate contact with reacting ammunition or explosives. If the source is a true high explosive, the casing usually ruptures into a large number of small primary fragments which can be projected at velocities up to several thousand feet per second by the explosion. For bomb and shell casings, typical weights of damaging fragments recovered in field tests are about 0.032 oz. These primary fragments, though irregular, are usually of "chunky" geometry, i.e., all linear dimensions are of the same order.

Containers or casings which fragment or burst during explosions are not the only sources of fragments and missiles. Other potentially damaging objects, known as "secondary missiles" or "secondary fragments" can also be produced due to the blast wave interaction with objects or structures located near the explosive source. These objects can be torn loose from their supports, if they are attached, and accelerated to velocities high enough to cause impact damage. The objects could be pieces of machinery, small tools, materials such as pipes and lumber, parts of buildings, or other structures disrupted by the explosions, and large pieces of equipment. Characteristics of both primary and secondary fragments (often referred to as secondary "debris" to distinguish them from primary "fragments") will be discussed in this section.

2-17 PRIMARY FRAGMENTS.

2-17.1 General.

The explosion of a cased donor charge results in the formation of primary fragments which are produced by the shattering of the explosive container. The container may be the casing of conventional munitions, the kettles, hoppers, and other metal containers used in the manufacture of explosives, or metal housing of rocket engines.

Primary fragments are characterized by very high initial velocities (in the order of thousands of feet per second), a large number of fragments, and relatively small sizes in comparison to secondary fragments and concrete fragments formed due to partial failure or total collapse of protective elements. The initial velocity and size of the fragments are functions of the thickness of the metal container, the shape of the explosive as a whole (spherical, cylindrical, prismatic), and the sections of the container (ends and middle) from which the fragments are formed. The size and shape of the

fragments will depend greatly on the metallographic history of the casing, its physical condition (such as dents, grooves, bends, or internal cracks or flaws), and the condition of joints, most notably welded joints.

Upon detonation of a cased explosive, the casing breaks up into fragments with varying weights and velocities. The destructive potential of these fragments is a function of their shapes, materials, momentum and kinetic energy distributions. Therefore, through testing or analysis, the velocity and weight of the "worst case" fragment must be determined and used for penetration analysis and as a design criterion for fragment barriers.

2-17.2 Initial Fragment Velocity.

2-17.2.1 Explosives with Uniform Cylindrical Containers.

The most common technique for calculating the initial velocity of fragments in contact with an explosive charge is the Gurney method. The initial velocity of primary fragments resulting from the detonation of a cased explosive is a function of the explosive output and the ratio of the explosive charge weight to casing weight.

The initial velocity of primary fragments resulting from a high-order detonation of a cylindrical casing with evenly distributed explosives is expressed as:

$$v_o = (2E')^{1/2}\left[\frac{W/W_c}{1+0.5W/W_c}\right]^{1/2} \qquad 2\text{-}32$$

and, applying a 20 percent factor of safety, the design charge weight is:

$$W = 1.2W_{ACT} \qquad 2\text{-}33$$

where

v_o = *initial velocity of fragments*
$(2E')^{1/2}$ = *Gurney Energy Constant from Table 2-5* (+)
W = *design charge weight*
W_c = *weight of casing*
W_{ACT} = *actual quantity of explosive*

The ratio of the Gurney energy constant to the heat of detonation, H_d,, represents the conversion efficiency of chemical energy to "Gurney" energy for a given high explosive material. This ratio can be assumed as a constant for many high explosives. Therefore, the values of the Gurney energy constant and heat of detonation for TNT can be used

to estimate the Gurney energy constant for another high explosive if its heat of detonation is known. 248

2-17.2.2 Explosives with Non-Uniform Cylindrical Containers.

Cylinders are the most common shape of cased explosives. Along the length of the cylinder, there may be a large variation in the thickness of the casing and its outside diameter. In such cases, the cylinder is divided into a series of equivalent cylinders. This method is further discussed in Section 2-17.3.2.

Gurney's equations were developed for cased high explosives (i.e., explosives that have a high-order detonation) where the explosive is in direct contact with the outer metal casing. Several conditions are illustrated in Figure 2-236 (+) where the explosive and outer casing are separated by an incompressible fluid. The initial velocity of primary fragments resulting from the detonation of such items may be approximated by using the Gurney equations with slight modifications. The actual weight of the explosive is increased by the required 20 percent factor of safety. The design charge weight is:

$$W = 1.2\, W_{ACT} \qquad 2\text{-}34$$

and, the weight of the casing is increased to include the weight of the fluid and the weight of the inner casing which surrounds the explosive, if present, or:

$$W_c = W_{CO} + W_{CI} + W_A \qquad 2\text{-}35$$

where

W = *design charge weight*
W_{ACT} = *actual quantity of explosive*
W_c = *total weight of casing*
W_{CO} = *weight of outer casing*
W_{CI} = *weight of inner casing*
W_A = *weight of fluid*

2-17.2.3 Explosives with Non-Cylindrical Containers.

Gurney formulas for some additional geometries are given in Table 2-6 (+/+). A plot of velocity versus casing to charge weight ratio for various geometries is shown in Figure 2-237 (+).

The shapes considered in Figure 2-237 (+) are assumed to have an evenly distributed explosive and a uniform container (casing) or plate thickness. However, for those cases where the shape is slightly non-uniform, the initial velocity of the resulting fragments may be estimated by using the average cross-sectional dimensions.

2-17.3 Fragment Mass Distribution.

2-17.3.1 Explosives with Uniform Cylindrical Containers.

The fragmentation pattern and the weight of the largest fragment resulting from the high-order detonation of an evenly-distributed explosive in a cylindrical metal case of uniform thickness have been calculated according to relationships developed on the basis of theoretical considerations confirmed with a large number of tests. The number of fragments produced by a cylindrical cased charge weighing more than a given design fragment is:

$$N_f = \frac{8W_c e^{-\left[W_f^{1/2}/M_A\right]}}{M_A^2} \qquad 2\text{-}36$$

and

$$M_A = Bt_c^{5/6}\ d_i^{1/3}\ (1 + t_c / d_i) \qquad 2\text{-}37$$

where

N_f = *number of fragments with weight greater than* W_f
W_c = *casing weight (lb)*
W_f = *design fragment weight (oz)*
M_A = *fragment distribution factor* ($oz^{1/2}$)
B = *Mott explosive constant from Table 2-7 (+)* ($oz^{1/2}in^{-7/6}$)
t_c = *average casing thickness (in)*
d_i = *average inside diameter of casing (in)*

The largest fragment produced by an explosion can be found by setting $N_f = 1$. Thus, the weight of the largest fragment is given by:

$$W_f = \left[M_A \ln\left(8W_c / M_A^2\right)\right]^2 \qquad 2\text{-}38$$

Setting the fragment weight W_f equal to zero, the following expression for the total number of fragments is obtained:

$$N_T = 8W_c/M_A^2 \qquad 2\text{-}39$$

where

N_T = *total number of fragments*

Hence, the average fragment weight can be found:

$$W'_f = 16W_c / N_T = 2M_A^2 \qquad 2\text{-}40$$

where

W'_f = *average fragment weight*

For design purposes, a confidence level C_L, where ($0 < C_L < 1$), can be defined as the probability that the weight, W_f, is the largest weight fragment released. The expression for the design fragment weight corresponding to a prescribed design confidence level (C_L) is given as:

$$C_L = 1 - N_f / N_T = 1 - e^{-\left[W_f^{1/2} / M_A\right]} \qquad 2\text{-}41$$

or rearranging terms:

$$W_f = M_A^2 \ln^2 (1 - C_L) \qquad 2\text{-}42$$

Equation 2-42 can then be used to calculate the design fragment weight for a prescribed design confidence level. Note that Equation 2-42 uses an infinite distribution to describe a physical phenomenon which has a finite upper limit. Equation 2-42 may be used for $C_L \leq 0.9999$. If $C_L > 0.9999$, use:

$$W_f = M_A^2 \ln^2 \left[1 - C_L \left(1 - e^{-\left[4(W_c)^{1/2} / M_A\right]}\right)\right] \qquad 2\text{-}43$$

The number of fragments with weight greater than W_f is:

$$N_f = N_T (1 - C_L) \qquad 2\text{-}44$$

It should be noted that Equations 2-41 through 2-44 are not applicable to casings designed to fragment in a specific pattern.

In order to facilitate design calculations, Figure 2-238 (+) is available for determining the quantity M_A/B for a given cylindrical casing geometry and Figure 2-239 (+) and Figure 2-240 (+) provide the value of W_f/M_A corresponding to a specified confidence level. Figure 2-239 (+)Plots/02_239.grf is applicable for a wide range of confidence levels ($0.3 \leq C_L < 1.0$) whereas Figure 2-240 (+) is applicable for high confidence levels ($0.986 \leq C_L \leq 1$).

To calculate the actual number of fragments with a weight greater than the design fragment weight, Equation 2-36 can be applied directly. Alternatively, Figure 2-241 (+) presents a plot of the quantity B^2N_T/W_c versus the casing geometry. The number of fragments with weight greater than W_f can then be calculated from Equation 2-44.

2-17.3.2 Explosives with Non-Uniform Cylindrical Containers.

The equations in Section 2-17.3.1 were developed assuming a uniform cross-section along the axis of the cylinder with evenly distributed explosive in direct contact with the outer casing. Actual cased explosives rarely conform to these ideal conditions. If there is only slight variation in the casing thickness and/or casing diameter, the fragment weight may be estimated using an average casing thickness and diameter in Equation 2-37.

If the cross-section varies greatly, the container is treated as a series of equivalent cylinders representing the actual shape as closely as possible (Figure 2-242 (+)). Using the average casing thickness and diameter of each section, the velocity and weight of the design fragment must be determined for each section. The worst case fragment of the equivalent cylinders is then taken as the design fragment for the entire container.

Cylindrical explosives with steel and hollow cores are shown in Table 2-6 (+/+). The fragment mass distribution may be estimated for these shapes using the uniform cylinder equations of Section 2-17.3.1. In applying these equations, the same procedures as outlined above for non-uniform cylinders are employed, except that the steel or hollow cores are neglected in the calculations.

Figure 2-236 (+) illustrates the cased explosive where the explosive and outer casing are separated by an incompressible fluid. The outer casing is much thicker than the inner casing which encloses the explosive. Here again, the fragment mass distribution may be estimated using the uniform cylinder equations of Section 2-17.3.1 except as indicated below. The heaviest fragment will fracture from the outer casing. Thus, W_c should be the weight of the outer casing only. The thin inner casing is neglected in the calculations. In addition, since the ratio of explosive weight to casing weight (W/W_c) is small, the fragment distribution factor (M_A) should be the larger of that given in Equation 2-36 and Equation 2-44 as follows:

$$M_A = At_c \frac{[d_i + t_c]^{3/2}}{d_i} \left[1 + \frac{W}{2W_c}\right]^{1/2} \qquad 2\text{-}45$$

where

A = explosive composition constant from Table 2-7 (+) and all other terms are as previously defined.

2-17.3.3 Explosives with Non-Cylindrical Containers.

Information is not presently available for evaluating the number and weight of fragments from charges other than those having a cylindrical casing.

The equations of Section 2-17.3.1 can only be employed to calculate masses of primary fragments which evolve from accidents involving an explosive detonation within a container of some sort, such as a casing, a storage tank, or a confining piece of machinery such as a centrifuge or press. Weights of fragments created as a result of a given quantity of explosive detonating while being machined or in an unconfined space must be estimated using other methods.

2-17.4 Variation of Fragment Velocity with Distance.

When an explosion is located close to an object (acceptor explosive or barrier), the velocity v_s at which a fragment strikes the object is approximately equal to the initial velocity v_o. However, if the detonation is located at a relatively large distance from the object, then the impact or striking velocity of the fragment may be substantially less than its velocity immediately after the explosion. This variation in velocities, which is primarily a result of air resistance, is also a function of the physical properties of the casing and the distance between the donor explosive and the object.

When the protective barriers are located 20 feet or less from a detonation, the variation between striking and initial velocities usually may be neglected. On the other hand, for determining the effects of primary fragment impact on structures further away from a detonation, the variation of fragment velocity with distance should be included in the design. The fragment velocity of major concern is the velocity with which the "design fragment(s)" (the worst case fragment(s) which the structure must be designed to withstand) strikes the protective structure. This striking velocity is expressed as:

$$v_s = v_o e^{-[12 k_v R_f]} \qquad \text{2-46}$$

and

$$k_v = 0.5(A/W_f)\ \rho_a\ C_D \qquad \text{2-47}$$

where

v_s = fragment velocity at a distance R_f from the center of detonation (ft/sec)
v_o = initial (maximum) fragment velocity (ft/sec)
R_f = distance from the center of detonation (ft)
k_v = velocity decay coefficient (in $^{-1}$)
A = presented area of the fragment (in^2)
W_f = fragment weight (oz)
A/W_f = fragment form factor
ρ_a = specific density of air
C_D = drag coefficient

The decay coefficient can be evaluated based on the following assumptions:

A/W_f = 0.78 /$W_f^{1/3}$ for a random mild steel fragment (in^2/oz)
ρ_a = 0.00071 oz/in^3
C_D = 1.2 for primary fragments

The resulting expression for the striking velocity is:

$$v_s = v_o e^{-\left[.004 R_f / W_f^{1/3}\right]} \qquad 2\text{-}48$$

Figure 2-243 (+) shows the variation of primary fragment velocity with distance. The term initial velocity refers to the maximum fragment velocity as the fragment is ejected from the charge. Due to the extremely high rates of fragment acceleration, this velocity is considered to be attained by the fragment prior to moving appreciably from its initial position.

2-17.5 Primary Fragments - Shape, Caliber Density and Impact Angle.

2-17.5.1 General.

In order to determine the damage potential of primary fragments, it is necessary to evaluate the caliber density, shape and angle of obliquity of the fragments, and the previously described weight and striking velocity. When a container fragments, a random distribution of fragment shapes results. Section 2-17.3 contained a method for determining the weight distribution of primary fragments. From the weight of the fragment and shape of the casing or containment vessel, one can estimate the size of individual fragments. This section discusses a method for performing an engineering estimate of a standard design fragment(s) for use in fragment impact damage.

2-17.5.2 Shape of Primary Fragments.

Two possible fragment shapes are shown in Figure 2-244 (+) for high explosives in contact with the outer casing. The blunt fragment shape in Figure 2-244 is considered as the standard shape in the design charts presented in the following section. While the standard fragment has a milder nose shape than the alternate fragment, the standard fragment is generally considered appropriate for use in design since (1) only a small number of fragments will strike the structure nose-on, and (2) only a small fraction of these fragments will have a more severe nose shape than the standard fragment. In addition, the length-to-diameter ratio of these fragments is considered more representative of an average fragment configuration. For convenience, a plot of fragment weight versus fragment diameter for these two fragment shapes is given in Figure 2-245 (+).

There is little data available concerning the shape of a fragment ejected from a cased explosive where the explosive is not in direct contact with the casing (Figure 2-236 (+)). Consequently, the worst possible shape is assumed, a thin rectangular or circular rod. The diameter of the cross-section (the thickness of a rectangular cross-section) is equal to the casing thickness at rupture.

The fragmentation pattern of this type of cased explosive somewhat resembles that of a ruptured pressure vessel. The casing diameter typically expands before rupturing and, therefore, to conserve mass, the casing thickness must be decreased.

It is assumed that the outside diameter expands to 1.5 times the original diameter. Thus, the adjusted inside diameter is:

$$d_i' = \left[1.25(d_i + 2t_c)^2 + d_i^2\right]^{1/2} \qquad \text{2-49}$$

where

d_i' = *adjusted inside diameter of casing*
d_i = *original inside diameter of casing*
t_c = *original casing thickness*

The adjusted or "necked-down" thickness is:

$$t_c' = 0.75\,(d_i + 2t_c) - 0.5d_i' \qquad \text{2-50}$$

where

t_c' = *adjusted casing thickness*

Assuming a circular cross-section, the length of the fragment is:

$$L_f = \frac{4W_f}{\pi\rho_c\left(t_c'\right)^2} \le L_{cyl} \qquad 2\text{-}51$$

where

L_f = *length of the fragment*
W_f = *weight of the fragment from Section 2-17.3*
ρ_c = *density of casing material*
L_{cyl} = *length of the cylinder or equivalent cylinder*

If assuming a circular cross-section, the length L_f calculated is longer than the length of the cylinder, then a rectangular cross-section is assumed where the width is equal to:

$$b_f = \frac{W_f}{\rho_c t_c' L_{cyl}} \qquad 2\text{-}52$$

where

b_f = *width of the fragment*

2-17.5.3 Caliber Density.

The influence of the fragment weight to fragment diameter ratio is expressed in terms of the caliber density of the fragment which is defined as:

$$D = W_f / d^3 \qquad 2\text{-}53$$

where

D = caliber density (see Figure 2-244 (+))
d = fragment diameter

2-17.5.4 Nose Shape Factor.

The nose shape factor expresses the influence of the shape of the primary fragment and is defined as:

For flat-nosed, solid fragments:

$$N = 0.72 \qquad 2\text{-}54$$

For fragments with special nose shapes:

$$N = 0.72 + 0.25\,(n - 0.2)^{1/2} < 1.17 \qquad 2\text{-}55$$

where

N = *nose shape factor*
n = *caliber radius of the tangent ogive of the assumed fragment nose (see Figure 2-244 (+))*

2-17.5.5 Impact Angle.

The angle of obliquity refers to the angle between the path of the fragment and a normal to the surface; thus, a normal impact corresponds to an angle of obliquity of zero degrees. A normal impact is usually assumed in penetration calculations in order to conservatively design for the worst case condition.

2-18 SECONDARY FRAGMENTS.

2-18.1 General.

The explosion of HE during some manufacturing or forming process (i.e., nitration, centrifuging, pressing, and machining on lathe) can result in a large number of secondary fragments which vary greatly in size, shape, initial velocity, and range. Each of these parameters affects the damage potential of an accidental explosion and, therefore, should be considered in the design of protective structures.

The current state-of-the-art for assessing damage potential requires that the design engineer estimate the conditions which are likely to exist at the time of the accident and perform a structural assessment of any equipment which will be involved. Some of the initial factors to consider are:

(1) Type and amount of HE.

(2) Configuration of HE (i.e., sphere, cylinder, cased, uncased).

(3) Location of HE (i.e., attached to lathe, resting on support table, contained in centrifuge, proximity to walls and other equipment).

(4) Type of propagation after initiation (i.e., high order, burning, partial detonation).

If the fragmentation pattern varies with the initial conditions, the Architectural Engineer must examine several likely scenarios to evaluate the damage potential.

To estimate the weight, shape, and velocity of fragments which result from detonation of an HE during a manufacturing or forming process, one would perform the following steps:

(1) Determine distance (R_i) from the center of the explosive to the expected fragment of interest (refer to structural details of the machine and/or architectural drawings).

(2) Determine the size and shape of the expected fragment (refer to structural details of the machine).

(3) Determine the fragment velocity (refer to Sections 2-18.2 and 2-18.3).

2-18.2 Velocity of Unconstrained Secondary Fragments.

To predict velocities of objects accelerated by an explosion, the interaction of blast waves with solid objects must first be considered. Figure 2-246 (+) shows the interaction of a blast wave with an irregular object. The interaction is shown in three phases as the wave passes over the object. As the wave first strikes the object, a portion is reflected from the front face, and the remainder diffracts around the object. In the diffraction process, the incident wave front closes in behind the object, greatly weakened locally, and a pair of trailing vortices is formed. Rarefaction waves sweep across the front face, attenuating the initial reflected blast pressure. After passage of the front, the object is immersed in a time-varying flow field. Maximum pressure on the front face during this "drag" phase of loading is the stagnation pressure.

To predict the effect of a blast wave on the object, it is necessary to examine the net transverse pressure on the object as a function of time. This loading, somewhat idealized, is shown in Figure 2-247 (+). After the time arrival t_a, the net transverse pressure rises from zero to a maximum peak reflected pressure P_r in time (T_1 - t_a). For an object with a flat face nearest the approaching blast wave, this time interval is zero. Pressure then falls linearly to drag pressure in time (T_2 - T_1) and decays more slowly to zero in time (T_3 - T_2).

The basic assumptions for unconstrained secondary fragments are (1) the object behaves as a rigid body, (2) none of the energy in the blast wave is absorbed in breaking the object loose from its moorings or deforming it elastically or plastically, and (3) gravity effects can be ignored during the acceleration phase of the motion. The equation of motion for the object is:

$$A\,p(t) = Ma \qquad 2\text{-}56$$

where

A = *area of object presented to blast front*
p(t) = *pressure-time history of blast wave acting on object*
M = *mass of object*
a = *acceleration of object*

Rearranging terms and integrating:

$$v(T_3) = \int (T_3 / t_a) a dt = \frac{A}{M} \int (T_3 / t_a) p(t) dt = \frac{A}{M} i_d \qquad 2\text{-}57$$

where

$v(T_3)$ = initial velocity of the object
i_d = *total drag and diffraction impulse*

The integral in Equation 2-57 is the area under the curve of pressure-time relationship. Equation 2-57 can be integrated explicitly if the pressure-time history can be described by suitable mathematical functions or it can be evaluated graphically or numerically if p(t) cannot be easily written in function form.

For intermediate strength shocks, the solution of Equation 2-57 can be determined from a rather long equation. For computational purposes that equation is presented here in graphical form as Figure 2-248 (+), where

P_{so} = *peak incident overpressure (psi)*
p_o = *atmospheric pressure (psi)*
C_D = *drag coefficient*
i_s = *incident specific impulse (psi-ms)*
a_o = *velocity of sound in air (ft/sec)*
K = *constant (4 if object is on the ground or reflecting surface and 2 if object is in the air)*
H = *minimum transverse dimension of the mean presented area of object (in)*
X = *distance from the front of the object to the location of its largest cross-section normal to the plane of the shock front (in)*
M = *mass of object (lb-ms^2)/in*
A = *mean presented area of object (in^2)*
v_o = *initial velocity of object (ft/sec)*

The peak incident pressure P_s and the incident specific impulse i_s can be determined from Figure 2-7 (+) knowing the scaled distance to the object. Values for the drag coefficient C_D for several common shapes are given in Table 2-8 (+). This analysis is

appropriate for objects "far" from the explosive charge; thus, the object is not in a high velocity flow field and C_D is essentially a constant. Figure 2-248 (+) can be used in most cases where the distance from the object to the center of a spherical charge is greater than 20 charge radii, which is normally considered to be "far" from the charge. For objects close to a charge, the initial velocity is a function of the impulse on the target, and the actual pressure-time variation across the object is unimportant. For this close-in range the impulse acting on the object is equal to the applied momentum.

$$i = MV / A \qquad \text{2-58}$$

Thus, the velocity in terms of the actual target shape is:

$$v_o = 1000 i ß A / (12M) \qquad \text{2-59}$$

where

i = *specific acquired impulse*
ß = *target shape factor from Figure 2-249* (+)
A = *area of the target*
M = *mass of the target*
v_o = *velocity of the target*

To calculate the specific impulse imparted to a close-in target, the following equations were developed based on experimental data:

\1

For spherical charges with $R/R_e \leq 5.07$:

$$\frac{i}{\beta R_{eff}}\left[R_e / R_t\right]^{0.158} = 47{,}690\left[R_e / R\right]^{1.4} \qquad \text{2-60}$$

and

$$R_{eff} = R_e \qquad \text{2-61}$$

For cylindrical charges with $R/R_e \leq 5.25$:

$$\frac{i}{\beta R_{eff}}\left[R_e / R_t\right]^{0.158} = 58{,}400\left[R_e / R\right] \qquad \text{2-62}$$

For cylindrical charges with $5.25 < R/R_e \leq 10$:

$$\frac{i}{\beta R_{eff}}\left[R_e / R_t\right]^{0.158} = 203{,}000\left[R_e / R\right]^{1.75} \qquad 2\text{-}63$$

/**1**/

and:

$$R_{eff} = 0.909\left[l_e / R_e\right]^{0.333} R_e \qquad 2\text{-}64$$

where

i = *specific acquired impulse (psi-ms)*
ß = *nondimensional shape factor of the target from Figure 2-249* (+)
R_{eff} = *effective radius (ft)*
R_e = *radius of the explosive (ft)*
R = *standoff distance (ft)*
R_t = *target radius (ft)*
l_e = *length of cylindrical explosive (ft)*

The effective radius R_{eff} is the radius of an equivalent sphere of explosive which could be formed from a cylinder of radius R_e and length l_e.

The specific impulse imparted to a target, as given by Equations 2-60, and 2-62 and 2-63 for spherical and cylindrical charges, respectively, is plotted in Figure 2-250 (+). This experimentally derived data should not be used beyond the distances shown in the figure. When these standoff distances are exceeded, the specific acquired impulse may be approximated by using the normal reflected impulse obtained from Figure 2-7 (+).

2-18.3 Velocity of Constrained Secondary Fragments.

The method used to predict initial velocities of a constrained secondary fragments close to an explosion must first consider the amount of energy applied to each fragment as well as the energy consumed in freeing the fragment from its support. This relationship can be expressed using the conservation of momentum and allowing the structural constraint to reduce the imparted impulse as follows:

$$I - I_{st} = mV_o \qquad 2\text{-}65$$

where

I = total impulse of the blast applied to the fragment
I_{st} = impulse consumed by the fragment support connection
m = mass of the fragment
V_o = velocity of the fragment after break away

The value of I_{st} must be established experimentally. Based on tests, an empirical expression has been developed for cantilever beams subjected to close-in effects:

$$V_o = \frac{1000}{12} \cdot \left[\frac{T}{p_f}\right]^{1/2} \left[C_1 + \frac{C_2 i b_f}{A[\rho_f T]^{1/2}} \left(\frac{2L_f}{b_f}\right)^{0.3}\right] \qquad \text{2-66}$$

where

V_o = velocity of fragment after break away (ft/sec)
T = toughness of material (area under the stress-strain curve) from Table 2-9 (+)
ρ_f = mass density of the fragment (lb-ms^2/in^4)
C_1 = constant equal to -0.2369
C_2 = constant equal to +0.3931
i = unit impulse acting on the member (psi-ms)
b_f = width of fragment exposed to the blast (in)
A = cross-sectional area in the plan perpendicular to the long axis of the fragment (in^2)
L_f = length of fragment exposed to the blast (in)

Equation 2-66 is adequate for determining the fragment velocity when:

$$\frac{i b_f}{A[\rho_f T]^{1/2}} \left[\frac{2L_f}{b_f}\right]^{0.3} \geq 0.602 \qquad \text{2-67}$$

When Equation 2-67 is less than 0.602, the magnitude of the velocity is equal to zero which indicates that disengagement of the fragment will not occur.

The constants in Equation 2-66 were derived from experimental data and can only be used for cantilevered beams of steel or aluminum.

An equation similar to that of Equation 2-66 has been developed for clamped-clamped fragments except that the value of C_1 is equal to -0.6498 and C_2 is equal to 0.4358.

A plot of Equation 2-66 for both cantilever and clamped-clamped fragments is presented in Figure 2-251 (+).

2-19 FRAGMENT TRAJECTORIES.

Once primary fragments or secondary missiles have been formed and accelerated by an explosion, they will move along a specific trajectory until they impact a target (receiver), or the ground. The forces acting on the fragments and affecting their trajectories are inertia, gravitation, and fluid dynamic forces. The fluid dynamic forces are determined by the instantaneous velocity of the fragment at each instant in time. Generally, fragments are quite irregular in shape and may be tumbling, so a completely accurate description of the fluid dynamics forces during flight is difficult, if not impossible. In the trajectory analysis for fragment flight, one usually resorts to some simplified description of the fluid dynamic forces, and uses the concepts from aerodynamics of division of these forces into components called drag (along the trajectory or normal to the gravity vector) and lift (normal to the trajectory or opposing gravity). Then the force components are given at any instant by:

$$F_L = C_L A_L (1/2)\, \rho\, v^2 \qquad 2\text{-}68$$

and

$$F_D = C_D A_D (1/2)\, \rho\, v^2 \qquad 2\text{-}69$$

where

F_L = *lift force*
F_D = *drag force*
C_L = *lift coefficient*
C_D = *drag coefficient*
A_L = *lift area*
A_D = *drag area*
ρ = *density of the medium through which the fragment is traveling*
v = *velocity of the fragment*

The lift and drag coefficients are determined empirically as a function of shape and orientation with respect to the velocity vector, and the magnitude of the velocity v. Fragments discussed in Sections 2-17 and 2-18 are generally of chunky shape, so that $C_D >> C_L$ for any flight orientation. Thus, they are called drag-type fragments. The lift force on drag-type fragments is very small and may be neglected.

In a simplified trajectory problem, where the fragment is considered to move in one plane, equations of motion can be written for acceleration in the X and Y directions.

The acceleration in the X direction (drag only) is:

$$a_x = A_D C_D \ddot{a}_o [v_x^2 + v_y^2] \cos \alpha / 2M \qquad 2\text{-}70$$

and for the Y direction (drag only):

$$a_y = -1.2 \times 10^{-5} g - A_D C_D \rho_o [v_x^2 + v_y^2] \sin \alpha / 2M \qquad 2\text{-}71$$

where:

a_x, a_y = *acceleration in the X and Y directions, respectively*
ρ_o = *mass density of the medium through which the fragment travels*
v_x, v_y = *velocity in the X and Y directions, respectively*
g = *gravity force (32.2 ft/sec^2)*
M = *mass of the fragment*
α = *trajectory angle*

At t = 0:

$$v_x = v_o \cos \alpha_o \qquad 2\text{-}72$$

$$v_y = v_o \sin \alpha_o \qquad 2\text{-}73$$

where

v_o = *initial velocity*
α_o = *initial trajectory angle*

The equations shown above can be solved simultaneously to eventually determine the distance traveled by the fragment. These equations are valid for fragment velocities up to Mach 1 for standard conditions. Figure 2-252 (+) summarizes the results of fragment range R for numerous sets of initial conditions for fragments affected only by drag forces. It should be noted that, in this curve, several initial trajectory angles were used in the analysis to obtain the maximum range R for the respective fragments. Thus, one need not know the initial trajectory angle of a fragment in order to use Figure 2-252Plots/02_252.grf.

Figure 2-236 Explosive Outer Casing Separated By Incompressible Fluid

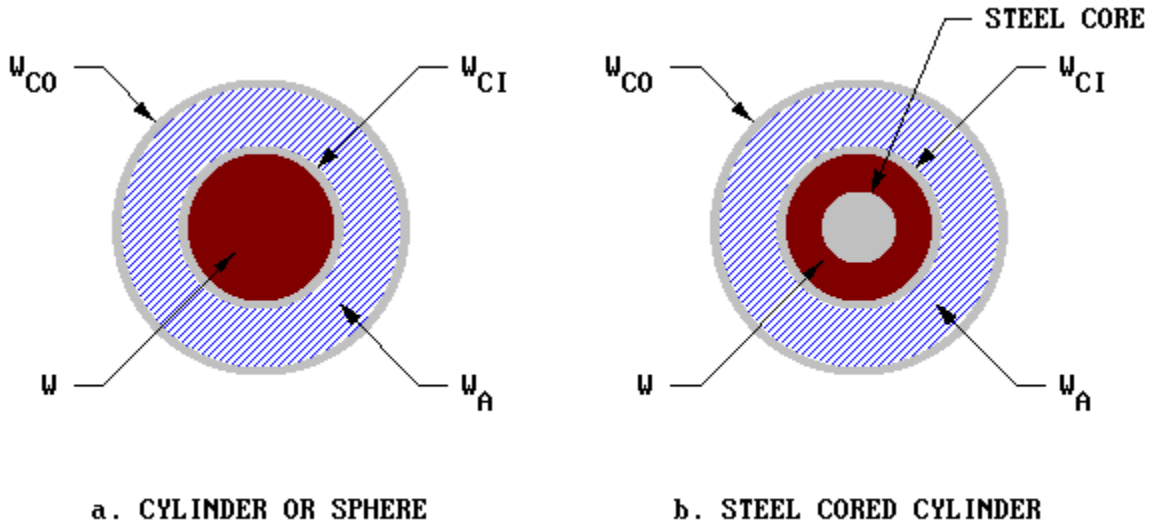

Figure 2-237 Initial Velocity of Primary Fragments for Various Geometries

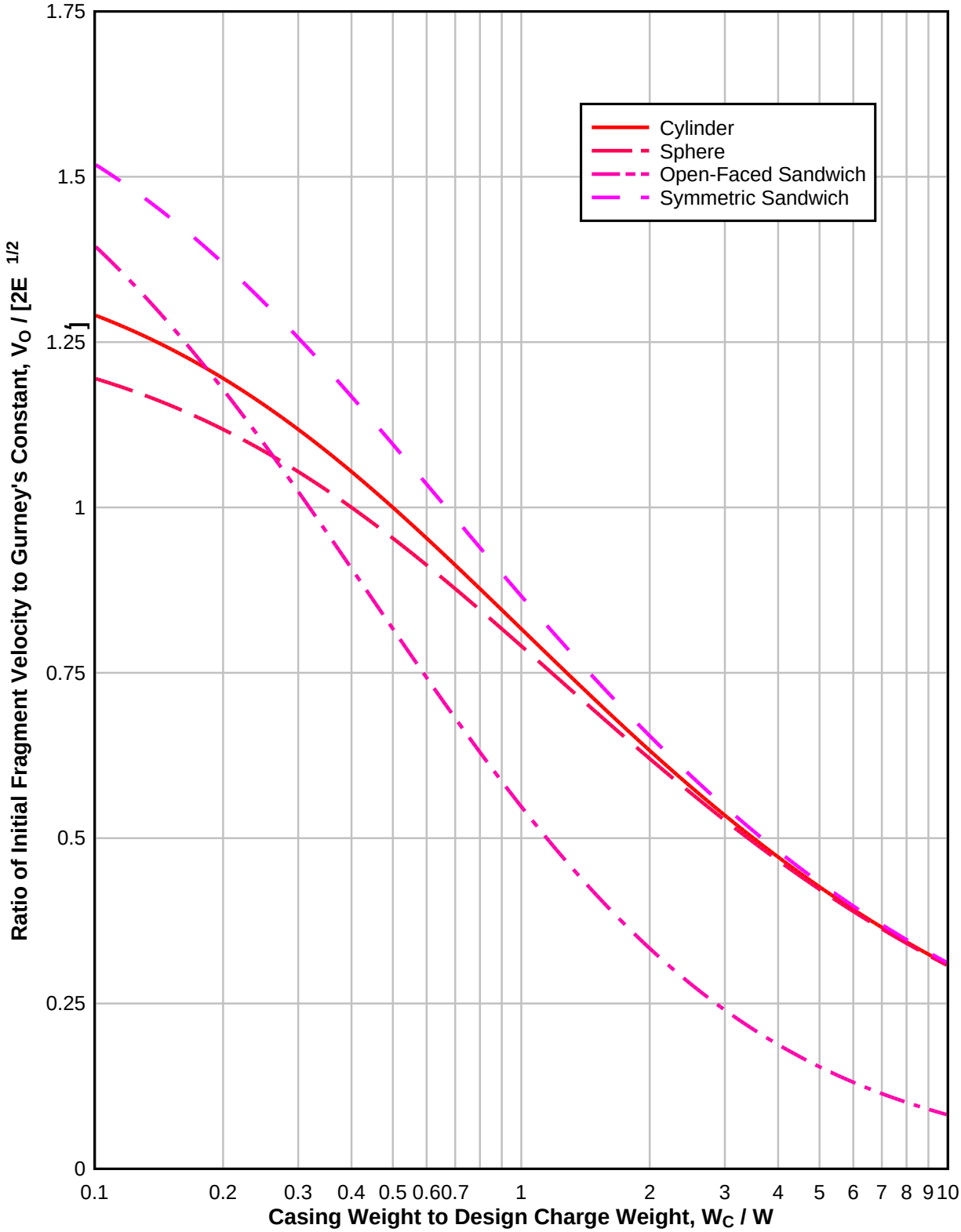

Figure 2-238 M_A/B versus Cylindrical Casing Geometry

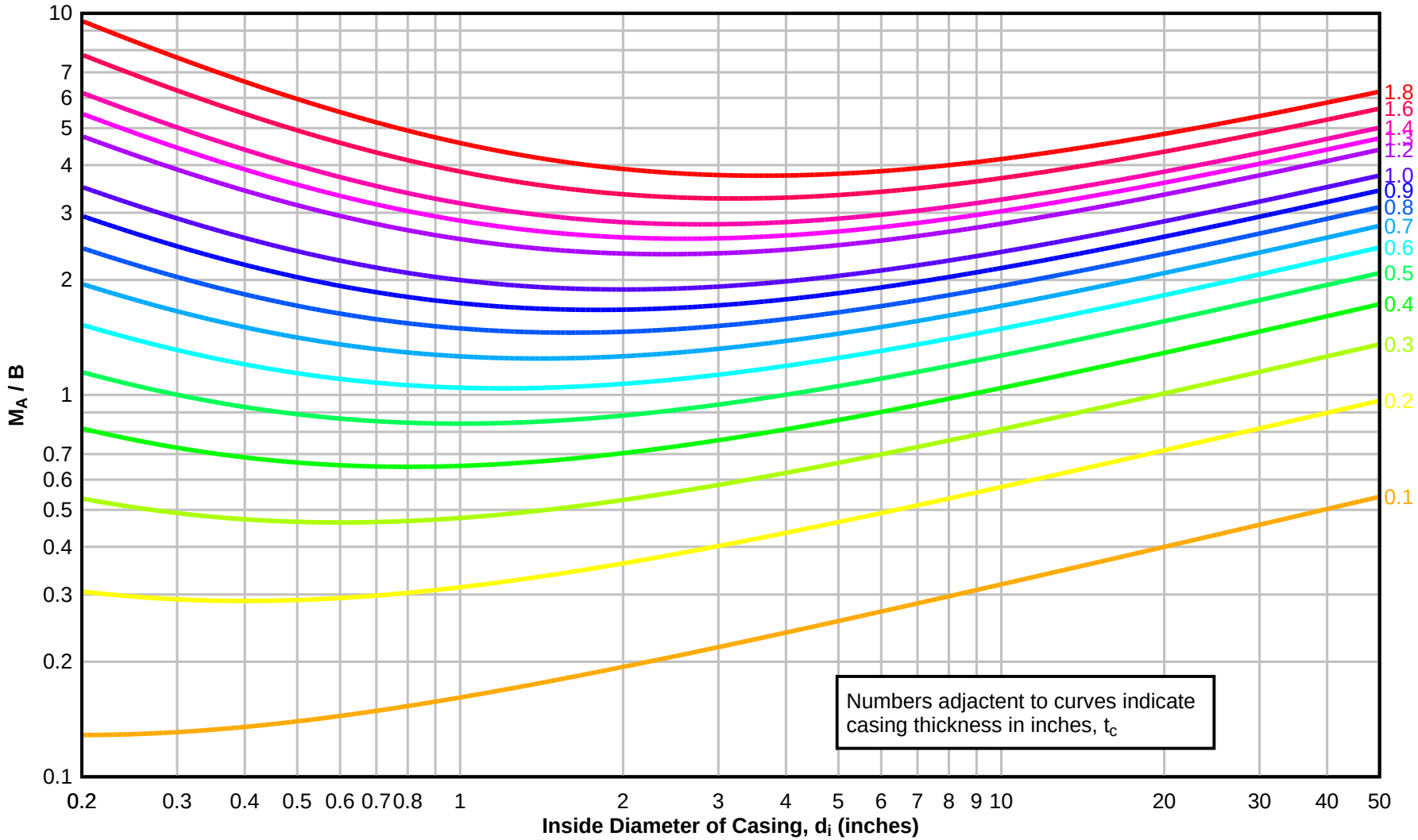

Figure 2-239 Design Fragment Weight versus Design Confidence Level ($0.3 \leq C_L \leq 1$)

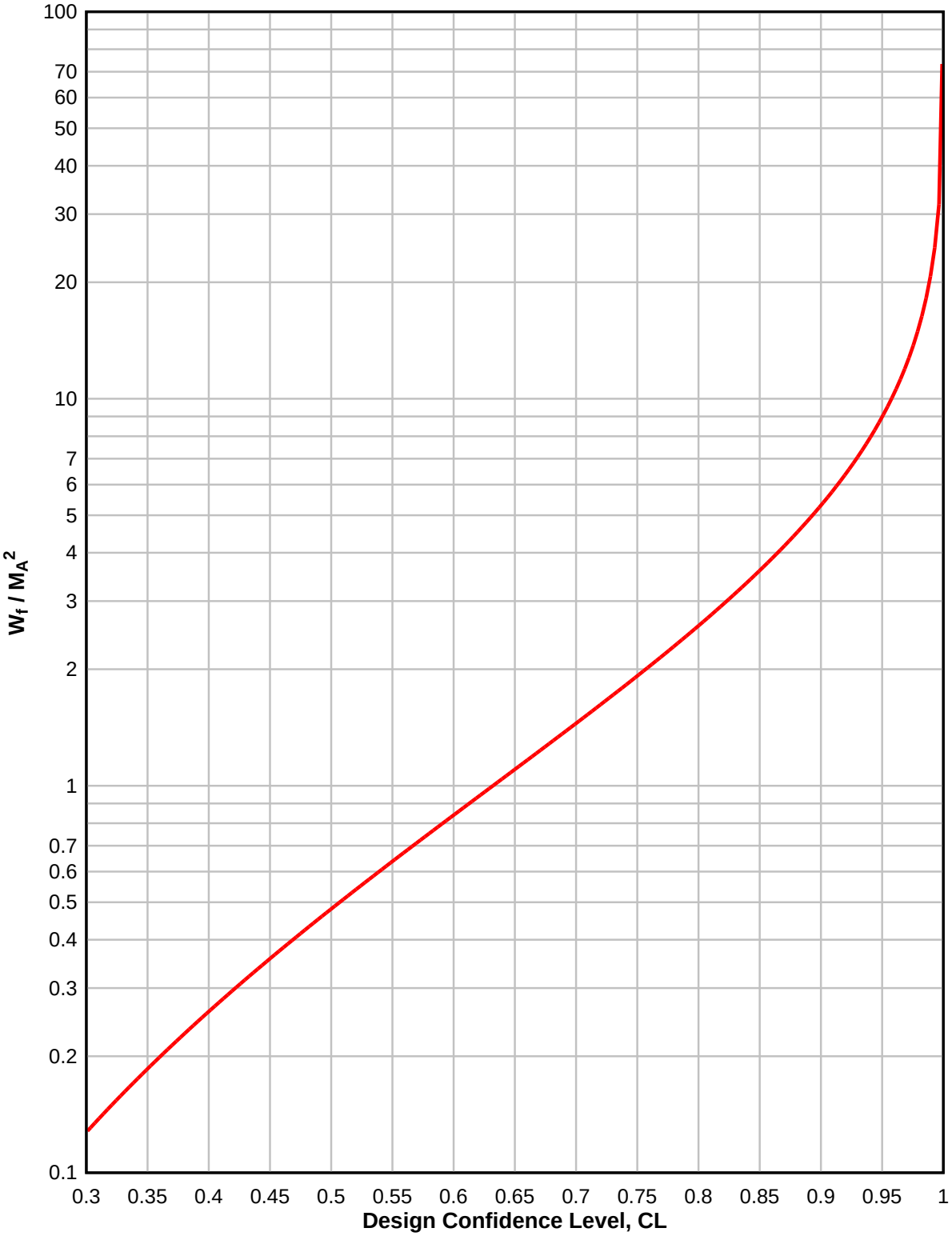

Figure 2-240 Design Fragment Weight versus Design Confidence Level ($0.986 \leq C_L \leq 1$)

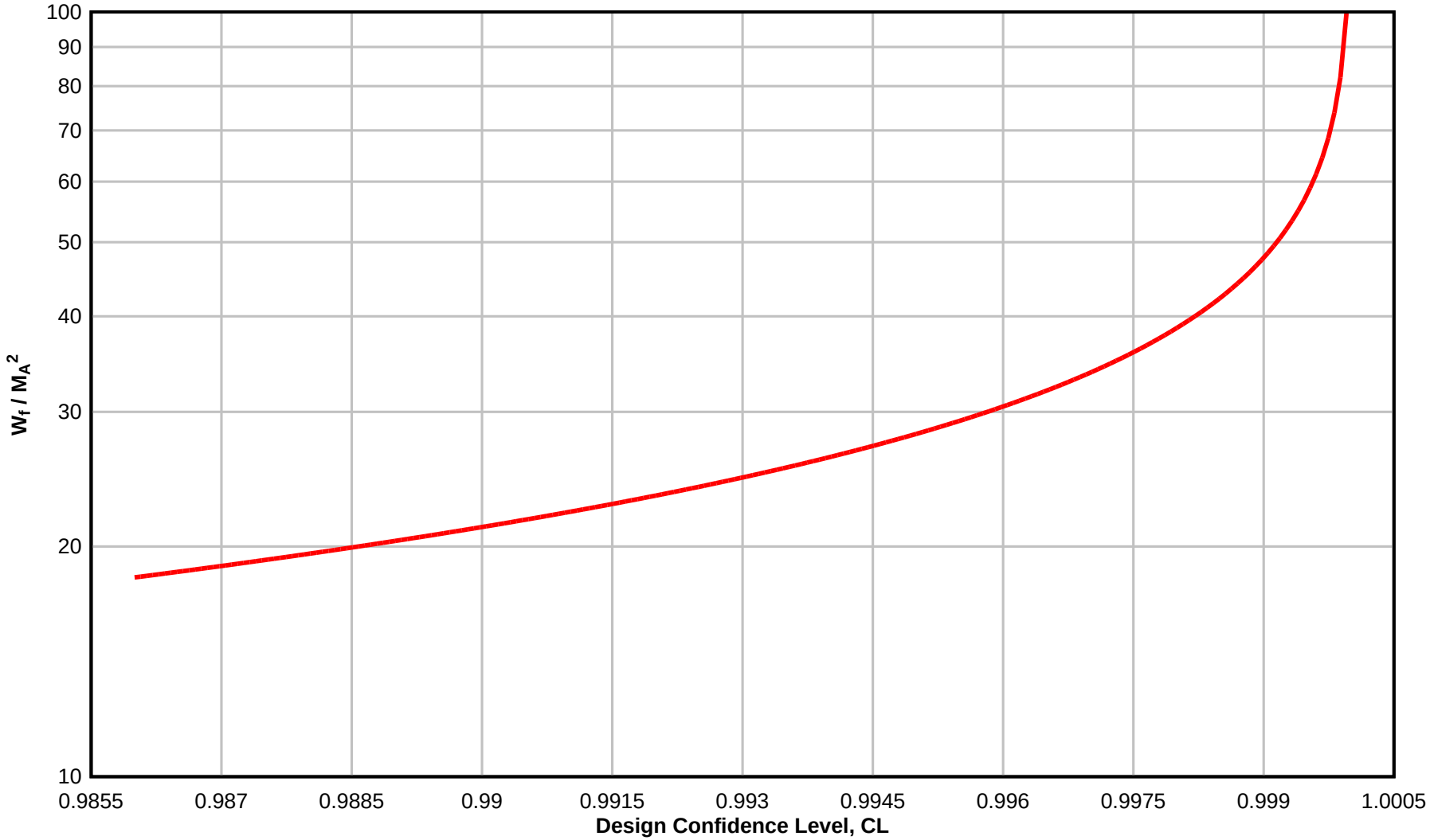

Figure 2-241 B^2N_T/W_C versus Casing Geometry

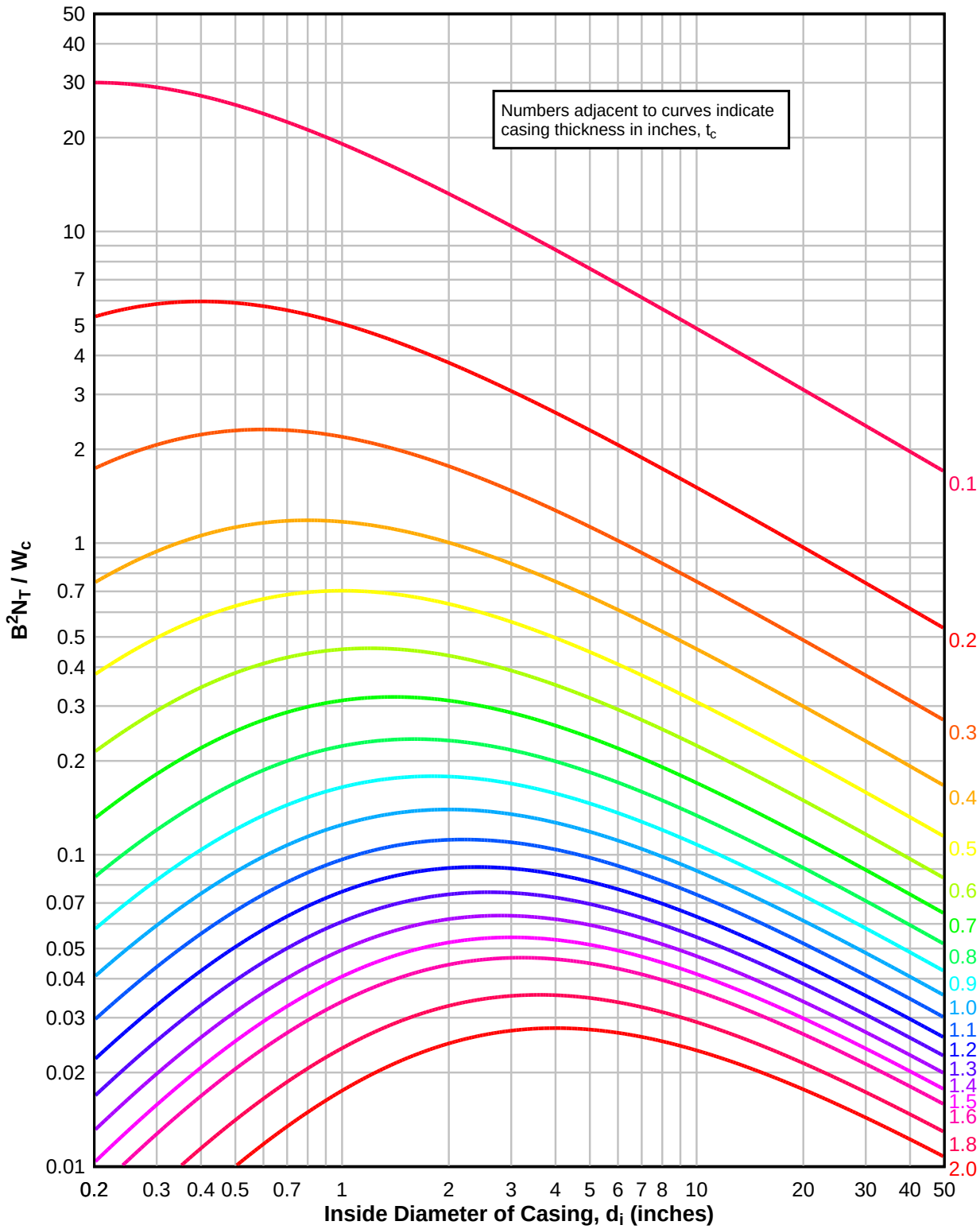

Figure 2-242 Equivalent Cylindrical Explosive Casings

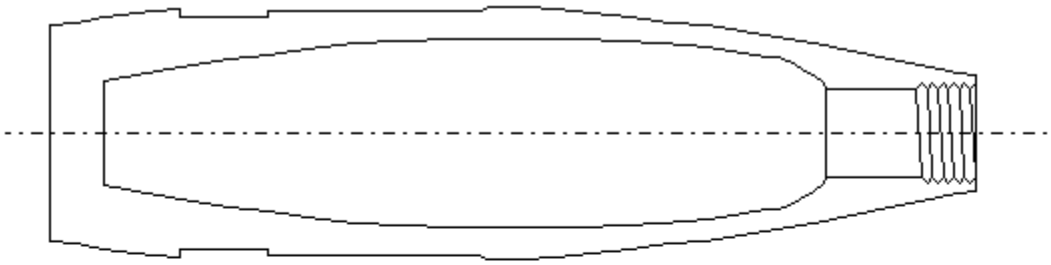

(a) ACTUAL CONFIGURATION

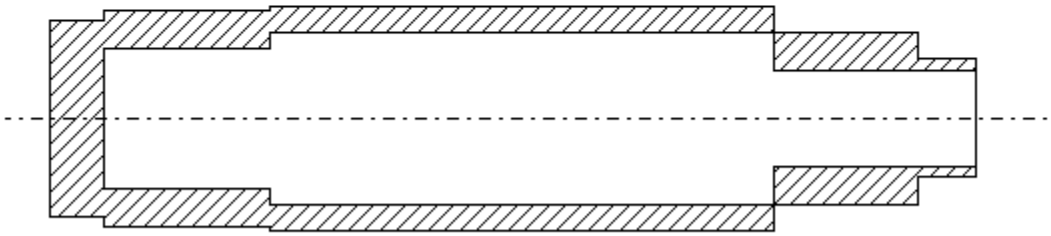

(b) IDEALIZED CONFIGURATION

Figure 2-243 Variation of Primary Fragment Velocity with Distance

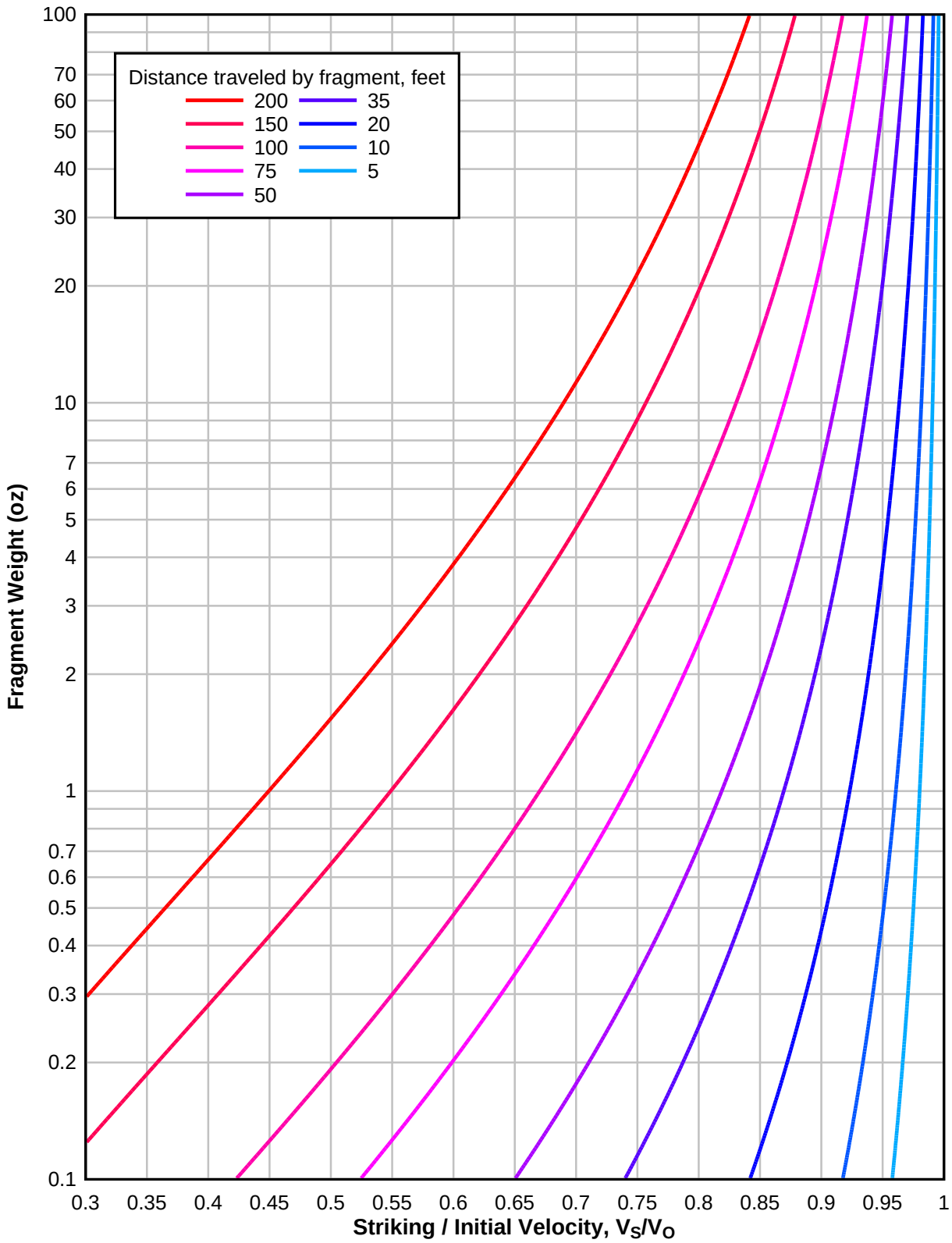

Figure 2-244 Primary Fragment Shapes

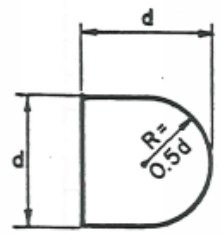

$n = 0.5$
$N = 0.845$
Volume $= 0.654d^3$
$W_f = 0.186d^3$
$D = 0.186$ lb/in.^{3}
$A = \pi d^2/4$

(a) Standard Fragment Shape

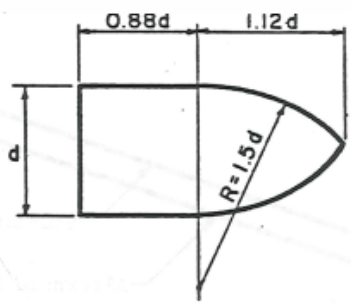

$n = 1.5$
$N = 1.00$
Volume $= 1.2d^3$
$W_f = 0.34d^3$
$D = 0.34$ lb/in.^{3}
$A = \pi d^2/4$

(b) Alternate Fragment Shape

NOTE:
N = Nose shape factor = $0.72 + 0.25\sqrt{n-0.25}$
n = Caliber radius of the tangent ogive of the fragment nose = R/d
D = Caliber density = W_f/d^3

Figure 2-245 Relationship between Fragment Weight and Fragment Diameter

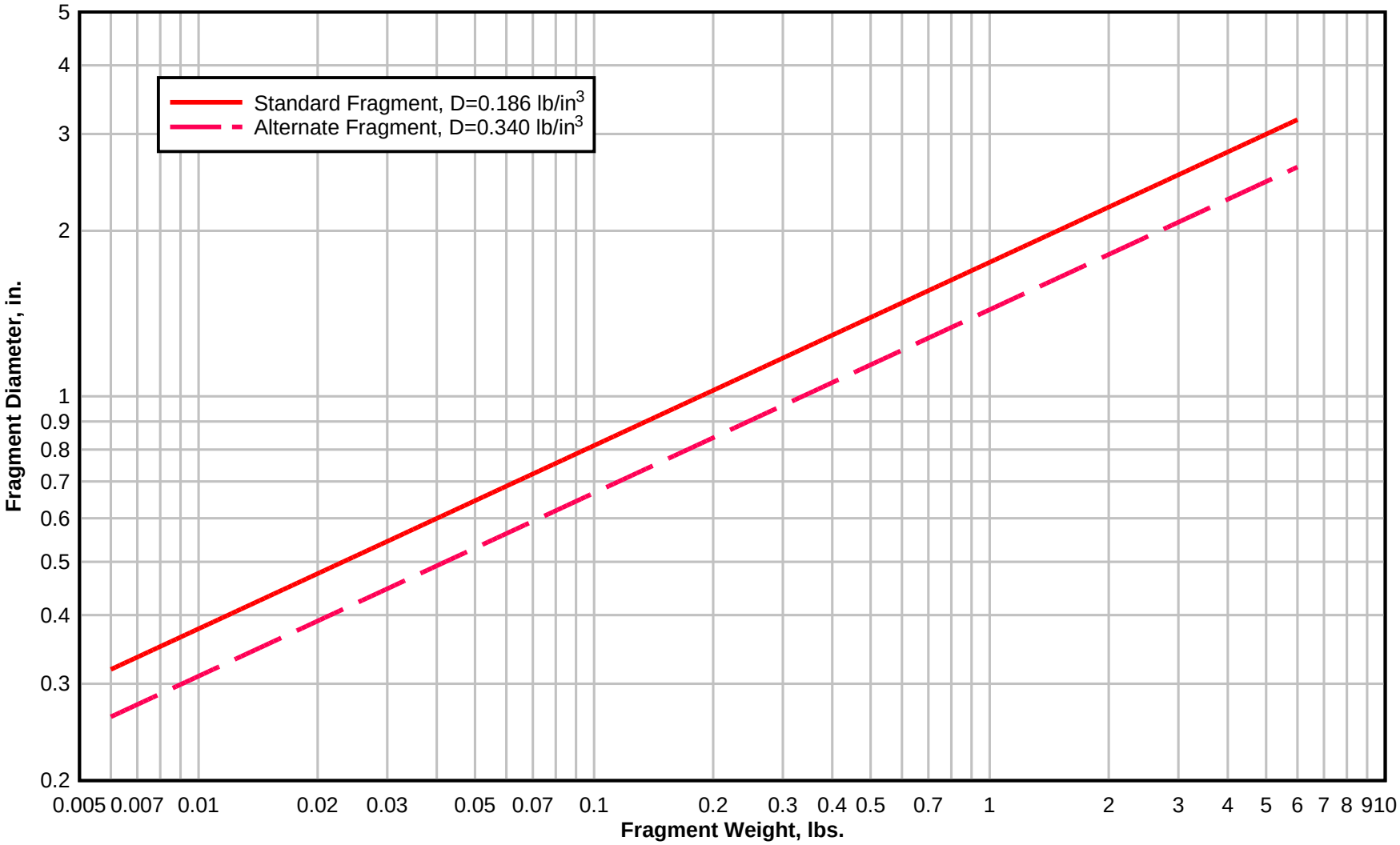

Figure 2-246 Interaction of Blast Wave with an Irregular Object

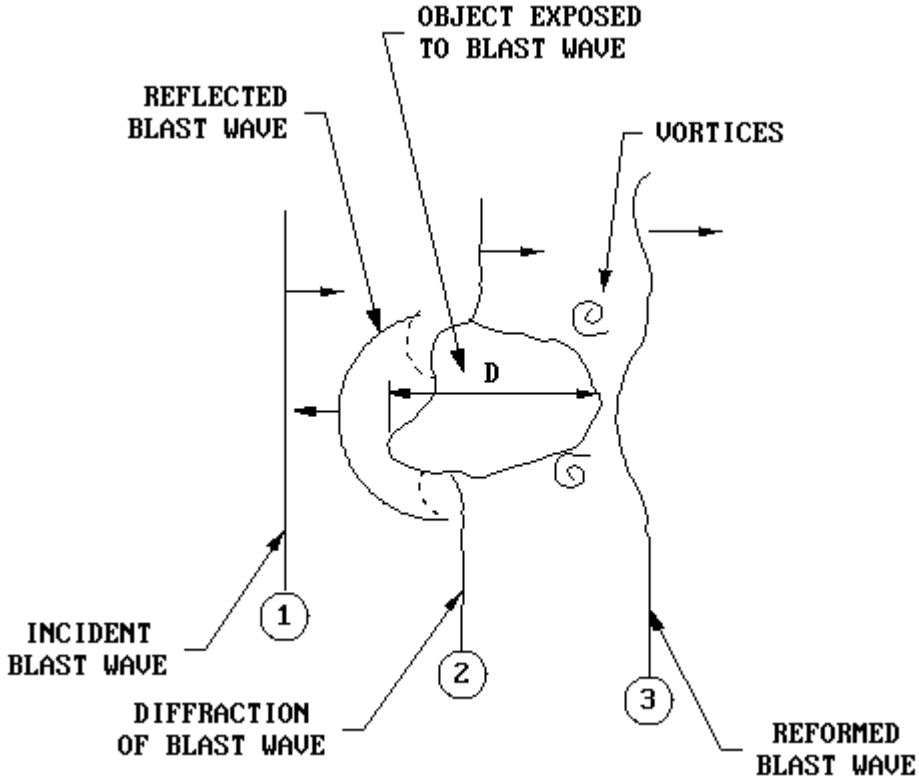

Figure 2-247 Idealized Pressure-Time Loading on an Irregular Fragment

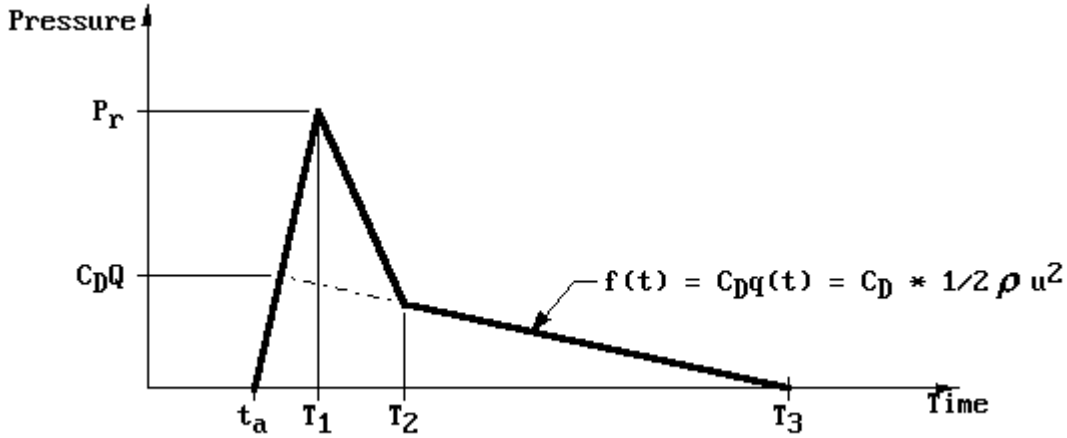

Figure 2-248 Nondimensional Object Velocity, $\overline{V}$, as a Function of Pressure and Impulse

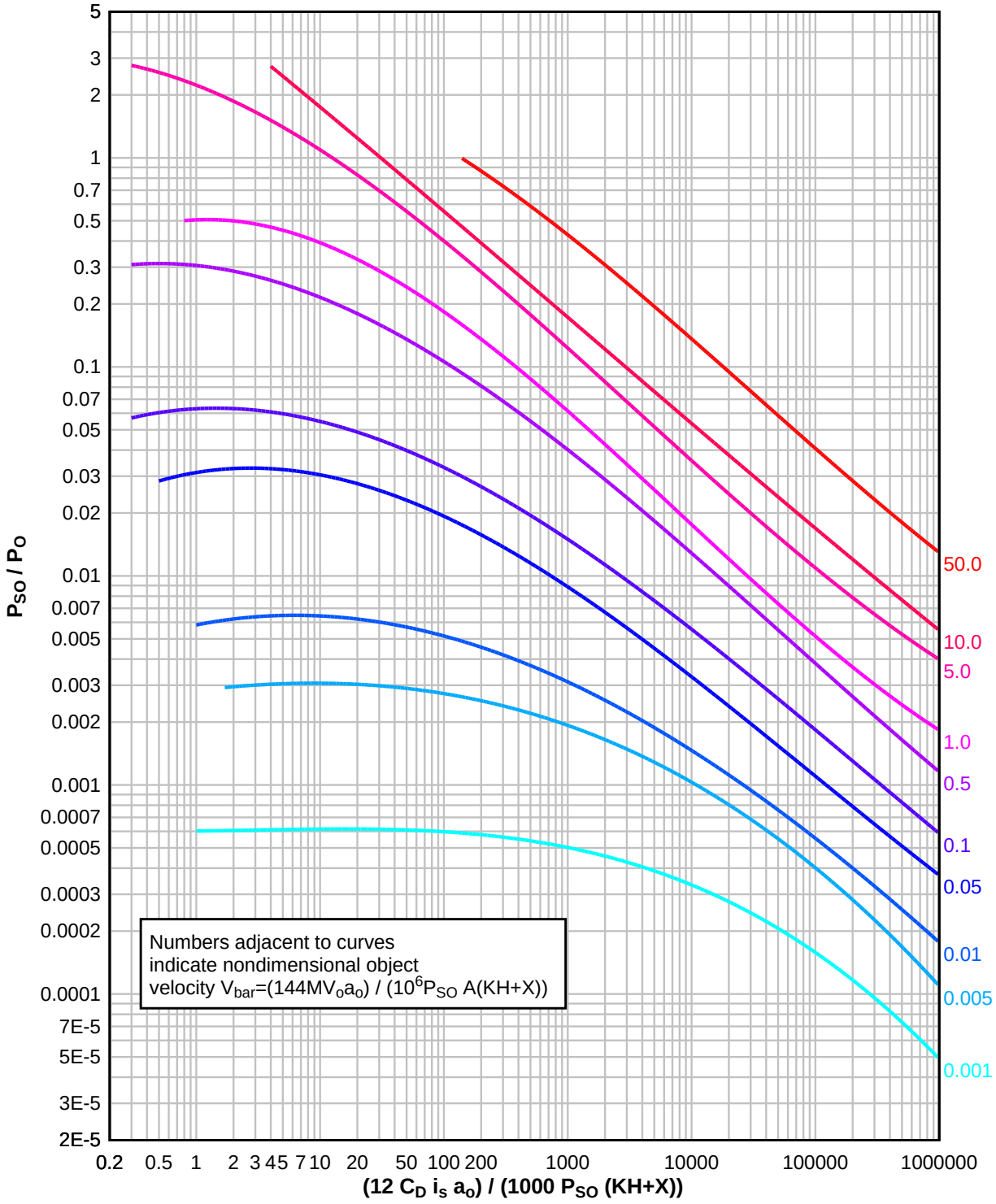

02_248.grf

Figure 2-249 Target Shape Factor for Unconstrained Fragments

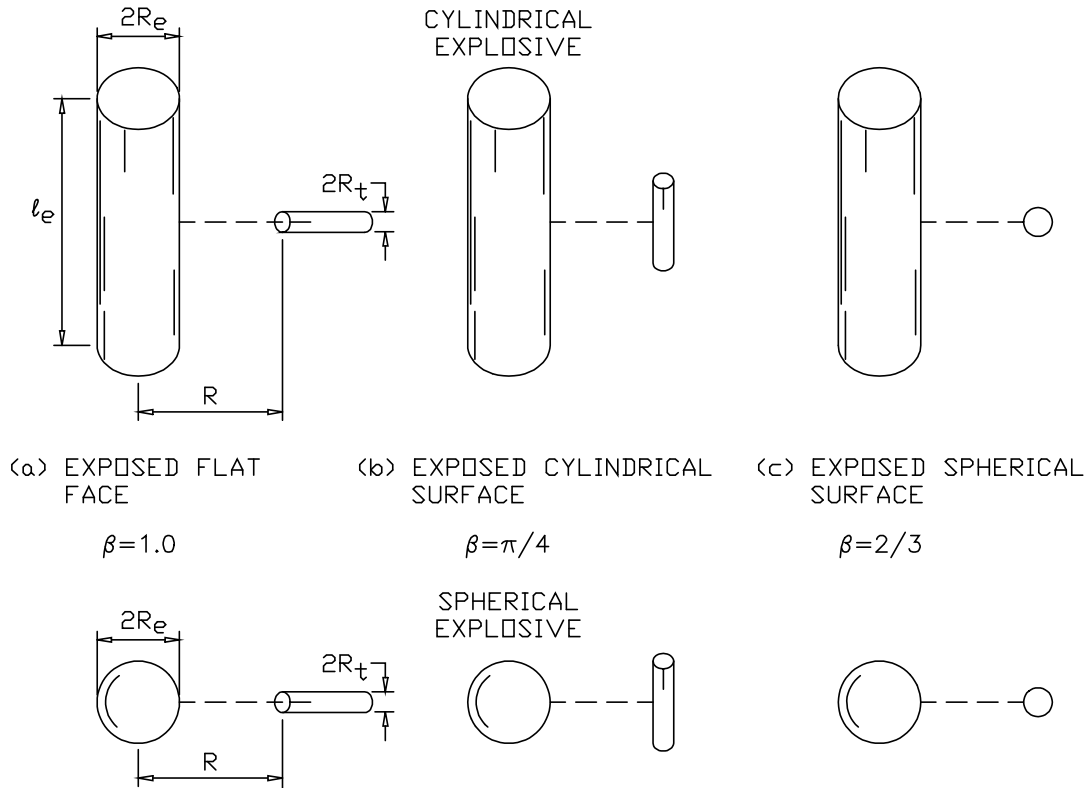

Figure 2-250 Specific Acquired Impulse versus Distance

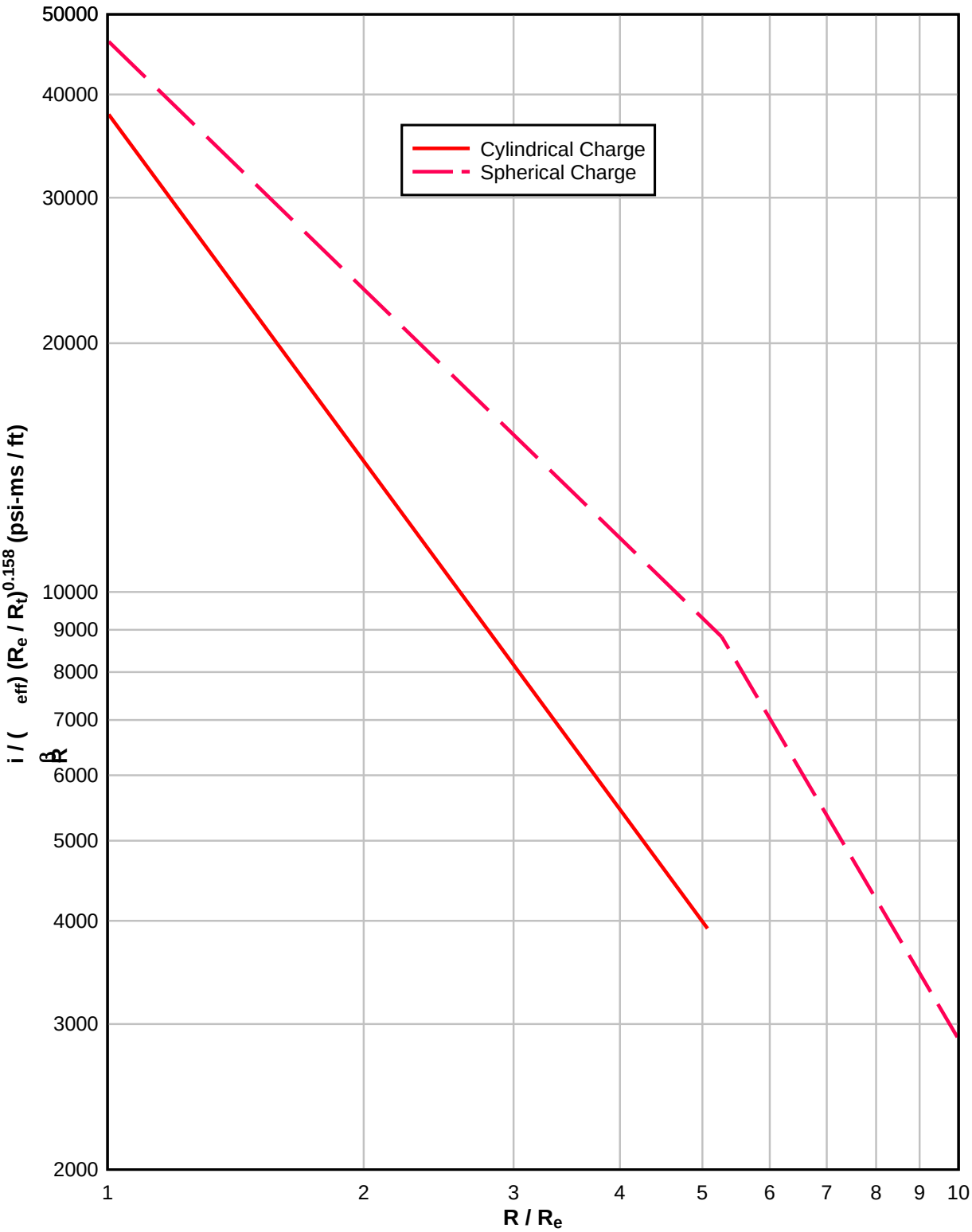

Figure 2-251 Scaled Fragment Velocities for Constrained Fragments

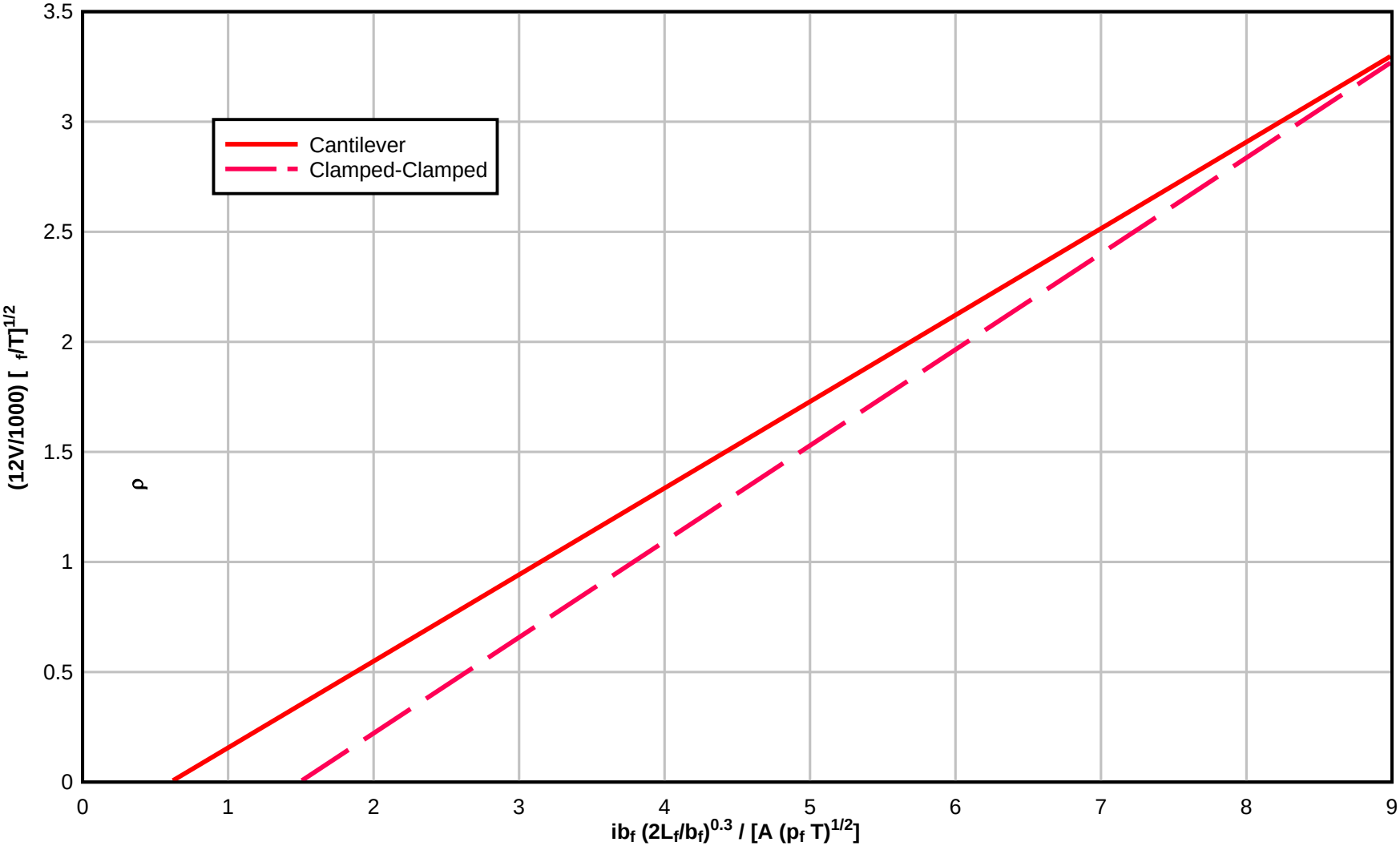

Figure 2-252 Fragment Range Prediction

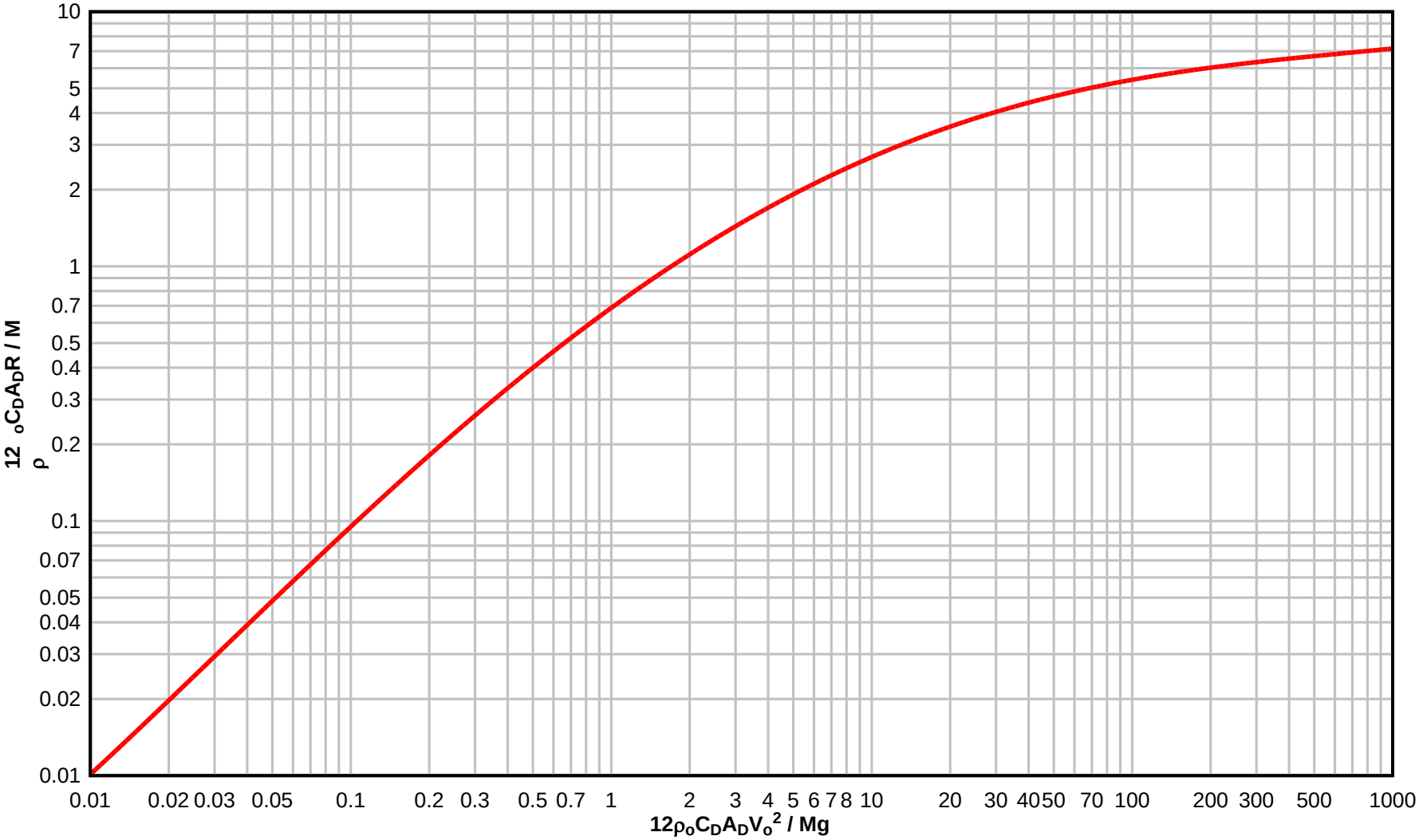

Table 2-5 Specific Weight and Gurney Energy Constant for Various Explosives

Explosive	Specific Weight (lb/in^3)	$(2E')^{1/2}$ (ft/sec)
Composition B	0.0621	9100
Composition C-3	0.0578	8800
HMX	0.0682	9750
Nitromethane	0.0411	7900
PBX-9404	0.0664	9500
PETN	0.0635	9600
RDX	0.0639	9600
TACOT	0.0581	7000
Tetryl	0.0585	8200
TNT	0.0588	8000
Trimonite No. 1	0.0397	3400
Tritonal (TNT/Al = 80/20)	0.0621	7600

Table 2-6 Initial Velocity of Primary Fragments for Various Geometries

Type	Cross-sectional shape	Initial fragment velocity v_o	Maximum v_o	Remarks
Cylinder	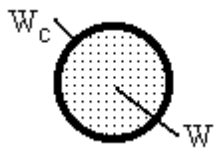	$\sqrt{2E'}\left[\dfrac{\dfrac{W}{W_c}}{1+\dfrac{W}{2W_c}}\right]^{1/2}$	$\sqrt{2E'}\sqrt{2}$	See Section 2-17.2
Sphere	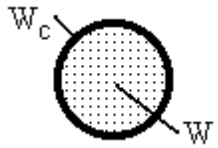	$\sqrt{2E'}\left[\dfrac{\dfrac{W}{W_c}}{1+\dfrac{3W}{5W_c}}\right]^{1/2}$	$\sqrt{2E'}\sqrt{\dfrac{5}{3}}$	
Steel cored cylinder	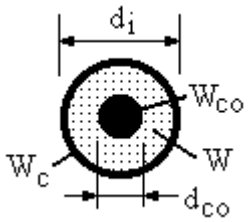	$\sqrt{2E'}\left[\dfrac{\dfrac{W}{W_c}}{1+\dfrac{(3+a)W}{6(1+a)W_c}}\right]^{1/2}$ $where\, a=\dfrac{d_{co}}{1.6d_i}$	$\sqrt{2E'}\sqrt{\dfrac{6(1+a)}{(3+a)}}$	If the steel core is many times more massive than the explosive, this expression for the initial velocity should be modified by multiplying it by the expression: $\sqrt{1-\dfrac{0.02W_{co}}{W}}$ where W_{co} is the weight of the steel core (lbs).
Plate	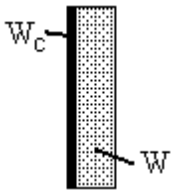	$\sqrt{2E'}\left[\dfrac{\dfrac{3W}{5W_c}}{1+\dfrac{W}{5W_c}+\dfrac{4W_c}{5W}}\right]^{1/2}$	$\sqrt{2E'}\sqrt{3}$	This expression applies for a rectangular explosive in contact with a metal plate having the same surface area. It is assumed that the entire system is suspended in free air and its thickness is small in comparison to its surface area so that the resulting motions are essentially normal to the plane of the plate.

Table 2-6 Initial Velocity of Primary Fragments for Various Geometries, Continued

Type	Cross-sectional shape	Initial fragment velocity v_o	Maximum v_o	Remarks
Hollow cylinder	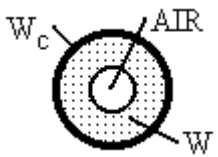	-	-	Although an expression to predict the velocity of fragments is not available, an upper limit of the initial velocity may be obtained using the expression for a solid cylinder and a lower limit from the expression for a single plate. The ratio of the explosive weight to the casing weight (W/Wc) of the hollow cylindrical charge is used in both expressions.
Sandwich plates	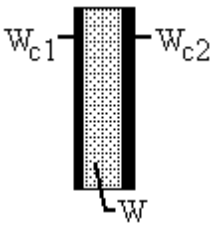	if $W_{c1} \neq W_{c2}$ $\sqrt{2E'}\left[\dfrac{W}{W_{c1}+W_{c2}g+\dfrac{W}{3}\left(1-g+g^2\right)}\right]^{1/2}$ $where\, g=\dfrac{W_{c1}+\dfrac{W}{2}}{W_{c2}+\dfrac{W}{2}}$ if $W_{c1}=W_{c2}=W_c$ $\sqrt{2E'}\left[\dfrac{\dfrac{W}{2W_c}}{1+\dfrac{W}{6W_c}}\right]^{1/2}$	$\sqrt{2E'}\sqrt{3}$	This expression applies for a rectangular explosive sandwiched between two metal plates having the same surface area as the explosive. It is assumed that the entire system is suspended in free air and its thickness is small in comparison to its surface area so that the resulting motions are essentially normal to the plane of the plates. Note: $W = E$ = Explosive weight $W_c = C$ = Casing weight W, W_c, W_{co}, W_{c1}, W_{c2} (lbs) v_o, $(2E')^{1/2}$ (ft./sec)

Table 2-7 Mott Scaling Constants for Mild Steel Casings and Various Explosives

Explosive	A ($oz^{1/2}$ $in^{-3/2}$)	B ($oz^{1/2}$ $in^{-7/6}$)
Baratol	-	0.512
Composition A-3	-	0.220
Composition B	0.214	0.222
Cyclotol (75/25)	-	0.197
H-6	-	0.276
HBX-1	-	0.256
HBX-3	-	0.323
Pentolite (50/50)	0.238	0.248
PTX-1	-	0.222
PTX-2	-	0.227
RDX	0.205	0.212
Tetryl	0.265	0.272
TNT	0.302	0.312

Table 2-8 Drag Coefficient, C_D, for Various Shapes

SHAPE	SKETCH	C_D
CIRCULAR CYLINDER (LONG ROD), SIDE-ON	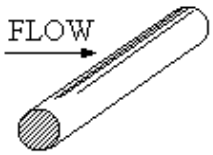	1.20
SPHERE	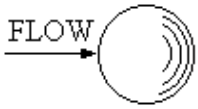	0.47
ROD, END-ON	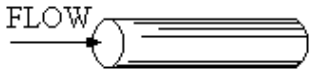	0.82
DISC, FACE-ON	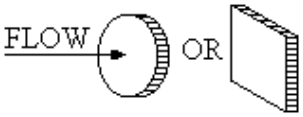	1.17
CUBE, FACE-ON	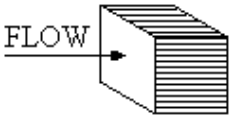	1.05
CUBE, EDGE-ON	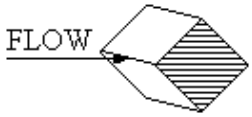	0.80
LONG RECTANGULAR MEMBER, FACE-ON	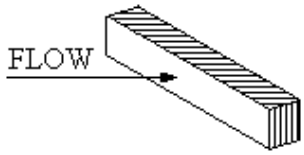	2.05
LONG RECTANGULAR MEMBER, EDGE-ON	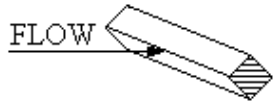	1.55
NARROW STRIP, FACE-ON	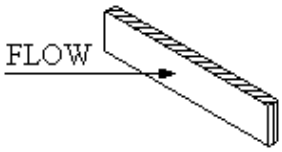	1.98

Table 2-9 Steel Toughness

Steel	Toughness in-lb/in^3
ASTM A 36	12,000
ASTM A 441	15,000
ASTM A514 Grade F	19,000

SHOCK LOADS

2-20 INTRODUCTION.

The strong air blast waves and high speed fragments are the primary hazards of accidental explosions. The exterior of a protective structure is designed primarily for the blast pressures. In some situations, the fragments may be just as important as the pressures in determining the configuration of a protective facility. While the contents of the structure are protected from the direct effects of blast pressures and fragments by the structure's exterior, the contents are subject to effects of the building's motion. These structure motions can cause injury to personnel, damage to equipment as well as dislodgement of the structure's interior components, including interior partitions, hung ceilings, light fixtures, ductwork, piping, and electrical lines.

Structure motions are caused by what is normally termed shock loads. These are loads which cause transient or short-duration vibratory motions of the ground surface and the structure. They do not cause significant structural damage but instead induce motion which, as stated above, can damage the structure's interior contents.

There are two distinct types of shock loads: ground shock and air shock. Ground shock results from the energy which is imparted to the ground by an explosion. Some of this energy is transmitted through the ground as direct-induced ground shock. Both of these forms of ground shock when imparted to a structure will cause the structure to move in both a vertical and horizontal direction. Air shock results from the blast overpressures striking the building. Vertical, horizontal and overturning motions result from the shock impact. The vertical and overturning motions are usually not significant and can be neglected while the horizontal motions must be considered. Large displacements can result when a structure slides relative to the ground surface.

The net motion of the structure is a combination of the motions due to the air induced and direct-induced ground shock, and the air shock. Curves which describe the ground motion (acceleration versus time, velocity versus time, and displacement versus time curves) are not readily calculated. However, these relationships are not required since the design of protective structures to resist shock loads is based on the peak values of the induced motion rather than the actual motion-time relationships.

The procedures presented in this section are applicable for uniform motions. The shock loads and resulting structure motions apply to rigid concrete structures located at the low- and intermediate-pressure design ranges. At distances corresponding to these pressures, the shock loads are uniform across the structure. A rigid concrete structure acts as a rigid body, that is, all components of the structure have essentially the same motion. The procedures can be applied to structures located close to an explosion and to non-rigid structures. However, the local effects associated with these conditions must be accounted for in the analysis.

2-21 GROUND SHOCK.

2-21.1 Introduction.

When an explosion occurs at or near the ground surface, ground shock results from the energy imparted to the ground by the explosion. Some of this energy is transmitted through the air in the form of air-induced ground shock and some is transmitted through the ground as direct-induced ground shock.

Air-induced ground shock results when the air-blast shock wave compresses the ground surface and sends a stress pulse into the underlying media. The magnitude and duration of the stress pulse in the ground depend on the character of the air-blast pulse and the ground media. Generally, the air-induced ground motions are downward. They are maximum at the ground surface and attenuate with depth. However, the presence of a shallow water table, a shallow soil-rock interface, or other discontinuities can alter the normal attenuation process. The properties of the incident overpressure pulse and the surface soil layer usually determine the character of air-induced ground shock on aboveground structures.

Direct-induced ground shock results from the explosive energy being transmitted directly through the ground. This motion includes both the true direct-induced motions and cratering-induced motions. The latter generally have longer durations and are generated by the crater formation process in cratering explosions. The induced ground motion resulting from both types have a longer duration than air-blast-induced ground shock and the wave forms tend to be sinusoidal.

The net ground shock experienced by a point on the ground surface is a combination of the air-blast-induced and direct-induced shock. The relative magnitudes and sequencing of the motions are functions of the media (air and soil) through which the shock travels and the distance from the point of detonation. At ranges close to the blast, the highly compressed air permits the air-blast shock front to propagate at speeds greater than the seismic velocity of the ground. In this region, the super-seismic region, the air blast arrives at a given point before the direct-induced ground shock. As the air-blast shock front moves farther from the point of detonation, the shock front velocity decreases, and the direct-induced ground shock catches and "outruns" the air blast. This latter region is called the outrunning region. Wave forms in the outrunning region are generally a complex combination of both types of induced shock. The combined motion can be obtained from consideration of the arrival time of each wave. The arrival time of the air blast is determined from the data presented for unconfined explosions. Whereas, the arrival time of the direct-induced ground shock can be estimated by assuming that the ground shock travels at the seismic velocity of the ground media. The combined ground motion in both the super-seismic and outrunning region are illustrated in Figure 2-253 (+).

2-21.2 Air Blast-Induced Ground Shock.

One-dimensional wave propagation theory is used to estimate air blast-induced ground shock. For surface structures located on ground media having uniform properties, the expressions to define this motion take very simple forms. Using this approach, the maximum vertical velocity at the ground surface, V_V, can be expressed as

$$V_V = P_{so} / (\rho C_p) \qquad 2\text{-}74$$

where

V_V = *maximum vertical velocity of the ground surface*
P_{so} = *peak positive incident pressure (Figure 2-15 (+))*
ρ = *mass density of the soil*
C_p = *compression wave seismic velocity in the soil*

The mass density, ρ, for typical soils and rock are presented in Table 2-10 (+) and the seismic velocities are presented in Table 2-11 (+).

The maximum vertical displacement, D_V, is obtained by integrating the above expression with respect to time. The integral of the pressure with respect to time is simply the total positive phase impulse so that:

$$D_V = i_s / (1000\ \rho C_p) \qquad 2\text{-}75$$

where

D_V = *maximum displacement of the ground surface*
i_s = *unit positive incident impulse (Figure 2-15 (+))*

The maximum vertical acceleration, A_V, is based on the assumption of a linear velocity increase during a rise time equal to one millisecond. The resulting acceleration is increased by 20 percent to account for nonlinearity during the rise time. Accelerations are expressed in multiples of the gravitational constant so that,

$$A_V = 100\ P_{so} / (\rho C_p\ g) \qquad 2\text{-}76$$

where

A_V = *maximum vertical acceleration of the ground surface*
g = *gravitational constant equal to 32.2 ft/sec^2*

The above equation is adequate for predicting the acceleration in dry soil. However, the equation underestimates the acceleration in saturated soils and rock. To approximate the acceleration of saturated soils and rock, it is recommended that the value of the acceleration obtained from the Equation 2-76 be doubled.

The maximum horizontal ground motions are expressed in terms of the maximum vertical motions as a function of the seismic velocity of the soil and the shock wave velocity so that

$$D_H = D_V \tan [\sin^{-1} (C_p / (12{,}000\ U))] \qquad 2\text{-}77$$

$$V_H = V_V \tan [\sin^{-1} (C_p / (12{,}000\ U))] \qquad 2\text{-}78$$

$$A_H = A_V \tan [\sin^{-1} (C_p /(12{,}000\ U))] \qquad 2\text{-}79$$

where U = shock front velocity (Figure 2-15 (+)).
1\

For $C_p/(12{,}000\ U) > 0.707$, horizontal and vertical motions are approximately equal. Therefore, it is recommended that for all values of the above function greater than 0.707, the horizontal motion is set equal to the calculated vertical motion. /**1**/

The equations which describe the air-induced ground shock are a function of the density and seismic velocity of the soil. However, a wide range of seismic velocities is given in Table 2-11 (+) for each of the soils listed. In a final design, soil tests are required to accurately determine the density and seismic velocity of the particular soil at the site. In lieu of tests, the mass density given in Table 2-10 (+) may be used. However, since the range of seismic velocities given Table 2-11Tables/02_011.PNG is so large, it is recommended that the lower bound value of the velocity be used to produce a conservative estimate of the induced motion.

2-21.3 Direct-Induced Ground Motion.

Empirical equations have been developed to predict direct-induced ground motions. The equations apply for TNT detonations at or near the ground surface. Three types of ground media have been considered; dry soil, saturated soil and rock. The ground shock parameters are expressed in terms of the charge weight and distance from the explosion.

The maximum vertical displacement (D_V) of the ground surface for a rock media is given by

$$D_V = 0.025\ R_G^{1/3}\ W^{1/3} / Z_G^{1/3} \qquad 2\text{-}80$$

in which

$$Z_G = R_G / W^{1/3} \qquad (2\text{-}81)$$

where

R_G = *ground distance from the explosion*
W = *weight of TNT charge*
Z_G = *scaled distance from the explosion*

and the maximum horizontal displacement D_H of the ground surface is equal to one-half of the maximum vertical displacement or

$$D_H = 0.5\ D_V \qquad (2\text{-}82)$$

When the ground media consists of either dry or saturated soil, the maximum vertical displacement is given by

$$D_V = 0.17\ R_G^{1/3}\ W^{1/3} / Z_G^{2.3} \qquad (2\text{-}83)$$

while the maximum horizontal displacement D_H is equal to the maximum vertical displacement or,

$$D_H = D_V \qquad (2\text{-}84)$$

The maximum vertical velocity (V_V) for all ground media is given by

$$V_V = 150 / Z_G^{1.5} \qquad (2\text{-}85)$$

and the maximum horizontal velocity (V_H) is equal to the maximum vertical velocity for all ground media or

$$V_H = V_V \qquad (2\text{-}86)$$

Finally, the maximum vertical acceleration (A_V) of the ground surface for all media is given by

$$A_V = 10{,}000 / (W^{1/3}\ Z_G^2) \qquad (2\text{-}87)$$

while for dry soil, the maximum horizontal acceleration, A_H, is equal to one- half of the maximum vertical acceleration, or

$$A_H = 0.5\ A_V \qquad (2\text{-}88)$$

however, for a wet soil or a rock media, the horizontal and vertical acceleration is equal, or

$$A_H = A_V \qquad (2\text{-}89)$$

2-22 AIR SHOCK.

2-22.1 Introduction.

When an air blast strikes an aboveground protective structure, motions are imparted to the building. The most severe motion is due to the response of the individual elements which make up the exterior shell of the structure. Procedures for the design of these elements are presented in subsequent chapters of this manual. This section is concerned with the gross motion of the structure on its supporting soil due to the impact of the air blast. This gross motion is in addition to the ground induced motions.

Vertical, horizontal and overturning motions are imparted to the structure by the air blast. However, since the vertical motion of the structure is restricted by the ground which is already compressed due to the dead load of the structure and its contents, vertical motions must necessarily be small and can be safely neglected. Overturning motions are also neglected in this section. These motions are most significant in tall structures with small plan dimensions which are not common in protective construction. This section is concerned solely with horizontal sliding motions which can be quite significant.

Horizontal motion results from an unbalanced blast load acting on the structure. The tendency of the structure to slide is resisted by the friction forces developed between the foundation and the underlying soil. For structures with deep foundations, additional resistance to sliding is afforded by active and passive soil pressures developed at the leeward side of the structure.

2-22.2 Method of Analysis.

The gross horizontal motion of a structure is computed in this manual using a method of numerical integration, namely, the acceleration-impulse extrapolation method. This method of dynamic analysis is comprehensively presented in Chapter 3. Briefly, the equation of motion for a single-degree-of-freedom system is given as

$$F - R - D = Ma \qquad (2\text{-}90)$$

where

F = *applied blast load as a function of time*
R = *resistance of the system to motion as a function of displacement*
D = *damping force as a function of velocity*
M = *mass of the single-degree-of-freedom system*
a = *acceleration of the system*

The numerical method of solving the equation of motion involves a step-by-step integration procedure. The integration is started at time zero where the displacement and velocity are known to be zero. The time scale is divided into small intervals. The values of *F*, *R* and *M* (*D* is not included) are calculated for each time step. The integration is started by first approximating the acceleration for the first time interval and progresses by successively calculating the acceleration at each time step. The change in velocity and displacement associated with each incremental acceleration is calculated. The accumulated velocity and displacement are obtained for each time step until the maximum values have been obtained.

The first step in the analysis is to describe the blast loads acting on the structure. The pressure-time variation of the blast load is computed as the shock front sweeps across the structure. The unbalanced load in the horizontal direction is computed as a function of the blast loads acting on the front and back walls (windward and leeward walls), respectively. The average blast load action of the roof of the structure is computed as the shock front traverses the building. The procedure used to describe these loading conditions have been presented in previous sections of this chapter.

The second step in the problem is the determination of the resistance of the building to horizontal motion. The tendency of the base of the structure to slide is resisted by friction forces on the foundation and earth pressure at the rear (leeward side) of the structure. For structures with shallow foundations, the resistance to sliding is afforded primarily by friction between the horizontal surfaces of the concrete foundation and underlying soil. The earth pressure resistance at the rear of the structure is small and can be conservatively neglected. For structures with deep foundations, the passive pressure at the rear of the structure is significant and greatly reduces the displacement of the building.

The friction force developed between the horizontal surfaces of the concrete foundation and underlying soil is given by

$$F_f = \mu F_N \qquad (2\text{-}91)$$

where

F_f = *frictional force resisting horizontal motion*

μ = *coefficient of friction between concrete and type of supporting soil*
F_N = *vertical load supported by the foundation*

The coefficient of friction μ for the horizontal surface between the concrete foundation and the underlying soil is given in Table 2-12 (+) for various types of soil. The coefficient is not a function of time or displacement. However, the structure must slide a finite amount before the frictional force is generated. The structure should slide approximately one-quarter of an inch before the frictional force is taken into account.

The vertical load F_N supported by the foundation consists of the dead weight of the structure, the weight of the building's interior contents, and the blast load acting on the roof of the structure. Since the blast load is a function of time, the building's resistance to sliding (frictional force F_f) is also a function of time. In addition, the blast load acting on the roof greatly increases the foundation loads, and consequently, significantly increases the building's resistance to sliding.

2-23 STRUCTURE MOTIONS.

2-23.1 Introduction.

The net motion of a structure is a combination of the motions due to the air-induced and direct-induced ground shock, and the air shock. Since the methods of analysis described in this section are applicable to rigid concrete structures located at comparatively large distances from an explosion, the structure motions are taken equal to the ground motions in the vicinity of the building. In the case of air shock, the structure motions are computed directly.

The motion of structures located at comparatively close distances to an explosion, as well as the motion of non-rigid structures, may also be determined. However, the local effects associated with these conditions such as motions due to cratering, fragment impact, etc. must be accounted for in the determination of the structure motions.

2-23.2 Net Ground Shock.

The net ground shock associated with an accidental explosion is a combination of the air-induced and direct-induced ground shock. The time at which the shock is felt at adjacent structures and the magnitude and duration of the motion are functions of the quantity of explosives detonating, the absolute distance between the detonation and adjacent structure, and the soil media at the site.

The air-induced ground shock is a function of the air blast. Consequently, the arrival time and duration of the ground shock may be taken equal to the arrival time t_A and duration t_o of the air blast. For an explosion occurring at or near the ground surface, the arrival time and duration are obtained from Figure 2-15 (+) for the scaled ground distance Z_G between the explosion and the structure. Figure 2-15 provides the blast parameters associated with the detonation of hemispherical TNT charge located on the ground surface.

The direct-induced ground shock is a function of the soil media. The arrival time of the shock load at the structure is a function of the seismic velocity in the soil and the distance from the explosion. The arrival time is expressed as

$$t_{AG} = 12{,}000\ R_G / C_p \qquad 2\text{-}92$$

where

t_{AG} = *arrival time of the ground shock*
R_G = *ground distance from the explosion*
C_p = *compression wave seismic velocity in the soil (Table 2-11 (+))*

As previously explained, the seismic velocity of the soil should be obtained from soil tests for a final design. In lieu of tests, it is recommended that the entire range of velocities given in Table 2-11 (+) be investigated to determine if the direct-induced ground shock can be in phase with the air-induced ground shock.

The actual duration of the shock load is not readily available. However, it is sufficient to realize that the duration is long, that is, many times larger than the duration of the air-induced shock.

The net ground shock is obtained from consideration of the arrival time and duration of each type of induced shock. If $t_A + t_o$ is less than t_{AG}, the structure is subjected to super-seismic ground shock (Figure 2-253 (+)). The air-induced ground shock arrives at the structure first and is dissipated by the time that the direct-induced ground shock arrives. The structure feels the effect of each shock separately. If t_A is greater than t_{AG}, the structure is subjected to outrunning ground shock (Figure 2-253). The direct-induced ground shock arrives at the structure first and, since its duration is long, the air-induced ground shock will arrive at the structure while the direct-induced ground shock is still acting. The structure feels the combined effects of the induced shocks. If t_A is slightly less than t_{AG} and $t_A + t_o$ is greater than t_{AG}, the air-induced ground shock will still be acting when the direct-induced ground shock arrives. For design purposes, this latter case should be treated as an outrunning ground shock.

2-23.3 Maximum Structure Motion.

The design of protective structures to resist the effect of shock loads is based on the peak values of the induced motion rather than the actual motion-time relationships. In fact, the actual time history of the motion is not known, nor can it be approximated with any degree of accuracy. Consequently, the phasing of the various shocks cannot be accomplished accurately. Therefore, for design purposes the peak values of the in-phase motions are added.

For the case of air-induced ground shock and air shock, the maximum values of horizontal displacement, velocity and acceleration are always added. These shock

motions must be in phase since they are caused by the same source, namely, the air blast.

In the case of super-seismic ground shock where the air-induced and direct-induced ground shock are completely separated, the maximum motion may be due to either source. The maximum value of displacement, velocity, or acceleration is the numerically larger value regardless of its source.

In the case of outrunning ground, the structure motion results from the combined effect of the air-induced and direct-induced ground shock as well as the air shock. The maximum motions in the vertical and horizontal direction is the algebraic sum of the maximum value of displacement, velocity, and acceleration from each source of motion in the vertical and horizontal directions.

2-24 SHOCK RESPONSE SPECTRA.

2-24.1 Introduction.

For the purposes of assessing the effects of shock on structures, one of the simplest interpretations of motion data involves the concept of the response spectrum. A response spectrum is a plot of the maximum response of a simple linear oscillator subjected to a given input motion against frequency. Hence, a response spectrum depicts only maximum response values, not a time-dependent history of the motion of the oscillator. The use of these maximum values is sufficient to ensure a reasonable and safe design for shock loads.

2-24.2 Definition of Shock Spectra Grid.

Response spectra are constructed from consideration of the response of a simple linear oscillator. For a protective structure subjected to shock loads, a piece of equipment or any interior component can be considered as the mass of a simple oscillator. The load-deflection properties of the structural system which connects the component to the protective structure determine the spring constant of the oscillator.

The maximum displacement of the mass (building component) relative to the base (protective structure) is called the spectrum displacement (D), and the maximum acceleration of the mass is called the spectrum acceleration (A). The maximum velocity of the mass is approximately equal to the more useful quantity called the spectrum pseudo-velocity (V) which is given by

$$V = 2\pi fD \qquad (2\text{-}93)$$

where

V = velocity of the mass
f = natural frequency of vibration of the oscillator
D = displacement of the mass

For an undamped system, the displacement and acceleration are related by

$$A = \frac{(2\pi f)^2 Dg}{387} \qquad 2\text{-}94$$

where

A = *acceleration of the mass in g's*
g = *gravitational constant*

When damping is present, the above relationship between acceleration and displacement is approximate. However, the relationship may still be used to develop shock spectra.

Plots of the three quantities, displacement *D*, velocity *V*, and acceleration *A*, against frequency *f*, are then shock spectra. They may be plotted individually or, more conveniently, on a single plot by means of the type of chart shown in Figure 2-254 (+). Any point on this logarithmic grid represents a simultaneous solution to Equations 2-93 and 2-94. The log-log grid must be proportioned to satisfy the solution of the equations. The grid is constructed from standard log-log paper on which a second log-log grid is superimposed and rotated 45 degrees. The width of a log cycle on this rotated grid is 0.707 times the width of a cycle on the standard grid.

2-24.3 Response Spectra.

A response spectrum is a plot of the maximum response of a single-degree-of-freedom system to a given input motion. The given input motions are the air shock and the air-induced and direct-induced ground shocks. Since the maximum values of the free-field displacement, velocity, and acceleration (input motion) are used to construct the spectra, a response spectrum envelope is produced. The spectrum takes a trapezoidal shape and is shown in Figure 2-254 (+) by the lines labeled *D*, *V* and *A*. The three sides of this trapezoid can be related to the maximum free-field input motion parameters of displacement, velocity, and acceleration.

Relationships between the spectrum envelope bounds and the characteristics of the time dependent free-field input motions (displacements, velocities, and accelerations) clearly indicate that as the variation of the free-field motion parameters versus time is defined, the definition of the corresponding spectrum envelope can be refined. However, in the general case of blast-induced motions, the variation of the input motions with time cannot visually be described in significant detail. Consequently, it is recommended that for the elastic response of systems, the spectrum be defined by the following three straight lines as illustrated in Figure 2-254 (+).

(1) Line "D" is drawn parallel to lines of constant displacement with a magnitude equal to the maximum free-field (building) displacement.

(2) Line "V" is drawn parallel to lines of constant velocity (actually pseudo velocity) with a magnitude equal to one and one-half (1.5) times the maximum free-field (building) velocity.

(3) Line "A" is drawn parallel to lines of constant acceleration with a magnitude equal to two (2) times the maximum free-field (building) acceleration.

A spectrum defined in this manner is clearly an approximation, however, its accuracy is considered to be consistent with the accuracy of the input free-field (building) motions on which it is based. In those cases where the input motions can be defined with greater confidence, the spectrum identified above can be defined to reflect the greater accuracy.

In most cases, interior components of the structure and/or equipment and equipment supports are designed elastically. Therefore, the shock spectra described above will suffice. However, when a very large explosion causes large structure motions, interior systems may require inelastic designs. These conditions will usually not arise for the charge capacities considered in this report. Therefore, methods for calculating inelastic shock spectra have not been presented. It is recommended that the bibliography given at the end of this chapter be consulted for further data on this subject.

Figure 2-253 Net Ground Motions Produced By an Explosion at the Ground Surface

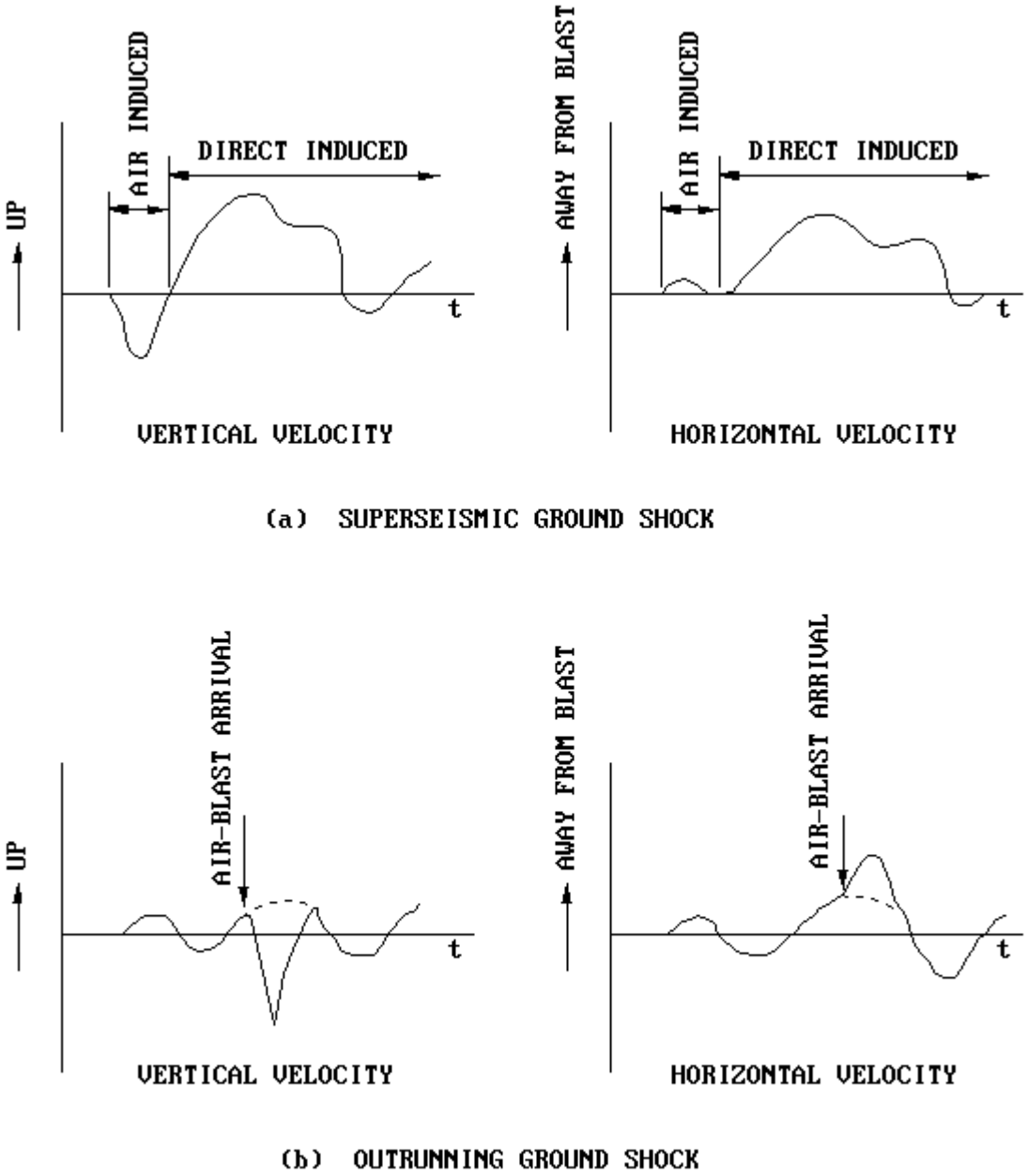

Figure 2-254 Typical Response Shock Spectra

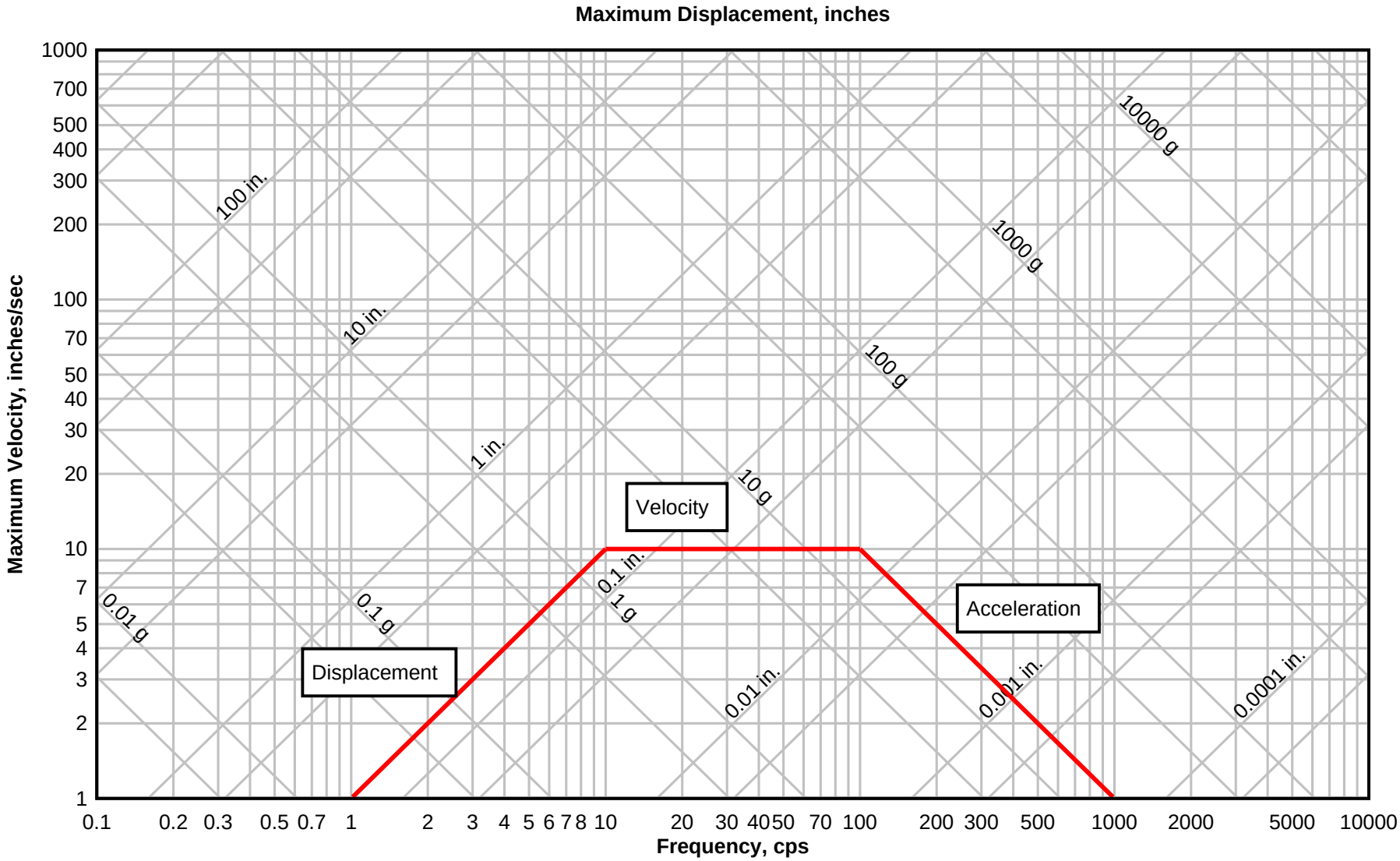

Table 2-10 Mass Density for Typical Soils and Rocks

Material	Mass Density, ρ (lb-sec^2)/in^4
Loose, dry sand	1.42 E-04
Loose, saturated sand	1.79 E-04
Dense, dry sand	1.65 E-04
Dense, saturated sand	2.02 E-04
Dry clay	1.12 E-04
Saturated clay	1.65 E-04
Dry, sandy silt	1.57 E-04
Saturated, sandy silt	1.95 E-04
Basalt	2.56 E-04
Granite	2.47 E-04
Limestone	2.25 E-04
Sandstone	2.10 E-04
Shale	2.17 E-04
Concrete	2.25 E-04

Table 2-11 Typical Seismic Velocities for Soils and Rocks

Material	Seismic Velocity (in/sec)
Loose and dry soils	7,200 to 39,600
Clay and wet soils	30,000 to 75,600
Coarse and compact soils	36,000 to 102,000
Sandstone and cemented soils	36,000 to 168,000
Shale and marl	72,000 to 210,000
Limestone-chalk	84,000 to 252,000
Metamorphic rocks	120,000 to 252,000
Volcanic rocks	120,000 to 270,000
Sound plutonic rocks	156,000 to 300,000
Jointed granite	9,600 to 180,000
Weathered rocks	24,000 to 120,000

Table 2-12 Coefficient of Friction for Concrete Foundation and Underlying Soils

Soil Material	Coefficient of Friction, μ
Clean sound rock	0.70
Clean gravel, gravel-sand mixture, coarse sand	0.55 to 0.60
Clean fine to medium sand, silty medium to coarse sand, silty or clayey gravel	0.45 to 0.55
Clean fine sand, silty or clayey fine to medium sand	0.35 to 0.45
Fine sandy silt, nonplastic silt	0.30 to 0.35
Very stiff and hard residual or preconsolidated clay	0.40 to 0.50
Medium stiff and stiff clay and silty clay	0.30 to 0.35